

SYNTHESIS AND CHARACTERIZATION OF ACTIVATED PITCH-BASED CARBON FIBERS

Michael W. Thwaites, Brian McEnaney and François D. Botha
University of Kentucky
Center for Applied Energy Research
3572 Iron Works Pike
Lexington, KY 40511

Brent E. McNeese and Michael B. Sumner
Ashland Carbon Fibers Division
P.O. Box 391
Ashland, KY 41114

Keywords: Carbon Fibers, Activated Carbon, Adsorption Studies

INTRODUCTION

Recently there has been an increase in interest in activated carbon fibers (ACF) produced from pitch precursors. These fibers offer a number of advantages and because of their novel properties may be more suitable in certain applications than granular and powdered activated carbons. Being fibrous in form, they can be incorporated more easily into fabrics, filters and other articles which would require special designs to include a powder or granular product. The isotropic nature of pitch-based fibers makes it possible to create high specific surface areas in the region of 700 - 2000 m²g⁻¹; because diffusion limitations are minimal, the fibers exhibit very high rates of adsorption and desorption, and they may be produced in a wide variety of woven and non-woven forms.

The adsorptive properties of petroleum pitch-based ACF are not as well-studied as other types of activated carbon fiber. This paper will discuss the manufacture and pore structure characterization by gas adsorption and mercury porosimetry of ACF derived from Ashland petroleum pitch.

MANUFACTURE OF ACTIVATED PITCH-BASED CARBON FIBERS

Figure 1 is a block diagram of the method for producing ACF from petroleum pitch. The starting material is a heavy petroleum fraction from catalytic cracking which must be purified to remove catalytic fines, ash and other impurities. Pitch is produced by distillation, thermal cracking, solvent extraction or combined methods. Pitch is a complex mixture of polynuclear aromatic hydrocarbon species, with sulfur and nitrogen incorporated into the aromatic structure as heteroatoms. Short aliphatic substituents are present on the "typical" petroleum pitch molecule. Softening temperature [1] is a common test method for characterization. The softening point must often be increased by further distillation prior to fiber forming by melt spinning or melt blowing. In these fiber forming processes, the pitch is melted to a carefully controlled viscosity and then forced through a number of fine capillaries to produce the fiber as the pitch re-solidifies. The diameter of the fiber is controlled by drawing the fiber and winding it onto a reel for the case of melt spinning. In melt blowing, a stream of air is used to blow the fiber onto

a moving belt as it forms into a random mat. Extreme care must be taken to control temperature and other fiber forming conditions.

Once formed, the "green" pitch fiber is still fusible. In order to withstand the high carbonization temperature without remelting, it must first be heated gradually and carefully in an oxidizing atmosphere to render it infusible. The fiber can then be carbonized under an inert atmosphere until it contains about 95% carbon by weight. Activation of the carbon fiber is accomplished in much the same manner as for other types of activated carbon: by steam, by carbon dioxide or by chemical oxidation. The resulting chemical reactions attack the fiber surface and form pores, which are classified by diameter: micropores (< 2 nm), mesopores (2 - 50 nm) and macropores (> 50 nm).

CHARACTERIZATION OF ACTIVATED CARBON FIBERS

Several methods have been established and used to characterize activated carbon fibers of several types [2-6]. Frequently studied is the adsorption of gases (especially nitrogen and carbon dioxide), and of solvent vapors (e.g. carbon tetrachloride, benzene or toluene). Activated coal-tar pitch fiber was characterized by Kaneko *et al* [3], who obtained adsorption isotherms of nitrogen, benzene, NO, SO₂ and NH₃, and then determined a number of surface characteristics. References were also cited in [3] on prior studies of activated fibers derived from cellulose, polyacrylonitrile (PAN) and phenol resin. Activated fibers derived from an unspecified pitch were characterized by Lee *et al* [4-5] and Ryu [6], who measured adsorption of nitrogen, CO₂, iodine and methylene blue. Also contained in reference [6] were detailed discussions of methods used and measurements of the degree of activation as a function of burn-off, or weight percent lost during activation. Finally in [6], pore size distribution plots were compared for phenol resin-based ACF and a granular activated carbon.

The present paper describes the surface characteristics of petroleum pitch-based ACF as determined by mercury porosimetry and adsorption of nitrogen at 77 K and carbon dioxide at 195 K.

EXPERIMENTAL

Isotropic petroleum pitch-based non-woven carbon fiber mat was activated using steam to yield activated fibers with varying degrees of burn-off as indicated in Table 1. A sample of powdered coconut shell activated carbon (Pica G210) was chosen for comparison.

Specific volumes (cm³g⁻¹) and surface areas (m²g⁻¹) of macropores and mesopores were determined by mercury porosimetry using a Quantachrome Autoscan-60 porosimeter that attained a maximum pressure of 60 000 psig. Nitrogen surface area measurements at 77 K were carried out using a Quantachrome Autosorb 6 apparatus to provide a 40 point adsorption and a 40 point desorption isotherm. Isotherms were also obtained using carbon dioxide at 195 K. Specific surface areas were calculated from both the nitrogen and the carbon dioxide isotherms using the Brunauer, Emmett and Teller (BET) theory [2].

Micropore volumes and mesoporous surface areas were determined from the nitrogen data using the α_s method [2]. A "notional" micropore surface area was taken as the BET surface area minus the mesopore surface area. Micropore volumes were also calculated from the N_2 and CO_2 adsorption data using the Dubinin-Radushkevich (DR) method [2].

RESULTS AND DISCUSSION

A Type 1 isotherm is observed for ACF 86-1 and G210 carbon, Figure 2; similar isotherms were found for the other ACF samples. The ACF isotherm shows slight hysteresis extending to low relative pressures; the G210 isotherm shows similar hysteresis but with a step at $p/p_0 \sim 0.45$. These results suggest that the ACF contain mainly narrow micropores with little mesoporosity. G210 powdered carbon is also mainly microporous, but with larger mesoporosity than ACF. These qualitative observations are supported by α_s analysis, Table 1, which shows that although S_{BET} values for the two carbons are similar, the mesoporous surface areas are 9 and 15 m^2g^{-1} for ACF 86-1 and G210 carbon, respectively. Table 1 shows that it is possible to vary BET and mesoporous surface areas of ACF by varying the degree of activation.

Estimates of micropore radii, r , were made using the Dubinin-Stoeckli (DS) equation [7]: $E_{or} = 14.8 \pm 0.6 \text{ kJ}\cdot\text{mol}^{-1}\cdot\text{nm}$, where E_o is the characteristic energy obtained by application of the DR equation to nitrogen adsorption isotherms. Values of r increase progressively with increase in burn-off of the ACF, Table 1. Similar trends have been inferred from studies of granular activated carbons [8] and our results are consistent with those reported by Kaneko *et al* [3] for pitch-derived ACF with progressively increasing surface areas.

Higher BET surface areas are obtained in all cases from adsorption of CO_2 , Table 2, showing that micropores in ACF and G210 carbon are more accessible to CO_2 than to N_2 . For both CO_2 and N_2 adsorption there is a linear correlation between S_{BET} and the extent of burn-off, Figure 3, as was also reported by Lee *et al* [4]; it follows from this that there is also a linear correlation between S_{BET} for CO_2 and N_2 . Micropore volumes for adsorption of N_2 obtained from the DR equation are comparable to those obtained by the α_s method. Although S_{BET} values for CO_2 at 195 K are greater than those for N_2 at 77 K, DR micropore volumes for N_2 are comparable with those for CO_2 . This trend has also been noted previously for granular carbons [9].

It was confirmed by mercury porosimetry that ACF samples contained no macropores, Table 3. In contrast, G210 carbon had a macropore volume of 0.28 cm^3g^{-1} . Mesopores are found in both types of carbon using mercury porosimetry, Table 3. For both ACF and G210 carbon estimates of the mesoporous surface areas by the α_s method are smaller than those estimated from mercury porosimetry at 60 000 psig. This may be due to breakdown of the pore structure under the high pressures used [10].

Results for a lower mercury pressure, 50 000 psig, Table 3, show better agreement for the ACF materials.

CONCLUSIONS

Activated petroleum-pitch-based carbon fibers are predominantly microporous, showing very little mesoporosity and no macroporosity. This is consistent with previously published results for ACF from coal-tar pitch and other sources. On the other hand, the mesopore and macropore structures of a powdered activated carbon are more highly developed. This work has shown that it is possible to vary BET and mesoporous surface areas of ACF by varying the degree of activation.

ACKNOWLEDGEMENTS

We thank Frank Derbyshire and Mark Stewart of the Center for Applied Energy Research, University of Kentucky, and Keith Friley of Ashland Carbon Fibers Division for valuable discussions.

REFERENCES

- [1] ASTM Standard Test D 3461-76: Softening Point of Pitches - Mettler Cup-and-Ball Method.
- [2] S. J. Gregg and K.S.W. Sing, Adsorption, Surface Area and Porosity, 2nd. Edition, Academic Press, London, 1982.
- [3] K. Kaneko, Y. Nakahigashi and K. Nagata, Carbon 26(3), 327 (1988).
- [4] D. W. Lee, J.K. Lee, B.S. Rhee and S.K. Ryu, Korean Inst. Chem. Eng. 27(6), 777 (1989).
- [5] S.K. Ryu, B.S. Rhee, J.K. Lee, N. Pusset and P. Ehrburger, Carbone '90 International Carbon Conference, Paris, France, p.96 (1990).
- [6] S.K. Ryu, High Temperatures-High Pressures 22, 345 (1990).
- [7] M.M. Dubinin and H.F. Stoeckli, J. Colloid Interface Sci., 75, 34 (1980).
- [8] F. Rodriguez-Reinoso, J.M. Martin-Martinez, M. Molina-Sabio, R Torregrosa-Macia and J. Garrido-Segovia, J. Colloid Interface Sci., 106, 315 (1985).
- [9] F.D. Botha, unpublished work.
- [10] J.M. Dickinson and J.W. Shore, Carbon, 6, 937 (1968).

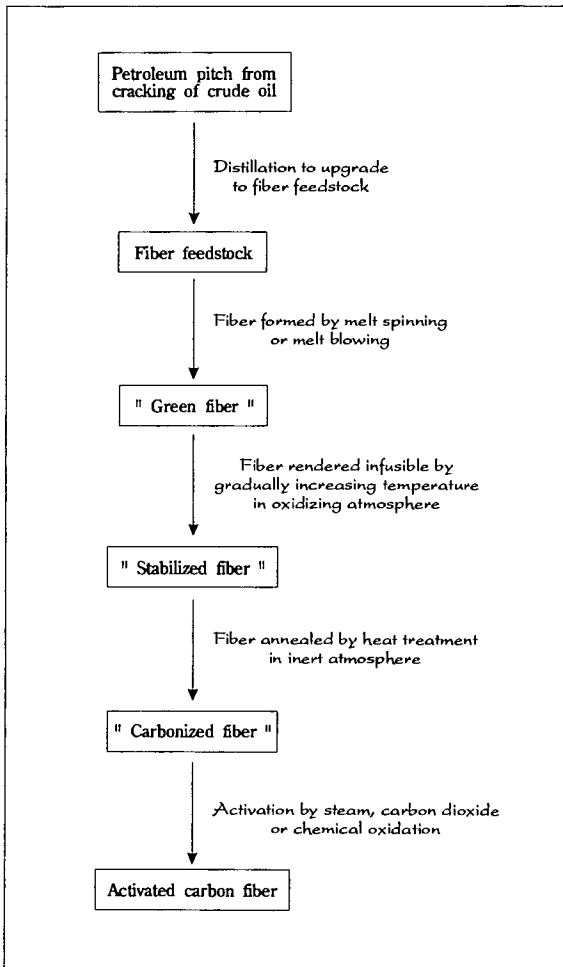


Figure 1 : Schematic diagram of the production of activated carbon fibers from isotropic petroleum pitch

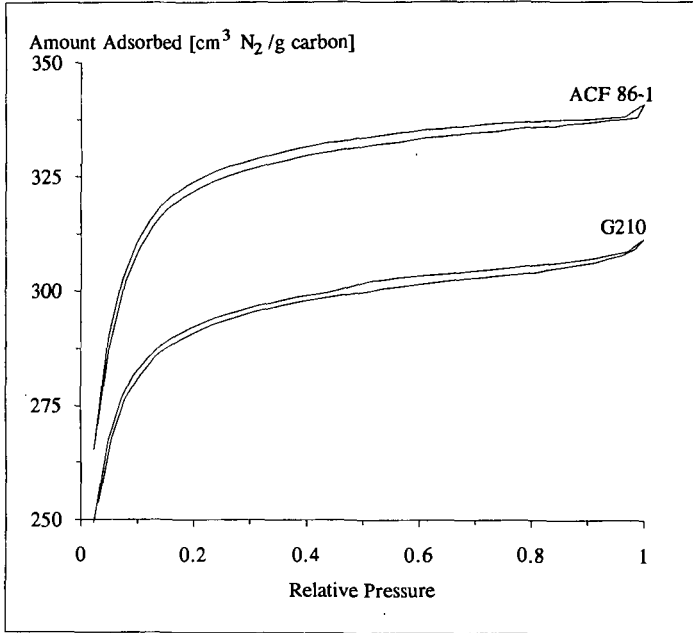


Figure 2 : Sorption isotherms for nitrogen at 77 K of G210 powdered activated carbon and ACF 86-1.

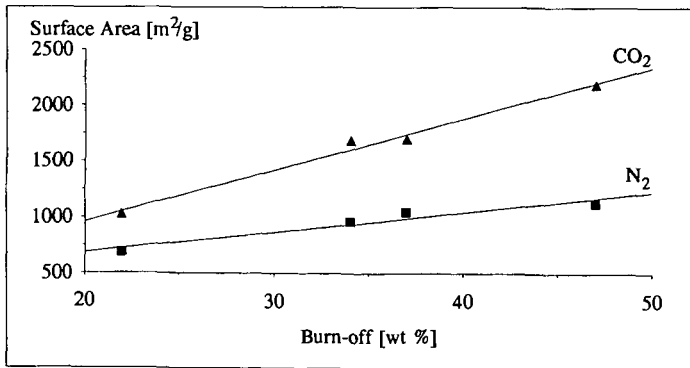


Figure 3 : BET surface areas from nitrogen (77 K) and carbon dioxide (195 K) adsorption on ACF as a function of burn-off.

Table 1. Pore structure analysis of activated carbons from N₂ adsorption data.

Sample	Burn-off (wt %)	BET Surface Area (m ² /g)	Mesopore Surface Area ¹ (m ² /g)	Notional Micropore Surface Area (m ² /g)	Micropore Volume ¹ (cm ³ /g)	Micropore Volume ² (cm ³ /g)	DS Mean Micropore Radius ³ (nm)
G210 Powdered Carbon	Not available	1193	15	1178	0.44	0.45	0.9
Carbon Fiber 41-1	22	685	2	683	0.26	0.26	0.4
Carbon Fiber 85-1	34	960	6	956	0.36	0.36	0.7
Carbon Fiber 70-1	37	1046	6	1040	0.39	0.40	0.8
Carbon Fiber 86-1	47	1123	9	1114	0.42	0.45	0.9

1 Calculated from the α_s method [Ref. 2]

2 Calculated from the Dubinin - Radushkevich (DR) equation [Ref. 2]

3 Calculated using the Dubinin - Stoeckli (DS) equation $E_{or} = 14.8 \pm 0.6 \text{ kJ.mol}^{-1}.\text{nm}$ [Ref. 7]

Table 2. Pore structure analysis of activated carbons from CO₂ adsorption data.

Sample	Burn-off (wt %)	BET Surface Area (m ² /g)	DR Micropore Volume ¹ (cm ³ /g)
G210 Powdered Carbon	Not available	1736	0.37
Carbon Fiber 41-1	22	1025	0.28
Carbon Fiber 85-1	34	1689	0.38
Carbon Fiber 70-1	37	1697	0.40
Carbon Fiber 86-1	47	2188	0.44

1 Calculated from the Dubinin - Radushkevich (DR) equation [Ref. 2]

Table 3. Pore structure analysis of activated carbons from mercury porosimetry.

Sample	Burn-off (wt %)	Macropore Volume (cm ³ /g)	Mesopore Volume (cm ³ /g)	Mesopore Surface Area 50 000 psig (m ² /g)	Mesopore Surface Area 60 000 psig (m ² /g)
G210 Powdered Carbon	Not available	0.28	0.08	37	55
Carbon Fiber 41-1	22	0	0	5	13
Carbon Fiber 85-1	34	0	0.04	6	21
Carbon Fiber 70-1	37	0	0.04	9	32
Carbon Fiber 86-1	47	0	0.05	13	49

Activated Carbons from Bituminous Coals by Reaction with H_3PO_4 : Influence of Coal Cleaning

Marit Jagtoyen, Brian McEnaney, John Stencil, Michael Thwaites
and Frank Derbyshire

University of Kentucky Center for Applied Energy Research
3572 Iron Works Pike, Lexington, KY 40511-8433

Keywords: Activated Carbon, Phosphoric acid, Coal cleaning

Introduction

Previous publications have described the results of research in this laboratory to investigate the conversion of coals to activated carbons through reaction with phosphoric acid (1-5). These studies have examined the compositional, morphological, and porosity changes in subbituminous and bituminous coals, resulting from reaction with H_3PO_4 at temperatures up to $650^\circ C$.

Most of the present studies has been concerned with the use of Illinois bituminous coals as activated carbon precursors. These coals have high sulfur and high mineral matter contents. Phosphoric acid reacts with both of these components, promoting the substantial removal of organic and inorganic sulfur as H_2S (5), and combining with mineral matter constituents, thereby increasing the ash content of the carbon.

The second of these effects is particularly undesirable from the standpoint of producing a quality adsorbent carbon. A possible solution is to lower the coal mineral matter content, by some physical separation process, prior to carbon synthesis. This paper describes the effects of coal cleaning by pentane agglomeration, for three bituminous coals with ash contents between about 8 to almost 40%, on the synthesis and properties of activated carbons.

Experimental

Three bituminous coals, IBC 101, IBC 104 and IBC 106, were studied as precursors. The coals were obtained from the Illinois Basin Coal Sample Program and were of high volatile C rank, as determined by vitrinite reflectance measurement. Properties of the coals are summarized in Table 1. The coals were selected to show significant differences in ash content and organic and inorganic sulfur: IBC 104 is a high ash content coal (39.3%) in which about two-thirds of the sulfur is in the pyritic form; IBC 101 and 106 both have lower ash contents (10.5 and 8.9%, respectively) but the first coal has a high proportion of organic sulfur and the second has an organic/pyritic sulfur ratio of about one.

The parent coals were ground to -20 mesh before reaction with phosphoric acid. Finer grinding (-200 mesh) was required for coal cleaning. Physically cleaned coal samples were produced using a laboratory scale flotation unit. Fuel oil or pentane was vigorously mixed with a coal/water slurry to render the coal particles hydrophobic and to selectively agglomerate them. The agglomerated slurry was then screened; the free ash particles flowed through the screen and the agglomerated coal was retained.

The procedure for preparing chemically activated carbons from both parent and cleaned coals has

been described in detail elsewhere (5). Briefly, a 20 g sample of coal was thoroughly mixed with 30 cm³ of 50% strength phosphoric acid solution. The mixture was then heated to 170°C and held at this temperature for 30 minutes in flowing nitrogen (80 ml.min⁻¹). Each sample was then heated to the higher heat treatment temperature of 550°C for 60 minutes in the same inert atmosphere. The solid products were leached with distilled water to pH=6 and vacuum dried at 110°C before further analysis.

Results and Discussion

The compositions of the cleaned coals are shown in Table 1. The reduction in ash content ranges from around 60%, for IBC 101 and IBC 106, to 90% for the high ash coal IBC 104. With all three coals, cleaning produces a significant rejection of pyritic sulfur. There is effectively no change in organic sulfur. For IBC 106, Si is also removed, and for IBC 104, there is substantial removal of both Si and Al.

The compositions of carbons produced from parent and cleaned coals by acid treatment, are shown in Table 2. In all cases, the carbons have much higher ash contents, by a factor of about two, than the corresponding precursor. Some increase is to be expected due to the loss of material to volatile products. However, the ash contents of the chemically-activated carbons are much higher than expected from devolatilization, and the trend is paralleled by increases in phosphorus content, as observed previously (5,6). Iron, silicon and aluminum can all form insoluble phosphates when reacted with phosphoric acid, and X ray diffraction data have shown that P is present as FePO₄, Si₂P₂O₇, Al(PO₃)₃ in carbons produced from both parent and clean coals. The formation of such species can account for the increased ash content and high phosphorus content of the synthesized carbons, even after extensive leaching.

The carbon phosphorus content is found to correlate almost linearly with both the total ash content of the parent coal and that of the carbon product, Figure 1, although the slopes of the curves differ. A high ash content is detrimental to the mechanical strength of the carbon product and its specific adsorptive capacity, and to the effective use of phosphoric acid: its consumption through these reactions means that less acid is available to promote the synthesis process, and less will be recoverable for recycle in an industrial process. The significant reductions in mineral matter, that are effected by coal cleaning, certainly help to minimize phosphorus retention and produce adsorbent carbons with much lower ash contents.

The data in Table 2 show that acid treatment causes extensive removal of sulfur: the concentrations of pyritic and organic sulfur are lowered by as much as 100% and 88%, respectively. The pyritic sulfur content is reduced to lower levels in the carbons from the parent coals and is almost completely eliminated in the carbons from the cleaned coals. More organic sulfur is also removed from the cleaned coals. The greater extent of S removal from the cleaned coals may relate to their smaller particle size and lower mineral matter content, both of which could facilitate access of the acid to the interior of the particles. The data for the parent high ash coal, IBC 104, provide evidence that the consumption of acid, by reaction with mineral matter, limits the extent of its reaction with the organic matrix, shown here by the extent of sulfur removal. After cleaning, the reduced mineral matter content allows more acid to be available for the removal of organic and pyritic sulfur, and other reactions involved in carbon synthesis.

The greater part of the coal sulfur is released in the form of H₂S, Figure 2. Approximately 60% of the sulfur in the starting coal is converted to H₂S for IBC 101, 47% for IBC 104, and 40% for IBC 106. This is considerably higher than can be attained by thermal treatment, as shown by other published data (5,7). Interestingly, the proportion of sulfur in the precursor that is removed as H₂S remains the same, irrespective of whether the coal has been cleaned or not.

Coal cleaning increases both the total (BET) surface area and the mesopore surface area of the synthesized carbons, Table 3. The bulk of the surface area is contained in the micropores. For the medium ash content coals, IBC 101 and IBC 106, the surface area is increased by 11 and 24%, respectively. However, for IBC 104, the surface areas of the carbon from the cleaned coal were about three times higher than for the carbon from the parent coal, corresponding to a major reduction in the ash content of the precursor from 39 to 4%.

The micropore, mesopore and macropore volumes are also significantly higher in the carbons from the cleaned coals, Figure 3. An exception is the macropore volume of IBC 106 which actually decreases after cleaning. The last observation may signify that, for this particular coal, the ash in the carbon made an appreciable contribution to the macroporosity.

One reason for the increased surface area and porosity in carbons from cleaned coals is considered to be that more of the phosphoric acid is available to react with the organic structure, since less will be consumed by reaction with coal mineral matter, as discussed. In the case of IBC 104, the high ash content of the parent coal could severely restrict the amount of available acid. Previous work has shown that acid concentration can be important to the development of porosity. By increasing the acid concentration from 15 to 50%, for the carbonization of coal IBC 101 at 550°C, the micropore volume was increased by a factor of four while the meso- and macropore volumes increased by a factor of two (6).

Mineral matter and ash constituents can also block the pore structure of coals and chars, which may also help to explain why coal cleaning prior to carbonization enhances porosity. Mahajan and Walker (8) examined the effects on pore structure of a number of coals by removing soluble inorganic constituents by acid washing of coals before carbonization, or the resulting chars. The results were apparently random with the surface area being increased in some cases and decreased in others, suggesting that the distribution of the mineral matter in the coal is an important parameter.

Ehrburger et al. (9) found that the micropore volume of chars was increased after demineralization of the parent coal. In these experiments, demineralization was effected by chemical treatment with HCl/HF prior to carbonization. Some of the increase in microporosity in these cases may well be due to the action of the acid on the organic structure of the coal, rather than simply the removal of mineral matter. The same authors found that acid pretreatment increased the carbonization yield which is indicative of the acid promoting crosslinking reactions. Similar phenomena may also account for some of the results obtained by Mahajan and Walker (8), where the coal structure is modified during acid washing, or during subsequent heat treatment in the presence of residual acid. It is known that acid treatment with HCl and HCl/HF modifies coal thermoplasticity and eliminates swelling during pyrolysis, Lee and Jenkins (10), Lu (11), and leads to increased microporosity in the carbon products.

It is supposed that the role of phosphoric and other acids is to initiate the cleavage of weak connecting bridges between coal structural units at sub-pyrolysis temperatures. Subsequently, bond cleavage reactions are followed by the re-combination of radical fragments to form stronger linkages or larger structural units, leading to the formation of a rigid crosslinked solid. This modified structure will be less susceptible to volume contraction upon heat treatment. Restricted shrinkage and limited volatile loss may facilitate the development, or perhaps more accurately, conservation of the elements of porosity that are present in the starting material. Consequently, factors that influence the availability of the reagent to the precursor will impact upon the pore structure of the carbon.

Summary

It has been shown that high mineral matter content can adversely influence the process of carbonization and the properties of carbons produced by chemical activation of coals. In thermal processing, it is desirable to keep the coal mineral matter content low as carbon is removed during carbonization and activation, thereby increasing the ash content. Around 8-10% ash in the activate is probably an acceptable maximum for many applications; higher concentrations can adversely affect the physical strength of the carbon and specific adsorption capacity. Ash constituents may also catalyze unwanted reactions when the carbon is in service and could reduce its ignition point.

In chemical activation with phosphoric acid, there are additional disadvantages in that acid is consumed by reaction with mineral matter. This leads to: reduced availability of acid for reaction with the organic structure, which may severely limit the extent of porosity development; the loss of recoverable acid for recycle; and an increase in the ash content of the carbon. Lowering the mineral matter content of the carbon precursor by coal cleaning techniques can provide a solution to these problems.

Acknowledgement

The authors wish to acknowledge the assistance of Jack Groppo and Danny Turner of the CAER, and the State of Kentucky and the Illinois Center for Research on Sulfur in Coal for financial support.

References

- 1) F. J. Derbyshire, M. Jagtoyen, B. McEnaney, S. M. Rimmer, J. M. Stencel and M. W. Thwaites, "Activated Carbon Preparation by Reaction of Subbituminous Coal with Phosphoric Acid", Proc. 20th Biennial Conference on Carbon, 23-28 June, 1991, Santa Barbara, CA, p52-53.
- 2) F. J. Derbyshire, M. Jagtoyen, B. McEnaney, J. M. Stencel and M. W. Thwaites, "The Adsorptive Properties of Activated Carbons Prepared by Phosphoric Acid Treatment of Subbituminous Coal", Proc. 20th Biennial Conference on Carbon, 23-28 June, 1991, Santa Barbara, CA, p2-3.
- 3) F.J.Derbyshire, M. Jagtoyen, B. McEnaney, S. M. Rimmer, J. M. Stencel, M. W. Thwaites, "Adsorbent Carbons form Coals by Chemical Activation", Proceedings 1991 ICCS Conference, 16-20 September, 1991, Newcastle, England, Butterworth-Heinemann Ltd.p480-483.
- 4) F. J. Derbyshire, M. Jagtoyen, B. McEnaney, A. R. Sethuraman, J. M. Stencel, D. Taulbee and M. W. Thwaites, "The Production of Activated Carbons from Coals by Chemical Activation", American Chemical Society, Fuel Division Preprints, 36 (3), 1072-1080, 1991.
- 5) F.J.Derbyshire, J. M. Stencel, B. McEnaney, M. W. Thwaites and M. Jagtoyen, "An Investigation of the Conversion of Illinois Coals to Activated Carbons". Final technical report to the Illinois Center for Research on Sulfur in Coal. Period 1st Sept. 1990 to 3rd Sept, 1991.
- 6) M. Jagtoyen, M. Thwaites, J. Stencel, B. McEnaney, and F. J. Derbyshire, "Adsorbent Carbon Synthesis from Coals by Phosphoric Acid Activation". Paper in preparation for Carbon.
- 7) Khan, M. R., "Prediction of Sulphur Distribution in Products during Low Temperature Coal Pyrolysis and Gasification", 1989, Fuel, **68**, 1439-1449.

8) Mahajan, O.P. and Walker, P.L., "Effect of Inorganic Matter Removal from Coals and Chars on their Surface Areas", 1979, Fuel, **58**, 333-337.

9) Ehrburger, P., Addoun, F. and Donnet, J.P., "Effect of Mineral Matter of Coals on the Microporosity of Charcoals", 1988, Fuel, **67**, 1228-1231.

10) Lee, C. W. and Jenkins, R.G., "Effect of Acid Treatment Atmosphere on the Thermoplasticity of a Low-Volatile Bituminous Coal", 1989, Energy Fuels, **3**, 703.

11) Lu, G.Q. and Do, D.D., "Structure Changes of Coal Reject Char during Pyrolysis at Low Heating Rates", Fuel Processing Technology, **28**, 1991, 247-258.

Table 1. Composition of parent and cleaned coals (wt.%).

Coal	ash	Fe	Si	Al	Pyr.S	Org.S	S
101	10.5	1.4	2.5	0.9	1.6	4.0	5.7
101 clean	4.1	0.8	2.5	1.2	0.8	3.6	4.4
104	39.3	3.2	10.8	3.6	4.4	3.0	7.5
104 clean	3.9	0.7	1.5	0.8	0.9	3.1	4.0
106	8.9	1.7	1.9	0.9	2.4	2.4	4.8
106 clean	3.7	0.8	1.1	1.3	1.0	2.4	3.4

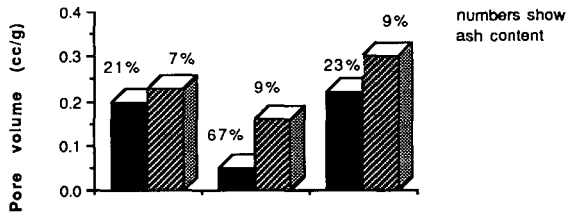
Table 2: Composition of carbons from parent and cleaned coals (wt.%).
(Carbons produced at HTT=550°C, 50% phosphoric acid)

Sample	ash	P	Fe	Si	Al	Pyr.S	Org.S	S
101	20.8	3.2	0.1	10.9	4.0	0.3	0.9	1.2
101 clean	7.0	1.3	0.3	0.1	0.2	0.1	0.8	0.9
104	67.0	8.7	2.5	34.8	8.8	2.3	2.0	4.4
104 clean	8.9	1.5	0.1	0.2	0.1	0.0	0.8	0.9
106	22.7	3.2	1.2	9.8	3.7	0.5	0.3	0.8
106 clean	9.2	1.7	0.2	0.3	0.1	0.1	0.3	0.5

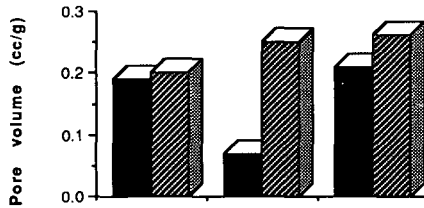
Table 3: Surface areas of carbons from parent and clean coals.
(Carbons produced at HTT=550°C, 50% phosphoric acid)

Sample	BET s.a. (m ² /g)	Mesopore s.a. (m ² /g)
101	575	87
101 clean	638	82
104	155	24
104 clean	652	98
106	660	92
106 clean	820	113

a) micropore volume



b) mesopore volume



c) macropore volume

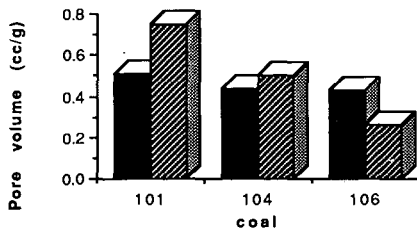


Figure 3: Pore volumes for carbons heat treated to 550°C, 50% acid.

■ carbons from parent coal ▨ carbons from clean coal

PRODUCTION OF CARBON MOLECULAR SIEVES FROM ILLINOIS COAL

Anthony A. Lizzio and Massoud Rostam-Abadi

Illinois State Geological Survey
615 E. Peabody Drive
Champaign, IL 61820

Keywords: coal, carbon molecular sieve, adsorption, gas separation

INTRODUCTION

Gas separations are a major production cost in the chemical industry today. Production of industrial gases by noncryogenic methods, e.g., pressure swing adsorption (PSA), is expected to grow much faster than by the conventional method, cryogenic distillation [1]. Although there is room for improvement in the design and operation of PSA processes for gas separation, most gains in process efficiency will likely come about from the development of new and improved adsorbent materials [2,3].

Carbon molecular sieves (CMS) have become an increasingly important class of adsorbents for application in the separation of gas molecules that vary in size and shape [1-6]. CMS are microporous materials with average pore dimensions similar to the critical dimensions of an adsorbate molecule. Selectivity for gas uptake by CMS is controlled by the relative rates of diffusion of the adsorbing gaseous species, as opposed to zeolites, which have separation efficiencies based primarily on their chemical affinity for a specific component in the gas mixture [6]. Gas molecules with only slightly varying critical dimensions, e.g., 0.2 Å, may be adsorbed by CMS at rates that vary by several orders of magnitude [7]. Thus, a small change in the average pore size can significantly affect the rate of diffusion of a gas molecule through the pore structure. Under controlled conditions of heat treatment [8-13] and activation [11-13], it has been possible to prepare carbonaceous adsorbents (chars) from coal which exhibit molecular sieve behavior. Pore structure modification can also be achieved by carbon deposition, i.e., the cracking of a suitable hydrocarbon gas within the pores of a carbon substrate [13-17].

The coal research program at the Illinois State Geological Survey has recently initiated a project to determine whether Illinois Basin coals are suitable feedstocks for the production of CMS and to evaluate the potential application of these products in gas separation processes. Data generated in this study will be used to design and engineer CMS with a proper pore size which will resolve a specific gas separation problem. This paper reports data on the kinetics of adsorption of oxygen, nitrogen, carbon dioxide, methane and hydrogen at 25°C on a series of chars prepared from an Illinois Basin coal under various pyrolysis and activation conditions. The effects of coal and char pretreatments such as preoxidation, demineralization, addition of potassium salt and carbon deposition on the molecular sieve properties of the char are also being investigated.

EXPERIMENTAL

Char Preparation: Chars were prepared from a Colchester (Illinois No. 2) hvC bituminous coal (sample IBC-102 of the Illinois Basin Coal Sample Program [18]). The coal is from a western Illinois preparation plant and is relatively low in organic and high in pyritic sulfur. The proximate and ultimate analyses for the coal and for the size fraction (12x40 mesh) used in this study are given in Table 1.

A microbalance reactor (Cahn RG) was used initially to prepare chars. Typically, 500 mg of coal was placed in a wire mesh basket and heated at 20°C/min in flowing N₂ (500 cm³/min) to a temperature between 600 and 1000°C and held for 0.5 h. The char was cooled in N₂, ground to -200 mesh and stored under N₂ for future characterization. A horizontal fixed-bed reactor was used to prepare larger quantities of char (up to 15 g) under similar conditions.

To enhance surface area development and increase the adsorption capacity of the char, both "physical" and "chemical" activation methods [19] were employed. Physical activation of the char was done in 1 atm CO₂ at 850°C. Upon reaching the desired conversion level, the reactant gas was switched to N₂ and the char sample cooled to 25°C. Chemical activation involved the addition of an alkali salt to the raw coal and subsequent heat treatment in inert gas. More specifically, the coal was physically mixed with potassium hydroxide (KOH) in a 1:1 ratio (by weight), ground with a mortar and pestle to -200 mesh, and pyrolyzed in N₂ at 800°C for 0.5 h. The char was cooled in N₂ to room temperature and washed with distilled water to remove the residual potassium. Since this char became noticeably warm upon removal from the furnace following pyrolysis, the char was submerged in water (quenched) to prevent any further oxidation.

Some chars were prepared by preoxidizing the coal at various O_2 partial pressures (0.2-1.0) and temperatures (130-220°C) prior to pyrolysis. In order to study the influence of mineral matter present in the coal on the molecular sieve properties of the char, a portion of the coal was acid-washed with 5 N HCl (60°C, 3 h); the ash yield was reduced from 3.2 to 1.2%.

The adsorption properties of the char were also modified by carbon deposition (CD). The char sample (1-3 g), placed in the horizontal tube furnace, was heated in flowing N_2 to 800 or 1000°C and held at this temperature for 0.5 h before switching to either 10% (balance N_2) or 100% CH_4 (300 cm^3/min). After a given CD time, N_2 was reintroduced to flush out any residual CH_4 before cooling to 25°C.

Char Characterization: Total surface areas of selected chars were determined from the amount of N_2 and CO_2 adsorbed at 77 and 195 K using a dynamic sorption method in conjunction with a single-point BET adsorption equation [20]. For comparison, a volumetric adsorption apparatus (Autosorb-1, Quantachrome Corp.) was used to obtain equilibrium adsorption data over the entire range of relative pressure. The N_2 (77 K) and CO_2 (273 K) surface areas, in this case, were determined using the multi-point BET and Dubinin-Radushkevich (DR) equations, respectively.

An experimental procedure was developed using the volumetric adsorption apparatus to determine the kinetics of adsorption (volume adsorbed vs. time) of a single gas, e.g., O_2 , N_2 , CO_2 , CH_4 , or H_2 , at 25°C. A typical run proceeded as follows: 0.3-1.5 g char was placed in a sample cell and outgassed (1×10^{-5} torr) at 180°C for 8 h. Helium was used to determine the dead volume of the sample cell. After outgassing again for several minutes, a known volume of gas was introduced into the sample cell (initial pressure of 350-500 torr) and the subsequent decrease in pressure monitored at 6 s intervals by a pressure transducer accurate to within ± 1 torr. After 10-30 min adsorption time, the sample was outgassed under vacuum at 25°C for 10 min and the same experiment repeated to ensure experimental reproducibility. Volumes adsorbed were calculated using the ideal gas law.

RESULTS AND DISCUSSION

Previously in this study [21], only values of N_2 and CO_2 equilibrium adsorption capacities were reported for our prepared chars. Differences in the N_2 and CO_2 surface area of each were attributed to the molecular sieving nature of the char; however, questions concerning how these materials would behave in an actual gas separation process remained. A knowledge of the kinetics of adsorption of select gases should allow us to better assess the potential usefulness of these materials in specific gas separation processes. In this section, three gas separation processes of commercial importance, N_2/O_2 , CO_2/CH_4 and CH_4/H_2 , are examined. Kinetic data obtained at 25°C for adsorption of these gases on selected chars are presented and discussed.

Oxygen/Nitrogen Separation: The demand for the two major industrial gases, oxygen and nitrogen, is on the rise due to their increased use in the combustion and gasification of coal [22] and in the steel and electronics manufacturing industries [23]. High purity N_2 can be produced using CMS in a PSA process. Nitrogen is the high pressure product and oxygen (35-50%) is produced as the low pressure product [2,3]. Air separation using microporous carbons relies on the fact that O_2 (kinetic diameter, 3.46 Å) diffuses into the carbon more rapidly than N_2 (3.68 Å) [24]. The kinetics of O_2 and N_2 adsorption at 25°C on the IBC-102 chars prepared at 600, 800, 900 and 950°C are shown in Figure 1. All chars adsorb more O_2 than N_2 and, thus, have some molecular sieving capability for air separation. Table 2 presents the O_2 and N_2 adsorption capacities of each char measured after 5 min and the ratio of both, or O_2/N_2 selectivity. Analysis of Figure 1 reveals that the O_2/N_2 selectivity decreases with time of adsorption, e.g., for the 800 and 900°C chars, the O_2/N_2 selectivities after only 30 s were 2.98 and 4.81, respectively, compared to 1.34 and 3.46 after 5 min. To be effective as a molecular sieve, the product should have a high selectivity ratio as well as a high adsorption capacity. A high selectivity indicates that the sieve readily discriminates between components in the gas mixture. A high adsorption capacity, of course, indicates that the molecular sieve will adsorb a large volume of gas. Table 2 shows that both the O_2 and N_2 adsorption capacities of the 800-1000°C chars decrease with increasing heat treatment temperature (HTT) while the O_2/N_2 selectivity increases from 1.34 to 4.10. Nandi and Walker [9] reported O_2/N_2 adsorption data (measured at 0.8 atm and 25°C) for several chars derived from lower rank coals. The extent of O_2 and N_2 adsorption showed a similar trend with HTT; however, their O_2/N_2 selectivities were substantially lower than those of the IBC-102 chars at any given HTT.

The IBC-102 char produced at 900°C seems to possess optimum molecular sieve properties for O_2/N_2 separation. A comparison of the the O_2/N_2 adsorption properties of this char with those of a coal-based carbon molecular sieve (CMS-A) used in air separation [12,17], a commercial CMS manufactured by Takeda Chem. Ind., Co. (measured at 1 atm and 25°C) [25] and a standard Linde type 4A zeolite is shown in Figure 1. The ability of each material to separate O_2 from N_2 is remarkably similar (except, of course, for the zeolite), suggesting that IBC-102 coal may, indeed, be a suitable feedstock for the production of CMS. No U.S. company currently manufactures CMS for commercial gas separation processes. Air

Products uses a coconut char-based CMS imported from overseas in its recently developed PSA process for production of N_2 from air [26,27]. A European patent [28] describes a process developed to manufacture CMS from coconut char. Typical values of O_2 adsorption capacity and O_2/N_2 selectivity obtained for a series of coconut char-based CMS were 4-6 cm^3/g and 6.5-8.5, respectively. In order to be competitive with currently available coconut char-based CMS, chars derived from coal should have comparable molecular sieve properties. Table 2 shows that our best product (900°C char) has an O_2 adsorption capacity of 4.46 cm^3/g and a selectivity of 3.46.

Table 2 presents O_2/N_2 adsorption capacities for two chars prepared from demineralized IBC-102 coal. For the 800°C char, acid-washing leads to a 1 cm^3/g decrease in the O_2 adsorption capacity, but a 40% increase in O_2/N_2 selectivity. For the 900°C char, there is a slight increase in the O_2 adsorption capacity, but the O_2/N_2 selectivity decreases by 18%. It seems there is no clear advantage in acid-washing this coal before pyrolysis. Table 2 presents O_2/N_2 adsorption data for two chars prepared from preoxidized IBC-102 coal. (Particle agglomeration, an eventual consideration in process scale-up, was not observed with these two chars, unlike the chars that were prepared from non-oxidized coal.) In both cases, the O_2 and N_2 adsorption capacities increase and O_2/N_2 selectivity decreases compared to the chars prepared from non-oxidized coal. The char yield from coal preoxidized at 220°C was about 35% compared to about 45% from coal preoxidized at 180°C. The more severely oxidized coal produces a char with less favorable O_2/N_2 molecular sieve properties. Table 2 also presents O_2/N_2 adsorption data for the 900 and 950°C chars activated to 14 and 10% conversion (X_2), respectively, in 1 atm CO_2 at 850°C. The O_2 adsorption capacity of both chars increases; however, this is offset by a substantial decrease in O_2/N_2 selectivity. Further work is needed to optimize coal preoxidation and char activation process conditions.

Table 2 presents O_2/N_2 adsorption data and Figure 2 shows the kinetics of O_2/N_2 adsorption for Carbonsieve, a CMS used in chromatographic applications. This material adsorbs slightly more N_2 than O_2 . Although Carbonsieve's (CO_2 -DR) surface area is about four times greater than that of the 800°C char, its O_2 adsorption capacity is only 40% greater, suggesting that total surface areas are not a good indicator of char adsorption capacity at room temperature. The closeness in value of the N_2 and CO_2 surface areas for Carbonsieve, however, does suggest their utility as a preliminary indicator of molecular sieving behavior. That is, carbons which do not exhibit large differences in CO_2 and N_2 surface areas do not make good sieves for the separation of N_2 and O_2 [9,24].

In another attempt to improve the molecular sieve properties of char made from IBC-102 coal, the coal was mixed with an alkali salt (KOH) prior to pyrolysis. Table 2 shows that there is a five-fold increase in the CO_2 -DR surface area of this char as compared to chars prepared without addition of KOH. The mesopore and total pore volumes of this "high-surface-area" (HSA) material were determined to be 0.20 and 0.80 cm^3/g , respectively. (Commercial CMS having 5-10 Å pores typically have total pore volumes no greater than 0.25 cm^3/g and surface areas which do not exceed 500 m^2/g [29].) Wennerberg and O'Grady [30] produced HSA carbons by mixing KOH with various carbon substrates, including petroleum coke and coal, and heat treating in inert gas. The physical and chemical properties of these materials have since been extensively studied by those investigators and others (see, for example, refs. 31-33). Whether these materials exhibit molecular sieving behavior, however, remains to be determined. Figure 2 shows that the HSA char adsorbs more N_2 than O_2 and its O_2/N_2 selectivity is quite low (0.40) compared to the chars prepared from untreated coal. Note that, although the CO_2 -DR surface area of the HSA char is five times greater than that of the char prepared at 800°C from untreated coal, its O_2 adsorption capacity is about the same. Figure 2 shows the kinetics of O_2 and N_2 adsorption to be very similar for Carbonsieve and the HSA char; neither appear to be a suitable adsorbent for air separation. It is interesting to note that the N_2 adsorption capacity (14.87) and N_2/O_2 selectivity (2.51) of the HSA char compare quite favorably with those of the commercial zeolite (8.26, 3.84).

In an attempt to improve the molecular sieve properties of the HSA char, carbon deposition was used to narrow the pores. Figure 2 shows the kinetics of O_2 and N_2 adsorption on the HSA char exposed to 10% CH_4 at 1000°C for 6 min. Depositing carbon in the pores of the HSA char is seen to have a significant effect on the kinetics and extent of O_2 and N_2 adsorption. The O_2 adsorption capacity nearly doubles while that of N_2 decreases by about one third. Table 2 lists the value of O_2/N_2 selectivity after 5 min adsorption time as 1.12, which is still lower than that of any of the chars prepared at 600-1000°C. Figure 2 shows the kinetics of O_2 and N_2 adsorption on the HSA char exposed to 10% CH_4 at 1000°C for 15 min. The rate of both O_2 and N_2 adsorption is considerably slower and the adsorption capacities less than those of the HSA char exposed to 10% CH_4 at 1000°C for 6 min. The O_2/N_2 selectivity, however, increases to 1.85 which is comparable to that of the untreated 800°C char. It is interesting to note that the O_2 and N_2 adsorption capacity of the 800°C char is about twice that of the HSA char (10% CH_4 , 1000°C, 0.25 h) even though they have similar surface areas. Further work is needed to optimize the carbon deposition conditions, most notably, the CD temperature, time and methane concentration (see, for example, ref. 34).

Figure 2 is also interesting in that it may help explain the unexpectedly low value of O_2 adsorption capacity obtained for the HSA char (see also Table 2). It shows the kinetics of O_2 and N_2 adsorption for the HSA

char produced by quenching the sample in H₂O upon removal from the furnace following pyrolysis. The quenched HSA char is seen to have adsorbed more than twice the amount of O₂ as the unquenched HSA char; its O₂/N₂ selectivity of 0.93 is similar to that of Carbosieve (see Table 2) and also some highly activated carbons tested by Nandi and Walker [9]. The reason for the higher O₂ uptake could be that the quenched char does not have a chance to chemisorb oxygen after its removal from the furnace since it is immediately quenched in water. The unquenched HSA char, on the other hand, was observed to chemisorb a considerable amount of oxygen upon exposure to air (i.e., it became noticeably warm) and, thus, most of the sites were already occupied by oxygen prior to an O₂ adsorption experiment at 25°C. This results in an apparently lower value of O₂ adsorption capacity being measured for the unquenched char. It is interesting to note that the O₂ adsorption capacity of the HSA char increases after CD (see Table 2) even though some of the pores were undoubtedly blocked by deposits of carbon formed by the cracking of methane at 1000°C. Recall that the HSA char sample was heated in N₂ at 1000°C for 0.5 h prior to a CD experiment, which would have removed most, if not all, of the oxygen present on the char surface as CO and CO₂.

Carbon Dioxide/Methane Separation: The incentive for developing more efficient CO₂/CH₄ separation processes, in particular, PSA using CMS, has increased with the recent advent of several innovative technologies [3]. The adsorption of CH₄ and CO₂ on CMS and activated carbon has been investigated by Schollner [35] for separation of CH₄ from fermentation gas via a PSA process. Methane is also found in combination with CO₂ and N₂ in some natural gas reservoirs (50% CH₄, 50% CO₂), in the effluent gas from oil wells undergoing CO₂ flooding for enhanced oil recovery (20-80% CO₂) and in municipal and industrial landfill gases (40-60% CO₂) [3]. Recovering methane as a medium- or high-BTU gas would be the primary aim of a CO₂/CH₄ PSA process. Significant progress in this area has been realized; both zeolites and CMS have been used as adsorbents [3,36].

The chars produced in this study were tested for their ability to separate CO₂ from CH₄, which have kinetic diameters of 3.3 and 4.0 Å, respectively. Figure 3 shows the kinetics of CO₂ and CH₄ adsorption and Table 3 lists the CO₂ and CH₄ adsorption capacities and CO₂/CH₄ selectivities of the chars prepared at 600-1000°C. The CH₄ adsorption capacity decreases significantly with increasing HTT, while the CO₂ adsorption capacity exhibits a maximum at a HTT of 800°C. Note that the CO₂ adsorption capacities of these chars are about one order of magnitude greater than the corresponding O₂ and N₂ adsorption capacities listed in Table 2. Also, the CO₂/CH₄ selectivity of the char is optimized at a HTT of 900°C and is quite high compared to its corresponding O₂/N₂ selectivity, 66.40 vs. 3.46. The CO₂ adsorption capacity of this char, however, is considerably less than that of the char prepared at 600 or 800°C; so, in effect, there is a tradeoff between high CO₂ adsorption capacity and high CO₂/CH₄ selectivity, i.e., one cannot achieve both by varying just the HTT. Due to the paucity of CO₂/CH₄ separation data in the literature, a comparison with other work is not possible at the present time. However, it is thought that these chars would show good potential for application in a commercial CH₄/CO₂ separation process.

Figure 4 presents the kinetics of CO₂/CH₄ adsorption and Table 3 lists CO₂ and CH₄ adsorption capacities and the CO₂/CH₄ selectivity for Carbosieve and the HSA char. It is interesting to note the similarity in the CO₂/CH₄ (as well as in the O₂/N₂) adsorption properties of these two materials. Both materials adsorb about the same amount of CO₂ at 25°C as the 800°C char even though their CO₂-DR surface areas (measured at 0°C) are greater by a factor of four. The CO₂/CH₄ selectivities of Carbosieve and the HSA char are only 2.86 and 2.57 compared to 13.50 and 66.40 for the 800 and 900°C chars. Apparently, the former two are not nearly as efficient as the latter two chars in separating CO₂ from CH₄. The high CO₂ adsorption capacity of the HSA char is desirable; however, its relatively low CO₂/CH₄ selectivity does not lend itself to being used in a commercial CO₂/CH₄ separation process.

Table 3 lists the CO₂ and CH₄ adsorption capacities and CO₂/CH₄ selectivity and Figure 4 also shows the kinetics of CO₂/CH₄ adsorption for the HSA char exposed to 10% CH₄ at 1000°C for 6 and 15 min. There is a slight increase in the CO₂/CH₄ selectivity (2.57 to 2.98) of the 6 min char while there is considerably more improvement in the CO₂/CH₄ selectivity of the 15 min char (2.57 to 7.09), but its CO₂ adsorption capacity decreases to one sixth its original value. The CO₂/CH₄ molecular sieve properties of these two chars still do not match those of the 600-950°C chars prepared from coal without added KOH.

Methane/Hydrogen Separation: Hydrogen is utilized in a variety of chemical and petrochemical processes. The demand for H₂ would be better met if an adsorbent material could be developed to more efficiently recover it from coke oven, steam reforming, or other coal utilization process gases. In general, all the gases produced in these processes have similar compositions, i.e., they contain principally H₂, along with N₂, O₂, CO, CH₄ and CO₂ in various proportions. The efficient removal of H₂ from this mixture is of considerable commercial importance [37].

Figure 5 shows the kinetics of adsorption of H₂ and CH₄ on the chars prepared at 600-1000°C. The diffusion rate of H₂ is quite high for the 600, 800 and 900°C chars and equilibrium is reached after only 20 seconds. Only the 1000°C char restricts, to some extent, entry of H₂ into its pore structure, i.e., equilibrium

is not reached even after 5 min. The H₂ adsorption capacities of the 600-1000°C chars are quite low and are essentially unaffected by HTT, contrary to the behavior previously observed (in most cases) for CH₄, O₂, N₂ and CO₂ adsorption. The CH₄ diffusion rate is highest for the 600°C char and monotonically decreases with HTT. The pore structure of the 900 and 1000°C chars has sufficiently closed to the point where the char now adsorbs more H₂ than CH₄. For adsorbing CH₄ from a CH₄/H₂ mixture, Table 3 shows that the 600°C char would probably be the best choice with both its relatively high CH₄ adsorption capacity and CH₄/H₂ selectivity. Jüntgen et al. [38] observed similar trends in the kinetics of H₂ and CH₄ adsorption on a "wide pore" CMS, "narrow pore" CMS, activated coal and a Type 5A zeolite. Hydrogen uptake by all four materials was essentially the same, i.e., a relatively high H₂ diffusion rate and low H₂ adsorption capacity were measured. Methane adsorption, on the other hand, varied according to the pore structure of the material. Their "narrow pore" CMS showed similar molecular sieving behavior to that of our 900 and 1000°C chars, whereas their "open pore" CMS displayed behavior similar to that of our 600 and 800°C chars.

Figure 6 presents the kinetics of CH₄ and H₂ adsorption on the HSA char at 25°C. Equilibrium for H₂ is reached within seconds. Table 3 shows that the extent of CH₄ and H₂ adsorption on this char is about three times greater than that on the 600°C char. The CH₄/H₂ selectivity of the HSA char was 39.5, highest among all the chars studied. For the HSA chars upon which carbon was deposited, Figure 6 and Table 3 show that the extent of both CH₄ and H₂ adsorption and the CH₄/H₂ selectivity decrease with increasing CD time. It is interesting to note the similarity in the kinetics of CH₄ and H₂ adsorption on the 800°C and the HSA (10% CH₄, 1000°C, 0.25 h) char (see Figures 5 and 6).

CONCLUSIONS

Chars were prepared from IBC-102 coal under various pyrolysis and activation conditions in a horizontal tube fixed-bed reactor. Chars having commercially significant BET surface areas of 1200-1700 m²/g were produced using select additives and heat treatment conditions. These high-surface-area (HSA) chars had more than twice the surface area of commercial molecular sieves. Experimental techniques were developed to study, at ambient temperature, the kinetics of adsorption of selected gases, e.g., N₂, O₂, CO₂, CH₄ and H₂, on these chars. The results were intriguing. A char prepared at 900°C was found to have similar N₂ and O₂ adsorption properties to those of commercial CMS used in air separation processes. On the other hand, the HSA char was found to adsorb more N₂ than O₂ and, therefore, was not considered a viable candidate (as is) for separating N₂ from O₂. Carbon deposition, using methane as the cracking gas, increased the O₂/N₂ selectivity of the HSA char; however, this was somewhat offset by a decrease in its O₂ adsorption capacity. Other gas separations of commercial interest studied included CO₂/CH₄ and CH₄/H₂. A char prepared at 800°C showed excellent molecular sieving properties for separating CO₂ from CH₄, i.e., both a relatively high CO₂ adsorption capacity and CO₂/CH₄ selectivity were achieved. The CO₂/CH₄ sieving ability of the HSA char was questionable. That is, although the CO₂ adsorption capacity of the HSA char was slightly greater than that of the 800°C char, its CO₂/CH₄ selectivity was lower by a factor of ten. With regard to CH₄/H₂ separation, the CH₄ adsorption capacity and CH₄/H₂ selectivity decreased with increasing HTT and CD time; H₂ adsorption was minimal and essentially independent of HTT. Future work will focus on optimizing the molecular sieve properties of the most promising chars for a given gas separation process using the char activation and carbon deposition methods employed in this study. Processing conditions will be sought which optimize molecular sieving behavior and minimize loss of adsorption capacity.

ACKNOWLEDGEMENTS

This work was funded in part by the Illinois Department of Energy and Natural Resources through its Coal Development Board and the Center for Research on Sulfur in Coal.

REFERENCES

1. Keller, G.E., in *Industrial Gas Separations* (ACS Symposium Series), (T.E. Whyte Jr., C.M. Yon and E.H. Wagner, eds.), American Chemical Society, Washington D.C., 1983, p. 223.
2. Ray, M.S., *Sep. Sci. Tech.* 21, 1 (1986).
3. Jasra, R.V., Choudary, N.V. and Bhat, S.G.T., *Sep. Sci. Tech.* 26, 885 (1991).
4. Jüntgen, H., *Carbon* 15, 273 (1977).
5. Jüntgen, H., Knoblauch, K. and Harder, K., *Fuel* 60, 817 (1981).
6. Walker, P.L., Jr., Austin, L.G. and Nandi, S.P., *Chem. Phys. Carbon* 2, 257 (1966).
7. Koresh, J. and Soffer, A., *J. Chem. Soc. Farad. I* 76, 2457 (1980).
8. Toda, Y., Yuki, N. and Toyoda, S., *Carbon* 10, 13 (1972).
9. Nandi, S.P. and Walker, P.L., Jr., *Fuel* 54, 169 (1975).
10. Miura, K. and Hayashi, J., *Carbon* 29, 653 (1991).
11. Patel, R.L., Nandi, S.P. and Walker, P.L., Jr., *Fuel* 51, 47 (1972).
12. Verma, S.K. and Walker, P.L., Jr., *Carbon* 28, 175 (1990).

13. Guo, S., Li, L. and Wang, A., *Fuel Sci. Tech. Conv.* 8, 545 (1990).
14. Moore, S.V. and Trimm, D.L., *Carbon* 15, 177 (1977).
15. Kamishita, M., Mahajan, O.P. and Walker, P.L., Jr., *Fuel* 56, 444 (1977).
16. Chihara, K. and Suzuki, M., *Carbon* 17, 339 (1979).
17. Verma, S.K., *Carbon* 29, 793 (1991).
18. Harvey, R.D. and Kruse, C.W., *J. Coal Qual.* 7, 109 (1988).
19. Rodriguez-Reinoso, F., in *Fundamental Issues in Control of Carbon Gasification Reactivity*, (J. Lahaye and P. Ehrburger, eds.), NATO ASI Series 192, Kluwer Academic, New York, 1991, p. 533.
20. Nelson, F.M. and Eggersten, F.T., *Anal. Chem.* 30, 30 (1958).
21. Lizzio, A.A. and Rostam-Abadi, M., Proc. Twentieth Biennial Conf. on Carbon, Santa Barbara, CA, 1991, p. 106.
22. Tsang, A.C., Dow Chemical, Private Communication to A.A. Lizzio, 1991.
23. Greek, B.F., *Chem. and Eng. News*, December 2, 1991, p. 13.
24. Nandi, S.P. and Walker, P.L., Jr., *Sep. Sci.* 2, (1976).
25. Schalles, D.G. and Danner, R.P., *AIChE Symp. Ser.* 84 (264), 83 (1988).
26. Armour, J., Air Products, Private Communication to A.A. Lizzio, 1991.
27. Armour, J., Proc. Twentieth Biennial Conf. on Carbon, Santa Barbara, CA, 1991, p. 40.
28. Sutt, R.F., Jr., Eur. Pat. 102, 902 (1983).
29. Vyas, S.N., Patwarthan, S.R. and Natraj, H.B., *J. Chem. Soc. Farad. Trans.* 86, 3455 (1991).
30. Wennerberg, A.N. and O'Grady, T.M., U.S. Patent 4,082,694, 1978.
31. Marsh, H. and Walker, P.L., Jr., *Fuel Proc. Technol.* 2, 61 (1979).
32. Marsh, H., Crawford, D., O'Grady, T.M. and Wennerberg, A.N., *Carbon* 20, 419 (1982).
33. Ehrburger, P., Addoun, A., Addoun, F. and Donnet, J.-B., *Fuel* 65, 1447 (1986).
34. Ismail, I.M.K., Rose, M.M. and Mahowald, M.A., *Carbon* 29, 575 (1991).
35. Schnoller, R., Franke, T. and Kluge, G., Proc. Fifth Conf. Appl. Chem., Balatonfuered, Hungary, Vol. 1, 1989, p. 123.
36. Sircar, S., *Sep. Sci. Tech.* 23, 519 (1988).
37. Kratz, W.C., Rarig, D.L. and Pietrantonio, J.M., *AIChE Symp. Ser.* 84 (264), 36 (1988).
38. Jüngen, H., Knoblauch, K., Münzner, H., Schröter, H.J. and Zündorf, D., Proc. Fourth London Inter. Carbon and Graphite Conf., 1974, p. 441.

Table 1. Proximate and Ultimate Analyses of IBC-102 Coal.

Proximate Analysis (wt%)	As-received	12x40 mesh
Moisture	13.9	10.6
Volatile Matter	35.3	37.8
Fixed Carbon	45.5	48.3
Ash	5.3	3.2
Ultimate Analysis (wt%)	As-received	12x40 mesh
Carbon	65.40	70.54
Hydrogen	6.03	6.05
Nitrogen	1.26	1.36
Oxygen	19.17	16.93
Sulfur	2.84	1.92
Sulfate	0.29	0.16
Pyritic	1.45	0.80
Organic	1.09	0.96

Table 2. O₂ and N₂ Adsorption Capacities, O₂/N₂ Selectivity and N₂-BET and CO₂-DR Surface Areas of Chars Prepared from IBC-102 Coal.

Sample	V _{O₂} (cm ³ /g)	V _{N₂} (cm ³ /g)	V _{O₂} /V _{N₂}	N ₂ -BET (m ² /g)	CO ₂ -DR (m ² /g)
Linde Type 4A Zeolite	2.15	8.26	0.26	35	316
CMS-A [12,17]	4.27	0.98	4.36	1	575
Takeda Type 3A CMS [25]	5.58	3.85	1.45	----	----
IBC-102, 600°C, 0.5 h	6.00	3.71	1.62	12	375
IBC-102, 800°C, 0.5 h	7.02	5.22	1.34	5	290
IBC-102, 900°C, 0.5 h	4.46	1.29	3.46	----	----
IBC-102, 950°C, 0.5 h	2.38	0.58	4.10	----	----
IBC-102, 1000°C, 0.5 h	0.17	0.00	----	2	5
IBC-102 Dem, 800°C, 0.5 h	6.17	3.21	1.92	----	----
IBC-102 Dem, 900°C, 0.5 h	4.67	1.62	2.84	----	----
IBC-102, 800°C, Preox., 220°C, 1 h, 100% O ₂	7.53	6.97	1.08	----	----
IBC-102, 800°C, Preox., 180°C, 2 h, 50% O ₂	10.05	8.27	1.21	----	----
IBC-102, 900°C, CO ₂ , X _c = 0.14	7.84	6.12	1.28	----	----
IBC-102, 950°C, CO ₂ , X _c = 0.10	6.12	3.80	1.61	----	----
Carbosieve	9.76	10.49	0.93	1040	1220
IBC-102 + KOH (1:1), 800°C, 0.5 h (HSA char)	5.93	14.87	0.40	1400	1690
HSA char, 10% CH ₄ , 1000°C, 0.10 h	11.40	10.19	1.12	710	980
HSA char, 10% CH ₄ , 1000°C, 0.25 h	3.39	1.83	1.85	15	240
HSA char, H ₂ O qucnch	13.75	14.74	0.93	1330	1550

Table 3. CO₂, CH₄ and H₂ Adsorption Capacities and CO₂/CH₄ and CH₄/H₂ Selectivities of Chars Prepared from IBC-102 Coal.

Sample	V _{CO2} (cm ³ /g)	V _{CH4} (cm ³ /g)	V _{CO2} /V _{CH4}	V _{H2} (cm ³ /g)	V _{CH4} /V _{H2}
IBC-102, 600°C, 0.5 h	78.42	19.22	4.08	0.56	34.32
IBC-102, 800°C, 0.5 h	93.85	6.95	13.50	0.64	10.86
IBC-102, 900°C, 0.5 h	29.88	0.45	66.40	0.56	0.80
IBC-102, 950°C, 0.5 h	12.68	0.30	42.27	0.62	0.48
IBC-102, 1000°C, 0.5 h	0.96	0.03	32.00	1.04	0.03
IBC-102 Dem, 800°C, 0.5 h	80.53	2.66	30.27	0.52	5.11
IBC-102 Dem, 900°C, 0.5 h	39.21	0.83	47.24	0.55	1.51
IBC-102, 900°C, CO ₂ , X _c = 0.14	111.05	8.64	12.85	0.60	14.40
IBC-102, 950°C, CO ₂ , X _c = 0.10	55.15	4.98	11.07	0.60	8.30
Carbosieve	118.41	41.40	2.86	----	----
IBC-102 + KOH (1:1), 800°C, 0.5 h (HSA char)	147.10	57.27	2.57	1.45	39.50
HSA char, 10% CH ₄ , 1000°C, 0.10 h	96.00	32.20	2.98	1.30	24.77
HSA char, 10% CH ₄ , 1000°C, 0.25 h	24.07	3.40	7.09	0.96	3.54
HSA char, H ₂ O quench	137.06	58.73	2.33	----	----

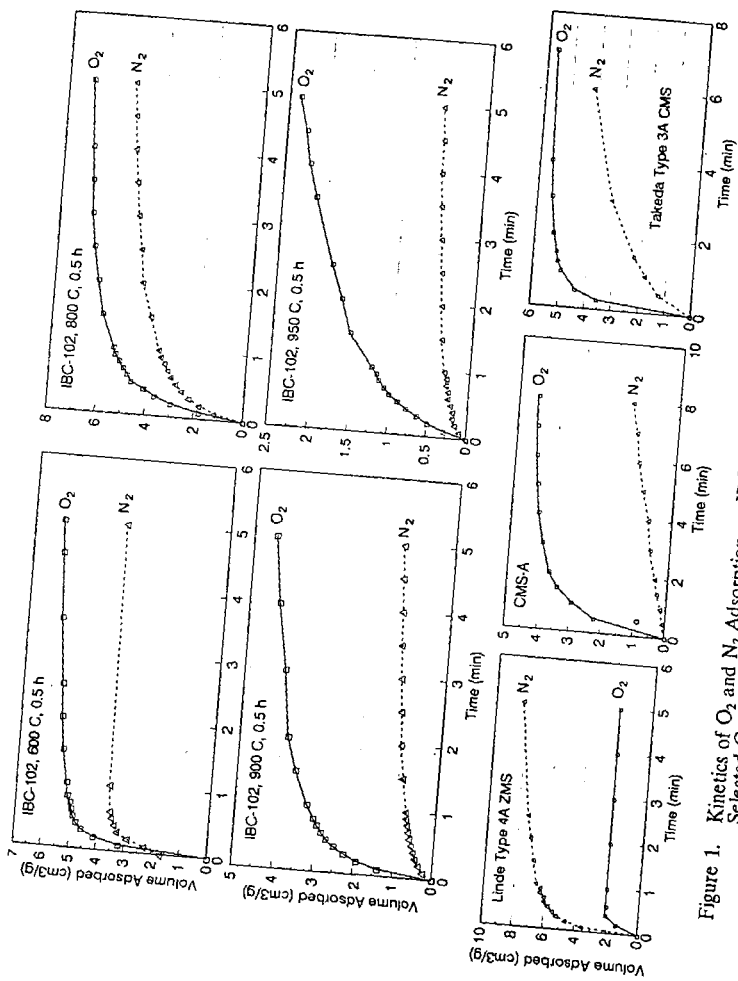


Figure 1. Kinetics of O₂ and N₂ Adsorption on IBC-102 Chars Prepared at 600-950°C and on Selected Commercial Molecular Sieves Used in Air Separation.

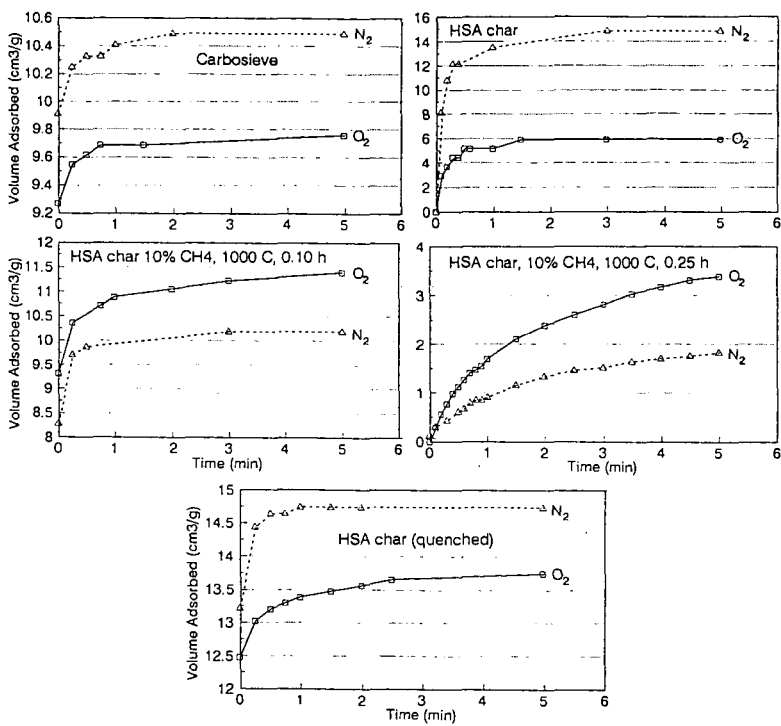


Figure 2. Kinetics of O_2 and N_2 Adsorption on Carbosieve and Selected HSA Chars.

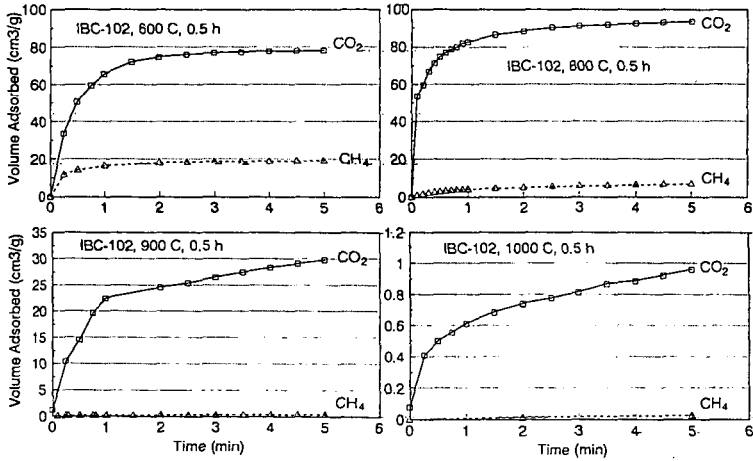


Figure 3. Kinetics of CO₂ and CH₄ Adsorption on IBC-102 Chars Prepared at 600-1000°C.

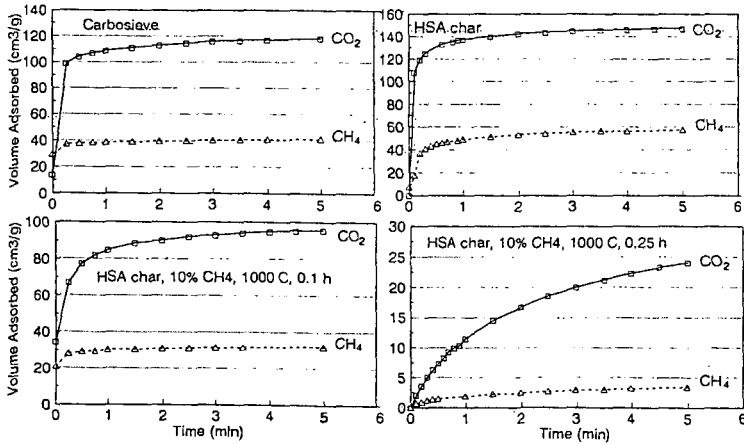


Figure 4. Kinetics of CO₂ and CH₄ Adsorption on Carbonsieve and Selected HSA Chars.

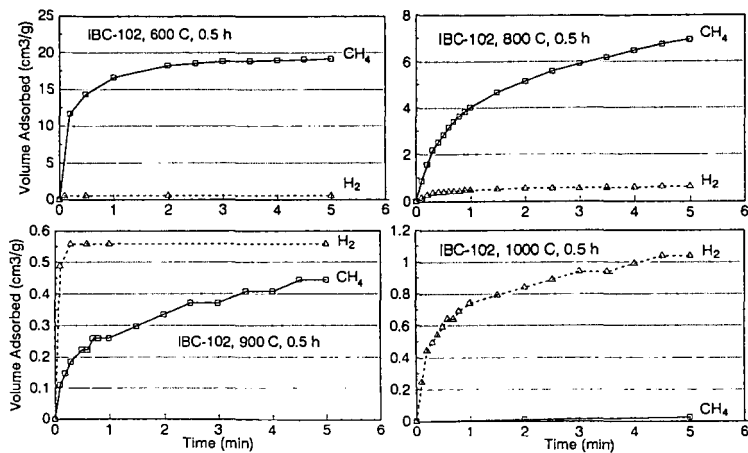


Figure 5. Kinetics of CH₄ and H₂ Adsorption on IBC-102 Chars Prepared at 600-1000°C.

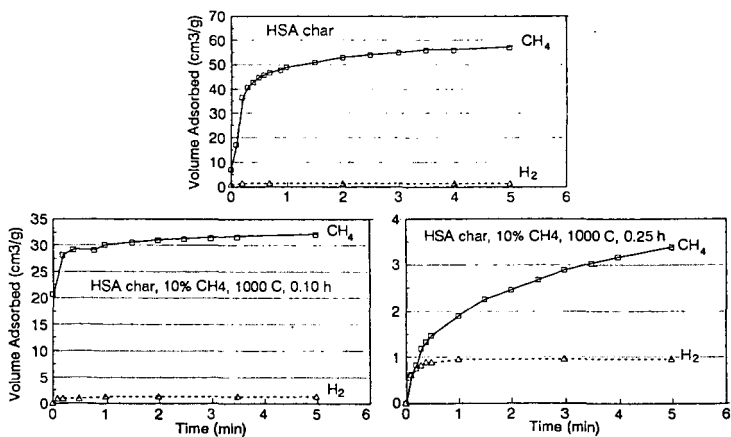


Figure 6. Kinetics of CH₄ and H₂ Adsorption on Selected HSA Chars.

SPECIALTY CHEMICALS AND ADVANCED MATERIALS FROM COALS: RESEARCH NEEDS AND OPPORTUNITIES

Chunshan SONG and Harold H. SCHOBERT

Fuel Science Program, Department of Materials Science and Engineering, 209 Academic Projects Bldg,
The Pennsylvania State University, University Park, PA 16802

Keywords: Coal Chemicals, Specialty Chemicals, Advanced Materials

1. Introduction

To use coals more efficiently as we move into the 21st century, it is important to explore the potentials and possible ways to develop high-value chemicals and materials from coals and coal liquids. This paper reports on our survey study, based mainly on literature and in part on our own experience. Our emphasis was placed on both the current status, including the applications and production level, and the future trends/growth rate of relevant chemicals and materials. The present study was guided by the following questions: What are the major problems and the future of industrial coal utilization? Is it necessary to develop coal chemicals now? What kinds of coal chemicals are more useful and competitive? Are there large-volume demands for coal chemicals? Is it really important to develop specialty chemicals and advanced materials? Are there large-volume applications of aromatic polymeric materials? How the aromatic specialty chemicals can be derived from coals and coal liquids? Are there new and better strategies for developing coal chemicals?

Discussed in this paper are 1) major problems facing the industrial utilization of coals such as carbonization, combustion and liquefaction, 2) the importance of developing coal chemicals, 3) new strategies for developing useful and competitive coal chemicals, and 4) some possible methods for developing several specialty chemicals such as 2,6-naphthalene dicarboxylic acid, and 5) some future research areas related to coal structural chemistry. Because units and pricing systems vary for different chemicals, both SI and English units are used but the conversion factors are given in appendix. Numerous abbreviations for long names were used, and they are listed in the appendix.

2. Worldwide Sources of Aromatic Chemicals

Petroleum and natural gas presently account for probably more than 90% of the organic chemicals [Sheldon, 1983; Speight, 1991]. They are the principal sources of the seven basic building blocks: ethylene, propylene, butadiene, benzene, toluene, xylenes and methanol. The principal sources of aromatic chemicals, however, include both petroleum and coal tar. About 3-4 % coal tars are produced as by-products from carbonization of coals in coke oven at about 1200 °C. In 1987 approximately 15-17 million tons (Mt) of coal tar and about 5 Mt of benzol were produced worldwide [Murakami, 1987; Mikami, 1988].

The annual consumption of aromatics in the world is about 25 Mt for BTX and 5 Mt for naphthalene, anthracene and other two- to four-ring aromatic compounds [Collin, 1985; Murakami, 1987]. About 95% of 2- to 4-ring polyaromatic and heterocyclic chemicals and about 15-25 % BTX chemicals come from coal tar (plus benzol) [Collin, 1985, Mikami, 1988]. In 1989, 7.5 Mt of coal tars was processed worldwide by distillation; about 950 thousand tons (Kt) naphthalene, 20 Kt anthracene, 10 Kt of methyl naphthalene, phenanthrene, acenaphthene, and pyrene were isolated for use in chemical industry; the remains were used as feedstocks for carbon blacks and for carbon materials [Kikuchi et al., 1989]. In Japan, about 2.5 Mt of coal tars are produced annually and 2 Mt tars are processed by distillation; and in Nippon Steel, about 0.6 Mt tars are processed annually [Okazaki and Nozaki, 1986]. With the rapidly growing engineering applications of aromatic polymer materials (Section 6), the demands for a number of 1-4 ring aromatic compounds will increase.

3. Current Status and Problems Facing Industrial Coal Utilization

Because of the 1990 Clean Air Act, switching of coal for combustion in electric utility boilers is expected and in the near future, more low rank coals, which have lower S and N contents, will be burned [Sondreal, 1991]. That humans are increasing the concentration of CO₂ in the atmosphere by burning fossil fuels, and the increased concern worldwide about global warming will certainly lead to pressure on use of all fossil fuels [Kasting, 1991]. Coal is by far the worst in terms of CO₂ production per unit energy production upon combustion. Coal is also a problem regarding NO_x, SO_x, and particulate emissions. It is likely that new laws will continue to mandate stricter controls on emissions of NO_x and SO_x, and in the near future, the control of CO₂ emission. Recent reserve estimates of natural gas suggest the reserve is much larger than heretofore thought. Natural gas produces half as much as CO₂ per J of energy as coal, and essentially no NO_x, SO_x or particulate. Thus natural gas is likely to be the fuel of choice for power generation in the future.

Another major industrial coal utilization is carbonization to produce metallurgical coke [Gray, 1989]. According to the data in 1987-1988, there are about 400 sets of coke ovens worldwide and approximately 450 Mt of bituminous caking coals are carbonized annually to produce about 350 Mt metallurgical coke (about 29 Mt in the USA in 1988); this coke production level account for the reduction of 800 Mt iron ores to produce approximately 450 Mt raw steel [Murakami, 1987; Patrick, 1991]. Coke production has been markedly reduced in recent years, and it appears this trend will continue. Reduced coke demand has come from reduced steel demand, which is largely due to competition from polymer materials, especially engineering plastics, and new technology of direct coal injection into blast-furnaces. By the end of 1989, 32 of Western Europe's 104 blast furnaces, and 23 out of 35 Japan's working blast furnaces were equipped for coal injection [Patrick, 1991].

It will become necessary to produce synthetic liquids from coals for transportation fuels and for chemicals. However, despite enormous strides in coal liquefaction research, and great effort at Wilsonville to reduce cost of coal-derived syncrudes, coal-derived liquid fuels are still not cost-effective with petroleum, and do not seem to be likely to compete with petroleum in near future. Moreover, the liquid fuels from coal must meet with the 1990 Clean Air Act Amendments. For this reason, the transportation fuels will be hydrogen-rich, highly aliphatic fuels. We need to realize that production of such fuels from coal-derived syncrudes will be considerably higher than those from petroleum crudes. This is because petroleum are originally aliphatic in nature, but coal-derived syncrudes are highly aromatic and contain primarily two- to four-ring polyaromatics; conversion to aliphatic transportation fuels would require extensive hydrotreating [Song et al., 1991a, 1991b].

4. Importance and Opportunities for Developing Coal Chemicals and Materials

The question why it is necessary to develop chemicals and materials from coals may be answered with respect to what is happening in the world around coal. The overall picture of the situation that emerges from the above is as follows: Significantly reduced coke demand will reduce the demand for bituminous coking coals and substantially reduce the production of by-product coal tar. However, coal tars are the sources of most polyaromatic and heterocyclic chemicals, which are the chemicals of great interest as feedstocks for specialty chemicals and advanced materials (Sections 2 and 6), and currently coal tar pitch is the major raw materials for coal-based carbon fibers and other carbon materials (Section 8). The demands for aromatic chemicals, aromatic polymer materials, engineering plastics, carbon-fibers and other carbon materials are remarkable and are rapidly increasing. Increased environmental concern about the greenhouse effects will result in significant environmental pressure on the use of coals as boiler fuels. Abundant supplies of cheap and clean natural gas will compete with coal-fired power generation. Synthetic fuels from coals do not seem likely to be competitive with petroleum for transportation fuels until 2010 or beyond.

From this situation, it is clear that we now need to explore other ways of using coals. We need to recognize that, primarily, coal is a hydrocarbon source, and this apparently has been often overlooked. As a hydrocarbon source, coal can also be used as feedstock for chemicals and materials, in addition to its use as fuel. The 70's and 80's have brought an explosive developments and applications of various organic materials, and the 90's and 21st century will definitely see the significant growth of these materials including aromatic polymers such as engineering plastics, liquid crystalline polymers, and high-temperature heat-resistant polymers, polymer blends, polymer membranes, carbon fibers, carbon-plastic composite materials, and other carbon materials.

A major shift in emphasis of developing new polymer materials is taking place, from aliphatic polymers to the polymers with benzene ring in the chains, and from benzene ring to naphthalene ring or from benzene ring to biphenyl ring. The incorporation of aromatic ring structures has led to higher melting polymers. Future use of polymer materials will involve a significant shift to polymers with two-ring aromatic groups in the chain. These significant developments will give rise to large-volume industrial demands in the 90's and 21st century for a number of 1-4 ring aromatic chemicals and specialty chemicals (Sections 6-7) such as 2,6-dialkyl-naphthalene (2,6-DAN) and 4,4'-dialkylbiphenyl (4,4'-DAB), and high-quality pitch feedstocks for carbon fibers and other carbon materials.

By developing the critical chemicals and substances for the advanced materials, coal chemical research could contribute significantly to high-technology development. The commercial and military importance of advanced polymer materials such as liquid crystalline polymers (LCP) resides in their unique properties. However, their commercial future and availability is intimately tied to lowering their cost. In turn, this is largely determined by the cost of the aromatic monomers [NRC, 1990]. Many of the aromatic monomers for newly developed high-performance materials are not readily available from petroleum.

This situation provides an excellent opportunity for starting to explore the potentials and possible ways to develop high-value chemicals and materials from coals and coal liquids. The coal liquids-to-coal chemicals research can be viewed

as an extension of, or product development part, of coal liquefaction research. Development of high-value chemicals from coal liquids could not only increase significantly the economic viability of coal liquefaction process, but also make coal liquids more competitive with petroleum because the former contains many chemicals which are not found in the latter [Song et al., 1991a]. For example, WI-MD contains many two- to four-ring aromatics, which can be converted into high-value specialty chemicals (Section 7). Heavier coal liquids can be transformed to fuels, chemicals, and carbon materials. The direct coal-to-chemical conversion is a new concept (Section 5) and has not been studied. The ideal target of the direct coal-to-chemical conversion research is to allow the structural units in various coals be transformed directly to useful chemicals. Research toward this end will contribute greatly to exploring new coal chemistry.

5. Chemicals from Coals - Old but New Approach

5.1 What Kinds of Chemicals from Coals ?

Several decades ago, the change from acetylene to ethylene brought about an explosive change from coal-based chemical technology to petroleum technology. Petrochemical industry based on ethylene and propylene is still a major industry, and there is no need for coal to be competitive for producing the basic chemicals. Our idea on coal-to-chemicals is to develop more valuable aromatic chemicals from coals, including those which are not readily available from petroleum but will be needed in relatively large volumes, and those which can be obtained both from coal and petroleum such as BTX and phenolic compounds. The "aromatization" trend of materials development and applications described in Sections 6 and 7 strongly supports this idea. In this way, both petrochemicals and coal-chemicals can find their uses, and this will contribute to the highly efficient utilization of these valuable resources.

5.2 How to Derive Chemicals from Coal ?

5.2.1 Traditional Approaches

The state-of-the-art of chemicals from coal has been reviewed recently by Schlosberg (1990). Among two general approaches to making chemicals from coal, in the first case, by-products such as carbonization tar could be subjected to some appropriate sequence of separation operations to produce eventually pure compounds of interest. The principal drawback is that the starting materials are often extremely complex mixtures. In tar from gasification of lignite, the most predominant compound type accounted for only 4.3% of one fraction. Thus, the sequence of separation steps needed to extract a particular compound becomes enormous. In the other approach, coal could be gasified to synthesis gas, the synthesis gas is converted via Fischer-Tropsch process to liquids, the liquids degraded to ethylene, and the ethylene used to synthesize desired chemical products. The technology for each of these processes is well known. Unfortunately, this route involves significant investment in plant equipment to manufacture what should ideally be a cheap commodity. Also, the overall procedure involves a degradation (gasification), followed by a synthesis (Fischer-Tropsch), followed by another degradation (cracking), followed by another synthesis (chemical manufacture). If one looks at the forest rather than the trees, this laborious tearing down and building up seems slightly crazy.

5.2.2 New Approaches

In regard to aromatic specialty chemicals, the liquids from advanced coal liquefaction, which retain mostly the original molecular components or ring structures of coals, may be theoretically more attractive as feedstocks for aromatic chemicals as compared to Fischer-Tropsch synthesis. This approach leads to aromatics, phenols, and heterocyclic compounds as chemicals. As compared to the distillate fractions of coal tars from coke oven which contain relatively simple and non-substituted aromatics, the disadvantage of chemicals from liquefaction is the presence of many, but not necessarily desirable, alkyl substituents on the ring systems. Two approaches can be taken to overcome this problem. The first is to use a simple liquefaction method followed by catalytic dealkylation of the coal liquids. The second approach is catalytic or thermal liquefaction at lower temperature to derive the aromatic compounds, followed by thermal dealkylation via hydropyrolysis at higher temperature to take off the alkyl substituents, producing relatively simple aromatics. The key factors are the conversion efficiency and the product separation. These approaches may become promising with the large-volume demands for aromatic chemicals, and can be economically competitive if improved separation methods emerge.

All the above-mentioned methods can be viewed as "indirect" coal-to-chemical conversion. An alternative is to explore introducing a reagent into the coal to cleave only a certain well-defined set of bonds, carefully cutting out the structures of interest. It is generally thought that a significant number of the aromatic systems in low rank coals such as lignites and subbituminous coals contain only 1- to 2-ring. Low rank coals therefore offer promise for production of phenol and catechol type chemicals as well as BTX (benzene, toluene, xylenes) and naphthalene. A careful oxidation should be able to produce large yields of benzene carboxylic acids. If long chain aliphatic units exist, as some investigators believe, neatly clipping the ends of the aliphatic chains may allow useful materials based on aliphatic carbon to be recovered.

5.3 Supporting Research in Fundamental Coal Chemistry

In the past ten years, there has been an accelerated development of our understanding of coal structures, reactivity, and reactions. What is needed more in order to assess the potential of this approach to chemicals from coals? First, more knowledge of the principal organic structural features is needed. Average parameters such as aromaticity are not very useful. To selectively obtain specialty chemicals, especially important knowledge is the number and specific position of substituents on aromatic rings in coals. When such knowledge is available, it should be possible to select specific coals and to select those types of bonds which are desired to cleave; and then knowledge is needed on the kinetics, mechanism, and the thermochemistry of the cleavage processes. Finally, better ways are needed of selecting appropriate solvents and adjusting the molecular size and polarity.

6. Aromatic Polymer Materials & Engineering Plastics Related to Coal Chemicals

We will review briefly the recent developments and applications of aromatic polymer materials and engineering plastic related to coal chemicals, namely, the polymers synthesized from aromatic monomers that can be made from coal and coal liquids. The world-wide consumption of synthetic polymers is now in the order of 70 Mt/yr, about 56% of which are plastics, 18% are fibers, and 11% synthetic rubber. The balance is made up of coatings and adhesives [Stevens, 1990]. The production of plastics is growing fast while the others are not. Assuming the industrial production indexes for synthetic polymer materials to be 100 in 1987, such indexes in 1990 are 115.8 for plastic materials, 92.7 for man-made fibers, and 88.6 for synthetic rubber [News-CI, 1991]. Numerous reviews on polymer materials have been published in recent years [Hall, 1981; Critchley et al., 1983; MacDermott, 1984; Bowden and Turner, 1987; Seymour, 1987; Stevens, 1990; Dyson, 1990; NRC, 1990; Weiss and Ober, 1990; Kroschwitz, 1991; Mark et al., 1992].

Engineering plastics are relatively higher in cost but have superior mechanical properties and greater durability, which make them competitive with metals, ceramics, and glass in a variety of applications. Engineering plastics is now a \$2 billion business in USA [Schlossberg, 1990]. More importantly, engineering plastics are rapidly growing market with consumption projected to increase up to 10% annually [Stevens, 1990]. The following are principal engineering plastics: polyamide / nylon (PA), polyacetal (PAL), polycarbonate (PC), polyphenylene oxides (PPO), thermoplastic polyester including polyethylene butylate (PBT) and polyethylene terephthalate (PET), polyarylate (PAR), polysulfone (PS); polyphenylene ether ether ketone (PEEK); and high-temperature heat-resistant polymers such as polyimides (PI) and polyamideimide (PAI). The top five are PA, PC, PPO, PAL, and PBT [Stevens, 1990]. The selling prices for the family of the 5 products was in the \$1.40-\$2.00 per pound (lb) range in 1985. It is forecast that consumption of thermoplastic polyester in North America will increase by 7.5% per year from 1.945 billion lb in 1990 to 2.79 billion lb in 1995, in which PET is the major player (from 1.73 to 3.425 billion lb) and the second is PBT (from 180 Mlb to 370 Mlb) [Vervain, 1991].

Polyimide-type heat-resistant polymers, as well as carbon fibers (Section 8) were developed initially for aerospace industry as better light-weight heat-resistant materials. They now have found wide commercial applications. Polyimides have experienced extremely rapid developments in recent years, the major emphasis being on engineering applications [Stevens, 1990].

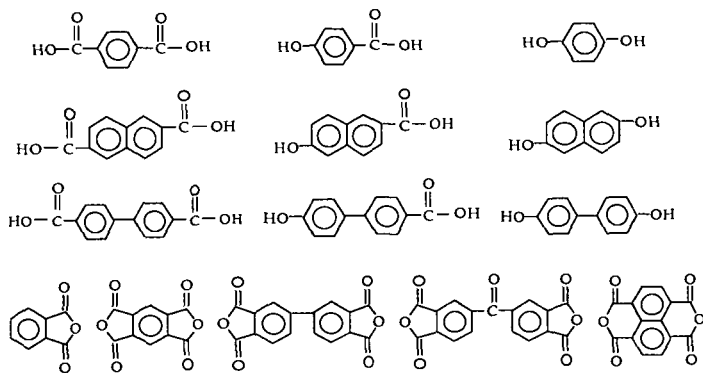
The liquid crystalline polymers (LCPs) containing naphthalene or biphenyl ring are capable of replacing metals and ceramics in many applications. Moldings of these rigid, rod-like, heat-resistant engineering polymers may be used in place of metals and ceramics for electronics, aerospace, and transportation applications [Seymour, 1987]. In 1989 worldwide production of LCP fibers is about 94 Mlb with an average market value of nearly \$10/lb; thermotropic LCPs about 10 Mlb (valued at about \$10/lb) of which about 5 Mlb was used in cookware [Weiss and Ober, 1990].

Most polymers are good insulators. However, some polymers such as poly-N-vinylcarbazole (PVCA) are photoconducting [Penwell et al., 1978]. Recently Hara and Toshima (1990) reported that the conductive and heat-resistant polymer films can be prepared by electrochemical polymerization of aromatic hydrocarbons such as naphthalene. Otani and co-workers reported that polyaromatics such as pyrene and phenanthrene can be used to make condensed polynuclear aromatics (COPNA) resin [Otani et al., 1986; Ota et al., 1988]. In addition, cyclic and short-chain linear phosphazenes with biphenyl as side chain [Allcock, 1991] may be viewed as biphenyl type organic-inorganic macromolecules.

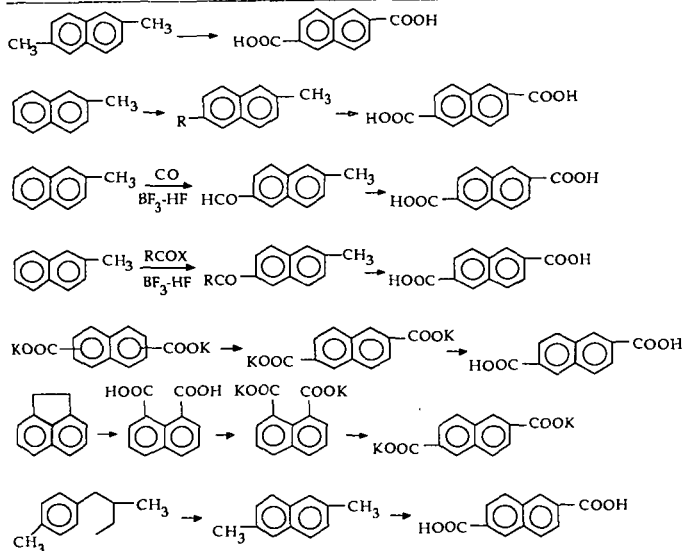
7. Monomers for High-Performance Polymers

Many aromatic and heteroatom-containing compounds can be converted into monomers for various polymers. Scheme 1 presents a list of important monomers for aromatic engineering plastics, liquid crystalline polymers (monomers in first 3 rows), and heat-resistant resins (monomers in the 4th row in Scheme 1). Because alkyl chains on aromatic rings can be readily oxidized to COOH or OH groups by using oxidizing agents or by heterogeneous catalytic oxidation, an

Scheme 1. Some Important Monomers for Aromatic Polymer Materials



Scheme 2. Possible Routes for Synthesis of 2,6-NDCA



important research subject is how to prepare the needed aromatics. For example, the oxidation of 2,6-DAN and 4,4'-DAB can readily give 2,6-naphthalene dicarboxylic acid (2,6-NDCA) and 4,4'-biphenyl dicarboxylic acid (4,4'-BDCA), respectively. Scheme 2 shows the possible routes for synthesis of 2,6-NDCA based on the chemicals that can be obtained from coal. By extending the methods used in catalytic synthesis of 1,4-xylene, terephthalic acid, and p-hydroxybenzoic acid, various methods seem to be available for the research and laboratory-scale synthesis of 2,6-disubstituted naphthalene and 4,4'-disubstituted biphenyl chemicals. However, because of the increase in the peripheral positions on the rings, the stereoselectivity is much more important, and in practice more difficult to control as compared to the situation of alkylbenzene.

Some of the coal-related important monomers for polyimides are pyromellitic anhydride (PMDA) and 1,4,5,8-naphthalene tetracarboxylic acid (NTCA) and its dianhydride (NTCADA) as well as the well known phthalic anhydride. Oxidation of pyrene produces NTCADA, which can be used for making some high-temperature heat-resistant resins. Phenanthrene and its derivatives are rich in coal-derived liquids, and can be obtained in relatively high yields from pyrolysis and carbonization tars. Considerable efforts have been devoted to finding the uses for it in the past decades, but its use is still very limited [Kurata, 1986]. During the Lewis acid-catalyzed hydrogenation of anthracene, sym-octahydrophenanthrene (sym-OHP) and phenanthrene were produced [Song et al., 1991c, 1989b]. sym-Octahydroanthracene (sym-OHA) was produced from phenanthrene over some acidic catalysts [Song et al., 1991 unpublished]. It is possible that sym-OHA can be formed from sym-OHP. Because sym-OHP can be obtained in considerably high yields by using supported NiW/Al₂O₃ or NiMo/Al₂O₃ catalysts [Shabtai, 1978; Song et al., 1988, 1991b; Ueda et al., 1990], it seems that one can hydrogenate phenanthrene and then isomerize sym-OHP to sym-OHA. The oxidation of sym-OHA and subsequent dehydration could produce PMDA, and dehydrogenation of sym-OHA can readily produce anthracene which is one of the most valuable chemicals and has found large-volume uses in dye industry as intermediate and in pulp industry as pulping agent (anthraquinone).

Biphenyl compounds are not as rich as naphthalene compounds in coal liquids. However, coal liquids contain phenanthrenes, fluorenes, dibenzofurans, and dibenzothiophenes. The latter three compounds can be converted to biphenyl type compounds by catalytic hydrocracking. Phenanthrene, may be used to produce diphenic acid and 4,4'-BDCA. Oxidation of phenanthrene can produce either phenanthraquinone or diphenic acid (biphenyl-2,2'-dicarboxylic acid). Diphenic acid may also be used for heat-resistant resins.

8. Advanced Carbon Materials from Coals and Coal Liquids

It is now well known that various useful carbon materials and composite materials can be made from coals, coal tars, coal liquids from liquefaction, and petroleum. It has been indicated in several recent reviews by Marsh [1989, 1991] and by Walker [1986, 1991] that the following are advanced or "old but new" carbon materials based on coal-derived feedstocks:

o Pitch-based carbon fibers	o Mesocarbon microbeads
o Mesophase-based carbon fibers	o Activated adsorbent carbons
o Carbon fiber reinforced plastic	o Activated carbon fibers
o Carbon whiskers or filament	o Metallurgical cokes
o Graphite and graphite-based materials	o Intercalation Materials
o Electrodes	o Fullerenes or bucky-balls
o Composite materials	o Diamond-like films
o Molecular sieving carbons	

Currently, coal tar pitch and bituminous coals (for making coke) are the major feedstocks of coal-based carbon materials. Coals ranging from low-rank coals to anthracites, and heavy liquids from coal liquefaction and tars from low temperature pyrolysis may be used for carbon materials in the future. The large-volume uses of coals for carbon materials can be stimulated significantly by the development of molecular sieving carbons (MSC) for gas separation and the adsorbent carbons for purifying water, air and medical and environmental applications. The application of MSC for air separation by PSA method is now commercially viable (Large-scale separation of CO from coal-derived gases may be carried out using COSORB method, provided care is taken to remove moisture and oxygen [Song et al., 1987, unpublished]). There are several recent review and original articles on coal-based carbon molecular sieves [Walker, 1986, 1990; Verma, 1991; Hashimoto, 1991] and adsorbent carbons [Marsh, 1989, 1991; Verheyen et al., 1991; Derbyshire and McEnaney, 1991a, 1991b].

The large-volume uses of coal liquids including those from carbonization and liquefaction may depend mainly on the development of technologies for producing general-purpose and mesophase-based carbon fibers, including activated carbon fibers for environmental protection uses, graphite electrodes, and mesophase microbeads-based materials. Several

reviews on carbon fibers are now available [Johnson 1989; Dorey, 1987; Anderson, 1987; Donnet, 1984]. Coal tar pitch-based carbon fibers are still in the development stage. Recently, commercialization of coal tar pitch carbon fibers has been announced by Mitsubishi Chemical (500 tons/yr) and Osaka Gas (300 tons/yr) through its subsidiary [Matsumura, 1989].

Coal-derived materials have higher N and O contents than petroleum feedstocks. Application of catalytic hydroprocessing for structural modification and heteroatom (especially N) removal of coal-derived carbonization feedstocks may become increasingly important for making mesophase-based carbon materials such as carbon fibers and graphite electrodes. Moderate hydrogenation and hydrodenitrogenation (HDN) of pitch feedstocks using large-pore [Song et al., 1991f, 1992f] hydrotreating catalysts can improve carbonization process; and perhaps more importantly, HDN of the feedstocks may significantly improve the properties of the coal-based mesophase carbon materials upon graphitization.

9. End of Beginning

Can we build a new basis in coal science for advanced and viable coal chemical industry? Would liquefaction of coals be commercialized in 21st century? Can we make break-through in coal-to-chemicals research to match the demands arising from rapidly developing polymer industry and carbon industry in the foreseeable future? Will it ever be possible to produce specific chemicals directly from coals? The future is not certain, particularly if the word "produce" carries the implication of a commercially viable process. Nevertheless, the potential exists, and the future may show handsome dividends from relatively modest investments in research on organic coal structures, reactivity, catalytic conversions, new pretreatments, novel reactions, supercritical extraction for the conversion processes such as direct coal-to-chemicals and coal liquids-to-chemicals tests coupled with advanced liquefaction method. While it may seem to be beyond the scope of "coal" science, the conversion of the coal aromatic chemicals to specialty chemicals such as 2,6-dialkyl-naphthalene is also important part, which determines the potential of coal chemicals as monomers for polymer materials.

Relevant Literature

(Due to space limit, some of the relevant references cited below were not mentioned in the text).

- Allcock, H.R.; Ngo, D.C.; Parvez, M.; Whittle, R.R.; Birdsall, W.J., *J. Am. Chem. Soc.* 1991, 113, 2628-2634.
- Anderson, B.W., *J. Phys. D: Appl. Phys.* 1987, 20, 311-314.
- Bacon, R. "Carbon Fibres from Rayon Precursors" in "Chemistry and Physics of Carbon", Vol. 9, (Eds. Walker, P.L. and Thrower, P.A.), Marcel Dekker, New York, 1975, pp.1-101.
- Bowden, M.J.; Turner, R.S. "Polymers for High Technology". *ACS Sym Ser.* 1987, No. 364, 466 pp.
- Borman, S., *C & EN*, 1992, Jan 6, p.26
- Chapoy, L.L. "Recent Advances in Liquid Crystal Polymers". Elsevier Appl. Sci. Pub: New York, 1985
- Chiba, K.; Tagaya, H., *Kagaku Kogaku* 1988, 52 (7), 520-525.
- Collin, G. Erdol und Kohle - Erdgas Petrochem. 1985, 38 (11), 489-496
- Critchley, J.P.; Knight, G.J.; Wright, W.W., "Heat-Resistant Polymers", Plenum Press: New York, 1983, 462 pp.
- Derbyshire, F.; McEnaney, B., *Energia*, University of Kentucky, 1991a, 2 (1), p.1-6.
- Derbyshire, F.; McEnaney, B., 1991 Int. Conf. Coal Sci., 1991b, Newcastle upon Tyne, pp.480-483.
- Donneu, J.B.; Bansal, R.P., "Carbon Fibers", Marcel Dekker: New York, 1984.
- Dorey, G., *J. Phys. D: Appl. Phys.* 1987, 20, 245-256.
- Dyson, R.W. "Engineering Polymers". Blackie (Chapman and Hall): New York, 1990
- Economy, J., *Mol. Cryst. Liq. Cryst.* 1989, 169, 1-22.
- Finkelmann, H., *Angew. Chem. Int. Ed.* 1987, 26 (9), 816-824.
- Gray, R.J., "Coal to Coke Conversion", in "Introduction to Carbon Science", H. Marsh Ed., Butterworths: London, 1989, pp.285-321.
- Hall, C., "Polymer Materials". John Wiley & Sons: New York, 1981, 198 pp.
- Haggin, J., *C&EN*, 1990, Aug. 6, p.29
- Hara, S.; Toshima, N., *Chemistry Letters* 1990, pp.269-272.
- Hirota; Nomura, M.; Song, C., "A Method for Manufacture of Aromatic Chemicals from Coals", Japan Patent Appl., 1989
- Jackson, W.J., Jr., *Mol. Cryst. Liq. Cryst.* 1989, 169, 23-49.
- Johnson, D.J., "Carbon Fibers: Manufacture, Properties, Structure and Applications". in "Introduction to Carbon Science", H. Marsh, Ed., Butterworths, London, 1989, pp. 198-228.
- Kamiya, T., *Aromatics (Japan)* 1988, 40, No.3-4, p.52-55.
- Kasahara, T.; Takamizawa, Y., *Kagaku Kogaku* 1988, 52 (6), 416-420.
- Kasting, J., Paper presented at Information Transfer Session, Cooperative Program in Coal Research, November 18-19,

- 1991, Pennsylvania State University, University Park, PA.
- Kikuchi, E.; Ariyoshi, J.; Sugi, Y.; Horida, Z.; Iwasaki, M., *Petrotech* 1989, 12 (2), 78-85.
- Komatsu, M., *Kagaku Kogaku* 1986, 50, (9), 614-618.
- Kroschwitz, J. Ed. "High Performance Polymers and Composites". Wiley : New York, 1991, 922 pp.
- Kurata, N., *Kagaku to Kogyo* 1988, 41 (1), 33-36.
- Kurata, N., *Kagaku to Kogyo* 1986, 60 (7), 274-280.
- MacDermott, C.P. "Selecting Thermoplastics for Engineering Applications". Dekker:New York, 1984.
- Margolis, J.M. (Ed.), "Engineering Thermoplastics: Properties and Applications". Dekker:New York, 1985.
- Mark, J.E.; Allcock, H.R.; West, R. "Inorganic Polymers". Prentice Hall, Englewood Cliffs, NJ, 1992.
- Marsh, H. "New and Traditional Carbon Materials from Petroleum and Coal Sources". Paper presented at Information Transfer Session, Cooperative Program in Coal Research, November 18-19, 1991, Pennsylvania State University, University Park, PA.
- Marsh, H. (Ed.), "Introduction to Carbon Science", Butterworths:London, 1989, 321 pp.
- Marsh, H.; Menendez, R., Butterworths:London, 1989, pp.38-73.
- Matsumura, Y., *Kagaku Keizai* 1989a, No.9, 33-41
- Matsumura, Y., *JETI* 1989b, 37 (No.9), 223-226.
- Mittal, K.L. Ed. "Polyimides". Plenum Press : New York, 1982.
- Mikami, K., *Aromatics* 1988, 40 (1-2), 26-29.
- Miura, K.; Hayashi, J.; Hashimoto, K., 1991 Int. Conf. Coal Sci., 1991, Newcastle upon Tyne, pp.560-563.
- Murakami, H., *Nenryo Kyokai-Shi* 1987, 66(5), 448.
- News-CI, *C&EN*, 1991, June 24, pp.28-69.
- News-CO, *C&EN*, 1992, Jan 6, p.12.
- News-LCP, *Speciality Chemicals* 1987, 11 (6), 12-19.
- News-LCP, *Speciality Chemicals* 1988, 12 (8), 17-22.
- News-NDCA, *Petrotech* 1989, 12 (7), p.513.
- News-PC, *C&EN* 1991, Dec. 23, p.8.
- News-PAR, *Kagaku Gijutsu-Shi MOL* 1988, No.3, p.20
- News-PBT, *Kagaku Gijutsu-Shi MOL* 1987, No.11, p.20-21
- News-PET, *Speciality Chemicals* 1988; 12 (10), 17-22.
- News-PET, *C&EN* 1991, Sept. 9, p.15.
- News-PS, *C&EN*, 1991, Dec.16, p.8.
- Nomura, M., *Kagaku*, 1986, 41 (7), 442-448.
- NRC National Materials Advisory Board. "Liquid Crystalline Polymers". National Academy Press, 1990, 106 pp.
- Okuda, K., *Petrotech (Japan)* 1982, 5 (1), 37-42.
- Ota, M.; Otani, S.; Iizuka, S.; Sawada, T.; Ota, E.; Kojima, A., *Nippon Kagaku Kaishi* 1988, No.3, 343-350
- Otani, S.; Raskovic, V.; Oya, A.; Kojima, A. *J. Mater. Sci.* 1986, 21, 2027.
- Okazaki, H.; Nozaki, M., *Fine Chemicals* 1986.6.15, 5-17.
- Patrick, J.W., *Energia*, University of Kentucky, 1991, 2 (5), p.1-6.
- Penwell, R.C.; Ganguly, B.N.; Smith, T.W., *Macromol. Rev.* 1978, 13, 63.
- Samulski, E.T. "Polymeric Liquid-Crystals". *Physics Today* 1982, 35 (5), 40-46.
- Sato, K., *Kagaku Keizai* 1987, No.11, 28-36.
- Schlosberg, R.H., "Chemicals from Coal", Chap. 24 in "Fuel Science and Technology Handbook", J.G. Speight Ed., Marcel Dekker: New York, 1990a, pp.763-773.
- Schlosberg, R.H., "Chemicals from Petroleum", Chap. 11 in "Fuel Science and Technology Handbook", J.G. Speight Ed., Marcel Dekker: New York, 1990b, pp.277-306.
- Schobert, H.H., Paper presented at the Twelfth Biennial Lignite Symposium, Grand Forks, North Dakota, May 18-19, 1983.
- Schobert, H.H.; Bartle, K.D.; Lynch, L.L. (Eds.), "Coal Science II", ACS Sym. Ser. 461, 1991, 337 pp.
- Schobert, H.H., "The Chemistry of Hydrocarbon Fuels", Butterworths: London, 1990, 348 pp.
- Seymour, R.B. "Polymers for Engineering Applications". ASM International, 1987, 198 pp.
- Shabtai, J.; Veluswamy, L.; Oblad, A.G., *Am. Chem. Soc. Div. Fuel Chem. Prepr.* 1978, 23 (1), 107-113.
- Sheldon, R.A. "Chemicals from Synthesis Gas", Reidel Pub. Co.: Boston, 1983.
- Shindo, A. *Osaka Kogyo Gijutsu Shikengo Koho*, 1961, 12, 110-119.
- Song, C.; Hanaoka, K.; Ono, T.; Nomura, M., *Bull. Chem. Soc. Japan* 1988, 61, 3788.
- Song, C.; Hanaoka, K.; Nomura, M., *Fuel* 1989a, 68 (3), 287-292.
- Song, C.; Ono, T.; Nomura, M., *Bull. Chem. Soc. Japan* 1989b, 62 (2), 630-632.
- Song, C., Eser, S.; Schobert, H.H. et al., "Compositional Factors Affecting Thermal Degradation of Jet Fuels", Annual Progress Report for the Period July 1990 - July 1991, DOE/Sandia National Laboratory, 78-0899-TPR-4, 1991a, 181 pp.
- Song, C., Schobert, H.H.; Matsui, H., *Prepr. Pap.-Am. Chem. Soc., Div. Fuel Chem.* 1991b, 36 (4), 1892-1899.

- Song, C., Nomura, M.; Ono, T., Prepr. Pap.-Am. Chem. Soc., Div. Fuel Chem. 1991c, 36 (2), 586-596.
- Song, C.; Schobert, H.H.; Hatcher, P.G., Proc. 1991 Int. Con. on Coal Sci., UK, 1991d, p.664-667.
- Song, C.; Nihonmatsu, T.; Hanaoka, K.; Nomura, M., Prepr. Pap.-Am. Chem. Soc., Div. Fuel Chem. 1991e, 36 (2), 542-550.
- Song, C.; Nihonmatsu, T.; Nomura, M., Ind. Eng. Chem. Res. 1991f, 30, 1726-1734.
- Song, C.; Schobert, H.H.; Hatcher, P.G., Energy & Fuels 1992a, in press.
- Song, C.; Schobert, H.H.; Hatcher, P.G., Prepr. Pap.-Am. Chem. Soc., Div. Fuel Chem. 1992b, 37, in press.
- Song, C.; Hatcher, P.G., Prepr. Pap.-Am. Chem. Soc., Div. Petrol. Chem. 1992c, 37, in press.
- Song, C.; Schobert, H.H., Prepr. Pap.-Am. Chem. Soc., Div. Fuel Chem. 1992d, 37, in press.
- Song, C.; Peng, Y.; Jiang, H.; Schobert, H.H., Prepr. Pap.-Am. Chem. Soc., Div. Petrol. Chem. 1992e, in press.
- Song, C.; Hanaoka, K.; Nomura, M., Prepr. Pap.-Am. Chem. Soc., Div. Fuel Chem. 1992f, 37, in press.
- Speight, J.G. (Ed.), "Fuel Science and Technology Handbook", Marcel Dekker: New York, 1990, 1193 pp.
- SRI International "1990 Directory of Chemical Products - United States of America", 1990, 1203 pp.
- Steveas, M.P., "Polymer Chemistry", Oxford University Press: New York, 1990, 633 pp.
- Sugi, Y.; Matsuzaki, T.; Hanaoka, T.; Takeuchi, K.; Arakawa, H., Shokubai 1989, 31 (6), 373-376.
- Sugi, Y., Kagaku Gijutsu Kenkyusho Hokoku 1990, 85 (8), 263-274.
- Taniguchi, K., Methods for Preparation of Dimethylnaphthalene", Japan Patent 49-86350, 1974, pp.323-327.
- Ueda, K.; Matsui, H.; Song, H.; Xu, W., J. Japan Petrol Inst. 1990, 33 (6), 413-417.
- Verheyen, T.V.; Guy, P.J.; Felber, M.D.; Perry, G.J., Energia, University of Kentucky, 1991, 2 (3), p.1-4.
- Verma, S.K., Carbon 1991, 29 (6), 793-803.
- Vervalin, C.H., Hydrocarbon Processing 1991, 70 (11), p.35
- Vogel, H.; Marvel, C.S., J. Polym. Sci. 1961, 50, 511.
- Vogel, H.; Marvel, C.S., J. Polym. Sci. 1963, A 1, 1531.
- Walker, P.L., Jr. "Review Article: Coal Derived Carbons", Carbon 1986, 24 (4), 379-386.
- Walker, P.L., Jr. "Carbon: An Old but New Material Revisited", Carbon, 1990, 28, 261-279.
- Weiss, R.A.; Ober, C.K. (Eds.) "Liquid-Crystalline Polymers". Am. Chem. Sym. Ser., 1990, No. 435, 32 chapters, 510 pp.
- Yokono, T.; Obara, T.; Sanada, Y.; Shimomura, S.; Imamura, T., Carbon 1986, 24, 29.

Abbreviations

BPL:	4,4'-Biphenol (p,p'-biphenol)
4,4'-BDCA:	4,4'-Biphenyl dicarboxylic acid
4,4'-DAB:	4,4'-Dialkylbiphenyl
2,6-DAN:	2,6-Dialkyl-naphthalene
ICI:	Imperial Chemical Industries
Lb:	Pounds (1 lb = 454 g)
LCP:	Liquid crystalline polymer
Kt:	Thousand tons (1 tons = 2204.6 pounds (lb))
Mlb:	Million pounds (1 Mlb = 453.59 tons)
MSC:	Molecular sieving carbon or CMS (carbon molecular sieves)
Mt:	Million tons (1 kg = 2.2046 lb)
2,6-NDCA:	2,6-Naphthalene dicarboxylic acid
sym-OHA:	1,2,3,4,5,6,7,8-Octahydroanthracene
sym-OHP:	1,2,3,4,5,6,7,8-Octahydrophenanthrene
PPO:	Polyphenylene oxide
PAR:	Polyarylate
PC:	Polycarbonate
PEEK:	Polyether ether ketone
PEN:	Polyethylene naphthalate
PET:	Polyethylene terephthalate
PBT:	Polybutylene terephthalate
p-HBA:	para-Hydroxy benzoic acid
PPTA:	Poly-p-phenylene terephthalamide (Du Pont's Kevlar LCP super-fibers)
PS:	Polysulfone
PSA:	Pressure-swing adsorption
PVCA:	Poly-N-vinylcarbazole
TPA:	Terephthalic acid
WI-MD:	Wilsonville middle distillates from catalytic two-stage coal liquefaction
3M:	Minnesota Mining and Manufacturing

REPROCESSING OF USED TIRES INTO ACTIVATED CARBON AND OTHER PRODUCTS

Hsisheng Teng, Michael A. Serio, Rosemary Bassilakis,
Philip W. Morrison, Jr. and Peter R. Solomon

Advanced Fuel Research, Inc.,
87 Church Street
East Hartford, CT 06108

Keywords: Used Tires, Activated Carbon, Pyrolysis

ABSTRACT

The disposal of used tires generated each year in the U.S. by landfill is increasingly becoming an unacceptable solution. A better solution from an environmental and economic standpoint is to thermally reprocess the tires into valuable products such as activated carbon, other solid carbon forms (carbon black, graphite, and carbon fibers), and liquid fuels. In this study, a high surface area activated carbon ($> 800 \text{ m}^2/\text{g}$ solid product) was produced in relatively high yields from pyrolysis of tires up to 900°C , followed by activation in CO_2 at the same temperature. The surface area of this carbon is comparable with that of commercial activated carbon. The efficiency of the activation process (gain in specific surface area/loss in mass) was greatest when the pyrolysis was done on unground pieces of tire. This approach was found to give the best results for the preparation of activated carbon from used tires, with a total surface area production as high as $138 \text{ m}^2/\text{g}$ (original tire). Oxygen pretreatment of tires appears to increase both the yield and surface area of carbon produced from this system. High pressure treatment of tires at low temperatures ($< 400^\circ\text{C}$) is an alternative approach if recovery of carbon black or fuel oils is the primary objective.

INTRODUCTION

The disposal of 280 million tires generated each year in the U.S. by landfill is increasingly becoming an unacceptable solution [1]. The tires take up large amounts of valuable landfill space and also represent a fire hazard. Recently, a large mountain of tires caught on fire in Canada with widespread environmental consequences due to the oils and gases generated from the decomposing tires. A better solution from an environmental and economic standpoint is to thermally reprocess the tires into valuable products [2]. The largest scale efforts employ tires either as a fuel [3] or as a filler for asphalt [4]. These two technologies consume about 5-6 million tires annually. However, tire burning has had repeated problems with feeding the tires and slagging, while the rubber asphalt costs 40% more than conventional material. An alternative is to reprocess the used tires into activated carbon and other solid carbon forms (carbon black, graphite, and carbon fibers), and liquid fuels. The key to producing such a product is controlling the chemistry of low temperature carbonization, which is the subject of this paper.

Pyrolysis has been widely used for converting solid fossil fuels, e.g. coal, into liquid and gaseous hydrocarbons, a process which results in a solid char residue. Coal pyrolysis has been extensively studied [5-7]. Used automotive tires contain polymeric aromatic structures which are similar to those of coal in some respects. Therefore, pyrolysis of waste tires to produce valuable products is currently receiving some attention. However, investigations of tire pyrolysis are rarely reported in the open literature.

The most commonly used vulcanized tire rubber is a styrene-butadiene-copolymer (SBR) containing about 25 wt.% styrene [8]. A typical composition for tire rubber is shown in Table 1. Also, a comparison of the structure and composition of tire rubber with that of a bituminous coal is shown

in Fig. 1. In most cases, tire pyrolysis studies were performed under inert conditions [8,9,10]. However, pyrolysis may be carried out in mildly oxidizing atmospheres, such as steam and carbon dioxide, to improve the quality of pyrolytic products [11,12,13].

Tire pyrolysis experiments have been conducted in the 500-900 C° range [8,9,11]. Similar to coal pyrolysis, the principal products from tire pyrolysis are gases, liquid oils and solid carbon residues. The following yields (as-received basis) of tire pyrolysis are typical: 33-38 wt.% char, 38-55 wt.% oil, and 10-30 wt.% gas. The product yields are affected by the pyrolysis conditions, such as pyrolysis temperature and heating rate. The literature work on the analysis of products from tire pyrolysis is summarized as follows:

Gas Analysis - Gases produced from tire pyrolysis are mainly hydrogen, carbon dioxide, carbon monoxide, methane, ethane and butadiene, with lower concentrations of propane, propene, butane and other hydrocarbon gases [8]. The temperature for the maximum evolution rate of each gas shifts to higher temperature levels as heating rate is increased. There was an increase in the total gas emission with heating rate and a corresponding decrease in oil yield [8]. Pyrolysis carried out in the presence of water increases the production of hydrogen and carbon monoxide [11]. This is thought to result from the occurrence of carbon gasification by steam, i.e., $C + H_2O \rightarrow CO + H_2$.

Oil Analysis - The yield of oil from tire pyrolysis is high (~50 wt % of initial tire rubber), reflecting the potential of tire rubber as a substitute for fossil fuel and chemical feedstocks. The oils have high aromaticity, low sulfur content, and are considered relatively good fuels [13]. The molecular weight range of the oils was up to 1600 with an average molecular weight in the 300-400 range [8]. The average molecular weight increases with increasing pyrolysis temperature and with decreasing heating rate. Infrared analysis of the oils indicated the presence of alkanes, alkenes, ketones or aldehydes, aromatic, polyaromatic and substituted aromatic groups [8]. An increase in pyrolysis temperature produced a decrease in the aliphatic fraction and an increase in the aromatic fraction [8]. Aliphatic hydrocarbons and alkylbenzenes are the major components of the oil if the pyrolysis is performed in the presence of water [11], and the average molecular weight of the aliphatic hydrocarbons was 164 and that of alkylbenzenes was 180. These average molecular weights are lower than the values for the oils from tire pyrolysis under an inert environment. This may indicate that the cracking of oil molecules during pyrolysis is promoted by the introduction of water.

The oil product from tire pyrolysis is a potential source of energy and chemicals. The oils may be used directly as fuel or added to petroleum refinery feedstocks [8]. The composition of the gasoline boiling fraction was reported to be comparable to that of petroleum gasoline [13]. The derived oils may also be an important source of refined chemicals, because it has been reported that they contain high concentrations of valuable chemical feedstocks, such as benzene, toluene and xylene [8].

Carbon Residue Analysis - The carbon residue would become a marketable product if its properties are similar to those of manufactured carbons. The simultaneous production of valuable solid products and gaseous and/or liquid fuels from what is currently a waste material would make tire pyrolysis economical if a large supply is readily available. This situation exists in many regions of the U.S.

Tire pyrolysis performed in an inert environment can produce 33-38 wt. % of carbon residue, as mentioned previously. It has been reported that the char yield increases with decreasing pyrolysis temperature and decreasing heating rate [8]. The surface area of the tire char also depends on pyrolysis temperature and heating rate. Williams et al. [8] reported that the surface area of the tire chars increases with both pyrolysis temperature and heating rate. However, Petrich [9] claims that chars prepared at too low of a temperature retain a large fraction of volatile material, resulting in lower surface areas, and those prepared at too high of a temperature tend to sinter and lose surface area. The surface area of a tire char produced by pyrolysis in an inert gas usually ranges from 30 to 90 m²/g [8,9,11].

Basically, there are two uses of tire chars: as a reinforcing filler and an adsorbent. Usually commercial carbon black is used for filling polymers and vulcanizates. Use of the tire char as an end product for the tire and printing ink industries has been reported to be unsatisfactory [8,9]. This is due to the high ash content of the tire char. Chars from tire pyrolysis contain as much as 15 wt. % of ash, with the majority of this ash being zinc oxide [9]. A means of removing the ash from tire char is an important issue in the process of producing useful carbon black from waste tires.

Carbon as an adsorbent is usually evaluated by its surface area. Measurement of surface area can be obtained by a gas adsorption method, for example nitrogen BET. Tire chars which had not been activated served well in removing mercury compounds from aqueous solution [13]. As mentioned above, the surface area of tire char is in the range of 30-90 m²/g, which is comparable with those of carbon blacks used in rubber products [8]. However, these values are too low for use of the char as activated carbon since commercial activated carbons have surface areas of around 1000 m²/g [8,9,11]. Therefore, an activation process is required to produce activated carbon from tire char. Carbons can be activated by mild oxidation with steam or carbon dioxide at high temperatures to develop internal surface area. The slow gasification kinetics of carbons in steam or carbon dioxide allows gas molecules diffusing into the carbon micropores to create or enlarge micropores. The activation process usually follows hydrocarbon pyrolysis performed in an inert environment, but it is possible to accomplish pyrolysis and activation in one stage by pyrolyzing under mildly oxidizing conditions [11].

Torikai et al. [10] pyrolyzed tires at 550°C for 30 minutes and activated the granulated char with CO₂ at 900°C. They found linear relationships between activation time and burn-off, burn-off and surface area, and burn-off and Methylene Blue value (an adsorption test). This activated carbon had a surface area up to 400 m²/g.

Ogasawara et al. [11] carried out the pyrolysis and activation of tires in one stage. In their study, water was continuously introduced to the sample with helium. The carbon residue from 1 hour steam activation at 900°C had a surface area of 1260 m²/g, while pyrolysis in helium gave a char with a surface area of 87 m²/g. The carbon residue produced from this "wet method" is as good as the commercial activated carbon in terms of surface area, but the carbon black yield was only 9 wt. % of the starting tire.

In studies on coal liquefaction and pyrolysis [14,15], it has been found that oxygen functional groups, such as carboxyl and hydroxyl appear to play a major role in promoting the crosslinking reactions between molecules in coal. These crosslinking reactions are usually encountered at low temperatures (< 200°C) prior to the occurrence of bond cleavage in liquefaction or pyrolysis. A lot of effort has been devoted to the reduction of oxygen functions of coal in order to increase the liquid yield for coal liquefaction. Conversely, an increase of the oxygen functional group content would be expected to result in an increased char yield from pyrolysis of coal.

In the study of tire pyrolysis, some workers [10,11] have already produced high surface activated carbons from tire chars. However, the product yields of their systems were very low, and this is a serious drawback from economic point of view. Therefore, a method to increase the char yield from tire pyrolysis is one of the most important issues in making activated carbon from waste tires. Since the chemical structures in the tire rubber are similar to structures found in the coal, an increase of the oxygen functional group content in tires would be expected to promote the crosslinking reactions between tire molecules, and thus enhance the char yield in pyrolysis. In this study, oxygen pretreatment of tires was carried out prior to pyrolysis, and the results were compared to those without oxygen pretreatment.

High pressure treatment of coal under wet (steam) conditions, has been reported to allow the breaking of hydrogen bonds, loosening of the coal matrix and stabilization of some of the reactive components of the coal [16]. The extraction of oils from tires by supercritical or subcritical water was

studied by Funazukuri et al. [12]. Under the current study, a limited number of runs was done on low temperature, high pressure treatment of tires under wet or dry conditions to study the "self-liquefaction" of tires to recover the carbon black and provide liquid fuels simultaneously.

EXPERIMENTAL

There were two tire samples used in this investigation: granulated and non-granulated. The granulated sample was prepared by crushing and grinding a large piece of frozen tire under cryogenic conditions. The particle size of the sample was -50 mesh. The non-granulated sample was prepared by cutting the tire rubber into a fixed size of 170 ± 5 mg, unless otherwise specified.

Most of the tire pyrolyses were carried out in a TG-FTIR system under an inert (helium) or a mildly oxidizing (carbon dioxide) environment [17]. Tire char produced from a fixed-bed reactor under an inert environment was prepared to compare with that produced from the TG-FTIR system. Flash pyrolysis of tire was also performed in a wire-grid reactor with direct electrical resistance heating in helium. The heating rate was as high as $20,000^\circ\text{C}/\text{min}$.

Various treatments of the tires were investigated in order to improve the quality of products. The granulated sample was used for these treatments. The tire treatment procedures are briefly described as follows: 1) Oxygen pretreatment: Sample was kept in the air at 140°C for 15 days; 2) Wet high pressure treatment: Sample was treated with water in an autoclave at 4000 psig and 400°C for 30 min.; 3) Dry high pressure treatment: Sample was enclosed in a 3500 psig helium filled autoclave at 400°C for 30 min.

The gases evolved during pyrolysis can be quantitatively measured in the TG-FTIR system [17]. The liquid oil product was analyzed as KBr pellets in a Nicolet FT-IR. For quantitative analysis of the oil FT-IR spectra, a curve analysis program is employed to synthesize the IR spectra [18-21]. The quantitative data derived from the spectral synthesis gives a good quantitative determination for aliphatic, aromatic, ether, carboxyl and hydroxyl functional groups and a qualitative determination of alkanes and alkenes [18-21].

The solid residues produced under various pretreatment and pyrolysis conditions were subject to surface area measurements. The measurements were carried out using a dynamic, continuous method. A commercial instrument (Quantasorb, Quantachrome Corp.) was used to determine N_2 BET surface areas. Prior to surface area analysis, all samples were outgassed in a flow of nitrogen at 300°C for 1 hour. The N_2 surface area was determined at 77 K.

A scanning electron micrograph (SEM) with an x-ray analysis instrument was used in this study to investigate the surface structure and sulfur content of different samples.

Tire chars produced from pyrolysis were activated in a flow of CO_2/He mixture at 900°C . The CO_2 partial pressure during activation was fixed at 0.08 atmosphere, unless otherwise specified. The activated chars with various burn-offs were prepared and subject to surface area analysis.

RESULTS AND DISCUSSION

1. Tire Sample Analysis

The results of proximate and ultimate analyses of the granulated tire are shown in Table 2. Since the ash content shown in Table 2 is higher than for the unground sample and those reported in the literature [8,11], it was concluded that the granulated tire sample was accidentally contaminated in the grinding and/or sieving process. By SEM/x-ray analysis, the contamination was found to be mainly iron. The non-granulated tire sample, which was not contaminated, has an ash content around 2.9 wt.%. This

is similar to what has been reported previously for tires [8,11]. The ash free composition of the non-granulated tire sample is the same as that of granulated sample shown in Table 2. The samples were supplied by Prof. Mark Petrich of Northwestern University from a batch of shredded (used) truck tires.

2. Product Composition from Tire Pyrolysis

Gas Products - The typical product evolution data during granulated tire pyrolysis, starting from room temperature with a heating rate of 30°C/min up to 900°C, are shown in Fig. 2. The principal gases evolved are H₂O, CH₄, CO₂, CO, SO₂, C₂H₄, and NH₃. The total yield of gases and tars increases with temperature up to 650°C, after which there is no significant change in product yield. Tar is the major product of tire pyrolysis. It evolves mainly between 350 and 500°C.

The product evolution during the pyrolysis of the oxygen treated sample is shown in Fig. 3. It is of interest to notice, by comparison of Fig. 3 with Fig. 2, that the gas yields during pyrolysis were significantly increased by oxygen pretreatment, whereas the tar yields were reduced. The comparison of the product yields of these two samples is shown in Table 2. There was no surprise to see the enhanced evolution of H₂O, CO, CO₂ and SO₂ due to oxygen pretreatment, since oxygen would react with the components in the tire, and result in the increase of oxygen containing products from pyrolysis. However, the interpretation of the observations of the increased evolution of CH₄ and C₂H₂ and the reduced production of tars resulting from oxygen pretreatment is not as straightforward. It has been reported that oxygen plays a major role in crosslinking and cleavage of the network structure of coals [14,15]. Our results obviously revealed that oxygen pretreatment promoted the cleavage reactions for producing small molecules, such as CH₄ and C₂H₂, and the crosslinking between macromolecules in tires to reduce tar evolution, with a corresponding increased char yield (see below). This is a very beneficial result for tire carbonization process, since the char yield is significantly raised (see Table 3) due to the crosslinking between macromolecules, whereas the production of gaseous fuels, CH₄ and C₂H₂, is also promoted.

Liquid Products - The condensable liquid products (tars) are the major products of tire pyrolysis. The compounds found in tire pyrolysis oils have been identified as largely consisting of benzene, toluene, xylene, styrene, indane, indene, naphthalene, methyl naphthalenes, biphenyl, fluorene, pyrene, anthracene, phenanthrene and various other 3, 4, 5 and 6 ring polyaromatic hydrocarbons and aliphatic compounds, including alkanes and alkenes [8]. Since the compounds in the oil are too numerous and diverse to recognize quantitatively, functional group compositional analysis was used to more clearly reveal the properties of the oil. The FT-IR absorbance spectrum of the tire oil is shown in Fig. 4. As shown in Fig. 4, the aliphatic C-H stretching vibrations at 2930 and 2850 cm⁻¹ and C-H deformation vibrations at 1350-1470 cm⁻¹ indicate the presence of alkanes. The C-H stretching at 3000-3100 cm⁻¹, 1600 and 1500 cm⁻¹ carbon-carbon stretching vibrations, C-H in-plane bending in the 1000-1100 cm⁻¹ region, and 700-900 cm⁻¹ (C-H out of plane bending) peaks indicate the presence of aromatic compounds. The C=O stretching vibrations at 1700 cm⁻¹ indicate the presence of ketones or aldehydes. The 1630 and 990 cm⁻¹ absorbance peaks are indicative of alkenes. The O-H stretching vibrations between 3200 and 3600 cm⁻¹ indicate the presence of hydrogen-bonded alcohols or phenols. The C-O stretching in the 1060-1300 cm⁻¹ range indicates the presence of alcohols, ethers, and carboxylic acids. The quantitative functional group analysis of the oil based upon the absorbance spectra in Fig. 4 is summarized in Table 4. It is indicated in Table 4 that the oils formed are mostly aliphatic.

Solid Products - The solid residue yield varied with pyrolysis conditions. The product yields of tire pyrolysis in helium under different pyrolysis conditions are shown in Table 5. These results show that the char yield increases with decreasing pyrolysis temperature. This is consistent with the results of other workers [8,11,12]. Table 5 also shows an increasing char yield with increasing heating rate, and this trend is opposite to that reported by Williams et al. [8]. This disagreement is probably due to the absence of a holding period at the final pyrolysis temperature in our study, whereas there was at least two hours of holding time at final temperature in the work of Williams et al. [8].

Tire pyrolysis performed in a fixed bed reactor shows no effect in promoting char yield. However, it is of interest to note that the char yield from pyrolysis of granulated tires was enhanced roughly 26% by oxygen pretreatment, as revealed in Table 5. As mentioned previously, this char yield enhancement may be attributable to the crosslinking between macromolecules in tire rubber due to the formation of oxygen functional groups during oxygen pretreatment. Oxygen pretreatment (at 140°C for 88 hours) of non-granulated tires shows little effect in increasing char yield. This may be due to the fact that oxygen cannot access the interior part of a large size tire rubber to promote the crosslinking between the molecules of the tire, or the pretreatment time was not long enough.

Tire pyrolysis performed under a mildly oxidizing (CO_2) condition was investigated. The comparison of char yields of tire pyrolysis in helium and CO_2 is shown in Fig. 5. These results show that char yields were higher when pyrolysis is carried out under a mildly oxidizing condition. Again, the existence of CO_2 during pyrolysis may provide oxygen to enhance the crosslinking reactions between tire molecules, and, therefore, increase the char yield. Since crosslinking enhancement has been mainly accomplished in the period of oxygen pretreatment, therefore pyrolysis carried out in CO_2 gives much less effect in the promotion of char yield for oxygen pretreated tires. Pyrolysis of non-granulated tires in CO_2 shows no effect in promoting char yield. This may also be due to the fact that CO_2 cannot easily diffuse into the interior part of a large piece of tire rubber to enhance the crosslinking reactions.

Zinc and sulfur have been reported to be the major components of the ash in tire chars [8,11]. Fig. 6 shows zinc and sulfur in the internal section of the solid residue from the pyrolysis of non-granulated tires in CO_2 , as measured by a SEM/X-ray microanalyzer. It shows, from the micrographs in Fig. 6, that zinc and sulfur grains are widely spread in the char and exist at the same locations, suggesting they are in a compound of zinc sulfide. Zinc sulfide is thought to be produced by the reaction between zinc oxide and the sulfur contained in tires [11].

Sulfur Distribution - Sulfur is used to cross link the polymer chains within the rubber. Therefore, due to environmental concerns, the emission of sulfur compounds from waste tire use has to be taken into account in the assessment of processes, such as tire pyrolysis, tire oil combustion, ..., etc. The distribution of sulfur in products after pyrolysis was investigated in this study. The sulfur contents of the gas and char from pyrolysis were determined by TG-FTIR and SEM/x-ray microanalysis, respectively. The quantity of sulfur contained in the liquid oil can be evaluated from the overall mass balance of sulfur of the tire pyrolysis. It is found that ~13% of tire sulfur is evolved in the gas phase ~9% is contained in the liquid oil, and ~78% is retained in the solid char. The results indicate that the sulfur within tire is preferentially retained in the char product after pyrolysis, since the char yield is typically 40% of the tire mass. This would imply that the cost of sulfur pollution control would be low in tire pyrolysis and for various uses of the tire oil.

High Pressure Treatments - High pressure treatment of automotive tires may hopefully result in the liquefaction of tire rubber and the recovery of carbon black. Table 6 presents the results obtained from wet and dry high pressure treatment of granulated tires. The overall mass balance is not 100% in Table 6. This deficiency in mass balance was also observed by Funazukuri et al. [12] in supercritical extraction of tire with water. The mass loss may be due to the evaporation of low boiling point oils during the process of product separation (separating solid and liquid). The product composition of wet and dry high pressure treatment are similar, and it shows roughly 35.9 ± 0.8 wt% solid residue, 45.4 ± 1.7 wt% oil, and 2.44 ± 0.89 wt% gas. The gaseous product is composed of CO_2 , CO , C_2H_4 , C_2H_6 and CH_4 , and its composition is shown in Table 7.

The results in Table 7 indicate that CO_2 is the main component of the gaseous products. The FT-IR absorbance spectra of the oils from high pressure treatment of tire are shown in Fig. 7, and the results of quantitative functional group analysis are shown in Table 8. Fig. 7 and Table 8 reveal that the property of the oils from high pressure treatment of tire is similar to that from tire pyrolysis shown in Fig. 4.

The solid residues from high pressure treatment (wet or dry) of tire contain carbon black, solid hydrocarbons and ash. The above results show that high pressure (wet or dry) pyrolysis of tires at low temperatures (<400°C) is an alternative approach if recovery of carbon black or fuel oils is the primary objective. However, additional analysis is required of the solid material recovered in order to confirm this conclusion.

3. Surface Area Analysis

Unactivated Tire Chars - Fig. 8 shows the surface areas of the chars formed from the pyrolysis of the granulated tire sample in helium up to 500 and 700°C at a heating rate of 30°C/min., and up to 900°C at various heating rates. The surface areas can be seen to increase with pyrolysis temperature. This result is in agreement with that of Williams et al. [8]. This observation says that chars prepared at lower temperatures retain a higher fraction of volatile material, resulting in lower surface areas. On the other hand, it is revealed in Fig. 8, that the surface area decreases with heating rate, and this trend is opposite to that observed in the study of Williams et al. [6]. As mentioned previously, this disagreement may be due to no holding period at final temperatures in our study.

Pyrolysis of non-granulated tires in helium up to 900°C also produced a char with a surface area of 97 m²/g. Surface areas of tire chars produced from the pyrolysis of both granulated and non-granulated tires in CO₂ were analyzed, and it shows no effect of CO₂ on the surface areas of char products. Pyrolysis of tires in a fixed bed reactor up to 700°C gave a char having a surface area of 79 m²/g, showing no significant improvement on creating char surface area. The surface area of char formed from the pyrolysis of O₂ pretreated tires in helium up to 900°C was measured, and it was found that the surface area of O₂ treated tire char was as high as 179 m²/g, which is almost twice as much as that of char from tires without any pretreatment under identical pyrolysis condition. Also, in the previous section, it showed that pyrolysis of O₂ treated tire gave the highest char yield. Therefore, considering both surface area and char yield, O₂ pretreatment of tires is very beneficial in producing high total surface area (in units of m²/(g tire)) carbon.

Fig. 9 shows the scanning electron micrographs of chars formed from pyrolysis of O₂ treated tires and tires with no pretreatment. It shows that the O₂ treated tire char has a very rough and dented surface, indicating that crosslinking or polymerization between rubber molecule and carbon black was enhanced by O₂ treatment and, therefore, the rubbers could not be totally volatilized during pyrolysis. On the other hand, the char from tires without any treatment shows a very smooth surface, indicating that most of the rubbers were volatilized during pyrolysis and the solid residue contains mainly carbon black and ash. The difference of char surfaces shown in Fig. 9 explains the higher surface area and yield of char produced from O₂ treated tires.

The above results show that the surface areas of chars formed from tire pyrolysis are comparable with the surface areas of carbon blacks in rubber products, including tires [7]. However, use of the char as activated carbon is not possible since commercial activated carbon has a higher surface area. An activation process is thus required for producing activated carbon from tire chars.

Activated Tire Chars - The surface areas of tire chars activated in CO₂ for various extents of burn-off are summarized in Table 9. It shows that the surface areas of tire chars increase monotonically with char burn-off, and pyrolysis conditions (including pyrolysis temperature, heating rate and gas environment) have little effect on the ultimate surface areas of activated tire chars. For granulated samples, similar to the results of unactivated chars, the O₂ treated tire chars gave the highest surface areas, i.e., up to 370 m²/g at 50% burn-off.

Table 9 shows that non-granulated samples gave much higher surface areas than the granulated. This can be attributable to the higher ash contents of granulated samples, since the surface area of ash is very low (8.6 m²/g). Having the value of ash surface area and the ash content allows us to calculate the specific surface area of dry ash free (d.a.f.) char. The calculated values for d.a.f. chars are also shown in Table 9. Table 9 reveals that the surface areas of granulated samples in terms of

daf mass are comparable to those of non-granulated samples. This is reasonable, since they were all derived from the same material.

For non-granulated samples, there was little size effect on surface areas of the activated chars, as revealed in Table 9. O_2 pretreatment of tires indeed increase the surface area of activated non-granulated char, but not as significantly as in the case of the granulated sample. Table 9 also shows that the surface area of non-granulated char was increased by performing activation under a higher partial pressure of CO_2 . Similar behavior was also reported for tire char activation in steam [11].

Torikai et al. [10] produced activated carbon from automotive tires by pyrolysis of the samples in an inert environment and activating the solid residue in a stream of CO_2 at $900^\circ C$. This activated carbon had surface areas of up to $400\text{ m}^2/\text{g}$ at 80% burn-off. Ogasawara et al. [11] prepared activated carbon from automotive tires from a wet thermal decomposition, and a $1260\text{ m}^2/\text{g}$ of carbon residue is obtained, however, with a yield of only 9 wt.% of the original tire sample. The total surface area of their product is $113\text{ m}^2/(\text{g tire})$. In our study, $813\text{ m}^2/\text{g}$ of activated carbon was produced with a yield of 17 wt.% of the original tire sample. The total surface area of this activated carbon was up to $138\text{ m}^2/(\text{g tire})$, a 20% increase when compared to the results of Ogasawara et al. [11]. This improvement could be partly due to differences in the starting tire samples.

The total surface area in units of $\text{m}^2/(\text{g tire})$ is actually a measure of activation (or burn-off) efficiency for producing activated carbon from tires. Fig. 10 shows the values of total surface area at various char burn-off. It shows no significant change with burn-off for granulated sample, indicating a low activation efficiency at higher burn-off. However, the total surface area of non-granulated sample increases significantly with carbon burn-off, indicating that the activation efficiency is high for this case. The reason for the better activation results for the char derived from larger tire pieces is not known. Since pyrolysis occurs from the outside of the particle to the center, a char layer will progressively move inward for larger pieces as the pyrolysis becomes less isothermal. This phenomenon may affect the development of the char morphology which in turn will affect how the material response to the activation process. This will be the subject of additional research.

CONCLUSIONS

1. Pyrolysis of granulated and non-granulated tires has shown recoveries of gases, liquid oils and solid char. The product yields vary with the variation of pyrolysis condition and pretreatment. The total yield of gases and tars increases with temperature up to $650^\circ C$, after which there is no significant change in product yield. The main gases evolved are H_2O , CH_4 , CO_2 , CO , SO_2 , C_2H_4 , and NH_3 . The derived oils are mostly aliphatic. The char yield increases with decreasing pyrolysis temperature and increasing heating rate. The char yield was found to be increased by performing pyrolysis under mildly oxidizing conditions, especially in the case of granulated tires. Both the gas and char yields of tire pyrolysis were increased by oxygen pretreatment, whereas the oil yield was reduced.
2. The sulfur within tires is preferentially retained in the char product after pyrolysis. This is an advantage for tire pyrolysis versus tire incineration, since the cost for sulfur emission controls would be low.
3. High pressure treatment of tires at low temperatures ($<400^\circ C$) is an alternative approach if recovery of carbon black or fuel oils is the primary objective.
4. The surface area of tire char is shown to increase with pyrolysis temperature and decrease with heating rate. O_2 pretreatment of tire shows beneficial results in promoting both char yield and surface area in tire pyrolysis, especially for granulated tires. The surface areas of tire chars are comparable with those of carbon blacks in rubber products, but too low if compared with that of commercial activated carbon. Therefore, an activation process is required for producing activated carbon from tire chars.

5. For production of a high specific surface area char directly from tire pyrolysis, the best results were obtained by O₂ pretreatment of granulated tires (~200 m²/g). However, in order to produce a commercial grade activated carbon an activation process is required and the efficiency of the activation process is best when non-granulated tire pieces are used. At 50% burnoff, specific surface areas close to 1000 m²/g (daf basis) were achieved in both cases. However, the net yield of activated carbon was significantly higher when starting with non-granulated tires. This is beneficial from an economic standpoint since the grinding costs are lower.

ACKNOWLEDGEMENTS

The financial support of the National Science Foundation under Grant No. ISI-9060297 is gratefully acknowledged. The Project Officer was Dr. Edward Bryan. The authors also acknowledge helpful discussions with Prof. Mark Petrich of Northwestern University, who supplied the tire samples, and the assistance of Prof. Eric Suuberg of Brown University with surface area analysis of the samples.

REFERENCES

1. *New York Times*, May 9, 1990, p. D1.
2. Schulman, B.L. and White, P.A., "Pyrolysis of Scrap Tires using the Tosco II Process - a Progress Report", *Solid Wastes and Residues: Conversion by Advanced Thermal Processes*, (J.L. Jones and S.B. Radding, Eds.), ACS Symposium Series #76, 1978, p. 274.
3. Oxford Energy Corporation, Modesto, CA.
4. Rubber Asphalt Producers, Phoenix, AZ.
5. Solomon, P.R., Hamblen, D.G., Carangelo, R.M., Serio, M.A., and Deshpande, G.V., *Energy and Fuel*, 2, 405, (1988).
6. Serio, M.A., Hamblen, D.G., Markham, J.R., and Solomon, P.R., *Energy and Fuels*, 1, 138 (1987).
7. Suuberg, E.M., Peters, W.A., and Howard, J.B., 17th Symp. (Int) on Combustion, The Combustion Institute, Pittsburgh, PA, 1979, p. 117.
8. Williams, P.T., Besler, S., and Taylor, D.T., *Fuel*, 69, 1474 (1990).
9. Petrich, M.A., "Conversion of Plastic Waste to Valuable Solid Carbons", Final Report of a Project in the Innovative Concepts Program, U.S. DOE, Jan., 1991.
10. Torikai, N., Meguro, T., and Nakamura, Y., *Nippon Kagaku Kaishi*, 11, 1604 (1979).
11. Ogasawara, S., Kuroda, M., and Wakao, N., *Ind. Eng. Chem. Res.*, 26, 2552 (1987).
12. Funazukuri, T., Takanashi, T., and Wakao, N., *J. Chem. Eng. Japan*, 20, 23 (1987).
13. Merchant, A. and Torkelson, J.M., "Pyrolysis of Scrap Tires", Chemical Engineering Dept., Northwestern U., Spring, 1990.
14. Serio, M.A., Solomon, P.R., Kroo, E., Bassilakis, R., Malhotra, R., and McMillen, D.F., *ACS Div. of Fuel Chem. Prepr.*, 35, (1), 61, (1990).
15. Serio, M.A., Solomon, P.R., Kroo, E., and Charpenay, S., *ACS Div. of Fuel Chem., Prepr.*, 36, (1), 7 (1991).
16. Bienkowski, P.R., Narayan, R., Greenkorn, R.A., and Choa, K.W., *I&EC Res.*, 26, 202&206(1987).
17. Carangelo, R.M., Solomon, P.R. and Gerson, D.J., "Application of TG-FTIR to Study Hydrocarbon Structure and Kinetics", *Fuel*, 66, 960 (1987).
18. Solomon, P.R., Hamblen, D.G. and Carangelo, R.M., *ACS Symp. Series*, 205, *Coal and Coal Products: Analytical Characterization Techniques*, Washing., DC (1982), pg. 77.
19. Solomon, P.R., Hamblen, D.G. and Carangelo, R.M., *Analytical Pyrolysis of Coal Using FT-IR*, 5th Int. Symp., on Analytical Pyrolysis, Colorado (1982).
20. Solomon, P.R. and Carangelo, R.M., *Fuel*, 61, 663 (1982).
21. Solomon, P.R. and Carangelo, R.M., *Fuel*, 67, 949 (1988).

Table 1. Composition of Tire Rubber [8,11]

Component	wt.% (as-received)
SBR	60 - 65
Carbon Black	29 - 31
Zinc Oxide	1.9 - 3.3
Sulfur	1.1 - 2.1
Extender Oil	~2
Additives	~0.7

Table 2. Composition of a Granulated Tire Sample.

Proximate Analysis (wt.%) (as-received)		Ultimate Analysis	
Moisture	0.4		
Volatile Matters	63.6	C, wt.% d.a.f.	88.1
Fixed Carbon	22	H, wt.% d.a.f.	7.9
Ash	14	N, wt.% d.a.f.	0.5
		S, wt.% d.a.f.	2.1
TOTAL	100	O, wt.% d.a.f.	1.4

* Supplied by Huffman Laboratories (Wheat Ridge, CO).

Table 3. Product Yields From Pyrolysis of Tires and O₂ Treated Tires in an Inert Environment.

	weight % (as received)								
	H ₂ O	CO ₂	CO	CH ₄	C ₂ H ₄	SO ₂	NH ₃	Tars*	Char
Granulated Tires	3.5	0.6	1.5	0.36	0.089	0.31	0.38	57	36
O ₂ Treated Granulated Tires	5.3	3.3	3.3	1.2	0.24	1.0	0.21	39	45

* Estimated from mass balance

Table 4. Functional Group Analysis of Liquid Oils Formed from Tire Pyrolysis.

weight % (dmmf)								
Hydrogen		Aromatic Hydrogen			Carbon	Oxygen		
H _{al}	H _{OH}	1 Adj	2 Adj	3 or more	(Aliphatic)	O _{Carbonyl}	O _{OH}	O _{Other}
13	0.045	0.44	0.44	0.40	81	0.84	0.75	0.58

Table 5. Product Yields (as-received basis) from Tire Pyrolysis in Helium Under Different Conditions

PYROLYSIS CONDITIONS								
Temp (°C)	Ramp (°C/min)	Pressure (atm)	Size	Reactor	Pretreat	Char Yield (%)	Gas (%)	Oil ⁺ (%)
500	30	1	granu.	TG	—	40	4.7	56
700	30	1	granu.	TG	—	38	5.6	57
900	20,000	1	granu.	Wire-Grid	—	38	—	—
900	100	1	granu.	TG	—	37	6.8	56
900	30	1	granu.	TG	—	36	7.0	57
900	3	1	granu.	TG	—	35	7.4	57
900	30	1	granu.	TG	Oxygen	45	15	39
700	30	1	granu.	Fixed Bed	—	37	—	—
900	30	1	non-granu.	TG	—	34	3.8	62
900	30	1	non-granu.	TG	Oxygen	35	—	—

⁺ Estimated from mass balance.

Table 6. Product Yields (as-received basis) of High Pressure Treatment of Tires.

	Solid (%)	Liquid (%)	Gas (%)	Mass Balance (%)
Wet	36.6	43.7	3.32	83.6
Dry	35.1	47.0	1.55	83.7

Table 7. The Gaseous Product Composition (by volume) from High Pressure Treatment of Tires

	CO ₂ (%)	CO (%)	C ₂ H ₂ (%)	C ₂ H ₄ (%)	CH ₄ (%)
Wet	90.6	—	2.9	3.8	2.6
Dry	60.3	8.7	9.0	13.5	8.5

Table 8. Functional Group Analysis of Liquid Oils Formed from High Pressure Treatments of Tires.

weight % (dmmf)									
	Hydrogen		Aromatic Hydrogen			Carbon	Oxygen		
	H _{sat}	H _{OH}	1 Adj	2 Adj	3 or more	(Aliphatic)	O _{Carbonyl}	O _{OH}	O _{ether}
Wet	13	0.045	0.18	0.37	0.40	76	1.0	0.75	0.65
Dry	13	0.040	0.14	0.38	0.40	80	0.79	0.65	0.23

Table 9. Surface Areas of Tire Chars and Activated Tire Chars

SUMMARY OF RESULTS													
PYROLYSIS CONDITIONS								SURFACE AREA					
Temp °C	M °C/min.	Press ATM	Size	Gas	Reactor	Pretreat	Char Yield ^a (%)	M ² /g (as-received)			M ² /g.daf (daf)		
								0%	30%	50%	0%	30%	50%
500	30	1	P	He	TG	—	40	41	135	—	58	281	—
700	30	1	P	He	TG	—	38	69	134	—	104	273	—
900	20000	1	P	He	Wire-Grid	—	38	57	—	293	85	—	1089
900	100	1	P	He	TG	—	37	85	117	—	131	245	—
900	30	1	P	He	TG	—	36	99	124	188	157	268	815
900	30	1	P	CO ₂	TG	—	37	78	—	185	120	—	734
900	3	1	P	He	TG	—	35	98	125	—	158	280	—
900	30	1	P	He	TG	O ₂	45	179	252	357	256	447	930
900	30	1	P	CO ₂	TG	O ₂	45	—	—	365	—	—	952
700	30	1	P	He	Fixed Bed	—	37	79	126	—	122	264	—
900	30	1	L	He	TG	—	34	97	—	732	105	—	882
900	30	1	L*	CO ₂	TG	—	34	113	423	703	123	481	847
900	30	1	L	CO ₂	TG	O ₂	35	—	—	793	—	—	952
900	30	1	L	CO ₂ *	TG	—	34	—	—	813	—	—	980

^a As-received basis.

* Smaller piece of non-granulated tire (10 mg).

⁺ Higher CO₂ partial pressure (1 atm).

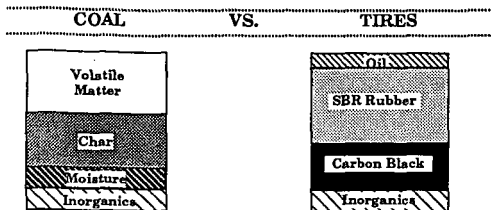
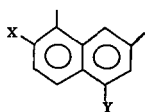


Figure 1. Comparison of Structure and Composition Between Coal and Tire Rubber.



ELEMENTAL ANALYSIS

C 82	C 88
H 5.5	H 8
O 8	O 2
N 1.7	N 0.5
S 2.4	S 1.5

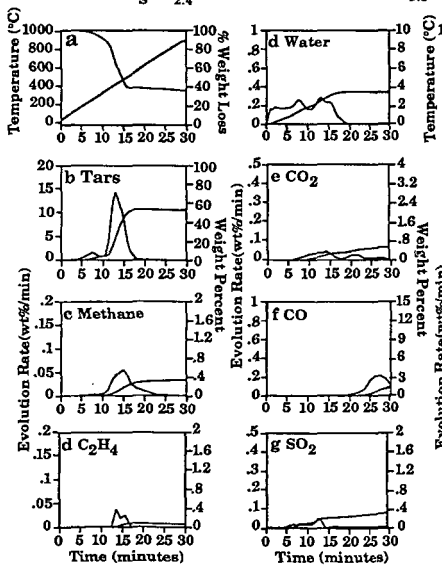


Figure 2. Product Evolution During the Pyrolysis Cycle of Granulated Tires.

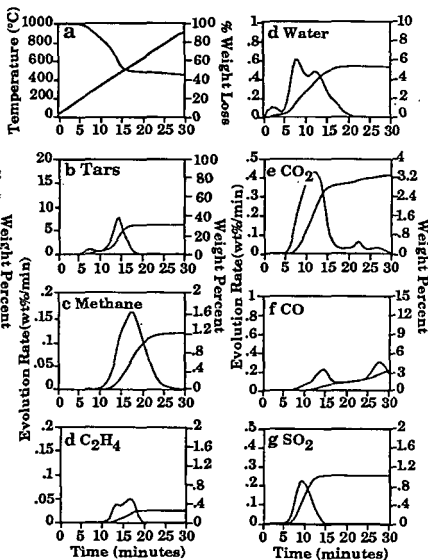


Figure 3. Product Evolution During the Pyrolysis Cycle of the Oxygen Pretreated Tires.

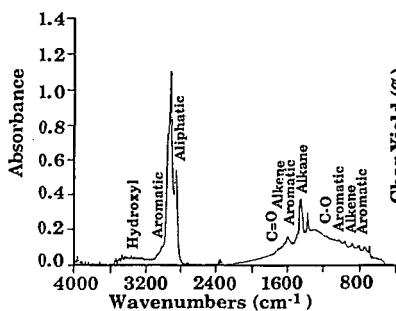


Figure 4. FT-IR Absorbance Spectrum of the Oils from Tire Pyrolysis.

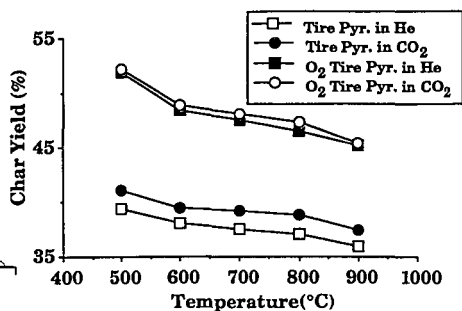


Figure 5. Comparison of Char Yields of Tire Pyrolysis in Helium and CO₂.

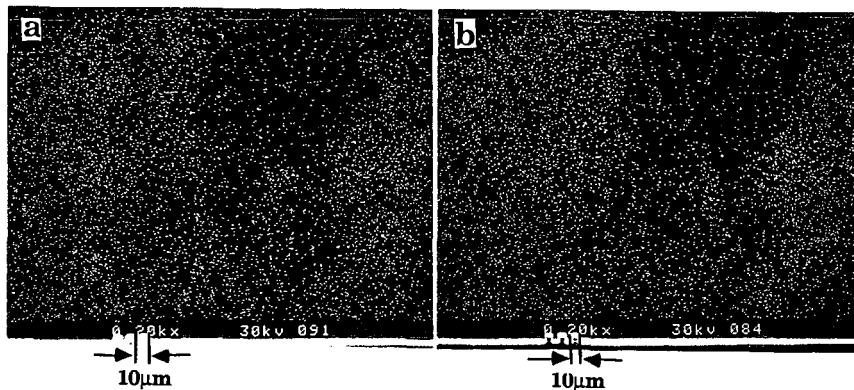


Figure 6. SEM/X-Ray Microanalysis of Zinc and Sulfur in a Carbon Residue. a) Zinc; b) Sulfur.

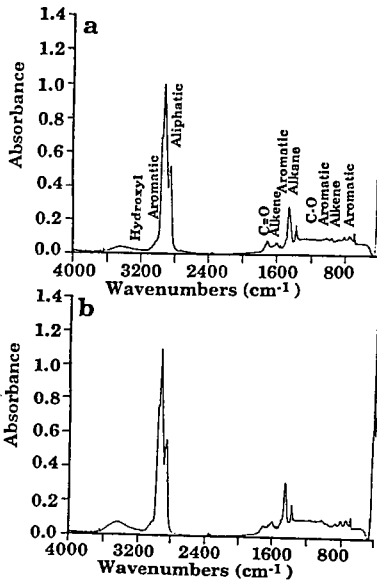


Figure 7. FT-IR Absorbance Spectra of Oils from High Pressure Treatments of Tires. a) Wet Process; b) Dry Process.

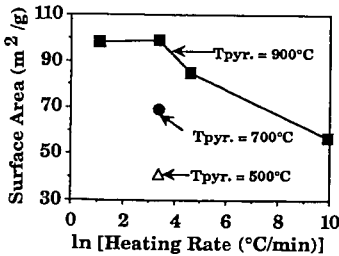


Figure 8. Surface Areas of Chars Formed from Different Pyrolysis Conditions.

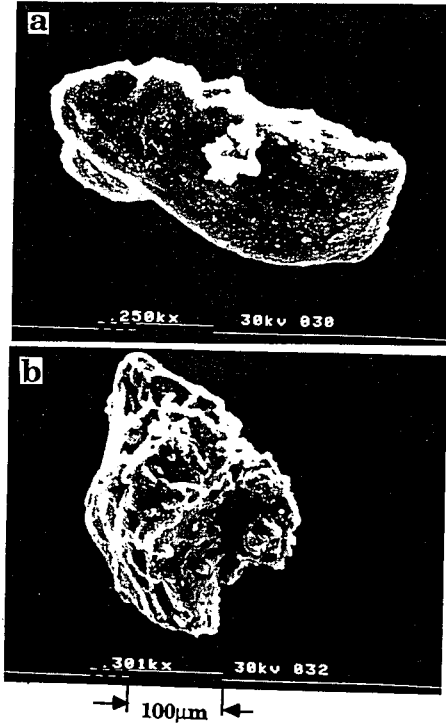


Figure 9. Scanning Electron Micrograph of 900°C Tire Chars from Tires. a) Without Pretreatment; b) Treated with Oxygen.

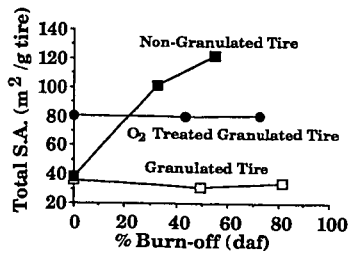


Figure 10. Total Surface Areas of Tire Chars at Various Extents of Carbon Burn-off.

ACTIVATED CARBONS FOR THE REMOVAL OF NITRIC OXIDES

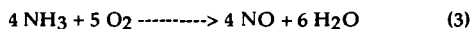
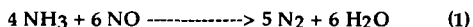
S. N. Ahmed, J. Stencel, F. Derbyshire and B. Baldwin*
Center for Applied Energy Research, University of Kentucky,
3572 Iron Works Pike, Lexington, KY 40511; *Colorado School
of Mines, Golden, CO 80401.

Keywords: Activated Carbon, Nitric oxide, and Reduction

INTRODUCTION

Nitrogen oxide (NO_x) emissions from stationary and mobile sources are precursors to acid precipitation, are important in the formation of ozone during interaction with hydrocarbons, and have been implicated as intermediates in greenhouse gas formation. The amount of NO_x emitted is distributed nearly equally between transportation, industry and power generation (1). For stationary sources, the recent Title III federal legislation will restrict NO_x emissions to levels of approximately 0.45 lb/MM Btu. As a result, it is anticipated that many coal fired power sources will be required to install some type of post combustion clean-up equipment to reduce NO_x emissions.

One of the commercially available technologies that has been used to control NO_x is selective catalytic reduction (SCR) using NH₃ as a reductant over oxide supported catalysts. It is called selective because with O₂ in the combustion flue gas, the following reactions are possible:



Reactions (1) and (2) are desired where as nonselective Reaction (3) would cause NO to be produced.

Currently, SCR technology using metal oxide catalysts has an optimum reaction temperature between 350-450°C. This range places restrictions on locating the catalyst bed for flue gas treatment in coal fired units. For example, if the catalyst bed is placed before the particulate and the sulfur oxide clean-up equipment, the flue gas temperature would be within the desired range but the catalyst life would be reduced because of high concentrations of particulates and catalyst poisons (2,3). If the catalyst bed is placed after the clean-up equipment, an additional source of heating is required to reheat the flue gas to a desired temperature.

To investigate catalysts for alternative lower temperature NO_x decomposition, we have initiated studies on the use of activated carbons and their modification. To date, these studies have concentrated on commercially available carbons and on comparisons with commercially available V₂O₅/TiO₂.

EXPERIMENTAL

A schematic diagram of the overall experimental setup is presented in Figure 1. Gas flow rates were controlled by Tylan model FC-280 mass flow controllers. Each stream was filtered through a 0.5 micron sintered metal filter before entering the flow controller. After passing through a block valve and a check valve, the gases entered the mixing chamber which was made up of a 2.54 cm od stainless steel pipe filled with 3 mm glass balls. This arrangement allowed a thorough mixing of gases before entering the reactor vessel. The reactor vessel was a 1.9 cm od stainless steel tube with a 1.22 cm id and was 30.45 cm in length. The catalyst bed was sandwiched between glass wool plugs which were supported by 3 mm glass beads. The reactor was enclosed in a tube furnace. After passing through the reactor, the product stream was analyzed by a non-dispersive infrared CO₂ detector, a chemiluminescence NO/NO_x detector and mass spectrometer.

Four commercial samples, originating from three different precursors have been obtained for this investigation. Their origins and surface areas are presented in Table I. Three of these samples (labelled SP1, SP2 and SP3) will be discussed here. They were used in a powdered form (50 - 100 mesh) and have characteristics shown Table II.

In the test runs, the temperature was varied from 100-300°C, the total gas flow rate was 1000 SCCM, and the catalyst weight was 3 g. An emphasis was placed on using the conditions similar to that of flue gas generated from power plants; hence, the NO and NH₃ concentrations were 700 ppm and O₂ was 4%. Prior to each test run, samples were heated for four hours at 300°C under a helium flow. For comparisons, a commercially prepared V₂O₅/TiO₂ catalyst was tested under the same conditions.

The pH of the samples was obtained using a standard procedure in which 3 g of the sample was mixed with 60 ml of distilled water and heated at 100°C for three minutes. The solution was then filtered, allowed to cool to room temperature, and its pH was measured.

RESULTS AND DISCUSSION

Figure 2 shows the NO conversion for the three samples as a function of temperature. SP1, which was produced from coal, had the highest activity and SP3, which was produced from peat, had the lowest activity. All samples showed a decrease in activity between 120°C and 200°C.

The NO conversion did not correlate with BET surface area, as shown in Figure 3. SP1 showed the highest activity but had the lowest surface area. Similarly, there was no correlation between pore volume and activity. Rather, NO conversion activity correlated inversely with pH and ash content, as displayed in Figure 4 and Figure 5. SP1, which had the lowest pH, showed the highest activity. This trend implies that a more acidic surface would maximize activity. The inverse correlation obtained for activity and ash contents of the samples might complement the inverse correlation between pH and activity. However, the mineralogy of the carbons have not been examined to define the influence of the ash on pH.

To examine further whether pH affects activity, SP3 was washed with distilled water for 24 hrs to reduce its pH from 9.55 to 8.23. This washing increased its activity at temperatures above 100°C (see Figure 6); no increase occurred at 100°C. This may imply that two conversion mechanisms are operative. One dominant at low temperatures and the other prevalent at higher temperatures.

The oxygen content of the carbons also was observed to correlate with activity. For example, as shown in Figure 7, SP1, which had the highest oxygen content, showed the highest activity. Hence, oxygen plays an important role in NO conversion. Perhaps, the amount of oxygen in the sample indicates the presence of acidic surface oxides, which decrease the sample's pH. SP1, which had the highest oxygen content, also had the lowest pH.

SP1 was also tested for the nonselective formation of NO by reacting NH_3 with O_2 in the absence of reactant NO (Reaction (3)). NO was not formed, thus suggesting that activated carbons promote NO reduction. In absence of reactant or gas phase oxygen, NO conversion was negligible.

A comparison of NO conversion activity for SP1 and $\text{V}_2\text{O}_5/\text{TiO}_2$ is shown in Figure 8. At low temperatures around 100°C, SP1 proved to be a better catalyst than $\text{V}_2\text{O}_5/\text{TiO}_2$. However, at temperatures higher than 150°C, $\text{V}_2\text{O}_5/\text{TiO}_2$ was more active than SP1.

SP3, which had shown the lowest activity, was further treated with sulfuric acid. Initial results have shown that its activity increased considerably. This could probably be due to the oxidation of the surface thus creating acidic functional groups on the surface. This possibility is under further investigation.

CONCLUSIONS

Activated carbons are potentially good catalysts for NO reduction. Low pH, activated carbons have higher activity for NO reduction implying that activated carbons which are acidic in nature are better catalysts for NO reduction. A higher oxygen content in the activated carbons increases their activity, whereas gas phase oxygen

is needed for NO conversion. Activated carbons can have a higher activity than V_2O_5/TiO_2 at low temperatures around $100^\circ C$.

REFERENCES

- 1) F. P. Boer, L. L. Hegedus, T. R. Gouker, K. P. Zak, *Chemtech*, **312**, May (1990).
- 2) H. Gutberlet, *VGB Kraftwerkstech*, **68**, 287 (1988).
- 3) I. S. Nam, J.W. Eldridge and J. R. Kittrell, *I & EC Prod. Res. Dev.*, **25**, 192 (1985)

TABLE I. SAMPLE'S BET SURFACE AREA

SAMPLE	PRECURSOR	BET SURFACE AREA m ² /g
SP1	Coal	466
SP2	Peat	1110
SP3	Coconut Shell	739
SP4	Peat	791

TABLE II. ULTIMATE AND PROXIMATE ANALYSIS

SAMPLE	C%	O%	H%	N%	S%	ASH %
SP1	91.54	4.77	0.47	1.17	0.70	2.05
SP2	91.55	3.87	0.17	0.54	0.46	3.44
SP3	91.54	2.55	0.46	0.51	0.02	4.92

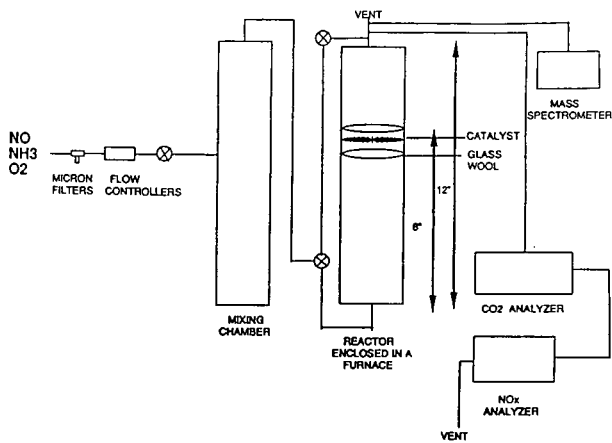


FIGURE 1. PROCESS FLOW DIAGRAM

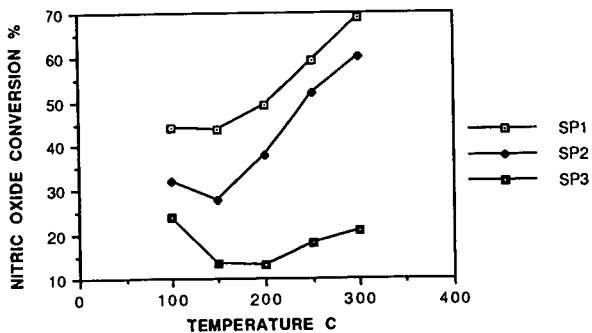


FIGURE 2. NO CONVERSION AT VARIOUS TEMPERATURES

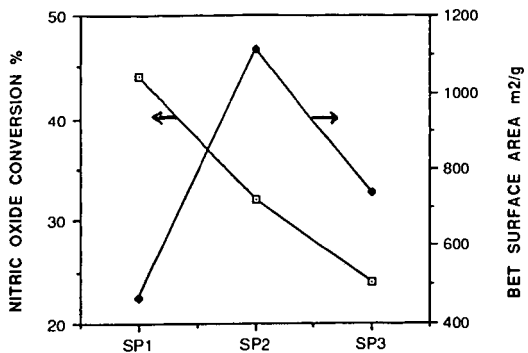


FIGURE 3. ACTIVITY (100C) VS BET SURFACE AREA

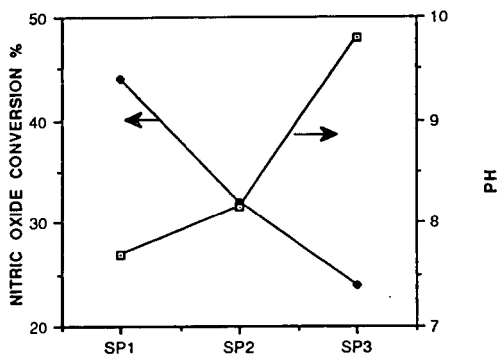


FIGURE 4. ACTIVITY (100 C) VS pH

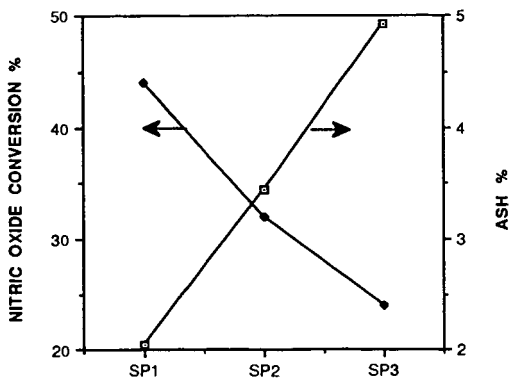


FIGURE 5. ACTIVITY (100C) VS ASH CONTENT

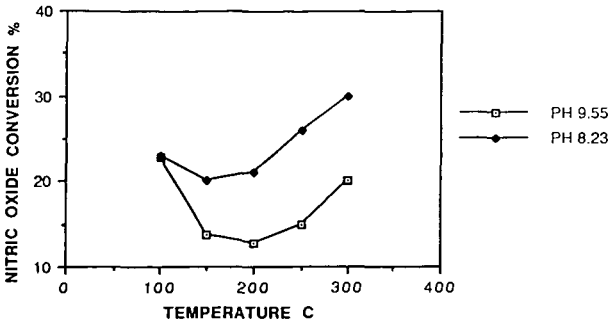


FIGURE 6. EFFECT OF pH ON THE ACTIVITY

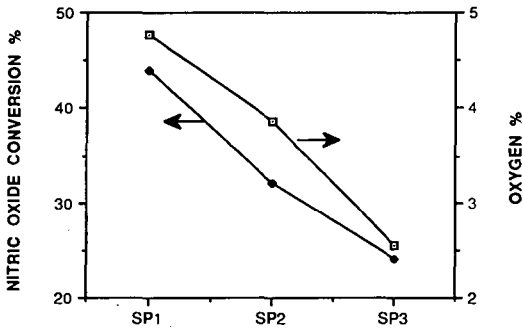


FIGURE 7. ACTIVITY (100 C) VS OXYGEN CONTENT

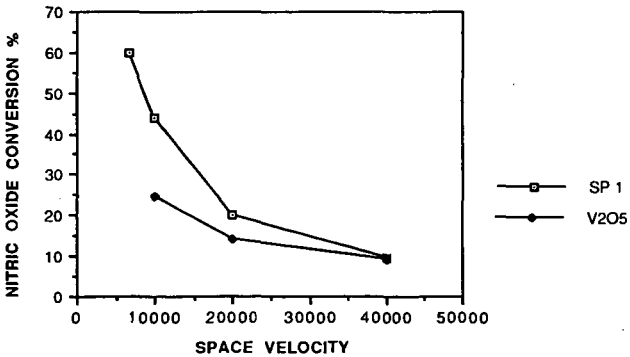


FIGURE 8. COMPARISON OF SP 1 AND V2O5/TiO2 (100C)

OXIDIZED COAL CHAR AS A CATALYST: I. CHARACTERIZATION

C.W. Kruse, M.I.M. Chou, C. Feizoulouf
Illinois State Geological Survey, Champaign, IL 61820

M. Fatemi, P. Beaulieu, and J. Schreiner
Amoco Corporation, Amoco Research Center, P.O. Box 3011 Naperville, IL 60566-7783

Keywords: coal, mild gasification, char, oxidized char, catalyst

ABSTRACT

Oxidizing the surface of carbonaceous materials at 500°C to 700°C in air was shown in the 1960s (1-3) to produce an excellent dehydrohalogenation catalyst. One goal of the current research was to prepare this catalyst from an activated mild gasification coal char having good sorptive properties, test its activity as a catalyst for other elimination reactions, and characterize the catalyst and its precursors. The pore surface area (nitrogen adsorption/desorption, BET) of a mild gasification (MG) coal char was raised from <5 to 475-580 m²/g by steam gasification at 870°C and the catalyst properties were imparted by controlled oxidation with 10% O₂/90% N₂ at 450°C. This material catalyzed not only dehydrochlorination but also dehydration and deamination reactions. Samples of the original coal and final oxidized activated char, as well as two intermediate samples (MG char and steam activated MG char) were fully characterized using Proximate and Ultimate Analysis, Inductively Coupled Plasma Analysis, X-Ray Diffraction, Nitrogen (BET) Surface Area, X-ray Photoelectron Spectroscopy, Diffuse Reflectance IR Spectroscopy, and Scanning Tunneling Microscopy.

INTRODUCTION

Gasification of coal under mild conditions produces char, coal-derived liquids and some gases. Economic viability of this approach to coal utilization is unquestionably dependent on the marketability of the char. To have a reasonable impact on coal utilization via mild gasification, any market considered for the char must be large and should have a projected price greater than coal's fuel value. The activated carbon market has the required price structure, more than \$1000/ton for a high quality product, and a potentially large volume. Activated carbon is used not only for air and water purification but also for cleanup of nonaqueous solutions or suspensions. More than 300 chlorinated organic compounds have been identified in chlorinated potable waters, cooling waters, and sanitary effluents. Systems are needed which will trap and destroy unwanted organic compounds, both those occurring in industrial streams and those that are introduced into drinking water by chlorination.

Carbonaceous materials were converted in the 1960s to effective dehydrochlorination catalysts by heating material, like char, to 500°C to 700°C in air. Some of these catalysts produced linear olefins from chlorinated n-alkanes with little rearrangement of the carbon skeleton. Other dehydrochlorination catalysts studied later were also effective for producing olefins from alcohols and amines by elimination of water and ammonia, respectively (4-8). Oxidized activated char might have the capacity not only to adsorb waste molecules from a variety of streams, but also to catalyze chemical transformations of the unwanted adsorbed compounds into more manageable or even useful chemicals. This work was undertaken to better characterize and define the properties and methods for making the oxidized char catalyst.

MATERIALS AND METHODS

Char preparation and activation - The mild gasification char was prepared in a pilot-scale, fixed-bed reactor at United Coal Co. (UCC), Bristol, Virginia, from a Herrin (Illinois No. 6) coal, IBC-103 in the Illinois Basin Coal Sample Program. This char was from a previous study on the burning behavior of partially devolatilized coal as a function of the amount of volatile matter (VM) in the char (9). Stepwise grinding and sieving of a composite of material having 11% and 15% VM produced 13.5 pounds of 10x30 mesh

particles, a size comparable to commercial granular activated carbon. This UCC char composite was subjected to additional pyrolysis in a 2.5-cm ID, batch, fluidized-bed reactor (FBR) (200-gram increments, N₂ gas, heated to 500°C at 20 C°/min) to drive off most of the VM. The pyrolyzed product is designated MG Char.

The FBR was used both for improving the porosity by steam gasification and for activating the material as a catalyst by oxidation with 10% O₂/90% N₂. In a typical steam gasification run, the MG char was heated in nitrogen to 870°C at a rate of 20 C°/min, and the fluidizing gas was switched to a 50:50 steam-nitrogen mixture. Fourteen steam-treatment runs, designated SA01 through SA14, were made. The SA01 and SA02 were used to determine the conditions for the final oxidation. Composites of SA03 through SA09 and SA10 through SA14 are designated SA3-9 and SA10-14, respectively. The catalyst surface was produced in the same reactor by heating batches in nitrogen to 450°C, and switching to 10% O₂/90% N₂ for 15 minutes. The gas was switched back to N₂ while cooling to room temperature in runs SA01 through SA09 but the flow of 10% O₂/90% N₂ was continued for SA10 through SA14. Composites from SA3-9 and SA10-14 are designated OSA3-9 and OSA10-14, respectively.

Testing as a catalyst - A 2.5 ml quantity of redistilled Wiley 3-chloro-3-methylpentane was heated 5 minutes at reflux temperature (120°C) in a 25 ml tube fitted with a micro reflux condenser before adding 0.25 g of the activated char to be tested. The temperature was maintained for another 10 minutes before the tube was removed from the heater. The liquid was separated from the char by filtration through a 10 ml gas-tight syringe connected to a filtration apparatus. The olefins in the filtrate were then analyzed using a Perkin-Elmer 8500 GC for a preliminary determination. A Hewlett Packard 5988A GC/MS (HP GC/MS) with a fused silica capillary column and a split (ratio 1:100) injection system was used for a molecular level identification. The preceding procedure was also used to dehydrate 2,3-dimethyl-2-pentanol.

Preliminary test data indicated that there was no catalytic activity exhibited by OSA3-9 for the deamination of t-butylamine or cyclooctylamine at a temperature lower than 220°C and a residence time of <10 minutes. Evidence that deamination requires a higher temperature than dehydrochlorination with other catalysts was found in the literature (5). Tests at higher temperatures were carried out in a Perkin-Elmer 8500 Gas Chromatograph equipped with a hot wire detector and liquid nitrogen trap. Helium was used as GC carrier gas. The GC injector glass liner was packed with 0.1 g of oxidized char and used as a catalytic column. The GC injector temperature was set at 295°C, the temperature found by Lycourghiotis to work. A 6' x 1/8" packed column was used as an analytical column for product separation. Deamination products eluted from the GC analytical column were collected at the exit of the detector at liquid nitrogen temperature. The expected olefins were identified on the HP GC/MS.

Surface Areas - Total surface area, micropore area and volume, and cumulative pore volume were determined from nitrogen adsorption data obtained at 77 K using a Micromeritics (ASAP 2400) apparatus. Adsorption isotherms were analyzed using the BET equation to obtain total surface area. Micropore area and volume were obtained from t-plots using the Halsey equation (10). Adsorption/desorption isotherms were analyzed using the BJH method (11) to calculate cumulative pore volumes.

RESULTS AND DISCUSSION

Catalyst activity. The oxidized char (OSA3-9 and OSA10-14) catalyzed the production of the expected olefins (identified by GC/MS) from 3-methyl-3-chloropentane at its boiling point, 2,3-dimethyl-2-pentanol at about the same temperature (120°C), and cyclooctylamine at 295°C. The methods used showed some differences in catalytic activity among char samples made by methods not described here, but better analytical procedures will be required to quantify the differences in catalytic activity.

Proximate and Ultimate analyses - Proximate analyses (Perkin Elmer TGA 7 thermogravimetric analyzer), and Ultimate analyses (Leco CHN-600 and Leco SC-132) appear in Table 1. There are significant differences among the samples. While the percent VM decreased from about 51% to 2.5% from coal to OSA char on a dry-ash-free basis (not shown in the table), the ash and fixed carbon

contents increased. The carbon content increased from a low of 80%, on a dry-ash-free basis, for the original coal to a high of 95% for the OSA char sample and, at the same time, the hydrogen decreased tenfold. The atomic H/C ratio was decreased from 0.87 to 0.28 by mild gasification and from 0.28 to the minimum of 0.07 when the MG char was steam treated (SA3-9 or SA10-14).

As expected, as the coal is pyrolyzed and gasified, it loses oxygen functional groups. Therefore, when IBC-103 was pyrolyzed to 500°C, it lost over 40% of its oxygen (from 9.27 to 5.24%, direct analysis) and then when this char (MG char) was steam gasified at 870°C, it lost another 60% to 75% of its oxygen content (down to 1.94% and 1.23% for SA3-9 and SA10-14). When this steam treated char was oxidized in air, to make it a catalyst, its oxygen content increased significantly (up to 3.32% and 3.33%, respectively). The cooling in the presence of 10% O₂/90% N₂ for OSA10-14 did not appear to increase the oxygen over that of OSA3-9.

Inductively Coupled Plasma (ICP) analysis - ICP spectroscopy determines the inorganic elements present in the bulk of a sample. Only the elements commonly present in the coal were determined. The data are shown in Table 2. As expected, the concentration of all metallic elements was increased as the original coal (IBC-103) was pyrolyzed to produce the MG char and even more as the char was steam treated to obtain SA3-9 or SA10-14.

X-Ray Diffraction (XRD) - All samples were found to be mostly amorphous and showed a graphite-like structure. Quartz (SiO₂) was the major crystalline phase in all samples. XRD data, like the data from ICP analysis, indicate that significant amounts of oxides of Si, Fe, Al and Ti are present in the oxidized chars (OSA3-9 and OSA10-14). In addition to phase and crystallinity information, XRD analyses provided some important correlations between the small-angle X-ray scattering (SAXS) intensity and microstructure of the samples. The SAXS intensity for the SA char was approximately 480 cps, and 550 cps for the OSA char samples OSA3-9 and OSA10-14, respectively. The conclusion one can reach solely on the basis of these two data sets is that the microporous structure in the OSA char is more fully developed than that for SA char. This is in contrast to the data on micropore volume, cumulative pore volume and average pore size radius data obtained from N₂ gas adsorption/desorption (BET) surface areas which indicated no significant differences between SA chars and the OSA chars.

Nitrogen (BET) surface area - Char activation has two purposes. One is to develop adsorption capacity, as estimated by pore surface area, and the other is to give the char the type of oxidized surface that catalyzes elimination reactions. Thermogravimetric analysis (TGA) was used for preliminary assessment of two methods for increasing surface area: 1) oxidation with 10% O₂/90% N₂ at 450°C and 2) steam gasification at 870°C. Because steam gasification generated higher nitrogen BET surface areas, steam was used. Adsorption/desorption data with N₂ at 77°K and the Brunauer, Emmett, and Teller (BET) equation were used to calculate pore surface areas and the micropore surface areas (Table 3). Due to the small surface area, the micropore area, micropore volume, cumulative pore volume and average pore radius were not measured for the original coal (IBC-103) and MG Char.

Steam activation raised the N₂ surface area from <5 m²/g in the mild gasification char (MG char) to 460 m²/g at 41% weight loss and to a high of 625 m²/g at 54% weight loss as measured at the ISGS. The average weight losses and pore surface areas generated were 51% and 542 m²/g for the 7 batches mixed to produce SA3-9 and 54% and 575 m²/g for the composite of 5 batches designated SA10-14. Amoco's values for these composites, 473 m²/g and 585 m²/g, respectively, confirmed order but showed a greater difference. The oxidized steam-activated (OSA) char having catalyst properties was made by oxidation at 450°C with 10% O₂/90% N₂ for 15 minutes. The pore surface areas of the catalyst composites, OSA3-9 and OSA10-14, were about equal, 557 m²/g and 552 m²/g, respectively, despite the difference in the pore surface areas and micropore surface areas of their precursors (473 m²/g and 187 m²/g for SA3-9 and 584 m²/g and 230 m²/g for SA10-14). The micropore surface area of the catalyst which during preparation was cooled in 10% O₂/90% N₂ to leave more oxygen on the surface (OSA10-14) had a lower micropore surface area than the one (OSA3-9) cooled in nitrogen (207 m²/g and 242, respectively).

Clearly the steam treatment and air oxidation steps opened up some very fine micropore structures in the MG char. This fine microstructure could account for the greatly increased surface area of the steam treated and final activated chars.

X-ray Photoelectron Spectroscopy (XPS) - Elemental surface composition (relative weight percent) and a summary of their binding energies (BE), as determined by XPS, are shown in Tables 4 and 5, respectively. Table 4 shows the concentration of several elements, including oxygen, on the surface of the samples which is typical for these types of materials. Binding energy data, Table 5, indicate the presence of hydrocarbon species such as C-C and C-H (284.6 ± 0.2 eV), oxidized carbon species such as C-O and C=O (286.2 ± 0.2 eV), and carbonate/carboxylic species O-C=O (289 ± 0.6 eV). The binding energy of 163.6 eV (± 0.6 eV) is typical for elemental sulfur and/or organic sulfur species such as mercaptans (R-SH), disulfides (R-SS-R) and thiophenes, and the binding energy of 168.0 eV (± 0.3 eV) is typical for species such as sulfonates (R-SO₃), alkylsulfonates (RO-SO-OR) and dialkylsulfates (RO-SO₂-OR). The nitrogen binding energies suggest the presence of amines (RNH₂) including alkylamines, aromatic (phenyl) amines and pyridine derivatives at 398.6 eV (± 0.6 eV), pyrolic nitrogen species at 400.4 eV (± 0.3 eV), and ammonium derivatives (RNH₃⁺) at 402.0 eV (± 0.4 eV) with one unidentifiable species at about 404.0 eV. However, numerous nitrogen-containing organic compounds (i.e. nitrobenzene and dinitrobenzene) fall into the binding energy range of 404-405 eV (± 5 eV). The presence of binding energies at approximately 711.5 eV (± 0.5 eV) for Fe, 103.0 eV (± 0.1 eV) for Si, and 75.0 eV (± 0.6 eV) for Al is most likely due to the respective oxides.

Based on the data in Table 5, the chemical species concentrated on the surfaces of the catalytic variety of char differ from those not oxidized. For example, while the concentration of hydrocarbon species such as C-C and C-H (284.6 ± 0.2 eV) on the surfaces of steam activated chars (SA3-9 and SA10-14) were 75% and 65%, respectively, the concentration of the same species on the surfaces of the air oxidized chars (OSA3-9 and OSA10-14) were 66% and 60%. On the other hand, the concentration of oxidized carbon species such as C-O and C=O (286.2 ± 0.2 eV) on the surfaces of steam treated chars were 16% and 23%, respectively, and on the surfaces of air oxidized chars were 23% and 30%. The concentration of carbonate/carboxylic species O-C=O (289 ± 0.6 eV) remained constant at about 10% for both steam treated and air oxidized chars.

The surface binding energies, Table 5, obtained from the XPS studies also suggest that the surface concentration of oxidized carbon species (C-O and C=O) is lower for OSA3-9 (23%) than for OSA10-14 char (30%), the sample that was cooled in 10% O₂/90% N₂ atmosphere rather than N₂. While four types of nitrogen species were identified on the surface of OSA3-9, only two were identified on the surface of OSA10-14, and this too may be the result of the cooling regime.

Diffuse Reflectance IR Spectroscopy - Spectra were obtained on a Mattson Cygnus 100 FTIR using a Harrick Diffuse Reflectance accessory. All spectra were acquired by co-adding 1024 scans at a resolution of 8 cm⁻¹. Powdered KBr was used as a background. Bands elucidated by second derivative treatment are broadly assigned as: 1867 cm⁻¹ and 1809 cm⁻¹, C=O, anhydride, probably cyclic and unconjugated; 1740 cm⁻¹, C=O, ester; 1707 cm⁻¹, C=O, possibly ketone, aldehyde, or COOH; 1655 cm⁻¹, C=O, highly conjugated, Ar-(C=O)-Ar; and 1613 cm⁻¹, highly conjugated, hydrogen bonded C=O. Mild gasification of the IBC-103 resulted in a higher ratio of aromatic C-H functional groups to aliphatic C-H functional groups which is consistent with a graphitization process. The pyrolysis process resulted in modest band shifts, which may be due to differences in electronegativity or level of conjugation in the substituents bonded to the various carbonyl groups. The spectrum obtained from the air oxidized char (OSA3-9) had features that were very faint and broad. A band centered near 1590 cm⁻¹ suggests the same aromatic character along with carboxylic acid salts. The former assignment is consistent with the broad feature centered near 3150 cm⁻¹ encompassing the aromatic C-H stretch region. A band near 1590 cm⁻¹ along with a very broad feature centered near 1170 cm⁻¹ may also be indicative of coordinated inorganic carbonate, which is consistent with the XPS results.

Scanning Tunneling Microscopy (STM) - STM and the newer technique for imaging and resolving surface detail at atomic and near atomic level, atomic force microscopy (AFM), are becoming increasingly

important in studies of molecules deposited on the surfaces of catalysts. The original coal sample (IBC-103) could not be imaged by STM, most likely because of the low intrinsic conductivity of the material. Chars had sufficient conductivity. Images were obtained with 1-2 nA tunneling current and 750 mV-1750 mV positive bias on the tip and sample at ground which is tunneling from occupied π states of the carbon to the probe tip. Images from the oxidized char (OSA3-9) suggest aggregated particles as large as several thousands of Angstroms which clearly are aggregates of still smaller particles. Particles were usually made of an aggregated state of several 200-400 Å particles. Increasing magnification indicated a further heterogeneity with smaller aggregates of size in the order of tens of Angstroms. At even higher magnification (less than 10 nm) an apparent lattice imaging became evident. The partially ordered region seen in this image was in the order 50x70 Å with a very poor registry. A well-ordered domain of size 20x40 Å was also seen at this magnification.

CONCLUSIONS

The oxidized, steam-activated (OSA) char catalyzed dehydration of an aliphatic tertiary alcohol and deamination of a primary aliphatic amine, in addition to dehydrochlorination of an alkyl halide. PS data indicated a significant amount of oxygen was in the surface of the OSA char. The ICP and XRD data indicated the presence of significant amounts of Si, Fe, Al and Ti oxides. In addition to phase and crystallinity information, XRD data provided an important correlation between the small angle X-ray scattering (SAXS) intensity and the microstructure of the samples. The strong presence of SAXS at low angles in OSA char is evidence that OSA char is a microporous material, and a comparison of intensity measurements suggests that the microporous structure becomes more fully developed during the oxidation of steam-activated (SA) char. XPS data suggest the chemical species concentrated on the surfaces of the chars are indeed different and these differences are expected to be related to variations in catalyst reactivity among samples. The surface binding energies from XPS work, and IR data supported the speculation that the cooling under N_2 atmosphere after the oxidation step causes the removal of some of the CO and C-O complexes.

Both IR and ^{13}C NMR data confirm that the ratio of aromatic C-H groups to aliphatic C-H groups increased significantly when volatile matter was removed during mild gasification. An oxidation index is defined as the ratio of the integrated area of the carbonyl region (1635-2000 cm^{-1}) to the integrated area of the region associated with the aliphatic and aromatic C-H stretches (2675-3135 cm^{-1}). The calculated oxidation index was about 0.48 and 1.09 for the coal and MG char, respectively. This index may prove useful in characterizing mild gasification chars and correlating final pore development with thermal histories.

In general, STM imaging of the samples revealed a highly aggregated hierarchical structure. A very fine sheet-like microstructure could be seen in steam-activated and oxidized steam-activated chars. STM data clearly support the BET data that the steam-activation opened up a very fine micropore structure on the originally small, several hundred Angstrom, features of MG char. Certainly, this fine microstructure could account for the greatly increased active surface area of the steam-activated char. The OSA chars have been shown to have good sorption properties and results will be reported in a subsequent publication.

ACKNOWLEDGEMENT

This work has received direct financial support from the Illinois Department of Energy and Natural Resources, through its Coal Development Board and the Center for Research on Sulfur in Coal CRSC, and from the United States Department of Energy through (CRSC). We also acknowledge in-kind contributions funded by the Alternative Feedstock Development (AFD) program of Amoco Corporation. Without this support and the encouragement of R. E. Lumkin (AFD), this work would not have been possible. The authors wish to acknowledge contributions by the following Amoco Research Center staff members in the areas specified: R. Roginski, Diffuse Reflectance IR Spectroscopy; B. Meyers, pore surface areas; G. Zajac, STM; and J. Faber, XRD. Assistance at the IGS included Sheng-Fu J. Chou, identification of compounds by GC/MS analysis; Robert Frost, surface area measurements; and M. Rostam-Abadi, directing the char activation portion of this study.

REFERENCES

1. Kruse, C.W.; Ray, G.C., U.S. Patent 3,240,834, March 15, 1966.
2. Mahan, J.E., Reusser, R.E.; Kruse, C.W., U.S. Patent 3,352,935, Nov. 14, 1967.
3. Kruse, C.W., U.S. Patent 3,437,695, April 8, 1969.
4. Lycourghiotis, A. *React. Kinet. Catal. Lett.* **1976**, *5*(4), 453-7.
5. Lycourghiotis, A.; Vattis, D.; Katsonos, N.A.; *Z. Phys. Chem. (Wiesbaden)*, **1981**, *126*(2), 259-67.
6. Suarez, A.R.; Mazzieri, M.R. *J. Org. Chem.* **1987**, *52*(6), 1145-7.
7. Mochida, I.; Watanabe, H.; Uchino, A.; Fujitsu, H.; Takeshita, K.; Furuno, M.; Sakura, T.; Nakajima, H. *J. Mol. Catal.* **1981**, *12*(3), 359-64.
8. Misono, M. *J. Catal.* **1973**, *30*(2), 226-34.
9. Rostam-Abadi, M.; DeBarr, J.A.; Chen, W.T. *Prepr. Pap.-Am. Chem. Soc., Div. Fuel Chem.* **1989**, *35*(4), 1264-71.
10. Halsey, G.D. *J. Chem. Phys.* **1948**, *16*, 931.
11. Barrett, E.P.; Joyner, L.G.; Halenda, P.P. *J. Am. Chem. Soc.* **1951**, *75*, 373-380.

Table 1. Proximate and Ultimate Analyses

	IBC-103 Coal	MG Char	SA3-9 Char	OSA3-9 Char	SA10-14 Char	OSA10-14 Char
<u>Proximate Analysis (wt%, as-received)</u>						
Moisture	3.35	1.01	2.28	0.93	2.01	1.62
Ash	5.92	10.42	19.81	21.81	21.43	24.58
V. Matter	49.2	16.02	12.36	2.44	11.38	2.72
Fixed C	41.53	72.55	65.55	74.82	63.18	71.08
<u>Proximate Analysis (wt%, dry)</u>						
Ash	6.12	10.53	20.27	22.02	21.87	24.98
V. Matter	50.91	16.18	12.65	2.46	11.61	2.76
Fixed C	42.97	73.29	67.08	75.52	66.52	72.26
<u>Ultimate Analysis (wt%, as-received)</u>						
%C	71.82	80.06	69.61	72.14	69.82	70.48
%H	5.63	1.98	0.65	0.53	0.67	0.58
%N	1.69	2.22	1.58	1.47	1.43	1.37
%S	2.2	1.84	1.23	1.21	1.19	1.24
%O ^a	11.39	5.54	3.54	3.39	2.73	3.9
<u>Ultimate Analysis (wt%, dry)</u>						
%C	79.16	90.39	89.35	93.37	91.2	95.5
%H	5.79	2.11	0.51	0.55	0.58	0.54
%N	1.86	2.51	2.03	1.9	1.87	1.86
%S	2.42	2.08	1.58	1.57	1.55	1.68
%O ^b	10.77	2.91	6.53	2.61	4.8	0.42
%O ^a	9.27	5.24	1.94	3.32	1.23	3.33
H/C	0.87	0.28	0.07	0.07	0.07	0.07

^aOxygen values were obtained by direct analysis.

^bOxygen values were obtained by difference (100 - (%C + %H + %N + %S) = %O).

Table 2. Metal Composition (Wt.%) Data from ICP Analyses

Sample I.D.	IBC-103 Coal	MG Char	SA3-9 Char	OSA3-9 Char	SA10-14 Char	OSA10-14 Char
Fe	1.04	1.59	4.1	2.85	3.14	3.27
Si	0.67	1.31	2.13	4.30	4.80	4.3
Al	0.74	1.38	2.72	2.45	2.95	2.92
Na	0.30	0.04	0.11	0.10	0.08	0.08
K	0.14	0.25	0.5	0.46	0.46	0.45
Ca	0.07	0.14	0.26	0.27	0.27	0.21
Mg	0.04	0.06	0.13	0.13	0.16	0.14
Ti	0.04	0.06	0.12	0.16	0.16	0.16

Table 3. Nitrogen Surface Area Data (Adsorption/Desorption)

	IBC-103 Coal	MG Char	SA3-9 Char	OSA3-9 Char	SA10-14 Char	OSA10-14 Char
N ₂ - BET Surface Area (m ² /g)	1.3	1.1	473	557	584	552
Micropore Area (m ² /g)	N.D. ^a	N.D. ^a	187	242	230	207
Micropore Vol (cc/g)	N.D.	N.D.	0.08	0.11	0.11	0.10
Cumulative Pore Vol (cc/g)	Ad.	N.D.	N.D.	0.17	0.19	0.22
	De.	N.D.	N.D.	0.18	0.20	0.23
Average Pore Radius (Å)	Ad.	N.D.	N.D.	20	20	20
	De.	N.D.	N.D.	18	18	19

^a Not Determined. Surface areas are too small to measure pore volumes by this technique.

Table 4. Surface Composition (Wt.%, Relative) Data from XPS Analyses

	IBC-103 Coal	MG Char	SA3-9 Char	OSA3-9 Char	SA10-14 Char	OSA10-14 Char
C	71.3	74.1	78.7	78.8	80.	80.
O	17.6	15.7	12.9	13.3	10.4	10.2
N	1.6	1.6	0.9	0.9	0.5	0.8
S	1.4	1.2	0.7	0.7	3.7	3.9
Al	2.8	2.4	2.1	2.3	1.6	1.6
Si	4.6	3.6	3.4	3.0	2.6	2.3
Fe	0.4	0.8	0.9	0.4	0.8	0.8
Mg	0.2	0.2	0.2	0.2	Tr.	Tr.
Ca	---	0.3	0.3	0.3	0.3	0.3

Table 5. Binding Energies (eV) Data from XPS Analyses

Sample Identification	C 1s	%	O 1s	Si 2p	Al 2p	S 2p	N 1s	%	Fe 2p	Ca 2p
IBC-103 (coal)	284.5	84	533.0	103.5	75.0	163.8	398.5	38	712.0	-----
	286.2	14				168.9	400.2	57		
	289.2	2					402.1	5		
MG Char (United Coal Company)	284.5	81	533.2	103.6	75.7	163.7	398.6	28	712.1	349.0
	286.4	16					400.4	62		
	288.8	3					402.4	10		
SA3-9	284.6	75	533.2	104.0	75.7	163.8	398.6	19	711.7	347.7
	286.3	16					400.7	68		
	288.7	9					402.3	13		
OSA3-9	284.6	66	533.2	104.1	75.7	163.9	398.4	13	711.2	347.7
	286.1	23					400.7	56		
	289.7	10					402.3	23		
SA10-14	284.6	65	533.2	103.6	75.4	163.9	398.6	22	711.6	348.2
	286.3	23					401.2	78		
	289.7	12								
OSA10-14	284.6	60	533.2	103.9	75.7	163.9	398.7	22	711.9	347.9
	286.0	30					402.3	78		
	290.0	10								

COAL AS A FEEDSTOCK FOR FULLERENE PRODUCTION AND PURIFICATION

Louis S.K. Pang, Anthony M. Vassallo and Michael A. Wilson
CSIRO Division of Coal and Energy Technology,
P.O. Box 136, North Ryde, NSW 2113, Australia

Keywords: fullerenes, coal, preparation, chromatography.

INTRODUCTION

Since the first availability of fullerenes in bulk,^{1,2} research on these materials has flourished rapidly. There is implication that these molecules are potentially useful³ as lubricants,⁴ superconductors, rechargeable batteries, diamond nucleators, catalysts and chemical feedstocks. Fullerenes are commonly produced by the electrical arcing of graphite in helium,¹ but can also form from benzene combustion in an Ar/O₂ mixture.⁵ Purification is usually performed by chromatography on silica.⁶ We have recently demonstrated that fullerenes can be produced by the electrical arcing of coke derived from coking coals.⁷ We have now extended the study using different Australian coals including brown coal and semi-anthracite and prepared coke from these coals by a number of different methods. Coal was also demonstrated to be a useful chromatographic material to purify C₆₀.

EXPERIMENTAL

Preparation of conductive coke rods

The primary requirement for production of fullerene from coal in this work is the preparation of conductive coke rods. Three methods of coke preparation were used.

1) laboratory coke. A finely ground coking coal was heated in an aluminium mould in an argon flow at 395°C for 24 h to form a semi-coke rod. This rod was carbonised at 1200°C in argon for 5h.

2) Coal-pitch composite. This method is suitable for both coking and non-coking coals. Finely ground coal and pitch (20 wt. %) mixtures were placed in a Swage-lok type stainless steel tube and sealed. The system was heated to 500°C for 24 h. A semi-coke rod was formed, which was carbonised at 1200°C in argon for 5 h. Additional carbonisation conditions (1200°C for 10 h, 1300°C for 1 h) was used for brown coal and neat pitch to induce electrical conductivity.

3) Oven coke. Finely ground coking coals were heated in a wall oven (0.42 m³) under sealed condition at 1010°C for 16-19 h. Samples of coke were cut into rods for electrical arcing.

Fullerene production

Fullerene was produced by electrically arcing the coke rods in a 250 torr helium atmosphere at 23-30 V and 80-130 A a.c. or d.c. in a stainless steel chamber. The soot produced by this process was Soxhlet extracted with toluene to give crude fullerenes.

Purification of C₆₀ on coal

For purification of C₆₀ on coal, Yarrabee semi-anthracite (H/C 0.74, O/C 0.013) was ground and size separated. The 63-125 μm size fraction was pre-washed in a Soxhlet extractor for 3 days with toluene to remove any soluble materials. A glass column was packed with this pre-washed coal (1.2 cm by 58 cm) using hexane, and crude fullerene (15 mg) was dissolved in toluene (3 ml) and loaded on the head of the column. After elution with hexane (800 ml) at a flow-rate of 2 ml/min, 8.7 mg of solid pure C₆₀ was obtained from the eluate.

RESULTS AND DISCUSSION

Table 1 lists the carbon contents and ash yields for the different cokes, and fullerene yields. Infrared spectroscopy showed absorption peaks characteristic of C₆₀ and C₇₀ fullerenes in similar ratios (ca. 10:1 for C₆₀ : C₇₀) reported for graphite as a source material¹. The ratios have been confirmed by solid-state ¹³C nuclear magnetic resonance spectroscopy.

All cokes tested so far produced fullerenes. Thus it appears that other conductive carbonaceous materials may also be able to produce fullerenes. An optimum fullerene yield of 8.6% was obtained from superclean Goonyella coke. This compares favourably with the yield of 9.3% obtained from graphite under identical conditions. Pitch (neat) yielded only 2% fullerenes, therefore, in the composite with coal in which pitch was present at a level 20%, the fullerenes were predominantly produced from the coal, since much higher yields were obtained from these

composites. Also, the use of d.c. current rather than a.c. appears to markedly increase the yield of fullerenes from both graphite and coal.

Although coking occurs readily at 1200°C, graphitisation does not usually occur below 2500°C on these time scales⁸. The results presented here show that graphitisation is not a requirement for fullerene production by the electrical arc method.

The presence of mineral matter (ash yield) in the coal does not inhibit fullerene formation from coke, however, its presence does result in a reduced yield of fullerene. Data in Table 1 indicate that poorer fullerene yield (around 3% or less) was obtained from the oven cokes and Coalcliff composite which have over 10% mineral matter. On the other hand, Loy Yang composite, Newvale composite and superclean Goonyella coke each has under 4% mineral matter and produces 6% or more fullerene yield. The electrical resistivities of the cokes do not appear to be directly related to mineral matter contents and no clear trend can be drawn between the electrical resistivities and fullerene yield.

It appears that the method of coke preparation may also affect fullerene yield. The data are scattered, but Table 1 shows that laboratory cokes (2.3-8.6%) produce comparable fullerene yield to carbonised coal-pitch composites (2-7.7%) while oven cokes (2-3.3%) give the poorest yield.

The presence of a small amount (below 4%, Table 1) of hydrogen and heteroatoms (O, S and N) in the coke does not inhibit fullerene formation. In addition, there is no simple relationship between the coal rank and fullerene yield. Semi-anthracite (Yarrabee coal) derived composite produced 5.0% fullerene, while Loy Yang brown coal composite produced 7.7% yield, which on a coal basis is at least equivalent to, if not higher than graphite at 5.8%.

A number of reports have appeared on fullerene generation by the laser ablation of coal, graphite and mesophase in an ion cyclotron resonance (ICR) spectrometer⁸⁻¹¹. These results showed that the laser power required to generate fullerenes increased from mesophase < brown coal < high rank coal < graphite. Higher laser power may be needed to break down some of the regular hexagonal structure in graphite, which then rearranges to form the five and six membered ring structure in C₆₀. On the other hand, the breakdown of the more disordered structure present in brown coal and mesophase may be accomplished with relative ease. Moreover, five and six membered rings are already present in these materials, which may assist in the formation of fullerenes. For comparison, a lower laser power requirement in the ICR experiment may relate to a higher fullerene yield in the electrical arc experiment. However, in our electrical arc experiment, a definite correlation between fullerene yield and coal rank or graphite could not be made.

CONCLUSIONS

The results presented here clearly show that a suite of coals of different ranks are capable of producing fullerenes. Moreover, for Yarrabee semi-anthracite a self-consistent process for producing fullerenes is possible. The coal can be used to produce fullerenes and also to separate pure C₆₀. The presence of mineral matter and heteroatoms does not inhibit fullerene formation but does reduce fullerene yield. The regular hexagonal carbon structure present in graphite is not a requirement for fullerene formation. In fact, a disordered carbon structure may be favourable. With the present cost of coal at \$100 per tonne or less, its use as an industrial material for fullerene may greatly improve the economics of large scale production.

REFERENECES

1. Kratschmer, W.; Lamb, L.D.; Fostiropoulos, K.; Huffman, D.R. *Nature* 1990, 347, 354-358.
2. Taylor, R.; Hare, J.P.; Abdul-Sada, A.K.; Kroto, H.W. *J.C.S. Chem. Commun.* 1990, 1423-1425.
3. Stoddart, J.F. *Angew Chem. Int. Ed. Engl.* 1991, 30, 70-71.
4. Meilunas, R.; Chang, R.P.H.; Liu, S.; Kappes, M.M. *Nature* 1991, 354, 271.
5. Howard, J.B.; McKinnon, J.T.; Makarovsky, Y.; Lafleur, A.; Johnson, M.E.; *Nature* 1991, 352, 139-141.
6. Ajie, H.; Alvarez, M.M.; Anz, S.J.; Beck, R.D.; Diederich, F.; Fostiropoulos, K.; Huffman, D.R.; Kratschmer, W.; Rubin, Y.; Schriver, K.E.; Sensharma, D.; Whetten, R.L. *J. Phys. Chem.* 1990, 94, 8630.
7. Pang, L.S.K.; Vassallo, A.M.; Wilson, M.A. *Nature* 1991, 352, 480.
8. Brooks, J.D.; Taylor, G.H. in "Chemistry and Physics of Carbon", Ed. Walker, P.H. Jr. p282, Marcel Dekker, N.Y., 1968.
9. Greenwood, P.F.; Strachan, M.G.; Willett, G.D.; Wilson, M.A. *Org. Mass Spec.* 1990, 25, 353-362.
10. Greenwood, P.F.; Strachan, M.G.; El-Nakat, H.J.; Willett, G.D.; Wilson, M.A.; Attalla, M.I. *Fuel* 1990, 69, 257-260.
11. Dance, I.G.; Fisher, K.J.; Willett, G.D.; Wilson, M.A. *J. Phys. Chem.* 1991, 95, 8425-8428.

Table 1. Electrical conductivities, fullerene yields, carbon contents and ash yields for coke^a and graphite.

source	electrical resistivity ohm/cm	fullerene yield (wt. %)	%C	%ash yield	%O+H+S+N ^b
I. Laboratory coke					
Goonyella ^{c,d}	.53	5.6	95.8	2.1	2.1
Goonyella ^{c,e}	.38	8.6	94.8	3.8	1.4
Goonyella ^{c,f}	.33	2.3	91.0	7.6	1.4
graphite ^c	.009	9.3			
graphite	.009	16.2			
II. Carbonised coal and pitch composite					
Coalcliff ^c	.07	2.0	85.2	14.5	0.3
Coalcliff	.07	3.2			
Newvale	.12	6.0	95.1	1.6	3.3
graphite ^g	.009	5.8			
Loy Yang	.38	7.7	96.5	1.8	1.7
Yarrabee	.26	5.0	95.7	4.2	0.1
pitch	.26	2.0	96.9	2.0	1.1
III. Oven coke					
Norwich Park	.10	3.3	84.2	12.1	3.7
Riverside	.09	2.5	85.4	12.0	2.6
Blackwater	.09	2.2	86.3	10.7	3.0
Goonyella	.46	2.3	85.3	11.0	3.7
Gregory	.12	2.8	85.4	11.5	3.1

a wt. % dry basis

b by difference

c electrical arcing was induced by a.c.; d.c. was used for the other experiments.

d from ultraclean coal

e from superclean coal

f from as received coal

g The fullerene generator was modified for these experiments, and the yield of fullerenes reduced significantly but consistently. Yield data for cokes below this column should be compared to this value.

EVIDENCE FOR ENTRAPMENT OF C₆₀ AND C₇₀

F. Hopwood, K.J. Fisher, I.G. Dance, G.D. Willett
Chemistry Department, University of New South Wales
PO Box 1, Kensington NSW 2033, Australia

M.A. Wilson*, L.S.K. Pang and J.V. Hanna
CSIRO Division of Coal and Energy Technology
PO Box 136, Ryde NSW 2113, Australia

Keywords: buckminsterfullerene, mass spectrometry, fullertubes

ABSTRACT

The carbon arc soot from coal produced in a fullerene generator has been exhaustively extracted with toluene and pyridine. Complete extraction of C₆₀ and C₇₀ was not fully achieved with toluene since the residue was shown to contain pockets of C₆₀ and C₇₀ some of which could subsequently be extracted by pyridine as demonstrated by negative ion laser desorption mass spectrometry, infra-red spectrometry and solid state nuclear magnetic resonance spectrometry. Threshold laser power experiments also indicated the presence of fullerenes to m/z 1800. These results clearly indicated the entrapment of C₆₀ by other fullerenes or fullertubes of higher molecular weight. When laser ablation techniques were used odd numbered cluster ions were observed indicating the presence of ruptured or chain substituted fullerenes.

INTRODUCTION

The isolation of stable carbon clusters including C₆₀ and C₇₀ fullerenes from carbon arc soot produced via the vaporisation of graphite in an inert gas atmosphere has recently been reported¹⁻⁶. For example, Diederich et al.⁴ and Ettl et al.⁵ have extracted arc soot with toluene and separated and identified C₇₆, C₇₈, C₈₄ and C₉₄ fullerenes. It is expected that a range of other fullerenes may be present in the soot and little is known about how C₆₀ and C₇₀ are formed and whether any are entrapped in the soot with other fullerenes. In this work we report the use of pyridine to extract the soot residue after toluene extraction. Both pyridine soluble and pyridine insoluble fractions have been characterised by FTICR mass spectrometry and FTIR spectrometry and in some cases also by solid state ¹³C NMR spectrometry.

EXPERIMENTAL

Preparation of fractions

The preparation of the fullerene soot from graphite and coal was carried out in a modified fullerene generator as reported elsewhere⁷.

The soot was generated from coal or graphitic rods using 25V and 100A d.c. We observed that holes drilled in the graphite rods increased the yield of soot for a given time and current.

Use of an inner water cooled chamber for the arcing process was designed to limit the penetration of the soot into the main chamber and thence its pumping system. The removal of the inner chamber also facilitated the easy recovery of the soot after each run for quantitative analysis and to limit the 'possible' health hazards that may arise handling this light fluffy material.

The resulting soot (3 g) was divided equally into two portions. One portion was Soxhlet extracted with toluene for 6 h. This yielded 85 mg of fullerene extract after solvent removal. After drying, the soot residue was Soxhlet extracted exhaustively with pyridine for 12 h (under nitrogen to prevent solvent decomposition). A clear brownish yellow solution was obtained. This yielded 65 mg of solid extract after solvent removal. This was dried in a vacuum oven at 80°C for 2 h to remove residual pyridine.

The second portion was Soxhlet extracted with pyridine for 11 h under nitrogen to yield a brownish yellow solution which gave 150 mg solid extract after solvent removal. After drying, the soot residue was Soxhlet extracted with toluene. A faint reddish solution was obtained which yielded a negligible amount (<5 mg) of solid fullerene residue.

Analysis

Details of the laser desorption FTICR mass spectrometry technique have been described previously⁸. Mass spectrometric studies were carried out using the fundamental frequency of a Nd YAG laser (1064 nm) and a Spectrospin CMS-47 Fourier transform ICR mass spectrometer. Careful variation of the laser power was carried out with neutral filters which allowed the determination of the threshold energies for laser desorption of the fullerenes. The laser power was determined using a Scientec power meter. Pressed samples of the soot were ablated in the ICR cell and the ions directly observed.

Fourier transform infra-red spectra (FTIR) were obtained on a Digilabs FTS 80 instrument. The soot was carefully pressed into KBr plates before observation. A sample of the material was mixed with KBr and then pressed in a 13 mm die at 9 t for 5 min.

Solid state nuclear magnetic resonance (n.m.r.) spectra were obtained on a Bruker CXP 100 instrument at 22.5 MHz for ¹³C. Spectra were obtained by single pulse (Bloch decay) techniques using a 4 μs pulse and 5 s recycle time⁹.

RESULTS AND DISCUSSION

The total amount of toluene extract and pyridine extract from the first portion of soot is identical to the total amount of pyridine extract and toluene extract from the second portion of soot. This shows that an equal amount of material can be extracted from the soot with these solvents irrespective of the sequence. Of this total, 57 wt. %

can be first extracted by toluene and a further 43 wt. % can be extracted by pyridine afterwards.

The soot and soot residue after solvent extraction have been examined by FTIR spectroscopy. Adsorptions from C_{60} can clearly be seen in the infra-red spectrum of the raw soot at 527 and 577 cm^{-1} . When the soot is extracted with toluene, the toluene extract contains C_{60} and C_{70} in the ratio of about 10:1 as reported previously by us and others^{1,3,7}. However when the extracted soot was examined by FTIR C_{60} resonances were still found to be present even though the soot had been exhaustively extracted with toluene. This result shows that much of the C_{60} is trapped in the soot in some way, so that it becomes unextractable. Pyridine extracts C_{60} . However after pyridine extraction the soot still contained C_{60} adsorptions showing that even pyridine cannot remove all C_{60} .

The pyridine extracted toluene insoluble material was studied in more detail. Its solid state n.m.r. spectrum showed a large resonance at 143 ppm and smaller resonances between 147 and 133 ppm with a small shoulder at 128 ppm. C_{60} resonates at 143 ppm in the solid state¹⁰ and hence this resonance can be ascribed to C_{60} . The other resonances although not fully resolved may be ascribed to C_{70} ¹⁻³.

Laser desorption studies at low laser powers (2 kW cm^{-1}) were in full agreement with the FTIR and N.M.R. results. Initial FTICR spectra of the residue from toluene extraction indicated the presence of C_{60} and C_{70} and smaller amounts of higher fullerenes on laser desorption. However when the experiment was repeated continually, the amount of C_{60} and C_{70} observed was found to be quite variable. This suggests successive desorption through the surface of the extract indicating that C_{60} and C_{70} were entrapped in various layers.

At higher laser powers (>100 kW cm^{-2}) ablation occurs. Positive ion spectra of the toluene residues indicated the presence of higher fullerenes (Figure 1). The most interesting observation from these experiments was the observation of odd numbered carbon clusters (see Figure 1). Thus some open ruptured fullerenes or fullerenes with odd chain length appendages must be formed. As far as we are aware this is the first reported observation of higher molecular weight odd numbered clusters.

As predicted from the infra-red data, the pyridine extracts were shown to contain both C_{60} and C_{70} by laser ablation. Negative ions were observed at threshold values of 2 kW cm^{-2} indicating the presence of fullerenes up to $m/z \sim 1800$ daltons (C_{150}). Increasing the laser power resulted in the appearance of fullerenes of m/z up to 2400 daltons (C_{200}), but further increase in power caused a loss of intensity in negative ions as reported previously for C_{60}/C_{70} mixtures⁸.

In summary, these results clearly show that during the formation of fullerenes by arcing techniques C_{60} and C_{70} fullerenes are often formed entrapped within other molecules, possibly other fullerenes. On laser ablation these other molecules can react either alone or possibly with C_{60} and C_{70} to form species that have odd numbered molecular weights. These species must be ruptured fullerenes or species containing

odd-numbered side chain lengths. These results are consistent with the hyperfullerene or Russian egg structure recently proposed by Curl and Smalley¹¹ for fullerene soot or an encapsulating tube model. In these structures C_{60} is encapsulated by fullerenes of higher carbon number.

REFERENCES

1. W. Kratschmer, L.D. Lamb, K. Fostiropoulos and D.R. Huffman, *Nature* 347 (1990) 354.
2. R. Taylor, J.P. Hare, A.K. Abdul-Sada and H.W. Kroto, *J.C.S. Chem. Commun.* (1990) 1423.
3. R.E. Haufler, J. Conceicao, L.P.F. Chibante, Y. Chai, N.E. Byrne, S. Flanagan, M.M. Haley, S.C. O'Brien, C. Pan, Z. Xiao, W.E. Billups, M.A. Ciufolini, R.H. Hauge, J.L. Margrave, L.J. Wilson, R.F. Curl and R.E. Smalley, *J. Phys. Chem.* 94 (1990) 8634.
4. R. Diederich, R. Ettl, Y. Rubin, R.L. Whetten, R. Beck, M. Alvarez, S. Anz, D. Sensharma, F. Wudl, K.C. Khemani and A. Koch, *Science* 252 (1991) 548.
5. R. Ettl, I. Chao, F. Diederich and R.L. Whetten, *Nature* 353 (1991) 149.
6. D. Ben-Amotz, R.G. Cooks, L. Dejarne, J.C. Gunderson, S.H. Hoke II, B. Kahr, G.L. Payne and J.M. Wood, *Chem. Phys. Lett.* 183 (1991) 149.
7. L.S.K. Pang, A.M. Vassallo and M.A. Wilson, *Nature* 352 (1991) 480.
8. P.F. Greenwood, I.G. Dance, K.J. Fisher, G.D. Willett, L.S.K. Pang and M.A. Wilson, *Org. Mass Spectros.*, 26, (1991), 920.
9. M.A. Wilson, *Techniques and Application of NMR in Geochemistry and Soil Science*, Pergamon Press, 1987.
10. C.S. Yannoni, R.D. Johnson, G. Meijer, D.S. Bethune and J.R. Salen, *J. Phys. Chem.*, 1991, 95, 9.
11. R.F. Curl and R.E. Smalley, *Scientific American* (1991) 32.

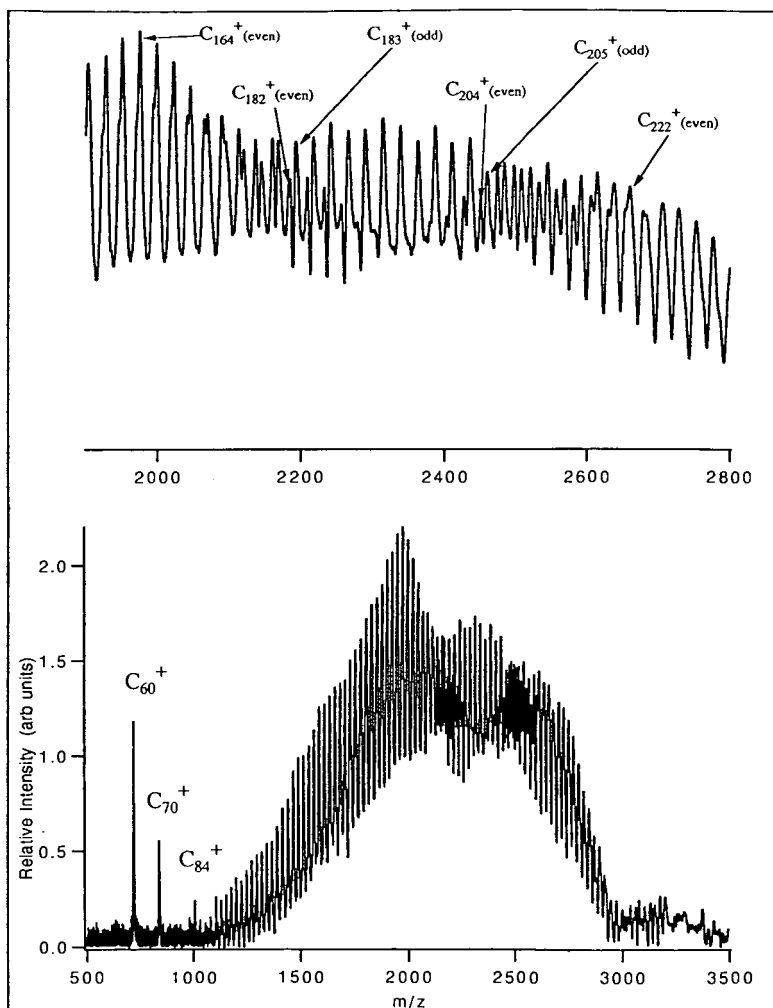


Fig. 1 Mass spectrum of the laser desorption ($\sim 4 \text{ k W cm}^{-2}$) of an insoluble residue

EVALUATION OF THE ASPHALT APPLICATION POTENTIAL
OF AN EASTERN US SHALE OIL

K. Mahboub¹, S. D. Carter³, R.E. Robertson⁴, P.M. Hamsberger⁴,
P. K. Oduroh², A. L. Simpson², and D. N. Taulbee^{*3}

¹Kentucky Transportation Center

²Dept. Civil Engineering

³Center for Applied Energy Research

University of Kentucky, Lexington
and

⁴Western Research Institute, Laramie, WY.

Keywords: Asphalt, shale oil, KENTORT II.

Abstract. A 3" fluidized bed retort was used to generate oil samples from a Devonian oil shale from Fleming County, Kentucky. Following distillation, samples of heavy end materials were subjected to a battery of tests aimed at evaluating their potential utilization as an asphalt cement, additive, or recycling agent. Due to the unusually rapid aging characteristics of the shale oil, emphasis was placed on the latter applications. Preliminary tests of the asphalt recycling potential were generally favorable, indicating that the eastern shale oil exhibits good dispersant and rejuvenation properties.

Introduction. This manuscript describes the results of a scoping study directed at evaluating the potential road paving applications for oils derived from the eastern U.S. oil shale deposits, more specifically, for eastern shale oils (ESO) produced in a KENTORT II prototype reactor.^{1,2} The KENTORT concept comprises a series of three fluidized bed reactors, i.e., pyrolyzer, gasifier, and combustor, that fully utilize the available carbon during oil shale processing. This process has been under continuing development at the CAER since about 1984 and has demonstrated that significant enhancements over Fischer Assay oil yield can be obtained using proven technology without resorting to high H₂ partial pressures. Further, this process was designed to mitigate many of the environmental concerns often associated with related technologies. However, in the present era of plentiful and reasonably priced petroleum, commercial production of motor fuels from oil shale is viewed as a high risk venture by those capable of lending financial support. Thus, the prospects for a near term commercial oil shale development is not promising.

Coincidental to the advances in oil shale technology of the past decade has been a continuing decline in both the quality and availability of road asphalts. The decline in availability has led to the recycling of road asphalts (milling and reapplication) in many areas of the country. The decline in quality, attributed primarily to advanced processing (e.g., fluid-cat crackers) used to recover more heating or motor fuel per barrel, has resulted in asphalts which do not have the desirable properties or longevity as asphalts from 3-4 decades past. Though this is bad news for motorists, this situation has created a potential niche market for shale oils,^{3,4} particularly since these materials often exhibit physical/chemical properties that suggest they may be a viable alternative to petroleum derived asphalts. Accordingly, a test program was implemented to evaluate KENTORT oils in three different paving applications; i.e., as an asphalt cement, an asphalt modifier, and an asphalt recycling agent. The study included a series of binder and mixture characterization procedures for evaluation of both

short- and long-term performance potential.

Details of the test methods along with preliminary results are described elsewhere^{5,6} and so only a brief description of test methods is given here. The conclusion from this earlier work was that unmodified ESO showed an unacceptable rate of 'aging' or hardening which would ultimately lead to pavement failure if used directly as an asphalt cement. However, the potential for use as an asphalt modifier and particularly, as an asphalt recycling agent showed more promise. Accordingly, these latter applications are the focus of this report.

Methods and Results. Study samples. Two oil streams, produced in a 5 lb/hr KENTORT prototype unit, were selected for study. The first was a highly viscous material (3440 P @60° C) recovered in an electro-static precipitator and is referred to as the 'hard' ESO. The second, referenced as the 'soft' ESO (8 P @60° C), was derived from a composite of the total oil product that was subjected to a vacuum distillation prior to testing. These two oils were deliberately selected for study since it is believed they represent the types of material that would be readily available and most likely to be utilized for asphalt production in a commercial operation. Both samples were derived from the Cleveland Member of the Ohio shale acquired from a freshly exposed outcrop in Rowan County, Ky. A detailed description of the oil shale sample and retort operation is given elsewhere.^{1,2}

Binder Characterization. If eastern shale oil is to be useful as an asphalt modifier, then the blend of asphalt and ESO must exhibit aging characteristics and rheological properties that are superior to the unmodified asphalt. Likewise, if ESO is to find application as an asphalt recycling agent, it must exhibit properties that are equivalent to or better than conventional agents. In an effort to determine if ESO could meet these criteria, the research was divided into two parts. The first part focused on evaluation of the 'hard' ESO as an asphalt additive and the second on evaluation of the 'soft' ESO as a softening agent for aged asphalt and aged asphalt mix (pavement recycling).

Evaluation as an asphalt additive involved determining the rheological properties of an AC-20 asphalt, a 7 wt. % blend of "hard" ESO and AC-20 asphalt, and neat "hard" ESO. The rheological properties of the three samples were also determined after they were subjected to an accelerated aging procedure. Evaluation of ESO as an asphalt recycling agent entailed measuring the viscosity of an asphalt extracted from a laboratory-aged pavement mixture, the "soft" ESO, and an AC-5 asphalt (representative of a commercial recycling agent). Two "recycle" blends, with a target viscosity of 10,000 poise at 60°C, were prepared by blending the laboratory-aged asphalt with 1) the "soft" ESO and 2) with the AC-5 asphalt. Rheological properties of the two blends were then examined.

Dynamic viscosity measurement were made on a Rheometrics RMS-605 mechanical spectrometer using a shear frequency range of 0.1 to 100 rad/sec at 25, 45, and 60°C from which the two components of shear modulus, G' and G'' , were determined. The storage modulus or the elastic component (G') quantifies the elastic rebound capability of the material. The loss modulus or viscous component, G'' , is a measure of damping capacity. Higher G' values indicate good resistance to permanent deformation (rutting) but greater susceptibility to cracking failure. Higher G'' values indicate the reverse behavior. Since there is always a trade-off between rutting performance and cracking performance, the term Tan Delta (ratio of G''/G') is used as a measure of the balance between damping and elastic properties. For a fresh asphalt, a Tan Delta value higher than 3 indicates better than average resistance to cracking but less than average resistance to rutting.⁷ Values less than 3 indicate the opposite.

Aged Asphalt Binder Rejuvenation. The 60°C viscosities of the laboratory-aged asphalt, the soft eastern shale oil, and the AC-5 asphalt as described above were determined to be 5.98×10^6 , 15, and 515 poise, respectively. Three trial blends each of the laboratory-aged asphalt/soft ESO and the aged asphalt/AC-5 were prepared in an effort to produce samples whose viscosity would bracket the 10,000 poise target value (see Fig. 1 and 2). Unfortunately, the trial blends did not bracket the target

viscosity for either blend series. Nonetheless, from the trial blends data, the mixing ratios required to produce 10,000 P blends were estimated to be 66% aged asphalt/34% soft ESO and 42% aged asphalt/58% AC-5 asphalt. The measured viscosity of the test blends prepared at these ratios are shown by the unfilled square symbols in Figures 1 and 2. The amount of soft ESO needed to achieve the target viscosity is considerably less than for the AC-5 due to the lower viscosity of the ESO.

Nearly identical viscosity-temperature relationships are shown for the test blends in Figure 3. Likewise, tan delta values were similar at all three temperatures with the AC-5/aged asphalt blend being slightly lower at 60°C and slightly higher at 25 and 45°C (Table 1). These results are favorable indicating good asphalt rejuvenation potential for the soft ESO both in terms of adequate dispersal of the aged asphalt and the ability to provide an equivalent viscosity as the AC-5 with less sample.

Mixture Characterization. The term mixture refers to a combination of asphalt and road aggregate. The mixture characterization program was designed so that the potential pavement performance of ESO modified asphalts could be related to that of an asphalt modified with a more conventional material with known field performance. This was accomplished by on-site sampling of ~40 Kg of hot mix (containing no modifier) during construction of an asphalt overlay research project during September 1990 (Pulaski County, Ky.). For this project, several test strips were constructed from a single asphalt blended with different commercial modifier agents. The test strips were placed on a long term monitoring schedule and samples of each asphalt/modifier blend were returned to the laboratory for testing. So, by blending the ESO with the same hot mix and subjecting this asphalt/ESO blend to the same lab tests as the field samples, a more realistic assessment of pavement performance could be obtained.

The field sampled hot mix was divided into two portions. The first portion was mixed with the "hard" ESO at the same proportions as the polymer modified mixtures. This was to compare the behavior of the hard ESO modified asphalt to the asphalts modified with commercial agents. The second portion was aged in a forced draft oven at 80°C for two weeks prior to mixing with the "soft" ESO. This was in order to test the soft ESO as a pavement recycling agent. An additional 4 Kg of the aged mixture was set aside for extraction and binder characterization. Mixture characterization included a series of mechanical response tests on compacted specimens (Marshall procedure; ASTM 1559) directed at evaluating the performance potential of the "hard" ESO modified asphalt mixture relative to the conventional polymer modified asphalts (brands "A" through "D"). All statistical comparisons were conducted at 95% level of confidence.

Tensile Strength Characterization. Fatigue and durability of asphalt pavements are believed to be related to tensile strength. It is customary to characterize tensile strength of pavement materials indirectly in accordance with ASTM-4123. Figure 4 shows the 'hard' ESO blend has tensile strength properties that are superior to the control mixture (unmodified, aged hot-mix) and are on par with two of the high tensile strength polymer modified asphalts. Taken alone, these results indicate desirable fatigue and durability performance potential for the "hard" blend ESO. However, previously reported results suggest that the aging characteristics of a 'hard' ESO blend that has not been subjected to some sort of pre-aging treatment may lead to early pavement failure.^{5,6}

Moisture Damage Characterization. Asphalt binder stripping from aggregate is a moisture induced effect. The potential for this type of damage is often characterized in the laboratory in accordance with the Root-Tunnicliff test⁸. The mean tensile strength data shown in Figure 4, along with statistical analyses of the data, indicates that the 'hard' ESO moisture damage susceptibility compares favorably with the control mixture and was not significantly different than at least two of the polymer modified mixtures. Nonetheless, the data show that 'hard' ESO modified asphalt is somewhat susceptible to binder stripping.

Freeze-Thaw Damage Characterization. The potential susceptibility to freeze-thaw damage was characterized, again using tensile strength as an index parameter. Mixtures were subjected to 100

cycles of freeze and thaw (3 hours at -18°C , followed by 3 hours at $+4^{\circ}\text{C}$). Cross comparisons (Figure 4), along with statistical data analyses, revealed no statistically significant change in tensile strength after 100 cycles of freeze-thaw. Evidently, more freeze-thaw cycles would be necessary in order to induce significant mixture differences.

Rejuvenated Mixture Characterization. Asphalt aging/oxidation severely reduces the tensile strength properties of an asphalt-aggregate mixture as demonstrated by the substantial decline in tensile strength of the aged control sample plotted in Figure 5. Addition of "soft" ESO to the aged mixture resulted in a notable increase in tensile strength, comparable to that from adding AC-5 asphalt. However, ESO addition did not restore the tensile strength to the level prior to aging. This phenomenon is not untypical and has led to a common practice of adding fresh hot mix to the recycled mixture along with the rejuvenating agent. Nonetheless, the mixture rejuvenation analysis shows the "soft" ESO to have potential asphalt recycling applications and merits further examination.

Summary. Two samples of eastern shale oil (ESO), one a hard ESO and the other a soft ESO, produced in the Kentort II process, were evaluated for potential use with paving asphalts. The hard ESO material was evaluated as an asphalt additive and the soft ESO was evaluated as an asphalt recycling agent to soften both an aged asphalt and an aged asphalt-aggregate mix.

The 'hard' ESO added at 7 wt. % to an AC-20 asphalt showed unfavorable susceptibility to moisture damage. An improvement in tensile properties of the aged asphalt mixture was achieved through addition of the hard ESO, however, this effect is likely to diminish rapidly with time due to previously reported aging characteristics.^{5,6}

Both soft ESO and AC-5 asphalt were used to soften a hardened asphalt extracted from a laboratory-aged pavement mixture. The rheological properties of the aged asphalt/soft ESO blend were essentially the same as those of the aged asphalt/AC-5 blend. This finding was verified by mixture rejuvenation analysis. The amount of ESO required to soften the aged asphalt was less than the amount of AC-5 due mostly to the lower viscosity of the soft ESO. However, the large negative deviation of the ESO blending curve suggests that even at equal viscosity, the soft ESO would exhibit more softening per unit weight. Overall, the soft ESO appears to have potential application as an asphalt rejuvenating agent.

Recommendations. Previously reported results indicate that the 'hard' ESO was unstable or reactive for some time following preparation. Measurement and control of this phenomenon is an important step that must be addressed prior to further testing since a chemically and thermally stable material is necessary for paving applications. Further mixture studies are needed to fully characterize both short-term and long-term performance potential of ESO modified/rejuvenated asphalts. Field trial projects are recommended for verification of laboratory test results.

Acknowledgements. The authors would like to express their appreciation to Mr. J. Button and Mr. S. Greer of TTI who extracted and recovered the aged asphalt, and to J.M. Wolf, and F.A. Reid of the WRI who conducted the blending and aging experiments under subcontract to the UK-CAER. Mr. R. Pemberton of Ashland Oil is acknowledged for supplying the AC-5 asphalt binder. This work was supported in part by the Morgantown Energy Tech. Ctr., USDOE, under Coop. Agreement DE-FC21-90MC27286 through subcontract with the UK-CAER (such support does not constitute an endorsement by the USDOE of the views expressed in this article).

References

1. Carter, S.D., Rubel, A.M., Taulbee, D.N., and Robl, T.L., The Development of the KENTORT II Process for Eastern Oil Shale: Final Report, Report to USDoE, Laramie Project Office, Coop. Agreement No: DE-FC21-86LC11086, Univ. of Ky.-Cir. for Appl. Energy Research, Lexington, KY, March, 1990, 208 p.
2. Carter, S.D., and Taulbee, D.N., *Proc.: 1989 Eastern Oil Shale Symp.*, Univ. of Ky. Inst. Mining and Minerals Res., pub., Lexington, Ky., **IMMR89/201**, 1990, 511-518.
3. Lukens, L.A., *22nd Ann. Oil Shale Symp. Proc.*, Colorado School of Mines, April, 1989, pp 199-206.
4. Sinor, J.E., DOE report **DOE/MC/11076-2759**, July 1989.
5. Mahboub, K., Simpson, A., Oduroh, P.K., Robertson, R.E., Harnsberger, P.M., Taulbee, D.N., Rubel, A.M., *Proc.: 1991 Eastern Oil Shale Symp.*, Inst. Mining & Minerals Res., Lexington, Ky., Nov. 1991, in print.
6. Mahboub, K., Simpson, A., Oduroh, P.K., Robertson, R.E., Harnsberger, P.M., Taulbee, D.N., Rubel, A.M., submitted to *Fuel*, Jan., 1992.
7. Goodrich, J.H., *Proc.: Assoc. of Asphalt Paving Tech.*, **57**, 1988.
8. Tunnickliff, D.G., and Root, R.E., Report #174, Ntl. Coop. Highway Res. Prog., Washington, D.C., 1987.

Table 1. Rheological Properties of Aged Asphalt Blended With Soft ESO and AC-5 Asphalt.

Binder	Dynamic Viscosity, 60°C, Poise	Tan Delta
66 wt.% Recovered Asphalt/34 wt.% Soft ESO	1.244 x 10 ⁴	6.112
42 wt.% Recovered Asphalt/58 wt.% AC-5	1.376 x 10 ⁴	5.973
Binder	Dynamic Viscosity, 45°C, Poise	Tan Delta
66 wt.% Recovered Asphalt/34 wt.% Soft ESO	1.576 x 10 ⁵	2.513
42 wt.% Recovered Asphalt/58 wt.% AC-5	1.627 x 10 ⁵	2.721
Binder	Dynamic Viscosity, 25°C, Poise	Tan Delta
66 wt.% Recovered Asphalt/34 wt.% Soft ESO	5.077 x 10 ⁶	1.582
42 wt.% Recovered Asphalt/58 wt.% AC-5	6.187 x 10 ⁶	1.738

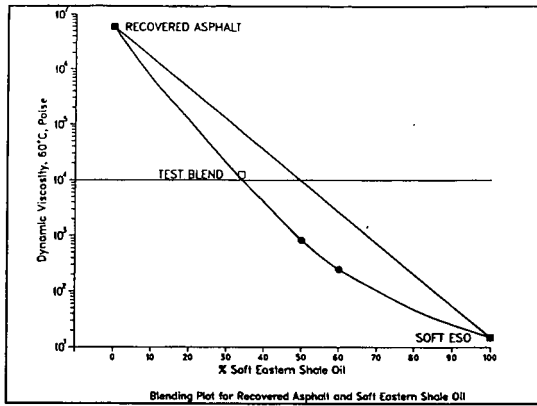


Figure 1. Viscosity of blends from aged asphalt/soft ESO blends.
 ●-trial blends; □-blend used for mechanical testing.

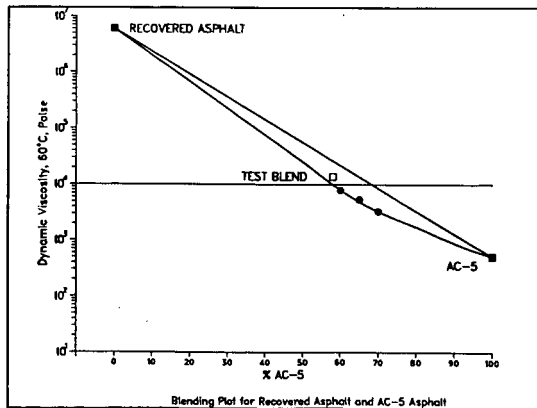


Figure 2. Viscosity of blends from aged asphalt/AC-5 blends.
 ●-trial blends; □-blend used for mechanical testing.

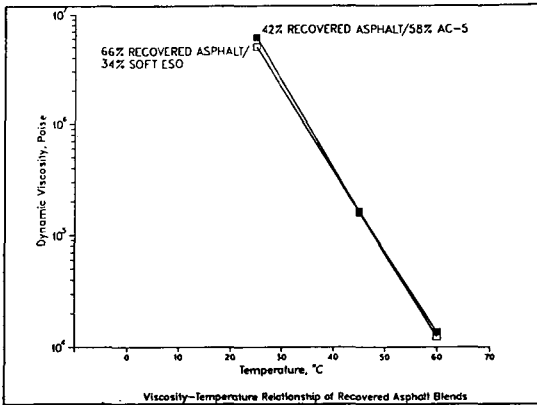


Figure 3. Viscosity-Temperature plots. □-soft ESO/aged asphalt (34%/66%); ■-AC-5/aged asphalt (58%/42%).

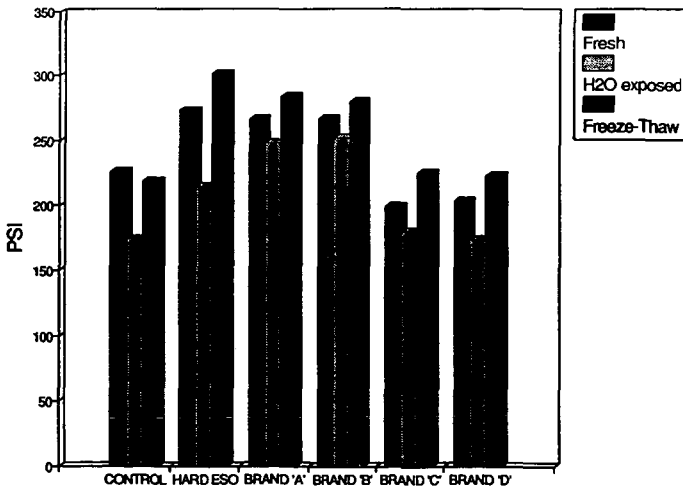


Figure 4. Tensile strength data for series of modified pavement mixtures. Samples were tested following preparation, moisture susceptibility analysis, and 100 freeze-thaw cycles. Control is pavement mixture without added modifier.

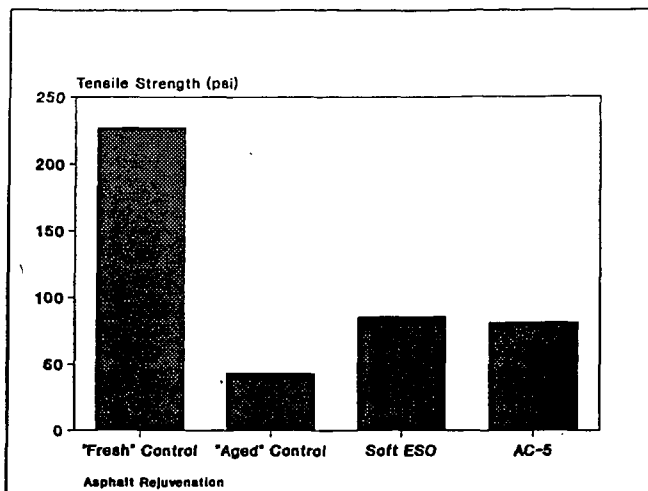


Figure 5. Tensile strength test series for fresh pavement mix, aged mix, and mix rejuvenated with either soft ESO or AC-5.

Market Enhancement of Shale Oil by Selective Separations

James W. Bunger, Prasad A. V. Devineni and Donald E. Cogswell
James W. Bunger and Associates, Inc.
Box 520037, 2207 West Alexander Street
Salt Lake City, UT 84152-0037

Joel B. DuBow, Huaying Huai and Jacek P. Dworzanski
Center for Microanalysis and Reaction Chemistry
University of Utah
Salt Lake City, UT 84112

Keywords: shale oil, separations, gc-ms

Introduction

The recent history of petroleum availability and price has shown that petroleum substitutes are not economically viable as long as there is a stable supply of conventional petroleum. The additional costs for recovery and upgrading are not sufficiently offset by product values to attract private risk capital without supports or subsidies. In order to create an economically viable synthetic fuels industry, it is becoming clear that some research must be directed at market enhancement technologies, in addition to the more traditional view of cost reduction (recovery and processing) technologies.

Recognizing this requirement, James W. Bunger and Associates, Inc. (JWBA), in concert with the Center for Microanalysis and Reaction Chemistry (MARC), at the University of Utah, has initiated a program aimed at technology for isolation and manufacture of high-value products from unconventional hydrocarbon resources. We refer to this technology as the Natural Products Extraction (NPX) technology. One such initiative is aimed specifically at high-value products from shale oil -- a U. S. natural resource of more than 1-trillion bbls-oil, in place. When compared with conventional crude oil, shale oil is characterized by its high percentage of heteroatom (N, S and O) containing molecules, its high level of mono- and di-cyclic compounds and relatively high percentage of vacuum gas oil.

For successful development of a high-value product slate from shale oil, we must focus on those structural characteristics which are present in higher concentrations in shale oil than in crude oil and which possess proven, or unique, chemical applications. Also, it is clear that isolation of distinctive structural types must, of necessity, adhere to fundamental thermodynamic principles. Therefore, separations process technology must be based on a fundamental understanding of shale oil composition and the relationship of that composition to partitioning during separation.

This paper reports results of our initial attempts to identify and isolate fractions from shale oil of potential market value, to confirm a suitable analytical methodology as a basis for process and product development, and to delineate the economic parameters of market enhancing technology.

Analytical Methodology

In prior work (1-3), it had been determined that thermodynamic properties of molecules correlate well with structural parameters 'n' and 'z' (defined by the formula $C_nH_{2n+z}N_uS_vO_w$) and 'i', a non-integer number which relates to isomeric variations. The indices 'n' and 'z' (with 'u', 'v' and 'w'), establish the molecular weight and define the essential skeletal structure. These parameters, which can be obtained from high resolution, parent peak mass spectroscopy, correlate well with enthalpic properties of the molecule. The parameter 'i', is a strong function of entropic properties. Preliminary evidence suggests that 'i' may be measured indirectly through chromatographic retention time (2).

The development of the classifying system and correlating functions has been collectively labeled the Z-Based Structural Index Correlation Method (Z-BASIC) (2). The Z-BASIC method allows, for the first time, the ability to track the separation behavior of individual species from shale oil. This provides the theoretical basis for process modeling on a molecular level. Coupled GC-MS-FTIR technologies available at the MARC, were used to demonstrate the viability of Z-BASIC for calculation of partition functions of molecular species.

Given the ability to develop separations technologies using fundamental molecular science, we organized a logical development strategy. Figure 1 shows the information flow for this strategy. The flow diagram shows that detailed analytical data is translated into mathematical terms which provide a rigorous basis for process simulation. The simulation becomes the controlling function for modifying the processes to manufacture a specification product. Where specifications cannot be met by

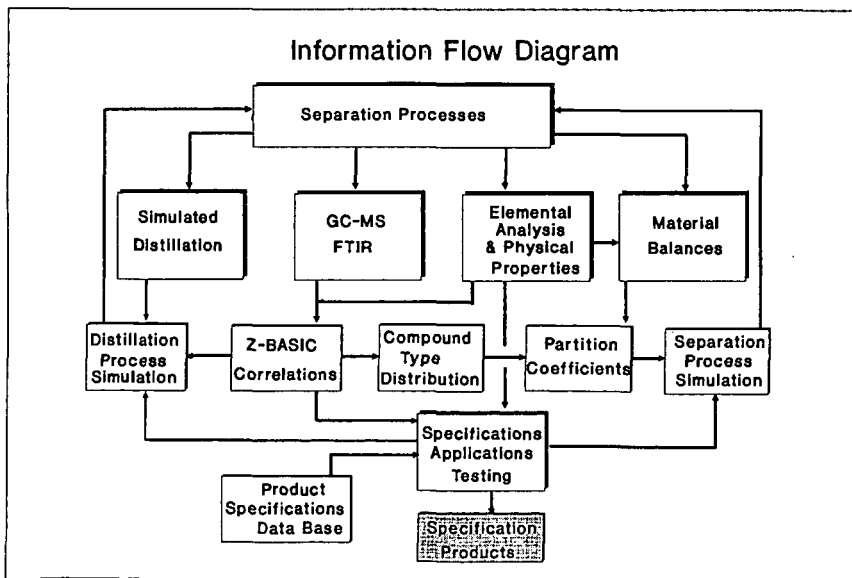


Figure 1

separations processing alone, a comparison between actual concentrate structure and desired concentrate structure will help delineate any additional processes required.

Separation of Shale Oil

Theoretical arguments suggest that attempts to separate a broad molecular weight mixture on the basis of polarity, will suffer from lack of definitiveness between molecular weight and polarity effects. Therefore, the logical initial step in a separation sequence is distillation, a process which provides fractions of narrower molecular-weight ranges.

Figure 2 shows the distillation scheme used in this study and the resulting weight percent yield of each fraction. Figure 3 shows the total ion chromatograms of the individual fractions showing the complexity of the fractions. In general, shale oil lacks homology on the basis of distillation alone, with the notable exception of the concentration of paraffins in the 350 - 440°C fraction.

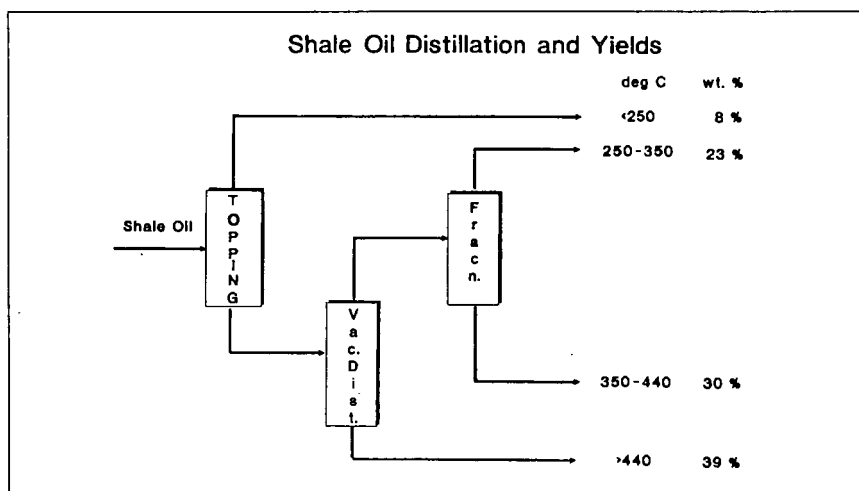


Figure 2

Figure 4 represents the heteroatom distribution as a function of boiling point and shows that while sulfur and oxygen are less dependent on boiling point, nitrogen increases significantly with boiling point. The unusual shape of the oxygen distribution is thought to be indicative of differing types dominating the lower-molecular-weight range as compared to the higher-molecular-weight range. These types have not been fully characterized.

Distillate fractions may be subjected to liquid-liquid extraction with polar solvents to separate concentrates according to polarity. Candidates for polar solvent separation include phenol, furfural, N-methyl-2-pyrrolidone and other polar solvents such as alcohols, ketones, organic and mineral acids, and organic bases. Two-phase partitioning was successfully achieved with several of the aforementioned solvent systems.

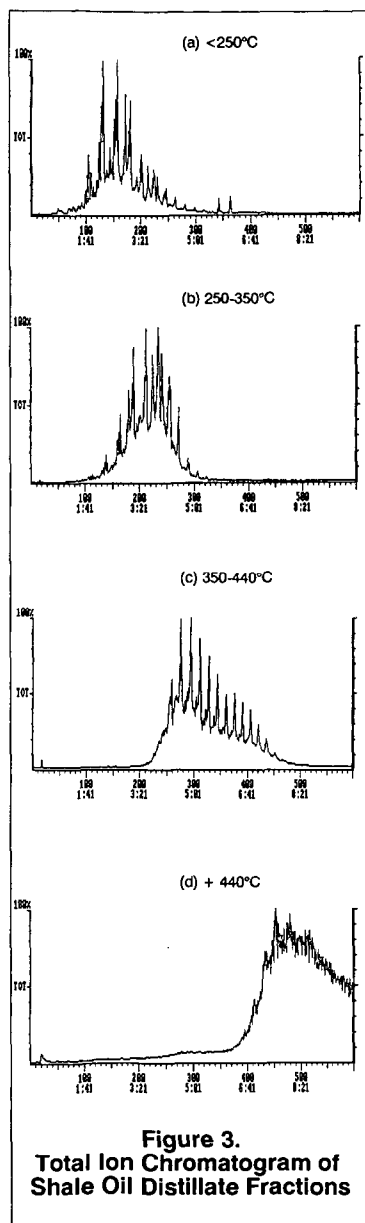


Figure 3.
Total Ion Chromatogram of
Shale Oil Distillate Fractions

Laboratory separations were conducted in a small-scale, batch-type processes and quantitative results must be further confirmed before publication. Laboratory conditions were designed to simulate commercially-realistic conditions, e.g., solvent-to-oil ratios of 1:1. In commercial practice, up to five sequential separation/distillation steps are envisioned.

The laboratory separations produced 16 specific concentrates covering four boiling ranges and four polarities. The overall yield and elemental composition of the fractions separated are given in Table 1. For purposes of illustration, the fractions were lumped according to similar polarities. The four major concentrates are labeled "White Oils and Waxes", "Aromatic Oils", "Low Polarity Nitrogen Compounds" and "High Polarity Compounds".

The elemental compositions of these concentrates illustrate the differences achievable with relatively straight-forward and inexpensive separations. The white oils and waxes are extremely low in heteroatoms, including sulfur. Oxygen is calculated by difference and is, therefore, subject to a wider margin of error. The aromatic oil fraction is particularly interesting because it possesses a low nitrogen content while constituting a significant portion of the shale oil barrel.

The major fraction is the low-polarity nitrogen compounds. These materials are of a higher molecular weight and thought to possess carbazolic and aromatic nitrogen. The high-polarity compounds are of a lower molecular weight and contain acidic, phenolic, nitrilic, pyrrolic and pyridinic functionalities.

Product Slate

Based on our laboratory separations and knowledge of the structural types present, a projected product slate for shale oil was constructed. The product slate is compared to current U. S. market volumes and prices. Results are shown in Table 2.

The product slate includes oils, waxes, aromatic oils, aromatics for manufacture of sulfonates, acids, bases and resins. Functionalized intermediates are compounds containing nitrogen or oxygen and which are thought to be of particular value as starting materials for derivatization to pharmaceuticals, industrial chemicals and other pure compound systems. Pure compounds are those with particularly high market

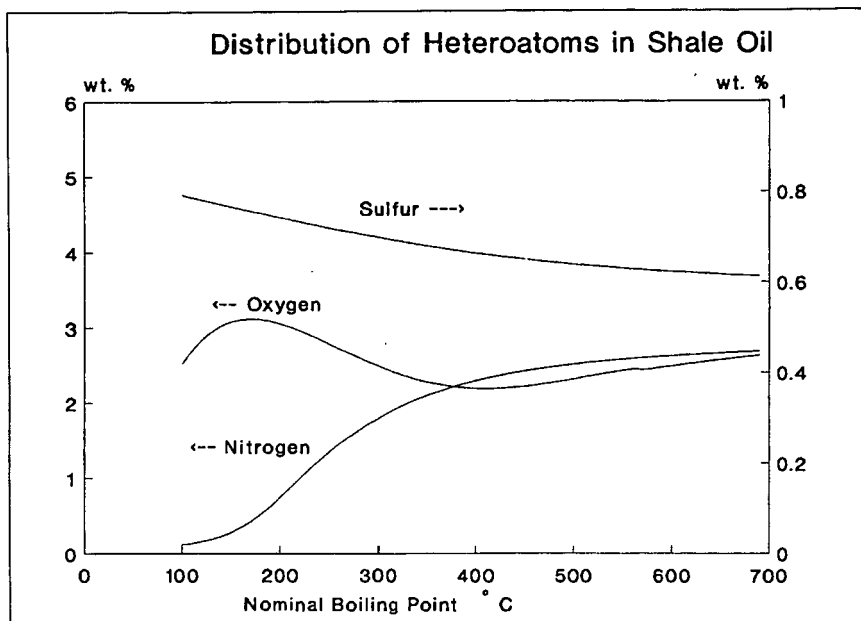


Figure 4

Table 1 Summary of Elemental Composition by Functional Concentrate							
Concentrate	Wt % of Shale Oil	C	H	N	S	O (Diff)	H/C
White Oils and Waxes	13	85.7	13.8	0.05	0.02	0.26	1.92
Aromatic Oils	22	87.0	12.1	0.2	0.6	0.5	1.66
Low-Polarity Nitrogen Com- pounds	35	83.6	10.4	3.2	0.7	3.4	1.47
High-Polarity Compounds	30	82.7	10.6	2.8	0.8	3.2	1.52

value that may be isolable in a pure form from shale oil. Target compounds include nitriles, pyridines, quinolines, amines, amides, phenols, naphthols and carboxylic acids.

The special applications concentrates represent mixtures of particular properties which makes the concentrate marketable in its mixed form. Examples include industrial antimicrobials, coatings, wood preservatives, industrial surfactants and asphalt additives. We currently project that less than 10% of the shale oil barrel may require marketing as a fuel or refinery feed.

Table 2
Demand and Value of Products
Output of SO/NPX = 170,000 Tons/year (3,000 bbl/day)

Product	Market Volume Tons/year	Recent Price \$/bbl-equivalent		SO/NPX Projected Yield Wt. % of Feed	% of Market	Revenue \$/feed-bbl
White Oils	4,575,000	84	Ref (4)	13.3	0.5	11.2
Waxes	882,000	133	Ref (4)	5.0	1.0	6.6
Aromatic/ Lubricating Oils	9,526,365	60	Ref (4)	30.5	0.5	18.3
Sulfonate Feeds	333,900	142	Ref (5)	11.7	5.9	16.6
Tar Acids and Bases	830,000	210	Ref (6)	4.0	0.8	8.4
Resins	542,000	120	Ref (7)	14.7	4.6	17.6
Functionalized Intermediates	130,000	178	Ref (7)	4.3	5.6	7.6
Special Application Concentrates	500,000	28	Ref (6)	10.3	3.5	2.9
Pure Compounds	200,000	135	Ref (7)	0.7	0.6	0.9
Fuels and Refinery Feeds	large	15	Ref (8)	5.5		0.8
Totals				100		\$90.90/bbl

The majority of the anticipated products are targeted for conventional commodity markets for which the market is well established. Maximum economic enhancement of a commercial shale oil facility will occur most readily when a large percentage of the shale oil product slate addresses large, well-established markets. The primary questions which remain and must be addressed in future research relate to the quality of the product and the finishing steps that are required to make the shale oil products market-acceptable.

It is recognized that certain products such as functionalized intermediates and special application concentrates may require significant market development. While this requirement may be an inhibiting factor in the short term, in the long term it raises exciting prospects for development of new materials, new chemical routes and new precursor chemicals, unique to shale oil.

Cost and Profitability Estimates

In order to establish the economic framework for our research, an attempt was made to estimate the process costs, and from projections of the product value, to estimate the profitability of a Shale Oil Native Products Extraction venture. The feed stream to the process facility is a raw, retorted shale oil which we charge to the facility, in the base case, at \$30/bbl.

The capacities of the unit operations required to produce the product slate shown in Table 2, were estimated based on conceptual flow diagrams (not shown). Costs for the unit operations were determined from analogy to commercially-practiced technologies. The results are given in Table 3.

Results show that process costs of approximately \$15/bbl are anticipated. Results also show that the shale oil barrel is subjected to an average of five process steps to make the product slate priceable at the values given in Table 2. Item -7 represents unspecified finishing steps through which the entire

Table 3
Estimated Process Costs for SO/NPX
(Basis: 1,065,000 bbl/year)

	Unit	Process Cost \$/bbl	Throughput bbl/yr	Operating Costs \$/yr
1.	Distillation	1.5	1,065,000	1.60
2.	Liquid-Liquid Extraction	2.7	1,065,000	2.88
3.	Adsorption	4.2	958,500	4.03
4.	Dewaxing	3.2	95,850	0.31
5.	High-Efficiency Separation	4.5	60,705	0.27
6.	Hydrofinishing	2.1	777,400	1.63
7.	Miscellaneous (Filtration, Precipitation, Crystallization, etc.)	4.0	1,065,000	4.26
Annual Manufacturing Costs				\$14.98M

output of the process facility is charged. This represents a contingency to account for currently unknown process requirements.

In order to account for marketing and distribution costs, a \$5/bbl charge is added to the operating costs. This allows for an average shipping radius of about 500-750 miles. Higher value products, e.g., \$100/bbl + , may be shipped further. Lower value products, e.g., asphalt additives, may be used locally or regionally.

Capital costs were estimated by summing the unit costs weighted for throughput capacities. A capital cost of \$120-million is projected for the 5,000 bbl/day case.

The profitability estimates are shown in Figure 5. Part a) shows the capital cost and return on investment as a function of capacity; parts b) and c) provide the sensitivity to the weighted average product value and raw shale oil costs, respectively; part d) shows the profitability analysis as a function of cost of raw shale oil and plant capacity. The profitability estimates have been made for the 100% equity case, using a 10% discount rate. The profit on investment for various debt-to-equity ratios can easily be estimated by multiplying the DCF/ROI for the 100% equity case by the ratio.

The economic assessments show that an increase in average product value rapidly offsets the process and raw material costs. The incremental price/cost differential promises significant profits on investment capital and a significant return on investment could be made, even if shale oil costs were \$40/bbl. Maximum profitability comes from the largest SO/NPX facility that the market will bear.

Conclusions

Commercial viability of synthetic fuels may be enhanced through technology for producing products of high market value. To pursue this objective, we have developed and demonstrated an analytical methodology which forms the basis for a process development strategy. This strategy promises an effective approach to maximizing the value of products isolable, or derivable, from shale oil.

Shale oil has been fractionated according to a simplified laboratory scheme using distillation, liquid-liquid extraction and liquid-solid adsorption, and the products have been characterized. Based on these results, a projected product slate has been constructed. The promised value of the product

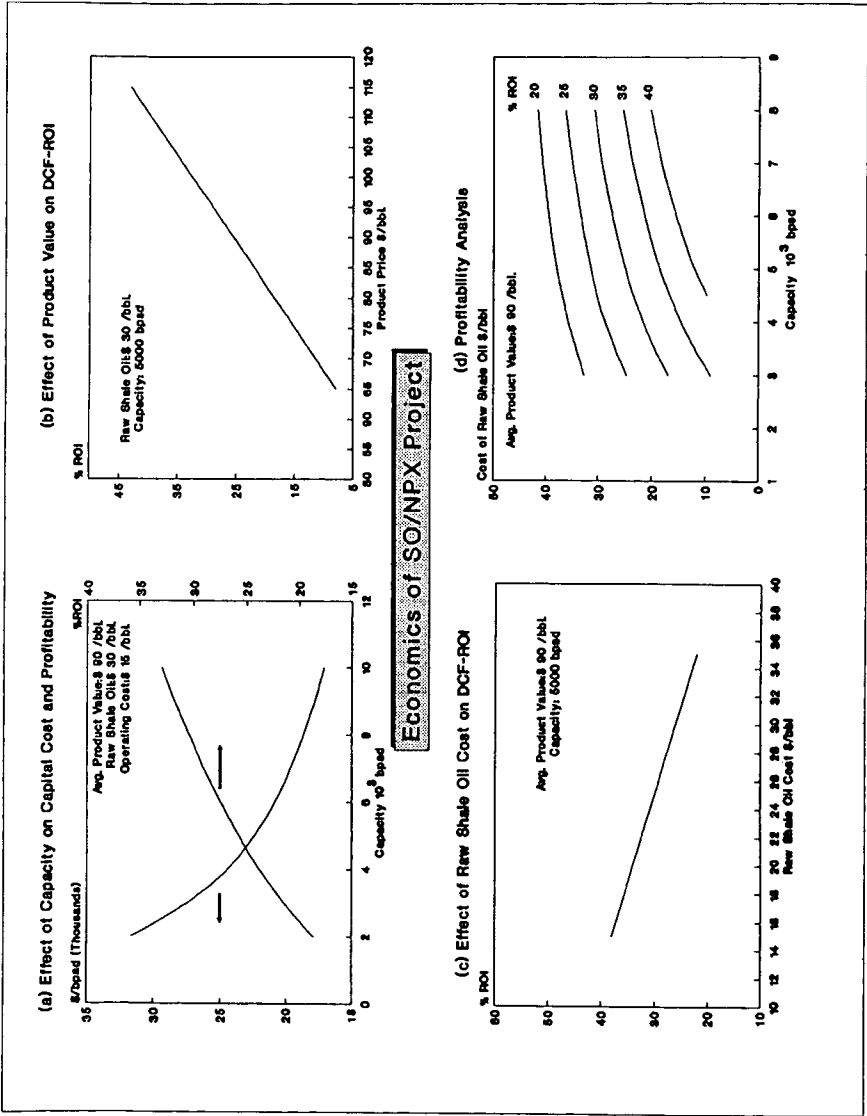


Figure 5

slate readily offsets the incremental process costs and shows promise for economic profitability. This work provides a sound basis for detailed process and product research and development.

Acknowledgments

The authors acknowledge Mr. J. W. Wisler for shale oil distillation, Dr. C. P. Russell for analytical and mathematical algorithms, and Mr. S. Valerio for technical assistance in laboratory separations, all of JWBA.

The authors also acknowledge Dr. J. D. Seader for consultation on thermodynamics and separations technology, and Mr. N. Chapman for GC-FTIR analysis, both of the University of Utah.

This work was supported through cooperative agreement DE FC21-90MC27084, between the U. S. Department of Energy and Occidental Oil Shale, Inc., under the project management of Dr. Ray Zahradnik. This support is gratefully acknowledged.

References

1. Bungler, J. W., Devineni, P. A. V., Russell, C. P., and Oblad, A. G., "Structure of Future Jet Fuels - A Model for Determining Physical and Chemical Properties from Molecular Structure", Preprints, Division of Petroleum Chemistry, 30(1), 1987.
2. Devineni, P. A. V., "A Model for Correlating Properties with Molecular Structure and Its Application to Fuel/Hydrocarbon Processing", Ph.D. Thesis, Dept. of Fuels Engineering, University of Utah, 1989.
3. Devineni, P. A. V., Bungler, J. W., and Russell, C. P., "Prediction of Optimum Structure for Jet Fuel Components Using the Z-BASIC Method", Preprints, Division of Petroleum Chemistry, 1989.
4. 1988 Report on U. S. Lubricating Oil Sales - National Petroleum Refiners Association.
5. Chemical Economics Handbook - SRI International, #543.8050A, 1987.
6. Sinor, J. E., "Niche Market Assessment for a Small Scale Western Oil Shale Project", Final Report, U. S. DoE, 1989.
7. United States Production and Sales, 1988 - Synthetic Organic Chemicals - U. S. International Trade Commission Publication.
8. Chemical Marketing Reporter, August 1990.

PROCESS FOR THE PRODUCTION OF PETROLEUM TAR PITCH FOR ANODE MANUFACTURING.

León Velasco,
Francisco García, Gustavo Velutini
Intevep, S.A. PO. BOX 76343
Caracas, Venezuela

Keywords: Petroleum tar pitch, Anode, Aluminium

INTRODUCTION

The aluminium production involves the consumption of petroleum coke and pitch, which are used in the manufacturing of anodes. Normally carbon consumption, as anode, lies between 0.4 and 0.48 Kg of carbon per Kg of metal produced¹. In the same manner, the amount of pitch used in preparing the anode lies between 14 and 18 mass %, and varies with the chemical composition of the pitch, the porosity and the structure of the petroleum coke.

The estimated amount of pitch required to meet the world aluminium production, for the early 90's, will be in the range of 1.2 million tonnes per year². Additionally, almost all binders used in the manufacturing of electrodes are derived from high-temperature coal treatment during the production of metallurgical coke. However the Environmental Protection Agency (EPA) regulations on the benzene emissions from coking oven equipment, have lead to recent announcements of numerous coking oven closures in the United States². According to PACE Consultants², metallurgical coke output in the US is expected to plummet to 17 million short tonnes by 1996 from 25 million short tonnes in 1990.

Coke battery closures in the US, resulting from the EPA mandates, should reduce the supply of good quality coal tar pitch in the US by as much as 25 to 30 %². One can assume that a similar trend should be observed in other major areas of coal tar pitch production.

Naturally, it is highly desirable to provide a continous closed-process for the production of high quality tar pitch suitable for electrode manufacturing. In this sense, INTEVEP the R&D Center of Petroleos de Venezuela, has carried out a research project to develop a process scheme for the production of a high quality petroleum pitch for use as a binder in anode manufacturing, using Fluid Catalytic Cracking Decanted Oil as feedstock. This paper presents results of this research as well as properties of the petroleum pitches obtained.

EXPERIMENTAL RESULTS

Feedstock selection and characterization: The main characteristic of coal tar pitch is that it is a highly condensed material with an aromatic content higher than 90 volume %. With this in mind, FCC decanted oil, a highly aromatic refinery stream, was selected as the feedstock. Table 1 presents the properties of this material.

Process Description: The process for the production of petroleum tar pitch was developed using Intevap's pilot plant facilities. The process route and product yields are shown in the fig.1 and table 2, respectively. The fresh feed, decanted oil, is fed to the filter so as to remove undesirable solids, mainly FCC catalyst particles, the clean filtered stream is thereafter fed to a preheater-coil heater where the temperature is increased to 430 °C. The heated feedstock is treated in a soaker type reactor, where sufficient residence time is provided for polymerization and condensation reactions to take place. Four different residence times were considered (TR1: 39 min, TR2: 78 min, TR3: 117 min, and TR4: 156 min). The stream leaving the soaker is sent to a high pressure separator, where C₄ minus hydrocarbons and light distillates are taken off from the top, and a heavier fraction is withdrawn from the bottom. The heavier fraction is finally sent to a reduced pressure pipe still so as to produce a gasoil and a petroleum pitch. By careful selection of pressure and temperature in this final stage a high quality petroleum tar pitch can be produced.

Pilot Plant yields and product characterization: Table 2 presents typical yields and product qualities obtained when the decanted oil is processed at a temperature of 430 °C and a pressure of 15.6 bar-a. Carbon value (CCR), density and softening point measurements showed that residence times TR1 and TR2 were not sufficient to yield a highly condensed petroleum pitch.

Petroleum pitch selection and preparation: From table 3, pitch TR3 has properties similar to those of a typical coal tar pitch used for anode manufacturing, on the other hand, pitch TR4 has higher softening point and viscosity values than those found for coal tar pitch. Nevertheless, its higher carbon content ought to yield a denser anode. In order to improve on these properties and still benefit from the high severity conditions at which this pitch was obtained, pitch TR4 was mixed with another aromatic and lighter petroleum fraction known as light cycle oil. The resultant mixture, TR4D contained 7 volume % of light cycle oil.

Finally, bearing in mind the importance of quinoline insolubles, as a coal tar pitch quality guideline, a fourth pitch TR4DNH was prepared by adding 7 mass % of carbon black to the TR4D pitch.

Evaluation of Intevap Petroleum Pitches: Four samples of petroleum pitch (TR3, TR4, TR4D and TR4DNH) were sent to a specialized laboratory in Switzerland, for analysis as a binder material for the production of carbon anodes for the aluminium industry. The work involved the determination of physical and chemical properties of each pitch as well as production and testing of a series of bench scale test anodes according to this particular laboratory's standard procedure. Physical and chemical properties of the pitches evaluated are presented in Table 3., together with corresponding values of a typical commercially available petroleum pitch and standard coal tar pitches used in the aluminium industry. For each pitch a series of 20 cylinders (50 mm in diameter) were produced at four separate pitch levels, these are 14, 16, 18 and 20 mass %. For each series mechanical properties, reactivity in CO₂ and air, and chemical analysis were performed.

DISCUSSION:

PITCHES

General: The main differences observed between coal tar and petroleum pitches are as follows:

- At comparable viscosity levels the softening point of the petroleum pitch is about 5 to 10 °C higher. This is due to the different temperature-viscosity interdependence of the two products.
- Petroleum pitches contain hardly no quinoline insolubles (QI). The QI present in coal tar pitches are due to the carry over from the coke oven during the carbonization process of mineral coal.
- The amount of QI in coal tar pitch reflects the severity of the pyrolysis and therefore, the pitch aromaticity, so that the aluminium industry specifies QI levels very closely. However, for petroleum pitches the aromaticity is independent of the QI content thus it is not relevant to consider this property in its specifications.
- Density in water of petroleum pitches is about 5-10 % lower than that for coal tar pitches (this being due to the different nature of the organic compounds) but is not detrimental as long as the coking value lies in an acceptable and comparable range to that of coal tar pitch. Furthermore, it is important to point out that previous work found in the literature has shown that anodes produced from petroleum pitches are inferior in baked density, strength and air permeability to those produced from traditional coal tar pitches. However, petroleum pitches have been successfully used as a binder in the aluminium industry where they have been specifically developed for a particular end user³

Softening point: TR4 pitch was found to be extremely hard and viscous, with a softening point that would make it unpractical for mixing in the paste plant.

TR3, TR4D and TR4DNH showed softening points that are more usual. The viscosities also fall within the typical values found for thermally cracked petroleum pitches.

Insolubles in toluene: Toluene insolubles is the most significant property for distinguishing between a thermally cracked and oxidized petroleum pitch. Values below 10 mass % for TR3, TR4, TR4D and the commercially available pet-pitch, illustrate the fact that they were produced by a thermal process. The higher value observed for the TR4DNH pitch is a result of the addition of about 7 mass % of carbon black, as artificial QI.

Insolubles in quinoline: This fraction is almost zero, as would be expected for a thermally cracked petroleum pitch. The TR4DNH sample has been blended with 7 mass % of carbon black, thereby allowing for the effect of artificial addition of QI to be quantified.

Coking value: The coking value was higher than typically expected for all four petroleum pitches under consideration. This is advantageous in anode production

since the greater the amount of residual coke, the higher the anode baked density (assuming all other parameters remain constant).

Distillation: The distillation of the TR4D and TR4DNH samples is their biggest drawback, as far as pitch properties are concerned, especially in the 0-270 °C range. The amount of these volatiles as well as their carcinogenic nature would pose significant problems in the paste plant. In the case of TR4D, this amount (6.57 mass %) in the 0-270 °C range is a direct result of the addition of a light cycle oil during the pitch preparation.

For TR3 and TR4, fractions obtained during distillation are much lower and can be considered more typical.

Density in water: TR3 pitch shows a value which is within the typical range for thermally cracked petroleum pitches, whereas the other three samples show lower but acceptable values for this property.

Elemental analysis: The elemental impurities of the four pitches are typical and would be acceptable to the aluminium industry.

BENCH SCALE ANODES AND PROPERTIES

Figures 2, 3, and 4 present the results of the evaluation of the bench scale anodes prepared with each of the INTEVEP petroleum pitches. Following is a discussion of the most relevant aspects of this evaluation:

TR3 Pitch (Fig. 2):

The optimum pitch content is around 14% this being 2% absolute less than for a typical coal tar pitch. This fact is of great financial consideration as the price of pitch is usually twice that of the coke. At this optimum the physical properties of anodes are within the range of those obtained with coal tar pitches. Although the compressive strength is at the lower end of the range this will not be too serious a problem if proper mixing, forming and baking conditions are chosen in an industrial scale plant.

As the permeability level (4.8 nPm at 14% pitch) is almost typical (3-4 nPm) for bench scale anodes and as the reactivities in CO₂ and air are quite normal, this pitch will give anodes having an acceptable burning behaviour in the pots.

TR4 (Fig. 3)

The poor wettability of this pitch, evident from the low green and baked apparent densities and the compressive strength, is a direct consequence of the high softening point and subsequent poor mixing during green paste manufacture. This effect becomes particularly evident at 20% pitch addition where the baking loss and shrinkage differ markedly from the trend observed at the lower pitching levels. The CO₂ reactivity is, despite the poor physical properties, better than typical and reflects the good quality of the baked pitch coke resulting from its higher anisotropy.

TR-4D (Fig. 4)

The physical properties of anodes made from this pitch are within the range of those measured for typical coal tar pitch based anodes, the only significant exceptions being air permeability, which is about twice the value typically expected and compressive strength which is at the lower end of the range. Although poor air permeability will result in a higher carbon consumption during electrolysis, this is offset to some degree by the lower CO₂ reactivity losses of the binder-matrix.

TR-4DNH

The addition of 7 mass % carbon black has severely affected the physical properties of the test anodes due principally to a blinding effect that has hindered the wettability of the pitch.

CONCLUSIONS

Intevep TR3

Of the four Intevep pitches tested this was found to be the most suitable as the majority of properties were within typical coal tar ranges. Although the compressive strength of the anodes were at the lower end of the range, a paste plant optimization would improve this behaviour. A significant "selling point" for this pitch is the lower optimum content needed in anode manufacture.

Intevep TR4

The TR4 pitch was unsuitable due to its high softening point resulting in inadequate fluidity and subsequently poor mixing.

Intevep TR-4DNH

The addition of 7 mass % carbon black to TR-4DNH was found to have a detrimental effect on the test anode properties.

Intevep TR-4D

The results indicate that the TR-4D pitch is promising although further investigations would be needed into production techniques that could improve its distillation behaviour, mechanical strength and air permeability.

REFERENCES

1. Grjothein, K. and B. J. Welch, "Aluminium Smelter Technology", 2th. edition, Aluminium Verlag Dusseldorf, Germany, chapter 4.
2. The pace consultants Inc. Petroleum Coke Markets Potential. November 1990.
3. R&D Carbon Ltd. Evaluation Program for Intevep Petroleum Pitches. April 90.

TABLE 1. FCC DECANTED OIL CHARACTERIZATION

SPECIFIC GRAVITY	1.078
API	-0.2
SULFUR % WT	2.6
CCR % WT	6.3
SOLIDS, PPM	15
ASH, PPM	41
FLASH POINT, °C	68
KINEMATIC VISCOSITY, cst	
KV @ 38°C	476
KV @ 60°C	118
AROMATICS, % WT	79
DISTILLATION D-1150	
% VOL	TEMP. °C
5	318
30	408
50	436
80	517

TABLE 2. TYPICAL YIELDS AND PRODUCT QUALITY

YIELDS	
GASES	9.3
LIGHT DISTILLATES	21.1
GASOIL	40.8
PITCH	28.8
LIGHT DISTILLATES CHARACTERIZATION	
SPECIFIC GRAVITY	0.8610
SULFUR, % WT	1.36
DISTILLATION:	
IBP	114
10	167
30	231
50	280
90	370
FBP	372
GASOIL CHARACTERIZATION	
SULFUR, %WT	3.8
SPECIFIC GRAVITY	1.1014
VISCOSITIES, cst	
KV @ 60°C	28.5
KV @ 100°C	5.9
FLASH POINT, °C	207.7
DISTILLATION	
IBP	261
10	334
30	366
50	390
90	442
FBP	490

TABLE 3. PITCH PROPERTIES

PROPERTIES	UNIT	COAL TAR PITCH	COMM PET. PITCH	TR-3	TR-4	TR-4D	TR-4DNH
		TYP. RANGE					
SOFTENING POINT METTLER.	°C	100-110	121.7	129.8	148.5	114.5	121.8
VISCOSITY BY 140 °C	cP	3000-6000	n.m	n.m	n.m	10'250	12'720
VISCOSITY BY 160 °C	cP	600-1500	2140	4280	n.m	1952	2590
VISCOSITY BY 180 °C	cP	150-300	406	696	4820	458	676
DISTILLATION 0-270°C	%	0.1-0.6	0.1	1.4	0.5	6.5	6.8
DISTILLATION 0-360°C	%	4-8	8.4	9.8	8.4	17.5	15.0
DENSITY IN WATER	Kg/dm ³	1.30-1.32	1.244	1.240	1.257	1.148	1.151
COKING VALUE	%	54-60	52.8	55.7	58.3	57.2	61.4
WATER CONTENT	%	0-0.2	<0.1	<0.1	<0.1	<0.1	<0.1
INSOLUBLE IN QUINOLINE	%	8-14	0.5	1.0	0.4	0.65	7.9
INSOLUBLE IN TOLUENE	%	28-36	8.5	8.9	8.2	10.0	17.5
ASH CONTENT	%	0.1-0.3					
ELEMENTS							
S	%	0.3-0.5	3.01	2.52	2.77	2.48	2.41
Na	ppm	100-400	110	98	82	70	97
Ca	ppm	20-80	21	25	23	17	38
Cl	ppm	100-300	41	34	30	30	37
Al	ppm	50-200	96	285	232	237	227
Si	ppm	50-200	74	271	276	284	398
Fe	ppm	50-300	63	199	146	166	191
Zn	ppm	100-600	15	17	4	5	5

FIGURE 2. BENCH SCALE ANODE EVALUATION USING PITCH TR3
 PITCH CONTENT: A = 14% B = 16% C = 18% D = 20%

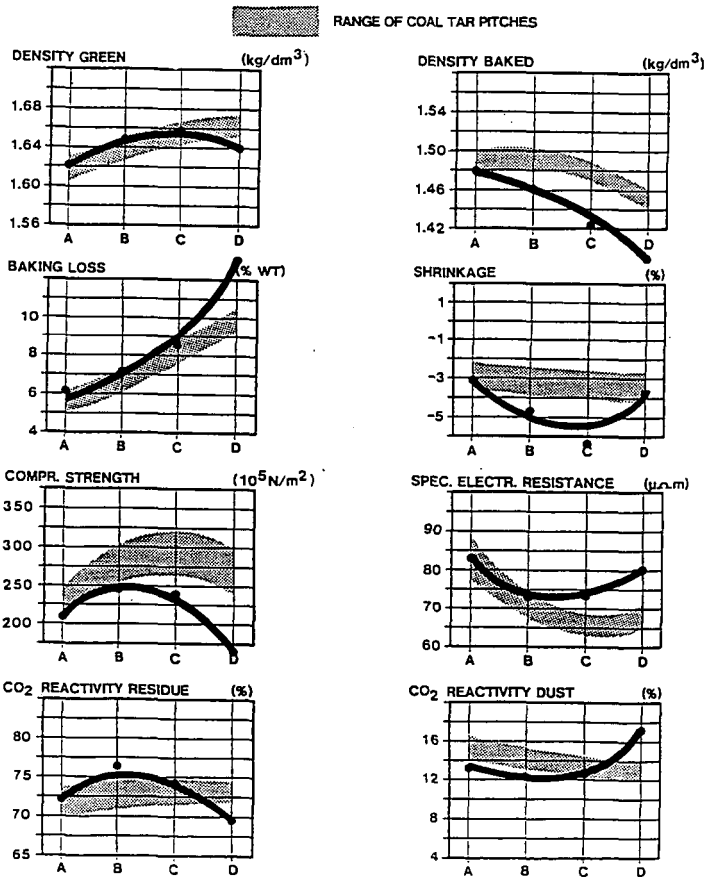


FIGURE 3. BENCH SCALE ANODE EVALUATION USING PITCH TR4
 PITCH CONTENT: A = 14% B = 16% C = 18% D = 20%

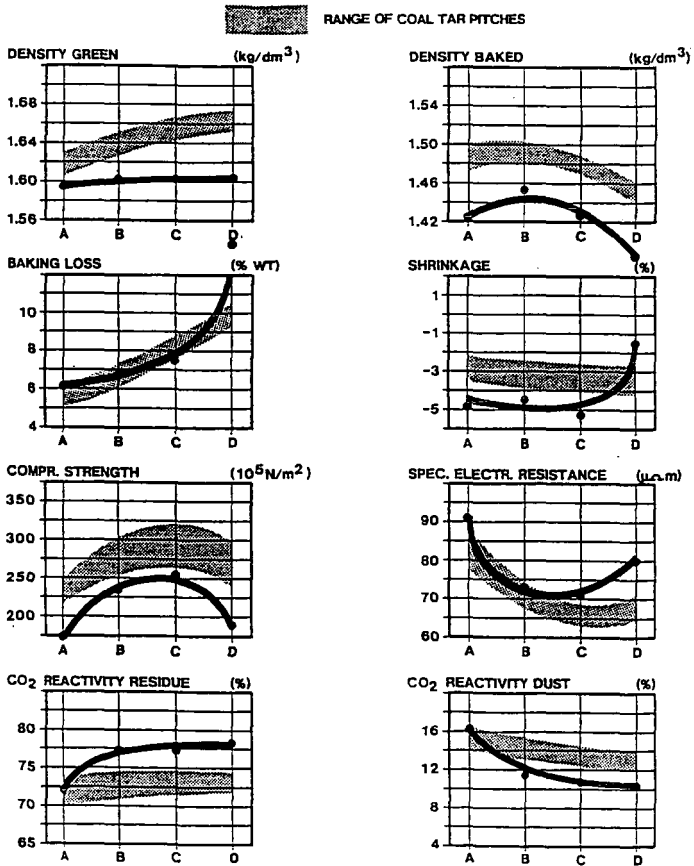
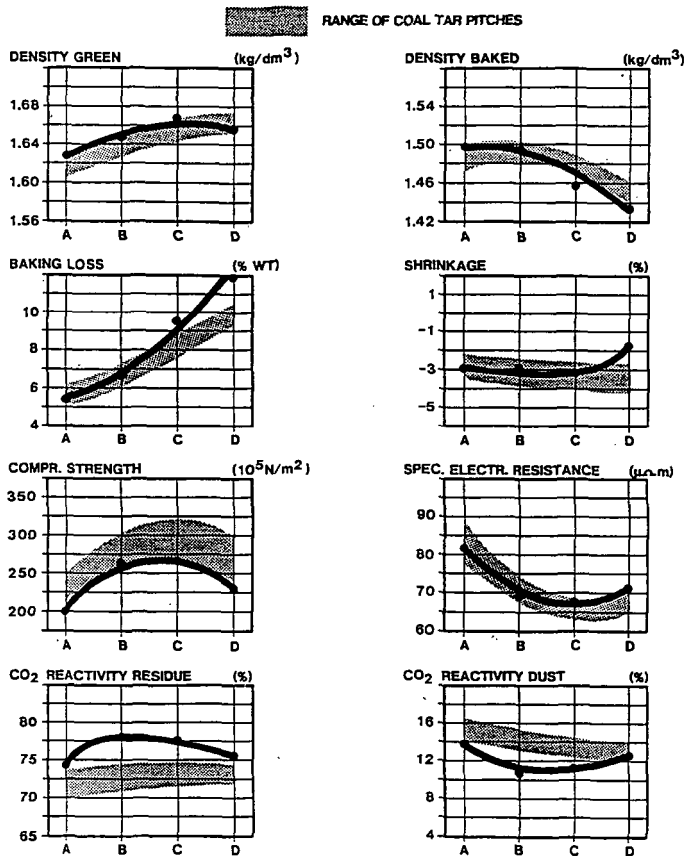


FIGURE 4. BENCH SCALE ANODE EVALUATION USING PITCH TR4D
 PITCH CONTENT: A = 14% B = 16% C = 18% D = 20%



PREDICTING PETROLEUM COKE QUALITY FROM FEEDSTOCK PROPERTIES

Joaquín Rodríguez, Carola Acuña,
Jorge Guerrero and León Velasco
Intevep, S.A.P.O. BOX 76343
Caracas, Venezuela

Keywords: Polarized light microscopy, NMR spectroscopy, coefficient of thermal expansion.

ABSTRACT

A method for predicting petroleum coke quality (Coefficient of Thermal Expansion, CTE) has been developed by correlating feed material properties such as aromatics carbons (wt. %) and optical size texture determined by ^{13}C NMR spectroscopy and polarized light microscopy, respectively.

Correlations used to develop this method are based on characterizations and studies of venezuelan feedstocks such as FCC Decanted Oil, Lube Oil Extract, Flexicoker Recycle Oil and several blends of these materials using the above mentioned analysis, as well as, an evaluation of needle grade coke obtained from the referred feedstocks.

INTRODUCTION

Needle grade coke is a special product obtained from the delayed coking of highly aromatic refinery streams. This special grade coke is used in the fabrication of electrodes for the electric arc furnace in the steel industry. Its a carbonaceous residue of a fibrous nature made up of needle like structures.

Feedstocks used in needle grade coke production are characterized by high aromatic content (>60 wt %), low sulfur content (<1wt %) and a relatively low Conradson Carbon (<10 wt %)¹.

One of the most important properties in assesing needle grade coke quality is the coefficient of thermal expansion (CTE).

In order to determine this property significant amounts of coke are required and pilot plant production of this material becomes necessary.

The fact that coke quality is strongly dependant upon the properties of the feedstock and the operating conditions and therefore on the growth of the mesophase^{2,3} which in turn determines the degree of crystallinity of the final product suggests that it should be possible to predict coke quality from feedstock properties at predetermined operating conditions.

The present paper presents the results of the evaluation of a variety of raw materials as potential feedstocks for needle grade coke production. The evaluation includes feedstock characterization by NMR⁴, observation of mesophase formation and

growth⁵ and pilot plant production, calcining and characterization (CTE) of needle grade coke.

The results establish that there is a relationship between the aromatic carbons in the feedstock and the CTE; and between the optical texture size and CTE.

EXPERIMENTAL

NMR spectra of the feedstocks to be evaluated were obtained from a Bruker 300 MSL spectrometer using deuterated chloroform as solvent and TMS as internal reference (0.0 ppm). ¹³C spectra of the liquid samples were taken at 75.468 MHz and those of ¹H at 300 MHz.

Mesophase growth and optical texture size were observed by polarized light microscopy. Samples placed in a micro cell (Figure 1) were subjected to a heat treatment at temperatures between 430°C and 470°C and a H₂ or N₂ pressure up to 2000 psig.

Additionally the feedstocks were used to produce delayed coke in a 4 litre drum capacity pilot plant with a feedrate between 1500-2000 gr/h, drum internal temp of 400-500°C and two operating pressures (60 and 140 psig).

Green cokes produced were later dried and crushed to 3 mesh in size and after calcined at 850/1250°C.

Several electrode recipes were prepared using the cokes, a coal tar pitch and puffing inhibitors with which 5/8" diameter and 5" long bench scale electrodes were made in order to determine the CTE.

RESULTS AND DISCUSSION

Characterization of the feedstocks evaluated (FCC decanted oil, lube oil extract and flexicoker recycle) are shown in table 1. FCC decanted oil subjected to thermal treatment and observed through polarized microscopy exhibits extended fluid domains.

On the other hand flexicoker recycle tends to yield coarse flow mosaics whereas Lube Oil Extract due to its low aromaticity gives rise to small mesophase spheres that do not generate mosaics.

Mixture of these feedstocks show intermediate behaviour. Optical texture size depends on the heating rate. Tables 2 and 3 show time of mesophase formation, coalescence period and the optical texture size of the feedstock considered, as well as values of CTE of the needle grade cokes produced from such feedstocks. It can be seen that the optical texture size is inversely proportional to the CTE of the cokes. This suggests that feedstocks that give rise to a greater degree of mesophase development yield higher quality cokes that is, less CTE. Figure 2 illustrates this point. This tendency can be accounted for by the fact that greater degree of mesophase development leads to a greater level of alignment in the aromatic layers which later form a microcrystalline structure that resembles graphite.

Furthermore, a relationship was found between the aromatic carbon content of the feedstock as determined by NMR and the quality of the needle coke. This dependence is shown in Figure 3. No relationship was observed between coke quality and the aromatics content determined by HPLC, which suggests that coke quality does not only depend on the amount of aromatic structures but also the type of structure.

CONCLUSION

Feedstocks evaluation by NMR spectroscopy and polarized light microscopy allows for the quality prediction of needle grade cokes produced at pilot plant scale.

REFERENCES

1. Feintuch, H.M. et al., in Handbook of Petroleum Refining, pp. 3-61, McGraw-Hill (1986)
2. Lewis, I.C. and Singer, in Polynuclear Aromatic Compounds, pp. 269-285, ACS (1988)
3. Marsh, H. and Smith, J., in Analytical methods for coal and coal products, Vol. 2, pp. 371-414, Academic Press (1978)
4. Gillet, S. et al., FUEL, 60 (3): 221-225 (1981)
5. Perrota, A.J. et al., High Temp. High Pres., 13(2): 159-166 (1981)

TABLE 1. CHARACTERIZATION OF FEEDSTOCKS

PROPERTY	FCCDO	LOE	FCR
API Gravity	6.9	14.6	6.3
KINEMATIC VISCOSITY			
at 60 °C, cSt	61.9	-	-
at 135 °C, cSt		11.0	45.8
Conradson Carbon, wt%	4.26	1.76	15.6
Sulfur, wt%	1.36	2.60	2.77
HPLC fractions, wt%			
Saturates	26.8	25.6	18.2
Aromatics	67.3	69.2	57.1
Polar aromatics	4.7	5.2	18.2
Asphaltenes	1.2	0.0	6.5
¹³ C NMR, wt%			
Paraffinic	25.00	42.94	37.41
Naphthenic	22.27	24.76	21.16
Aromatic	52.73	29.30	41.43
-protonated	27.75	11.86	15.54
-quaternary	24.98	17.44	25.89
¹ H NMR, wt%			
Aliphatic	73.8	64.6	70.3
Aromatic	26.2	35.4	29.7

TABLE 2. EFFECT OF MIXING FCC DECANTED OIL AND FLEXICOKER RECYCLE

FCC wt%	Mesophase formation min.	Coalescence period min.	Size μm	CTE $10^{-7}/\text{C}$
20 °C/min. (450°C)				
0	2	5	157	4.1
30	6	10	140	7.3
50	9	12	140	7.6
100	>9	> 17	<50	17.3
50 °C/min. (450°C)				
0	2	3	250	4.1
30	10	7	380	7.3
50	16	9	<3	7.6
100	9	13	<50	17.3

TABLE 3. EFFECT OF MIXING FCC DECANTED OIL AND LUBE OIL EXTRACT

Lube Oil wt%	Mesophase formation min.	Coalescence period min.	Size μm	CTE $10^{-7}/\text{C}$
20 °C/min. (450°C)				
0	2	5	157	4.1
30	3	6	150	5.3
50	na	na	na	7.3
100	no	no	no	na
50 °C/min. (450°C)				
0	2	3	250	4.1
30	5	no	80	5.3
50	na	na	na	7.3
100	no	no	no	na

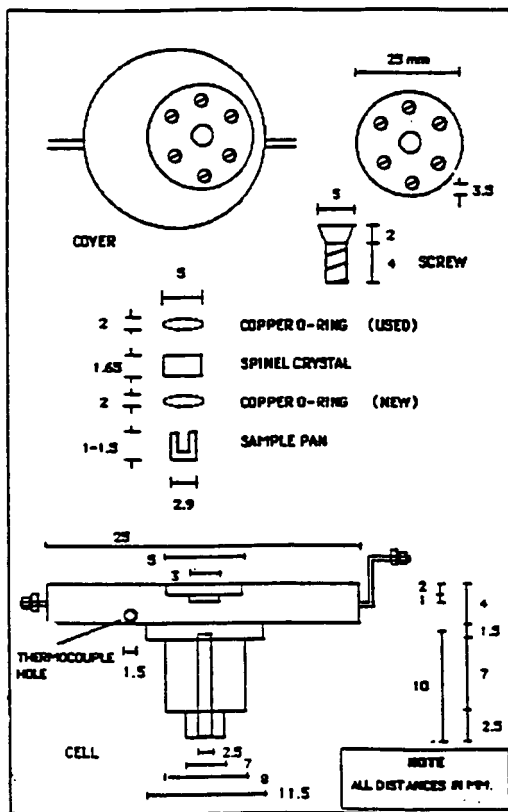


Figure 1. High temperature high pressure micro-cell

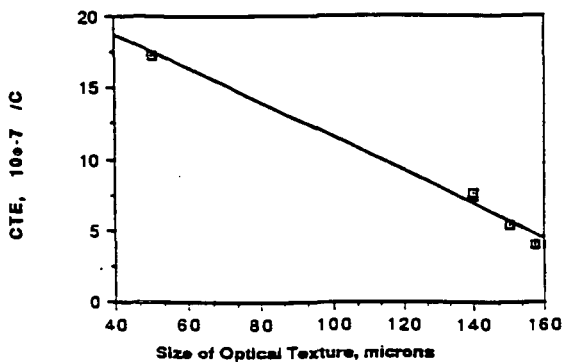


Figure 2.

Relation between Optical Size Texture of mesophase and the Coefficient of Thermal Expansion of cokes

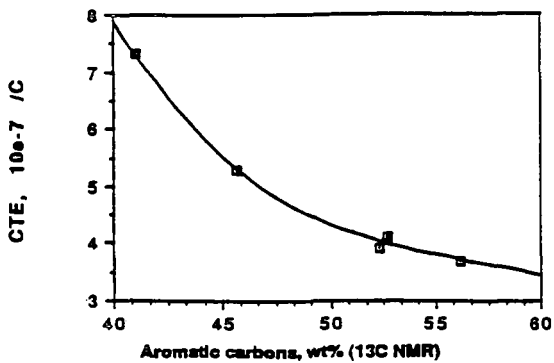


Figure 3.

Relation between NMR characterization of feedstocks and Coefficient of Thermal Expansion of cokes

SELF REDUCED IRON ORE PELLETS USING FLEXICOKE AS REDUCTANT

María Specht
Carlos Seaton and Arianna Morales

INTEVEP, S.A. Apdo. 76343, Caracas, Venezuela
Simon Bolívar University (Dept of Materials
Science). Caracas, Venezuela

INTRODUCTION:

The use of flexicoque as a replacement of higher valued raw materials, has been considered, since the implamentetion of flexicoking technologies for upgrading heavy Venezuelan crude oil would increase the production of this by product.

One of the most promissing alternatives is to use this material as reductant of iron ore, because of the large amount of this mineral in Venezuela and the high demand of reduced iron for steel production.

This work is concerned with the use of flexicoke as solid reducing agent for producing direct reduced iron ore in pellet form and with the evaluation of the product obtained by the fusion of these reduced pellets.

REDUCTION OF IRON ORE USING SOLID REDUCING AGENT:

The direct reduction of iron oxides by carbon has been extensively investigated in recent years. The work done has demonstrated that such process occurs via the gaseous intermediates CO and CO₂. Initially the carbon monoxide is produced by a reaction of carbon with oxygen from the oxide in contact with the carbonaceous materials. This carbon monoxide reduces the oxides, producing carbon dioxide which reacts with carbon to form more CO; thus restoring the reducing potential of the gas phase that allows the reduction to continue. According to Baldwin [1], the chemical reactions associated with the process are as follows:



Previous investigation work related with the reduction of iron oxide with carbonaceous materials: charcoal, carbon, graphite, lignite coke [2, 3, 4, 5, 6, 7 and 8] have reported that the variables of major influence on this type of reduction process are: temperature, carbon content and reactivity of the carbonaceous materials. Also they demonstrated that the rate of reduction, increases with: increasing reduction temperature, increasing carbon percentage and decreasing particle size.

PRODUCTION OF COLD BOND SELF REDUCING PELLETS (SR-PELLETS):

SR-pellets are produced when carbon is incorporated in the mixture with iron ore and binders. Then an internal solid-solid reduction occurs according to the following general reactions [9].

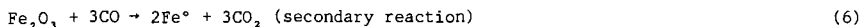


Fig. 1, illustrates the different mechanisms involved in the reduction of a self-reducing pellet and a conventional one reduced with external carbon [9]. Here it can

be seen that the rate and percentage completion of reduction, is higher for the self-reducing pellet than for the conventional pellets with external carbon.

Fig. 2 shows schematically the different steps for producing self-reduction pellets (SR-pellets). The self-reduced pellets can not be hardened thermally, because the reduction process would occur before the temperature for pellet induration is achieved (conventionally, $\sim 1300^{\circ}\text{C}$), since reduction reactions of iron ore by carbon may start at temperatures higher than 600°C . Therefore, SR-pellets must be produced by other pellet hardening processes i.e without firing. Such processes are designated as cold bond pelletizing.

The binders in the cold bond processes play an important role, because they must have the ability to improve green ball formation as well as the mechanical properties of green, dry, and indurated pellets [9]. Four types of binders are evaluated in this work; Portland cement, Ca(OH)_2 , a cellulose base binder called Peridur [13] and SiO_2 (clay).

EXPERIMENTS

Methodology used

The experimental procedure is shown schematically in Fig. 3.

The reductibility of the iron oxide in the presence of flexicoke, was determined experimentally by using a thermogravimetric set up (continuous tests) and the tubular furnace (discontinuous tests) as shown in Figs. 4 (a) and (b), respectively. The removal of oxygen was measured by the loss in weight of the sample, this is known as the Loosing - weight method. By plotting the percentage loss in weight or the lost weight fraction versus time, a measure of the of the reductibility can be obtained.

For the evaluation of flexicoke as a solid reducing agent of iron ore and for determining the optimum mixture for manufacturing SR-pellets, briquettes of 10 mm in diameter and 5 mm height, were prepared by using a compressive strength of 2700 kg/cm^2 . Two parameters were considered in the reduction of the samples, flexicoke percentage and its particle size. The experiments were performed at the same temperature (1050°C). This temperature was selected, since it was found high conversion rate at this temperature when reacting it with CO_2 [12]. Fifteen mixtures of iron ore plus flexicoke were tested, with three types of binders: hydrated lime, peridur and clay. Portland cement was evaluated as binder by making SR-pellets of iron ore and flexicoke [10]. Once was the optimum mixture determined, the effect of temperature on the reduction processes was analysed. Each experiment was run out three times for checking results reproducibility.

The SR-pellets reduction experiments were carried out using an inert atmosphere (argon), and five different temperatures: 950°C , 1000°C , 1050°C , 1100°C and 1150°C . The fraction of weight lost of the reduced samples were determined as a function of the maximum weight loss, in order to compare the behaviour of the pellets reduced at these different temperatures.

The remnant carbon content after reduction was determined by a carbon and sulphur analyser LECO. A qualitative analysis of reduction products, was carried out by X-ray diffraction, using a diffractometer PHILLIPS, model 1840, with the following experimental conditions: 35kv, 20mA, 0,03 \emptyset seg with Ni filter. The metallic iron oxide phases present in the reduced products were determined by Mosbauer spectroscopy. The values for metallic iron obtained by this technique were used to determine metallization percentage (%MET) according to the following relationship:

$$\% \text{MET} = [\text{MFe}^{\circ} / \text{MFe}_{\text{tot}}] \times 100 \quad (9)$$

Where: %MET = percentage of metallization.
MFe° = iron mass.
MFe_{tot} = total iron mass as obtained by chemical analysis.

The mechanical compressive strength (crushing strength) of self-reduced pellets was determined by using a universal mechanical test equipment INSTRON of 500 kg capacity. The fracture surface of reduced products was also observed using a scanning electron microscope (SEM): PHILLIPS model 505. Attached to it a X-ray energy dispersive system (EDAX) and a wave length spectrometer of X-ray (WDAX) for qualitative and semiquantitative analysis.

The characteristics of the raw material used in the present work are shown in Table 1.

RESULTS AND DISCUSSION

FLEXICOKE AS IRON ORE REDUCTANT:

It was found that flexicoke acts as solid reducing agent of iron ore and the reduction rate increases with flexicoke content up to 17% (see Fig. 5). The curve shape indicates that there is an initial high rate of weight lost, and 15 to 30 minutes after the test started the slope of the curve tends to zero. The initial stage of the curve is related to loss of the water contained in the SR-pellets, the pyrolysis of the volatile materials present in the flexicoke and the reduction of hematite to magnetite and magnetite to wustite by CO_(g) generated by the flexicoke gasification, according to Boudouard reaction (4). The second stage of the curve is related to the reduction of wustite to iron. Fig. 6 (a) shows the effect of reduction temperature on the reduction of iron ore, from these curves it can be observed that the higher the reduction temperature, the higher the fraction of weight lost, and hence, the higher the reducibility. Fig. 6(b) shows the effect of reduction temperature on the presence of magnetite, wustite and iron. Also it was found that decreasing flexicoke particle size, increases reduction rate.

MANUFACTURE AND EVALUATION OF COLD BOND SELF REDUCING PELLETS (SR-PELLETS):

Table 2 shows the mixtures used for SR-pellets manufacturing, and also pellets quality before and after reduction tests at 1150°C for 90 minutes. Here it can be observed that the SR pellet manufactured with cement as a binder showed the highest strength 20,4 kg/pellet, although this value is lower than the required for the thermally indurated pellets (320 kg/pellets). The reduced SR pellets showed cracks, peeled surface, double structure (layer-core), and the mechanical strength decreased in 82%.

On the other hand, the SR-pellets with Ca(OH)₂, as a binder, showed an increment of 214% in mechanical strength after reduction. Although this value obtained: 40 kg/pellet, is lower than the required by steel making industry for reduced pellets (60 kg/pellet).

Peridur and SiO₂ binders were used to evaluate the possibility of improving mechanical strength, however no improvements were noted when using them. Therefore the evaluation was focused on SR-pellets with cement and Ca(OH)₂ as binders.

The highest percentage of metalization was obtained for the SR-pellets with Ca(OH)₂ as binder.

STRUCTURAL CHANGES OBSERVED IN SELF REDUCED PELLETS:

The fractured area of SR-pellets with cement, as binder, reduced at 950, 1000, 1100 and 1150°C showed an internal structure of interconnected pores giving a "sponge" like appearance, which indicated high degree of particle decohesion.

Whiskers or fibers of iron emerging from the oxide phases were present (see Fig. 7). The iron fibrous growth tended to be favored in the areas of oxide phases close to flexicoke particles, similar results were reported by Seaton, et al. [8]. When using charcoal as iron ore reducing agent. Internal fusion was also observed (see b in same figure), which may have occurred when the carbon was transferred from the gaseous phase to the reduced iron, producing an eutectic which fusion point is close to 1000°C [11].

Similar morphology was observed in the fractured area of SR-pellets with Ca(OH)_2 as binder, when they were reduced at 950 and 1000°C (see Fig. 8a). This phenomena could be accounted for by a low rate in the reaction of carbon gasification (4) and combined with a decrease in the wustite activity by the presence of calcium oxide, inhibiting iron nucleation [8].

The scanning photomicrograph of the SR-pellet with Ca(OH)_2 , reduced at 1100°C (see Fig. 8b) showed isolated porous in a continuous matrix, indicating a more compact structure (compare with Fig. 8a).

Table 3, indicates, the volumen contraction of pellets containing Ca(OH)_2 as binder and the incidence of whiskers. Here it can be observed that the presence of whiskers is associated with either swelling or low volume contraction of the reduced pellets, and that these whiskers tend to disappear as the massive iron sinterization takes place at longer periods of residence time, and at higher reduction temperatures. Also, from here can be inferred that the strengthening mechanism of SR-pellets is the massive iron sinterization during reduction. If this process does not occur the reduced pellet is highly porous and easily disintegrable, which was the case of the SR pellets with cement as a binder. The lack of massive iron sinterization is associated with the high amount of coarse remnant flexicoke particles, and to phases rich in calcium (from the high percentage of cement used as a binder) which act as barriers for iron nucleation. This lead to iron whiskers growth which are unable to sinterize each with other, promoting swelling and cracks in the reduced pellets.

FUSION TESTS RESULTS:

Table 4 shows the metallic charge patterns used for performing the fusion tests in the induction furnace, and the chemical analysis of the fusion products. If fusion 1 and 2 are compared, it can be seen that the product obtained from fusion 1, contains the double amount of carbon, vanadium and sulphur with respect to fusion 2. This is due to the fact that the remnant carbon content in SR-pellets with cement, is larger, and also that in the manufacture of these pellets a combination of two types of flexicoke (low and high vanadium content) were used.

In general, a relative high carbon and vanadium content could be acceptable, depending on the final use of the pellets, for example: as raw material for foundry (grey iron) or alloyed steels of high carbon content, providing the use of a desulphurizer during fusion process.

The fusions 3 to 7 were performed using only SR-pellets containing Ca(OH)_2 as binder. It can be observed that the amount of carbon and sulphur, increase with the amount of pellets in the metallic charge, except in fusion 7, where the volume of slag generated did not allow good interaction of the added pellets with the liquid phase.

Fig. 9, shows the optical photomicrographs indicating the microstructure of the fusion products, Fig. 9(a) corresponds to fusion 1, the light areas correspond to ferrite which are distributed along boundaries of very coarse prior austenite grains, and as plates within the grains; the matrix is fine perlite, a morphology characteristic of medium carbon steels. Fig. 9(b) corresponds to fusion 2 where can be observed Widmanstätten patterns of proeutectoid ferrite in a matrix consisting of ferrite and fine perlite. This type of microstructure is characteristic of low carbon steels.

CONCLUSIONS:

The results of this investigation lead to the following conclusions:

- Flexicoke acts as solid reducing agent of iron ore and is effective at temperature >1100 °C.
- It is possible to agglomerate the iron ore with flexicoke by using cement, Ca(OH)_2 , clay and perdur as binders, and manufacture cold bond self reducing pellets. The hardening mechanism is the massive iron sinterization during reduction, however these pellets do not fulfill the minimum value required for conventional pellets mechanical properties, because of the lack of a stable skeleton for binding together all the particles and the sufficient strength to support handling and transportation conditions prior to reduction; as well as sufficient compressive strength to overcome the pressure of conventional metallurgical reactors (rotary kiln or shaft type) during reduction process.
- Self reduced pellets with flexicoke as iron oxide reductant can be used as raw material for producing gray iron, or carbon steels.

RECOMMENDATIONS:

An alternative for the reduction of SR-pellets with flexicoke, would be the rotary grid or a rotary open hearth furnace under isothermal conditions with high heating rates that warranties no temperature gradient in the pellets. Under these circumstances the SR-pellets residence time, in the low temperature zones would be diminished and the problems of disintegration by abrasion would be overcome. Fig. 10 shows schematically the suggested process for reducing SR-pellets. But further investigation is required to determine optimum operational conditions.

REFERENCES:

1. BALDWIN, B. G. J. Iron Steel Inst., 179, 101 (1955).
2. OTSUKA, K. and KUNII, D. J. Chem. Eng. Japan, 2, 46, (1969).
3. ABRAHAM, M. and GOSH, A. Iron Making and Steelmaking, N 1, 14, (1979).
4. RAO, Y. K. Met. Trans. B., 8B, 279, (1979).
5. FRUEHAN, R. J. Met. Trans. B., 8B, 279 (1977).
6. GOSH, P. C. and TIWARI, S. N. J. Iron Steel Trans. B. 8B, 171 (1979).
7. SRINIVASAN, N. S. and LAHIRI, A. K. Met Trans. B., 6B, 269, (1975).
8. SEATON, C. E.; FOSTER, J. S. and VELASCO, J. Trans. ISIJ, 23, 497, (1983).
9. GOKSEL, M. A. Agglomeration, ASM, Vol. 1, Chap. 52, 877, 1981.
10. SPECHT, M. I.; MORALES, A. and SEATON, C. "Evaluation of Pellets Manufactured by Lurgi Gm6H Using Flexicoke as Solid Reducing Agent", INTEVEP, S.A., INT-EPTM,00030,87, July, 1987.
11. GOSH, P. C. and TIWARI, S. N. J. Iron Steel Trans. B, 8B, 46, 1969.
12. SEATON, C.; SPECHT, M. I.; ESTELLER, D.; CONTRERAS, G. and MORALES, A. "Potential Uses of Flexicoke in the Venezuelan Steel Industry", Iron Making Conference Proceedings, 1989.
13. From Dreeland Colloids Inc., 1670 Broadway Suite 3335, Denver, Colorado.

Table 1. Characteristics of the raw material used (weight).

Analysis	Flexicoke		Iron ore		Cement Portland		Binders (*)	
	(Bed)	(Filter)					Hydroted lime	
Fixed C	88,4	39,22	Fe ₂ O ₃	94,33	CaO	64,0	CaO	70,00
			Al ₂ O ₃	0,64	SiO ₂	20,0	MgO	0,90
S	2,4	2,3	P	0,065	Al ₂ O ₃	5,0	A ₂ O ₃	0,60
V	1,34	16,22	S	<0,03	TiO ₂	0,3	SiO ₂	1,10
Ni	0,39	0,46	SiO ₂	1,24	P ₂ O ₅	0,1	Fe _{tot}	0,10
Volatile material	3,1	11,6	Fe _{tot}	64,3	Fe ₂ O ₃	2,5		
As h	4,1	30,2			Mn ₂ O ₃	0,1		
High Heating value (Cal/gr)	7305	5265			MgO	1,5		
					Na ₂ O	0,2		
					K ₂ O	0,9		

(*) Peridur is a cellulose base binder (13)
Clay was from Guárico Mines (Venezuela)

Table 2. Mixture patterns for manufacturing SR-pellets (weight %):

Binders	13,2 cement	2,0 Ca(OH) ₂	0,08 Peridur	0,9 SiO ₂
Iron ore	65,8	80,77	82,43	81,67
Flexicoke	5,3 (bed)	17,23 (bed)	17,49 (bed)	17,34 (bed)
	15,8 (filter)	-	-	-
Hardening time	7 days	-	-	-
Crushing Strength (kg/pellet)	20,4	1,78	1,64	1,60
Reduction results: (argon atmosphere at 1150°C).				
% Fe°	96,9	82,94	49,82	36,16
% Metalization	75,9	89,90	55,17	45,90
% Remnant Carbon	9,7	2,00	-	-
% FeO	13,0	6,27	26,02	11,45
Crushing strength (kg/pellet)	3,7	40	-	-

Table 3. Incidence of iron whiskers and volumen contraction percentage for reduced pellets containing Ca(OH)₂ as binder.

Reduction temperature (°C)	Residence time (min)	Presence of iron whiskers		Partial volume changes percentage
		yes	no	
950	5	x		0.65
	60	x		-13.58
	90	x		3.56
1000	5	x		-7.22
	60	x		6.91
	90	x		13.34
1050	5	x		1.73
	60		x	25.69
	90		x	34.69
1100	5	x		-6.23
	60		x	27.82
	90		x	46.06
1150	5	x		-4.38
	60		x	50.68
	90		x	51.16

Table 4. Metallic charge patterns for fusion tests and chemical analysis of fusion products.

		Fusions							
Metallic charge pattern	Self-reduced pellets	1 (*)	2 (**)	3 (**)	4 (**)	5 (**)	6 (**)	7 (**)	
		(weight %)	13.1	13.1	15	15	30	30	45
		(g)	500	500	522	522	867	867	878
		Scrap (Steel SAE 1010)	3316.2	3316.2	3048	3048	2036	2036	2968
	(g)								
Elements									
Chemical composition of fusion products (Weight %)	C	0.51	0.25	0.60	0.37	0.64	0.53	0.03	
	S	0.13	0.09	0.09	0.08	0.22	0.23	0.29	
	Mn	0.20	0.12	0.29	0.16	0.14	0.20	0.05	
	Ni	0.06	0.04	0.04	0.04	0.04	0.05	0.05	
	Si	0.03	0.06	0.09	0.08	<0.01	0.05	<0.01	
	V	0.15	0.03	0.04	0.05	0.08	0.08	0.04	
	P	0.03	0.02	0.03	0.02	0.03	0.03	0.04	

* Self-reduced pellets containing cement as binder

** Self-reduced pellets containing Ca(OH)₂ as binder.

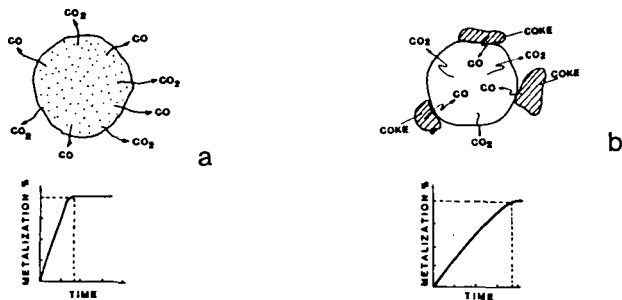


Fig. 1. (a) Self reducing pellet. Reaction (5) and (6) occurs internally.
 (b) Conventional pellet with external carbon. Reaction (5) occurs at the pellet-carbon contact area and (6) inside the pellet by diffusion.

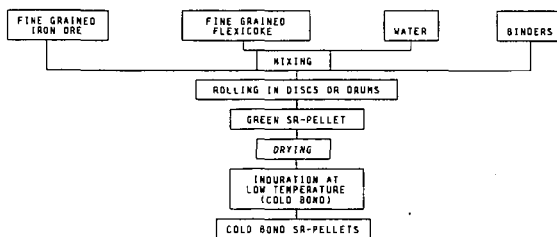


Fig. 2. Steps for producing cold bond self-reduced pellets.

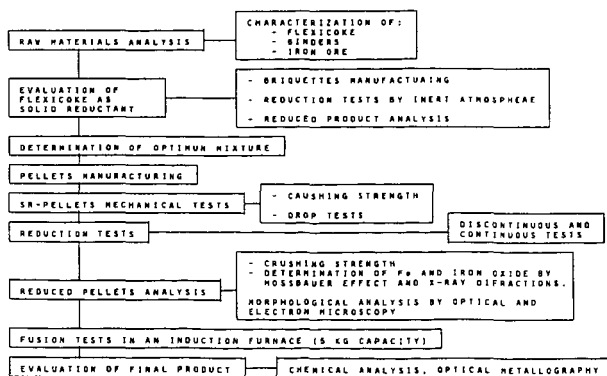


Fig. 3. Methodology used.

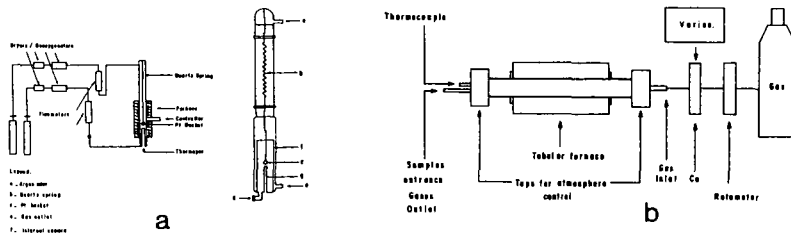


Fig. 4. (a) Thermogravimetric set up for continuous tests
(b) Tubular furnace for discontinuous tests.

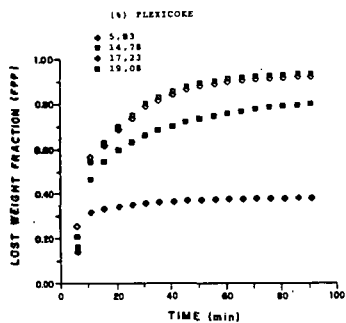


Fig. 5. Effect of flexicoke content in the reduction of iron ore.

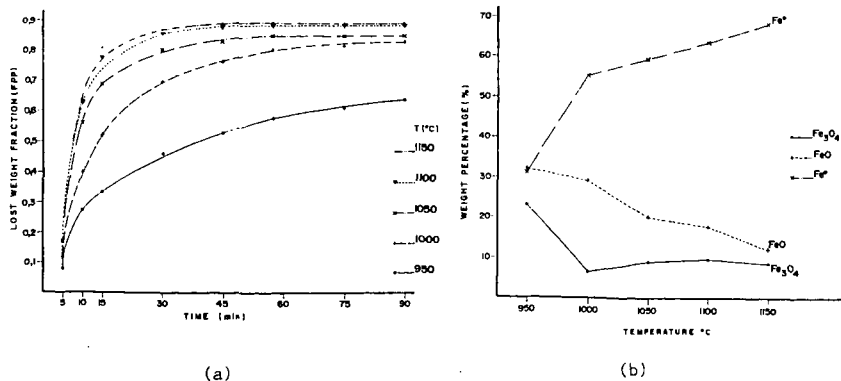


Fig. 6. Effect of temperature on (a) reduction rate (b) the presence of magnetite, wustite and iron.

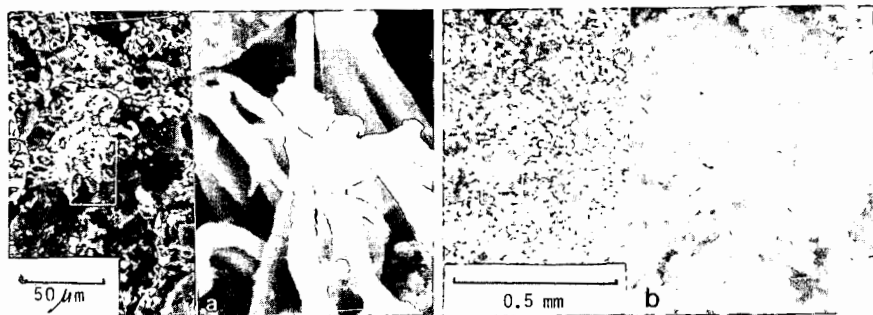


Fig. 7. (a) Scanning photomicrograph showing whiskers of iron, found in reduced pellets containing cement as a binder. (Reduction temp. 950°C).
 (b) Scanning photomicrograph showing internal fusion when these pellets were reduced at 1150°C.

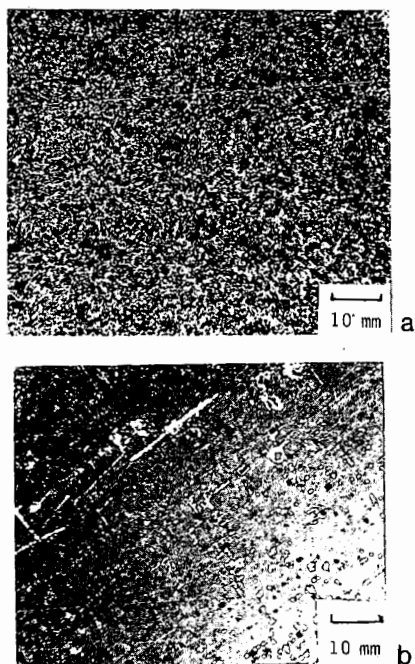


Fig. 8. SR-pellet containing Ca(OH)_2 as a binder. (a) reduction temp. 950°C (b) 1100°C.

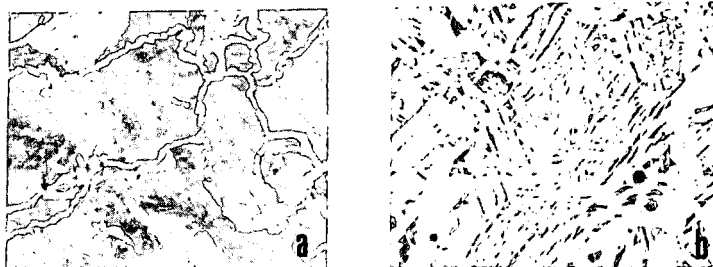


Fig. 9. (a) Optical photomicrograph of fusion 1 (100x).
 (b) Optical photomicrograph of fusion 2 (100x).

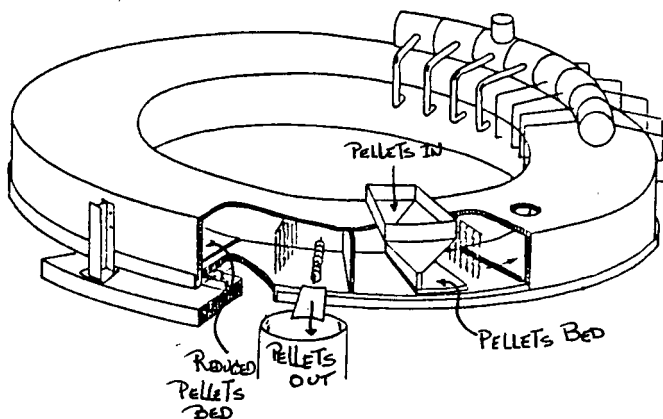


Fig. 10. Schematic view of a rotary open hearth furnace.

FLEXICOKE APPLICATIONS IN THE VENEZUELAN STEEL MAKING INDUSTRY

Druso Esteller SIDOR (Centro de Investigación). Matanzas, Edo. Bolívar, Venezuela
María Specht INTEVEP, S.A. Apdo. 76343, Caracas, Venezuela

INTRODUCTION:

In 1983 the oil refinery of LAGOVEN in Amuay installed a noncatalytic conversion process of heavy feedstock called Flexicoking. The plant has been in operation for seven years producing a by product known as flexicoke, at an approximate rate of 300 metric tons per day. As a result, approximate 400 thousand metric tons of solid are currently stored, posing serious problems of solids waste disposal. The flexicoke has a high carbon content, low volatile material and high heating value which makes it attractive for metallurgical applications. In 1987 a research group conformed by SIDOR (Venezuelan Steel Making Plant), INTEVEP (Venezuelan oil research institute) and LAGOVEN started activities oriented to investigate the different possibilities of flexicoke metallurgical applications. Among the possibilities studied were: flexicoke as pyroconsolidating agent, (added during pelletizing) and as foaming slag promoter for steel electric arc furnaces. The work reported here has been performed at laboratory, pilot plant and industrial scales. The laboratory work dealt with the characterization of the flexicoke. The pilot plant work dealt with the production of iron ore pellets using flexicoke as an additive to improve the pyroconsolidating process and the mechanical behaviour of the iron oxide pellets. And the industrial work dealt with the evaluation of flexicoke as a foaming slag promoter.

EXPERIMENTAL PROCEDURE:

The experimental procedure followed in this work is shown esquematically in Fig. 1. The main characteristics of the flexicoke used in this work is shown in Table 1. If this material is compared with the metallurgical coke, used by SIDOR (see Table same) it can be observed that the main difference is the sulphur content which may impose limitations to flexicoke applications in the steel making industry. The main objective of the investigation was to determine up to which level flexicoke could substitute metallurgical coke.

Besides the chemical and physical analysis of the flexicoke given in Table 1, a morphological characterization and element distribution was performed by using scanning and transmission microscope analysis in order to have a better understanding of flexicoke behaviour in these particular metallurgical applications.

In order to evaluate flexicoke as pyroconsolidating agent, the procedure shown schematically in figure 2 was followed. The chemical analysis of the iron ore, dolomite, hydrated lime and sand used are indicated in Table 2.

The mixture patterns are given in Table 3. It was added 8% of water to the mixture and pelletized in a 120 cm diameter disc at 14 rpm, this configuration has a pellet production of 60 kg/h. During pelletizing more water was added up to achieve 10% in the pellet. The compression strength and drop resistance were the two parameters evaluated in the product obtained (ie, green pellet). The drop resistance test consists of register the number of times a pellet drops from 46 cm height before it presents cracks. The reported value is often the mean value among 10 pellets. The compression strength, also called crushing strength is the force applied on a pellet up to it breaks, it is generally reported as kg/pellet.

The pellets were burnt in a pot grate. The temperature ranged between 1260°C and 1320°C; for 30 to 45 minutes. The parameters considered for the burnt pellets evaluation were compression strength, porosity, drum abrasion index and pellet

reducibility. The criteria of acceptance or rejection of these pellets were the same considered by SIDOR for their conventional iron oxide pellets (ie, with no carbon addition). The reducibility tests were performed in a vertical reactor when 500 g of burnt pellets were heated up to 850°C in a N₂ atmosphere. When achieved this temperature a reducing atmosphere composed of CO, CO₂, H₂, H₂O was run for 90 minutes. During this period the loss weight fraction was recorded to calculate the metallization percentage according to the following equation:

$$\% \text{ Met} = (\text{iron mass/total iron mass as obtained by chemical analysis}) \times 100.$$

The drum abrasion index was determined by reducing 500 g of burnt pellets at 550°C for 2 h in a rotary tubular furnace (Linder type). The heating up and cooling down of the sample was performed with a flow of N₂. The cold reduced sample was screened and the percentage < 6,35 mm was taken as the drum index, according to SIDOR, this must be less than 10%.

For the evaluation of flexicoke as foaming slag promoter the procedure shown in figure 3.

The slag in the steel making electric arc furnace has not only the function of trapping steel impurities but also as thermal barrier. The heat introduced inside the furnace is from typically three carbon electrodes arc, where temperatures higher than 3500°C are generated. This is much higher than the melting point of the furnace refractory lining. Therefore, after the furnace metallic charge is melted, the furnace sidewalls are exposed to this intense radiation except for the portion of the arc that can be submerge below the slag cover that is created on top of the molten metal. The common practice is to add CaO not only for sulphur and phosphorous removal, but for covering the arc as much as possible.

In order to increase SIDOR electric arc furnace operability and decrease refractory consumptions refrigerated panels were installed on the outside walls of the furnaces, this modification implies the use of a foaming slag promoter. When carbonaceous materials such as graphite, metallurgical coke, lignite coke, etc, react with the ferrous oxide contained in the slag, CO gas is generated, the entrapped CO bubbles tend to increase the slag volume, covering in this manner the electric arc and dissipating the heat radiation that erode the refractory lining.

Previously, SIDOR tested fine metallurgical coke (mean particle size approximately 1 mm) by injecting it through the system showed schematically in figure 4 but the usage of this material implied high consumption of valves, hoses and conexions due to its high abrasivity. Taking this into consideration, it was decided to test with flexicoke. The parameters considered during the evaluation were: operability of the injection and remnant sulphur content in the steels, since flexicoke has a sulphur content of 2,6% (62% higher than metallurgical coke).

120 metric tons of flexicoke were charged to a silo of 150 tons capacity through an air pneumatic system, at a pressure of 6 kg/cm² by a hose and pipe of 101,6 mm diameter. The flexicoke was injected on the incipient slag already formed in the electric arc furnace due to the melting of the initial metallic charge. Two electric arc furnaces were used one of 150 tons of steel capacity, where carbon steels for bars are produced, here the maximum sulphur content in the steel is 0,030%. The other, was 200 tons of steel capacity where carbon steels for slabs are produced, here is programed the production of steels with maximum sulphur content of 0,010%; 0,015% and 0,025%. Approximately 1 or 2 tons of flexicoke per steel heat where injected. A total of 85 steel heats were evaluated.

RESULTS AND DISCUSSION

CHARACTERIZATION OF FLEXICOKE:

The flexicoke is formed during thermal cracking of the heavy residues. The break down of the large hydrocarbon molecules occurs at the surface of the heated solid particles (seed). As a result, light hydrocarbons are produced and the seeds grow in size due to the continuous deposition of carbon, sulphur and metallic compounds: vanadium and nickel. A fraction of these particles stay within the reactor and the heater of the flexicoking unit, exiting the process at the elutriator when they reach an approximate mean size of 100 microns. This fraction constitute the bed coke particles and represents 80% of the total flexicoke production, their typical shape is shown in figure 4 as, can be seen, they are rounded with smaller protuberances on their surface. The inner structure of the bed coke is shown in figure 4b where also can be observed, the metals and sulphur distribution in the particle. Notice the onion like structure produced by continuous deposition of heavy, inorganic and organic substances on the solid substrate during the reactor-heater, heater-reactor cycle. Also, it can be observed that sulphur and nickel are homogeneously distributed in the particle, while vanadium tends to concentrate in the inner of the particle. The sulphur is present as organic compound as it is revealed by the transmission electron micrograph in figure 5.

FLEXICOKE AS PYROCONSOLIDATING AGENT:

Table 3 summarizes the results obtained when using flexicoke as an additive in the manufacture of iron oxide pellets. Here, it can be observed that pellets mechanical properties have increased with the addition of flexicoke up to 1%. After it, the mechanical properties decrease abruptly.

Figure 6 (a) and (b) show that the production rate and the productivity of the pelletizing process increases with additions of flexicoke up to 1%. SIDOR plans to increase the pellet plant production from 6,6 million tons/year up to 8,0 million tons/year. Flexicoke additions to pellets manufacturing would help to increase the productivity of this plant with minor equipment modifications, that would represent the installation of a flexicoke feeder. This represents to SIDOR a consumption of 80 thousand tons/year of flexicoke.

FLEXICOKE AS FOAMING SLAG PROMOTER:

The operability of the injection system was 100%, after being used 120 tons of flexicoke, a visual inspection of the valves, hoses and conexions revealed no erosion of the internal parts.

The flexicoke was injected during the fusion period, parallel to reduced sponge iron feeding. The optimum rate of injection was 30-40 kg/min. With this value the "swelling" of the slag was continuous improving furnace operation and decreasing noise level. At higher flexicoke injection rates, explosion between the electrodes and incontrollable flames were observed that led to decrease the furnaces between working power and the feeding rate of sponge iron.

With respect to the sulphur and carbon transference from the slag to the molten steel due to flexicoke injection; it was found that in the 150 tons capacity steel making electric arc furnace, 30% of the heats evaluated, the sulphur increments were from 0.001 up to 0.007%. The distribution of these sulphur increments in the steel heats are indicated in figure 7. In the 70% of the heats no sulphur increments were detected, on the contrary, it tend to decrease due to the simultaneous addition of CaO.

The carbon content was also evaluated, but in the 92% of the heat, no increments were detected, mainly because the flexicoke injection was on the incipient slag and flexicoke low density and high reactivity did not allow to get into the molten steel.

In the 200 tons steel capacity electric arc furnace, 66% of the heat evaluated showed increments from 0.002 up to 0.008 of sulphur. The distribution of these sulphur increments are indicated in figure 1, where it can be observed that 61% of the heats showed sulphur increments less than 0.004%. Since in this furnace, steels with more sulphur restrictions are produced, it was recommended to inject flexicoke for steels with maximum sulphur content of 0.025%. For those steels with maximum sulphur content of 0.015% the injection of flexicoke should be only during first stage of fusion period. And for those steels with maximum sulphur content of 0.010% not to use flexicoke as foaming slag promoter.

The potential consumption of flexicoke for this particular application in SIDOR is 31 thousand tons/year (11 thousand tons for 20 tons steel capacity electric arc furnace and 20 thousand tons for the 150 tons steel capacity furnace).

Only in this two applications 121 thousand tons of flexicoke per year has to be handled and transport through 18000 km distance from LAGOVEN Amuay to SIDOR through marine transportation. Although there is proven technical feasibility of using flexicoke in the steel making industry. The transportation of high tonnage of this material with 100 micros mean particle size is critical, due to powder emissions to the atmosphere. The handling and transportation involves pneumatic systems increasing its costs. The evaluation of agglomerate flexicoke in briquettes is considering now in order to diminish transportation costs and reduce environment impact. These results will be published later on.

CONCLUSIONS:

Flexicoke can be used in the venezuelan steel making industry as pyroconsolidating agent for iron oxide pellet manufacturing, improving its mechanical strength, level of porosity and reducibility when added up to 1%. The pellet plant production and productivity is also increased with flexicoke additions.

Flexicoke can be used as foaming slag promoter in the steel making electric arc furnace, but its sulphur content restricts its application to steel production of 0.025% - 0.030% S maximum.

Flexicoke can partially substitute metallurgical coke in these particular applications. But the handling and transportation of this material with such a fine particle size remains a critical point.

RECOMENDATION:

An economical study must be performed in order to evaluate the investment costs for handling and transportation of flexicoke in its original particle size and if it comparable to metallurgical coke price in powder form. Also the option of agglomerating flexicoke in briquettes must be considered from technical and economical point of view.

Table 1. Characteristics of flexicoke and metallurgical coke (traditionally used by SIDOR).

Analysis	Flexicoke (Bed coke)	Metallurgical coke
%C	91,7	88,0
%S	2,6	<1,0
%V	1,58	-
%N	0,36	-
Volatile material	2,6	<3,0
Ash	3,3	40
Density	1,89	-
Heating value (cal/g)	7305	7337
Mean particle size	100 microns	>3mm

Table 2. Chemical analysis of iron ore, binders and other additives.

Analysis (w%)	Iron ore	Dolomite	Hydrated lime	Sand
Fe _{tot}	66,21	2,11	2,13	0,728
SiO ₂	1,34	4,30	1,53	95
CaO	0,03	31,96	63,68	0,61
MgO	0,02	15,44	2,83	0,11
Al ₂ O ₃	0,51	0,33	0,32	1,46
P	0,035	-	-	-
S	-	-	-	-

Table 3. Mixture patterns (weight %).

Flexicoke	Iron ore	Dolomite	Hydrated lime	Sand
0	94,96	2,72	1,89	0,73
0,5	94,51	2,84	1,89	0,76
1,0	96,51	2,84	1,89	0,76
1,5	94,51	2,84	1,89	0,76
2,0	94,51	2,84	1,89	0,76

Table 4. Summary of the results obtained when using flexicoke as an additive for iron oxide pellet production.

% Flexicoke	Green pellets		Burnt pellets			
	Crushing strength (kg/pellet)	Crushing Strength (kg/pellet)	Abrasion Index	Drum Index	Porosity	Reducibility K(10 ⁻² /min)
0	2.45	221	5.26	91.20	15.2	2.6
0.5	1.97	321.3	4.78	93.10	20.49	2.85
1.0	1.80	375.0	4.75	93.54	19.43	3.25
1.5	2.27	144.67	5.19	92.31	-	-
2.0	2.6	100.5	5.49	87.96	-	-

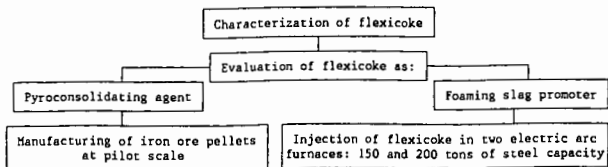


Fig. 1. Experimental procedure.

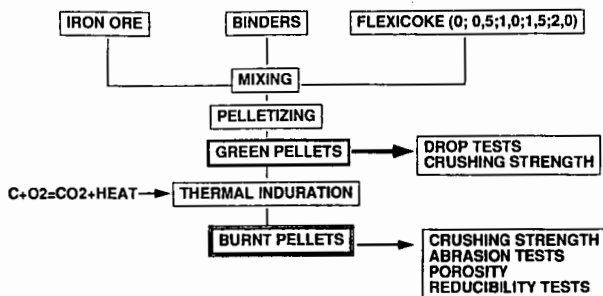


Fig. 2. Procedure followed for manufacturing iron ore pellets with flexicoke as pyroconsolidating agent.

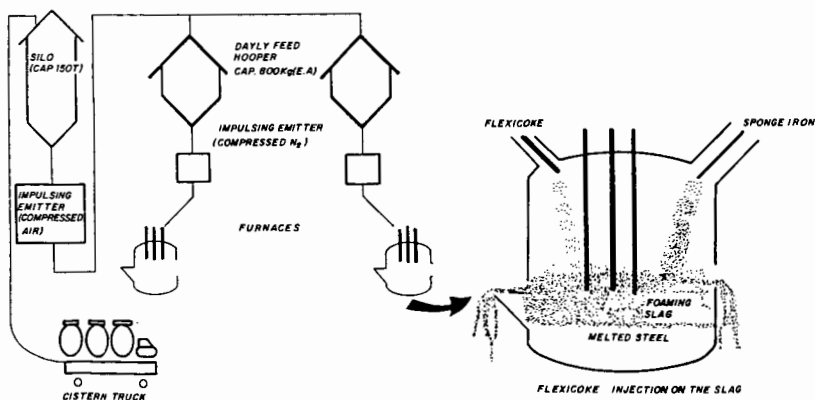


Fig. 3. Procedure for evaluation of flexicoke as foaming slag promoter.

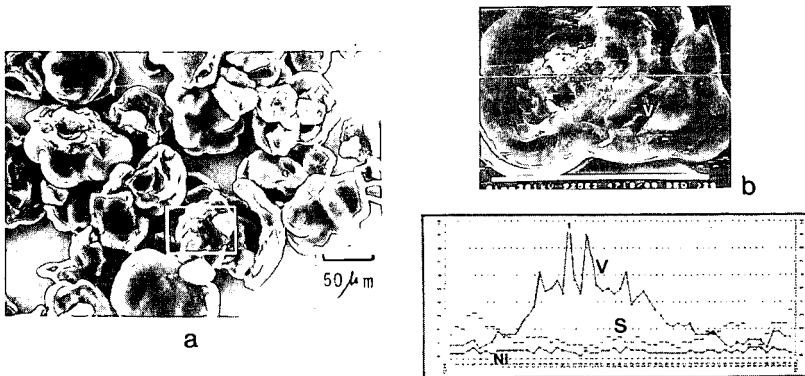


Fig. 4. (a) Scanning photomicrograph of flexicoke (bed coke). (b) V, Ni and S profile. On the photomicrograph the vanadium concentration profile is superimposed.

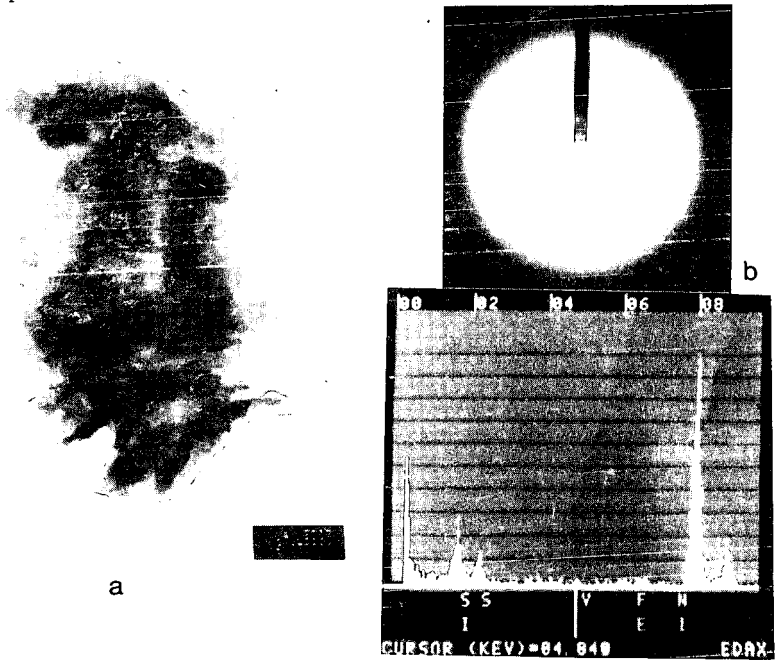


Fig. 5. Transmission photomicrograph of a bed coke particle (a). Diffraction pattern of the organic sulphur compound (b).

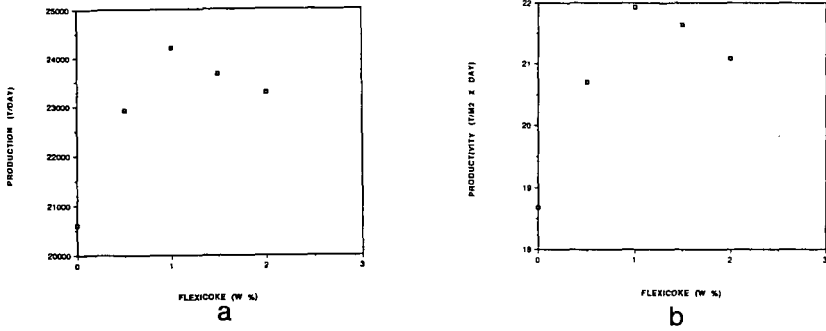


Fig. 6. (a) Production behaviour with flexicoke additions (b) Productivity.

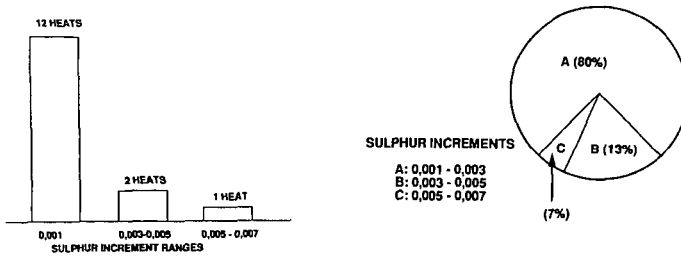


Fig. 7. Distribution of sulphur increments in the evaluated steel heats produced in the electric arc furnace 150 tons of steel capacity.

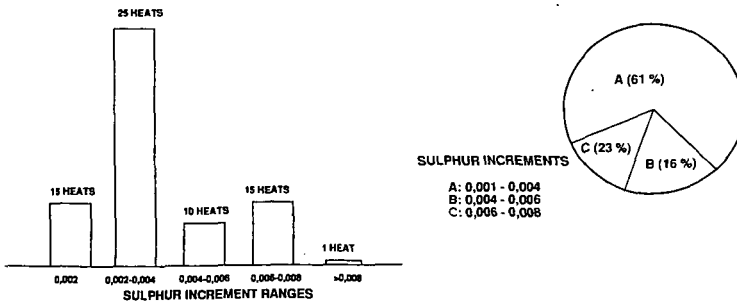


Fig. 8. Distribution of sulphur increments in the evaluated steel heats produced in the electric arc furnace 200 tons of steel capacity.

¹H PULSED SOLID-STATE NMR T₂ RELAXATION STUDIES OF MACROMOLECULAR STRUCTURES OF ARGONNE PREMIUM COALS

X. Yang, A. R. Garcia, J. W. Larsen, and B. G. Silbernagel
Exxon Research and Engineering Company, Annandale, NJ 08801

Keywords: Coal Structures, NMR Relaxation, Argonne Premium Coals

Abstract

NMR studies of free induction decay (FID) have been made for as received and dried samples of North Dakota, Illinois #6 and Pittsburgh #8 coals.

Modifications of the NMR measurement and data treatment lead to an unambiguous separation of the FID signal into three components: two gaussians and one lorentzian. The two gaussians can be related to the macromolecular structures of coal, and their relaxation behaviors are comparable with model polymer systems. The lorentzian is almost entirely due to absorbed water, and the water content determined for the coals as received agrees very well with those reported using other methods.

High vacuum dried coal samples are also studied, and the results are compared with those of as-received coals. The drying is very effective, evidenced by almost complete loss of the lorentzian component. Interestingly, neither T_2 nor $I_2(0)$ is changed after drying, indicating that the drying process does not have a damaging effect on coal structures.

Introduction

The determination of moisture in coals, the investigation of effective ways for coal drying, and the evaluation of the effect of the drying process on coal structures are both of fundamental importance in coal science and of commercial value in industry applications.

Several experimental methods have been developed in the analysis of moisture in coals, e.g., ASTM (1) and ¹⁸O isotope dilution (2). NMR relaxation measurement has been used for a long time in water quantification in coals (3). A recent work by Wroblewski et al. (4) using ³¹P NMR relaxation technique not only provided a new method for coal moisture quantification, but also presented an excellent review and comparison among different techniques and results in the literature on coal moisture determination.

Coal drying is often the first step in coal experiments and coal treatment both in laboratory and industry scale. However, contrary to the studies of wet coals, much less work has been done for dried coals. Although both wet and dried coals were

studied using solid-state NMR a long time ago (5), much of the attention lately have been given to the kinetics of the drying process (6). In other words, there is a need of a systematic evaluation of the effectiveness of various drying methods, and a investigation of the impact of the drying processes on coal structures.

Recently, we have conduct a series of experiments on as-received, dried (in different ways), and solvent swelled Argonne Premium coals using pulsed solid-state NMR techniques (7). Here, we present part of these results, i.e., ^1H NMR T_2 relaxation measurement of as-received and high vacuum dried Illinois #6, Pittsburgh #8 and North Dakota coals. The main purpose of this paper is to demonstrate:

- (1) a new method for coal moisture quantification,
- (2) a establishment of the relationship between NMR relaxation behaviors and coal structures, and
- (3) an evaluation of the effectiveness of drying, and its impact on coal structures.

Experimental

The as-received samples were prepared by directly transferring well-shaken 100 mesh Argonne premium coals from the original ampules to a 5 mm NMR tube under nitrogen atmosphere. The dried coal samples are prepared using high vacuum pumping at about 1×10^4 torr for 48 hours. The NMR tube was sealed under a vacuum of 1×10^2 torr while the sample was frozen with liquid nitrogen. The sealed tube is about same length as that of the NMR probe coil (2 cm), and about two-thirds of it is filled with the sample.

The relaxation measurements were carried out on a Bruker MSL-360 spectrometer operated at 360 MHz. A two-pulse (the output of the RF pulse is about 1kW) $90_x - \tau - 90_y$ solid-echo sequence was used in order to get the entire FID. The signal is recorded by a Bruker BC-131 transient digitizer with a sampling speed of $0.2 \mu\text{s}$. The data was stored in an Aspect 3000 computer and treated with the Lotus-123 data spreadsheet. The parameters used in the measurement, e.g., pulse width D1, pulse spacing τ , repetition time D0, and number of scans NS were systematically optimized, and the typical values used in the data collection are $1.0 \mu\text{s}$, $4.0 \mu\text{s}$, 6s and 512 for D1, τ , D0 and NS respectively.

Effort was made to shim the NMR magnet to reduce the inhomogeneity as much as possible. With liquid cyclohexane, the line width measured is less than 100 Hz.

A Kel-f probe base was made to reduce the background proton signal to about 0.3% relative to the intensity of dried coals (the original Bruker probe base gives a background proton signal of about 4% due to absorbed water).

Results and Discussion

The coal structure is complex. The protons measured by ^1H NMR can be of different structural origins. In terms of the free induction decay, these 'different' protons can relax to equilibrium by different mechanisms and at different rates. Thus, a proper deconvolution of the FID into different components is crucial, and also valuable, in understanding coal structures. Following, a brief discussion of the fitting routine used in the present experiment is given.

In this work, a step-by-step least-linear-square analysis of the natural logarithm of the FID intensity was used to deconvolute the FID signal. For both as-received and dried coals, the FID signal can be fitted best by minimum of two gaussian and one lorenzian functions:

$$I = I_{g1}(0) \text{EXP}[-(t/T_{2g1})^2/2] + I_{g2}(0) \text{EXP}[-(t/T_{2g2})^2/2] + I_l(0) \text{EXP}(-t/T_{2l}) \quad [1]$$

where T_2 is the transverse relaxation time and $I(0)$ is the intensity extrapolating to $t=0$ for any one of the components. The subscriptions g and l abbreviate gaussian and lorenzian respectively.

It was found previously (8) that, by using a nonlinear-least-square fitting method, the FID signal can be fitted by either two gaussians and one lorenzian or two lorenzians and one gaussian (those authors chose the later). However, we find that our fitting procedure provides an unambiguous deconvolution of the FID signal into two gaussians and one lorenzian, as demonstrated in Figure 1 for as-received Illinois #6.

In Figure 1(A), the long decaying component is clearly a lorenzian function. After subtracting the lorenzian component, the natural logarithm of the rest of the signal is plotted in Figure 1(B) as a function of t (lorenzian) and in Figure 1(C) as a function of t^2 (gaussian). The lorenzian fitting in Figure 1(B) for the second component would lead to an erroneous extrapolation to $t=0$, while the gaussian fitting in Figure 1(C) not only gives a reasonable value to $I_{g2}(0)$, but also leads to an almost-perfect gaussian fitting for the last component in Figure 1(D).

All the measured relaxation parameters defined in Equation 1 are listed in Table 1 for both as-received and dried coals. By inserting the values of Table 1 into Equation 1, it can be easily verified that the three components are indeed well separated in each of their time regions. Generally, the accuracy in determination of the relaxation time T_2 is greater than that of $I(0)$ since the former is derived from the slope of the plots as showed in Figure 1, while the later is obtained from the extrapolation to $t=0$ where fluctuation at the beginning of the decay could cause more uncertainty. For the dried coals, uncertainty in both T_{2l} and $I_l(0)$ can be even higher since water concentration in dried coals is so low. Nevertheless, the accuracy in present experiment is good enough for the following discussions.

From Table 1, it can be seen clearly that water has a profound effect on the relaxation dynamics of coals, mainly the lorenzian component. A slow lorenzian decay is usually due to protons with high isotropic rotational mobility. The fact that the lorenzian component for the coals as received is almost completely gone after drying leads to a speculation that this lorenzian component is entirely due to the contribution from physically absorbed water protons. This speculation is strengthened by the fact that the weight percentage of water in coals $W\%$, derived from $I_t(0)$ in the present experiment, compares very well with those obtained using other established methods for coal moisture determination. The comparison is made in Table 2, where the literature values of $W\%$ are listed and compared with ours derived from $I_t(0)$ using the following equation:

$$W\% = \frac{I_t(0) \times 18/2}{I_t(0) \times 18/2 + [100 - I_t(0)] / H_{\text{coal}}} \quad [2]$$

where H_{coal} is the weight percentage of proton in dried coal obtained from elemental analysis (1). Thus, the ^1H NMR relaxation measurement not only serves for understanding coal structures, but also provides a new method for quantitative determination of moisture in coals.

It is known that strongly coupled rigid-lattice structures usually give a FID signal of gaussian shape (9). The coal structure, which is represented by the two gaussian components, seems indeed a tight one. As shown in Table 1, neither wetting nor drying has a significant effect on the structure, which evidenced by the fact that almost same values of T_{2g} and $I_t(0)$ are obtained for both as-received and dried coals.

The shorter time gaussian component is dominant, accounting for more than 90% of the FID signal, and its T_2 values are nearly same for all of the three coals. It has been proposed that the coal structure consists mainly of a three-dimensional cross-linked polymer network (10). The present experimental observations are consistent with this picture. Further support for this model comes from the fact that similar NMR experiments on a cross-linked polystyrene in this laboratory (7) gives just one gaussian component with a T_2 of 9.7 μs which is very close to the T_{2g1} values for the first gaussian component of the coals.

The second gaussian component also presents part of the coal structure not only because the decay has a gaussian form, but also because the relative intensity of this component, $I_{22}(0)$, is independent of the water present in the coals. The clear correlation between T_{2g1} and T_{2g2} (a ratio about 1/2) indicates that certain kind of relationship exists between the two types of coal structures. It has been suggested (11) that the restricted rotation of methyl groups and hydrocarbon chains in the macromolecular framework of coals is likely responsible for this component of higher mobility. Further experiments on model polymers might lead to a more definite structural identification.

Conclusions

A step-by-step least-linear-square fitting in the present work leads to an unambiguous deconvolution of the FID signal into two gaussian and one lorentzian components. The lorentzian arises from the protons of physically absorbed water in coals, and the quantitative measurement of the lorentzian component provides a new way for the moisture determination in coals.

More than 90% of the coal structure behaves as a rigid-lattice. The relaxation time measured for coals is very similar to that of cross-linked model polymer. Less than 10% of the coal structures shows higher mobility, and a possible source for this intermediate component may be the hindered rotation of methyl groups or hydrocarbon chains of the coal macromolecular structure.

The drying by high vacuum pumping is almost complete, and no significant structural change in coal was observed during the drying process.

Acknowledgement

We thank Philip Mulieri of Lehigh University for preparing the high vacuum dried samples.

References

1. Vorres, K. S. "User's Handbook for the Argonne Premium Coal Sample Program", U.S. Department of Energy, October 1, 1989. See also: Vorres, K. S. *Energy and Fuel* 1990, 4, 420.
2. Finseth, D. *Prepr. Pap. - Am. Chem. Soc., Div. Fuel Chem.* 1987, 32, 260.
3. Lynch, L. J. and Webster, D. S. *Fuel* 1979, 58, 429.
4. Wroblewski, A. E.; Reinartz, K.; Verkade J. G. *Energy and Fuel* 1991, 5, 786.
5. Gerstein, B. C.; Chow, C.; Pembleton, R. G.; Wilson, R. C. J. *Phys. Chem.* 1977, 81, 565.
6. For example, Vorres, K. S. and Kolman, R. *Prepr. Pap. - Am. Chem. Soc., Div. Fuel Chem.* 1988, 33, 7.
7. Yang, X; Garcia, A; Larsen, J. W.; Silbernagel, B. G., unpublished results.
8. Gerstein, B. C., unpublished results.
9. For example, see Abragam, A. "The Principles of Nuclear Magnetism", Clarendon Press: Oxford, 1961.
10. Larsen, J. W.; in "New Trends in Coal Science", Yürüm, Y. Ed., Kluwer Academic Publisher: New York, 1988, 73-84.
11. Kamieński, B; Pruski, M; Gerstein, B. C.; Given, P. H. *Energy and Fuel* 1987, 1, 45.

Table 1: Summary of the ^1H NMR relaxation measurements

Coals		Gaussian 1		Gaussian 2		Lorenzian	
		$T_{2g1}^{\#}$	$I_{g1}(0)$	T_{2g2}	$I_{g2}(0)$	T_{2l}	$I_l(0)$
Pittsburgh #8	as*	10.1	90	19.6	5	23.3	5
	dried	10.1	95	20.6	5	25	1
Illinois #6	as	9.9	76	18.8	5	155	19
	dried	10.0	95	20.9	5	27	1
North Dakota	as	9.5	35	16.5	9	258	56
	dried	9.6	91	19.8	7	25	2

[#] The unit for T_2 is 10^{-6} sec.

* as = as received.

Table 2: Moisture in coals (W%) determined with various methods

Coals	H_{coal}	^{31}P NMR	Moisture W%		
	(Dry%) Ref(1)		ASTM Ref(1)	^{18}O dilt. Ref(2)	^1H NMR This work
Pittsburgh #8	4.83	2.85	1.65	2.5	2.2
Illinois #6	4.23	9.35	7.94	9.6	8.2
North Dakota	4.36	31.05	32.24	34.4	33

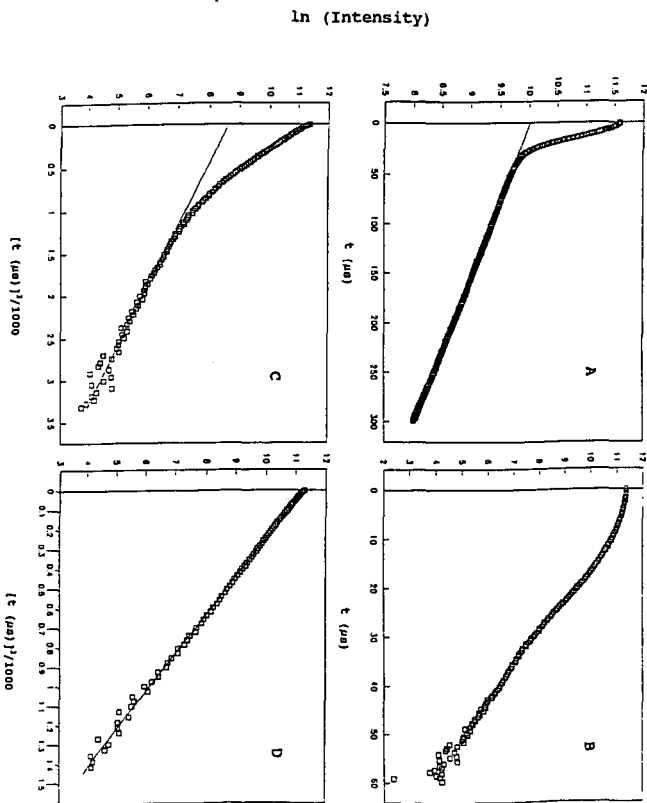


Figure 1: The natural logarithm of the FID intensity of as-received Illinois #6 as a function of relaxation time t and t^2 . D is the experimental data point and the solid line is the least-square fitting. (A) the original FID, (B) after subtracting the lorentzian component from (A), (C) same as (B) except plotted as function of t^2 , and (D) after subtracting the intermediate gaussian component from (C).

CARBON RADICAL RELAXATION PROPERTIES IN ARGONNE PREMIUM COALS

M. Bernardo, B.G. Silbernagel, and H. Thomann
Exxon Research and Engineering Co.
Annandale, NJ 08801

Key Words: Electron Paramagnetic Resonance, Relaxation, Coal

ABSTRACT

We have applied Electron Spin Echo (ESE) spectroscopy to the analysis of demineralized samples of Argonne Premium Coals. The goal of the present work has been to examine the detailed form of the magnetization recovery in spin lattice relaxation (T_{1e}) and phase memory decay measurements and to trace the temperature dependence of the T_{1e} processes to get a clearer understanding of the mechanisms responsible for carbon radical relaxation. The demineralized coal samples have been chosen for this study because the presence of paramagnetic transition metal ions tends to obscure the effects in the starting coal samples. We find a significant degree of non-exponentiality in the recovery of the carbon radical magnetization, to the best of our knowledge the first of such observations in coals. Such a result could have three sources: spectral spin diffusion among the radical species, a distribution of T_{1e} values due to inequivalent structures for the radicals, or non-uniform spatial distributions of the radicals. A comparison of the T_m and the temperature dependence of these properties suggests that this non-exponentiality is intrinsic to the radicals.

INTRODUCTION

There has been considerable recent interest in the application of transient Electron Paramagnetic Resonance (EPR) techniques to the studies of a variety of materials [1]. These techniques are widely varied, including Electron Spin Echo (ESE) determinations of the relaxation properties of the paramagnetic species as well as more elaborate Electron Nuclear Double Resonance (ENDOR) techniques. Recent studies in coal samples indicate a significant potential for important results in these areas [2, 3]. The present report will focus on the former of these advanced transient EPR techniques: a study of the functional dependence of the magnetization dynamics for carbon radicals in coal using ESE techniques.

The early work in this laboratory on the ESE properties of carbon radicals in coal was performed on a series of coal macerals (vitrinites, exinites, and inertinites) isolated from the starting coal by gravity density centrifugation techniques [4]. In this previous survey [5], the magnetization recovery of the samples was found to be closely approximated by an exponential. For the vitrinite members of this series, the phase memory decay rate, T_m^{-1} , the analog of the spin-spin relaxation time in nuclear magnetic resonance, was found to be proportional to the density of the carbon radicals in the sample, suggesting that the T_m relaxation arose from dipolar coupling. The spin-lattice relaxation rate for the radicals, T_{1e}^{-1} , was found to increase dramatically for higher rank coals, the increase initiating in the vicinity of ~ 82% carbon. It was suggested that this increase in T_{1e}^{-1} resulted from the onset of short range local order with increasing rank for the aromatic molecules which serve as the hosts for the radicals.

While these results were encouraging, there was some concern about whether they reflected the intrinsic properties in the native coal. These materials were prepared from samples of coal from the Penn State (PSOC) coal bank. The history and storage conditions of these samples were not carefully documented. Furthermore, these materials were exposed to air during the grinding and centrifugation processes. At the time, conventional EPR techniques were used

to trace variations in g -value, linewidth, and lineshape of the radicals at each stage of the process [6]. While no major changes were noted, there were still concerns about the chemical nature of the as-received PSOC samples and the chemical forms of the carbon radicals. Finally, the scale of the centrifugation process, as practiced at that time, produced very small amounts of material (~ 10 mg) which severely affected the signal to noise in the ESE experiments.

The availability of the Argonne Premium Coal samples [7] has provided the opportunity to address these concerns about the nature of the radical chemistry. Prior to receipt in this laboratory, the samples have been handled to avoid air exposure. However, a previous survey [3] indicated that the g -values, linewidths, radical densities, and relaxation properties for these samples—as received—were not consistent with the chemical variations expected during the maturation process. An EPR survey of the samples indicated high levels of transition metal ions, especially Fe^{3+} , in the as-received samples, with the effect being particularly pronounced in the highly functionalized lower rank coals. Subsequent removal of the transition metal impurities, by acid wash (e.g. with citric acid) or by HCl/HF demineralization, removed these transition metal ions and produced a much more consistent carbon radical behavior [8]. Now that these mineral effects are understood, we are returning to a detailed study of the organic matter in coal. There have been concomitant advances in the ESE systems in which the experiments are performed. In particular, the introduction of loop gap resonators provides higher microwave power levels and approximately a hundred fold increase in sensitivity for the ESE signals, greatly improving the precision of a study of the functional dependence of the magnetization dynamics.

EXPERIMENTAL

Samples of the demineralized Argonne Premium Coal samples have been examined at room temperature by the ESE techniques. For the radical spin-lattice relaxation measurements, a distinctly non-exponential magnetization recovery is observed. We will characterize this recovery in the following form:

$$(1) \quad (M_z(t) - M_0)/M_0 = \exp\{-(t/T_1')^\beta\},$$

where T_1' is a relaxation time (not a T_{1e}) and β is the exponent of the magnetization recovery. An example of this magnetization recovery is shown in Figure 1. In examinations of Beulah-zap, Illinois #6, and Pittsburgh #3 samples from the Argonne Premium Coal series, values of β ranging from ~ 0.5 to ~ 0.8 have been observed.

To test for possible instrumental effects, we have examined the effect of sample size and position in the resonator. The results suggest that we are not observing an instrumental effect.

DISCUSSION

In addition to these effects, there are several other sources for non-exponential magnetization recovery during spin-lattice relaxation measurements. Spectral spin diffusion among the radicals during the magnetization recovery process can lead to the effect. Alternatively, a distribution in T_{1e} values among the radicals in the sample could also lead to non-exponentiality, since in that case:

$$(M_z(t) - M_0)/M_0 = \int \rho(\alpha) \exp\{-\alpha t\} d\alpha \quad (2)$$

where α represents the T_{1e} value for a given class of radicals and $\rho(\alpha)$ represents the

probability distribution for radicals with that T_{1e} value in the coal sample. This distribution in radical types might not be so prominent in weathered coal samples like the isolated coal macerals observed previously. A third alternative might be that the *spatial distribution* of the radicals in the coal might be causing a distribution in recovery properties, which has been examined in some detail for other systems (e.g. γ -irradiated frozen solutions) [9]. The spatial inhomogeneity will influence both T_{1e} and T_m , and is currently under investigation.

ACKNOWLEDGEMENTS

We would like to thank Dr. R.A. Flowers of Lehigh University for the preparation of the demineralized samples and A.R. Garcia of this laboratory for the sample preparation.

REFERENCES

- 1 Keijzers, C.P., Reijerse, E.J., and Schmidt, J. Pulsed EPR: A New Field of Applications, North Holland, Amsterdam, 1989.
- 2 Thomann, H. and Bernardo, M. in Magnetic Resonance of Solid Carbonaceous Fuels (R.E. Botto, ed.), ACS Advances in Chemistry Series 229, (1992).
- 3 Silbernagel, B.G., Gebhard, L.A., Bernardo, M. and Thomann, H. in Magnetic Resonance in Solid Carbonaceous Fuels (R.E. Botto, ed.), ACS Advances in Chemistry Series 229, (1992).
- 4 Dyrkacz, G.R., and Horwitz, E. Energy and Fuels, 1982, 61, 3-12.
- 5 Thomann, H., Silbernagel, B.G., Jin, H., Gebhard, L.A., Tindall, P., and Dyrkacz, G.R. Energy and Fuels, 1988, 2, 333-339.
- 6 Silbernagel, B.G., Gebhard, L.A., Dyrkacz, G.R., and Bloomquist, C.A.A. Fuel, 1986, 65, 558-565.
- 7 Vorres, K.S. Energy and Fuels, 1990, 4, 420-426.
- 8 Silbernagel, B.G., Gebhard, L.A., Flowers, R.A., and Larsen, J.W. Energy and Fuels, 1991, 5, 561-568.
- 9 For a discussion of non-exponential magnetization recovery, see, e.g. Bowman, M.K., and Kevan, L. in Time Domain Electron Spin Resonance (L. Kevan and R.N. Schwartz, eds.), John Wiley and Sons, New York, 1979, 73-80.
- 10 For a discussion of the effects of the spatial distribution of paramagnetic species, see, e.g. Salikov, K.M. and Tsvetkov, Yu.D. in Time Domain Electron Spin Resonance (L. Kevan and R.N. Schwartz, eds.), John Wiley and Sons, New York, 1979, 258-271.

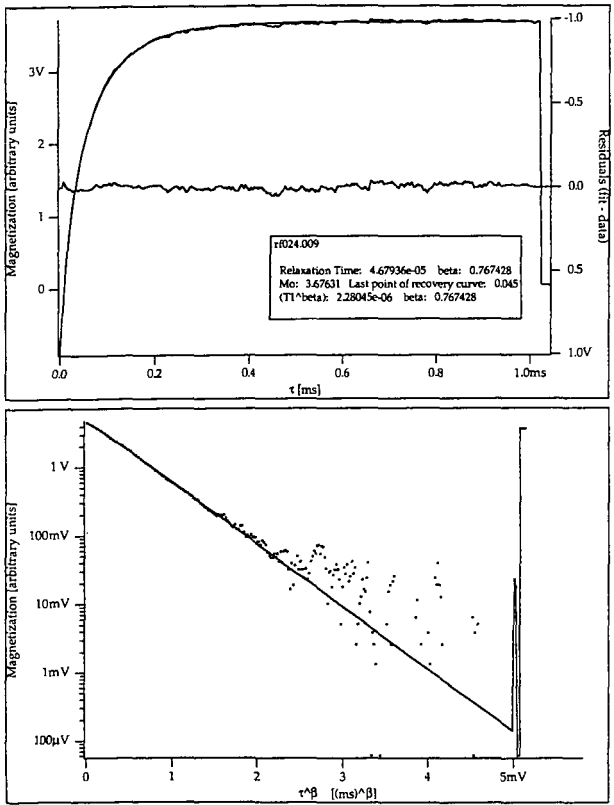


Fig 1 Non-exponential magnetization recovery for a sample of Pittsburgh #3 coal. An exponent of $\beta = 0.767$ is observed in this case. The residuals shown in the upper portion of the figure provide some measure for the goodness of fit for the data.

Solid-State CPMAS ^{13}C NMR and Pyrolysis-GC-MS Studies of Coal Structure and Liquefaction Reactions

Chunshan Song, Harold H. Schobert and Patrick G. Hatcher

Fuel Science Program, Department of Materials Science and Engineering, 209 Academic Projects Building, The Pennsylvania State University, University Park, PA 16802, USA

Keywords: Solid-state C-13 NMR, Pyrolysis-GC-MS, Coal Liquefaction

Abstract

The objective of this work is to delineate the chemical reactions during liquefaction of low rank coal by characterizing the resultant structural changes in coal macromolecular network, using cross-polarization magic angle spinning (CPMAS) solid-state ^{13}C NMR and flash pyrolysis-GC-MS (Py-GC-MS). We analyzed the THF-insoluble residues from liquefaction of a Montana subbituminous coal at different final temperatures ranging from 300 to 425°C in three different solvents under temperature-programmed (TPL) and non-programmed (N-PL) conditions. The combined use of CPMAS ^{13}C NMR and Py-GC-MS on the residues from TPL revealed a progressive loss of oxygen-containing species, and the gradual loss of aliphatic-rich species from the coal macromolecular network with increasing temperature from 300 to 425°C. The higher efficiency of TPL in the presence of H-donor, compared with conventional runs, is closely associated with H-transfer from tetralin to reactive species and removal of specific oxygen functional groups such as carboxyl and catechol groups from the coal during the programmed heat-up. Loss of these specific functional groups in early stage of TPL probably moderates or minimizes the occurrence of retrogressive reactions, thus increasing the conversion.

Introduction

Modern solid state nuclear magnetic resonance (NMR) spectroscopy originated in 1970s when cross-polarization (CP) and magic angle spinning (MAS) techniques were developed and combined (CPMAS) [1-3]. Since the first paper on NMR of coals was published by Vander Hart and Retcofsky in 1976 [4], solid-state NMR has been applied extensively in characterization of coals. The techniques of CPMAS and dipolar dephasing MAS (DDMAS) ^{13}C NMR can provide useful structural information on insoluble organic solids. In recent years, solid-state NMR has rapidly become one of the most important non-destructive techniques for studying the structure of solid coal, coal macerals, coal-derived products, geochemical samples, and other organic solids [5-12]. Flash pyrolysis-gas chromatography-mass spectrometry (Py-GC-MS) is also an important analytical technique for structural study of polymeric materials [13-16]. Py-GC-MS is relatively simple in theory, and can be viewed as a combination of the well known MS techniques with pyrolysis-GC [17,18]. While these techniques have been applied in many investigations, very few applications have been made in coal liquefaction studies.

The present work is a part of our research on temperature-programmed liquefaction of low rank coals, and involves the spectroscopic study of coal structure and liquefaction reactions using the combination of CPMAS ^{13}C NMR and Py-GC-MS [19-21]. The NMR technique has an advantage of providing the information related to the type and distribution of aromatic and aliphatic carbons in a non-destructive and quantitative fashion. Its disadvantage is that the information from NMR does not provide a direct picture of the molecular components and their environments. This is partly because the coal organic matrix is a complex mixture, whose individual components can not be resolved by NMR. Py-GC-MS is a very useful technique for studying the molecular components or structural units of polymeric organic solids. Py-GC-MS is also a fingerprinting technique [16]. However, the major drawback to Py-GC-MS is that the proportion of coal that can be volatilized and analyzed by GC-MS is relatively small. For many coals more than half of the organic material remains as a residue. Since each technique has advantages and disadvantages, we can make complementary use of these techniques by using them in tandem. The combined use of solid state NMR and Py-GC-MS has the potential to provide both average structural information and specific molecular components, and when applied to properly selected samples, can provide insights into the major and minor changes in coal structures and structural transformations involved in coal liquefaction processes [19,20].

Experimental

The coal used was a Montana subbituminous coal obtained from the Penn State Coal Sample Bank (DECS-9 or PSOC-1546). The characteristics of this coal are as follows: 33.5% volatile matter, 37.1% fixed carbon, 4.8% ash, 24.6% moisture, on a raw coal basis; 76.1% C, 5.1% H, 0.9% N, 0.3% organic S, and 17.5% O, on a dmmf basis. The coal was dried in a vacuum oven at 95°C for 2 h before use. The vehicle used was tetralin, a known H-donor. Liquefaction was carried out in 25 ml microautoclaves using 4 g coal (< 60 mesh) and 4 g tetralin under 6.9 MPa H₂. After the reaction, the liquid and solid products were separated by sequential extraction with hexane, toluene and THF.

The THF-insoluble residues were analyzed by solid state ¹³C NMR and Py-GC-MS. Our preliminary tests showed that a trace amount of THF remains in the residue even after vacuum drying at 100 °C for over 6 h, which significantly interferes with the spectroscopic characterization using CPMAS ¹³C NMR and Py-GC-MS. Therefore, prior to analyses, all the THF-insoluble residues were washed first by using acetone and then n-pentane, followed by vacuum drying at 100°C for 6 h. This procedure was found to be very effective for removing trace amount of THF.

The NMR spectra were acquired on a Chemagnetics M-100 NMR spectrometer by using the combined high power proton decoupling, cross-polarization and magic-angle-spinning (CPMAS) techniques. The measurements were carried out at a carbon frequency of 25.1 MHz. About 0.4-0.6 g of a sample was packed in a bullet-type Kel-F rotor (0.4 ml capacity); the spinning speed of the rotor was about 3.5 kHz. The experimental conditions for all the samples are as follows: a cross-polarization contact time of 1 ms and a pulse delay time of 1 s. An instrumental calibration test was performed with the rotor containing hexamethylbenzene, which was adjusted to the magic angle (54.7°) to give the correct chemical shifts. To assure good spectra with high signal-to-noise ratios, the number of pulses accumulated for obtaining a spectrum was at least 10,000, and most of the spectra were obtained with numbers of scans between 20,000 to 35,000.

Py-GC-MS analysis was performed on a Du Pont 490B GC-MS system fitted with a 30 m x 0.25 mm i.d. capillary column DB-17 coated with 50% phenylmethylsilicone stationary phase with a film thickness of 0.25 μm, and interfaced to a Chemical Data Systems Pyroprobe-1000 pyrolyzer. Helium was used as a carrier gas. The data acquisition and data processing were controlled through a computer-aided system. Prior to the start of data acquisition, the samples were flash-pyrolyzed at 610°C for 10 seconds, during which the pyrolysates (pyrolysis products) were retained in the close-to-inlet part of the capillary column by colling with liquid nitrogen. The column was held at 40°C for 5 minutes and subsequently programmed to 280°C at a rate of 4°C/min. The mass spectrometer was operated in the electron impact mode at 70 eV. In order to derive information related to the macromolecular network, the low molecular species in the coal and coal liquefaction products were removed by THF extraction prior to Py-GC-MS analysis. The other experimental details about the NMR and Py-GC-MS are similar to those described elsewhere [7].

Results and Discussion

Characterization of DECS-9 Subbituminous Coal

Because the liquefaction residues are THF-insoluble, it was necessary to obtain a corresponding baseline spectrum with the THF-insoluble residual part of the raw coal. Figure 1 shows the CPMAS ¹³C NMR spectra of the fresh DECS-9 coal and the unreacted but THF-extracted DECS-9 coal. It is interesting to note that the THF-extracted coal, which lost about 8 % THF-soluble materials, gave a spectrum similar to that of the raw coal in terms of the aromaticity and functionality (see below). Integration of the spectra gives only a slightly higher aromaticity (fa) value for the THF-extracted coal than for the raw coal. It should be noted that for some coals, the THF-extracted samples may display substantially different spectra. In addition, a general observation is that these NMR spectra are relatively poorly resolved, as compared to the spectra of pure materials, primarily because of the presence of a large number of different molecular species that have only slightly different chemical shifts.

Figure 2 shows the total ion chromatogram (TIC) obtained from Py-GC-MS of the THF-extracted raw coal. With the aid of computer-based data processing, it is now possible to perform a compound type analysis of coal pyrolysis products by using the selective ion monitoring technique in Py-GC-MS, as has been used for hydrocarbon type analysis of liquid fuels by GC-MS [22]. Low rank coals are known to have higher oxygen functionalities [23], and therefore we have examined the oxygen compounds in the pyrolysis products by using the characteristic ion masses for phenol (m/z 94), cresol (m/z 108), xylenol (m/z 122), and catechol (m/z 110). Figure 3 shows the total ion chromatogram (TIC) and selected ion chromatograms (SIC) in the extended retention time (RT) region of 2-22 min, which is a part of Figure 2. Within this range, the four most predominant peaks in the TIC are all phenolic compounds. Also found in this sample are catechol and methylcatechol. The two relatively large peaks around RT of 3 min are p- and o-xylene, in that order. It should be noted that there are a number of major hydrocarbon peaks which appeared between 0 to 2 min (Figure 2) and whose intensities are higher than the largest peak phenol in Figure 3. Those peaks are C₅-C₈ alkanes plus

alkenes, which are not well separated, and toluene, the second largest peak. There are many other small peaks appeared over the whole RT region, and selective ion monitoring at m/z 71 indicates that they are long-chain alkanes and alkenes. Overall, these results show that the DECS-9 coal contains significant amounts of oxygen-containing structural units such as phenol and alkylphenols as well as alkylbenzenes. It is also interesting to note that the long-chain aliphatics still exist after long time Soxhlet extraction with toluene and THF.

Characterization of Liquefaction Residues

CPMAS ^{13}C NMR

The temperature-programmed liquefaction (TPL) of DECS-9 Montana subbituminous coal was carried out at final temperature ranging from 300 to 425°C. Detailed discussion of the TPL may be found elsewhere [21]. For the sake of comparing the amount of organic materials in the THF-insoluble residues, Figure 4 shows the yields of THF- and toluene-soluble products plus gas from duplicate runs of Montana coal, as a function of final TPL temperature.

Figure 5 presents the NMR spectra. The spectrum of THF-extracted unreacted coal serves as a baseline. The THF-insoluble residue from TPL at final temperature of 300°C has a spectrum (Figure 5B) similar to that of the THF-extracted coal (Figure 5A). In this spectrum, an intense peak is present for aliphatic carbons (0-60 ppm) which may also include trace amounts of aliphatic ether (-C-O-X). This aliphatic peak becomes progressively smaller with increasing severity of liquefaction. The aromatic region has three peaks: an intense peak around 130 ppm (aromatic C), and two shoulders, one at about 142 ppm (possibly catechol-like C), and another at 152 ppm (phenolic or aromatic ether C). A peak at 181 ppm (carboxyl C), and a broad band around 212 ppm (ketone or aldehyde C) define the rest of the spectrum. The peaks at 142 and 212 ppm almost disappear after TPL at 350°C, and the peak at 181 also diminishes after TPL at 375°C. A decrease in intensity of the peak at 152 ppm is only observed after 375°C, and this is accompanied by further loss in aliphatic carbons. Concomitant with the decrease in total aliphatic carbons, the relative contribution from methyl carbons (0-25 ppm) increases. In general, the intensity of the aliphatic region (0-60 ppm) decreases, and the aromaticity increases with an increase in severity of TPL. Integration of the ^{13}C NMR spectra shown in Figure 5 indicates a progress increase in carbon aromaticity of the remaining organic materials in the residue. We are currently exploring the ways to quantitatively calculate the contents of different carbons both in the aromatic and aliphatic regions, and their changes with the TPL temperature by using the curve-fitting methods with the aid of computer-software.

Pyrolysis-GC-MS

Figure 5 shows the selected retention time region of 2-22 minutes of the Py-GC-MS chromatograms of the THF-extracted raw coal (A) and the residue from TPL at 300°C, the major peaks in which are identified in Table 1. Phenol, alkyl phenols, alkylbenzenes, catechols as well as alkanes and alkenes are formed from flash pyrolysis of the THF-extracted raw coal. Relative to this sample, there is apparent change in Py-GC-MS profile of the residue from TPL at 300°C. The appearance of a major peak for naphthalene and disappearance of catechol differentiate the latter from the former. This is especially interesting, since the NMR spectra of these two samples (Figure 4) and the corresponding yields of THF-solubles (7-9%) are similar to each other. From these results, it is clear that the reaction at 300°C did cause some structural change. The naphthalene peak in Figure 3 is due mainly to the use of tetralin solvent, because this peak was found to be very small with other solvent or without solvent. Since the residue has been extracted by THF for over 24 h, washed by acetone and pentane (to remove THF completely) and dried in vacuum at 90-100°C for 6 h, the naphthalene/tetralin remained in the residue must be either chemically bound to other species or physically entrapped in solvent-inaccessible micropores or closed pores which can not be removed by solvent extraction.

Also, it appeared that Py-GC-MS can detect some subtle differences in coal structure which are not easily detectable by CPMAS NMR. Combination of the NMR and Py-GC-MS data suggests that the original coal contains considerable quantities of catechol-like structures, which seem to disappear in the liquefaction residues above 300°C, and carboxyl groups, which almost disappear after 350°C, and also phenolic structures which diminish in concentration with increasing temperature. The analytical results point to the progressive loss of oxygen functional groups and aliphatic species from the macromolecular network of the subbituminous coal during its depolymerization in tetralin under TPL conditions. The higher conversions in TPL runs (relative to the conventional runs in tetralin) suggest that the removal of carboxylic and catechol groups from the coal during the programmed heat-up ($\leq 350^\circ\text{C}$) in tetralin may have contributed to minimizing the retrogressive crosslinking at higher temperatures.

Low-rank coals are characterized by low aromaticities and high oxygen functionalities. It seems possible from comparative examination of the coal conversion data and spectroscopic data that the TPL conditions may facilitate the reduction of crosslinking reactions of the thermally sensitive groups such as oxygen-functional groups at low temperatures in H-donor. Further work on the quantitative evaluation of coal structural change during liquefaction is

now in progress.

ACKNOWLEDGEMENTS.

C. Song gratefully acknowledges the financial support of this work (Fund No. 424-04-2404 LG-4-91) by the Cooperative Program for Coal Research at the Pennsylvania State University. We thank Mr. J. McConnie for assistance with some liquefaction experiments, and Mr. L. Hou for measuring some of the NMR spectra.

REFERENCES

1. Pines, A.; Gibby, M.G.; Waugh, J.S., *J. Chem. Phys.* 1972, 56, 1776; 1973, 59, 569.
2. Schaefer, J.; Stejskal, E.O., *J. Am. Chem. Soc.* 1976, 98, 1031
3. Yannoni, C.S., *Acc. Chem. Res.* 1982, 15, 201
4. Van Der Hart, D.L.; Retcofsky, H.L., *Fuel*, 1976, 55, 202
5. Alemany, L.B.; Grant, D.M.; Pugmire, R.J.; Alger, T.D.; Zilm, K.W. *J. Am. Chem. Soc.* 1983, 105, 2142.
6. Wilson, M.A.; Pugmire, R.J.; Karas, J.; Alemany, L.B.; Woolfenden, W.R.; Grant, D.M., *Anal. Chem.* 1984, 56, 933-943.
7. Hatcher, P.G., Wilson, M.A., Vassallo, A.M. and Lerch III, H.E. *Int. J. Coal Geol.* 1989, 13, 99.
8. Dennis, L.W.; Maciel, G.E.; Hatcher, P.G., *Geochimica et Cosmochimica Acta* 1982, 46, 901-907
9. Yoshida, T.; Maekawa, Y., *Fuel Processing Technol.* 1987, 15, 385-395.
10. Supaluknari, S.; Larkins, F.P.; Redlich, P.; Jackson, W.R., *Fuel Processing Technology* 1989, 23, 47-61.
11. Botto, R.E.; Wilson, R.; Winans, R.E., *Energy & Fuels* 1987, 1, 173.
12. Solum, M.S.; Pugmire, R.J.; Grant, D.M., *Energy & Fuels* 1989, 3, 187-193.
13. Nip, N.; de Leeuw, J.W.; Schenck, P.H.; Meuzelaar, H.L.; Stout, S.A.; Given, P.H.; Boon, J.J., *J. Anal. Appl. Pyrol.* 1985, 8, 221-240.
14. Philip, R.P.; Gilbert, T.D., *J. Anal. Appl. Pyrol.* 1987, 1, 93-108.
15. Hatcher, P.G.; Lerch, H.E.; Koura, R.K.; Verheyen, T.V., *Fuel* 1988, 67, 1069-1075.
16. Saiz-Jimenez, C.; De Leeuw, J.E., *J. Anal. Appl. Pyrol.* 1986, 9, 99-119.
17. Gallegos, E.J., "Pyrolysis Gas Chromatography", in "Chromatography in Petroleum Analysis", K.H. Altgelt and T.H. Gouw Eds., Marcel Dekker, New York, 1979, pp.163-184.
18. Meuzelaar, H.L.C.; Haverkamp, J.; Hileman, F.D., "Pyrolysis Mass Spectrometry of Recent and Fossil Biomaterials", Elsevier, Amsterdam, 1982, 287pp.
19. Song, C.; Schobert, H.H.; Hatcher, P.G., *Proc. 1991 Int. Conf. Coal Sci. U.K.*, 1991, p.664
20. Song, C.; Schobert, H.H.; Hatcher, P.G., *Energy & Fuels* 1992, in press.
21. Song, C.; Schobert, H.H., *Am. Chem. Soc. Div. Fuel Chem. Prepr.* 1992, 37, in press.
22. Song, C.; Hatcher, P.G., *Am. Chem. Soc. Div. Petrol. Chem. Prepr.* 1992, 37, in press.
23. Schobert, H.H., *Resources, Conservation and Recycling*, 1990, 3, 111-123.

Table 1 Major identified peaks in Figure 6

No.	MW	Identified Compound
1	106	p-Xylene
2	106	o-Xylene
3	120	C ₃ -benzene
4	120	C ₃ -benzene
5	94	Phenol
6	108	o-Cresol
7	108	m- + p-Cresol
8	122	Dimethylphenol
9	122	Ethylphenol
10	128	Naphthalene
11	136	C ₃ -phenol
12	110	Catechol
13	124	Methylcatechol
14	142	Methylnaphthalene
15	124	Methylcatechol

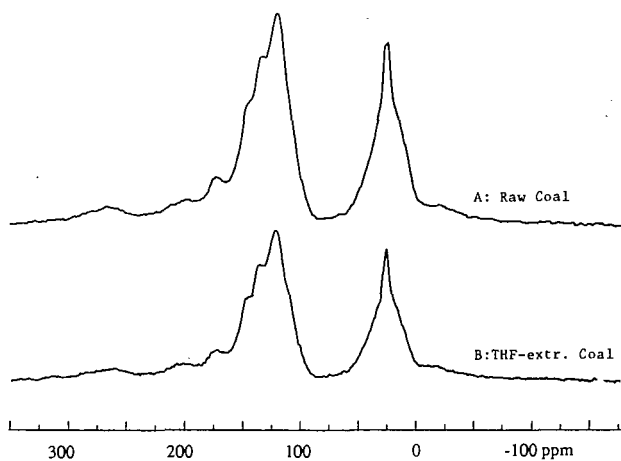


Figure 1 CPMAS ^{13}C NMR spectra of DECS-9 Montana subbituminous coal (A) and the THF-extracted coal (B).

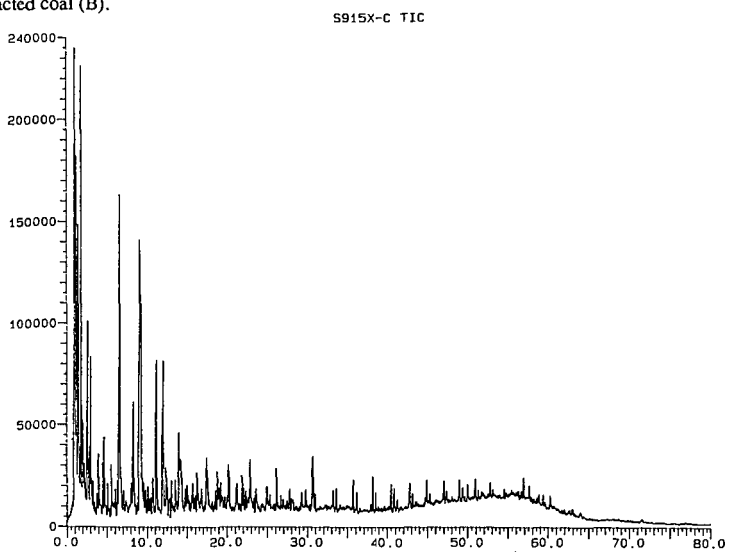


Figure 2 Total ion chromatogram for pyrolysis-GC-MS (610°C for 10 s) of THF-extracted DECS-9 Montana coal.

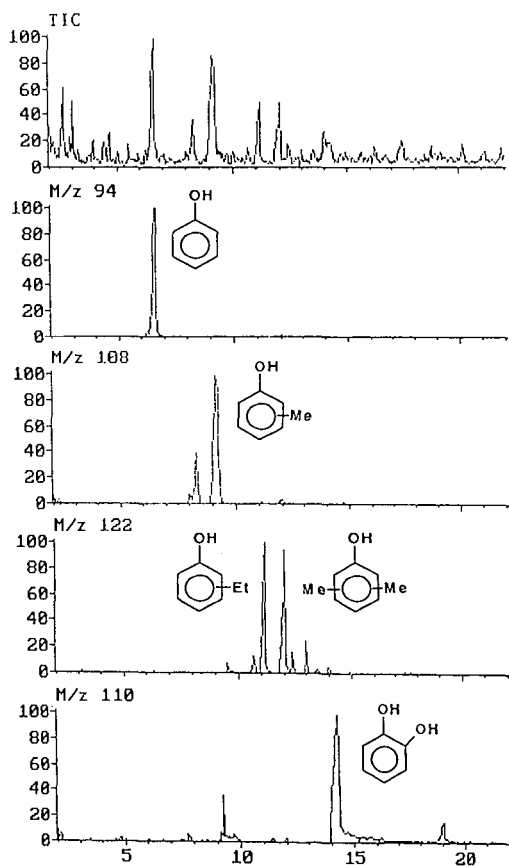


Figure 3 Specific ion chromatograms (SIC) and TIC from Py-GC-MS of THF-extracted, unreacted DECS-9 Montana subbituminous coal (pyrolysis at 610°C for 10 s)

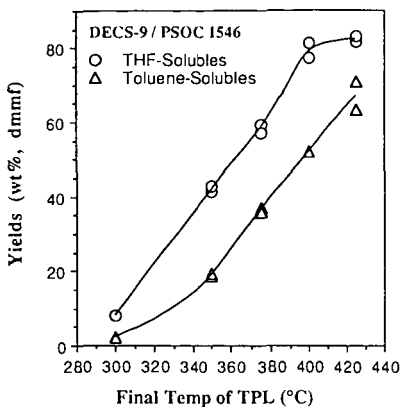


Figure 4 Conversion of DECS-9 Montana coal to THF- and toluene-solubles as a function of final temperature of temperature-programmed liquefaction (TPL) in tetralin.

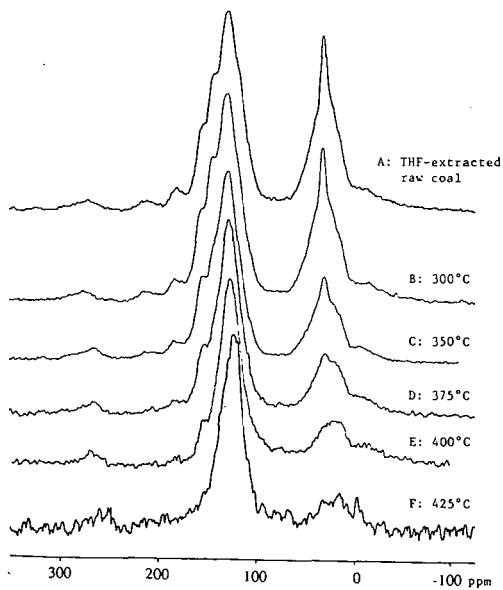


Figure 5 CPMAS ^{13}C NMR spectra of THF-insoluble residues from TPL of DECS-9 Montana coal in tetralin at different final temperature.

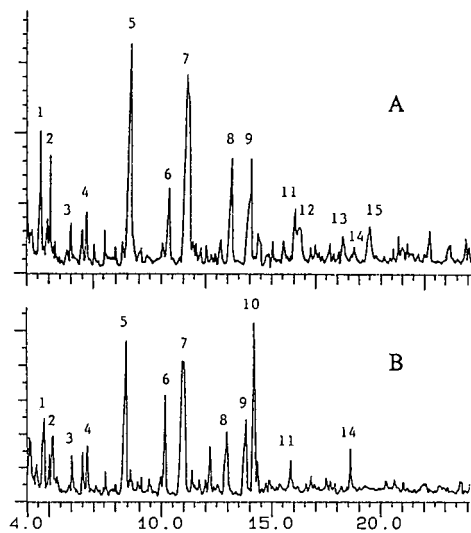


Figure 6 Py-GC-MS profiles of THF-extracted unreacted DECS-9 Montana subbituminous coal (A) and the residue (B) from TPL at final temperature of 300°C (pyrolysis at 610°C for 10 s).

Selective Saturation and Inversion of Multiple Resonances in High Resolution Solid State ^{13}C CP/MAS Experiments

Jian Zhi Hu,* Ronald J. Pugmire,+ Anita M. Orendt,* David M. Grant,* and C. Ye**

Department of Chemistry*, and Department of Fuels Engineering,+
University of Utah, Salt Lake City, Utah 84112, U.S.A.

**Wuhan Institute of Physics, Chinese Academy of Sciences, Wuhan
430071, The People's Republic of China

Abstract

Taking advantage of the long ^{13}C T_1 values generally encountered in solids, selective saturation and inversion of more than one resonance in ^{13}C CP/MAS experiments can be achieved by sequentially applying several DANTE pulse sequences centered at different transmitter frequency offsets. A new selective saturation pulse sequence is introduced composed of a series of 90° DANTE sequences separated by interrupted decoupling periods during which the selected resonance is destroyed. Applications of this method, including the simplification of the measurement of the principal values of the ^{13}C chemical shift tensor under slow MAS conditions are described. The determination of the aromaticity of coal using a relatively slow MAS spinning rate is also described.

Keywords: DANTE, multiple offset DANTE, coal structure, ^{13}C NMR

INTRODUCTION

It is well known that high resolution isotropic chemical shift spectra in solids can be obtained by applying high power heteronuclear decoupling in combination with MAS at a spinning rate larger than the width of the chemical shift anisotropy (CSA). Although isotropic chemical shifts are very useful in determining chemical structure, they come at a high price as the sample spinning averages the tensorial parameters which provide a great deal of information about the local electronic environment of the nuclei and molecular dynamics. However, when the sample spinning rate is less than the width of the chemical shift anisotropy (i.e., the slow MAS condition), the CSA powder pattern collapses to a group of spinning sidebands (SSB) spaced at the sample rotation rate with the center band located at the isotropic chemical shift position. As was demonstrated by Herzfeld and Berger (1), the tensorial principal values can be retrieved through digital simulation of the intensities of just a few spinning sidebands. However, when there are several chemically inequivalent nuclei in a molecule, the spinning sideband patterns are superimposed in the classical one dimensional CP/MAS experiment and it becomes very difficult to separate the individual sideband patterns and measure accurate intensities due to overlapping of lines. In order to simplify this measurement, a few two dimensional MAS experiments have been developed in which the isotropic chemical shift is obtained in one dimension while the spinning sideband patterns for each spin are separated in the second dimension (2,3). However, these methods suffer from either the need for specialized equipment and relaxation difficulties in the case of the switched speed method (2) or from intensity distortion problems in the case of the TOSS-Reversed TOSS method (3). It will be shown in this paper that undistorted spinning sideband patterns for only the aliphatic carbons can be readily obtained by saturating the entire aromatic, carbonyl and carboxyl sideband families using several DANTE sequences at different transmitter offset frequencies.

There are basically three categories of selective pulses; 1) the soft pulse (4-6) which is a single long, weak rectangular pulse; 2) the shaped pulse (7,8); and 3) the DANTE pulse sequence which consists of a series of short intense rf pulses (9-11). It has been known for a decade that selective excitation experiments in liquid state high resolution spectroscopy are quite informative (12). In solid state experiments, attention has initially been focused on selective excitation of multiple quantum coherence in quadrupolar systems (13-17) and on the application of selective excitation to either a static or high speed MAS sample. In both cases no spinning sidebands need be considered (18). In 1983, Caravatty et al. (19) demonstrated the usefulness of selective irradiation under slow MAS conditions and concluded that uniform excitation of one spinning sideband family can be achieved by synchronizing the pulse train of the DANTE sequence with sample rotation. It is possible to saturate the longitudinal magnetization of an entire sideband family by selective irradiation of one of its sidebands, while it is not possible to excite the whole sideband family via selective sideband irradiation. An example of this important feature is provided by Tekely et al. (20), where an incomplete elimination of the broad aromatic band and its spinning sidebands in a ^{13}C CP/MAS spectrum of coal at high magnetic field was achieved by applying a long DANTE sequence. Recently, Tekely et al (21) have reported a new selective pulse sequence named SELDOM; this sequence employs the normal 90° hard pulse and takes advantage of the short T_2 values generally encountered with solids. This pulse sequence preserves the magnetization of the preferred spin along the z axis while destroying all components of magnetization corresponding to the other spins presented in the spectrum. Selective pulses have also been successfully applied to simplify ^{13}C CSA measurement in 1D MAS-OFFMAS switched-angle experiments (22-23).

However, selective experiments to date have mainly focused on the selective excitation or saturation of one particular resonance or chemical shift range in the spectrum. If more than one resonance or chemical shift range could be inverted or saturated before the detection period, these experiments would have a broad range of applications. Some efforts have been made in the past to selectively excite more than one resonance. In the Double-DANTE sequence (11), selective excitation at two arbitrary frequencies can be achieved by the modulation of the phase of the DANTE sequence. Another demonstration provided by Ashida et al (23) in their 1D switched angle experiment showed that the inversion of two signals can be realized by sequentially applying two long soft pulses at different frequencies.

It will be demonstrated in this paper that selective saturation or inversion of multiple resonances can be achieved in spin systems with long spin lattice relaxation times by sequentially applying multiple DANTE sequences at different transmitter frequency offsets. In addition, a variation of the basic DANTE sequence which efficiently saturates the selected resonance is introduced. Several applications will be presented of this multiple resonance selective method which we will denote as "multiple offset DANTE". Experiments presented include spectra of complex organic compounds containing only one or two sideband families by saturation of the remaining resonances. This allows for more accurate determination of the sideband intensities and resultant principal components of the chemical shift tensor through removal of overlapping lines. The carbon aromaticity of coals can also be determined by the saturation of the entire aromatic region. Finally, with the addition of standard dipolar dephasing techniques to the multiple offset DANTE method, a spectrum containing only the spinning sideband family of a single aromatic carbon type (i.e., protonated, substituted, condensed, or phenolic) of a low rank coal can be obtained.

EXPERIMENTAL

All of the ^{13}C CP/MAS and selective irradiation experiments were performed on a Varian VXR-200 NMR spectrometer with a ^{13}C frequency of 50.318 MHz, using a CP/MAS probe from Doty Scientific Inc. A 50 KHz rf field strength was applied during the cross polarization period for both the ^{13}C and ^1H spin systems. When either higher decoupling rf field or higher selectivity for the DANTE sequence was necessary, the transmitter power levels of both channels were switched to the required level separately.

The basic pulse sequence used to perform the multiple offset DANTE is shown in Figure 1a. It starts with a classical cross polarization procedure to enhance the sensitivity of the observed rare nuclei (^{13}C), followed by a nonselective 90° pulse used to rotate the prepared magnetization back along the z axis. This is then followed by a series of DANTE sequences in which the transmitter frequency offset is changed. For the i th DANTE sequence, the parameters are as follows: transmitter frequency offset ω_i , pulse width T_{pi} , pulses interval T_{di} , and number of pulses N_i . Each DANTE sequence is, as shown in Figure 1b, a series of small tip angle pulses. If the cumulative total of the small tip angles is 180° , the net effect is inversion of the selected resonance whereas the selected resonance is saturated or destroyed by a long pulse train. An interrupted decoupling period DD_i is inserted between the DANTE sequences to allow the residual transverse magnetization to be fully destroyed before the next DANTE sequence starts; this delay time also serves for the switching time of the transmitter frequency offset. At the end of the DANTE group, a nonselective 90° pulse is used to return the magnetization to the x-y plane. Data acquisition then starts under the condition of high power proton decoupling.

In order to understand how these sequences work, several important features of the DANTE sequence must be reviewed. The selectivity of irradiation, ν_i , is approximately determined by the average rf strength $\nu_i = \gamma H_1 [T_{pi} / (T_{pi} + T_{di})]$, where γH_1 is the pulse field strength in Hz. The magnetization corresponding to those non-selected spins is nearly unperturbed at the end of each individual DANTE sequence, i.e., after the first DANTE sequence they remain at their original longitudinal position. The second DANTE sequence acts in an identical manner, preparing the magnetization situated at ω_2 from its longitudinal position to its predesignated state, while the other resonances outside the selectively irradiated range, including the resonance at ω_1 , remain unperturbed. The first irradiated resonance still remains in its prepared state as long as its T_1 is relatively long compared to the length of the DANTE sequence. In the same manner, additional resonances can be prepared by the application of more DANTE sequences at different transmitter offsets.

A variation of the DANTE sequence which has been found to be very powerful in performing saturation in solids is shown in Figure 1c. In this variation the classical long DANTE sequence, shown in Figure 1b, is replaced by a group of sub-DANTE sequences with the cumulative flip angle for each sub-DANTE sequence set to 90° . A dipolar dephasing period inserted between each of the sub-DANTE sequences destroys the transverse magnetization selectively produced by each sub-DANTE sequence. The dephasing time needed depends on the strength of the C-H dipolar coupling; however, a longer time can be used since the magnetization of the spins of interest remains along the z axis during these dephasing periods. This variation of the normal DANTE sequence is called the "dephased DANTE" sequence in the following discussion. It functions in a manner opposite to the SELDOM pulse sequence (21), by destroying only the longitudinal magnetization corresponding to the resonance line selected while leaving the remaining resonances unperturbed.

Hexamethylbenzene (HMB) and 1,2,3-trimethoxybenzene (TMB) were obtained from Aldrich and used as received. The Lewiston Stockton coal sample is from the Argonne Premium Coal Sample Bank. Simulation of the intensity pattern of a spinning sideband family was performed using a program similar to that described in the literature by Fenzke et al (24).

RESULTS AND DISCUSSIONS

The efficiency of the dephased DANTE sequence, demonstrated on HMB, is shown in Figure 2. In this test case the resonance for the methyl carbons in HMB is saturated by using both the classical long DANTE pulse train (Figure 2b) and the dephased DANTE sequence (Figure 2c). It is obvious that the longitudinal magnetization of the methyl carbons is still appreciable after the application of 400 pulses using the classical DANTE sequence, whereas 60 pulses are sufficient to destroy the magnetization with the use of the dephased DANTE sequence. The dephased DANTE sequence can be used to replace the individual DANTE sequence in Figure 1a to perform signal saturation. It should be noted that the efficiency of the dephased DANTE sequence decreases as the number of spinning sideband of the saturated resonance increases unless synchronized sample rotation is used.

A typical example of the multiple offset DANTE method is given in Figure 3. Figure 3a is the ^{13}C CP/MAS spectrum of TMB under fast spinning conditions. There are four peaks in the aromatic region with isotropic chemical shifts of 105, 124, 138 and 154 ppm. Figure 3b shows the resultant spectrum obtained by inverting the two outer peaks using the classical 180° -DANTE at $t_{01}=105$ and $t_{02}=154$ ppm and saturating the two inner peaks using the dephased DANTE sequence at $t_{03}=124$ and $t_{04}=138$ ppm. It is clear that the multiple offset DANTE pulse sequence works.

The application of this pulse sequence in cases of slow MAS spinning in order to retrieve the shielding tensor components is shown in Figure 4. Figure 4a is the classical ^{13}C CP/MAS SSB spectrum of TMB obtained at a spinning rate of 1106 Hz. This spectrum is very crowded and the sidebands from the aromatic carbons and aliphatic carbons overlap as expected. By using three DANTE sequences at different transmitter frequency offsets, one is left with the spinning sideband spectrum containing only the three methyl carbons and the C2 aromatic carbon (138 ppm), as shown in Figure 4b. The frequency offset is chosen such that the selectively irradiated frequency is on one of the spinning sidebands with relatively high intensity in the selected sideband family. In addition, this irradiated sideband should not be superimposed with the sidebands from any of the carbons whose magnetization is to be preserved. Figure 4c contains only the sideband patterns from the methyl carbons and was obtained by saturation of all of the aromatic carbon resonances using four DANTE sequences. In order to avoid perturbation of the methyl groups, the transmitter frequency offsets were set to the downfield first sideband positions instead of the central isotropic peaks for the two protonated carbons (105 and 124 ppm). The chemical shift tensor principal values for the three methyl carbons, obtained by simulation of the intensity distribution patterns, along with the values obtained from a single crystal study (25) are listed in Table 1. The two sets of data are consistent within experimental error. It should also be noted that the SSB pattern for the unsaturated C2 aromatic carbon in Figure 4b looks very similar to that in the classical CP/MAS spectrum (Figure 4a), demonstrating the selectivity of the pulse sequence. The intensity of the lines in Figure 4b for the non-saturated C2 are not perturbed even though there are sidebands of this carbon within 300 Hz of the saturating frequency. The principal values for C2 obtained for both experiments are within the experimental error for this technique, and these values are also close to the single crystal results (see Table 1). Similar

experiments were performed to isolate the sideband pattern of the other aromatic carbons, with the resulting tensor components also reported in Table 1. Thus, this multiple offset DANTE method can be used to perform tailored excitation to obtain the tensor components of carbons in complex solids where either a single crystal or 2D experiments were previously required.

The application of the multiple offset DANTE sequence to an even more complex sample is demonstrated in Figure 5 for a Lewiston-Stockton coal sample. This coal has been well characterized by NMR measurements in our laboratory (26) as well as by other researchers (27). In this case, the experiments are performed under conditions of moderate (2-4 KHz) spinning rates in order not to attenuate the cross polarization magnetization transfer mechanism for carbons with weak dipolar interactions (28). However, at this spinning rate the sidebands produced by the aromatic carbons will be superimposed on the aliphatic signal as is shown in Figure 5a. A second spectrum, Figure 5b is obtained by total elimination of the aromatic spinning sideband family using four DANTE sequences with transmitter frequency offsets of 110, 126, 138, 150 ppm (26). It is clear from this figure that the elimination of the aromatic signal is complete. Figure 5c is the difference between Figures 5a and 5b, and shows only the signal from the aromatic carbons. From the integrated signal intensities of these spectra a carbon aromaticity of 0.77 is calculated, in good agreement with the value of 0.75 obtained from a Bloch decay measurement performed at 100 MHz with a spinning rate of 4 KHz (29). This agreement again lends confidence in the high degree of selectivity of this method.

This type of tailored excitation is even more efficient for extracting the ^{13}C CSA information from a complex compound such as a low rank coal under slow MAS condition when combined with the dipolar dephasing technique. In this case, a rotational synchronized dipolar dephasing sequence (30) is incorporated into the pulse sequence in Figure 1a to suppress the signal from protonated carbons. The data in Figures 6a and 6b were obtained in the same fashion as in Figures 5a and 5b on the Lewiston Stockton coal but with the addition of a 50 μs dephasing period to suppress the signal from the protonated carbons. Only the sideband families from the nonprotonated aromatic carbons as well as the mobile methyl resonances remain in Figure 6a and only the mobile methyl carbons remain in Figure 6b. Figure 6c is obtained by inserting a 50 μs dipolar dephasing time followed by three DANTE sequences centered at 155, 145, and 138 ppm in order to achieve complete saturation of the rather large chemical shift range of the phenolic and substituted carbons. The resulting spectrum contains signals due to the condensed aromatic carbons (i.e., bridgehead), and the mobile methyl carbons. A 50 μs dephasing time is again inserted and followed by four DANTE sequences with transmitter frequencies at 150, 125, 120 and 110 ppm, respectively, in order to saturate the phenolic and inner aromatic carbons, leaving essentially only the signal from the substituted aromatic carbons along with that from the mobile methyl carbons (Figure 6d). By a linear combination of the spectra in Figures 5 and 6, it is possible to obtain the sideband patterns for the protonated, the condensed, as well as the substituted aromatic carbons. For example, the condensed aromatic sideband family is obtained by subtracting 6b from 6c, and the substituted aromatic sideband family can be isolated by subtracting 6b from 6d. The ^{13}C CSA tensor principal values obtained by digital simulation of these sideband patterns for each type of carbon are listed in Table 2. These values are similar to those reported in coals by using static powder pattern simulation and variable angle spinning experiments (31).

Now, let us consider the limitations of the multiple offset DANTE discussed above. First, the prepared magnetization before the last DANTE sequence will relax to its equilibrium state according to its individual spn-lattice relaxation time, T_1 . It generally takes 5 to 20 ms to prepare each resonance, thus limiting the number of resonances that can

be prepared. Fortunately, ^{13}C T_1 values in solids are generally very long, ranging from seconds to tens of seconds. If different values of T_1 exist, the resonance with the longest T_1 should be selectively irradiated first while the resonance with the shortest T_1 should be selected last. A second limitation arises from using normal rectangular pulses in the DANTE sequence which cause excitation not only at the center frequency, but also at other frequencies determined by the pulse length and spacing applied (10). This leads to a slight intensity loss at these other frequencies, or to a distortion in the baseline. Although this loss is small, it can become significant as the number of DANTE sequences increases. This loss could be reduced or eliminated with the use of a more selective pulse, such as shaped pulses (7-8).

CONCLUSIONS

Multiple resonance saturation and inversion in a solid state spin system with relatively long T_1 values can be easily achieved by using multiple DANTE pulse sequences at different transmitter frequency offsets. A powerful saturation pulse sequence (i.e., the dephased DANTE sequence) is proposed. This type of multiple resonance saturation method can be successfully applied to perform the spinning sideband separation in slow MAS experiments, including tailored excitation of a spinning sideband family of a single aromatic carbon type in a low rank coal. This method can also be applied to additional problems in solids, such as monitoring the spin diffusion process among carbons. In addition, the selective pulse sequence is not limited to the DANTE sequence; other sequences such as a soft pulse or a shaped pulse could be used in place of the DANTE sequence. This type of multiple resonance method based on changing the transmitter frequency offsets should also be useful in high resolution liquid state NMR, as long as the spin system under investigation has relatively long spin-lattice relaxation times.

ACKNOWLEDGMENT

This work is supported by the Pittsburgh Energy Technology Center through the Consortium for Fossil Fuel Liquefaction Science (Contract No. DE-FC22-89PC89852). Mr. Fu Ruqiang is acknowledged for providing the spinning sideband simulation program.

REFERENCES

1. Herzfeld, J. and Berger, A.E. *J. Chem. Phys.* 1980, 73 (12), 6021.
2. Kolbert, A.C.; DeGroot, H.J.M. and Griffin, R.G. *J. Magn. Reson.* 1989, 85, 60.
3. Kolbert, A.C. and Griffin, R.G. *Chem. Phys. Letts.* 1990, 166 (1), 87.
4. Alexander, S. *Rev. Sci. Instrum.* 1961, 32, 1066.
5. Freeman, R. and Wittekoek, S. *J. Magn. Reson.* 1969, 1, 238.
6. Freeman, R.; Wittekoek, S. and Ernst, R.R. *J. Chem. Phys.*, 1970, 52, 1529.
7. Silver, M.S.; Joseph, R.I. and Hoult, D.I. *J. Magn. Reson.* 1984, 59, 347.
8. McCoy, M.A. and Warren, W.S. *J. Magn. Reson.* 1985, 65, 178.
9. Morris, G.A. and Freeman, R. *J. Magn. Reson.* 1978, 29, 433.
10. Xi-Li Wu; Ping Xu; Friedrich, J. and Freeman, R. *J. Magn. Reson.* 1989, 81, 206.
11. Geen, H.; Xi-Li Wu; Ping Xu; Friedrich, J. and Freeman, R. *J. Magn. Reson.* 1989, 81, 646.
12. Freeman, R. *Chem. Rev.* 1991, 91, 1397.
13. Vega, S. and Pines, A. *J. Chem. Phys.* 1977, 66, 5624.
14. Polak, M. and Vaughan, R.W. *Phys. Rev. Lett.* 1977, 39, 1677.

15. Vega, S. and Naor, Y. *J. Chem. Phys.* 1981, 75, 75.
16. Brunner, P.; Reinhold, M. and Ernst, R.R. *J. Chem. Phys.* 1980, 73, 1086.
17. Reinhold, M.; Brunner, P. and Ernst, R.R. *J. Chem. Phys.* 1981, 74, 184.
18. Vanderhart, D.L. *J. Magn. Reson.* 1989, 72, 13.
19. Caravatti, P.; Bodenhausen, G. and Ernst, R.R. *J. Magn. Reson.* 1983, 55, 88.
20. Tekely, P.; Brondeau, J.; Marchal, J.-P.; and Delpuech, J.-J. *Fuel*, 1986, 65, 997.
21. Tekely, P.; Brondeau, J.; Elbayed, K.; Retourmard, A. and Canet, D. *J. Magn. Reson.* 1988, 80, 509.
22. Iwamiya, J.H.; Davis, M.F. and Maciel, G.E. *J. Magn. Reson.* 1990, 88, 199.
23. Ashida, J.; Nakal, T. and Terao, T. *Chem. Phys. Letts.* 1990, 168, 523.
24. Fenzke, D.; Maeb, B. and Pfeifer, H. *J. Magn. Reson.* 1990, 88, 172.
25. Carter, C.M.; Facelli, J.C.; Alderman, D.W. and Grant, D.M. *J. Chem. Soc., Faraday Trans. 1*, 1988, 84 (11), 3673.
26. Solum, M.S.; Pugmire, R.J. and Grant, D.M. *Energy & Fuels*, 1989, 3 (2), 187-193.
27. Wind, R.A.; Jurkiewicz, A. and Maciel, G.E. *Fuel*, 1989, 68, 1189.
28. Snape, C.E.; Axelson, D.E.; Botto, R.E.; Delpuech, J.J.; Tekely, P.; Gerstein, B.C.; Pruski, M.; Maciel, G.E.; Wilson, M.A. *Fuel*, 1989, 68, 547.
29. Solum, M.S.; Yi Jiang, Jian; Pugmire, R.J.; Grant, D.M. Manuscript in preparation.
30. Munowitz, M.G.; Griffin, R.G.; Bodenhausen, G. and Huang, T.H. *J. Am. Chem. Soc.* 1981, 103, 2529.
31. Orendt, A.M.; Solum, M.S.; Sethi, N.K.; Hughes, C.D.; Pugmire, R.J.; and Grant, D.M. "Measurement of ^{13}C Chemical Shielding Anisotropy in Coal", in "Techniques in Magnetic Resonance: Advances in Chemistry Series No. 229". Botto, R.E. and Sanada, Y. Editors (1992) ACS Publications.

Table 1. Principal values of ^{13}C chemical-shift tensors obtained through digital simulation of sideband intensity patterns^a

Assignment	σ_{11}	σ_{22}	σ_{33}	σ_{avg}
1,2,3-trimethoxybenzene				
M ₁	82(83)	72(71)	9(9)	54
M ₂	87(88)	84(83)	10(10)	60
M ₃	81(82)	71(70)	13(13)	55
C _{1,3}	221(218)	168(172)	72(73)	154
C ₂ ^b	174(179)	169(164)	71(71)	138
C ₂ ^c	172	171	71	138
C _{4,6}	190(187)	119(123)	10(7)	106
C ₅	229(227)	133(136)	11(10)	124

^aData in parentheses are single crystal results (25).

^bObtained using sideband intensities from Figure 4a.

^cObtained using the sideband intensities in Figure 4b.

Table 2. Principal values of ^{13}C chemical shift tensors obtained through digital simulation of sideband intensity patterns for the Lewiston Stockton Coal

Assignment	σ_{11}	σ_{22}	σ_{33}	σ_{avg}
Protonated	230	126	14	123
condensed	192	184	2	126
substituted	238	158	18	138

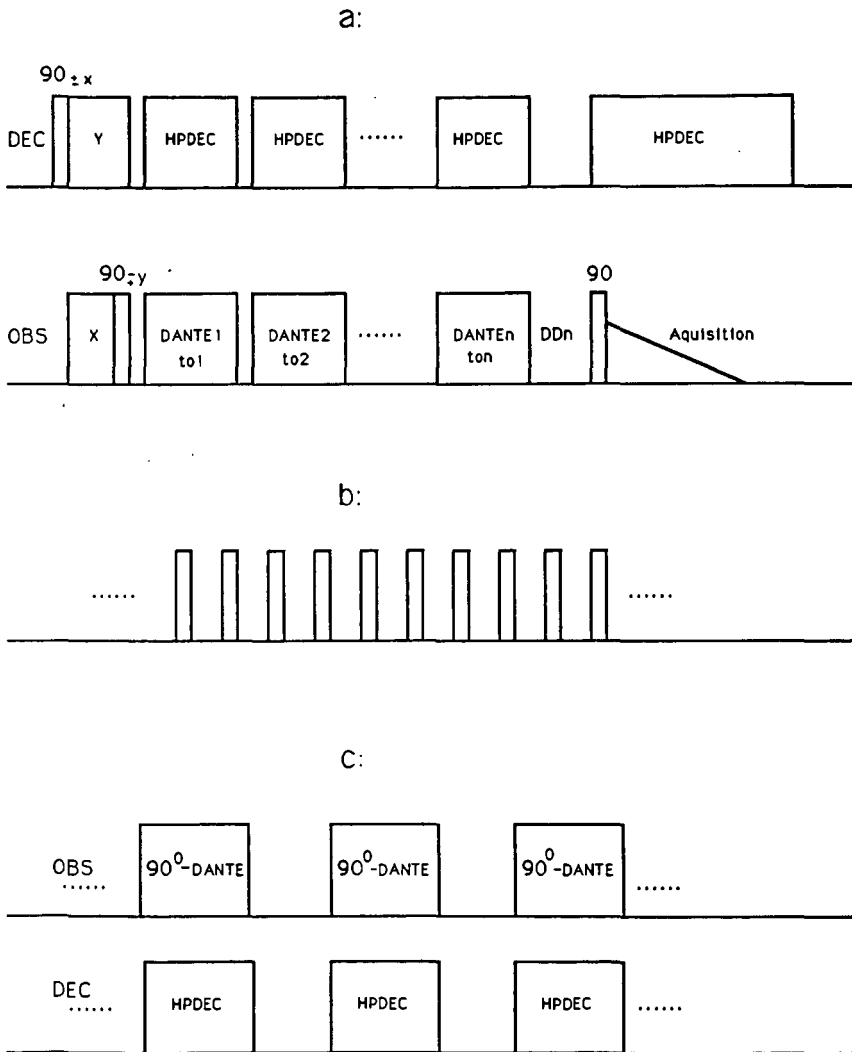


Figure 1. Pulse sequences: a) the general pulse sequence used to perform multiple resonance saturation and inversion, with the parameters for the i th DANTE sequence: transmitter frequency offset ω_i , pulse width T_{pi} , pulse interval T_{di} , and the number of pulses N_i ; b) the classical DANTE sequence; c) the dephased DANTE sequence.

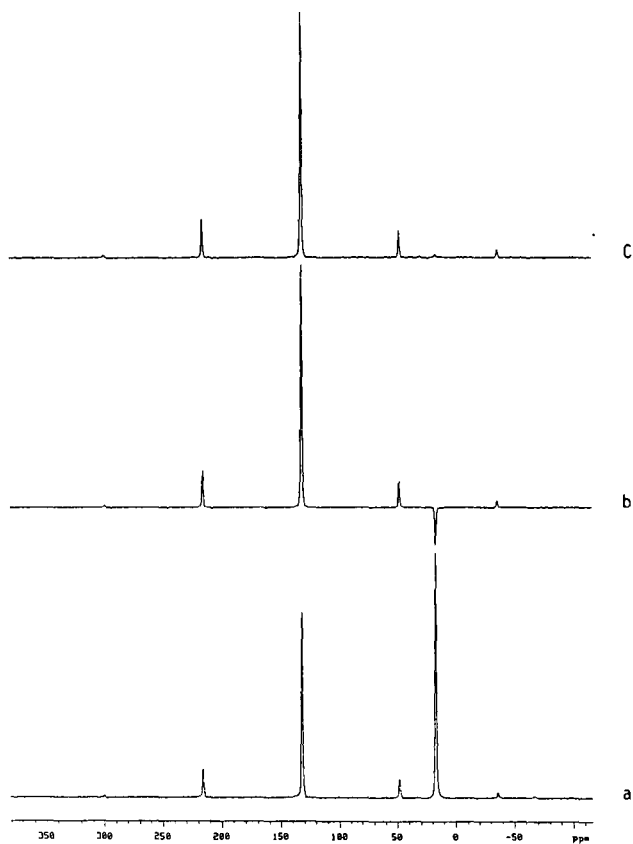


Figure 2. ^{13}C CP/MAS spectra of HMB obtained with sample spinning rate of 4.2 KHz, contact time of 3 ms, and 64 scans: a) the normal ^{13}C CP/MAS spectrum; b) saturation of the methyl carbon using the classical DANTE sequence with 400 hard pulses, pulse width $0.25\ \mu\text{s}$ and the interval between pulses $50\ \mu\text{s}$; c) saturation of the methyl carbon using the dephased DANTE sequence with three sub-DANTE sequences, each containing 20 hard pulses with the same parameters as in b, and a dephasing time of 16 ms.

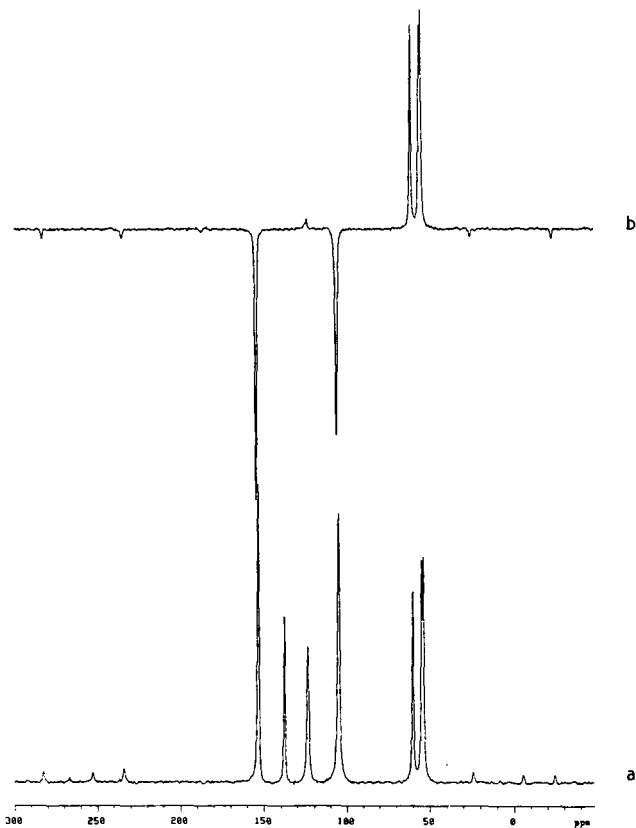


Figure 3. ^{13}C CP/MAS spectra of 1,2,3-Trimethoxybenzene (TMB) obtained with sample spinning rate of 6.0 KHz, contact time of 4 ms: a) the normal ^{13}C CP/MAS spectrum; b) spectrum obtained using the sequence in Figure 1a. The inner two aromatic resonances were saturated using the dephased DANTE sequence with offset frequencies centered at $\tau_1=124$ ppm and $\tau_2=138$ ppm and the outer two aromatic resonances were inverted using two 180° DANTE sequences with offset at $\tau_3=154$ ppm and $\tau_4=104$ ppm. Each dephased DANTE contains three 90° -DANTE of 20 pulses with pulse width 0.25 μs and a dephasing time between the sub-DANTE sequences of 16 ms.

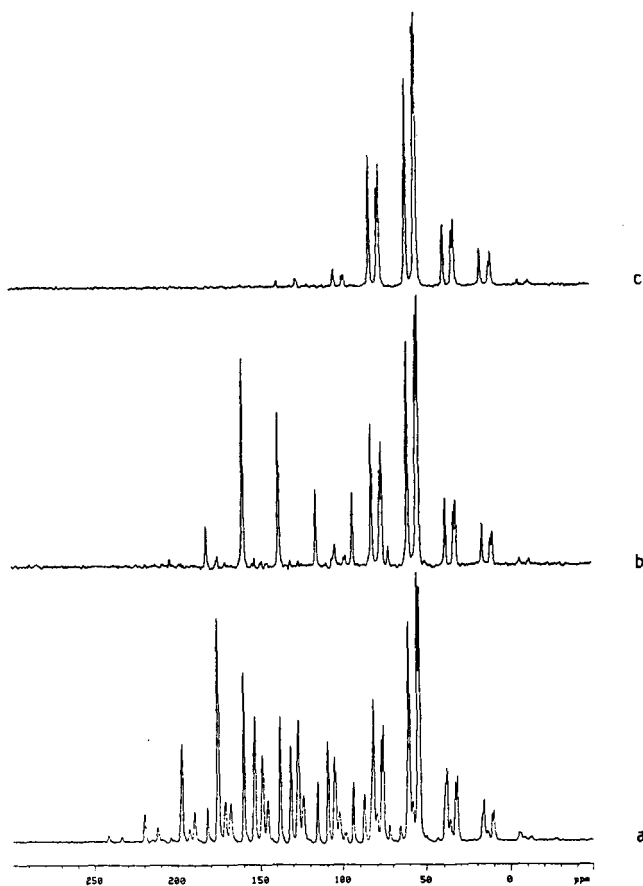


Figure 4. Spectra of TMB obtained with sample spinning rate 1106 ± 5 Hz and contact time of 4 ms: a) normal ^{13}C CP/MAS spectrum; b) spectrum obtained using three long DANTE sequences at transmitter frequency offsets of 126, 146 and 154 ppm in order to saturate these three spinning sideband families; c) spectrum obtained using four long DANTE sequences at 126, 146, 138, and 154 ppm to saturate the entire aromatic sideband family. The parameters for each long DANTE sequence are $T_{pi}=0.25 \mu\text{s}$, $T_{di}=100 \mu\text{s}$, $N_i=150$ and $DD_i=8$ ms.

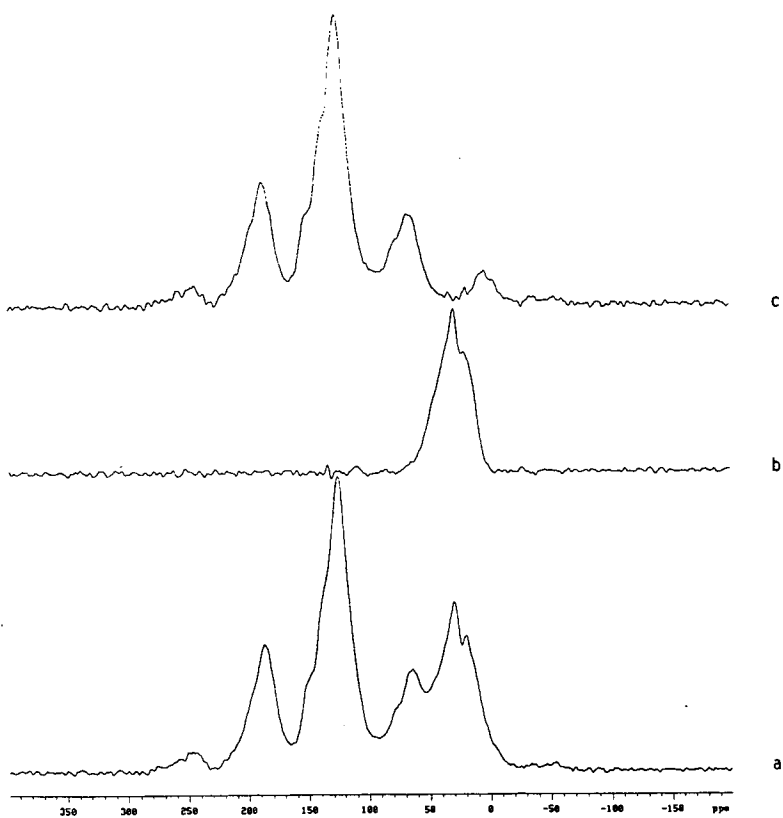


Figure 5. ^{13}C CP/MAS spectrum of Lewiston Stockton coal obtained with a sample spinning rate 3000 ± 30 Hz, and 1 ms contact time: a) the classical ^{13}C CP/MAS spectrum; b) application of four long DANTE sequences at 110, 126, 138 and 150 ppm to saturate the entire aromatic carbon spinning sideband family; c) subtraction of a from b. The parameters for each DANTE sequence are: $T_{pi}=0.5 \mu\text{s}$, $T_{di}=30 \mu\text{s}$, $N_i=150$, $DD_i=2$ ms;

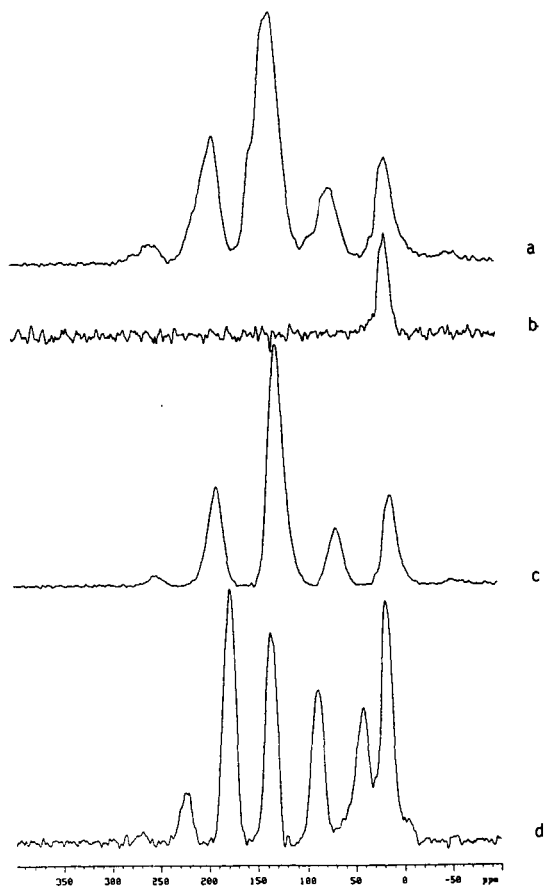


Figure 6. Tailored excitation of the spinning sideband family for various types of carbons in Lewiston Stockton coal by combining the multiple offset DANTE method with the dipolar dephasing technique with a contact time of 1 ms, recycle delay time of 4s and sample spinning rate 3000 ± 30 Hz (6d with sample spinning rate 2100 ± 50 Hz), and $T_{pi}=0.5 \mu s$, $T_{di}=30 \mu s$, $N_i=150$, $DD_i=2$ ms; a) dipolar dephasing spectrum with dephasing time of $50 \mu s$; b) spectrum obtained in a similar manner to Figure 5b except with a dephasing time of $50 \mu s$ inserted between the contact time and the first 90° pulse in the pulse sequence shown in Figure 1a; c) spectrum obtained in a similar manner to (b) except with three DANTE sequences at 138, 145 and 155 ppm used to saturate the phenolic and substituted aromatic sideband families; d) spectrum was again obtained in a similar manner to (b) but with four DANTE sequences used at 110, 120, 125 and 150 ppm to saturate the sideband families of the condensed and phenolic aromatic carbons. The remaining signals are due to methyl and substituted aromatic carbons.

QUANTITATIVE DECONVOLUTION OF ^{13}C NMR SPECTRA OF ILLINOIS #6 COAL

M.A. Jacintha,^a C.R. Dybowski,^a W.H. Calkins,^b W.D. Provine,^b M.T. Klein^b

Center for Catalytic Science and Technology

^aDepartment of Chemistry and Biochemistry

and

^bDepartment of Chemical Engineering

University of Delaware

Newark, DE 19716

Keywords: coal, deconvolution, ^{13}C NMR

INTRODUCTION

The quantification of chemical functionality is necessary to construct a picture of the structure of coal. The aromaticity of coal has been determined in a relatively quantitative manner using solid-state ^{13}C NMR spectroscopy,¹ although there has been a great deal of discussion about how this process can be carried out.² In this study, we discuss how one might further deconvolute the carbon spectrum of coal, into various aromatic and aliphatic components.

EXPERIMENTAL

Illinois #6 coal was obtained from the Argonne Premium Coal Sample Bank. The solid coal was analyzed by variable-contact-time solid-state ^{13}C CPMAS NMR spectroscopy, with a Chemagnetics m100S spectrometer operating at 25.1 MHz for carbon. Samples were kept in Kel-F[®] spinners to avoid spurious resonances from spinner material. Typical spinning speeds were 3 kHz. The acquisition time was 50 ms with a ^1H 90° pulse width of 6.5 μs and a pulse delay of 1 s. Quantification of both the original and the deconvoluted spectra were performed by fitting the integral intensities to the magnetization-recovery equation.³ The CPMAS spectra obtained at the various contact times were digitized using a TANDY Digitizer Pad, corrected for baseline roll and analyzed with the Peakfit[®] computer fitting program.

RESULTS

Various combinations of functions were tried. Of the many sets tried, only the combination of Lorentzian and Voigt functions given in Tables 1 and 2 fit the CPMAS spectra

obtained at various contact times over the full range of contact times. The aromatic region was resolved into three Lorentzians and one Voigt function. Similarly, the aliphatic region was resolved into two Lorentzians and two Voigts. The chemical-shift range, type of line-shape function, $T_{1\rho H}$, T_{CP} and ρ for each of the aromatic and aliphatic components are listed in Tables 1 and 2, respectively.

From the data in Tables 1 and 2, one sees that the parameters determining the cross-polarization behavior of the various components vary by up to a factor of 4 for $T_{1\rho H}$, and by a factor of 15 for T_{CP} . With such a wide variation of the values of the parameters for various components of the coal, it is readily understandable why integration of a CP-MAS spectrum taken at a single contact time cannot properly represent the distribution of carbon as accurately as possible. These results are related to the usual time constants determined for the aromatic and aliphatic regions, in that weighted averages of the $1/T_{1\rho H}$ and $1/T_{CP}$ of the components in a region are equal to those determined by variation of the integrals with contact time.⁴

In Figure 1, a simulated spectrum of this coal (based only on CPMAS-derived parameters) is compared with a fully relaxed Bloch-decay (BD) spectrum of the same coal. While the BD spectrum is relatively noisy, the simulated spectrum closely approximates its features. The BD spectrum was obtained with a pulse delay of 120 s. We have found that, to obtain fully relaxed spectra one must wait much longer than the suggested pulse delay of 20 s.⁵

One may be tempted to assign the components generated by this process, through comparison of the mean chemical shifts to those of pure model compounds. However, this is an oversimplification of the speciation. The range of shifts for each component as indicated by the half-width in the Tables is rather wide. In these ranges fall many different carbon functionalities. Thus, an analysis of this type will only coarsely describe the results. For example, the two downfield aromatic components may be associated with carbon-oxygen linkages. One possible solution to assigning the NMR components is correlation of these results with other measures of the coal structure (obtained by wet-chemical analysis or other spectroscopic investigation) using the techniques of factor analysis.⁶ To do this requires the analysis of many different coal samples such as the Argonne Premium Coal Samples. We are exploring this possibility.

References

1. Maciel, G.E.; Sindorf, D.W. *J. Am. Chem. Soc.* **1980**, *102*, 7607.
2. Snape, C.E.; Axelson, D.E.; Botto, R.E.; Delpuech, J.J.; Tekely, P.; Gerstein, B.C.; Pruski, M.; Maciel, G.E.; Wilson, M.A. *Fuel* **1989**, *68*, 547.
3. Botto, R.E.; Winans, R.E. *Energy and Fuels* **1987**, *1*, 173.
4. Solum, M.; Pugmire, R. J.; Grant, D. M. *Energy and Fuel* **1989**, *3*, 187.
5. Snape, C.E.; Love, G.D. *Prepr. of the Fuel Chem. Div.* **1991**, *36*, 877.
6. Malinowski, E.F.; Howery, D.F. *Factor Analysis in Chemistry*; Wiley: New York, 1980.

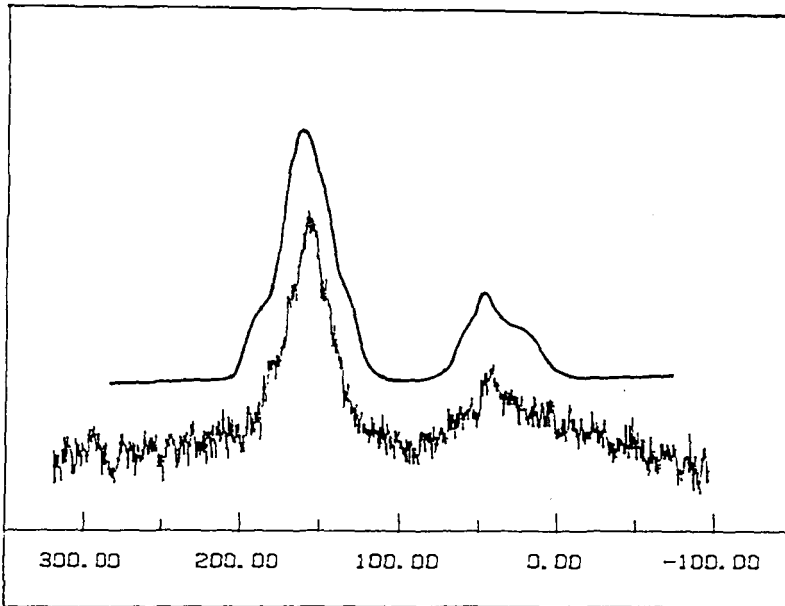
Table 1. Aromatic Components of Argonne Illinois #6 Coal

$\langle \delta \rangle$ (ppm)	Function	$T_{1\rho H}$ (ms)	T_{CP} (ms)	f
170 ± 5	Lorentzian	1.7 ± 0.05	0.39 ± 0.004	0.14 ± 0.02
160 ± 7.5	Lorentzian	3.0 ± 0.05	0.43 ± 0.004	0.16 ± 0.02
150 ± 12	Voigt	6.0 ± 0.05	0.30 ± 0.004	0.27 ± 0.02
125 ± 5	Lorentzian	3.5 ± 0.05	0.13 ± 0.004	0.12 ± 0.02

Table 2. Aliphatic Components of Argonne Illinois #6 Coal

$\langle \delta \rangle$ (ppm)	Function	$T_{1\rho H}$ (ms)	T_{CP} (ms)	f
75 ± 5	Lorentzian	4.0 ± 0.05	0.05 ± 0.004	0.07 ± 0.02
65 ± 7.5	Voigt	3.8 ± 0.05	0.18 ± 0.004	0.12 ± 0.02
50 ± 7.5	Lorentzian	7.0 ± 0.05	0.14 ± 0.004	0.09 ± 0.02
25 ± 2	Voigt	1.0 ± 0.05	0.75 ± 0.004	0.04 ± 0.02

Figure 1. Comparison between a simulated fully-relaxed spectrum and a Bloch-decay spectrum



¹³C NMR ANALYSIS OF MODEL SULFONIUM SALTS

T. K. Green, W. G. Lloyd, L. Gan, P. Whitley, K. Wu

Department of Chemistry, Western Kentucky University
Bowling Green, KY 42101

INTRODUCTION

The speciation and quantification of organic sulfur forms in fossil fuels is an area of research which has received much attention in recent years (1). Most of the techniques employed either chemically change the sulfur structures or fail to fully detect sulfur structures due to their nonvolatility. Exceptions are X-ray absorption spectroscopy (XAS) and X-ray absorption near edge spectroscopy (XANES) used recently by Gorbaty et al. to quantify sulfur forms in coals and heavy petroleum (2,3). This paper describes a new, nondestructive NMR method which offers potential for identifying and quantifying sulfur forms in fossil fuels. The method is based on the methylation of sulfur compounds to form sulfonium salts. We demonstrate that the ¹³C chemical shift of the added methyl carbon is very sensitive to the nature of the sulfur atom to which it is bonded. Thus, in principle, dialkylsulfides, alkylarylsulfides, diarylsulfides, benzothiophenes and dibenzothiophenes can be distinguished by this technique. A preliminary study using crude petroleum is presented to illustrate the potential of this technique for identifying sulfur compounds in fossil fuels.

EXPERIMENTAL

Methylation of Model Compounds

The procedure for methylation is similar to that given by Acheson and Harrison (4). Approximately 1 mmol of the sulfur compound and 1.2 mmol of AgBF₄ were dissolved and stirred in 3.0 mL of dichloroethane under argon. Methyl iodide (2.0 mmol) was added via syringe to the stirred solution. A yellow precipitate (AgI) immediately formed in all cases. The reaction was allowed to stir overnight after which the solution was filtered to remove AgI. The AgI precipitate was washed with acetonitrile. The filtrate was then rotovaporized at 40-50 °C to remove excess solvent. The residue was triturated with ether to give a precipitate. In some cases an oil formed which could not be precipitated, in which case the oil was dissolved in d₃-acetonitrile or d₆-acetone and analyzed directly by NMR. If a precipitate formed, it was filtered and washed with ten drops of water to remove excess AgBF₄. The solid was then dissolved in acetonitrile. Ether was then added until the solution became slightly turbid. The solution was then cooled in dry ice/acetone to effect crystallization. The yields ranged from 40 to 80%.

Methylation of Crude Petroleum

The same basic procedure was used to effect methylation of an Arabian crude petroleum sample. The sample was obtained from Ashland Oil and contains 2.8% sulfur. The amounts of the reagents were the same except that 1 g of petroleum was used in place of the sulfur compound. The solution was stirred overnight and then the AgI was filtered off. The solvents were removed by rotovaporization at 40-50°C and the residue was then placed in a vacuum oven overnight at room temperature. A small amount of residue (100 mg) was then dissolved in about 1 mL of d₃-acetonitrile. Not all of the residue dissolved so the solution was filtered and then placed in an NMR tube for analysis.

FT-NMR Analysis

¹³C spectra were obtained at 270 MHz using a JEOL CPF 270 FT-NMR. A pulse width of 2.8 us and a pulse delay of 3.0 sec were used. The number of transients ranged from 1500-5000 for the petroleum samples, depending on the concentration.

RESULTS AND DISCUSSION

Model Compounds

Sulfur is an excellent nucleophile. As such, sulfides and thiophenes react with alkyl iodide to yield sulfonium ions as shown below (5,6).



The reaction is favored by polar solvents such as acetonitrile and acetone. Since iodide is also a good nucleophile, the reaction is reversible. However, if the reaction is carried out in the presence of silver tetrafluoroborate (AgBF_4), silver iodide is precipitated, leaving the poor nucleophile tetrafluoroborate as the solute anion. Alkyl and aryl sulfides and thiophenes have all been successfully alkylated by this method.

Only limited ^{13}C chemical shift information exists on methyl sulfonium salts (7,8). Therefore, we prepared models for examination by NMR spectroscopy. The results are shown in Table I, where the chemical shifts of the added methyl carbon (relative to TMS) are listed.

The S-CH₃ chemical shifts cover a 15 ppm range for the model compounds examined. Among the sulfides, the chemical shift increases with the number of aryl groups bonded to the sulfur atom. This same trend is observed for the thiophenes, with the chemical shift increasing with increased aryl substitution about the central thiophenium ring. Comparing the chemical shifts of the S-methylbenzo[b]naphtho[2,1d]thiophenium (7) and S-methyldibenzothiophenium cations (6) reveals the effect of an additional fused ring - a slight upfield shift. Although more model compound work is required, these initial results indicate the potential for speciation of sulfur forms by the NMR technique.

Methylation of Crude Petroleum

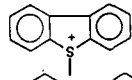
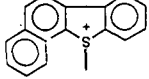
To demonstrate the usefulness of this approach, we have methylated an Arabian crude petroleum sample. The aliphatic region of the ^{13}C NMR spectrum of the crude dissolved in CDCl_3 is shown in Figure 1 (spectrum A). The major peak in the spectrum is at approximately 30 ppm (relative to TMS). This peak is attributed to aliphatic methylene groups by distortionless enhanced polarization transfer techniques (DEPT). The spectrum of the product from S-methylation using ordinary methyl iodide as methylating reagent is shown above this spectrum (spectrum B). The solvent is this case was d_3 -acetonitrile. This spectrum is very similar to that of the original crude, with the same set of major peaks. The small differences in chemical shifts might be attributed to a solvent effect. There is no apparent evidence of added methyl groups in the spectra of the methylated crude.

The spectrum of the product using 99% ^{13}C -enriched methyl iodide is also shown in Figure 1 (spectrum C). This spectrum is strikingly different than the other two spectra. The difference is most logically attributed to added methyl groups whose signals are enhanced due to the isotopic enrichment of the methyl iodide. This spectrum is expanded in Figure 2 to illustrate more detail. Although complex, this spectrum was highly reproducible in a duplicate run. Some of the peaks can be attributed to the original petroleum and are indicated with an asterisk (*).

Obviously, the spectrum in Figure 2 contains a considerable amount of information most of which is presently not interpretable. However, some preliminary assignments can be made. The region from 32.0 to 36.0 ppm is expanded and shown in Figure 3. There are six major peaks in this region with only one peak at 32.7 attributed to the original petroleum. In order to make possible assignments for these peaks, we have spiked the sample with known samples of S-methyldibenzothiophenium and S-methylbenzo[b]naphtho[1,2d]thiophenium tetrafluoroborate salts (compounds 6 and 7, Table I, respectively). The spectrum of the spiked sample is shown above the unspiked sample. The peaks at 34.9 and 34.2 ppm are seen to grow, indicating that these peaks correspond to compounds 6 and 7, respectively. Thus a tentative assignment can be made to these two peaks in the spectrum.

TABLE I

NMR Data on Model Sulfonium Salts

Cation ^a	δ , ppm (CH ₃) ^b
(1) $\text{CH}_3\text{CH}_2-\overset{+}{\text{S}}(\text{CH}_3)-\text{CH}_2\text{CH}_3$	21.0, 19.8 ^c
(2) $\text{C}_6\text{H}_5-\overset{+}{\text{S}}(\text{CH}_3)-\text{C}_6\text{H}_5$	25.0
(3) $\text{C}_6\text{H}_5-\overset{+}{\text{S}}(\text{CH}_3)-\text{C}_6\text{H}_5$	28.4
(4) 	28.3
(5) 	31.7
(6) 	34.9
(7) 	34.2

^a Tetrafluoroborate salts^b Relative to TMS^c Reference 7

CONCLUSIONS

We have determined the S-CH₃ ¹³C chemical shifts for a variety of model sulfonium salts. The data reveal that the chemical shift is very sensitive to the nature of the sulfur atom bonded to the methyl group. Thus a variety of model sulfur compounds can be readily distinguished by S-methylation with subsequent NMR analysis. The ¹³C NMR spectrum of methylated crude petroleum using isotopically-enriched methyl iodide reveals a number of peaks, most of which are unidentified at this time. More model compound work is obviously needed in order to more fully interpret the spectrum. However, it is clear that the technique offers potential for speciation of sulfur forms in fossil fuels. The technique might be particularly useful for analyzing sulfur forms in coals, since many of the sulfur-containing compounds are nonvolatile and are not readily analyzed by other techniques.

ACKNOWLEDGEMENTS

TKG acknowledges the Faculty Research Committee at WKU for a grant to initiate this study. We thank Howard Moore of Ashland Oil for the petroleum sample.

REFERENCES

1. Stock, L. M.; Wolney, R.; Basdrichna, B. Energy Fuels 1989, **3**, 651-61.
2. George, G. N.; Gorbaty, M. L., J. Am. Chem. Soc. 1989, **111**, 3182
3. George, G. N.; Gorbaty, M. L.; Keleman, S. R.; Sansone, M. Energy Fuels 1991, **5**, 93-97.
4. Acheson, R. M.; Harrison, D. R. J. Chem. Soc. C 1970, 1764.
5. Lowe, P. A. in "The Chemistry of the Sulphonium Group," Stirling, C. J. M.; Patai, S.; Eds.; John Wiley, New York, 1981, Chapter 11.
6. Trost, B. M.; Melvin, L. S., "Sulfur Ylids," Academic Press, New York, 1975.
7. Barabrella, C.; Dembach, P.; Garbassi, A. Tetrahedron Lett. 1980, **21(21)**, 2109-12.
8. Heldeweg, R. F., Hogeveen, H. Tetrahedron Lett. 1974, (1), 75-78.

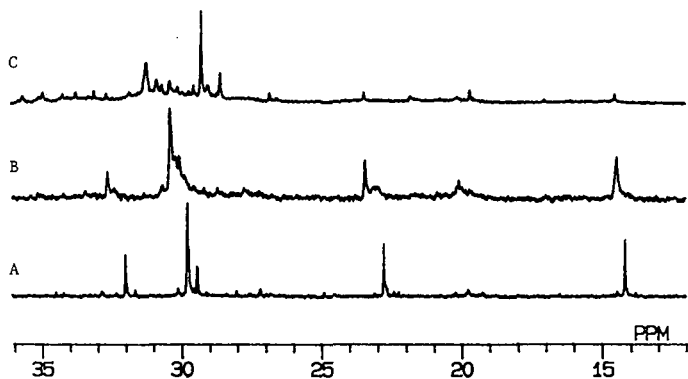


Figure 1. ^{13}C NMR Spectra of Arabian Crude. A - original crude in CDCl_3 . B - methylated crude in d_3 -acetonitrile. C - methylated crude in d_3 -acetonitrile using 99% ^{13}C -enriched methyl iodide.

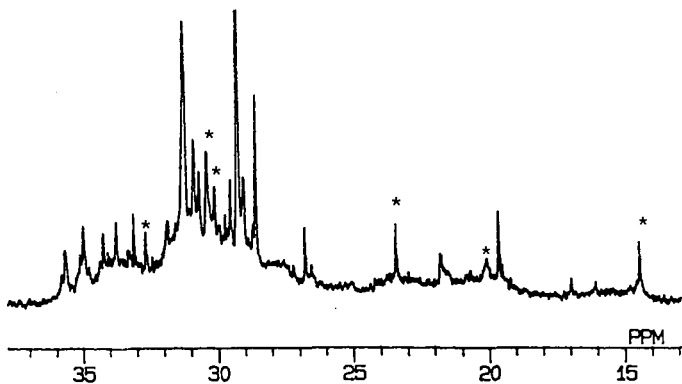


Figure 2. ^{13}C NMR Spectrum of Methylated Arabian Crude using 99% ^{13}C -enriched methyl iodide. Asterick indicates peak attributed to original crude.

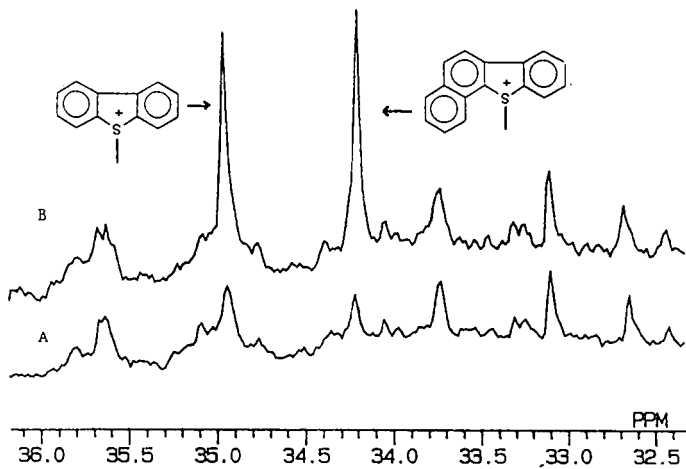


Figure 3. ^{13}C NMR Spectrum of Methylated Arabian Crude using 99% ^{13}C -enriched methyl iodide. A - unspiked sample. B - sample spiked with Compounds 6 and 7.

¹³C NMR SPECTROSCOPIC STUDIES OF ILLINOIS #6 COAL AND THE PRODUCTS OF ITS LIQUEFACTION

W.D. Provine,^a M. A. Jacintha,^b M.T. Klein,^a W. H. Calkins,^a and Cecil Dybowski^b

Center for Catalytic Science and Technology

^aDepartment of Chemical Engineering
and

^bDepartment of Chemistry and Biochemistry
University of Delaware
Newark, DE 19716

Keywords: coal, liquefaction, short contact time, ¹³C NMR

INTRODUCTION

The direct liquefaction of coal involves the cleavage of a variety of bonds, both covalent and otherwise, having a wide range of activation energies.^{1,2} The weaker bonds of lower activation energy are expected to break first, forming somewhat different products than are formed later in the process. As the coal becomes liquefied, the liquid products are also subject to further reaction. A practical application of these concepts is the observation that higher yields of liquids are obtained when the liquefaction process is carried out in two or more stages under somewhat different conditions.³ While the specific bonds that are first broken is still not known, examination of the process at very low conversions even before the coal has become a liquid should be of great interest. To do this, one requires a sampling system capable of providing samples at very short, well-defined reaction times (low conversions) of less than one minute to perhaps 5 to 15 minutes with mass and heat transfer not limiting and temperature and residence times accurately known. It is to report the preliminary results of such a study using solid-state NMR spectroscopy that this paper is presented.

EXPERIMENTAL

Reactor and sampling system. The system selected for study is a 1 liter CSTR (continuous stirred tank reactor) [Fig. 1] with a constant flow of tetralin (7 liters/hour) as a hydrogen-donor solvent in a 900psig nitrogen atmosphere (450 sccm nitrogen) at a selected temperature (390°C). 50-gram charges of coal in a tetralin slurry (1:2 coal to solvent) are injected through a rupture disk almost instantaneously by diverting the pressurized solvent into the charging bomb. Isothermal and isobaric conditions are achieved within 20s after injection. Product samples taken in an automated sampling manifold at 2, 23, 55, 87, 119, and 155s after injection are quenched to

150°C with a countercurrent water heat exchanger. The system was tested with samples of dibenzylether (with the inert biphenyl run as a blank) to check the behavior of a compound with well-known kinetics in the system and to determine the distribution of residence times. More details about the reactor system can be found in another paper.⁴

Sample work-up. The solids were filtered and washed with methylene chloride and dried in a vacuum oven. The liquefaction products were placed in a rotary evaporator to remove tetralin and lower-boiling products. The light fraction was analyzed by GC/MS and the heavy fraction by NMR spectroscopy.

Ash measurements. Conversion of the coal was determined by measuring the low-temperature ash content of the solid residue and comparing it to that of the unreacted coal. A low-temperature asher [LFE Corporation, LTA-302] was operated around 75-100 watts. The oxygen flow rate was kept at 100 cc/min.

NMR spectroscopic experiments. Residual solids were analyzed by variable-contact-time solid-state ¹³C CPMAS NMR spectroscopy,⁵ with a Chemagnetics m100S spectrometer operating at 25.1 MHz for carbon. Samples were kept in Kel-F[®] spinners to avoid spurious resonances from spinner material. Typical spinning speeds were about 3 kHz. The acquisition time was 50 ms with a ¹H 90° pulse width of 6.5 μs and a pulse delay of 1 s. Carbon aromaticities were derived by fitting integrated signal intensities for the aliphatic and aromatic carbon bands to the magnetization-recovery equation.⁶ We checked this procedure on known model compounds (hexamethylbenzene, adamantane and high-molecular-weight polystyrene), and in each case found that we could determine the relative fraction of intensity in one NMR peak to within ±0.01 of the known stoichiometric value. The Bloch-decay experiments were done with pulse delays of 5 s, 20 s and 120 s.

ESR experiments. ESR spectra were recorded on a Varian E-109 spectrometer at 9.1 GHz with 100 kHz modulation. All spectra were recorded at ambient temperature (295 ± 2 K) and DPPH was used as an external spin standard.

RESULTS

All of the experiments reported here were carried out on an Illinois #6 coal obtained from AMOCO Corporation.

One point of concern in measurements with NMR spectroscopy of solids is that the presence of paramagnetic centers may render some of the carbon NMR-invisible.⁶ If that process affected one carbon type more than another, aromaticities determined with NMR techniques could be skewed so that they do not reflect actual changes in the carbon, but rather the increase in paramagnetic centers. To address this point, we determined the paramagnetic concentrations in a set of residual solids as a function of residence time, as well as the aromaticity. These data are plotted against each other in Figure 2. As can be seen, the concentration of paramagnetic centers did change by more than a factor of four with processing. [The spin density is reported as the ratio of that in the residue to that of the unprocessed Illinois #6 coal.] The comparison of the ¹³C-derived aromatic fractions with the spin densities shows that there is very little, if any, correlation between these two variables. We assume,

therefore, that for this system the changes in aromaticity with residence time are not attributable to changes in paramagnetic concentrations.

Another issue regarding quantitation is the contention that Bloch-decay experiments give reliably quantitative information on the aromaticity of coal as compared to the variable-contact-time CPMAS experiments. When a Bloch-decay experiment was performed with a pulse delay of 20 s, the aromaticity value obtained was 0.77, whereas with a pulse delay of 120 s, the aromaticity value obtained was 0.66. The larger relative aromaticity value obtained in the experiment with a shorter pulse delay may be due to insufficient aromatic carbon nuclear relaxation toward equilibrium magnetization. The value of 0.66 is within experimental error, the same value found by fitting the entire build-up and decay curve in a CPMAS experiment.

The f_a values for Illinois #6 and the residual solids obtained upon liquefaction are given in Fig. 3 (as determined by fitted carbon magnetization curves) as a function of residence time. Conversions are reported as a function of residence time in Table 1.⁷ The graph in Fig. 3 is roughly divided into three regions: (a) a very early, almost instantaneous, decrease in aromatic fraction, (b) an intermediate regime in which the aromatic fraction increases and (c) a regime in which the aromatic fraction again decreases with time. The initial sharp decrease in aromaticity (after a residence time of only 2s) may be attributed to the removal of small aromatic moieties not covalently bound to the coal structure. An increase in the number of condensed aromatic protons in the liquid phase, as determined by NMR, (Fig. 4) is consistent with these results. The light fraction of the liquid products was found by GC/MS to contain only tetralin and its degradation products, to any measureable degree. An explanation for the intermediate regime, in which the aromatic fraction of the solid increases, is not clear. Aliphatic side chains may be removed⁸ or internal transfers of protons to liquefying fragments⁹ may produce an increase in aromaticity of the solid material. At residence times greater than about 2 minutes, the aromaticity of the residual solids is again seen to decrease. This decrease in aromaticity is probably due to hydrogen transfer from tetralin to the aromatic structures as the dominant process.¹⁰

CONCLUSIONS

Preliminary coal liquefaction experiments in a specially designed CSTR using NMR spectroscopy of the residual solid and the liquid products show that the kinetics of this process are very complex. There are at least three regimes that can be distinguished, with several different processes contributing to the overall process. These are readily distinguished by their effects on the aromaticity as determined by NMR techniques. Such processes as the flash desorption of small aromatics not covalently bonded to the framework, disruption of the coal with release of aliphatic material, proton transfer within the coal and from tetralin to the coal all presumably contribute to the observed changes.

REFERENCES

1. Szladow, A. J.; Given, P. H. *Ind. Eng. Chem. Proc. Res. Dev.* **1981**, *20*, 27-33.
2. Shabtai, J.; Skulthai, T.; Saito, I. *ACS Fuel Div. Preprints* **1986**, *31 (4)*, 15.
3. *Coal Liquefaction, A Research Needs Assessment: Technical Background*, DOE/ER-O400; volume II, pp. 4-89 to 4-115.
4. Provine, W. D.; Porro, N. D.; LaMarca, C.; Foley, H. C.; Bischoff, K. B.; Scouten, C. G.; Cronauer, D. C.; Tait, A. M.; Klein, M. T., "Development of a Pulse-Injection CSTR coal Liquefaction Flow Reactor," presented at the AIChE National Meeting, Chicago, IL, November, 1990.
5. Maciel, G. E.; Sindorf, D. W. *J. Am. Chem. Soc.* **1980**, *102*, 7607-7608.
6. Botto, R. E.; Wilson, R.; Winans, R. E. *J. Energy and Fuels* **1987**, *1*, 173.
7. Shou, J.K.; Pitts, W.S. *Fuel* **1977**, *56*, 343.
8. Calkins, W.H.; Tyler, R. J. *Fuel* **1984**, *63*, 1119.
9. Finsath, D. H.; Bockrath, B. C.; Illig, E. G.; Thames, B. M. *ACS Fuel Div. Preprints* **1986**, *31(4)*, 124.
10. Bockrath, B. C.; Illig, E. G.; Hough, M. *ACS Fuel Div. Preprints* **1990**, *35(1)*, 232.

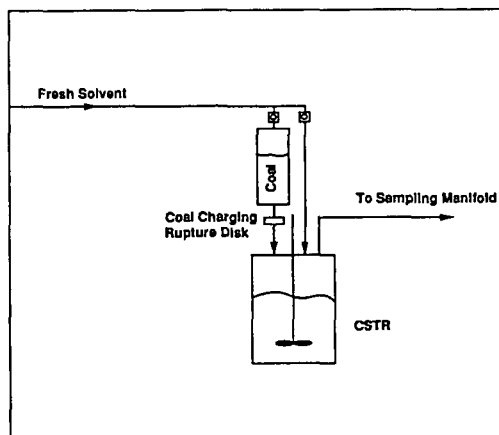


Figure 1 Schematic diagram of the CSTR.

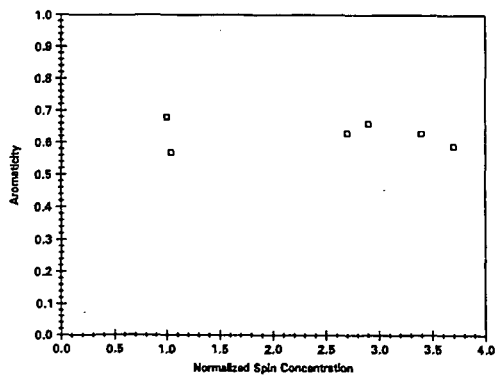


Figure 2 Aromaticity versus spin concentration for several solid residues.

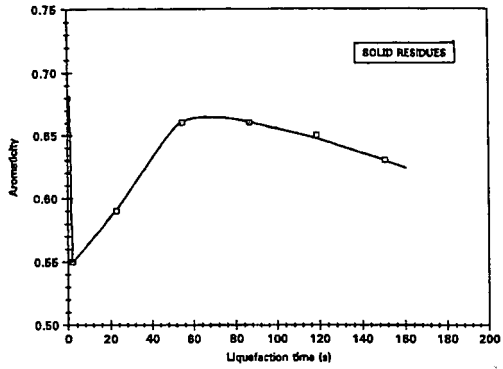


Figure 3 Aromaticity of solid residues as a function of liquefaction time.

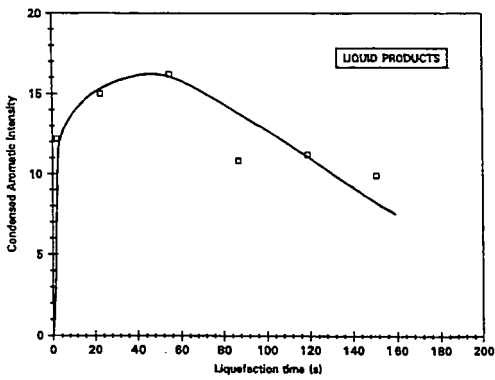


Figure 4 Aromaticity of liquid products as a function of liquefaction time.

Table 1. Weight % Conversion as a Function of Residence Time

Residence time (s)	Weight % Conversion
2	5.0
23	9.5
55	16.4
87	19.5
119	17.6
151	20.1

$$\text{Weight \% Conversion} = \frac{(A_t - A_0)}{A_0(1 - A_0)} \times 100$$

A_0 = Ash fraction of coal at time, $t = 0$

A_t = Ash fraction of coal at time, t

Chemical Structure of Char in the Transition from Devolatilization to Combustion

Thomas H. Fletcher*
Chemical Engineering Department
Brigham Young University, Provo, UT, 84602

Mark S. Solum, David M. Grant, and Ronald J. Pugmire
Departments of Chemistry and Fuels Engineering
The University of Utah, Salt Lake City, UT, 84112

Introduction

Recent coal devolatilization efforts have focused on relating coal devolatilization behavior to the chemical structure of the parent coal.¹⁻⁶ Gas and tar yields, as well as tar molecular weights, can be predicted based on correlations related to elemental compositions or from measured chemical characteristics of the parent coal. However, char is an important product produced during coal devolatilization, and must be characterized as a function of temperature and heating rate in a manner similar to volatile devolatilization products. Quantitative measurements of chemical structure are performed on the coals and chars using ¹³C nuclear magnetic resonance (NMR) techniques described by Solum and coworkers.⁷

The chemical structures of char and tar during devolatilization for an Illinois #6 coal and a lignite were published previously, and discussed relative to devolatilization behavior.^{8,9} These data showed that during the tar release period, the percentage of aromatic carbon for the bituminous coal char changed by less than 5%, while the carbon aromaticity in the lignite char changed in the early stage of pyrolysis. The carbon aromaticities for both sets of chars ultimately reached comparable values, but the parent lignite had a lower carbon aromaticity value ($f_a' = 0.57$) than the parent bituminous coal ($f_a' = 0.67$). The number of aromatic carbons per cluster indicated restructuring of the aromatic species earlier in the lignite than in the Illinois No. 6 coal.

In this work, the chemical structure of chars from five coals of different rank are examined, and implications on char reactivity are discussed. Chars were obtained as a function of residence time in two flow reactors generally used for devolatilization and char combustion experiments, respectively. The examination of five coals and their respective chars from two reactors allows better distinction of trends than was possible with the limited data previously published.

Experimental Approach

Char samples were collected as a function of residence time in an entrained flow, laminar reactor in the Sandia Coal Devolatilization Laboratory (CDL) in 100% nitrogen to isolate the pyrolysis reactions, with typical particle heating rates of 2×10^4 K/s, gas temperatures of 1250 K, and particle temperatures as high as 1200 K.^{2,3} Additional char samples were collected in an entrained flow, laminar flow reactor in the Sandia Char Combustion Laboratory (CCL), with a laminar CH₄/H₂/O₂/N₂ flat flame providing a high temperature environment (maximum gas temperature = 1600 K).¹⁰ Stoichiometric conditions were used in the flame, yielding less than 50 ppm O₂ in the post-flame gases. Char samples in the CCL were collected subsequent to the visible region of coal devolatilization, with particle heating rates of about 5×10^4 K/s and particle temperatures of

* Experiments performed at the Combustion Research Facility, Sandia National Laboratories, Livermore, CA.

approximately 1300 to 1500 K, depending on residence time and oxygen concentration.¹⁰ Common coal samples were used in the coal devolatilization and char oxidation experiments discussed here.

Helium-quench probes were used to collect char samples,^{2,10} and chars were analyzed for organic and inorganic elemental composition. The experiments in the CCL with no post-flame oxygen required modifications to the sampling system to aerodynamically separate tars, soot and aerosols from char particles. The extent of mass release from the char particles was determined from the trace mineral species (Si, Al, Ti, and total ash). Samples were obtained in the CDL at different residence times in the 1250 K gas condition, with residence times ranging from 20 to 250 ms. Samples were taken just subsequent to the pyrolysis zone (47 ms, 6.4 cm above the burner) in the CCL.

Results

The elemental compositions of the five coals used in these experiments are shown in Table 1, along with their total volatiles yields in the two reactors. The coals range in rank from a lignite to a low-volatile bituminous coal. The volatiles yields in the CCL are slightly higher than those in the CDL, and are much higher than the ASTM analyses.¹¹ Results of the ¹³C NMR chemical structure analyses of CDL chars are presented first, followed by data for the CCL chars.

Table 1
Elemental Analyses of Coals Used

PSOC-	Coal	Size Fraction (μm)	C (% daf)	H (% daf)	O (% daf)	N (% daf)	S (% daf)	Ash (% dry)	CDL Volatiles Yield (% daf)	CCL Volatiles Yield (% daf)
1507D	Beulah Zap (lignite)	75-106	66.56	4.26	25.16	1.12	2.89	18.7	53.7	58.6
1445D	New Mexico Blue (subbituminous)	106-125	75.6	5.26	17.33	1.32	0.49	3.48	53.4	56.2
1493D	Illinois No. 6 (hvb bituminous)	106-125	74.12	4.96	13.18	1.45	6.29	11.30	53.5	58.3
1451D	Pittsburgh No. 8 (hva bituminous)	63-75	84.23	5.54	7.56	1.65	1.01	3.73	53.1	52.2
1508D	WV Pocahontas (lv bituminous)	106-125	88.83	4.37	5.14	1.06	0.6	16.72	15.9	17.4

A. Chemical Structure of Coal Chars from the CDL

Attachments per Cluster. Attachments to aromatic clusters consist of alkyl groups and oxygen functional groups (e.g., phenols and/or alkyl and aryl ethers). These attachments are either bridges and loops between aromatic clusters or side chains. The bond strengths of the aromatic rings are much greater than the bond strengths of the labile bridges and loops. During devolatilization the labile bridges break, generating finite-size fragments containing one or more aromatic clusters. The light fragments are released as tar, while the heavier fragments stay in the char as metaplast and eventually reattach to the infinite char matrix. Broken bridge fragments (i.e., side chains)¹ are eventually released as light gas. In this analysis, it is assumed that the broken bridge fragments may be distinguished from intact bridges by the presence of methyl groups. Hence, the number of side chains per cluster can be estimated together with the number of intact bridges and loops per cluster. It is important to note that aliphatic carbons still remain at the end of the pyrolysis process and represent the presence of stable aliphatic bridge material and/or side chains that have not been expelled at the pyrolysis temperatures employed.

The total number of attachments per cluster (referred to as the coordination number, $\sigma+1$) is shown in Fig. 1 for char samples from all five coals. The coordination number either remains relatively constant or decreases slightly during devolatilization for all five coals. This means that no new attachment sites are generated during pyrolysis; any reattachment of metaplast occurs at existing side chain sites. Decreases in the coordination number can be explained by the release of side chains with no subsequent crosslinking at that site.

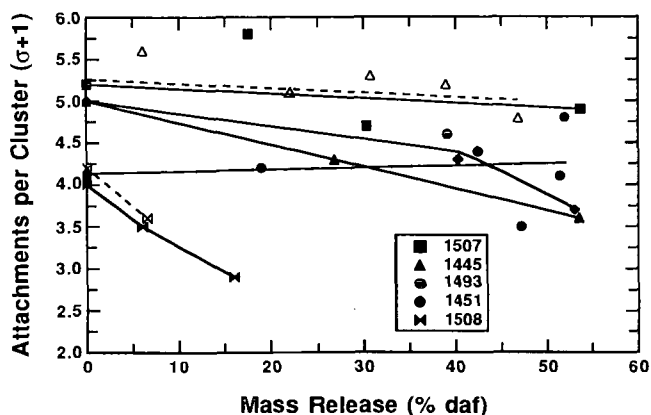


Figure 1. The total number of attachments per cluster vs. the extent of mass release due to devolatilization for chars collected at different residence times in the 1050 K (dashed lines and open symbols) and 1250 K (solid lines and filled symbols) gas temperature conditions.

The number of bridges and loops (i.e., bridges between aromatic rings and aliphatic loops on aromatic rings, such as tetralin) per cluster does not change significantly in the Illinois #6 coal char until the end of the mass release period, as shown in Fig. 2. The increase in the number of bridges and loops per cluster is an indication of the extent of crosslinking that occurs between neighboring aromatic clusters. The total number of attachments per aromatic cluster ($\sigma+1$), however, does not change significantly, indicating that bridge material is released at a rate proportional to the formation of crosslinking bridges. These stable char bridges likely are formed at the site of the original bridge. These data at rapid heating conditions clearly indicate that the average molecular structure of the Illinois No. 6 coal does not undergo major changes in functional group distribution until after most of the tar is released, at which time reactions occur in the char/metaplast that are associated with gas release.

The crosslinking behaviors of the chars from other coals, as indicated by the NMR data, are different from that observed in Illinois No. 6. The changes in the number of bridges and loops per cluster in the late stages of mass release for the other bituminous coal (PSOC-1451) are more scattered, and do not exhibit the clear indication of crosslinking observed in the Illinois #6 coal (PSOC-1493). In the lignite, the initial number of bridges and loops is slightly higher than in the bituminous coals, and increases in a monotonic progression with the extent of mass release, as reported earlier.⁹ The lignite data reflect the early crosslinking that is observed in solvent swelling measurements of lignites as compared to the high volatile bituminous coals.^{12,13} This early crosslinking is only indicated in Fig. 2 for the lignite; none of the other coals show significant increases in the number of bridges and loops

per cluster until the late stages of mass release (including the subbituminous coal). The highest rank coal (PSOC-1508 Pocahontas lv bituminous) shows a slight decrease in the number of bridges and loops per cluster as mass release proceeds.

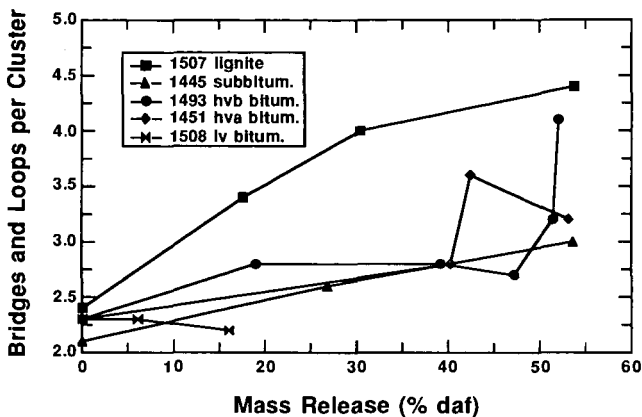


Figure 2. The number of bridges and loops per cluster vs. the extent of mass release due to devolatilization for chars collected at different residence times in the 1250 K gas temperature condition.

Coordination numbers for char samples obtained in the 1050 K gas condition in the CDL are shown as dashed lines and open symbols in Fig. 2. In the 1050 K gas condition, the coordination number determined for the chars from the subbituminous coal (PSOC-1445) does not decrease as much with mass release as indicated at 1250 K. The lower temperature condition does not permit the same degree of gas release as the higher temperature condition, and hence more side chains remain attached to the clusters. The coordination number data at 1050 K for the high rank coal (PSOC-1508) follow the data indicated at 1250 K. In general, the data at 1050 K support the conclusion inferred from the 1250 K data; no increases in the number of attachments per cluster are seen, indicating that crosslinking occurs only at existing side chain sites.

Carbon Aromaticity. The carbon aromaticities of the fully-devolatilized chars only range from 79% for the subbituminous coal to 88% for the Pittsburgh No. 8 and the Pocahontas coals, whereas f_a' in the parent coals range from 53% for the subbituminous coal to 77% for the Pocahontas coal. The carbon aromaticity measured for the subbituminous coal and char is uniformly lower than measured in the other four coals (and their chars). The carbon aromaticities of the fully-devolatilized chars from the other four coals lie in a narrow range from 84% to 88%.

Cluster and Attachment Molecular Weights. The average cluster molecular weight determined from the NMR analyses includes the aromatic carbons per cluster plus the attachments (bridges and side chains) to the cluster, i.e., the contributions from both the aromatic and aliphatic material in the vicinity of a cluster. Cluster molecular weights of chars collected in the CDL at the 1250 K gas condition as a function of residence time are shown in Fig. 3. The average cluster molecular weight for parent coals ranges from 270 amu for the Illinois No. 6 coal to 440 amu for the Zap lignite, as shown in Fig. 3 at a

residence time of 0 ms. However, as these coals are heated and the volatiles are released, average cluster molecular weights for the chars of these different coals become very similar.

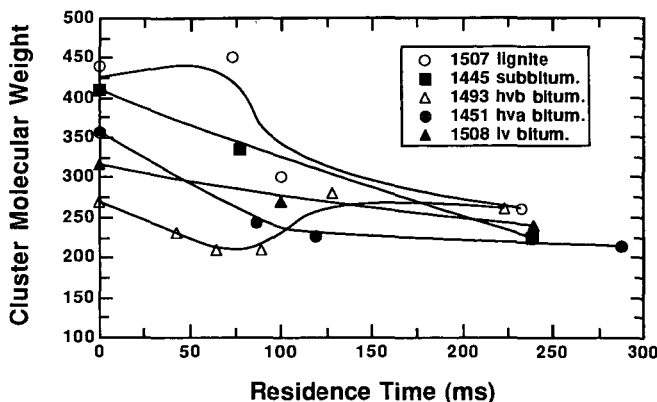


Figure 3. Average cluster molecular weights in coals and chars collected in the 1250 K gas condition in the CDL, determined from ^{13}C NMR analyses. Parent coals are represented at 0 ms residence time.

Another comparison of chemical structure as a function of coal rank is the average molecular weight of attachments to clusters in the parent coal. Attachments to clusters include labile bridges (ξ), char bridges (c), and side chains (δ). The molecular weight of attachments m_{att} can be calculated from the cluster molecular weight by subtracting the mass in the aromatic fused structure (the number of aromatic carbons per cluster multiplied by the molecular weight of carbon) and dividing by the number of attachments per cluster:

$$m_{att} = \frac{M_{clust} - C_{clust} M_C}{\sigma + 1} \quad (1)$$

The definition of the molecular weight per cluster (M_{clust}) used here includes the mass in the aromatic part of the cluster plus the surrounding aliphatic material. The cluster molecular weight therefore includes the mass of side chains, and one-half the molecular weights of labile bridges and char bridges attached to the cluster, as follows:

$$m_{att} = \frac{\xi \frac{m_b}{2} + c \frac{m_{char}}{2} + \delta m_\delta}{\xi + c + \delta} \quad (2)$$

where ξ , c , and δ represent the populations of labile bridges, char bridges, and side chains, respectively. The factor of 2 in the m_b and m_c terms reflects the fact the only one-half of an intact bridge is attributed to a cluster. Unreacted coals contain very few char bridges (i.e., $c = 0$), and hence Eq. 2 reduces to the relation $m_{att} = m_\delta$, assuming that $m_\delta = m_b/2$. For fully-devolatilized chars, $\xi = 0$.

Attachment molecular weights have been thus determined for all five coals examined in the Sandia devolatilization experiments, as well as for chars at different residence times, as shown in Fig. 4. Attachment molecular weights for other parent coals are also shown, as reported by Solum, et al.⁷ for the Argonne premium coals¹⁴ and for three coals examined at Advanced Fuel Research (AFR).¹⁵ The continuous lines in this figure represent linear correlations of the data. The oxygen content of the parent coal is an indicator of coal rank; the oxygen content of the parent coal decreases as coal rank increases. The attachment molecular weights of the parent coals exhibit a definite trend as a function of coal rank; values of m_{att} range from 52 amu in the lignite and subbituminous coal (25% daf oxygen) to 13 amu for the highest rank coal (Pocahontas #3 lv bituminous, Argonne sample).

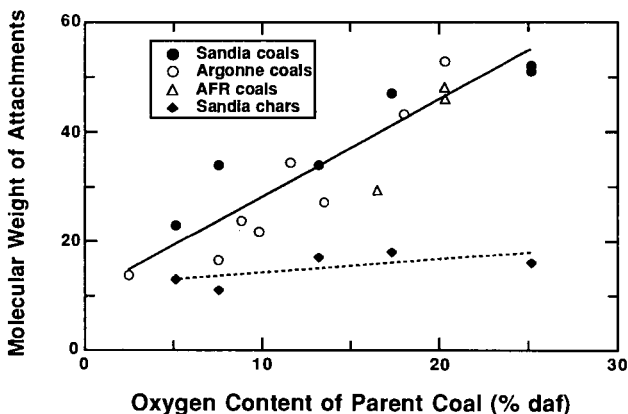


Figure 4. Average molecular weight of attachments to aromatic clusters in unreacted and fully-devolatilized coals as a function of coal type. Data for non-Sandia coals are taken from Solum, et al.⁷. Fully-devolatilized chars are from the longest residence time (~ 250 ms) in the 1250 K gas condition in the CDL.

The fully-devolatilized chars in Fig. 5 are from the longest residence time (~ 250 ms) in the 1250 K gas condition in the CDL (in 100% N₂). The molecular weights of attachments for the fully-devolatilized chars vary from 18 to 11 amu, which is not a significant dependence on coal rank. The fully-devolatilized chars do not contain any labile bridges, and hence the attachments to the cluster consist solely of char bridges and side chains. The fact that the average molecular weight of attachments to aromatic clusters in the fully-devolatilized chars is low enough (11 to 18 amu) to compare with bridges consisting of one atom (12 amu for carbon, 16 amu for oxygen) suggests that low molecular weight side chains may consist mainly of methyl groups (15 amu) and OH groups (17 amu), which are more stable than longer side chains such as COOH or ethyl groups (C₂H₅).

Stable char bridges are thought to mainly consist of three types: (a) biphenyl bridges, where a bridge is formed between neighboring carbons on different aromatic clusters (Ar-Ar); (b) ether-type bridges where a single oxygen atom forms a bridge between neighboring clusters (Ar-O-Ar); and (c) a carbon bridge, thought to mainly consist of single carbon atoms between clusters (Ar-C-Ar). The molecular weights of these three types of bridges are low enough to be consistent with the NMR data: 0 amu for the biphenyl bridge; 16 amu for the oxygen bridge; and 14 amu for the carbon bridge.

Discussion of CDL Data. It is well known that the physical structures (i.e., apparent densities and internal surface areas) of these chars vary significantly, causing a difference in the *apparent* reactivities of these chars (based on external surface area). However, the similarity in chemical structure of the fully-devolatilized chars from different coals may imply that the *intrinsic* chemical reactivities of these chars may be similar. The exact relationship between cluster molecular weight, carbon aromaticity, and intrinsic chemical reactivity is not yet clear. The fact that the chemical structure of these chars are similar is somewhat surprising because the chemical compositions of these chars are different. The carbon contents of the fully-devolatilized chars vary from 83% on a dry ash-free (daf) basis for the lignite char to 92% daf for the Pocahontas char. The oxygen contents of these chars range from 9.9% daf for the lignite char to 3.3% daf for the Pocahontas char. The NMR chemical structure data on chars should be compared in the future with physical structure and reactivity data.

B. Chemical Structure of Coal Chars in the CCL

Char samples from five coals collected at 47 ms residence time in the CCL with 0% post-flame oxygen were analyzed by ^{13}C NMR spectroscopy. The chars taken from the CCL-0 condition are very similar in chemical structure to the chars taken immediately after tar release in the CDL experiments at 1250 K (residence times of approximately 70 to 100 ms). In the CDL, these chars have finished releasing tar, and are beginning the slower gas release phase. The chars in the CCL-0 condition at 47 ms have just completed tar release as well, and hence should be followed by a slower light gas release region. The similarity in chemical structure of chars from the 1250 K gas condition in the CDL and from the CCL-0 condition is shown in Fig. 5. The solid lines in these figures represent the CDL data at different residence times, while the dashed line represents data from the CCL-0 experiments. Residence time for a given coal is in the vertically upward direction.

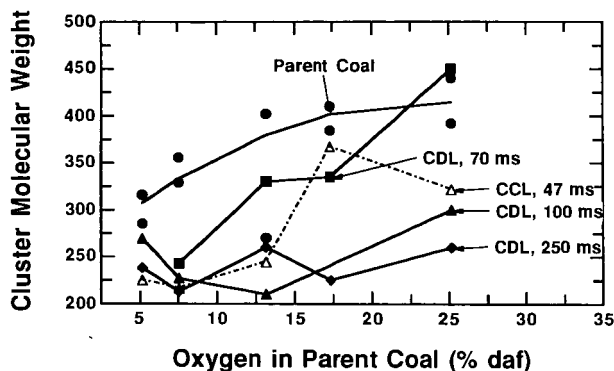


Figure 5. Comparison of cluster molecular weights in char samples from the CCL-0 condition and the 1250 K gas condition in the CDL (see caption to Fig. 6).

The cluster molecular weights (Fig. 5) in the CCL-0 chars from the low rank coals generally lie between the values observed in the chars collected at 70 and 100 ms in the CDL. In contrast, the cluster molecular weights in CCL-0 chars from the high rank coals are most similar to the CDL chars collected at 100 ms. Similar trends were observed in the carbon aromaticities of the chars from the CDL and CCL.

Quantitative measures of chemical structure (e.g., carbon aromaticities, cluster molecular weights) for the CCL-0 chars always lie close to the values observed in the chars collected at 70 or 100 ms in the CDL, and do not approach the values observed at 250 ms in the CDL. The chemical structure data for the CCL-0 chars therefore indicate that tar release in the CCL is complete at 47 ms, but that further release of light pyrolysis gases is still underway in the early stages of char combustion. Simultaneous char combustion and light gas evolution occur as the char ignites, and both must be considered in the determination of reactivities early in the char combustion process.

Conclusions

The chemical structures of chars from an electrically-heated laminar flow reactor (CDL) and a flame-driven flow reactor (CCL) show remarkable similarities. The CCL chars are similar to the chars that were collected in the CDL immediately after tar release, but before the further release of light gases. This indicates that char combustion occurs concurrently with the late degassing stage of devolatilization. The fully-devolatilized chars from the CDL exhibit similar chemical structure characteristics, such as molecular weight per cluster and attachment molecular weight, even though the parent coal structures are quite different. The similarity in chemical structure of the chars is in contrast to the general trend in char reactivity (in oxygen); low rank coals are generally more reactive than high rank coal chars. This implies that the principal cause of differences in char reactivity is physical structure (e.g., internal surface area, porosity) rather than chemical structure.

Acknowledgements

The pyrolysis work carried out at the Sandia Livermore Combustion Research Facility was supported by the DOE/PETC Direct Utilization AR&TD Program. NMR work was supported through the Advanced Combustion Engineering Research Center at Brigham Young University and the University of Utah which is supported by the NSF, 23 industrial firms and DOE/PETC. Additional support was provided through the Consortium for Fossil Fuel Liquefaction Science by DOE/PETC.

References

1. Grant, D. M., Pugmire, R. J., Fletcher, T. H., Kerstein, A. R.: *Energy and Fuel*, 3, 175 (1989).
2. Fletcher, T. H.: *Comb. Sci. & Tech.*, 63, 89 (1989).
3. Fletcher, T. H.: *Comb. & Flame*, 78, 223 (1989).
4. Niksa, S. and Kerstein, A. R.: *Energy and Fuels*, 5, 647 (1991).
5. Solomon, P. R., Hamblen, D. G., Carangelo, R. M., Serio, M. A. and Desphande, G. V.: *Energy and Fuel*, 2, 405 (1988).
6. Ko, G. H., Sanchez, D. M., Peters, W. A., and Howard, J. B.: 22nd Symp. (Int.) on Comb., The Comb. Inst., Pittsburgh, PA, 115 (1988).
7. Solum, M. S., Pugmire, R. J., and Grant, D. M.: *Energy and Fuels* 3, 187 (1989).
8. Fletcher, T. H., Solum, M. S., Grant, D. M., Critchfield, S., and Pugmire, R. J.: 23rd Symp. (Int.) Comb., The Comb. Inst., Pittsburgh, PA, 1231 (1990).
9. Pugmire, R. J., Solum, M. S., Grant, D. M., Critchfield, S., and Fletcher, T. H.: *Fuel*, 70, 414 (1991).
10. Mitchell, R. E.: 22nd Symp. (Int.) on Comb., The Comb. Inst., Pittsburgh, PA, 69 (1988).
11. Fletcher, T. H. and Hardesty, D. R.: Milestone Report for DOE's Pittsburgh Energy Technology Center, contract FWP 0709, in press (1991).
12. Suuberg, E. M., D. Lee, and Larsen, J. W.: *Fuel*, 64, 1668 (1985).
13. Solomon, P. R., Serio, M. A., Deshpande, G. V., and Kroo, E.: *Energy & Fuels*, 4, 42 (1990).
14. Vorres, K. S.: *ACS Div. Fuel Chem. prepr.*, 32:4, 221 (1987).
15. Serio, M. A., D. G. Hamblen, J. R. Markham, and Solomon, P. R.: *Energy & Fuels*, 1, 38 (1987).

CORRELATION OF STRUCTURE AND REACTIVITY IN ALKYLARENE THERMOLYSIS

C. Michael Smith, Minda M. McNally and Phillip E. Savage*
University of Michigan, Department of Chemical Engineering
Ann Arbor, MI 48109-2136

KEYWORDS: Alkylarenes, Bond Cleavage, Reactivity Indices, Pyrolysis, Hydrogenolysis

INTRODUCTION

There is an industrial trend toward developing molecular-level process models for the conversion of hydrocarbon-containing feedstocks. The development of such models has been motivated by a desire for more efficient processes and improved product quality, and to an extent by environmental regulations. Recent and continuing advances in analytical chemistry, which provide increasingly detailed structural descriptions of complex materials, and advances in computing have fueled the formulation of these increasingly complex models. An integral part of such models is a set of correlations that relates the reactivity (e.g., kinetics and product distributions) of a given portion of the feedstock to its chemical structure.

Polycyclic n-alkylaromatic moieties are important structural features of feedstocks such as crude oils, bituminous sands, kerogens, asphaltenes, and coals,¹⁻⁵ and recently the thermal chemistry of representative model compounds has been explored.⁶⁻¹¹ An interesting observation that arose from these pyrolysis experiments was that the very strong aryl-alkyl C-C bond was susceptible to hydrogenolytic cleavage. We developed a quantitative correlation that related the rate of this aryl-alkyl bond cleavage in long-chain n-alkylarenes to the respective localization energies through Dewar reactivity numbers calculated from perturbational molecular orbital (PMO) theory.⁸ In this paper we extend the previous analysis to develop a similar structure-reactivity correlation for methylarenes based on the set of methylaromatics displayed in Figure 1.

EXPERIMENTAL

1-Methylnaphthalene (1-MN), 1-methylanthracene (1-MA), 2-methylanthracene (2-MA), and 9-methylanthracene (9-MA) were pyrolyzed at temperatures between 350°C and 450°C. All chemicals were obtained from Aldrich. The pyrolyses were conducted in constant-volume, 316 stainless steel, micro-batch reactors. The reactors were constructed from one Swagelok port connector and two Swagelok end caps, and they had a nominal volume 0.6 ml. Previous work established that the reactor material did not alter the experimental results.¹⁰ As an additional test for catalytic activity by the reactor walls, we conducted several pyrolyses in the presence of stainless steel filings and saw no appreciable effect on conversion and product selectivities.

The batch reactors were typically loaded with 10 mg of the model compound and 10 mg of an internal standard and sealed in a nitrogen-filled glovebox. After being loaded and closed, the reactors were placed in an isothermal, fluidized sandbath. Upon reaching the desired holding time, the reactors were removed from the fluidized bath, and the reaction was quenched. The products were recovered by repeated extraction with benzene.

The reaction products were analyzed by gas chromatography (GC) and gas chromatography-mass spectrometry. The GC analysis used a Hewlett Packard 5890 instrument equipped with a flame ionization detector (FID). The reaction products were identified by comparing their GC retention times with those of authentic standards and by inspection of their mass spectra. Product molar yields, calculated as the number of moles of product formed divided by the number of moles of the reactant initially loaded in the reactor, were obtained from the GC analyses using experimentally determined FID response factors. We estimate the uncertainty in these yields to be about 20%. Further analytical details have been given previously.⁶⁻¹⁰

RESULTS

In the following section, we present the results from the pyrolysis of 1-MA, 2-MA, and 9-MA. Tables I-III give representative data for these compounds in terms of the yields of the major products and selected minor products.

1-Methylanthracene (1-MA): The neat pyrolysis of 1-MA was conducted at 400°C, 425°C, and 450°C for batch holding times up to 300 minutes. Table I provides representative experimental data obtained under different reaction conditions. The products from 1-MA pyrolysis were anthracene, 9,10-dihydroanthracene (DHA), 1,2,3,4-tetrahydroanthracene (THA), 1-methyl-9,10-dihydroanthracene (1-MDHA), 9-methylanthracene, 5 dimethylanthracene (DMA) isomers, and benzene-insoluble char. We were not able to determine the specific locations of the methyl groups in the dimethylanthracene isomers so we have simply identified these isomers as I, II, III, IV, and V.

Anthracene was the most abundant product at all reaction conditions, and its molar yield generally increased with batch holding time at all three temperatures. The highest anthracene yield was 31%, which was obtained at a batch holding time of 120 minutes for the pyrolysis at 450°C. At conversions less than 50%, 1-MDHA was the second most abundant product, but at higher conversions its yield was low. For example, at 425°C the molar yield for 1-MDHA reached a maximum value of 2.9% at a holding time of 60 minutes, and it subsequently decreased to 1.4% at 300 minutes. This same behavior (i.e., the presence of a maximum) was also observed for each of the dimethylanthracene isomers and 9-methylanthracene. Such behavior was not observed for the yields of the remaining minor products, DHA and THA. Rather, the molar yields of these products were very low at short batch holding times, but they increased steadily with time to become significant minor products. For example, at 425°C the molar yields of DHA and THA were 0.5% and 0.1%, respectively at 60 minutes, but these yields increased to 3.5% and 2.2%, respectively, at 300 minutes.

2-Methylanthracene (2-MA): Table II lists the products' molar yields obtained from the pyrolysis of 2-MA at 400, 425, and 450°C. The major products were anthracene and 2-methyl-9,10-dihydroanthracene (2-MDHA). The minor products included three dimethylanthracene isomers. A benzene-insoluble char was also observed. The highest conversion of 2-MA, 87%, occurred at the most severe reaction conditions employed (200 minutes at 450°C).

The molar yield of anthracene steadily increased with batch holding time. The highest molar yield (20%) for this compound was obtained at 450°C for a batch holding time of 200 minutes. The behavior of the 2-MDHA yield was analogous to that of the 1-MDHA yield in 1-MA pyrolysis. For example, at 450°C the molar yield of 2-MDHA increased to 5.8% at 75 minutes and subsequently decreased thereafter.

9-Methylanthracene (9-MA): The neat pyrolysis of 9-MA was conducted at 350, 375, and 400°C for batch holding times up to 180 minutes. Table III provides representative data from these experiments. The major product from 9-MA pyrolysis was always anthracene. The highest yield of anthracene, 42%, was obtained at the most severe conditions (90 minutes at 400°C), and the corresponding conversion of 9-MA was 85%. DHA and two dimethylanthracene isomers were observed as minor products. The molar yield of DHA increased with batch holding time until it reached a maximum, and then it subsequently decreased. At 400°C, for example, the maximum molar yield for this compound was 5.1% at 30 minutes.

PYROLYSIS PATHWAYS

We used the Delplot technique to deduce a general reaction network for the pyrolysis of the methylanthracenes studied.¹² This methodology determines the order of appearance of products in a reaction network through the examination of their initial selectivities, where the selectivity is calculated as the molar yield divided by the reactant conversion. These initial selectivities are determined as the y-intercept of the selectivity versus conversion curve for each product. Typically, products that have a non-zero initial selectivity are primary products (those that arise directly from the reactant), and they are the first to appear in the reaction network. Products that have zero initial selectivities are generally secondary and higher order products.

Figure 2 displays the Delplots for 1-MA pyrolysis. The discrete points are the experimental data, and the curves are drawn to convey the trends in these data. Figure 2a presents the selectivities to anthracene, DHA, and 1-MDHA as a function of conversion. Analysis of the y-intercepts for each of the products reveals that anthracene and 1-MDHA have initial selectivities of 0.19 and 0.14, respectively, and that the initial selectivity for DHA is essentially zero. This signifies that anthracene and 1-MDHA are primary products, and DHA is a secondary or higher order product. Figure 2a also shows that the selectivity to 1-MDHA decreases with conversion, which implies that 1-MDHA undergoes secondary decomposition at higher conversions. In this light, it is interesting to observe that the DHA selectivity increases with conversion, and that one possible route to its formation is dealkylation of 1-MDHA.

The Delplots for the five dimethylantracene isomers are displayed in Figure 2b. The initial selectivity for each of these compounds is non-zero, which indicates that each is a primary product. The selectivity to each of these compounds decreases with the 1-MA conversion, which may indicate that secondary decomposition occurs.

We conducted similar reaction pathway analyses using the pyrolysis product data for the other two methylantracenes to develop a general reaction network for the pyrolysis of methylantracenes. This pyrolysis network is shown in Figure 3. The network includes the primary conversion of each of the methylantracenes to anthracene and to dimethylantracene isomers. This portion of the pathway involves reversible steps. 1-MA and 2-MA can also undergo primary reaction to 1-MDHA and 2-MDHA, respectively, and DHA can form through the secondary reactions of 1-MDHA, 2-MDHA, and anthracene.

STRUCTURE AND REACTIVITY

Our development of a structure-reactivity correlation for the compounds in Figure 1 will focus on the pathway through which the aryl-alkyl C-C bonds are cleaved. The mechanism responsible for this cleavage involves a hydrogenolysis reaction in which the methyl substituent is displaced by hydrogen,^{6,7} but the mechanistic details remain unresolved. Possible mechanisms include hydrogen atom ipso-substitution,¹³ molecular disproportionation,^{14,15} and radical hydrogen transfer.^{16,17} Each of these mechanisms involves the transfer of a hydrogen atom from a donor to the *ipso* position of the methylantracene thereby engendering aryl-alkyl bond cleavage. Thus, in essence, this reaction involves a substitution reaction in which the methyl group is replaced by a hydrogen atom.

For aromatic substitution reactions involving a family of arenes, the differences in the activation energies are likely due to the changes in the differences between the energies of the delocalized electrons in the reactants and in the transition state (i.e., $\Delta E_{\pi}^{\ddagger}$, the delocalization energy of activation). From PMO theory and the Evans-Polanyi principle, we expect the differences in activation energies to be proportional to the differences in the energies of reaction, which in turn can be attributed to the change in energy of the delocalized electrons (π -energy of the system, ΔE_{π}) provided there is little or no change in energy of the localized bonds and in solvation.¹⁸⁻²⁰ The result of this analysis allows us to write Equation 1, where α is the Evans-Polanyi factor.

$$\Delta E_{\pi}^{\ddagger} \cong \Delta E_a = \text{constant} + \alpha \Delta E_{\pi} \quad (1)$$

For even alternant hydrocarbons, ΔE_{π} can be calculated readily from PMO theory as

$$\Delta E_{\pi} = 2\beta(a_{0r} + a_{0s}) = \beta N_t \quad (2)$$

where β is the resonance integral, and a_{0r} and a_{0s} are the coefficients of the non-bonding molecular orbitals at the positions adjacent to the position of substitution, which is denoted by the subscript t .^{18,19} The value of β should be the same for a given reaction family since the structures of the transition states should be similar. The quantity $2(a_{0r} + a_{0s})$ is defined as the Dewar reactivity number, N_t , and the values for the compounds used in the present study were given in Figure 1. These Dewar numbers are for the aromatic position bearing the methyl substituent.

Combining Equations 1 and 2 shows that

$$\Delta E_a = \text{constant} + \alpha \beta N_i \quad (3)$$

Equation 3 suggests that a semilog plot of the reaction rate constants for aromatic substitution reactions as a function of the Dewar reactivity number, N_i , should be linear. We desired to employ the Dewar reactivity number as a correlating parameter, but we could not calculate the value of the rate constant because the precise form of the hydrogenolysis rate law is unknown. Thus, we chose to employ initial rates in the correlation. These rates were calculated as the initial slope of the arene molar yield vs. time curve. Figure 4 displays the natural logarithm of this initial rate of aryl-alkyl bond cleavage at 400°C as a function of the Dewar reactivity number for the methylarenes used in this study and for 1-methylpyrene (1-MP).⁹

Two linear correlations exist for the data presented in Figure 4. The first is for the methylarenes in which the position bearing the methyl group and the position with the lowest Dewar number (i.e., most reactive position) coincide, and the second is for the three methylanthracenes, compounds in which these positions do not necessarily coincide. These two distinct lines emerge because there are two key features that principally control the rate of hydrogenolysis. The first is the rate at which hydrogen is added to and CH_3 removed from the substituted position in the methylarene. This rate should correlate with the Dewar number of the position bearing the substituent. The second feature is the rate at which hydrogen is added to any position on the methylarene to form potential radical hydrogen donors, which can subsequently engender hydrogenolysis. This rate, to a first approximation, should correlate with the Dewar number of the most reactive position in the methylarene. Thus, the two key Dewar numbers for a polycyclic alkylarene are the one for the substituted position and the one for the most reactive position (i.e., the lowest one). For compounds where these numbers coincide, a single line is expected. Thus, the data for 9-MA, 1-methylpyrene (1-MP), and 1-methylnaphthalene (1-MN) fall on a single line. For an alkylarene in which these Dewar numbers differ (i.e., 1-MA, 2-MA) a different correlation is expected. This expectation is realized by the methylanthracene data in Figure 4.

Each peripheral carbon atom in a polynuclear aromatic can accept hydrogen from a donor, and each carbon atom has its own susceptibility for hydrogen addition, which is dependent upon its intrinsic reactivity. The Dewar reactivity number provides a numerical measure of the ease of hydrogen addition to a given position. Positions with lower Dewar numbers accept hydrogen more readily than do positions with higher Dewar numbers. Thus, the rates of hydrogenolysis for methylarenes having the methyl group at the position possessing the highest reactivity (e.g., lowest Dewar number) should correlate with the Dewar number of that position because a majority of the hydrogen addition will be to the ipso-position. This correlation appears as line 1 in Figure 4.

For methylarenes in which the methyl group is not substituted on the position of highest reactivity, hydrogen adds more rapidly to non-ipso positions to form hydroaromatic radicals than it adds to the ipso position. These hydroaromatic radicals can engender subsequent hydrogenolysis through radical hydrogen transfer steps. Thus, methylarenes with highly reactive non-ipso positions can undergo hydrogenolysis at a rate that is higher than expected from the Dewar number of the ipso position. The presence of these more reactive non-ipso positions provides additional modes for engendering hydrogenolysis. This behavior is exhibited in the methylanthracenes because the 9-position is highly reactive, and it can readily accept hydrogen to form a 9-hydroanthracyl radical. These hydroaromatic radicals can then transfer hydrogen to the ipso position, via RHT for instance, and engender hydrogenolysis. This increase in the H-donor pool concentration increases the rate of demethylation above what it would be if the highly reactive 9 position were absent. Thus, the rates of aryl-alkyl C-C bond cleavage for 1-MA and 2-MA fall above line 1 in Figure 4.

The insight gained from Figure 4 can be used for predictive purposes. Consider two methylarenes that have identical Dewar numbers for the position bearing the methyl substituent. In the first compound the position of highest reactivity and the position bearing the substituent coincide, whereas in the second compound they do not. The rate of demethylation

will be greater in the second compound because additional modes of hydrogen transfer involving hydroaromatic radicals are available.

SUMMARY AND CONCLUSIONS

1. The pyrolysis of methylanthracenes leads to anthracene as the major product. Minor products include methyl-9,10-dihydroanthracenes, 9,10-dihydroanthracene, and dimethylanthracenes.
2. Anthracene, dimethylanthracenes, and methyl-9,10-dihydroanthracenes were primary products of methylanthracene pyrolysis. Dihydroanthracene and methylanthracene isomers were secondary products.
3. The rates of aryl-alkyl bond cleavage for methylanthracene pyrolyses were correlated with the Dewar reactivity numbers for the peripheral aromatic carbon bearing the methyl group. A second correlation was deduced for the rate of demethylation of 9-methylanthracene, 1-methylpyrene, and 1-methylnaphthalene. The existence of two distinct structure-reactivity correlations is consistent with the governing hydrogen transfer mechanisms.

ACKNOWLEDGEMENTS

This work was supported in part by the Link Foundation, the Shell Faculty Career Initiation Fund, and the National Science Foundation (CTS-8906859). Acknowledgement is also made to the donors of the Petroleum Research Fund (ACS-PRF # 23744-AC4), administered by the ACS, for the partial support of this research. We also thank Scott Schnieder for conducting the 1-methylnaphthalene experiments.

LITERATURE CITED

1. Ali, L. H.; Al-Ghannam, K. A. and Al-Rawi, J. M. *Fuel* **1990**, *69*, 519-521.
2. Kolandaisamy, M; Betts, B; Smith, J. *Fuel* **1990**, *69*, 1322-1325.
3. Strausz, O. *AIChE Symp-Ser* **1989**, *273*, 1-6.
4. Waller, P. R.; Williams, A.; Bartle, K.D. *Fuel* **1989**, *68*, 520-526.
5. Speight, J. G. *Prepr.-Am. Chem. Soc., Div. Pet. Chem.* **1989**, *34*, 321-328.
6. Smith, C. M.; Savage, P. E. *Ind. Eng. Chem. Res.* **1991**, *30*, 331-339.
7. Smith, C. M.; Savage, P. E. *Energy and Fuels*, **1991**, *5*, 146-155.
8. Smith, C. M.; Savage, P. E. *AIChE Journal* **1991**, *37*, 1614-1624.
9. Smith, C. M.; Savage, P. E. *Energy and Fuels* **1992**, *in press*
10. Savage, P.E.; Jacobs, G.E.; Javanmardian, M. *Ind. Eng. Chem. Res.* **1989**, *28*, 645-652.
11. Freund H.; Matturo, M. G.; Olmsted, W. N.; Reynolds, R. P.; Upton, T. H. *Energy & Fuels* **1991**, *5*, 840-846.
12. Bhole, N. A.; Klein, M. T.; Bischoff, K. B. *Ind. Eng. Chem. Res.* **1990**, *29*, 313-316.
13. Vernon, L. W. *Fuel* **1980**, *59*, 102-107.
14. Billmers, R.; Brown, R. L.; Stein, S. E. *Int. J. Chem. Kinet.* **1989**, *21*, 375-389.
15. Billmers, R.; Griffith, L. L.; Stein, S. E. *J. Phys. Chem.* **1986**, *90*, 517-523.
16. Malhotra, R.; McMillen, D. F., *Energy and Fuels*, **1990**, *4*, 184-193.
17. McMillen, D. F.; Malhotra, R.; Chang, S.J.; Olgier, W.C.; Nigenda, E; Fleming, R. H. *Fuel*, **1987**, *66*, 1611-1620.
18. Dewar, M. J. S.; Dougherty, R. C. "*The PMO Theory of Organic Chemistry*" Plenum Press, New York, **1975**.
19. Dewar, M. J. S. "*The Molecular Orbital Theory of Organic Chemistry*" McGraw Hill, New York, **1969**.
20. Streitwieser, A. "*Molecular Orbital Theory for Organic Chemists*" John Wiley & Sons, New York, **1961**.

Table I: Product Molar Yields from 1-Methylanthracene

Temp (°C)	400	400	400	400	400	425	425	425	425	425	425	450	450	450	450	450
Time (min)	60	150	200	240	300	30	60	150	300	425	425	30	90	120	150	300
Anthracene	2.9%	9.3%	4.8%	10.3%	16.7%	4.0%	10.8%	16.4%	23.8%	26.8%	14.7%	26.3%	30.9%	28.8%	23.3%	
DHA	0.0%	0.6%	0.2%	0.7%	1.5%	0.0%	0.5%	1.2%	2.7%	3.5%	0.9%	2.6%	3.4%	3.2%	3.4%	
THA	0.0%	0.2%	0.0%	0.3%	0.8%	0.0%	0.1%	0.5%	1.4%	2.2%	0.2%	1.1%	1.7%	1.6%	1.7%	
DMA I	0.3%	0.9%	0.5%	1.0%	1.2%	0.4%	1.0%	1.2%	1.0%	0.5%	1.1%	1.0%	0.6%	0.9%	0.0%	
DMA II	0.3%	1.1%	0.5%	1.2%	1.8%	0.4%	1.2%	1.7%	2.1%	1.3%	1.5%	2.1%	1.4%	0.9%	0.0%	
DMA III	0.7%	2.0%	1.1%	2.2%	2.6%	0.9%	2.3%	2.5%	2.1%	0.7%	2.5%	2.0%	0.0%	0.0%	0.0%	
DMA IV	0.1%	0.3%	0.1%	0.2%	0.3%	0.1%	0.2%	0.3%	0.3%	0.0%	0.4%	0.4%	0.3%	0.0%	0.0%	
DMA V	1.0%	1.3%	1.4%	1.0%	0.7%	1.3%	1.5%	0.7%	0.4%	0.0%	0.9%	0.3%	0.0%	0.0%	0.0%	
1-MDHA	2.3%	3.4%	2.7%	2.9%	3.3%	2.0%	2.9%	2.3%	2.2%	1.4%	2.3%	1.9%	1.4%	1.1%	0.1%	
9-MA	0.0%	0.5%	0.1%	0.5%	0.9%	0.0%	0.6%	0.8%	0.9%	0.3%	0.6%	0.8%	0.3%	0.3%	0.0%	
1-MA	74.9%	56.3%	75.6%	47.4%	36.6%	81.4%	66.1%	32.7%	22.1%	9.5%	43.3%	20.7%	9.5%	8.2%	2.7%	

Table II: Product Molar Yields from 2-Methylanthracene

Temp (°C)	400	400	400	400	400	425	425	425	425	425	450	450	450	450	450
Time (min)	15	60	90	120	130	30	45	60	150	200	60	75	90	160	200
Anthracene	0.1%	0.2%	0.7%	1.0%	1.2%	2.5%	3.8%	4.3%	6.7%	8.9%	6.5%	9.5%	11.3%	14.6%	19.7%
DMA I	0.1%	0.4%	0.7%	0.9%	0.8%	0.7%	1.7%	2.1%	0.8%	1.2%	0.7%	1.1%	1.3%	0.0%	1.6%
DMA II	0.1%	0.1%	0.1%	0.1%	0.0%	0.1%	0.2%	0.0%	2.9%	3.3%	2.5%	3.1%	3.7%	0.0%	0.0%
DMA III	0.2%	0.4%	0.4%	0.5%	0.4%	0.4%	1.1%	1.4%	1.7%	1.4%	1.6%	0.0%	1.6%	0.0%	0.0%
2-MDHA	1.7%	2.5%	3.4%	3.8%	3.5%	1.3%	3.4%	4.7%	5.9%	4.7%	4.9%	5.8%	5.3%	4.6%	0.0%
2-MA	100.6%	95.0%	87.6%	82.3%	66.7%	81.8%	78.8%	70.2%	67.0%	53.5%	67.2%	61.2%	44.7%	37.0%	13.3%

Table III: Product Molar Yields from 9-Methylanthracene

Temp (°C)	350	350	350	350	350	375	375	375	375	375	400	400	400	400	400
Time (min)	15	30	60	100	180	15	30	45	60	90	15	30	45	60	90
Anthracene	7.2%	1.9%	2.9%	3.4%	4.6%	6.4%	11.6%	15.3%	20.9%	20.6%	9.0%	17.9%	34.5%	33.1%	42.0%
DHA	1.0%	0.0%	0.2%	0.6%	0.2%	0.5%	0.8%	1.1%	1.2%	1.1%	2.6%	5.1%	2.2%	2.3%	1.1%
DMA I	0.7%	0.0%	0.0%	0.4%	0.5%	0.8%	1.4%	2.0%	2.3%	1.9%	1.6%	2.5%	2.4%	1.4%	1.0%
DMA II	2.5%	0.7%	1.1%	1.1%	1.7%	0.7%	2.6%	2.5%	2.4%	0.8%	1.0%	1.4%	2.5%	1.9%	1.9%
9-MA	94.3%	122.0%	115.7%	106.0%	129.0%	84.0%	78.3%	78.3%	61.8%	39.9%	53.4%	34.8%	30.8%	18.1%	15.3%

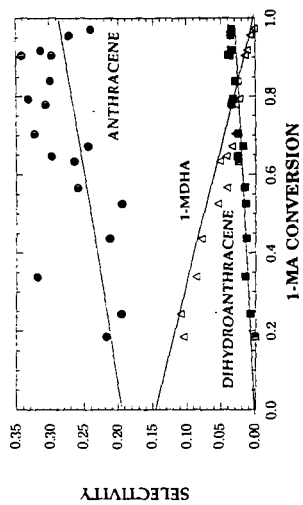


Figure 2a: 1-MA Selectivity to Anthracene, 9,10-Dihydroanthracene (DHA), and 1-Methyl-9,10-dihydroanthracene (1-MDHA).

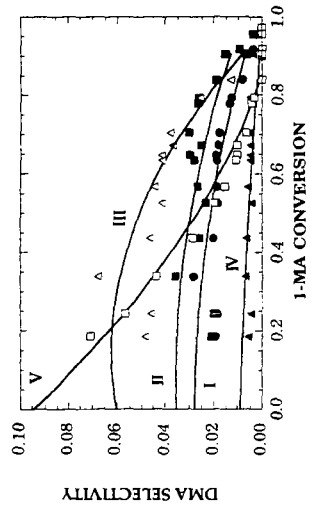


Figure 2b: 1-MA Selectivity to Dimethylanthracene (DMA) Isomers (I-V).

Model Compounds	Name	Dewar Number
	1-Methylnaphthalene (1-MN)	1.81
	1-Methylantracene (1-MA)	1.57
	2-Methylantracene (2-MA)	1.89
	9-Methylantracene (9-MA)	1.26
	1-Methylpyrene (1-MP)	1.51

Figure 1: Heavy Feedstock Model Compounds.

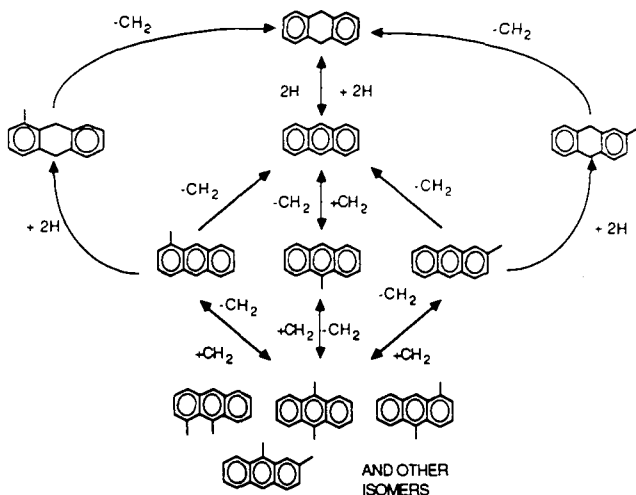


Figure 3: Pyrolysis Network for Methylanthracenes.

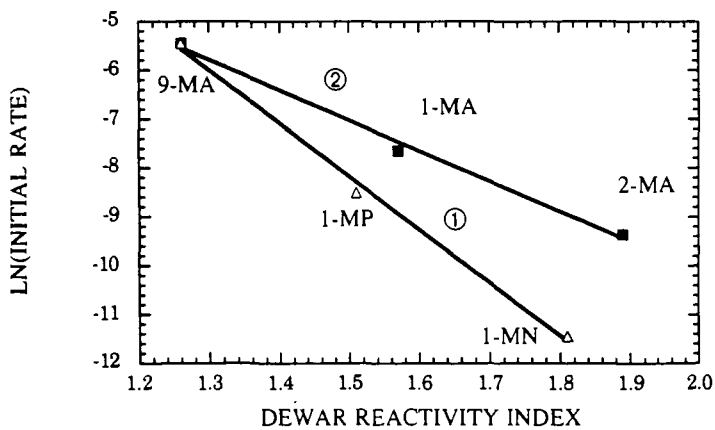


Figure 4: Correlation of Initial Rate of Demethylation in Methylarene Pyrolysis with Dewar Reactivity Numbers

CHARACTERIZATION OF COALS, OTHER KEROGENS, AND THEIR EXTRACTS BY THERMAL MASS SPECTROMETRY

R. E. Winans, P. E. Melnikov, and R. L. McBeth
Chemistry Division, Argonne National Laboratory
9700 S. Cass Avenue, Argonne, IL 60439

Keywords: DCI mass spectrometry, coal extracts, coal structure

INTRODUCTION

The objective of this study is to elucidate the nature of the medium size molecules derived from coals by a succession of stronger extraction conditions. The Argonne Premium Coals have been extracted with pyridine, binary solvents and with KOH/ethylene glycol at 250 °C. Thermal desorption and pyrolysis mass spectrometry were the major approaches chosen to provide detailed information on structure and heteroatom composition. Soft ionization techniques including desorption chemical ionization (DCI) and fast atom bombardment (FAB) were combined with high resolution and tandem MS techniques. This paper will focus on the comparison of the nature of the unextracted coals, the pyridine extract and the extracted coal residue. With this approach the desorption-pyrolysis yields of the extracts and residues combined were greater than the yields from the starting material. Although molecule weight distributions had a minor dependence on rank, the nature of molecules with the same nominal mass varied greatly with rank.

Pyrolysis combined with a variety of mass spectrometric techniques has been used extensively to study coals and separated coal macerals. High resolution mass spectrometry elucidated the distribution of heteroatoms in vacuum pyrolysis products resulting in the discovery of a large number of products containing multiple heteroatoms.¹ The more volatile pyrolysis products have been examined by PyGCMS and PyMS methods. Thermogravimetric MS techniques yield quantitative data with rather slow heating rates.² Field ionization MS (FIMS) is a technique widely used to provide molecular weight distributions of volatile tars.³ Data are available for all eight of the Argonne Premium coals^{4,5} and will be compared to the results by other MS techniques. In addition, Meuzelaar, Schulten and co-workers have compared the results of PyFIMS, low voltage PyMS and TGAMS and discovered similar patterns in the low mass regions.⁶ Recently, FABMS has been applied to the characterization of coal vacuum pyrolysis products yielding data similar to FIMS.⁷ Initial results using the DCIMS approach on demineralized and extracted Argonne coals have been presented⁸, and this paper will extend this study to include the pyridine extracts. Also, tandem MS is used to elucidate the structure of larger molecules. The problem of secondary reactions occurring due to the pyrolysis step is reduced by focussing on extracts.

EXPERIMENTAL

A complete discussion of the characteristics of the coals used in this study has been reported.⁹ Selected elemental analysis values and results from vacuum pyrolysis, and extractions are given in Table I. Details on how the coals were treated are shown on the flow diagram in Scheme 1. A complete description of the KOH in ethylene glycol treatment has been reported.¹⁰

The DCIMS studies have been performed on a Kratos MS 50 triple analyzer with isobutane as the reagent gas. The solids and extracts were heated directly in the source of the mass spectrometer on a small platinum wire coil. The wire was heated from 200° C to 700° C at 100° C/min with the source body kept at 200° C.

In addition to the three-sector MS 50, tandem MS data have been obtained on a four-sector instrument located at the University of Manchester, Institute of Science and Technology (UMIST). The spectrometer is a combination of two Kratos Concept-H's, each with a 10,000 mass range. The sensitivity in MS-2 where the daughter spectra are obtained is enhanced by using an array detector.

Scheme 1

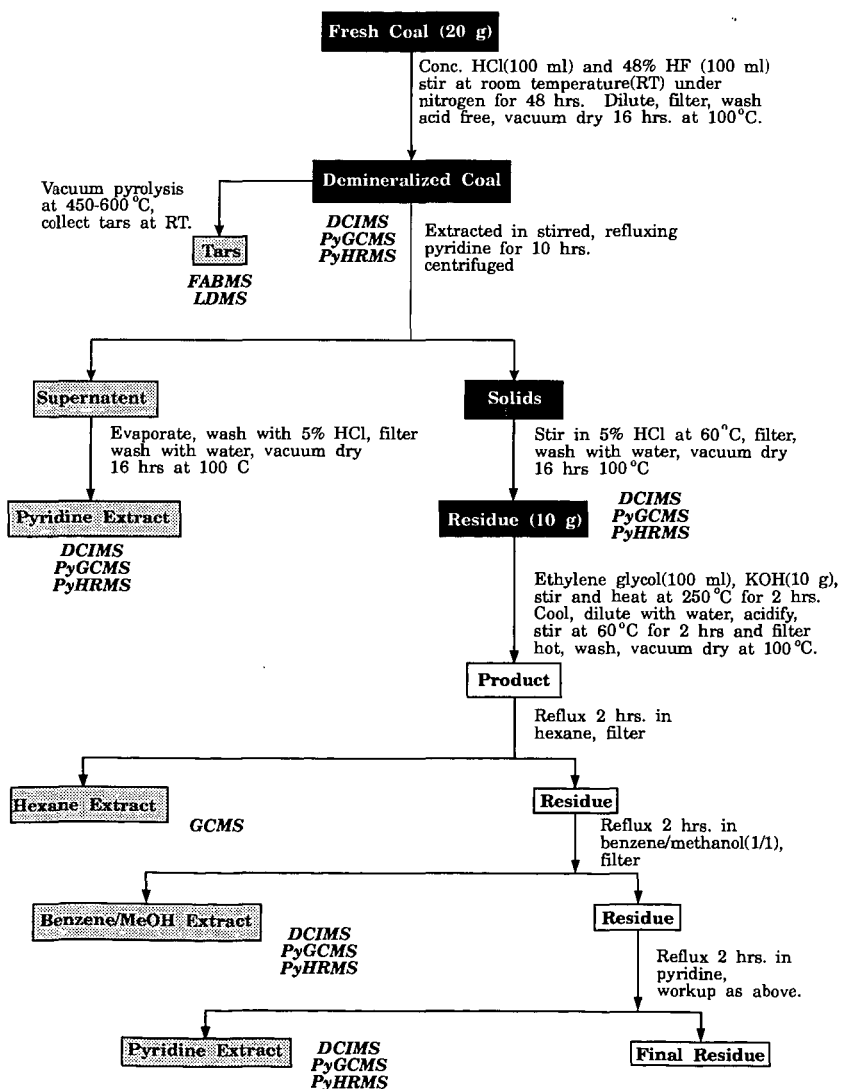


Table 1. Elemental Analysis and Yields for the Coal Samples, Ordered by Carbon Content.

Sample	Name	%C dmmf*	Per 100 Carbons		Yields (Wt%, dmmf*)		
			H	O	Pyrolysis	Pyridine Extract	KOH/Glycol Solubles
8	Beulah-Zap Lignite	74.1	79.5	20.9	23.6	17.9	84.1
2	Wyodak-Anderson SubB	76.0	85.6	18.0	39.3	29.3	79.0
3	Illinois No. 6	80.7	77.2	13.0	36.8	29.0	71.1
6	Blind Canyon hvBB	81.3	85.7	10.8	50.2	25.0	
4	Pittsburgh hvAB	85.0	76.7	7.96	16.2	24.4	
7	Lewiston-Stockton hvAB	85.5	76.3	8.93	22.9	16.9	
1	Upper Freeport mvB	88.1	66.0	6.59	14.3	3.6	
5	Pocahontas lvB	91.8	58.5	2.04	12.1	2.6	

*dry mineral matter free

RESULTS AND DISCUSSION

From examination of Table 1 it is apparent that the batch pyrolysis yields and the pyridine extract yields parallel each other, except for the Blind Canyon coal (APCS 6). This coal is rich in liptinites which may account for the greater pyrolysis yield. However, the yields of products observed in the DCIMS experiments as a function of time and temperature for the coal and the extract differed significantly. This is shown for the Blind Canyon coal in Figure 1. The extract exhibits a much more bimodal character with a significant yield of volatiles at the lower temperature. In addition, the high temperature peak is shifted to higher temperatures for the extract compared to both the unextracted and extracted coal. This is a general phenomena for all the coals but becomes more pronounced with the higher rank coals. These data suggest that the thermally extractable material as discussed by Meuzelaar, et al.,⁹ may be a subset of the potentially extractable material. In addition, the extracts appear to be more thermally stable compared to the solids. This may be due to a transport problem of moving the volatiles through the pore structure where secondary reactions can occur. Also, it may be that there is more donatable hydrogen available in the extracts.¹¹

In some cases the extracts yielded higher molecular weight products and a different set of compounds compared to the whole coal. Figure 2 shows an example of this result for the Lewiston-Stockton coal

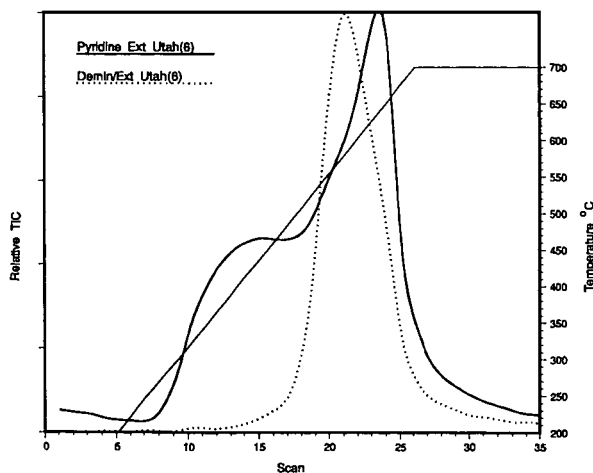


Figure 1. Total ion pyrograms from DCIMS of Blind Canyon (APCS 6) pyridine extract and demineralized and extracted residue.

(APCS 7). Note that the whole coal spectrum shows well defined series at $m/z < 250$ while the extract contains two sets of series of peaks at $m/z=250-400$ and $m/z=500-600$. The high mass set is expanded in Figure 2b. There are pairs of peaks separated by two mass units and repeating every 14 units (methylene). What is even more interesting is that these products appear across the whole temperature range as is shown in Figure 3. Initially, it was thought that these peaks could be a series of M+1 ions

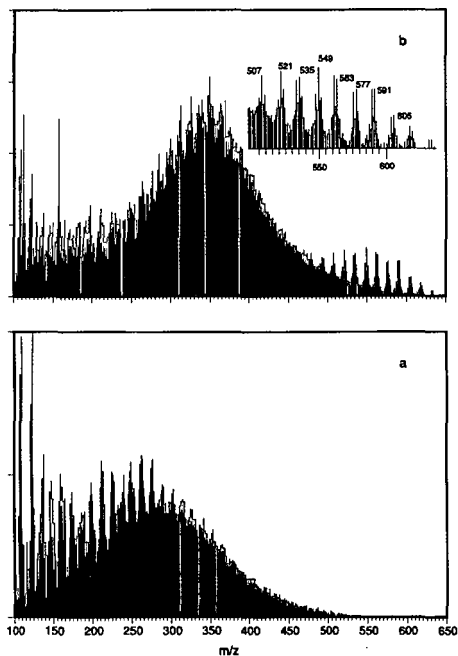


Figure 2. Averaged DCI mass spectra for (a) demineralized Lewiston-Stockton coal (APCS 7) and (b) pyridine extract of the same coal.

resulting from porphyrins. Because of the unusual nature of these ions, we felt it was worth further investigation by tandem MS. The daughter spectrum of $m/z=535$ is shown in Figure 4. It is a fairly complicated spectrum with a large number of aliphatic fragments. It is not a porphyrin or a very large ring number polycyclic aromatic compound. There is the possibility that it could be an aromatized terpenoid with the partial structure shown in Figure 4 for the fragment at $m/z=255$. A very different daughter spectrum is observed for parent ion $m/z=533$, demonstrating that these pairs of peaks are apparently not related.

The thermal stability of the extracts is seen also in the average molecular weight of the volatiles. An example is shown in Table 2 for the Lewiston-Stockton coal (APCS 7). The average molecular weight did not vary over a large temperature range for the coal while for the extract varied significantly. It started out high with the release of the large non-polar molecules, decreased at the start of the pyrolysis, and then increased with temperature.

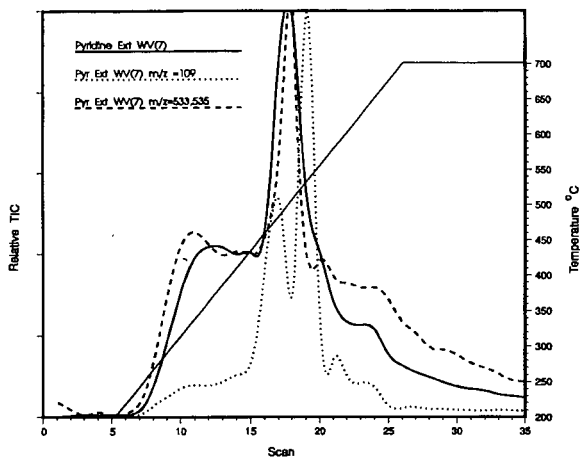


Figure 3. Total and selected ion pyrograms for DCI MS of pyridine extract of Lewiston-Stockton coal (APCS 7): solid - total ion, dotted - $m/z = 109$ and dashed - sum of $m/z = 533, 535$.

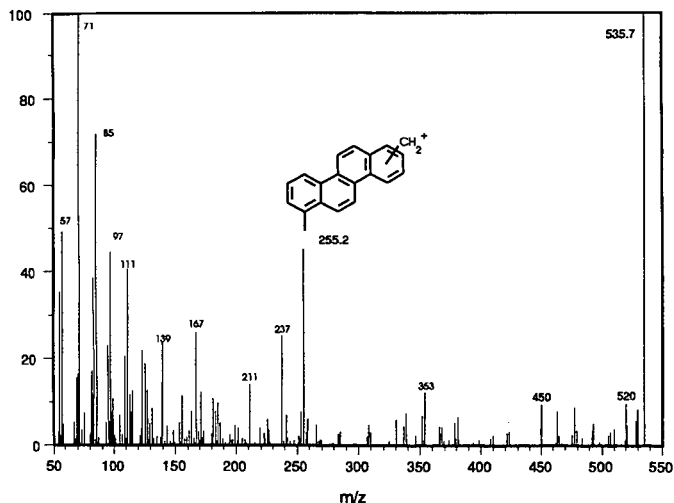


Figure 4. Daughter spectrum from parent $m/z = 535$ from CIMS of pyridine extract from Lewiston-Stockton coal (APCS 7) taken on UMIST four-sector instrument.

Table 2. Average Molecular Weights for Lewiston-Stockton (APCS 7) from DCIMS.

Sample	Temperature (°C)	M_n	M_w
Deminerized	475	240	283
	650	253	290
Pyridine Extract	375	316	345
	500	298	334
	650	319	356
	700	342	374

M_n = number average molecular weight; M_w = weight average molecular weight

Another interesting result is the suggestion from the extract data that large molecules derived from lignin sources are soluble in pyridine. In Figure 3, it is shown the selected ion ($m/z=109$) curve which would represent alkylphenol fragments. There is very little yield at the lower temperatures, but as soon as high temperature pyrolysis begins these fragments are observed. From some initial experiments with the base solubilized material, it is interesting to note that the most abundant products in the low rank coals are C_2 and C_3 alkylphenols derived from lignin. This helps to demonstrate the concept that coals are not a simple two phase system; however, they are more likely a continuum of increasing molecular weight species.

CONCLUSIONS

This work demonstrates that future work should place emphasis on the extracts and mild degradation products. Thermally extractable molecules and solvent extractable molecules are likely to be different with the former possibly a subset of the latter. Large lignin-derived fragments exist in the pyridine extractables which suggest that these extracts may be quite representative of the whole coal (vitrinite).

ACKNOWLEDGEMENTS

This work was performed under the auspices of the Office of Basic Energy Sciences, Division of Chemical Sciences, U.S. Department of Energy, under contract number W-31-109-ENG-38. Assistance of M. Morris (UMIST), D. W. Tudge and S. Evans (Kratos) in obtaining the 4-sector MSMS spectra is appreciated.

REFERENCES

1. Winans, R.E. and Neill, P.H. In *Geochemistry of Sulfur in Fossil Fuels*, W.L. Orr and C.M. White, Eds., ACS Symposium Series 429, ACS, Washington, D.C., 1990, Ch. 15, p. 249-259.
2. Szabo, P.; Varhegyi, G.; Till, F.; Szekeley, T. *Thermochimica Acta*, 1990, 170, 167-177.
3. Schulten, H.-R. and Marzec, A. *Fuel*, 1986, 65, 855-860.
4. Solomon, P.R.; Serio, M.A.; Despanda, G.V.; Kroo, E. *Energy Fuels*, 1990, 4, 42-54.
5. Malhotra, R.; McMillen, D.F.; Huestis, D.L. *Preprint, Division Fuel Chem., ACS*, 1991, 36(3), 1252-1258.
6. Yun, Y.; Meuzelaar, H.L.C.; Simmler, N.; Schulten, H.-R. *Energy Fuels*, 1991, 5, 22-29.
7. Winans, R.E. *J. Anal. Appl. Pyrolysis*, 1991, 20, 1-14.
8. Winans, R.E.; McBeth, R.L.; Hunt, J.E.; Melnikov, P.E. *Proceedings, 1991 International Conf. Coal Sci.*, 1991, 44-47.
9. Vorres, K.S. *Energy Fuels*, 1990, 4, 420-425.
10. Winans, R.E.; Hayatsu, R.; McBeth, R.L.; Scott, R.G.; Moore, L.P.; Studier, M.H., In *Coal Structure*, Gorbaty, M.L., Ouchi, K. Eds.; Adv. Chem. Series 192, ACS, 1981, 161-178.
11. Solomon, P.R., private communication.

STRUCTURE/REACTIVITY STUDIES OF SINGLE COAL PARTICLES AT VERY HIGH HEATING RATES BY LASER PYROLYSIS GC/MS

Walced S. Maswadeh, Y. Fu, Joel Dubow and Henk L.C. Meuzelaar
Center for Micro Analysis & Reaction Chemistry
University of Utah, Salt Lake City, Utah 84112

KEYWORDS: high heating rate devolatilization, laser devolatilization/GC/MS technique, coal devolatilization kinetics

INTRODUCTION

Recently, Maswadeh et al. [1] reported on the design, construction and testing of a single particle levitation/laser devolatilization apparatus featuring an on-line gas chromatograph/mass spectrometer (GC/MS) system, enabling coal devolatilization experiments at heating rates in the 10^5 - 10^6 K s⁻¹ range. Analysis of bituminous coal particles revealed a high degree of qualitative correspondence with pyrolysis patterns obtained at much slower (10^2 - 10^0 K s⁻¹ range) TG/MS heating rates [1], thus providing mechanistic justification for extrapolating kinetic parameters obtained by slow pyrolysis techniques (e.g., TG/MS or TG/IR) to the high heating rates characteristic of full scale, suspension fired coal combustors.

A second observation made with the aid of laser pyrolysis GC/MS was that the distribution of devolatilization products observed at very high heating rates was not measurably influenced by the presence or absence of air [1]. A subsequent redesign of the system permitted the use of electron microscopy (EM) grids to support individual coal particles, thereby simplifying the experimental set up, improving collection efficiency of volatile products and facilitating optical alignment of the particles (microscopy, optical micropiprometry) as well as retrieval of residual char particles [2].

EXPERIMENTAL

Materials

Bculah Zap and Illinois #6 coal samples were obtained from the Argonne Premium Coal Sample Program. Minus 100 mesh samples were carefully sieved and the subfraction passing through a #170 mesh screen but retained by a #230 mesh screen was used for further analysis. Several coal particles were picked up by means of a glass rod and transferred over to the EM grid (see Figure 1). A single particle was then selected visually under the microscope and centered manually with the help of the two HeNe laser guide beams shown in Figure 1.

Two Color Micropiprometer

Since the temperature-time history of the particle is necessary for describing tar evolution kinetics, the two color micropiprometer depicted in Figure 1 was constructed. Light emitted from the hot particle is collimated in a Cassegrainian objective (Ealing x 15/.28) and subsequently chopped at 2 kHz (Stanford Research Systems chopper, model SR540, Palo Alto, CA). A 5.066-5.364 micron IR band pass filter transmits the 5 micron band to a 15x Cassegrainian objective focussed on the first IR detector and reflects the remainder of the beam through a 1.84-2.11 micron band pass filter (both filters from Optical Filter Corp. Natick, Mass.) to a 15 X Cassegrainian objective focussed on the second IR detector. The two detectors are dewar mounted, liquid nitrogen cooled InSb photodiodes (Barnes Engineering, Stamford Conn.). The flip mirror shown in Figure 1 is a manually controlled mirror inserted into the optical path when the video camera is employed.

Signal chopping is employed to eliminate and to take into account the d.c. drift in the measurements, to operate in the frequency region of maximum D^* for the detectors and facilitate an increase in the signal to noise ratio for the measurement system [3]. The detector current outputs are converted to voltages, fed to two filtered preamplifiers (Tektronix, model AM 502) and recorded by means of a Hewlett Packard Model 5183 dual channel, 4 Mhz storage oscilloscope. The filters eliminate spurious signals arising from pulsing the CO_2 laser.

Laser Py-GC/MS

Single, 60-120 μm dia. particles of Beulah Zap lignite were analyzed by means of CO_2 laser Py-GC/MS using single laser pulses ranging in duration from 2-20 msec. The particles were mounted on copper EM grids, as shown in Figure 1. Volatile products were sampled into a 6 ft long, 180 μm i.d. fused silica capillary GC column coated with DB5 (0.40 μm) using a valveless, automated vapor sampling (AVS) device (U.S. patent 4,970,905). In these experiments, the AVS was set to "inject" a 2 sec long vapor pulse into the capillary "transfer line" column 0.1 sec after the laser pulse. Subsequently, the capillary GC column was heated ballistically from ambient to 200 C over a 2 minute period while volatile pyrolysis products were being eluted directly into the high vacuum of the Finnigan MAT ion trap mass spectrometer (ITMS). Approximately 1,200 mass spectra were recorded at a rate of 4 spectra per second after each laser pyrolysis of a single coal particle.

RESULTS AND DISCUSSION

Two Color Micropyrometer Measurements

Following Spjut et al. [4] the single channel and two channel transient responses were calculated. These showed that the intrinsic 2-color pyrometer response time was on the order of 0.1 microsecond and that the 5 micron channel was nearly a factor of two faster than the 2 micron channel. However, parasitic impedances and impedance mismatches between the detectors and the preamplifiers slowed the response time considerably, so that chopping at frequencies of 1 Khz and above caused a degradation in response, especially in the 5 micron channel. This effect led to a small but systematic underestimation of the temperature in these data but has recently been eliminated using techniques to increase system electronic bandwidths. In order to minimize systematic errors, careful temperature calibration was performed over the 300-1100 K range using a specially constructed 0.88 mm dia. black body cavity radiator. This calibration is extrapolated to higher temperatures using standard radiation pyrometry theory. The results are shown in Figure 2.

As shown in Figure 3, two Beulah Zap lignite particles (63-90 μm) produced maximum temperature readings in the 1700-1850 K range, which is directly comparable to the characteristic operating temperatures of full scale pulverized coal combustors [5]. The temperature history profiles suggest a two step heating behavior with initial heating rates of approx. 2.10^5 K s^{-1} giving way to lower heating rates (approx. 4.10^4 K s^{-1}) after 6-7 milliseconds. Laser beam intensities are known to remain essentially constant ($\pm 5\%$) throughout the duration of the pulse (after an initial 1 millisecond stabilization period). Partial obscuration of the particle surface by the rapidly expanding and cooling cloud of volatiles, combined with evaporative surface cooling effects could be the source of the observed temperature variations in the 6-15 millisecond range. Similar temperature profiles were obtained for a series of Illinois #6 particles (not shown here).

Laser Py-GC/MS Analysis

A typical GC/MS profile of the volatile laser pyrolysis products of a single Beulah Zap coal particle is shown in Figure 4, illustrating the good signal to noise ratio obtained in spite of the small particle size and the relatively low tar yields (<10% daf coal) of lignites. The largest GC peaks seen in the

total ion chromatogram (TIC) profile after the initial "air peak" in Figure 4a consist of toluene ($M^+ = m/z$ 91), phenol (m/z 94), cresols (m/z 108), C2 phenols (m/z 122), naphthalene (m/z 128), and methyl guaiacol (m/z 138), as further detailed by the selected ion chromatogram (SIC) profiles in Figure 4b-d illustrating the useful degree of chromatographic pre-separation achieved by the short capillary "transfer line" GC column. All major isomers are readily identifiable, thus providing a sensitive way of comparing pyrolysis mechanisms at high heating rates with those observable at much lower heating rate, e.g., in TG/MS experiments, as reported previously [1,2]. It should be noted here that the observed pyrolysis profiles of most Beulah Zap lignite particles are quite similar to the profiles obtained from the much slower (10^2 - 10^3 K s⁻¹) Curie-point Py-GC/MS experiments (not shown here), e.g., with regard to the dominant (alkyl) phenol series. As discussed before [1], however, the highly polar and reactive dihydroxy benzenes tend to be absent or underrepresented in laser Py-GC/MS profiles of low rank coals, presumably as a result of mass transfer limitations resulting in condensation reactions of the dihydroxybenzenes inside the char particle. The less reactive methoxyphenols characteristic for lignites and thought to represent typical building blocks of fossilized lignin [7] are readily detected as shown by the prominent methyl guaiacol peaks in Figure 4a.

By performing laser Py-GC/MS analysis of Beulah Zap coal particles at 8 different laser pulse durations and summing the quantitative response of the dominant tar components at m/z 108 (C1 phenols) and m/z 122 (C2 phenols) for each laser experiment, it proved possible to construct the tar evolution profile shown in Figure 5. Note that each point represents the average of 3-4 laser Py-GC/MS analyses. From previous experience it was expected that 20 milliseconds would suffice to obtain complete devolatilization. As demonstrated in Figure 5, however, the tar yield still seems to be increasing at 20 milliseconds, probably due to a somewhat reduced laser power output. Unfortunately, we omitted to determine remaining volatile matter content at 20 milliseconds by subjecting each remaining char particle to a second laser pulse of ample long duration. From the shape of the profile and the intensities of the mass spectra obtained, the tar yield at 20 milliseconds is assumed to be 60-80% of the maximum tar yield obtainable.

Kinetic Considerations

The tar evolution profile in Figure 5 invites the question whether kinetic parameters can be extracted from these data. In view of the relatively small number of data points and the large number of potential sources of error in this type of experiment the authors decided not to attempt a direct extraction of kinetic parameters (which involves differentiation of the curve in Figure 5) but rather to compare the measured profile with predicted yield profiles derived from low heating rate data, using appropriate kinetic models. Beulah Zap tar evolution profiles obtained by three different laboratories (Advanced Fuels Research, using TG/FTIR at 30 K min⁻¹ [8] and 10 K min⁻¹; and Lawrence Livermore National Laboratory, using Py-MS/MS at 4 K min⁻¹ [9]) are represented in Arrhenius plot format (Figure 6). All profiles show excellent agreement (max. 25 K difference in temperatures, corresponding to less than a factor 2 in rate constant difference, when correcting for variations in heating rate) in spite of the very different experimental set-up. The two TG/MS curves (Nie et al., unpublished data) were recorded in our laboratory with a new system operating at ambient pressure and featuring a molecular leak type quartz probe positioned within 5 mm of the TG crucible. When ignoring the minor temperature offsets between the curves, the average slopes and curvatures are quite similar with the possible exception of the TG/FTIR curve. In other words, three of the four curves appear to represent the same set of activation energies.

This brings up the important question how to interpret the observed curvature of all four profiles in the Arrhenius plot. Three possible options are: (1) multiple parallel reactions characterized by a particular distribution of activation energies [10]; (2) a continuously variable (conversion dependent) activation energy (see appendix); and (3) a single, constant activation energy with a heat or mass transfer controlled reaction rate. Most likely, we are dealing with a combination of all three scenarios. There is little doubt that multiple parallel reactions are involved in coal pyrolysis, as can be readily observed by time-resolved pyrolysis MS experiments [11, 12]. Similarly, it is well understood that continuous chemical alteration of the coal matrix takes place throughout the pyrolysis process, gradually transforming the original coal particle into a fully developed char particle. In other words, the chemical structure and composition of the coal particle halfway through the pyrolysis reaction are fundamentally different from that of the unreacted particle as can be readily determined by interrupting the pyrolysis process [13]. Obviously, the activation energy (and its distribution) are unlikely to remain constant throughout the entire process. Finally, evidence of mass transfer limitations (e.g., caking!) is readily observable in TG experiments, especially at heating rates above 5-10 K min⁻¹, depending on coal type and rank. Although all three phenomena: distributed activation energy, continuously variable activation energy and mass transfer limitations can readily explain the observed curvatures in the Arrhenius plot, each assumption leads to different rate and yield predictions at very high heating rates, as illustrated for the DAE (distributed activation energy) and VAE (variable activation energy) models in Figure 7. The numerical procedures used to obtain Figures 6-8 will be explained in detail elsewhere [6]. No attempt was made to predict the effects of transfer limitations due to the particle size dependence and the lack of information on the exact particle size distribution in the various experiments.

Interestingly, the DAE and VAE assumptions each lead to quite different predicted rate constants at high heating rates, thus opening up the possibility of direct experimental verification! Figure 8 compares the DAE and VAE predictions to the observed tar evolution profile. Although our VAE prediction appears to produce a better fit with the observed data, the current lack of quantitative information on the effect of transport limitations on the results of the devolatilization experiments at slow as well as at fast heating rates precludes the possibility of reaching a firm conclusion. Figures 5-8 merely illustrate that the experimental and numerical tools are in hand to start answering some of these questions and that experimental results obtained with different techniques and in different laboratories are starting to converge in a highly promising manner. Foremost among the problems that remain to be addressed however, appears to be the need to conduct systematic studies on the effects of heat and mass transfer limitations under slow as well as rapid coal devolatilization conditions.

ACKNOWLEDGEMENTS

The authors wish to thank N. Rappaport, X. Nie and N.S. Arnold for their valuable help and advice. This work was supported by the Advanced Combustion Engineering Research Center. Funds for this Center are received from the National Science Foundation, the State of Utah, 23 industrial participants and the U.S. Department of Energy.

LITERATURE REFERENCES

1. Maswadeh, W.; Huai, H. and Meuzelaar, H.L.C.; *ACS Preprints, Div. of Fuel Chem.*, 36(2) 733-740, 1991.
2. Maswadeh, W.; Meuzelaar, H.L.C.; *Proc. 39th ASMS Conf. on Mass Spectrom. All. Top.*, 1991, 192-193.
3. Wolff, W., and Zissis, G., *The Infrared Handbook*, Office of Naval Research, Dept. of the Navy, Arlington, VA, 1978.

4. Spjut, R.E., and Balsaitis, P., *Mat. Res. Soc. Symp.* 87, 295-302, 1987.
5. Smoot, D., and Smith, P. in: *Coal Combustion and Gasification*, D. Luss (ed.) Plenum Press, NY, 37-75 (1985).
6. Maswadeh, W.; Meuzelaar, H.L.C.; Dubow, J.S to be submitted to *Energy & Fuels*.
7. Nip, M.; de Leeuw, J.W.; Schenck, P.A.; Meuzelaar, H.L.C.; Stout, S.A.; Given, P.H.; Boon, J.J., *J. Anal. Appl. Pyrol.*, 1985, 8, 221-239.
8. Solomon, P.R.; Serio, M.A.; Carangelo, R.M.; Bassilakis, R. *Energy & Fuels*, 1990, 4, 319-333.
9. Burnham, A.K.; Oh, M.S.; Crawford, R.W.; *Energy & Fuels*, 1989, 3, 42-55.
10. Braun, R.L.; Burnham, A.K.; *Energy & Fuels*, 1987, 1, 153-161.
11. Chakravarty, T.; Windig, W.; Hill, G.R.; Meuzelaar, H.L.C. *Energy & Fuels*, 1988, 2, 400-405.
12. Yun, Y.; Meuzelaar, H.L.C. *ACS Preprints, Div. Fuel Chem.*, 1988, 33(3), 75-84.
13. Pugmire, R.J.; Solum, M.S.; Grant, D.M.; Critchfield, S.; Fletcher, T.H. *Fuel*, 1988, 2., 1991, 70, 414-423.

Appendix - VAE Calculation

1. From experimental rate $\left(\frac{dX}{dT}\right)$ versus temperature (T), integration is performed from $T_0 \rightarrow T$ to obtain conversion $X(T)$.
2. An Arrhenius plot is made which is a plot of $\text{Ln} \left(\frac{dX/dT}{1-X}\right)$ versus $\left(\frac{1}{T}\right)$.
3. The first derivative of this Arrhenius plot at different temperatures yields $(-Ea/R)$ and the intercept is equal to $\text{Ln}(A_0)$. These are plotted versus T.
4. From the plots of $-Ea/R$ versus T and X versus T a plot of (Ea) versus X is made.
5. A polynomial fit is made for the apparent activation energy (Ea) versus conversion X in Step 4.

$$Ea(X) = a_0 + a_1x^1 + a_2x^2 + a_3x^3 + \dots$$
 and the resulting frequency factor determined $(Ea = a \ln A_0 + b)$.
6. The relationship from step 5 is matched with the experimental rate using the standard equation below:

$$\frac{dX}{dT} = \left(\frac{Ea(X)-b}{a m}\right) e^{-\frac{Ea(X)}{RT}} (1-X)$$
7. The above equation is plotted for high heating rates using the $Ea(X)$ function obtained at low heating rates and compared to the high heating rate experimental data.

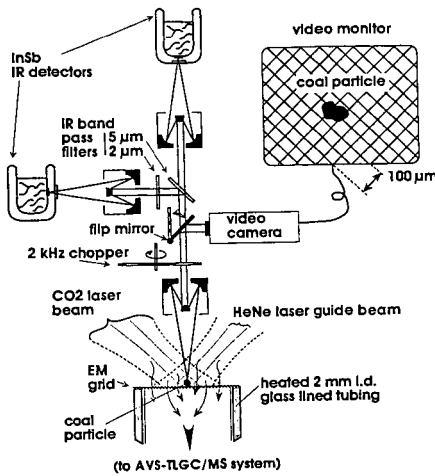


Figure 1. Schematic overview of two-color micropyrometer module with grid supported coal particle, incident dual CO₂ and HeNe laser beams, and inlet to AVS-TLGC/MS system.

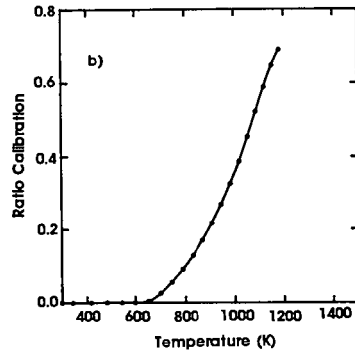
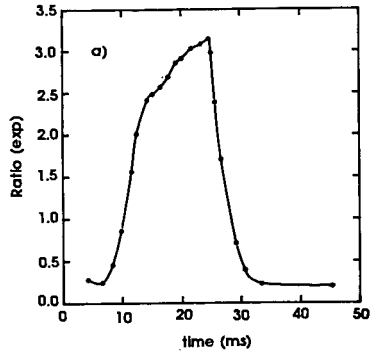


Figure 2. Pyrometer Calibration. The ratio of the outputs from the signal channels at 2.0 microns and 5.2 microns, as shown in (a), is converted to temperature using black body calibration, as depicted in (b). Above 1100 K, temperature is extrapolated using calibration and two channel pyrometry theory.

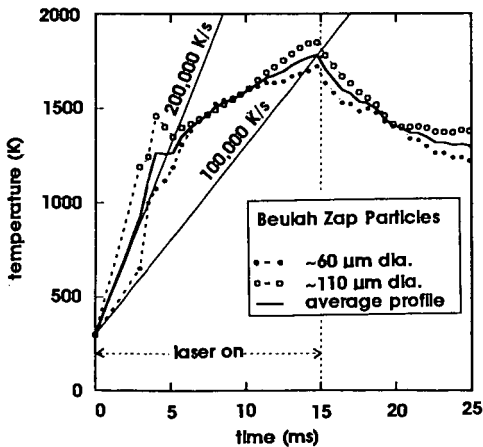


Figure 3. Temperature/time profiles of 2 Beulah Zap lignite particles during 15 millisecond CO₂ laser heating pulse and subsequent 10 millisecond passive cooling period.

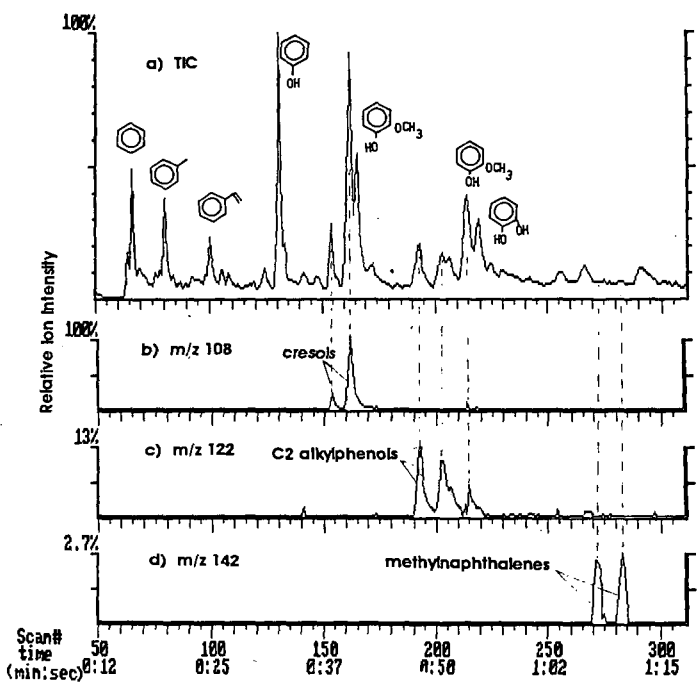


Figure 4. Typical laser Py-GC/MS profile of a 100 μm dia. Beulah Zap particle at 20 msec pulse duration. Note highly useful GC separation within approx. 70 seconds as well as dominant hydroxyaromatic signals (in agreement with low coal rank). Integrated area signals at m/z 108 and 122 were used to calculate "tar yields" shown in Figures 5 and 8.

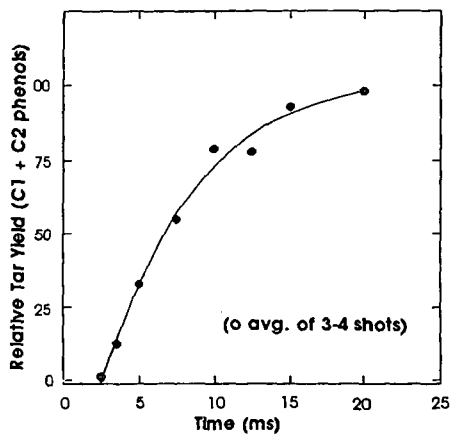


Figure 5. Relative tar yields (normalized to 20 ms yields) of 60-100 μm dia. Beulah Zap lignite particles at 8 different laser pulse times. Note that devolatilization still appears incomplete at 20 ms. Compare with Figures 3 and 4.

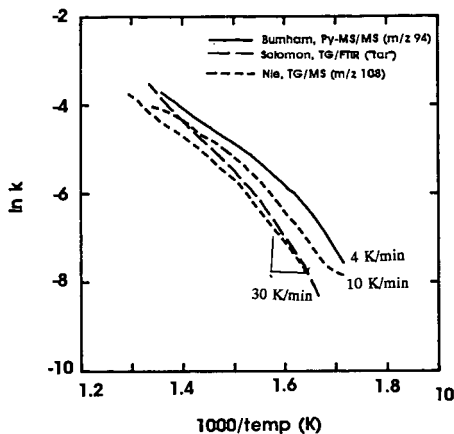


Figure 7. Comparison of VAE and DAE predictions of tar evolution kinetics at typical laser heating rates based on the 30 K min⁻¹ TG/MS profile shown in Figure 6. Note DAE model fit (42 ± 4 kcal/mol). For details of VAE prediction calculation, see Appendix.

Figure 6. Arrhenius plots showing very good agreement of literature data (Burnham, Solomon) on Beulah Zap tar evolution kinetics with our TG/MS data in spite of marked differences in experimental technique (and some variation in "tar" definition), especially when correcting for variations in heating rate. Note that entire tar evolution profiles were plotted (see Appendix).

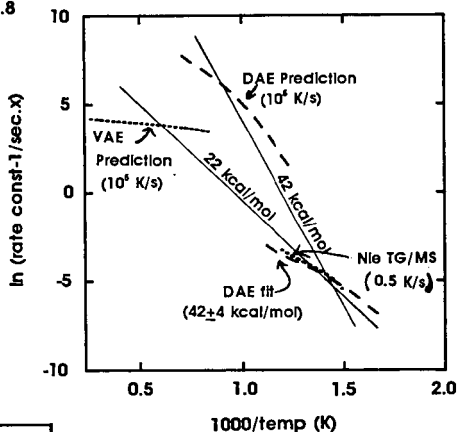
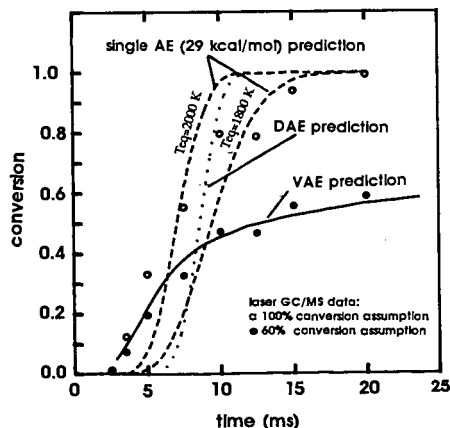


Figure 8. Measured and predicted relative tar yields of Beulah Zap coal particles. Note that VAE prediction indicates only 60% relative tar yield within 25 milliseconds. Measured points (o, o) represent averages of 3 or 4 laser shots. Single Ea (SAE) and Variable Ea (VAE) predictions use measured temp profiles (see Figure 3), DAA prediction uses linear heating rate (10^5 K s⁻¹).



Analysis of Coals from the San Juan Basin by Programmed Temperature Micropyrolysis

John G. Reynolds and Alan K. Burnham

Lawrence Livermore National Laboratory
University of California
Livermore, CA 94551

Abstract

Eighteen coals from the San Juan Basin of the southwestern U.S. were analyzed by micropyrolysis at constant heating rates for temperatures of maximum evolution (T_{max}) and pyrolysis yields. T_{max} values increased with maturity (as measured by vitrinite reflectance [% R_m]). The pyrolysis yields increased with increasing maturity until approximately R_m of 0.9% after which the yield declined rapidly.

A subgroup of coals from the Fruitland seam of the San Juan basin was also analyzed by micropyrolysis at several constant heating rates to determine laboratory pyrolysis kinetics. The kinetic calculations yielded the energy of activation by the approximate method (E_{approx}) and the principal energy of activation by the discrete method (principal $E_{discrete}$) in the range of 55 to 57 kcal/mol for the coals in the R_m range of 0.4 to 0.9%. However, the coal with the highest R_m (1.30%) had E_{approx} and principal $E_{discrete}$ around 63 kcal/mol.

These Fruitland seam coals were also extracted with organic solvents and the residual coals were analyzed to determine laboratory pyrolysis kinetics. The results were within experimental error of the kinetic values calculated for the corresponding unextracted coals.

Key words: San Juan Coals, Pyrolysis Kinetics, and Yield

Introduction

The San Juan Basin in the southwestern U. S. (Four Corners area) is a major producer of natural gas. Recently, there has been activity in the exploration for gas in the upper cretaceous Fruitland seam, which is the major deposit of coal in the basin. The Fruitland seam is considered to have the potential of 50-56 tcf of gas production, as well coal reserves of approximately 200 billion tons.¹

Most of the production is probably due to the thermal maturation over geological time. To assist in the understanding of this hydrocarbon production, we have been studying thermal maturation of source materials in the laboratory by pyrolysis techniques,² such as the Pyromat II micropyrolyzer.³ With this technique, the pyrolysis kinetics are measured, and through selected models, these kinetic

parameters measured have been extrapolated to produce relevant maturation parameters.

This report summarizes pyrolysis kinetic analysis of selected coals from the San Juan Basin by the Pyromat II micropyrolyzer. A more complete listing and analyses of this data will be reported elsewhere.⁴

Experimental

Kinetic Analysis. The method of kinetic analysis using the Pyromat II has been described in detail elsewhere.³ Briefly, the kinetics were determined from multiple runs at constant heating rates on approximately 4 to 10 mg samples. Generally three - 50°C/min, one - 7°C/min, and two - 1°C/min runs were performed. If T_{max} values and profile shapes were not in agreement, more runs at these heating rates were performed.

Yield Analysis. Yield analysis was performed on all samples by comparing to the yield of AP22 oil shale. This yield has been determined from Fisher Assay to be 88 mg of pyrolysate/gram oil shale. Two furnaces were used for these measurements. The yields were determined by two methods: 1) the yield was determined for the coal from two or three runs at the nominal heating rate of 25°C/min, from 250°C to 700°C using the old furnace. The AP22 standard was run twice daily and a single calibration factor was determined for the entire set of runs (over a period of four days). 2) For the four samples used in the kinetic analyses, several determinations were performed using the new furnace. To assure more accurate yields, the standard was run immediately before each coal sample. The standard values were then averaged each day, providing a daily calibration factor.

Samples. All samples were received run-of-mine condition, sealed in plastic bags. The whole allotment (5 to 10 grams) was ground with mortar and pestle in a nitrogen purge glove bag to inhibit oxidation. Homogeneity problems were encountered with some samples and these were reground.

Eighteen samples were received from various parts of the San Juan Basin - Fruitland formation, 12; Menefee formation, 4; Hog mountain tongue, 2. Table 1 shows the formation, the sample identification symbols, the well and depth (feet), and the vitrinite reflectance values (mean random reflectance values). The samples range from essentially subbituminous rank to medium-volatile bituminous. The depths of the Fruitland samples vary considerably and are not directly correlated with rank because of non-uniform heating due to an intrusion in the formation and the different well locations through out the field. For Henry AGC Fed #1, the shallower samples are from the Fruitland formation, and the deeper samples are from the Menefee formation (the well probably passes through the Pictured Cliffs and Cliff House sandstone formations). For Champ #5, the shallower sample is from the Fruitland formation, probably more north than the Henry AGC Fed #1 well, the intermediate samples are from the Hog Mountain tongue, and the deepest

samples are from the Menefee formation. The maturity of the Menefee formation samples from these two wells is only slightly higher than that of the shallower Fruitland samples.

Extraction. 0.2 to 0.5 g of the coal sample were extracted in a micro-soxhlet extractor for 36 hours using either the 92% CH₂Cl₂/8% MeOH azeotrope or 100% tetrahydrofuran (THF) as the extraction media. After the extraction was complete, the extracted coal was dried *in vacuo* and the solvent with the extracted bitumen was removed under a stream of N₂ gas. Mass balances exhibited over 98% recovery for the CH₂Cl₂/MeOH extractions. The THF extraction exhibited over 100% recovery after extensive drying, indicating some permanent incorporation of the solvent into the sample.

Elemental Analyses. Table 2 lists the C, H, N, CO₂, and TOC (total organic carbon) analyses (there was not enough CH₅D sample to analyze). Most of the coals have TOC levels which fall in the range of 30 to above 60 wt%, with KB5B being the richest. Two are less than 30 wt% and one, CU2A, is extremely lean in organic matter. This coal exhibits anomalous evolution behavior (see below). The coals are also very low in carbonate content (%CO₂).

T_{max} and Yield Data

Relationship between T_{max} and vitrinite reflectance. Figure 1 shows the T_{max} values at the nominal heating rate of 25°C/min measured directly on the coal samples from the San Juan Basin as a function of maturity (measured by vitrinite reflectance). Included are not only the Fruitland seam coals, but also coals from the other seams.

Except for the two coals with the lowest R_m values, all the T_{max} values fall nicely on a slightly curved line which has a positive slope with increasing R_m values. This behavior includes coals from the Fruitland, Menefee, and Hog Mountain seams. Generally two runs were performed on each coal and both runs were in good agreement, except for CU2A. The T_{max} of this coal was particularly susceptible to sample size.⁵ Ten runs were made to obtain reasonably reproducible data. This coal has a very low TOC (see Table 2), and mineral matter, sample inhomogeneity, as well as a high percentage of the TOC being bitumen, could be causes for variations in the pyrolysis behavior.⁶

The coals with the lowest R_m, CH5A and HAFA, have T_{max} values which do not fall in line with the rest of the T_{max} values. Measurements on these coals and GR3A and KBSA were repeated to check reproducibility, and the results were found to be comparable to the original data. (The latter data was taken on the Pyromat II after the furnace was replaced) No reason for the outlying behavior of CH5A and HAFA is obvious from the little data we have on other properties of the coals. However, both these coals are found at the shallowest depth (300 ft above the others). In addition, the CH5A sample was from above the Hog Mountain tongue, and both

HAFa and CH5A samples are from above the Menefee formation (see Table 1). It is important to note that Michael et al.⁷ found a linear relationship between R_m and T_{max} for Rock Eval measurements on coals from the San Juan basin. This result would suggest CH5A and HAFa as being well behaved and that the Menefee and Hog Mountain coals (see Figure 1) do not follow the trend.

Relationship between yield and vitrinite reflectance. The yields were also measured at the nominal heating rate of 25°C/min on the coals from the San Juan Basin, and are shown in Figure 1 as the open symbols (corresponding to the closed symbols for the T_{max} values). Because the Pyromat II has no direct method of measuring yield, these values were measured by using an AP22 standard (see experimental). For most of the data shown in Figure 1, the calibration factor from the AP22 standard was an overall average (yield method 1). For selected coals, the yields were checked more carefully, particularly if the value appeared to not follow the trend in Figure 1 (yield method 2).

The yield data shown in Figure 1 exhibits scatter, particularly for the low R_m coals. However, the yields appear to decrease with increasing R_m , with a noticeable change in the curvature around R_m of 0.9%. This is even more noticeable when considering only the Fruitland formation coals. (GR3B does not really follow this trend as well as one determination for CU2A. We had significant problems with every aspect of CU2A, and have little confidence in the reproducibility. Alternatively, it may contain primarily migrated bitumen.) The trend of decreasing yield above R_m of 0.9% has been seen for the Fruitland seam previously.⁶

Effect of bitumen extraction on pyrolysis yields. Four Fruitland coals, CH5A, MOAB, KB5B, and CU5A, were extracted with organic solvents to remove native bitumen and the pyrolysis yields were determined. Table 3 shows a summary of these data and compares them with the data on the corresponding unextracted coal. In all cases, the extraction reduces the pyrolysis yield. The magnitude depends upon the coal and the extraction solvent. The extracted pyrolysis yields as percentage of unextracted pyrolysis yield are: CH5A, 79; CH5A (THF extraction), 82; MOAB, 92; KB5B, 95; CU5A, 65. The extraction appears to have less effect with increasing R_m except for CU5A, which has the highest R_m of the samples studied. This behavior is opposite to the pyrolysate yields themselves which exhibit a decrease around R_m of 0.9%.

Because we had no previous experience with these coals, we selected 92% CH_2Cl_2 /8% MeOH as the extraction solvent because of its: effectiveness in extracting shales, the reduced likelihood of coal structure damage due to swelling, and minimal irreversible binding. The extraction yields using this solvent calculated from the weight of extracted bitumen were: CH5A, 4.4%; MOAB, 4.1%; KB5B, 4.8%; CU5A, 4.2%. However, these yields seem relatively low compared to bitumen yields for other coals, so THF was selected as an alternate. This solvent has a higher solubility parameter, and could possibly extract more native bitumen. The yield for CH5A using 100% THF as the extraction solvent was 6.9%, which is not a

significantly higher to cause re-extraction of the samples. Solvents such as pyridine were ruled out because of their destructive interactions with the coal structure and the noted irreversible binding.⁷

Qualitatively, the native-bitumen extraction yields are consistent with the amount the pyrolysis yields are reduced upon extraction for all the coals except CU5A. For this coal, the pyrolysis yield is reduced substantially more than would be expected from the extraction yield. The reasons for this are not clear. CU5A is the most mature sample of the group and has one of the lowest pyrolysis yield based on bitumen recovery. In addition, all the extractions of CU5A (four) showed a mass balance of over 100%, unlike the other samples, indicating solvent was incorporated into the coal structure, and suggesting the coal network was being much more affected by the extractions than the other coals.

Kinetics of Evolution of Organic Materials by Pyrolysis

Fruitland Coals. Four Fruitland coals, CH5A, MOAB, KB5B, CU5A, were examined to determine their kinetic parameters for hydrocarbon evolution. These coals were picked because their range in R_m covers from the least to most mature of the samples (see Table 1). Figure 2 shows the kinetic parameters for the discrete and approximate analyses from the best kinetic sets for each coal. The best kinetic set was chosen from multiple runs and multiple determinations, primarily from the agreement of the approximate and the discrete parameters, as well as the least squares analysis of the fits.

The best kinetic sets show some interesting trends. The parameters for the lower rank coals are all very similar. CH5A has E_{approx} and principal E_{discrete} slightly higher than MOAB and KB5B. CU5A stands out as having the highest R_m of the samples studied and distinctly different kinetic parameters (higher E_{approx} and principal E_{discrete}). This appears to follow the behavior seen before in the kinetic studies of Argonne premium coals,⁸ which show a decrease in activation energy with increasing rank for the lower rank coals, and an increase in activation energy with increasing rank for the higher rank coals.

Figure 2 also shows the fits of the evolution data using the discrete distribution model. The fits for CH5A, MOAB, and KB5B look very good. However, the fits for CU5A look significantly poorer. This will be discussed below.

Extracted Fruitland Coals. To understand the effects of native bitumen on the kinetics parameters of these coals, CH5A, KB5B, MOAB, and CU5A were extracted with organic solvents and the pyrolysis kinetics were determined from multiple-heating rate experiments. The best kinetic sets are listed in Table 4.

As in the case for the unextracted coals, the lower rank coals all have very similar kinetic parameters. E_{approx} and principal E_{discrete} are slightly higher for CH5X. As the rank increases, E_{approx} and principal E_{discrete} are slightly lower for both MOAX

and KB5X, and then is significantly higher for CU5X. This behavior is almost identical to the behavior of the unextracted coals.

Comparing the parameters in Figure 2 and Table 4 shows the kinetics for the unextracted and corresponding extracted coals are within experimental error. CH5X and CH5A show the most difference. Noting the possibility of compensating A values for the lower activation energy values for CH5X, the discrete kinetic parameters were recalculated for CH5X holding the A value fixed at 1.74×10^{15} . Table 5 shows these results. Although the least squares fits were not as good as for the CH5X kinetic set, the resulting discrete parameters were almost identical to those of the unextracted CH5A coal.

The similarity of the parameters for the unextracted coals and the corresponding extracted coals indicates the extraction does little to effect the kinetic parameters. The biggest differences are seen in the calculated T_{max} values at the heating rate of $25^{\circ}\text{C}/\text{min}$. The extracted coals yield values which are slightly higher for the lower ranks, and essentially identical for the higher rank coals. However, this difference is probably not significant enough to confidently say the extraction affects laboratory pyrolysis evolution kinetics, or that extraction is necessary in these cases to obtain valid kinetics.

This was not the case for CU5A, where the kinetic determinations were not as easy to interpret. The choice for the best kinetic set required several determinations, as well as considering the extracted data also. Figure 3 shows a comparison of extracted and unextracted CU5A at the nominal heating rate of $25^{\circ}\text{C}/\text{min}$. Obvious is the removal of the low temperature evolving material in the extracted sample. This had a significant effect on discrete kinetic parameters. Also, the σ values in Figure 2 and Table 4 show this extraction affects the peak width of evolving materials in the kerogen pyrolysis range.

As stated in the yield section, CH5A was also extracted with THF. The best kinetic set is shown in Table 5, which shows that the THF extraction had little effect on the kinetic parameters, where the values are within experimental error of the $\text{CH}_2\text{Cl}_2/\text{MeOH}$ extraction parameters.

Conclusions

For the San Juan Basin coals in this study:

- 1) T_{max} increases systematically with increasing maturity (as measured by vitrinite reflectance).
- 2) Total pyrolysate yield increases with increasing maturity until a R_m of approximately 0.9%. After this, the yield begins to decrease rapidly.

For the Fruitland seam coals in this study:

- 1) Extraction with 92% CH₂Cl₂/8% MeOH removes approximately 4% by weight of total sample. This qualitatively agrees with the reduction of pyrolysis yield upon extraction, except for CU5A.
- 2) Extraction of CH5A with 100% THF showed modest increase in bitumen yield over the 92% CH₂Cl₂/8% MeOH extraction, but showed no decrease in pyrolysis yield. This suggests THF is being incorporated into the coal.
- 3) Kinetic calculations of CH5A, MOAB, and KB5B, showed similar kinetic parameters. CU5A, however, had much higher activation energies.
- 4) Kinetic calculations of the extracted CH5A, MOAB, and KB5B showed similar kinetic parameters. Extracted CU5A, however, had much higher activation energies.
- 5) Kinetic parameters of the extracted CH5A, MOAB, and KB5B coals were almost identical to the parameters of the corresponding unextracted coal indicating extraction does little to effect the coal structure and is probably not necessary for these determinations.
- 6) Kinetic calculations for CU5A showed large differences between approximate and discrete parameters. The kinetic parameters of the extracted data set were used to resolve these discrepancies which suggests extraction is necessary for this coal.

Acknowledgments

We thank Edward L. Jones and Ann M. Murray for experimental assistance and Vido Nuccio of the U. S. Geological survey for the samples and the corresponding vitrinite reflectance data. This work was performed under the auspices of the U. S. Department of Energy by the Lawrence Livermore National Laboratory under contract number W-7405-ENG-48.

References

1. D. D. Rice, C. N. Threlkeld, A. V. Vuletich, and M. J. Pawlewicz, *Oil and Gas J.*, Aug 13, 60-61 (1990).
2. R. L. Braun and A. K. Burnham, *Energy and Fuels*, 4, 132-146 (1990).
3. R. L. Braun, A. K. Burnham, J. G. Reynolds, and J. E. Clarkson, *Energy and Fuels*, 5, 192-204 (1991).
4. J. G. Reynolds, LLNL Report UCRL-ID-XXXXXX (1992).
5. J. G. Reynolds and A. M. Murray, LLNL Report UCRL-ID-106505 (1991).

6. H. Dembicki, Jr., B. Horsfield, and T. T. Y. Ho, A.A.P.G. Bulletin, 67(7), 1094-1103 (1983).
7. G. E. Michael, D. E. Anders, and B. E. Law, manuscript to be published.
8. D. D. Whitehurst, T. O. Mitchell, and M. Farcasiu, Coal Liquefaction, (1980), Academic Press, New York.
9. A. K. Burnham, M. S. Oh, R. W. Crawford, and A. M. Samoun, Energy and Fuels, 3, 42-55 (1989).

Table 1. Selected information on coals from the San Juan Basin.

Sample ID	Formation	Depth (feet)	Vitrinite Reflectance (%R _m)
HAFa ^a	Fruitland	1528-1534	0.46
HAFB ^a	Menefee	3049-3054	0.57
HAFC ^a	Menefee	3800-3810	0.58
CH5A ^b	Fruitland	950-960	0.44
CH5B ^b	Hog Mountain	1880-1890	0.52
CH5C ^b	Hog Mountain	1910-1920	0.49
CH5D ^b	Menefee	3170-3180	0.54
CH5E ^b	Menefee	3210-3220	0.54
MOAA ^c	Fruitland	2927-2937	0.76
MOAB ^c	Fruitland	3085-3106	0.82
KB5A ^d	Fruitland	3046-3056	0.82
KB5B ^d	Fruitland	3169-3184	0.93
GR3A ^e	Fruitland	2520-2540	0.62
GR3B ^e	Fruitland	2540-2550	0.66
CU2A ^f	Fruitland	3960-3990	1.08
SJ8A ^g	Fruitland	3150-3160	1.22
SJ8B ^g	Fruitland	3148-3158	1.24
CU5A ^h	Fruitland	4180-4200	1.30

Wells:

a. Henry AGC Fed #1 (Yates Petroleum Co.). b. Champ #5 (Dugan Petroleum Co.). c. Moore A #8 (Amoco Production Co.). d. Kernaghan B #5 (Amoco Production Co.). e. Grenier #103 (Meridian Oil). f. Carracas Unit 23A #2 (Nassau Resources). g. San Juan 32-5 #108 (Meridian Oil). h. Carracas Unit 17B #15 (Nassau Resources).

Table 2. Selected elemental analyses for coals from the San Juan Basin.

Sample	%C	%H	%N	%CO ₂	TOC
HAF A	41.81 (0.35)	3.78 (0.14)	1.26 (0.10)	0.96	41.55
HAF B	40.22 (0.09)	3.63 (0.03)	1.26 (0.22)	0.53	40.08
HAF C	59.74 (1.33)	4.69 (0.06)	1.43 (0.22)	0.47	59.61
CH5 A	51.88 (0.20)	3.99 (0.06)	1.12 (0.09)	2.65	51.15
CH5 B	61.86 (0.06)	4.83 (0.19)	1.49 (0.24)	0.62	61.69
CH5 C	46.08 (1.19)	3.73 (0.12)	1.08 (0.01)	0.72	45.88
CH5 D	na	na	na	na	na
CH5 E	26.11 (31.7)	2.30 (0.10)	2.19 (0.09)	0.63	25.94
MO A A	38.27 (3.83)	3.10 (0.06)	1.10 (0.16)	2.31	37.64
MO A B	63.21 (1.93)	4.12 (0.07)	1.53 (0.04)	0.88	62.97
KB5 A	60.23 (1.67)	4.41 (0.26)	1.43 (0.19)	1.41	59.85
KB5 B	64.09 (1.08)	4.48 (0.14)	1.89 (0.27)	1.35	63.72
GR3 A	18.41 (0.34)	1.95 (0.01)	0.63 (0.04)	1.76	17.93
GR3 B	55.69 (2.28)	4.96 (0.89)	1.62 (0.06)	1.65	55.24
CU2 A	1.93 (0.06)	0.52 (0.08)	nd	2.91	1.14
SJ8 A	36.35 (0.56)	2.65 (0.13)	1.17 (0.09)	0.95	36.09
SJ8 B	33.42 (1.29)	2.37 (0.06)	0.88 (0.03)	1.33	33.06
CU5 A	56.29 (0.58)	3.26 (0.06)	1.19 (0.07)	0.12	55.75

na. Not enough sample to analyze. nd. Analyzer problem with N determination

Table 3. Summary of yield data by Pyromat II micropyrolysis for selected coals and bitumen-extracted coals from the San Juan Basin at the nominal heating rate of 25°C/min.

Coal	Extraction Solvent	Yield, mg pyrolysate/ g coal	Yield, mg pyrolysate/ g TOC
CH5A	none	131	255
CH5A	92% CH ₂ Cl ₂ /8% MeOH	104	na
CH5A	100% THF	108	na
MOAB	none	191	303
MOAB	92% CH ₂ Cl ₂ /8% MeOH	175	na
KB5B	none	192	303
KB5B	92% CH ₂ Cl ₂ /8% MeOH	182	na
CU5A	none	91	163
CU5A	92% CH ₂ Cl ₂ /8% MeOH	59	na

na = not enough sample to measure TOC

Table 4. Approximate and discrete kinetic parameters from the best kinetic sets selected for extracted CH5A (CH5X), MOAB (MOAX), KB5B (KB5X), and CU5A (CU5X) coals.

Sample	CH5X	MOAX	KB5X	CU5X
Approximate E, ^a kcal/mol	55.9 (0.05)	55.2 (0.09)	55.2 (0.09)	63.2 (0.20)
Approximate A, 1/sec	4.83 X 10 ¹⁴	9.7 X 10 ¹³	8.64 X 10 ¹³	5.52 X 10 ¹⁵
Approximate σ , % of E	3.14	2.34	2.40	3.16
Discrete E, % of Total				
41 kcal/mol			0.09	
42 kcal/mol	0.49			
43 kcal/mol	0.33		0.25	
44 kcal/mol	0.66	0.11	0.67	
45 kcal/mol		0.01	0.63	
46 kcal/mol	0.24	0.44	1.00	
47 kcal/mol	0.29	0.19	1.07	0.80
48 kcal/mol	0.42	1.41	1.31	
49 kcal/mol	0.05	0.23	1.44	0.56
50 kcal/mol	1.03	1.86	1.84	0.74
51 kcal/mol	0.38	0.40	1.02	0.80
52 kcal/mol	1.74	0.89	1.71	0.78
53 kcal/mol	3.65	3.42	1.13	0.68
54 kcal/mol	5.26	0.35	8.15	1.78
55 kcal/mol	16.70	26.26	25.63	0.39
56 kcal/mol	21.12	22.30	20.77	2.72
57 kcal/mol	16.08	17.21	12.04	0.18
58 kcal/mol	11.98	5.17	4.56	1.67
59 kcal/mol	4.91	5.79	6.54	0.89
60 kcal/mol	3.41	3.17		10.45
61 kcal/mol	3.17	1.77	4.83	15.21
62 kcal/mol	2.03	2.10	0.10	16.02
63 kcal/mol	1.36	0.43		11.71
64 kcal/mol	2.55	3.02	4.74	8.99
65 kcal/mol				5.99
66 kcal/mol	0.89			3.03
67 kcal/mol	1.73	3.47		2.86
68 kcal/mol				6.11
69 kcal/mol				
70 kcal/mol				
71 kcal/mol				7.65
Discrete A, 1/sec	6.47 X 10 ¹⁴	1.65 X 10 ¹⁴	1.13 X 10 ¹⁴	2.40 X 10 ¹⁵
T _{max} , °C, at 25°C/min	468.06	491.78	494.94	514.51

a ± error in kcal/mol in parentheses

Table 5. Approximate and discrete kinetic parameters from the best kinetic sets selected for CH5A, CH5X (92% CH₂Cl₂/8% MeOH extracted CH5A), CH5X with fixed A (from CH5A determination), and CH5T (THF extracted CH5A).

Sample	CH5A	CH5X	CH5X fixed A	CH5T THF extracted
Approximate E, ^a kcal/mol	56.7 (0.07)	55.9 (0.05)	55.9 (0.05)	55.7 (0.03)
Approximate A, 1/sec	9.99 X 10 ¹⁴	4.83 X 10 ¹⁴	4.83 X 10 ¹⁴	4.06 X 10 ¹⁴
Approximate σ , % of E	3.58	3.14	3.14	3.05
Discrete E, % of Total				
42 kcal/mol		0.49		1.14
43 kcal/mol		0.33		0.85
44 kcal/mol		0.44	0.28	0.18
45 kcal/mol			0.66	1.95
46 kcal/mol		0.46		0.68
47 kcal/mol		0.29	0.24	
48 kcal/mol		0.42	0.23	0.99
49 kcal/mol		0.05	0.39	
50 kcal/mol	2.41	1.03	0.15	1.65
51 kcal/mol	1.42	0.38	0.68	0.13
52 kcal/mol	2.76	1.74	0.79	3.32
53 kcal/mol	1.53	3.65	1.02	3.34
54 kcal/mol	5.92	5.26	3.48	10.56
55 kcal/mol	5.87	16.70	4.28	23.76
56 kcal/mol	12.80	21.12	11.59	15.41
57 kcal/mol	19.60	16.08	20.41	16.20
58 kcal/mol	14.07	11.98	17.40	4.57
59 kcal/mol	16.02	4.91	13.97	4.90
60 kcal/mol		3.41	7.40	3.51
61 kcal/mol	7.72	3.17	3.97	0.98
62 kcal/mol	0.40	2.03	2.79	2.62
63 kcal/mol	3.52	1.36	3.49	0.87
64 kcal/mol	0.04	2.55		
65 kcal/mol	2.39		3.88	2.38
66 kcal/mol		0.89	0.03	4.71
67 kcal/mol	1.85	1.73		0.82
68 kcal/mol	0.21		2.84	7.97
69 kcal/mol				
70 kcal/mol	1.48			
71 kcal/mol				7.27
Discrete A, 1/sec	1.74 X 10 ¹⁵	6.47 X 10 ¹⁴	1.75 X 10 ¹⁵	4.06 X 10 ¹⁴
T _{max} °C, at 25°C/min	464.48	468.06	468.06	468.87

a \pm error in kcal/mol in parentheses

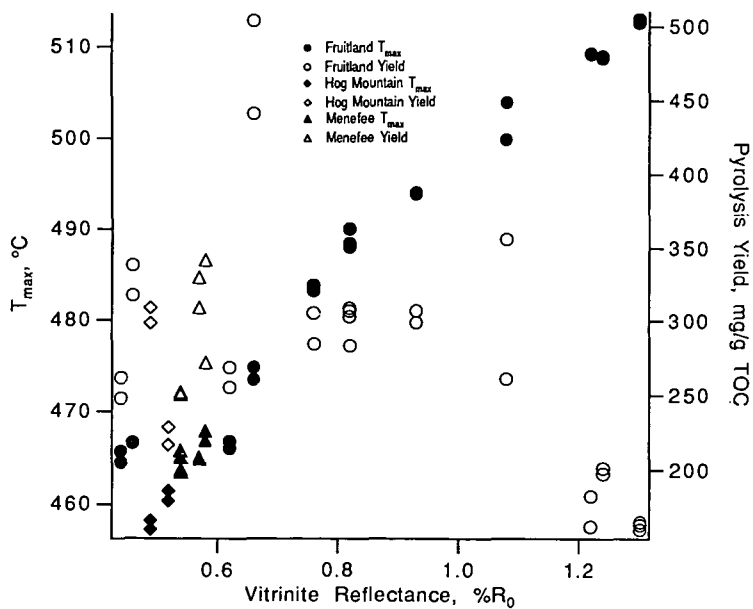


Figure 1. Relationship of maximum rate of evolution (T_{max}) and pyrolysis yield (mg/g TOC) with vitrinite reflectance ($\%R_m$) at the nominal heating rate of 25°C/min for selected coals from the San Juan Basin.

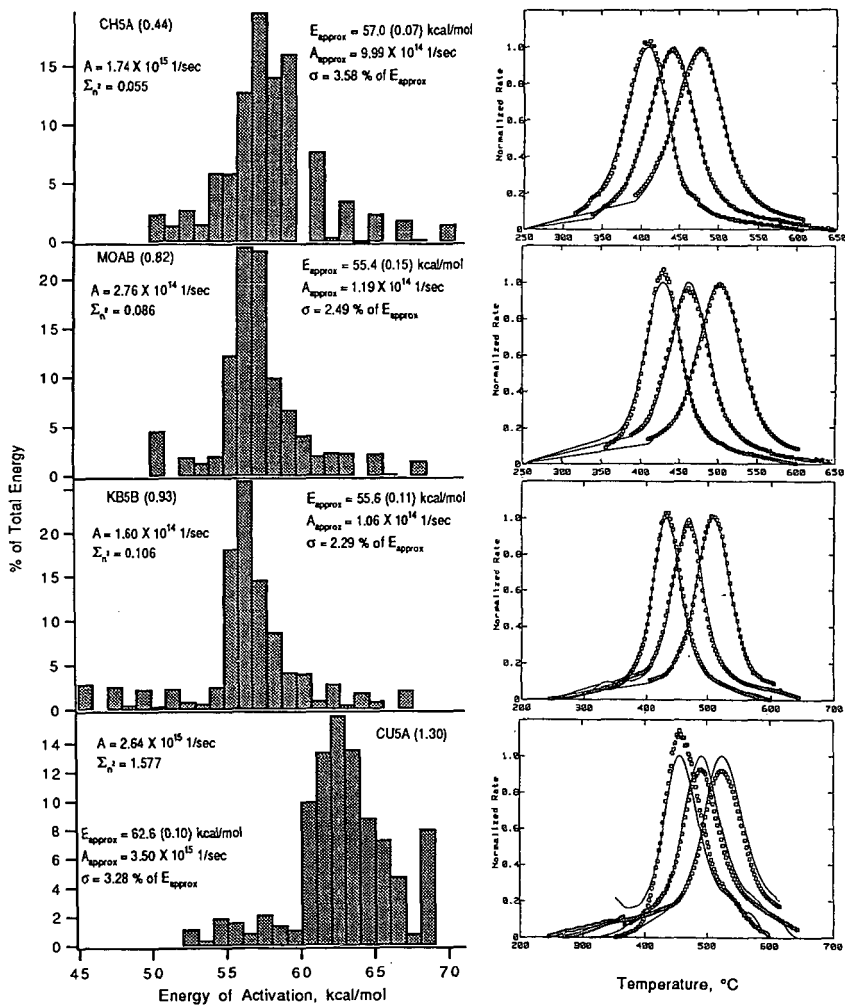


Figure 2. Approximate and discrete kinetic parameters for CH5A, MOAB, KB5B, and CU5A coals (left side) and corresponding evolution data fits from the discrete kinetic analysis (right side).

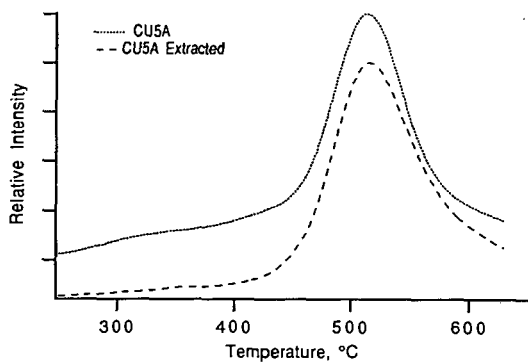


Figure 3. Evolution profiles for CU5A and extracted CU5A coals at the nominal heating rate of 25°C/min.

CURIE-POINT PYROLYSIS MASS SPECTROMETRY OF SHANXI COALS

Huaying Huai, Alec F. Gaines+ and Peter J.J. Tromp++
Center for Micro Analysis and Reaction Chemistry, University of Utah,
Salt Lake City, Utah 84112
+ Middle East Technical University, Institute of Marine Science, P.O. Box 28,
33731 Erdemli - ICEL, TURKEY
++ Institute of Chemical Engineering, University of Amsterdam,
Nieuwe Achtergracht 166, 1018 WV Amsterdam, The Netherlands

Keywords: pyrolysis mass spectrometry, coal structure, Chinese coal

ABSTRACT

Seven Shanxi (PRC) coals, having carbon contents from 80.5% to 94.2%wt (daf), have been studied by the Curie-point pyrolysis mass spectrometry technique. Markham Main (British) coal, 83.5 %C and Bulli (Australian) coal, 89.3 %C, have been used as references. As reported by other workers [1,2] studying very different depositions, three major groups of compounds, aliphatic hydrocarbons (e.g. alkenes), aromatic hydrocarbons (e.g. alkylbenzenes, alkylnaphthalenes, alkylpolyaromatics) and oxygen containing aromatics (e.g. alkylphenols, dihydroxybenzenes), were prominent amongst the pyrolysis products. The relative proportions of oxygen containing compounds and aromatic hydrocarbons, illustrated by the ratio of the intensities of the m/z 156/108 peaks, change with rank. The spectra are consistent with the low lignite content and the moderately low sulfur contents of Shanxi coals.

INTRODUCTION

Pyrolysis-mass spectrometry (Py-MS) was first introduced as a promising technique for the study of polymers in 1948 [3,4]. In 1973, Meuzelaar et al. [5] designed a Py-MS system in which products from a Curie-point pyrolyzer were ionized by low energy electrons so that molecular, rather than fragment, ions were formed and passed directly into a quadrupole mass spectrometer. Since then many studies of solid fuels have been reported [1,6,7,12-18]. These studies have shown coal pyrograms to be dominated by series of ions representing several groups of aromatic and aliphatic hydrocarbons as well as heteroaromatic compounds. Differences between the spectra were shown to correlate with rank (maturity) [1,3], maceral composition [12,14] and reactivity towards liquefaction [10,11].

Thus, the method gives detailed, and at least semiquantitative information about the structures of the complex but volatile products obtained from the pyrolysis of solid fuels at rather fast rates of heating. Moreover, there is a sufficient bank of existing data in the literature that the nature of the products from any individual coal can be related to such parameters as its maceral group composition, its deposition and its rank.

The North China Block (tectonic plate), approximately coincident with Shanxi Province, gives rise to about one third of China's current production of coal. As part of a study to delineate the organic geochemistry of Shanxi coals and to relate the chemistry of these coals to their present and potential use, seven Shanxi bituminous coals, covering a range of rank from 80.5 to 94.2 %C (daf) have been studied by means of Curie-point Py-MS. The results have been compared with those from well characterized coal deposited in Euramerica (Markham Main coal, Britain) and another deposited in Gondwanaland (Bulli coal, New South Wales, Australia).

EXPERIMENTAL

Sample Preparation

Nine coals were sampled for this study. Seven of these were mined from six coalfields of Shanxi Province, PRC [19]. Markham Main and Bulli coals were mined in Yorkshire (Britain) and in New South Wales (Australia), respectively. The elemental composition of the coals is given in table 1. The samples were ground in a nitrogen - filled glove box to a particle size smaller than 63 μm , dried in a vacuum oven at 70 C for 3 hours, sealed under nitrogen and kept in a deep freeze until needed. The samples for each experiment were taken from a coal/water slurry, prepared by impregnation of the ground coal sample with deionized water until the pore volume was filled. Aliquots ($\sim 50 \mu\text{m}$) from these slurries were applied with a spatula to ferromagnetic pyrolysis wires on which they were air-dried.

Pyrolysis Mass Spectrometry Analysis

The Curie-point Py-MS technique has been described elsewhere [2]. Within 1 hour of coating, the wire samples were pyrolyzed at a Curie-point temperature of 770 K (pure iron wires), previously found to be optimal for the pyrolysis of coal samples. The pyrolysis conditions were: vacuum, $\sim 10^{-4}$ Pa; heating time, 0.1 sec; and heating rate, ~ 7000 C/sec. The mass spectrometer conditions were: temperature of the expansion chamber, 200 C; electron energy, 15 eV; mass range scanned, m/z 25-225; scan speed, 10 scans/sec; and total number of spectra averaged, 200. Each coal slurry was analyzed in triplicate.

RESULTS AND DISCUSSION

The pyrolysis mass spectra of the coals, including the Markham Main and Bulli coals, are shown in Figure 1 in order of increasing rank of coal. The spectra include peak sequences apparently representing suites of limited numbers of homologous compounds. The chemical structures and corresponding mass numbers of the most important species are given in table 2.

The differences between the spectra in Figure 1 appear to be related primarily to rank. In agreement with the known effects of rank on the chemical composition of coals, the relative intensities of aromatic compounds which do not contain oxygen functional groups, such as alkylbenzenes (m/z: 78, 92, 106, etc.), alkylnaphthalenes (m/z: 128, 142, 156, etc.), and alkylphenanthrenes/anthracenes (m/z: 178, 192, 206, etc.) increase with rank, whereas the intensities of such oxygen containing aromatic hydrocarbons as alkylphenols (m/z: 94, 108, 122, etc.) decrease. Since relatively few samples were used in this study, factor and/or discriminant analysis were not applied. However, the ratio of the relative intensities of the m/z 156 (C2-naphthalenes) and the m/z 108 (C1-phenols) peaks as functions of the carbon content and the atomic ratio of oxygen/carbon (Figure 2 and 3, respectively) illustrates the rank dependence. Due to very low absolute amounts of ions generated, the results from the anthracite, Fenghuang Shan coal, are not included in the Figures 2 and 3. It is to be noted that the results from Bulli coal differ from those of Shanxi coals of similar rank. Bulli coal contained 74.5% of inertinite with a rather large amount of fusinite [19]. Consequently, the spectra of Bulli coal, containing prominent alkylbenzenes, resemble the fusinite spectra obtained by Larter [6]. Other features of the mass spectra derived from Shanxi coals are: (1) low H_2S formation (m/z 34) consistent with the moderately low sulfur content indicated by the elemental analyses (Table 1), and (2) low formation of alkanes (m/z: 58, 72, 86, etc.) consistent with the low liptinite content of these coals [19].

Finally, the coherence of the pyrolysis mass spectra of coals from depositions on different tectonic plates and in different climatic conditions is part of the evidence that the whole coal family, which may now be taken to include the Shanxi coals, shares a common system of structural chemistry [2]. Differences in pyrolysis mass spectra are caused by variations in the rank of the coal (that is, by differences in the geochemical temperatures to which the coals were subjected [20]) and, to a lesser extent, by differences in their maceral group composition (that is, by variations in the original flora and the degree to which it was preserved by the deposition). That being written, it should be understood that the volatile products examined by Py-MS may have structures which are the result of secondary, retrogressive reactions as well as of the structures in the original coals. Relatively few of the mass spectra generated by the Shanxi coals contained hydroaromatic structures characteristic of vitrinite [21] and the presence of alkanes is direct evidence of cracking.

CONCLUSIONS

Curie-point pyrolysis of seven coals from the North China Block generated volatiles in which alkenes, alkylaromatics, alkylphenols and dihydroxylbenzenes were prominent. The ratio of the C2-naphthalenes to the C1-phenols produced by the pyrolyses increased with the rank of the coals. The pyrolysis products, though they may have suffered retrogressive, secondary reactions, are nevertheless consistent with the coals from the North China Block having the structures expected of lipinite poor, bituminous coals.

ACKNOWLEDGEMENTS

This work was conducted in the FOM Institute for Atomic and Molecular Physics (The Netherlands) and partially funded by Taiyuan University of Technology (PRC) and the SEDC (UK). The authors would like to thank Professors Colin D. Flint and Jacob A. Moulijn for their encouragement.

REFERENCES

1. Meuzelaar, H.L.C.; Harper, A.M.; Hill, G.R.; Given, P.H. *Fuel*, 1984, 63, 640.
2. Tromp, P.J.J. *Ph.D. Thesis*, 1987, University of Amsterdam, The Netherlands.
3. Madorsky, S.L.; Strauss, S. *Ind. Eng. Chem.*, 1948, 40, 848.
4. Wall, L.A. *J. Res. Nat. Bur. Stand.*, 1948, 41, 315.
5. Meuzelaar, H.L.C.; Kistemaker, P.G. *Anal. Chem.*, 1973, 45, 587.
6. Larter, S.R. *Ph. D. Thesis*, 1978, University of Newcastle upon Tyne, U.K.
7. Meuzelaar, H.L.C.; Harper, A.M.; Pugmire, R.J. *ACS Preprints, Div. Fuel Chem.*, 1983, 28(1), 97.
8. Meuzelaar, H.L.C.; Hoesterey, B.L.; Windig, W.; Hill, G.R. *Fuel Proc. Tech.*, 1986, 15, 59.
9. Huai, H.; Lo, R.; Yun, Y.; Meuzelaar, H.L.C. *ACS Preprints, Div. Fuel Chem.*, 1990, 35(3), 816.
10. Meuzelaar, H.L.C.; Wood, R.W.; Futrell, J.H.; Wojcik, L.H. *Proc. 28th Ann. Conf. Mass Spectrom. All Topics*, New York City, 1980, 460.
11. Meuzelaar, H.L.C.; McClennen, W.H.; Tomlinson, J.H.; Pope, D.L. *Proc. Int. Conf. Coal Sci.*, Dusseldorf, 1981, 816.
12. Meuzelaar, H.L.C.; Harper, A.M.; Pugmire, R.J.; Karas, J. *Intl. J. Coal Geol.*, 1984, 4, 143.
13. van Graas, G.; De Leeuw, J.W.; Schenck, P.A. *J. Anal. Appl. Pyrol.*, 1980, 2, 265.
14. Nip, M.; De Leeuw, J.W.; Schenck, P.A. *Geochim. Cosmochim. Acta*, 1988, 52, 637.
15. Nip, M. *J. Anal. Appl. Pyrol.*, 1987, 11, 125.
16. Nip, M.; De Leeuw, J.W.; Schenck, P.A.; Windig, W.; Meuzelaar, H.L.C. *Geochim. Cosmochim. Acta*, 1989, 53, 671.
17. Chaffec, A.L.; Johns, R.B.; Baerken, M.J.; De Leeuw, J.W.; Schenck, P.A.; Boon, J.J. In: *"Advances in Organic Geochemistry, Org. Geochem."* (Schenck, P.A.; De Leeuw, J.W.; Lijmbach, G.W.M. Eds.), 1983, 6, 409.

18. Eglinton, T.I.; Larter, S.R.; Boon, J.J. *J. Anal. Appl. Pyrol.*, 1991, 20, 25.
19. Huai, H. *Ph.D. Thesis*, 1989, University of London, U.K.
20. Teichmuller, M.; Teichmuller, R. In: "*Stach's Textbook of Coal Petrology.*" (Stach, E.; Taylor, G.H.; Mackowsky, M-Th.; Chandra, D.; Teichmuller, M.; Teichmuller, R. Eds.), Gebruder Borntraeger, Berlin, 3rd Edition, 1982, pp. 5-86.
21. Davis, M.R.; Abbott, J.M.; Cudby, M.; Gaines, A.F. *Fuel*, 1988, 67, 960.

Table 1. Elemental Composition of Coal Samples

Sample	Weight % daf					
	C	H	N	S	O(diff)	O/C
Pinglu Erpu coal	80.5	4.9	1.3	0.6	12.7	0.118
Markham Main coal	83.5	5.1	1.4	1.0	9.0	0.081
Datong Jueqiang Buxiang coal	83.9	5.2	0.9	0.9	9.1	0.083
Xuangang Jiaojia Zhai coal	86.2	5.2	1.7	1.8	5.1	0.044
Xishan Gujiao coal	86.9	5.0	1.6	1.4	5.1	0.044
Fenxi coal	89.9	5.1	1.5	0.5	3.0	0.025
Bulli coal	89.3	4.9	1.7	0.5	3.6	0.030
Jishuigou coal	89.6	4.8	1.2	1.2	3.2	0.027
Fenghuang Shan coal	94.2	2.9	0.9	0.9	1.1	0.009

Table 2. Chemical Structures and Corresponding Mass Numbers of the Most Important Compounds and Groups of Homologous Compounds, Present in the Mass Spectra of the Coals

Groups of homologous compounds	Chemical Structures with corresponding mass numbers
Alkenes	$C_2H_4(28)$; $C_3H_6(42)$; $C_4H_8(56)$; $C_5H_{10}(70)$; etc.
Benzenes	 (78);  (92);  (106);  (120); etc.
Naphthalenes	 (128);  (142);  (156); etc.
Phenanthrenes &	 (178);  (192);  (206); etc.
Anthracenes	 (178);  (192);  (206); etc.
Phenols	 (94);  (108);  (122); etc.
dihydroxybenzenes	 (110);
Sulfur compounds	$H_2S(34)$; $CH_3SH(48)$;

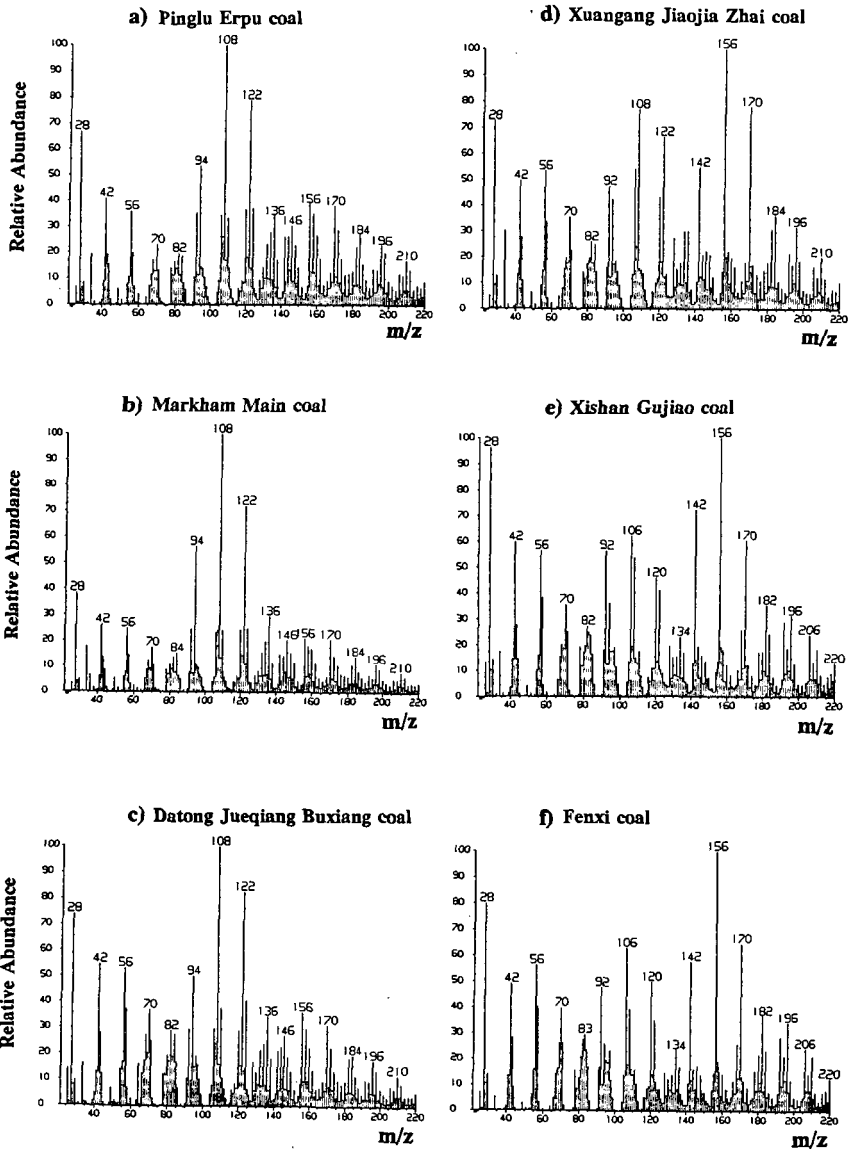


Figure 1. Average mass spectra of coals.

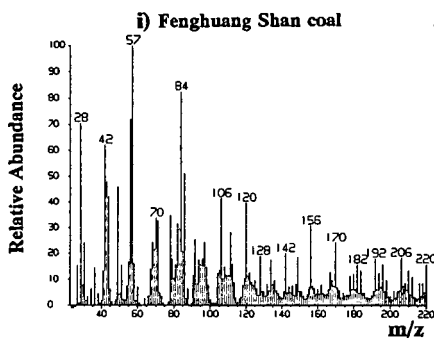
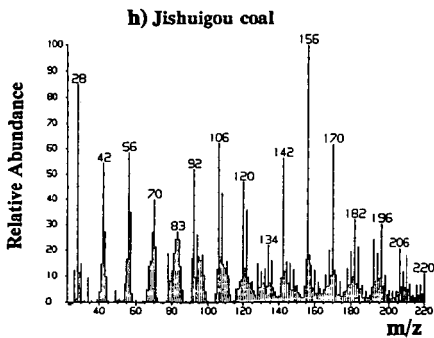
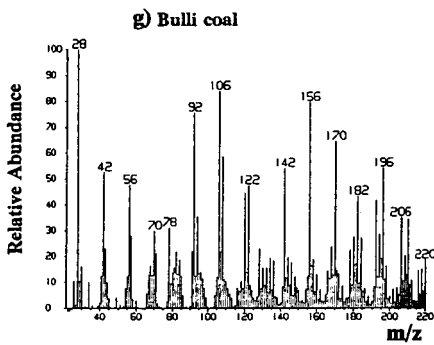


Figure 1. (continued).

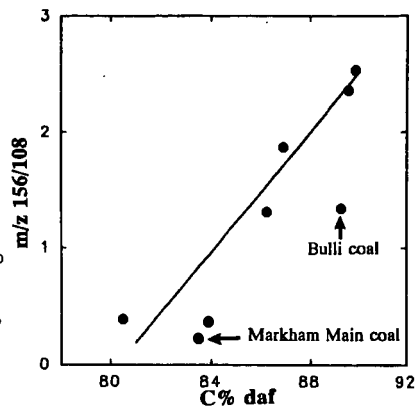


Figure 2. Variation of the ratio of m/z 156/108 from Py-MS with carbon content of coals.

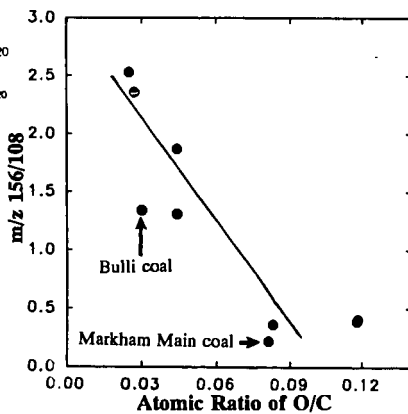


Figure 3. Variation of the ratio of m/z 156/108 from Py-MS with atomic ratio of O/C of coals.

FT-I.R. STUDY OF OXYGENATED FUNCTIONAL GROUPS DISTRIBUTION
DURING DRY-PHASE OXIDATION OF COALS.

V. Calemma, P. Iwanski, R. Rausa and E. Girardi
Eniricerche SpA, 20097 San Donato Mil.se, Milan, Italy

Keywords: coal, oxidation, FT-i.r.

INTRODUCTION

When coal is oxidized with air in dry-phase conditions at temperatures higher than 150 °C, besides the well known alteration of several coal properties [1], a mixture of base extractable substances is formed in considerable yields after a few hours [2]. These substances are generally referred to as regenerated humic acids (RHA). Although details of chemical changes in coal "molecule" caused by air oxidation are only partially understood, the results of spectroscopic and chemical studies on dry oxidized coals are consistent with a preferential oxidation of the aliphatic part of coal structure, leading to a more aromatic product and to a concomitant formation of various oxygenated functional groups (-COOH, C=O, CO-O-CO, etc.) [3,4]. In a previous FT-ir study [4], performed on a subbituminous B coal oxidized between 175 and 275 °C, only the overall trend of carbonyl groups was presented and no considerations about the behavior of hydroxyl groups were made owing to the complexity of regions where oxygenated functional groups absorb. The objective of this work was to detect and determine, the formation and relative changes in concentration of various oxygenated functional groups as a function of oxidation time by applying the curve-resolving procedure and acetylation of coal samples. The aim was to gain a better understanding of the structural modification which occur during the formation of RHA.

EXPERIMENTAL

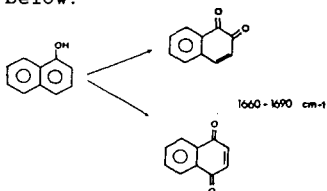
Two U.S coals (M. Rosebud and a subbituminous B) were used in this study. Their ultimate and proximate analyses are given in table 1. The as received coals were crushed, sieved and the fraction 106-250 µm was used throughout this investigation. Oxidation tests were performed in a steel fluid bed reactor, at 200 °C, with air pressure of 0.2 MPa and reaction times up to 4 hours. For each run the reactor was charged with 30 g of dried coal heated (in flowing N₂) and pressurized. Subsequently the coal sample was reacted switching over the nitrogen flow with a controlled flowrate of preheated air. For all runs the gas superficial velocity was 5.1 cm/sec. After reaction, oxidation was stopped by feeding nitrogen and after that the reactor was depressurized and cooled to room temperature. Finally, the oxidized coal samples were subjected to elemental analysis, characterized by FT-ir spectroscopy and selected samples were acetylated to determine hydroxyl groups. Experimental procedures used for preparing KBr pellets and obtaining FT-ir spectra of coal samples have been described elsewhere [4]. The latter were obtained on a Digilab ETS/15 FT-ir spectrometer. The

characterization of region between 1900 and 1450 cm^{-1} , was achieved through curve-fitting procedure, performed using the software supplied with the Data General processing system. The parameters requested in deconvolution procedure are mainly the number of bands, their positions, the gaussian coefficient and the base line intercepts. The gaussian coefficient was fixed at 0.3. The number of bands was determined after a critical examination of the second derivative of the spectra. Their position was recalculated iterating the fitting procedure. For each spectrum the base line was drawn between two points where no absorption occurs, namely around 1800 and 730 cm^{-1} . Acetylation of raw and oxidized coal samples was conducted following the procedure set up by Blom et al.[5]. No attempt was made to demineralize the coal samples prior acetylation.

RESULTS AND DISCUSSION

Figure 1 shows FT-ir spectra of Montana Rosebud coal at various oxidation degrees. From a general point of view the evolution is similar for both coals and as observed by other investigators [6] the most remarkable changes are those occurring in the regions 3000-2700 cm^{-1} (aliphatic C-H₁ stretching), 1800-1600 cm^{-1} (C=O stretching) and 1300-1000 cm^{-1} (-C-O-C- stretching, phenolic and alcoholic C-O stretching, OH bending, etc.). As the reaction time increases the absorption due to aliphatic groups decreases while the absorption bands due to C=O stretching and present in the region 1300-1000 cm^{-1} display a noteworthy increase. Figure 2 shows the FT-ir spectrum of subbituminous B coal between 1870 and 1450 cm^{-1} and its second derivative. Upon examination, fig.2 reveals the presence of three well defined maxima (1770, 1718 and 1608 cm^{-1}) and shoulders or secondary maxima to be distinguished from possible artifacts. This situation was verified to be valid for each spectrum of coal samples examined. As an example of the results obtained through curve fitting procedure, fig. 3 shows the infrared spectrum of a oxidized coal sample curve-resolved into nine bands. The choice of number and position of component bands was made on the basis of the second derivative of spectrum, FT-ir measurements on ion exchanged and acetylated coal samples and results obtained by other investigators in similar works [7,8,9]. Assignments of component bands are given in table 2. In this connection it is important to stress that owing to unavoidable interference of adjoining bands, the presence of different molecular situations and its modifications caused by oxidation, the absorption frequency of bands resulting from the curve fitting procedure have undergone slight shifts (generally $\pm 5 \text{ cm}^{-1}$) during reaction. The structural changes observed were similar for both coals examined and the most remarkable concerned the bands at 1771, 1734, 1711, 1684 and 1648 cm^{-1} whose evolution is reported in figures 4 and 5. On the contrary bands located at 1608, 1585, 1568 and 1542 cm^{-1} as expected did not display significant variations. The results presented in the figures 4 and 5 show that the evolution of different functional group containing C=O is qualitatively similar for both coals and as the reaction proceeds the concentration of each group increases. However significant differences exist between the two coals as regards the formation rates and relative concentration of various C=O groups during reaction. Previous results obtained by FT-ir and ¹³C-NMR [4,10] showed that at 200 °C the oxidation occurs almost exclusively on the aliphatic part

of coal structure. Therefore the formation of different oxygenated functional groups detected by I.R. spectroscopy can be explained in terms of oxidative destruction of aliphatic structures. Considering the Wisser model of coal structure [11], where polyaromatic and hydroaromatic units are joined by short aliphatic chains and various ether linkages to form a three-dimensional network, it is possible to single out some structural units, which through the oxidation of aliphatic part, can give rise to the formation of detected oxygenated functional groups. Some possible reaction pathways, worked out on the basis of the results obtained, and considering the different reactivity of various structures towards the oxygen, are given in figure 6. The changes in hydroxyl groups content (alcoholic and phenolic) upon oxidation at 200 °C was determined by measuring the area of the peaks centred at 1367 cm^{-1} (CH_2 bending) and 1187 cm^{-1} (-C-O- stretching) of acetylated coal samples. Before discussing the data it is important to stress that the bands used to follow the hydroxyl behavior are due to phenolic and alcoholic group. However literature data[9] show that the content of the latter is much lower than that of phenolic group. In addition, some results of curve fitting procedure of the complex spectral band due to the C=O stretching of acetyl group indicate that the R-OH/Ar-OH ratio remains almost constant during reaction at 200 °C. Therefore the trend observed should reflect the behavior of phenolic group. The trend reported in figure 7 shows a noteworthy decrease of hydroxyl groups contents in the first hour of oxidation followed by a levelling off at longer reaction times. It is known that the presence of hydroxyl groups activate the aromatic ring towards oxidation and that phenols are easily oxidized to quinones, which subsequently can evolve to carboxyl through rupture of benzenic ring [12]. Therefore the observed trend can be interpreted by the reaction scheme given below:



Furthermore, the disappearance of hydroxyl groups can also be a result of condensation reactions between hydroxyl and carboxyl or hydroxyl groups to form esters and ethers bonds respectively. The latter might have a negative effect on RHA formation for the alkaline hydrolysis of ether bond occurs with difficulty and demands more drastic conditions than those used to determine the alkali solubility of oxidized coal [2,13].

CONCLUSIONS

The changes of coal structure caused by molecular oxygen at 200 °C have been evaluated by FT-ir spectroscopy and acetylation of coal samples. The results indicate that the oxidative process leads to the formation of different oxygenated functional groups such as carboxyls, ketones, conjugated carbonyls and various type of esters. Their evolution with time as well as the trend of hydroxyl groups

has been determined. On these grounds some reaction pathways which explain the oxygenated functional group formation in terms of oxidative attack of aliphatic structure have been presented. Keeping in mind the coal structure proposed by Wiser [11], a major conclusion of this work is that formation of RHA should be mainly associated with the break-down of aliphatic structure which lead to smaller fragments (through oxidation of links between aromatic and hydroaromatic clusters) and to a concomitant increase of oxygenated functional groups which make these substances soluble in alkali solution.

REFERENCES

1. M.Rashid Khan and R.G. Jenkins in "Chemistry of coal weathering" Ed. by C.R. Nelson, Elsevier, Amsterdam, 1989, chapter 5.
2. V. Calemma, R. Rausa and E. Girardi, Proc. of the 1989 Int. Conf. on Coal Science, Tokyo, Japan, vol.1, pg. 233.
3. J.R. Havens, J.L. Koenig, D. Kuehn, C. Rhoads A. Davis and P.C. Painter, Fuel 62, 936, (1983).
4. V. Calemma, R. Rausa, R. Margarit and E. Girardi, Fuel 67, 764, (1988)
5. L. Blom, L. Edelhausen and D.W. van Krevelen, Fuel 38, 537, (1959)
6. J.K. Kister, M. Guiliano, G. Mille and H. Dou, Fuel 67, 1076, (1988).
7. C.A. Rhoads, J.T. Senftle, M.M. Coleman, A. Davis and P.C. Painter, Fuel 62, 1387, (1983)
8. P. Painter and C. Rhoads, ACS., Fuel Chem. Div. Prep. 26(1), 35, (1981)
9. P. Painter, M. Starsinic and M. Coleman, in "Fourier Transform Infrared Spectroscopy", Ed. by J.R. Ferraro and L.J. Basile, Academic Press, 1985, vol. 4, chapter 5.
10. R. Rausa, V. Calemma, S. Ghelli and E. Girardi, Fuel 68, 1168, (1989)
11. W.H. Wiser, ACS Symp. Ser. 71, 29, (1978)
12. M. Lj. Mihailovic and Z. Cekovic in " The Chemistry of Hydroxyl Group", Ed. by S. Patai, John Wiley & Sons (Interscience), 1971, part 1, chapter 10, pg.505
13. E. Staude and F. Patat in " the Chemistry of ether linkage", Ed. by S. Patai, John Wiley & Sons (Interscience), 1969, chapter 2, pg. 46.

	Sub.B*	M. Rosebud*	Wavenumber (cm^{-1})	Assignment
%C	63.5	63.0	1770	Ar-O-CO-R (1775-1765)
%H	4.7	4.1	1734	R-O-CO-R (1750-1735)
%N	1.1	1.0		Ar-CO-OR; Ar-O-CO-Ar (1740-1715)
%S	0.9	0.7		
%O (by diff.)	20.5	14.7	1711	-COOH (1720-1705)
%Ash	9.6	16.5	1684	Ar-CO-R (1700-1670)
%V.M.	44.1	39.4	1648	Ar-CO-Ar (1680-1640)
				Quinones as: 2 C=O in two rings (1655-1635)
			1608	aromatic stretching
			1585	aromatic band [9]
			1562	$-\text{COO}^- \text{M}^+$
			1541	$-\text{COO}^- \text{M}^+$

* moisture free basis

Table 1. Characteristics of utilized coals

Table 2. Band Assignments

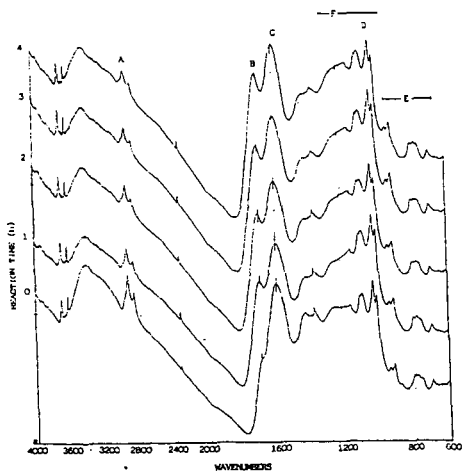


Figure 1. FT-ir spectra of Montana Rosebud coal at various oxidation degrees. A: aliphatic; B: C=O stretching; C: aromatic stretching; D: mineral matter; E: aromatic C-H out of plane bending; F: C-O stretch., C-C stretch., OH bending, etc.

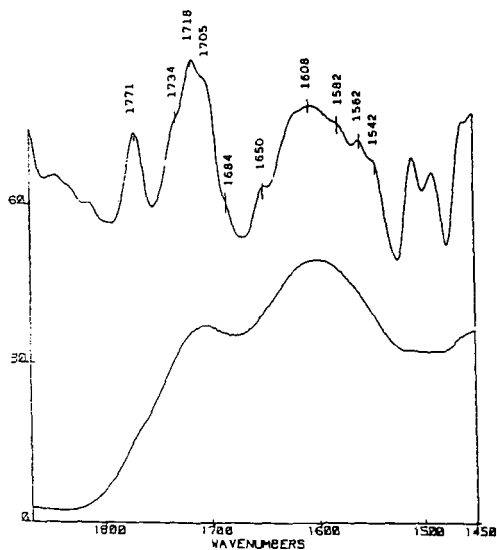


Figure 2. Bottom : FT-ir spectrum of oxidized subbituminous B coal between 1850 and 1450 cm^{-1}
 Top: Second derivative of spectrum

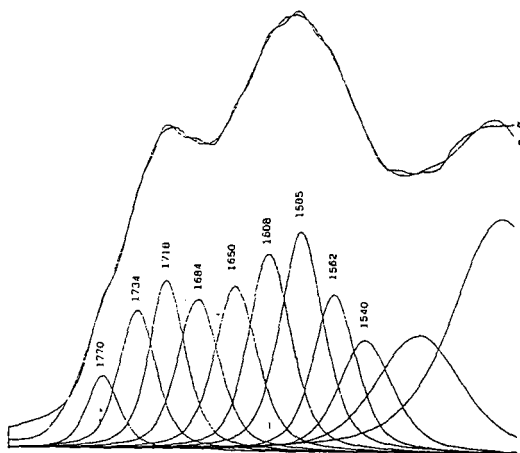


Figure 3. FT-ir spectrum of oxidized Montana Rosebud coal between 1850 and 1450 cm^{-1} and component bands from curve fitting procedure.

Figure 4. M. Rosebud coal, evolution of various oxygenated functional groups containing C=O

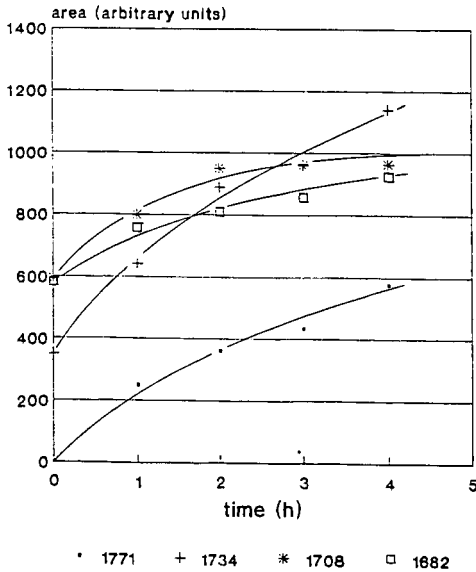
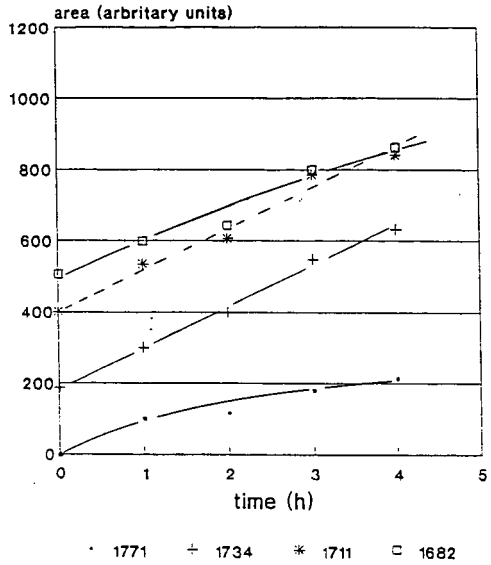


Figure 5. Subbituminous B coal, evolution of various oxygenated functional groups containing C=O

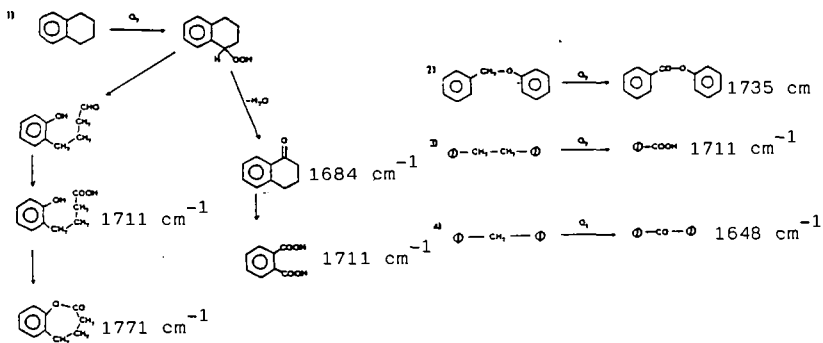


Figure 6. Scheme depicting the proposed reaction pathways that may occur during the oxidation on the grounds of FT-ir results.

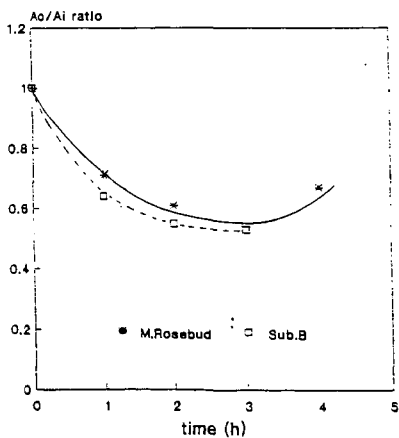


Figure 7. Graph of the fractional change in the peak area (1187 cm^{-1}) of hydroxyl groups versus oxidation time.

EVOLUTION OF VOLATILE SULFUR COMPOUNDS DURING TEMPERATURE-PROGRAMMED
PYROLYSIS-COMBUSTION WITH A QUADRUPOLE GAS ANALYZER

K.C. Hackley and C.-L. Chou
Illinois State Geological Survey
615 East Peabody Drive
Champaign, IL 61820

Keywords: coal pyrolysis-combustion, volatile sulfur species, quadrupole gas analyzer

The evolution of sulfur species during combustion of pyrolysis volatiles from coal IBC-109 (1.13% sulfur, 0.42% chlorine) of the Illinois Basin Coal Sample Program has been studied using a pyrolysis-combustion apparatus in conjunction with a quadrupole gas analyzer (QGA). This work is part of an on-going project which investigates the role of sulfur and chlorine in coal in boiler corrosion. A better understanding of the behavior of these elements in coal during combustion may help elucidate the mechanism of boiler corrosion. The experimental conditions are designed to simulate the formation of sulfur compounds during coal combustion.

The pyrolysis-combustion apparatus used with the QGA to study the release of gases from coal is capable of heating the coal sample from the ambient to about 850°C at different heating rates. Major components include a quartz tube reactor, a gas flow controller, two split-tube furnaces, a programmable temperature controller, 50- μ m capillary tubing connecting a Dycor QGA to the pyrolysis system, and a microcomputer (Fig. 1). Approximately 0.5 gram of coal is heated nonisothermally under a controlled atmosphere (air, nitrogen, oxygen, or other gases) in the quartz-tube reactor which consists of two consecutive chambers. The coal is pyrolyzed in the first chamber under a nitrogen atmosphere and the volatile products are carried to the second chamber where they are combusted at 850°C under a constant flow of oxygen. The gaseous products are sampled through the capillary tube and monitored with a quadrupole gas analyzer. The different gaseous species are determined in the QGA by monitoring the atomic mass associated with different species, such as mass 64 for SO₂ and 44 for CO₂. The data from the QGA and temperature controller are transmitted to a microcomputer and stored as ASCII files on the hard disk.

The release of sulfur compounds from the coal was monitored as the temperature was increased from the ambient to 850°C at a heating rate of 50°C/min. Sulfur dioxide (SO₂) was released from coal IBC-109 primarily between 250° and 650°C (Fig. 2). The SO₂ profile showed a small initial release of sulfur between 250° and 400°C followed by a main peak between 400° and 550°C with a maximum at 510°C, and then by a small peak close to 625°C. The main SO₂ peak is associated with the release of volatile matter from the coal. The smaller higher temperature peak is probably associated with the release of pyritic sulfur^{1,2}. The initial small broad peak of SO₂ is unusual relative to other SO₂ profiles from Illinois coals² but may be characteristic of this sample. Perhaps there is a significant amount of weakly bonded organic sulfur compounds which are released in the initial volatilization of IBC-109.

When the combustion atmosphere was changed to a reducing condition, gaseous COS and H₂S were detected. Figure 3 compares the profiles for SO₂ and COS under an oxidizing condition where the excess oxygen concentration in the combustion chamber never fell below 5 percent (Run 3) to where a reducing condition occurred in the combustion chamber during the major release of volatiles (Run 4). An

obvious peak was obtained for COS in Run 4. The H₂S profile is more difficult to comprehend because of the presence of oxygen isotope ¹⁸O in the oxygen flow. The combination of ¹⁸O and ¹⁶O gives a mass of 34 for oxygen (¹⁶O¹⁸O), the same as H₂S. Thus the profile of mass-34 will mimic that of O₂ (mass 32). When O₂ is consumed, the oxygen (mass 32) will drop to background levels as will the ¹⁶O¹⁸O profile (mass 34). Figure 4 shows this effect for masses 32 and 34 of a blank run where the oxygen flow was shut off between 400° and 625°C. If H₂S is present under a reducing condition, a peak should occur in the mass-34 profile during the period of O₂ depletion. Figure 5 shows typical profiles of sulfur species, including mass 34, obtained when the O₂ was consumed during the experiment. The H₂S peak is observed in the trough of the mass-34 profile. As the rate of volatile gases released from the coal sample decreases, the O₂ concentration is no longer completely consumed and the reduced gas species disappear.

For this high-chlorine coal, we also attempted to monitor the evolution of HCl gas (mass 36) with QGA. Only a very weak peak was obtained for mass 36 during complete combustion with sufficient oxygen however, when the combustion atmosphere was under a reducing condition, a better gas release profile was obtained for the species of mass 36. This improved profile of mass-36 is probably not due to HCl. With the occurrence of H₂S under the reducing condition, the enlarged peak of mass-36 (Fig. 5) is most probably a result of the presence of the naturally occurring heavy sulfur isotope ³⁴S in the hydrogen sulfide (H₂³⁴S, total mass = 36).

Thus, the sulfur species formed in the combustion gas are controlled by the oxidizing condition in the combustion chamber. The experiments indicate that sulfur dioxide (SO₂) is the predominant sulfur species observed during combustion of pyrolysis volatiles. In some of the experiments, during the major release of volatiles, between 450° and 550°C, all oxygen in the pyrolysis system was consumed and a reducing condition occurred which resulted in the detection of additional sulfur species (COS and H₂S).

This work has been sponsored by the Illinois Department of Energy and Natural Resources through its Coal Development Board and Center for Research on Sulfur in Coal, and the U.S. DOE.

References

1. Oh M.S., Burnham A.K. and Crawford R.W., ACS Fuel Chemistry Division Preprints 33 (1), 274 (1988).
2. Hackley K.C., Frost R.R., Liu C.-L., Hawk S.J. and Coleman D.D., Illinois State Geological Survey Circular 545, 33 p. (1990).

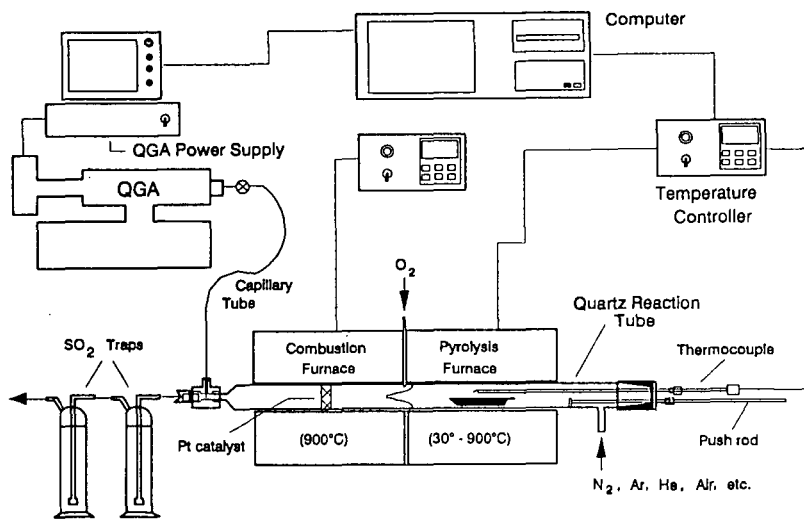


Figure 1. The experimental setup of a temperature-programmed pyrolysis-combustion system in conjunction with a quadrupole gas analyzer.

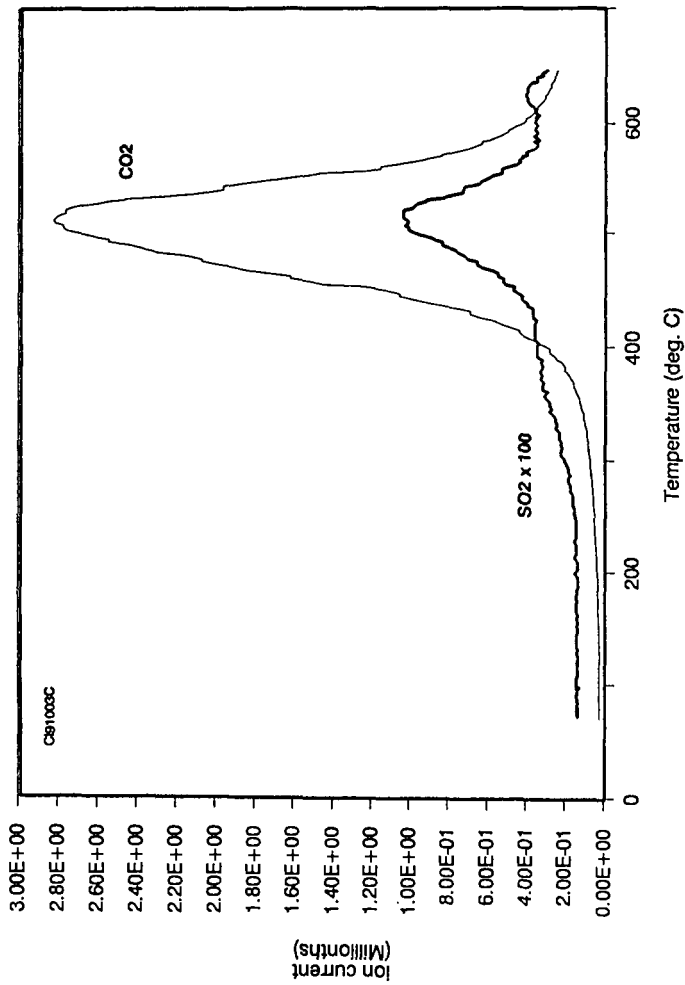


Figure 2. Profiles of CO₂ and SO₂ (X100) in combustion gas under an oxidizing condition at a heating rate of 50°C/min.

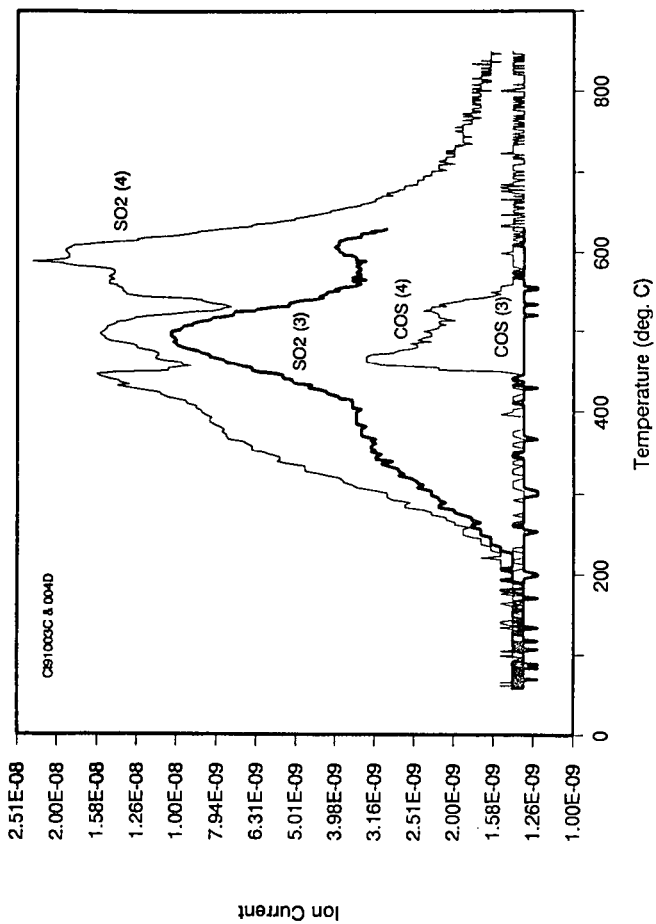


Figure 3. SO_2 and COS profiles when combustion chamber was under oxidizing (Run 3) and reducing (Run 4) conditions.

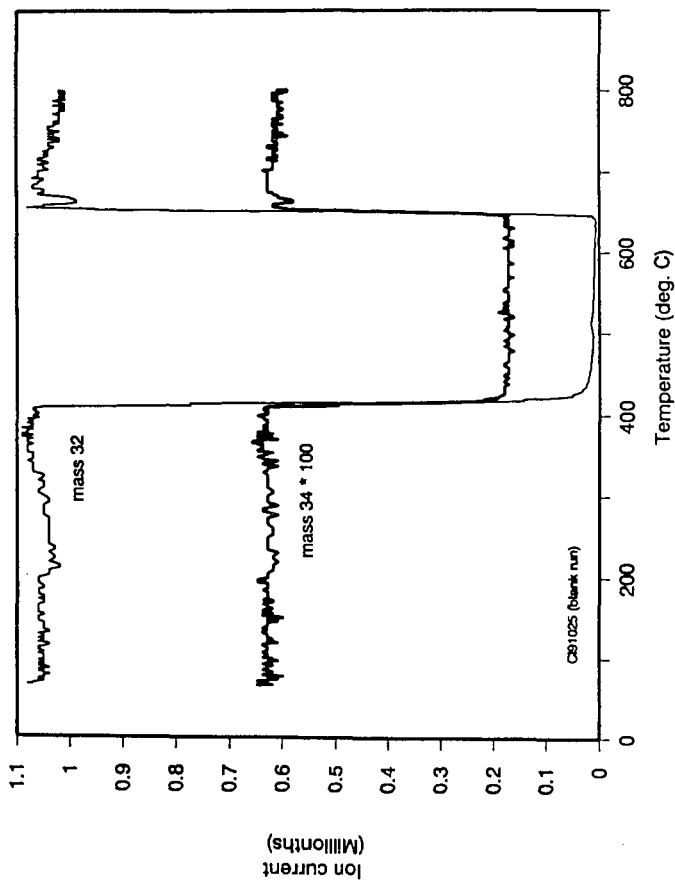


Figure 4. Profiles of masses 32 and 34 ($\times 100$) during a blank run where O_2 flow was shut off between 400° and $625^\circ C$.

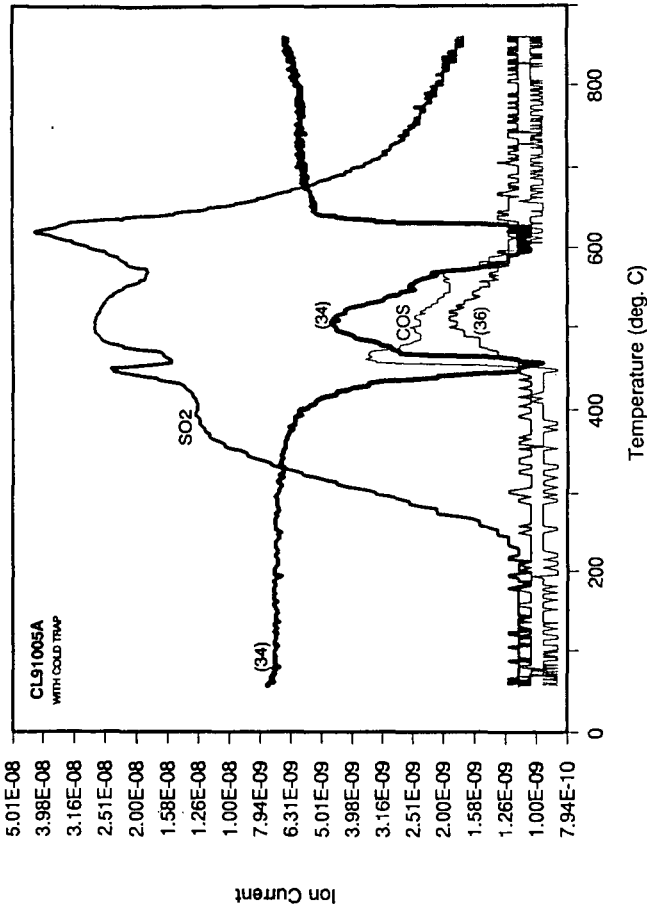


Figure 5. Gas release profiles obtained when combustion chamber was under a reducing condition. Mass numbers in parentheses are used for profiles that possibly represent more than one gaseous species.

SECONDARY PYROLYSIS AND COMBUSTION OF COAL VOLATILES

D. Marlow, S. Niksa, and C. H. Kruger
High Temperature Gasdynamics Laboratory
Stanford University
Stanford, CA 94305

Keywords: Coal Volatiles, Combustion, Burning Velocity

INTRODUCTION

During the initial stages of pulverized fuel (p. f.) firing devolatilization converts about half of the injected coal mass into gases, including many fuel compounds. The subsequent secondary pyrolysis and combustion of these volatile compounds accounts for large portions of the heat release, pollutant formation, and soot evolution during coal combustion. This study focuses on the combustion of the volatiles. Noncondensable volatiles, without tar or soot, from the pyrolysis of a bituminous coal were mixed with O_2 and N_2 and burned in a constant volume combustion bomb. The resulting laminar burning velocity determinations provide a means of estimating global combustion rates. Laminar burning velocities are reported as a function of equivalence ratio and unburned gas temperature for a single pyrolysis condition, in which most of the tar had converted to soot.

APPARATUS

As seen in Fig. 1, the volatiles are generated by entraining pulverized coal particles in N_2 , and passing the suspension through an induction furnace. At the exit of the furnace, a fraction of the N_2 /volatiles stream is diverted from the main stream of gas and char, and drawn through a heated filter to an evacuated storage tank. The stored gas is then pumped to the combustion bomb, where it is mixed with O_2 and N_2 , and ignited by an electric spark.

Design details and performance characteristics of the radiant coal flow reactor are given elsewhere.^{1,2} Briefly, the coal suspension passes through a quartz tube within an inductively heated cylinder of graphite maintained at temperatures from 1000 K to 1850 K. Radiation from the graphite heats the coal particles at $10^4 - 10^5$ K/sec. The N_2 carrier gas is transparent to radiation, and can only be heated by convection from the coal suspension and the quartz tube. Since the coal suspension supplies much of the heat to the carrier gas, the gas temperature can be kept low to minimize secondary reactions among the volatiles by operating with very dilute suspensions (about 100 particles/cc). However, to obtain the flammable mixtures for this study the coal loading was increased to 2400 particles/cc. At this condition, secondary pyrolysis of the volatiles is virtually complete.

Gas concentrations were determined with gas chromatography (for H_2 , CO , CH_4 , C_2H_6 , C_2H_4 , C_2H_2 , C_3H_6 , and light oils) and non-dispersive infrared analysis (for CO_2 and H_2O). Hydrogen and CO were sampled with a gas-tight syringe and measured with a thermal conductivity detector after separation on Molecular Sieve 5A. Chromatography for these compounds was conducted immediately after sampling to avoid diffusive loss of H_2 . Methane, C_2H_6 , C_2H_4 , C_2H_2 , and C_3H_6 were sampled into a multiposition valve and measured with a flame ionization detector (FID) after separation on Silicalite. The remaining hydrocarbons in the gas stream were grouped as light oils and measured by direct injection of the gas stream into the FID. The resulting total signal included the signals from $C_1 - C_3$ hydrocarbons, which were subtracted out; the remainder was then converted to a light oil concentration using the conversion factor for pentane, which has a molecular weight similar to the oils'.

The combustion bomb is a spherical pressure vessel (15.24 cm diam.) constructed from 316 stainless steel, and equipped with 10 access ports. Copper electrodes form a 1 mm spark gap at the center of the spherical chamber. Three ionization gages spaced about the chamber wall monitor the arrival time of the flame to check for flame sphericity (an assumption in the data reduction). The transient

pressure rise from combustion is monitored by a water-cooled piezoelectric pressure transducer mounted at the bomb wall. Laminar burning velocities are determined from the transient pressure trace. But this determination is complicated by the fact that the pressure rise is related both to the rate at which volatiles enter the flame, and the rate at which the unburned gas is compressed by the expansion of the products behind the flame. A computational procedure has been adapted to separate these two effects, and is explained elsewhere.³

EXPERIMENTAL

An HVA bituminous coal (Illinois #6, IBCSP 105) distributed by the Illinois Basin Coal Sample Program was used. The coal was ground under liquid nitrogen and dry-sieved to produce a 75-106 micron size fraction. The 75 micron cutoff was then improved by sedimentation of the coal in water. An ultimate analysis of the sized coal gave 64.8 % C, 4.9 % H, and 1.4 % N on a moisture free basis. Before each use, the coal was dried overnight at 330 K under 15 kPa of N₂.

The radiant coal flow reactor was operated at 1640 K and a nominal residence time of 200 msec. The large amounts of soot observed at the furnace exit confirmed extensive secondary pyrolysis of the volatiles. Soot and condensed volatiles were removed on a glass fiber filter maintained at 330 K. The filtered noncondensable volatiles were stored at 450 K, and pumped to the combustion bomb through lines heated to 380 K.

The combustion bomb was operated at an initial pressure of 0.07 MPa, which is sufficiently low to keep inordinate uncertainties in the initial section of the pressure trace from obscuring the behaviour at 0.1 MPa. The bomb was preheated to the two initial temperatures of 493 K (5 runs) and 579 K (4 runs). Compression heats the unburned gases to 540 K and 635 K, respectively, by the time the bomb pressure has reached 0.1 MPa. Oxygen was added to the volatiles to obtain fuel lean equivalence ratios (defined in terms of fuel/O₂ ratios) from 0.5 to 0.9, where the fuel comprises H₂, CH₄, C₂H₆, C₂H₄, C₂H₂, C₃H₆, light oils, and CO. Nitrogen was also added to maintain a constant diluent/O₂ ratio of 4.3 +/- 0.25 on a mole/mole basis; N₂, CO₂, and H₂O are the diluents.

RESULTS

Table I gives the measured species concentrations for two fills of the storage tank. The first mixture provided the results at 540 K, while the second mixture was used at 635 K. While H₂, CH₄, and CO are the most abundant fuel species, the remaining hydrocarbons contribute about half of the heat release of combustion. In fact, the light oils alone contribute about a quarter of the heat release. Because of their higher molecular weights, very small mole fractions of these higher hydrocarbons contribute significant amounts of energy release.

Fig. 2 shows the volatiles burning velocities measured for two unburned gas temperatures. The magnitude of the measured velocities is much smaller than that for H₂/air combustion at similar conditions ($S_u = 720$ cm/sec in air at an equivalence ratio of 0.9 and an unburned gas temperature of 635 K), but similar to that for CH₄/air (see correlations in Fig. 2).⁴ Note, however, that the correlations are for air, which has a diluent/O₂ ratio of 3.76, while the volatiles measurements are for a diluent/O₂ ratio of 4.3; CH₄ burning velocities for the same diluent ratio would tend to be 10 to 20 % lower. While CH₄ and volatiles burning velocities compare favorably for the conditions of this study, this result cannot be generalized. Further secondary pyrolysis leads to higher levels of H₂ and CO than observed here and lower levels of heavy hydrocarbons,² so that such volatiles mixtures might be expected to burn faster. Also, lower rank coals produce more H₂O, CO₂, and CO than observed here, and these species can be expected to play more important roles in the combustion of volatiles from these coals. Finally, the condensable tars absent from this study can contribute more than half of the heat release of combustion, and can be expected to introduce additional rank effects into the combustion rates of volatiles.

SUMMARY

A facility has been constructed to study the effects of primary and secondary pyrolysis on the combustion rates of the volatiles from coal. Concentration measurements for an HVA bituminous coal show that under significant secondary pyrolysis H₂, CH₄, and CO are the most abundant noncondensable fuel species; but other hydrocarbons, especially light oils, contribute significantly to the heat release. For the conditions of this study, the measured burning velocities are similar to those of methane. However, we do not anticipate this similarity in subsequent studies in which coal rank and extent of secondary pyrolysis are varied, and tar is left in the volatile fuel mixture.

ACKNOWLEDGEMENT

Support for this program is provided by the United States Department of Energy's Morgantown Energy Technology Center under Grant DE-FG22-86PC90511.

REFERENCES

1. Chen, J. C., Chang, Y. Cleo, and Niksa, S., Proc. 1989 Int'l Coal Science Conf., IEA, Tokyo, p. 503.
2. Chen, J. C., Castagnoli, C., and Niksa, S., Paper No. 90-48, WSS/CI Fall 1990 Mtg., San Diego, CA, October 1990.
3. Metghalchi, M., and Keck, J. C., Combust. Flame, 1980, **38**, 143.
4. Iijima, T., and Takeno, T., Combust. Flame, 1986, **65**, 35.

Table I: Measured Species Concentrations of Stored Volatiles.

		Mole % of Stored Volatiles									
	H ₂	CH ₄	C ₂ H ₆	C ₂ H ₄	C ₂ H ₂	C ₃ H ₆	Light Oil	CO	CO ₂	H ₂ O	N ₂ [#]
1	4.9	2.3	0.079	0.61	0.61	0.16	0.84	2.28	0.34	3.0	84.9
2	4.6	1.9	0.050	0.49	0.55	0.16	0.50	1.88	0.32	3.0 [*]	86.6

* Estimated. Not measured.

By difference.

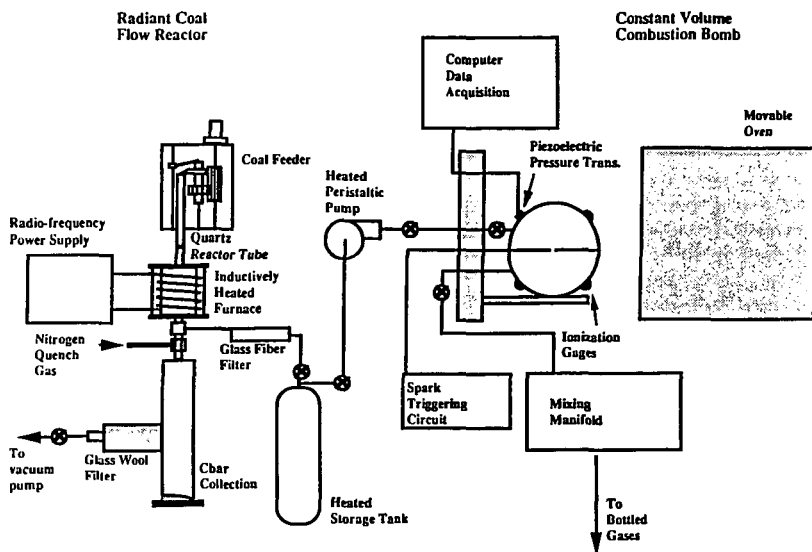


Fig 1: Schematic of the radiant coal flow reactor, the means of transporting volatiles, and the constant volume combustion bomb.

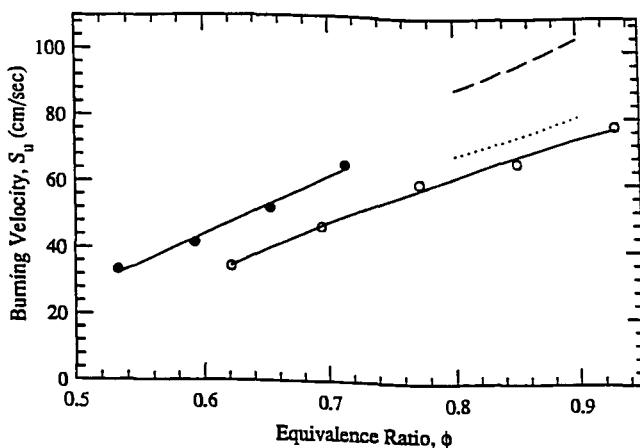


Fig 2: Burning Velocities, S_u , for the noncondensable volatiles of Table 1 as a function of stoichiometry for unburned gas temperatures of 540 K (○), and 635 K (●). The burning velocities for CH_4/air combustion are indicated by 540 K, and --- 635 K. Schematic of the radiant coal flow reactor, the means of transporting volatiles, and the constant volume combustion bomb.

Microscopic Studies on the Dispersion of Iron/Molybdenum Bimetallic Catalysts in Argonne Coals

David A. Sommerfeld, Jumpol Jaturapitpornsakul,
Larry Anderson and Edward M. Eyring
Dept. of Chemistry and Dept. of Fuels Engineering
University of Utah
Salt Lake City, UT 84112

Keywords: catalyst dispersion, bimetallic catalysts, EPMA

Abstract

The dispersion and reactivity of an iron/molybdenum coal liquefaction catalyst was investigated in three Argonne coals. Three coals (Blind Canyon, Wyodak and Pittsburgh #8) were impregnated with a 1 wt% Fe and 1 wt% Mo liquefaction catalyst using both ultrasonic and incipient wetness techniques. The yields of THF solubles in demineralized Blind Canyon coal indicate no significant advantage in the use of ultrasound as the impregnation technique. Results of electron probe microanalysis (EPMA) reveal that the catalyst is coated on the surface of the particles prior to hydrolysis at 350 °C and 2000 psig H₂. EPMA micrographs indicate that the catalyst occupies the interior of the coal particles after hydrolysis. Our results suggest that coal catalyst mobility occurs during hydrolysis and may be due to the liquid phase present in the coal and the amount of porosity.

Introduction

Catalyst dispersion remains an area in coal liquefaction research requiring a more thorough understanding.¹ Common sense suggests that the more evenly dispersed and the finer the size of the catalyst the more efficient the coal liquefaction. In other words, both the form of the catalyst and the manner in which it is introduced into the coal affect the coal liquids yields.

In this study we examine the role of the catalyst impregnation technique upon coal hydrolysis by comparing the incipient wetness technique with ultrasonic impregnation. A series of bimetallic catalysts were studied in three coals from the Argonne Premium Coal Sample Program. The dispersion of the catalyst was followed with electron probe microanalysis (EPMA) as in previous studies.² Electron probe microanalysis is a microscopic technique that allows one to examine on the micron scale the distribution of elemental species by detecting characteristic X-rays (Fig. 1).^{3,4}

Experimental

Samples of 100 mesh Blind Canyon, Wyodak and Pittsburgh #8 coals were obtained from the Argonne Premium Coal Sample Program

and stored at 0 °C until impregnation. In some studies involving Blind Canyon coal the coal samples were demineralized. The demineralization process occurred under nitrogen using warm (about 60 °C) solutions of concentrated HCl followed by concentrated HF and then concentrated HCl.

The following catalyst systems were studied: 0.05% Mo, 1% and 0.01% Fe, 1% and 0.01% Ni, 1% and 0.01% Fe/0.05% Mo and 1% and 0.01% Ni/0.05% Mo (note: these are all in wt%). Two methods of catalyst impregnation were compared: incipient wetness and ultrasound. For bimetallic catalysts the impregnation was done sequentially from aqueous solutions using first the ammonium tetrathiomolybdate, followed by the iron(III) chloride hexahydrate or nickel(II) nitrate hexahydrate. Hydropyrolysis was done in a shaken tubing bomb reactor in which samples were reacted for one hour at 350 °C and 2000 psig of H₂. In order to determine the product yields, the samples were Soxhlet extracted with tetrahydrofuran (THF) after hydropyrolysis.

Samples for electron probe microanalysis were prepared with Petropoxy, polished to a smoothness suitable for EPMA, and sputter coated with carbon to reduce point charging of the surface. Visual images of the samples were obtained from the secondary electron and back-scattered electron images with a CAMECA Model SX-50 detector (Courbevoie Cedex, France). The catalyst dispersion in the samples was determined by collecting the characteristic X-rays for iron, nickel, molybdenum and sulfur with an energy dispersive spectrometer detector. X-ray analysis was done using a Digimap program. Sample magnification was x1000 or x1500.

Results

The resulting yields are summarized in Tables 1 and 2. The first set of experiments involved the use of demineralized Blind Canyon coal. These first experiments were run in order to determine which method of impregnation was better, incipient wetness or ultrasound, and whether preextracting the coal with THF improved the yields. As seen in Table 1 no significant advantage exists for either impregnation technique and preextraction with THF actually decreases the yields of THF solubles upon hydropyrolysis. The rest of the experiments were all done with coals that had not been preextracted and had been impregnated by the incipient wetness technique and were performed in order to determine the efficiency for producing THF solubles of various Fe/Mo and Ni/Mo bimetallic catalysts. The results show that the bimetallic catalysts are much more efficient than either metal alone (Table 1). More importantly, even when the loading of the Fe/Ni promoters is decreased by two orders of magnitude significant amounts of THF solubles are still produced.

These images are of samples that have been impregnated with 1 wt% Mo because the 0.05 wt% loading of Mo results in a Mo concentration too close to the detection limits of the EPMA for accurate micrographs. The EPMA images for iron, nickel and molybdenum show that all three of the cationic species behave in

a similar manner. Before hydropyrolysis the catalyst species are located on the surface of the coal particles (Fig. 2). After reaction the catalyst species occupy the interior of the coal particles (Fig. 3). This is true for the iron, nickel and molybdenum catalytic species.

The second set of experiments involved three different Argonne coals: Wyodak, Pittsburgh #8 and Blind Canyon and were done in order to determine whether the choice of catalyst impregnation technique seriously affected the yields of THF solubles. The coals were used as received from the Argonne Premium Coal Sample Program. The catalyst system used was 1 wt% Fe/1 wt% Mo with the same reaction conditions as given previously. For the Pittsburgh #8 and Blind Canyon coal samples there was no significant difference in the yields of THF solubles between samples impregnated by incipient wetness or by ultrasound (Table 2). A significant difference occurs for Wyodak coal. The samples impregnated by incipient wetness exhibit a 13% higher yield of THF solubles. As described in the case above, before hydropyrolysis the catalytic species are found on the surface of the coal particles. After hydropyrolysis these species are found in the interior of the coal particles.

Discussion

Sulfided molybdenum can provide a reasonably efficient coal liquefaction catalyst.^{5,6} Recently, Li and coworkers,⁷ using a fixed-bed reactor, found that a MoS₂ loading of 0.5% produces a 35% oil yield under hydropyrolysis conditions of 3 M Pa and 798 K for 30 minutes. As they note in their conclusion, a Mo loading of 0.5% is commercially unrealistic due to its high cost and the sulfur added to the hydropyrolysis products.⁷

The yields reported in the present study (Tables 1 and 2) result from a procedure using lower Mo loadings (0.05%) and mild hydropyrolysis conditions. The presence of the iron/nickel promoters appears to increase the efficiency of hydropyrolysis (Table 1). These results seem to indicate that one of the most promising routes to commercially feasible coal liquefaction involves the use of bimetallic catalyst systems with loadings of less than 1% and the use of mild hydropyrolysis conditions. The mild conditions would permit a catalytic rather than thermal breakdown of the coal structure.

The EPMA experiments lead to two main conclusions: First, catalyst mobility occurs during hydropyrolysis for these coals and catalytic species. Second, because these catalysts are mobile species during hydropyrolysis, the choice of catalyst impregnation technique probably will not significantly affect the coal liquefaction yield.

What does affect the liquefaction yield is the rank of the coal. The best yields were obtained from a subbituminous coal, Wyodak coal, which is 75% C.⁸ Blind Canyon coal, a high volatility bituminous coal which is 81% C, provided the next best yield of THF solubles. Pittsburgh #8 with a carbon content of 83% provided the lowest yields of THF solubles (Table 2). As has been pointed out

by Derbyshire,⁹ the rank of a coal and its carbon content correlate with the porosity of the coal structure. Upon heat treatment the open pore structure of low rank coals is preserved whereas higher rank coals undergo increasing degrees of graphitization. We believe this effect helps to explain our results. If, as we surmise, catalyst mobility occurs during hydroxyprolysis then a more efficient catalyst dispersion process will occur in the low rank coals resulting in a higher yield of THF solubles. Higher rank coals will have less efficient catalyst dispersion during hydroxyprolysis and hence lower THF soluble yields. This is precisely what we find for the yields of Wyodak versus Blind Canyon and Pittsburgh #8 coals (Table 2).

Acknowledgment

Financial support by the U.S. Department of Energy, Fossil Energy Division, through the Consortium for Fossil Fuel Liquefaction Science, Contract No. UKRF-4-21033-86-24, is gratefully acknowledged. Ray Lambert provided generous technical assistance.

References

1. Derbyshire, F.J. Catalysis in Coal Liquefaction, IEA Coal Research: London, 1988, p. 17.
2. Wang, H.P.; Lo, R.; Sommerfeld, D.A.; Huai, H.; Pugmire, R.J.; Shabtai, J.; Eyring, E.M. Fuel, in press.
3. Newbury, D.E.; Fiori, C.E.; Marinenko, R.B.; Myklebust, R.L.; Swyt, C.R.; Bright, D.S. Anal. Chem. (1990), 62, 1159 A.
4. Newbury, D.E.; Fiori, C.E.; Marinenko, R.B.; Myklebust, R.L.; Swyt, C.R.; Bright, D.S. Anal. Chem. (1990), 62, 1245 A.
5. Derbyshire, F.J.; Davis, A.; Lin, R.; Stansberry, P.G.; Terrer, M.-T. Fuel Proc. Technol. (1986), 12, 127.
6. Snape, C.E.; Bolton, C.; Dosch, R.G.; Stephen, H.P. ACS Div. Fuel Chem., prep. (1988), 33, 351.
7. Li, B.-Q.; Braekman-Danheux, C.; Cypres, R. Fuel (1991), 70, 254.
8. Vorres, K.S. Energy & Fuels (1990), 4, 420.
9. Derbyshire, F.J. Fuel (1991), 70, 276.

Table 1. Catalytic Hydropyrolysis of Blind Canyon Coal
THF^c

Catalyst ^a	Impregnation ^b	Sol.	Insol.
0.05% Mo	U	40	52
0.05% Mo	I	42	52
1% Fe + 0.05% Mo	I	55	41
0.01% Fe + 0.05% Mo	I	50	43
1% Ni + 0.05% Mo	I	50	46
0.01% Ni + 0.05% Mo	I	52	45

^aCatalyst loadings are given in wt%

^bImpregnation: U=ultrasound, I=incipient wetness

^cYields are given as % of maf coal

Table 2. Comparison of Yields and Impregnation Technique
THF^b

Coal	Impregnation ^a	Sol.	Insol.
Wyodak	U	55	36
Wyodak	I	68	20
Pittsburgh #8	U	53	45
Pittsburgh #8	I	56	42
Blind Canyon	U	62	36
Blind Canyon	I	63	38

^aImpregnation: U=ultrasound, I=incipient wetness

^bYields are given as % of maf coal

Electron Probe Microanalysis Schematic

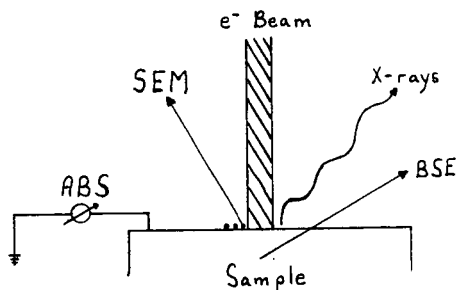


Figure 1. This illustration portrays the various signals generated by EPMA. An e^- beam of 10-30 keV impinges upon the sample surface resulting in three "visual" signals and characteristic X-rays. The secondary electron image (SEM) results when the incoming electron beam causes the loosely bound surface electrons to leave the sample. Back-scattered electrons (BSE) have entered the sample and through atomic interactions are emitted from the sample. The absorption image (ABS) is read as a current from the sample and accounts for those electrons of the incoming electron beam that are not back-scattered.

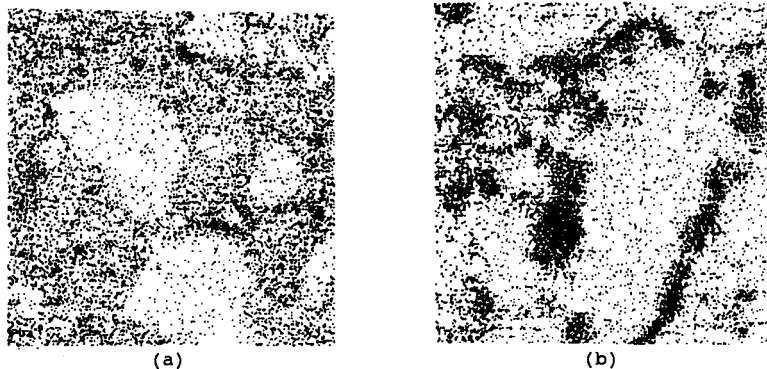
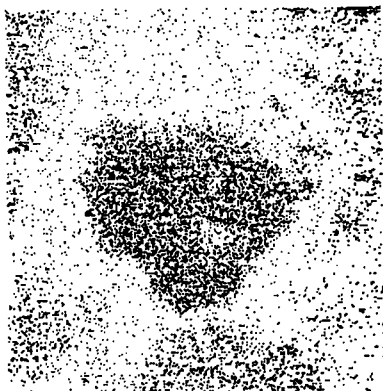


Figure 2. These EPMA micrographs are 97×97 microns. Figure 2a is of 1 wt% Fe impregnated Blind Canyon coal before reaction. Figure 2b is of 1 wt% Ni impregnated Blind Canyon coal before reaction. The cationic species have not entered the particles, they are located on the surfaces of the coal particles as seen by the rings and ghost images of particles.



(a)



(b)

Figure 3. The EPMA images here are 97×97 microns. Figure 2a is an image of Blind Canyon coal after impregnation with 1 wt% Fe and hydrolysis. The iron is now evenly dispersed throughout the coal particle in the center of the image. Figure 2b is an image of Blind Canyon coal after impregnation with 1 wt% Ni and hydrolysis. The nickel species has entered the coal particle in the lower-right corner of the image and is less evenly dispersed.

XPS STUDY OF CATALYSTS AND CATALYST IMPREGNATED COAL

P.J. Reucroft and J.Y. Kim

Dept. of Material Science & Engineering,
University of Kentucky, Lexington, KY 40506

INTRODUCTION

The highly dispersed forms of certain catalysts are believed to be very active in the conversion of coal to liquids via direct liquefaction.¹⁻³ A catalyst with a higher specific surface area and fine particulate size can be utilized at small concentrations to achieve better performance in terms of overall coal conversion and selectivity to lighter products (oils) in direct coal liquefaction.⁴

X-ray photoelectron spectroscopy (XPS) has been used to study the surface characteristics of six catalysts and a catalyst impregnated Illinois #6 coal. This technique provides the surface elemental distribution and chemical information about the outermost 3-4 nm of the exposed solid surface. This characterization has shown that the concentration of elements at the outermost layer measured by XPS is different from that in the bulk determined by chemical analysis. The oxygen concentration was enriched in the surface regions of all the samples. The oxidation states of these elements were generally identified.

XPS depth profiling studies also have been carried out to determine if there are any differences in the distribution of the major components in catalyst II (Mo/FeOOH/SO₄²⁻) and catalyst I (FeOOH/SO₄²⁻) impregnated Illinois #6 coal. A systematic trend towards lower weight concentrations of both oxygen and sulfur was observed for both samples as the sputtering time increased (i.e. when going from surface to the bulk).

EXPERIMENTAL

Six catalysts and catalyst I (FeOOH/SO₄²⁻) impregnated Illinois #6 coal were investigated in the surface characterization studies. These samples were obtained from the Univ. of Pittsburgh⁵ and are shown in Table 1. The powdered samples were examined in their as-received form and their particle sizes were less than -100 mesh.

The powdered samples were mounted on the spectrometer probe tip by means of double-sided adhesive Scotch insulating tape. The samples were pressed with the aid of a metal spatula and the excess that had not adhered was tapped off. To exclude the possibility of recording contaminants associated with the tape, the tape was also analyzed separately. It was found that the constituents of tape were not detected by XPS, and that the photoionization signals are characteristic of the catalyst and coal samples alone.

The samples were examined by XPS on a Kratos XSAM 800 spectrometer using Mg K α (1253.6 eV) radiation. The spectrometer was run in fixed retarding ratio (FRR) mode at a pass energy of 13 kV and 15 mA. Under these conditions, the full width at half maximum (FWHM) of the Ag (3d_{5/2}) peak is ≈ 1.1 eV. Spectra were recorded at $< 5 \times 10^{-7}$ torr.

Radiation damage to the sample from long-term exposure to the X-ray beam was not observed. All binding energies were referred to carbon (1s) at 285 eV to compensate for

sample charging. Elemental concentrations were obtained from peak areas and corrected for atomic sensitivity factors.

The peak was deconvoluted using a peak synthesis procedure which employed a Gaussian line shape at fixed binding energies determined from model compound studies.⁶ The data system permitted the intensity of the components and their FWHM to be varied in order to obtain the best fit between the experimental and the synthesized spectra.

Ar⁺ sputtering of the powdered sample was carried out with the Ar⁺ gun operating at 3.5 kV (estimated etching rate of ca. 20 Å/min, as determined from a SiO₂ standard film). Each charge compensation was referred to the C 1s peak at 285 eV.

RESULTS AND DISCUSSIONS

Surface Compositions

The XPS spectra showed a distinct peak for major elements, oxygen, iron, and tin, as well as the minor component, sulfur, in each catalyst sample. The C 1s peak was observed in all catalysts and can be ascribed to carbon contamination. Cl 2p was only observed in the tin oxide catalyst (III). This occurs because chlorine was introduced as SnCl₄·5H₂O in the starting materials that were used for the preparation of the tin oxide catalysts. This excess chlorine was left at the surface after sample preparation. The quantitative analysis results are shown in Table 2.

To determine the oxidation states of Fe, Mo, and Sn, narrow survey scans were carried out. The binding energies of the Fe 2p, Mo 3d and Sn 3d levels showed the expected values for the most stable oxidation states of these elements. Multiple splitting was observed in the transition elements, such as Fe and Mo. Figures 1a and b show the results for Fe 2p and Mo 3d, respectively. This is the result of spin interaction between an unpaired electron from the photoionization process and other unpaired electrons present in the system. The point of real interest is that the separation between the two peaks varies depending upon the environment of the atom concerned. In Fig. 1a, the Fe 2p peak shows the 13.6 ± 0.05 eV splitting between the 2p_{1/2} and 2p_{3/2} peaks. This was observed in all iron oxide containing catalysts. The observed splitting corresponds well with the Fe 2p peaks of Fe₂O₃ and/or FeOOH (Goethite) in model compound studies.⁶ The Fe compound shown in the surface of the catalyst samples can thus be ascribed to either Fe₂O₃ or FeOOH.

Mo 3d showed the 3.2 eV splitting between the 3d_{3/2} and 3d_{5/2} peaks in the catalyst II, IV, and V samples. Molybdate (MoO₄²⁻) was used as a starting material in the preparation of these catalysts. This anion is readily oxidized at the surface and produces the stable oxidation state MoO₃ at the catalyst surface. Sn 3d also showed the multiple splitting of 8.45 eV. This can be ascribed to SnO₂ and is shown in Fig. 1c. Emphasis has been focused on the S 2p peaks of raw coal samples in earlier reports.⁷ It was shown that the S 2p peak always displays two photolines with a separation of 5.6 eV in raw coal samples. However, the XPS spectrum of S 2p in the catalyst samples showed only one S 2p peak at 168.8 eV, corresponding to SO₄²⁻. This result is shown in Fig. 1d where a catalyst spectrum is compared with that of catalyst impregnated coal. In the upper spectrum, the peak at 164 eV can be ascribed to sulfide in the coal.

From the above results, it was concluded that all major elements showed the most stable oxidation states at the surface of all catalysts and catalyst impregnated coal samples.

Depth Profile Studies

In order to show if there is any difference in the distribution of the elements and chemical changes between the surface and bulk, the samples have been analyzed by combining Ar^+ sputtering with XPS measurements. Due to the edge effect associated with the unetched sample surface, the depth profiles for materials in powder form were difficult to obtain. Preferred areal sputtering was carried out to reduce this effect. Although different features such as preferential sputtering, atomic mixing, particle size effects, etc., can effect the etching profiles, sputtering was performed in the present studies for comparative purposes on samples where such effects were expected to be very similar.

Figures 2a and b show depth concentration profiles for the most abundant elements in catalyst I and catalyst I impregnated Illinois #6 coal samples, respectively. A systematic trend towards lower weight concentrations of both oxygen and sulfur was observed for both samples as sputtering time increased. A relatively high oxygen concentration was determined initially at the surface by XPS before etching, but a sharp drop in oxygen concentration was subsequently observed as shown in Fig. 2a. This surface enrichment of oxygen can be ascribed to air oxidation and the oxidized layer thickness was estimated to be 40-50 Å. In Fig. 2a, Fe shows an enrichment as the etching proceeds from the surface to the bulk of catalyst I. This was also observed in catalyst II. From these results, which show a decrease in oxygen and an increase in iron concentrations with increased etching, it can be concluded that the surface iron particles are covered with an oxide layer. However, no change was observed in the iron concentration in the case of the catalyst impregnated coal sample shown in Fig. 2b. It can thus be concluded that the iron particles, in catalyst I impregnated Illinois #6 coal, are encapsulated by organic materials from the coal.

Chemical state changes for sulfur were observed as the etching proceeded in both samples. The surface sulfur showed a binding energy of 168.8 eV, indicating sulfate (SO_4^2-) and no peaks were observed in the sulfide region (164 eV) in the case of the catalyst I sample. As sputtering time increased, however, the sulfate peak decreased and finally disappeared. A sulfide or elemental sulfur peak was then observed. These results are shown in Figs. 3a and b. This can be ascribed to the removal of oxidized sulfur at the surface by the etching procedure. No chemical state changes were observed for Fe and Mo states as a result of etching.

SUMMARY AND CONCLUSIONS

It is apparent from this study that XPS can be used to obtain surface chemistry information and elemental identifications on the exposed solid surface. The major elements showed the most stable oxidation states. Sputtering with Ar^+ is a useful tool in determining depth concentration profiles along the outermost sample surfaces. However, in the case of chemical state changes during etching procedures, the interpretations tend to be inconclusive, unless extensive, time-consuming data accumulation can be performed.

ACKNOWLEDGEMENT

We gratefully acknowledge financial support from the Consortium for Fossil Fuel Liquefaction Science, Univ. of Kentucky under Dept. of Energy Contract no. DE-FC22-90 PC 90029. We also thank Dr. G.P. Huffman for his interest in this work.

REFERENCES

1. F.J. Derbyshire, Catalyst in Coal Liquefaction: New Direction for Research, IEA Coal Research, London, 1988, IEA CR-08
2. A.V. Cugini, R.G. Lett, I. Wender, *Energy & Fuels*, 3, 1989, 120-126
3. S. Weller, M.G. Pelipetz, *Ind. Eng. Chem.*, 43, 1951, 1243-1246
4. T. Suzuki, H. Yamada, P. Sears, Y. Wadanabe, *Energy & Fuels*, 3, 1989, 707-713
5. Catalyst samples were supplied by V.R. Pradham and I. Wender, Univ. of Pittsburgh
6. C.D. Wagner, W.M. Riggs, L.E. Davis, J.F. Moulder, and G.E. Muilenberg, *Handbook of X-ray Photoelectron Spectroscopy*, Perkin Elmer Corp. Phys. Elec. Div., Norwalk, CT, 1979
7. P.J. Reucroft, J.Y. Kim, Annual report for CFFLS, 1989-1990

Table 1. Summary of Materials

Catalyst	Symbol	Elemental Analysis
FeOOH/ SO ₄ ²⁻	I	3.0 wt% Sulfur
Mo/FeOOH/ SO ₄ ²⁻	II	1.0 wt% Mo and 2.0 wt% Sulfur
FeOOH/SnO(OH) ₂ / SO ₄ ²⁻	III	
Mo/ Fe ₂ O ₃ / SO ₄ ²⁻	IV	0.5 wt% Mo and 1.3 wt% Sulfur
Fe ₂ O ₃ / MoO ₄ ²⁻	V	2.0 wt% Mo
SnO ₂ / SO ₄ ²⁻	VI	
FeOOH/ SO ₄ ²⁻ on Ill. #6		10.0 wt% Fe and 2.0 wt% Sulfur

Table 2. Bulk and Surface Concentrations (wt%) for Catalysts

Element	I		II		IV		V		III	VI
	Bulk	XPS	Bulk	XPS	Bulk	XPS	Bulk	XPS	XPS	XPS
Fe	57.85	40.79	59.12	40.43	68.87	40.71	67.61	34.69	27.09	
O	34.15	52.24	37.88	48.65	31.34	46.22	30.09	39.97	30.55	19.07
S	3.00	6.97	2.00	4.51	1.30	6.34			0.46	2.05
Mo			1.00	6.40	0.50	6.74	2.00	25.94		
Sn									41.89	78.88

FeOOH/ SO₄²⁻ on Ill. #6 --- C:43.46, O:38.54, Fe:6.67, S:1.87, Al:3.48, Si:3.97
 Raw Coal (Illinois #6) ----- C:66.58, O:22.53, S:1.52, Al:3.99, Si 4.3

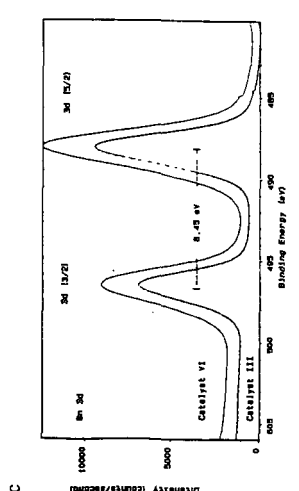
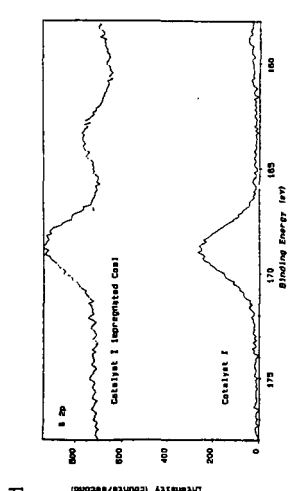
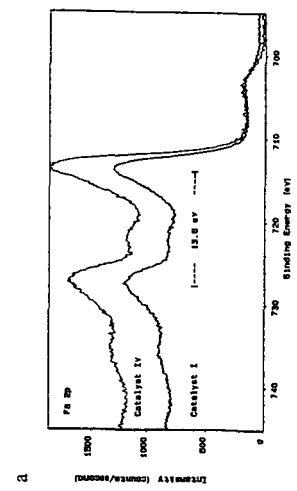
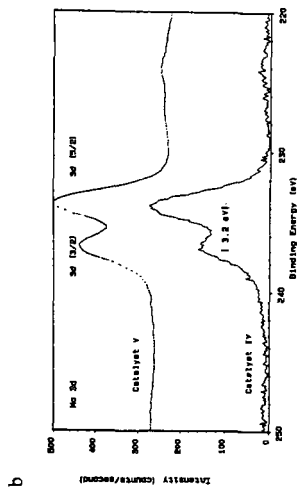


Figure 1. Typical XPS narrow scan spectra for (a) Fe 2p for catalysts I & IV, (b) Mo 3d for IV & V, (c) Sn 3d for III & VI, and (d) S 2p for catalyst I and catalyst I impregnated on Illinois #6 coal

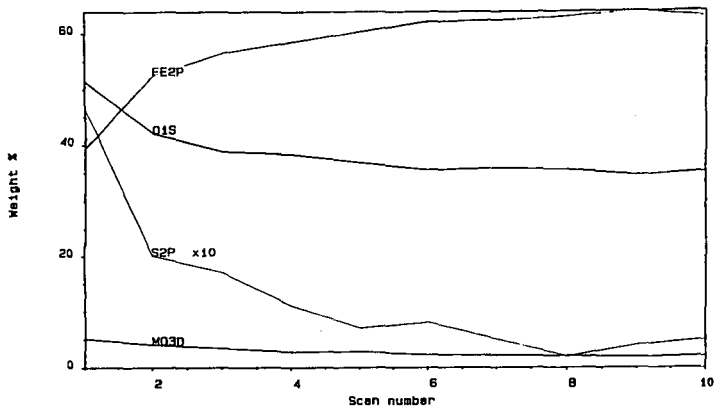


Figure 2-a. XPS depth profile of Catalyst I

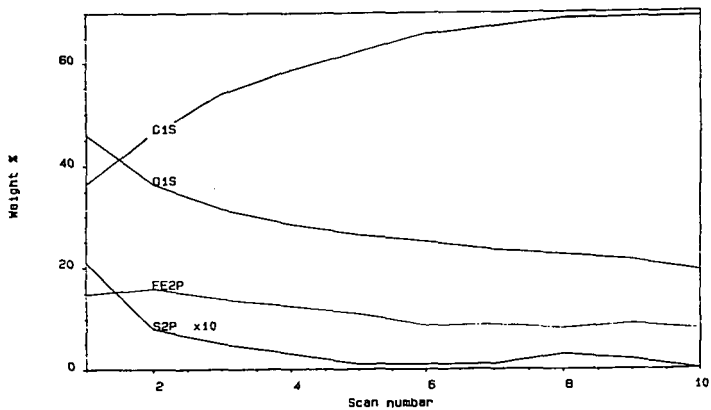


Figure 2-b. XPS depth profile of Catalyst I impregnated on Illinois #6 coal

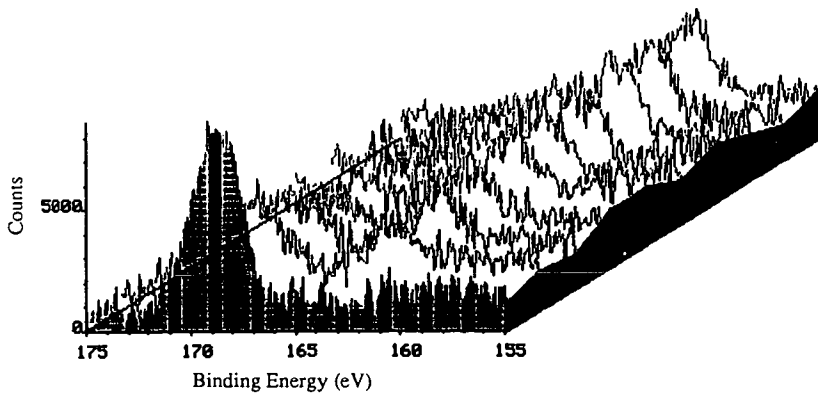


Figure 3-a. XPS depth profile of Sulfur in Catalyst II

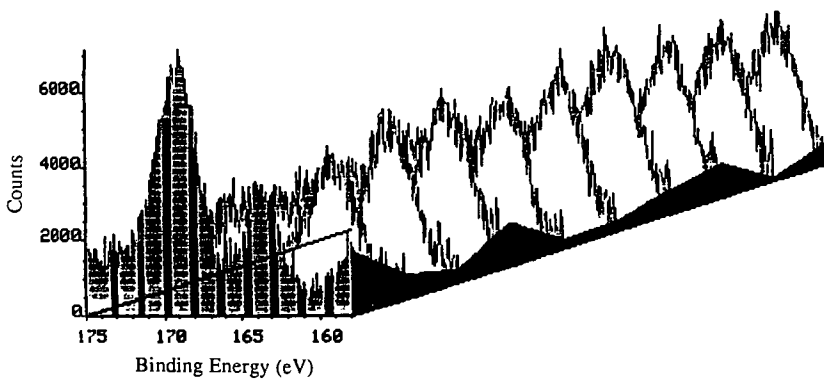


Figure 3-b. XPS depth profile of Sulfur in Catalyst I impregnated Illinois #6 coal

THE EFFECTS OF CHLOROBENZENE PRE-TREATMENT ON THE LOW-SEVERITY LIQUEFACTION BEHAVIOUR OF PITTSBURGH No.8 COAL

C.A. McArthur, A.J. Mackinnon, P.J. Hall and C.E. Snape

University of Strathclyde, Dept. of Pure & Applied Chemistry, Thomas Graham Building, 295 Cathedral Street, Glasgow G1 1XL

Keywords: Conformational changes, macromolecular structure, tetralin extraction, hydrogenation.

ABSTRACT

Recent work has demonstrated that pre-treating coals, particularly with polar solvents, can give rise to significantly improved yields under relatively low-severity liquefaction conditions. Although accessibility is undoubtedly improved, interpretation of these phenomena in terms of changes in the macromolecular structure of coals is complicated by the fact some organic matter is being removed at the same time that conformational changes may be occurring. Chlorobenzene has the advantage of extracting virtually no organic matter from coals and, in this study, the effects of chlorobenzene treatment on short contact time tetralin extraction and dry hydrogenation with and without a dispersed sulphided molybdenum (Mo) catalyst for the Pittsburgh No. 8 Argonne Premium Coal Sample have been investigated. While the chlorobenzene treatment significantly improved the yields from tetralin extraction and non-catalytic hydrogenation due to improved accessibility of solvent and hydrogen gas respectively, reduced yields were obtained in catalytic hydrogenation presumably due to the oil diffusing more effectively out of the remaining macromolecular framework and reducing the effectiveness of hydrogen atom transport from the catalyst.

INTRODUCTION

It was established by Brown and Waters ⁽¹⁾ during the 1960s that chloroform-extractable material within the macromolecular structure of coking coals markedly affects their ability to swell during carbonisation. A close correspondence was found between the release of chloroform-soluble material and pore accessibility with increasing temperature. More recently, the effect of pre-swelling and pre-extracting coals in both polar and non-polar solvents on conversions in direct liquefaction has begun to receive considerable attention ⁽²⁻⁷⁾ as it is particularly important to overcome mass transfer limitations to maximise yields. For extraction in hydrogen-donor ^(2,5) and non-donor ^(5,7) solvents and for dry (solvent-free) hydrogenation ⁽⁸⁾, significant improvements in overall conversions to pyridine/tetrahydrofuran (THF)-soluble material and in oil yields have been achieved. The study by Joseph ⁽⁴⁾ in which tetrabutylammonium hydroxide (TBAH) was the most effective swelling solvent used has demonstrated that the beneficial effect is evident in hydrol liquefaction both with and without a dispersed catalyst. As well as pre-swelling or pre-extracting coals in polar solvents, contacting coals at elevated temperatures with non-polar liquefaction solvents including 1-methylnaphthalene ⁽⁷⁾ and 9,10-dihydrophenanthrene ⁽⁵⁾ has given rise to significant improvements in conversion in short contact time liquefaction and in fluidised-bed pyrolysis ⁽⁹⁾. In contrast, removal of chloroform-extractable material has resulted in lower conversions in fluidised-bed pyrolysis ⁽¹⁰⁾ and in high temperature extraction with phenol ⁽¹¹⁾.

Clearly in the above cases where improved liquefaction yields have been achieved, the accessibility of solvents within the highly porous macromolecular structure of coals has been improved, particularly during the initial stages of liquefaction where retrogressive reactions need to be avoided. However, interpretation of the above phenomena in terms of changes in the macromolecular structure of coals is complicated by the fact some organic matter is being removed at the same time that conformational changes may be occurring and, in the case of polar solvents and pre-treatments at elevated temperatures, hydrogen bonds are being disrupted. Chlorobenzene has the advantage of extracting virtually no organic matter from coals ⁽¹²⁾ but it is non-polar and does not significantly disrupt hydrogen bonds at relatively low temperatures (<150°C). Therefore, in principle, it is possible to decouple the effects of conformational changes and extraction for this non-polar solvent. Indeed, it has already been demonstrated that chlorobenzene treatment markedly affects mass transfer phenomena in Upper Freeport coal ⁽¹³⁾ (Argonne Premium Coal Sample). Although the

CO₂ surface area remained constant at 180 m² g⁻¹, the time to reach equilibrium decreased from about 6 hours to only 5 minutes. Moreover, there was a significant change in the fractal dimension derived from SAXS. This parameter is a measure of the overall smoothness of the pores and varies between D=2 for a flat plane and D=3.0 for a surface so convoluted that it effectively fills a three dimensional volume. The change in D from 2.8 to 2.5 indicates that the chlorobenzene treatment is smoothing the pores and, as the CO₂ equilibration times demonstrate, this has a significant effect on mass transport within the macromolecular structure.

If the effect of chlorobenzene for Upper Freeport coal is general for most bituminous coals, significant changes in liquefaction behaviour can be anticipated due to the improved accessibility of solvents into the microporous structure and also the ability of coal-derived oil to possibly diffuse more effectively out of the remaining macromolecular framework. In this study, the effects of chlorobenzene treatment on short contact time tetralin extraction and dry hydrogenation with and without a dispersed sulphided molybdenum (Mo) catalyst for the Pittsburgh No. 8 Argonne Premium Coal Sample are reported and the results are discussed in light of the recent work on solvent pre-treatments (2-8).

EXPERIMENTAL

Pittsburgh No.8 coal was treated in chlorobenzene under nitrogen for 1 week in a Soxhlet apparatus. The extracted coal was then dried *in vacuo* at 50°C.

The following liquefaction experiments were conducted in duplicate on the original and chlorobenzene treated samples. For extractions in a hydrogen-donor solvent, 1 g of sample used and 2 g of tetralin were loaded into a microreactor which was submerged in a fluidised sandbath at 400°C for 15 minutes and was agitated using a flask shaker. The heat-up period for the thin-walled 1/2" O.D. microreactors was less than 2 minutes. After extraction, the reactor contents were recovered by filling the microreactor with dichloromethane (DCM) and placing it in an ultrasonic bath. The DCM washings were refluxed and filtered using phase separating paper and the DCM-solubles were recovered by evaporating the filtrate to dryness. The DCM-insolubles were weighed after drying *in vacuo* and were then refluxed in pyridine and filtered to determine the yield of pyridine-insolubles.

The dry or solvent-free hydrogenations were carried out with and without a sulphided Mo catalyst in a 9/16" O.D. microautoclave (*ca* 10 cm³) constructed of Autoclave Engineer high pressure fittings. For the catalytic experiments, the samples were loaded with 1% Mo (daf basis) by impregnation with a methanolic/water solution of ammonium dioxodithiomolybdate (14). 0.3 g of sample was loaded into the microautoclave which was pressurised to 70 bar with hydrogen. A sandbath at 400°C was raised to fully submerge the microautoclave for 60 min., the heat-up period being *ca* 5 min. The reactor contents were recovered and fractionated as described above for the tetralin extractions.

RESULTS AND DISCUSSION

Tables 1 and 2 list the yields of DCM-solubles, pyridine-solubles/DCM-insolubles and pyridine-insolubles from the duplicate tetralin and hydrogenation experiments, respectively, carried out on the initial and chlorobenzene-treated coal, the repeatability being *ca* ± 1% daf coal. The mean values are presented in Figures 1 and 2.

Tetralin Extractions

To highlight mass transfer effects during the initial stages of coal dissolution, tetralin was chosen as the solvent because it is largely in the vapour phase at 400°C and a relatively short contact time of 15 minutes was selected. Table 1 and Figure 1 indicate that chlorobenzene treatment has significantly improved the yield of DCM-solubles or oil. The fact that the total conversions to pyridine-solubles are extremely high would suggest that, for Pittsburgh No.8 coal which will undoubtedly soften to a considerable extent at 400°C, given that the free swelling index is 8, solvent accessibility is not too critical a factor affecting the initial dissolution. However, the vast increase of 20% daf coal in the yield of DCM-solubles clearly indicates improved solvent transport has been achieved with more hydrogen being available to promote the thermal breakdown of pyridine-soluble/DCM-insoluble material into oil.

The increase in oil yield is broadly comparable to that of 14% reported by Joseph ⁽⁴⁾ for tetralin extraction (with a hydrogen over-pressure) of an Illinois No.6 pre-treated with TBAH. Increases of only 5% were obtained for THF and methanol, but, nonetheless, pre-swelling with both these weakly-basic solvents increased the overall conversions to THF-solubles more than with TBAH. However, their boiling points are considerably lower than that of 132°C for chlorobenzene and, although some disruption of the hydrogen-bonding network in coals would undoubtedly have occurred as the coal swells to a significant extent, it is uncertain whether the glass transition temperature would have been lowered sufficiently to allow the coal to adopt a lower energy configuration. It is likely that the chlorobenzene treatment will also lead to significant improvements in primary conversions for non-hydrogen-donor polynuclear aromatic compounds in light of the fact THF extraction achieved this for a UK bituminous coal ⁽⁵⁾.

Hydrogenation

It is well-established that dispersed catalysts, such as sulphided Mo, significantly improve oil yields in solvent-free hydrogenation. At 400°C, yields of chloroform-solubles have been found to increase from 10-20% to 50-60% (daf basis) for bituminous and sub-bituminous coals upon catalyst addition ⁽⁵⁾. Interestingly, opposite conversion trends have been found after chlorobenzene treatment with and without catalyst for Pittsburgh No.8 coal (Table 2 and Figure 2). Without catalyst, the treatment increased the DCM-soluble yield from 19 and 31% and reduced the pyridine-insoluble yield from 40 to 20% indicating that transport of hydrogen gas into the depolymerising coal has been improved. Perhaps surprisingly at first sight, catalytic hydrogenation of the treated coal gave 25% less oil (DCM-solubles) and 12-13% more pyridine-solubles/DCM-insolubles and pyridine-insolubles (Table 2 and Figure 2).

The results with catalyst would appear to be contrary to both those of Joseph ⁽⁴⁾ and Artok *et al* ⁽⁸⁾ who both achieved increased yields in catalytic hydroliquefaction after pre-swelling in polar solvents. However, the experiments by Joseph were carried out in the presence of tetralin and the dominant effect could be the improved transport of the solvent into the macromolecular framework resulting in both more effective hydrogen donation and the transfer of dissociated hydrogen atoms from the catalyst particles. Further, the use of polar solvents which swell the coal considerably may have improved the dispersion of the Mo catalyst, although there is little evidence from hydropyrolysis studies on THF-extracted coals that this is the case ⁽¹⁵⁾. Without solvent, the transfer of hydrogen atoms is dependent on the bitumen or the oil generated by hydrogenation. However, it is likely that the transport of the oil out of the remaining macromolecular structure has also been improved by chlorobenzene treatment and, therefore, the effectiveness of the catalyst is reduced due to the less bitumen remaining in the pore structure to transport hydrogen atoms to reaction sites. Although Artok *et al* ⁽⁸⁾ found improved conversions in catalytic hydrogenation of Blind Canyon coal and two lignites, the experiments were conducted at 275°C and, not surprisingly at this low temperature, total conversions were less than 30% meaning that the amounts of oil available to transfer hydrogen atoms were small. Therefore, it is probable that the principal effect of pre-swelling in TBAH was to improve access of hydrogen gas into the macromolecular structure and thus limit retrogressive reactions.

General discussion

This investigation has reinforced other recent work ⁽²⁻⁸⁾ which indicated that pre-treatments can greatly enhance liquefaction yields, particularly in relatively low-severity regimes. However, much of the other work was concerned with pre-swelling coals in polar solvents where the dominant effect is undoubtedly the disruption of hydrogen bonding. Conversely, chlorobenzene is a low-swelling solvent and does not disrupt coal hydrogen bonding. However, as mentioned earlier, it acts as a plasticizer and, as such, lowers the glass transition temperature thus inducing conformational changes in the coal macromolecule during treatment. The nature of the conformational changes have yet to be elucidated but they are different to those induced by polar solvents and could well involve the disruption of non-covalent bonding between aromatic moieties. Indeed, our continuing research will investigate whether the conformational changes are general or occur to vastly differing extents for coals of varying rank and whether similar changes occur for other non-polar solvents, particularly polynuclear aromatic and hydroaromatic compounds found in vehicle solvents used in coal liquefaction. Circumstantial evidence discussed earlier would indeed suggest that this is the case ^(5,7) and more suitable contact between solvent and coal prior to liquefaction could prove to be extremely beneficial from a processing standpoint.

ACKNOWLEDGEMENT

The authors thank the British Coal Utilisation Research Association and the Science & Engineering Research Council for financial support.

REFERENCES

1. H.R. Brown and P.L. Waters, *Fuel*, 1966, **45**, 17.
2. R.M. Wham, *Fuel*, 1987, **66**, 283.
3. N.R. Pollack, G.D. Holder and R.P. Warzinski, *Prepr. Am. Chem. Soc. Div. Fuel Chem.*, 1991, **36**(1), 15.
4. J.T. Joseph, *Fuel*, 1991, **70**, 139 and 459.
5. C.E. Snape, F.J. Derbyshire, H.P. Stephens, R.J. Kottenstette and N.W. Smith, *Fuel Process. Technol.*, 1990, **24**, 119.
6. J.M. Rincon and S. Cruz, *Fuel*, 1988, **67**, 1162.
7. N.K. Narain, H.R. Appell and B.R. Utz, *Prepr. Am. Chem. Soc. Div. Fuel Chem.*, 1983, **28**(1), 161.
8. L. Artok, H.H. Schobert, G.D. Mitchell and A. Davis, *Prepr. Am. Chem. Soc. Div. Fuel Chem.*, 1991, **36**(1), 36.
9. C. Riemer and C.E. Snape *GB Patent No. 2,204,877A*, 1988.
10. J.W. Larsen, T.L. Sams and B.R. Rogers, *Fuel*, 1980, **59**, 666.
11. R.J. O'Brien, J.R. Gibbons and R. Kandiyoti, *Fuel Process. Technol.*, 1987, **15**, 71.
12. M. Nishioka and J.W. Larsen, *Energy and Fuels*, 1990, **4**, 100.
13. P.J. Hall and J.W. Larsen, *Energy and Fuels*, 1991, **5**, 228.
14. C.E. Snape and C.J. Lafferty, *Prepr. Am. Chem. Soc. Div. Fuel Chem.*, 1990, **35**(1), 1.
15. C.E. Snape, C. McArthur and S. Mitchell, unpublished results in *Final Report to EC on Project No. EN3V-0048-UK(H)*, 1992.

Table 1 Tetralin Extraction Results

	DCM sols	% daf coal Pyr sols/DCM insols	Pyr sols
Initial coal	43.0	54.1	2.6
	42.7	55.1	1.7
CB Treated coal	62.9	32.0	3.0
	62.7	30.0	2.7

CB Treated coal is chlorobenzene extracted coal

Table 2 Hydrogenation Results

	DCM conv*	% daf coal DCM sols	Pyr sols/DCM insols	Pyr insols
Non-catalysed Initial	22.0	17.5	30.7	40.5
	23.7	19.9	31.1	40.8
CB Treated	30.1	26.3	45.8	17.4
	29.7	27.9	46.2	19.1
Catalysed Initial	62.4	58.2	29.4	5.1
	62.1	57.9	30.9	5.4
CB Treated	36.0	31.5	44.0	18.1
	35.5	31.4	42.6	17.4

* DCM sols + gas + water

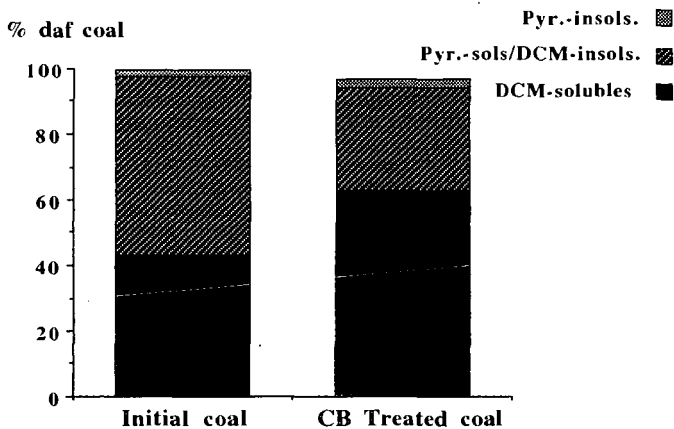


FIGURE 1 YIELDS FROM TETRALIN EXTRACTIONS

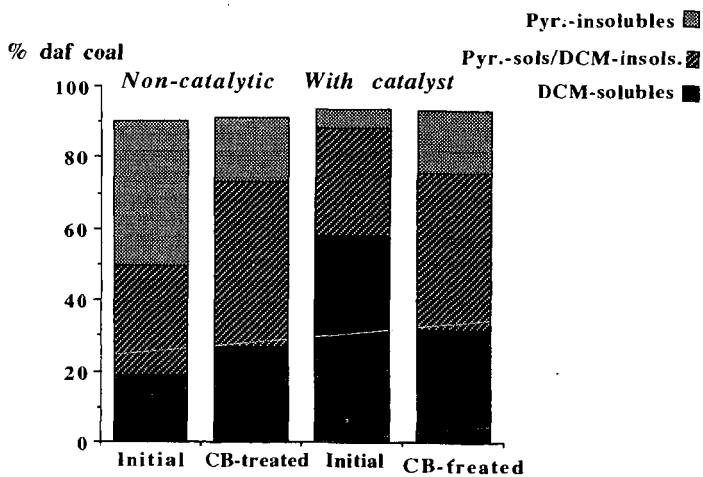


FIGURE 2 HYDROGENATION YIELDS

REACTIVITY OF COALS UNDER COPROCESSING CONDITIONS

Jasna Tomić and Harold H. Schobert
Fuel Science Program,
Department of Materials Science and Engineering,
The Pennsylvania State University,
University Park, PA 16802

Key words: coprocessing, coal reactivity, thermoplastic properties

INTRODUCTION

In the recent years greater interest has developed for processes involving coal and petroleum fractions to produce distillate fuels. Coprocessing is especially attractive as a direct liquefaction process because it involves the use of heavy petroleum fractions, so both coal and heavy petroleum resids are upgraded simultaneously. The main distinction of coprocessing from other direct liquefaction processes is that coprocessing is more complex from a chemical standpoint than direct liquefaction processes which use traditional solvents, due to the greater variety of hydrocarbons (aromatics from the coal and aliphatics from the petroleum) present in the system. Therefore, need arises for better understanding of the chemical and physical interactions during coprocessing (1).

The aim of the present study is to examine the influence of reaction conditions, coal and petroleum resid properties as well as the compatibility of the coal/petroleum resid pairs in terms of structural components on total coal conversion. Special focus will be given to the reactivity of coals and interactions of the coal and resid which lead to anisotropic coke.

EXPERIMENTAL

Five coal samples, ranging in rank from subbituminous B through high volatile A bituminous, from the Penn State Coal Sample Bank were used in this project. The coals were ground to -100 mesh and stored under nitrogen. Three petroleum resid samples were used. The West Texas (FHC-470) and Blend (FHC-571) resids were obtained from Amoco Co. and Hondo resid was obtained from Unocal. Analytical data for the coal and petroleum feedstocks are shown in Tables 1 and 2.

Prior to the reaction, the coal samples were dried to a 1% moisture under vacuum. The petroleum resid samples were used as received. A mixture of resid and coal (2.5g coal + 5g resid) was placed in a 20ml stainless steel vertical tubing bomb (microautoclave) reactor. The air was evacuated from the reactor by carefully flushing with nitrogen before pressurizing with nitrogen or hydrogen gas. The starting cold gas pressure was approximately 3.5 MPa. Reactor vessels were immersed in a fluidized sand bath which was previously preheated to 350°, 400° or 450°C and was vigorously shaken during the reaction. The reaction time was usually 30 min but some additional reactions were carried out at 15, 45, and 60 min. At the end of the reactions the microautoclave was cooled nearly instantaneously by immersing it in water.

The products were washed out from the reactor with tetrahydrofuran (THF) and separated into THF-solubles and THF-insolubles. The insoluble matter was transferred to a Soxhlet thimble and was extracted under a nitrogen atmosphere for 24 h. The THF was removed from the soluble portion in a rotary evaporator and the solid residue rinsed with acetone and pentane to remove any residual THF. Both the soluble and insoluble portions were dried under vacuum for 12 h. Total coal conversion was defined on basis of the final weight of THF-insoluble matter.

In addition to coprocessing reactions, a series of baseline experiments were performed. Thermal stability tests of the petroleum resids were carried out in order to assess the amount of THF-insoluble matter resulting from the petroleum resids directly and similarly coal was reacted alone (in the absence of a solvent) under the same reactions conditions. Unreacted (raw) coal was also extracted with THF to determine the extractable amount of coal. The amount of THF-insoluble was corrected for the amount produced from resid thermal stressing before calculating the coal conversion.

The petroleum resids were fractionated into pentane-soluble and pentane-insoluble. The pentane-solubles were analyzed by GC and, when possible, with GC-MS. The coal and the solid residue were characterized by CPMAS. The insoluble residue samples were embedded in an epoxy resin and their surfaces were polished for optical microscopy. An optical microscope with reflected polarized light was used to identify anisotropic structures in the produced solid residues.

RESULTS AND DISCUSSION

Reactions were conducted in nitrogen and hydrogen atmospheres in order to determine the influence of molecular hydrogen on coal conversion. The increase in coal conversion due to hydrogen gas was estimated by the difference of the results of coal blank (no solvent) experiments under hydrogen and nitrogen at a given temperature of reaction. These results are shown in Table 3. The first observation is that presence of hydrogen increased the conversion of the two lower rank coals more than the conversion of the higher rank coals, especially at 450° C. The lower rank coals also seem to be least sensitive to molecular hydrogen at 400° C. These results agree with the observations reported by Mochida et al. (2) that higher rank coals prefer lower temperatures, while the lower rank coals prefer higher reaction temperatures. The authors relate this to the structure of the coals and the strengths of the bonds which are inversely proportionate to the preferred reaction temperature.

We previously reported (3) the results of reactions of coal with model compound solvents. For all coals, the conversions were highest at 400° C with the exception of reactions involving pyrene. Reactions with pyrene gave the highest conversion compared to the alkylated benzenes and n-alkanes, but overall, the conversions with any solvent were better than in the absence of a solvent. Also we observed that different coals reacted differently in a hydrogen and nitrogen atmosphere in the presence of a solvent. The lower rank coals actually gave higher conversions at 400° C (and in some cases at 450° C) under nitrogen, while the higher rank coals benefited from the presence of hydrogen gas. These observations indicate that coals of different rank react differently and have different response to hydrogenation and solvation conditions. Non-donor solvents under H₂ overpressure decreased the conversion for the lower rank coals compared to the blank runs and compared to the reactions under N₂. It has been reported in the literature that lower rank coals require a better hydrogen donor especially at elevated temperatures, due to the greater number of reactive species resulting from the broken crosslinks (2) and because of the smaller size of the polyaromatic structures in these coals (4).

The results of coal conversion for the coal/resid reactions based on solubility in THF are presented in Table 4. Similarly as in the model compound studies, the coprocessing experiments yielded highest conversions at 400° C. The reactions at this temperature seem to be governed by the nature of the coal, because there is little influence of the different petroleum resids. Even between the different coals there is not significant difference at 400° C. This fact is emphasized because of the great range in results when the reaction temperature is increased to 450° C. In this case the influence of the resid feedstock is evident as well as the interactions between the coal/resid pairs. The conversions at 450° C decrease compared to the previous temperature for all coal/resid pairs

but there is obviously an influence of the resids as shown by the differences between the values in Table 4 for one coal compared to those between different coals. Figures 1 and 2 show the variation of coal conversion with temperature and coal/resid feedstock pairs.

The interactions in a coprocessing system are both physical and chemical. At 350° and 400° C the dominant effect is the dissolution of the coal particles in the solvent. At these temperatures it is predominantly a physical process because no effect of the petroleum resid (solvent) is noticed and the range of coal conversion values is small. Whether the solvent (resid) acts as a donor or a non-donor is still not a significant effect at these temperatures (5). As the temperature increases the physical dissolution of coal particles reaches a limit, and the petroleum resid undergoes chemical changes at the elevated temperature. (Note that the resids produced significant amounts of THF-insolubles only at 450° C.)

We had reported earlier (3) that the coal conversion results of the coal/resid reactions were similar to those when pyrene was in the system. This would imply that the resids act as hydrogen shuttlers. Other reported investigations indicate that indeed petroleum resids act as shuttlers rather than donors (6). The aromatic compounds present in petroleum resids can act as hydrogen shuttlers. The aromaticities of the petroleum resids used in this project, determined by NMR are shown in Table 2.

In addition to following the degree of conversion by solubility of the products in THF, optical microscopy was used to study the morphology of the solid residues. The polarized light enabled identification of isotropic versus anisotropic material. Optical microscopy of the THF-insoluble residue show that the solids are in most part isotropic when the temperature of reaction is 350° and 400° C. Anisotropic structures are detected in the solid residue from coal/resid reactions that has seen temperatures of 450° C. A closer examination of the anisotropic structures indicates that anisotropy occurs at the contact between the coal and petroleum resid particles. The resid particles surround the coal particles, which later fuse. Figure 3 shows the optical micrograph of the THF-insoluble residue obtained from reaction of PSOC 1488 subbituminous coal with Blend resid at 450° C. The lighter spots represent the anisotropic structures surrounding isotropic coal particles which are fused together. Anisotropic structures formed solely from petroleum the resid are present also. Davis et al (7) compared the THF-insoluble residue of a high volatile A and high volatile C coal and found anisotropy only in the case of the high volatile A coal. Therefore, the anisotropic structures found in the residue of the coprocessing reactions, regardless of the coal rank are attributed to the presence of the petroleum resids in the system and the coal/resid interactions.

The optical textures of the solids exhibit differences depending on the coal used in the reaction. Differences observed can be correlated to the thermoplastic properties of the coals. The higher rank coal (PSOC 1504) with a FSI of 5.5 produced solids which had pores as a result of swelling. Figure 4 shows the optical micrograph of the THF-insoluble residue obtained from reactions of PSOC 1504 with Blend resid at 400° C. The isotropic coal particles contain pores which are a result of swelling. The lower rank coal (PSOC 1488) has a FSI of 0 and does not pass through a plastic range so the solid particles under the microscope showed mostly sharp cracks as a result of devolatilization. This can be correlated with the degree of coal conversion. Namely, the coal exhibiting strong thermoplastic properties (PSOC 1504) under same reaction conditions achieves higher coal conversion than the coal that does not pass through a plastic range. These result again indicate that the structural components of the coals play an important role in the interactions during coprocessing and ultimately enhance or reduce the formation of undesirable semi-coke structures.

CONCLUSIONS

The results from coprocessing of five coals of different rank with three petroleum resids indicate that the degree of coal conversion depends on the nature of the coal as well as the nature of the resids. The conversions were optimum at 400° C where the reactions seem to be governed strongly by the coal. At temperatures up to 400° C the results indicate that the dominant effect is the dissolution of the coal particles in the solvent. The nature of the resid and especially its donor abilities, effect the conversion at temperatures higher than 400° C. The petroleum resid has undergone chemical changes above this temperature and the interactions of the coal and petroleum resids become an important factor in the conversion to light weight products. This is evident under an optical microscope where anisotropic structures were detected especially at the contact between the coal and petroleum resid particles. The morphology of the particles in the insoluble residue also indicate that thermoplastic properties of coals can be related to their reactivity under coprocessing conditions. The coal exhibiting stronger thermoplastic behavior also showed to be more reactive for coprocessing. Higher thermoplasticity is an indicator of greater mobility of structural fragments leading to higher coal conversions.

ACKNOWLEDGEMENTS

The authors are pleased to acknowledge the financial support for this research provided by the U.S. Department of Energy. The assistance of Dr. Semih Eser with optical microscopy results is greatly appreciated. We are also grateful for the assistance of Dr. O.P. Mahajan of Amoco Corporation and Dr. G.E. Dolbear of Unocal in obtaining the resid samples. We have also enjoyed useful discussions with Drs. Bruce Utz and Karl Schroeder of the Pittsburgh Energy Technology Center (DOE).

LITERATURE CITED

1. Curtis, C. W., and R. A. Winschel, in "Coal Liquefaction : A Research Needs Assessment Technical Background" DOE/ER-0400, Final Report, Vol II, February 1989.
2. Mochida, I., Kishino, M., Sakanishi, K. Korai, Y., and Takahashi, R., *Energy & Fuels*, 1987, 1, 343.
3. Tomic, J., and H. H. Schobert, *Am.Chem.Soc.,Div. Fuel. Chem. Preprints*, 1991, 36(2), 617.
4. Malhotra, R., and D. McMillen, *Energy & Fuels*, 1990, 4, 184.
5. Neavel, R., *Fuel*, 1976, 55, 237.
6. Rahimi, P. M., W. H. Dawson, and J. F. Kelly, *Fuel*, 1991, 70, 95.
7. Davis, A., Mitchell, F. J., Derbyshire, F. J., Rathbone, R. F., and R. Lin, *Fuel*, 1991, 70, 352.

Table 1. Analyses of Project Coals.

Coal (rank)	PSOC 1488 subB	PSOC 1498 hvCb	PSOC 1501 hvBb	PSOC 1504 hvAb	PSOC 1448 hvAb
%C (dmmf)	76.56	78.24	81.17	82.88	85.20
%H	5.27	5.50	5.32	5.86	6.12
%N	0.95	1.83	1.56	1.77	1.86
%O	17.22	14.43	11.95	9.49	6.81
FSI	0.0	0.5	2.0	5.5	8.0
max fluid, T°C	n/a	n/a	421	433	438

Table 2. Analyses of Petroleum Feedstock.

	Hondo	W. Texas FHC-470	Blend FHC-571
Oils (wt.%)	43.9	39.4	21.4
Resins	40.2	59.1	62.8
Asphaltenes	15.9	0.5	14.8
%C	83.40	86.39	83.91
%H	11.80	11.23	10.26
%S	5.10	0.68	4.8
C _{ar} (%) ^a	25.4	28.5	32.3
H _{ar} (%) ^a	8.1	8.2	9.3

^a determined by NMR

Table 3. Increase in coal conversion (wt%) by hydrogenation at three temperatures.

Coal	350°	400°	450°
PSOC 1488	5.49	5.11	11.7
PSOC 1498	4.06	1.9	7.9
PSOC 1501	1.81	3.26	1.92
PSOC 1504	2.75	1.11	3.59
PSOC 1448	4.5	3.58	2.26

Table 4. Total coal conversion for coal/resid reactions at 30 minutes.

Resids	350°	400°	450°	350°	400°	450°
	N ₂			H ₂		
	PSOC 1488					
Hondo	17.61	28.63	6.86	5.46	27.29	9.93
Blend	17.73	28.46	3.45	17.35	31.32	-13.54
W.Texas	14.81	28.87	19.31	19.95	33.03	16.99
	PSOC 1498					
Hondo	12.41	22.53	3.21	7.88	22.79	48.68
Blend	11.41	24.83	0.17	11.56	27.93	-2.7
W.Texas	9.92	23.61	21.08	16.5	26.82	12.83
	PSOC 1501					
Hondo	14.99	29.92	13.4	13.36	28.89	12.41
Blend	12.36	29.5	-0.39	14.75	31.75	20.99
W.Texas	15.2	29.51	26.91	20.89	31	25.85
	PSOC 1504					
Hondo	19.14	36.54	16.53	17.38	31.3	16.66
Blend	13.73	31.94	2.54	16.48	33.94	0.52
W.Texas	13.36	33.66	26.99	14.73	31.98	28.91
	PSOC 1448					
Hondo	17.33	31.87	14.37	16.45	36.2	15.26
Blend	16.24	33.85	-0.46	14.07	32.78	6.88
W.Texas	17.5	32.35	25.99	15.26	36.39	29.05

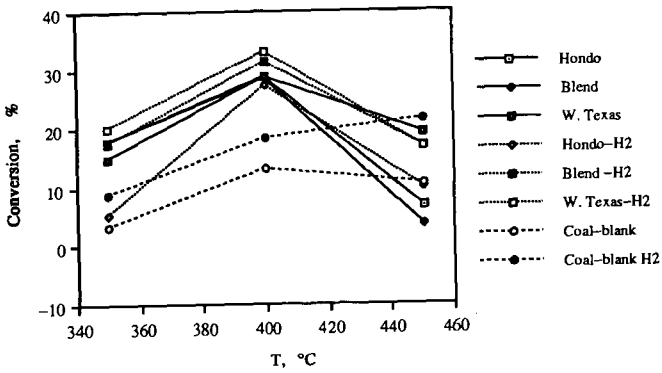


Figure 1. Coal conversion of subB coal (PSOC 1488) at three reaction temperatures under hydrogen and nitrogen atmospheres with three petroleum resid.

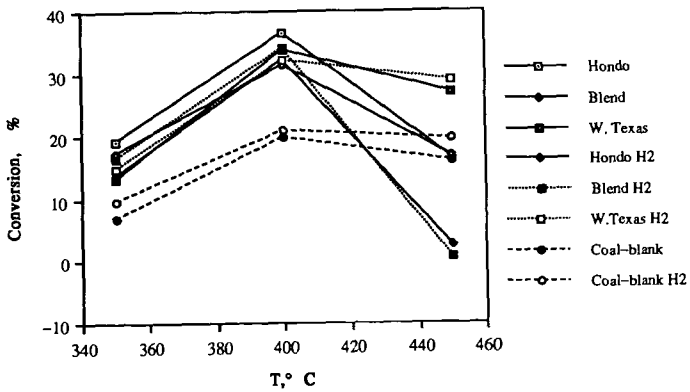


Figure 2. Coal conversion of hvAb coal (PSOC 1504) at three reaction temperatures under hydrogen and nitrogen atmospheres with three petroleum resid.

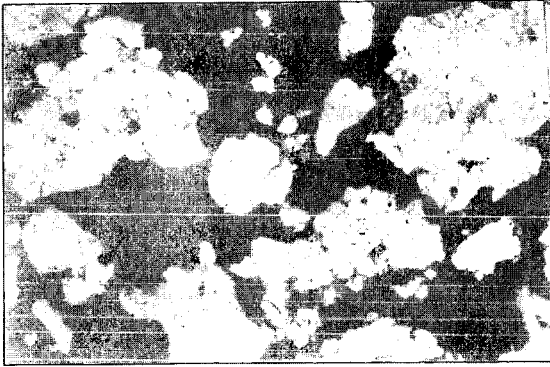


Figure 3. Optical micrograph of the THF-insoluble residue obtained from PSOC 1488 (subB) with Blend resid at 450° C.



Figure 4. Optical micrograph of the THF-insoluble residue obtained from PSOC 1504 (hVCb) with Blend resid at 450° C.

THE FLUIDIZED BED PYROLYSIS CHARACTERISTICS OF MOROCCAN OIL SHALE

U. M. Graham¹, O. Bekri² and T. L. Robl¹.

¹Center for Applied Energy Research, University of Kentucky,
3572 Iron Works Pike Lexington, KY 40511;

²Office National De Recherches Et D'Exploitations
Petrolieres, Rabat, Morocco.

Keywords: Fluidized bed, oil yields, material balances.

ABSTRACT. Pyrolysis characteristics of oil shales from the Timahdit and Tarfaya deposits were investigated in fixed bed, nitrogen swept fixed bed and fluidized bed pyrolysis. The objectives of this work were to determine the effects of pyrolysis conditions on product yields and distribution of the pyrolysed shales. Samples representative of two lithologic units (M_1 and T_4), which comprise part of the richest zone of the Timahdit oil shale formation and samples representative of five zones (R_0 , R_1 , R_2 , R_3 and R_4) of Tarfaya deposit were examined. The shales are primarily carbonates, averaging 12.9 (Timahdit) and 11.3 (Tarfaya) percent organic carbon. Modified Fischer assay for the shales resulted in oil yields ranging between 13.2 and 20.4 gal/ton. Fluidization resulted in shale oil yields ranging from 133 - 157 percent of modified Fischer Assays.

INTRODUCTION. Large deposits of oil shales exist in Morocco. Extensive exploration and processing research has been conducted over the past decades (1). Moroccan oil shale deposits, discovered in the 1960's (1) include those at Guir, Ganntour, Mescala, Oulad Abdown, Tanger, Tarfaya and Timahdit (1-6). Because oil shales are the only abundant indigenous source of fossil fuel in Morocco an extensive resource assessment program has been conducted by Office National de Recherches et D'Exploitations Petroliers (ONAREP). The entire shale oil resources were estimated to amount to 50 billion barrels (2).

Organic carbon contents for Moroccan shales, averaging between 11 and 13 percent, are very similar to both western and eastern US oil shales (2). When western US oil shale technologies are applied to Moroccan shales, a significant amount of carbon is left on the spent shales (2, 4) and large amounts of off-gases are generated. This is similar to the case for eastern US oil shale, where coking and cracking reactions result in high residual carbon and large off-gas volume (7, 8). Fluidized bed retorting has been shown to enhance oil yields when applied to eastern US oil shale by minimizing retrograde oil reactions. This is accomplished by providing rapid heat up and product sweep.

Thus, the objectives of this study are to determine if fluidized bed retorting will enhance oil yields from Moroccan shale and to determine the nature of products produced from the shale. Oil shales from the Timahdit and Tarfaya deposits were selected and the pyrolysis characteristics were investigated using fixed bed, nitrogen swept fixed bed and fluidized bed conditions.

CHARACTERIZATION OF TIMAHDIT AND TARFAYA OIL SHALE DEPOSITS. The Cretaceous Timahdit and Tarfaya oil shale have been under intensive study since 1974 as potential sources of domestic oil (1 - 6). The Timahdit and Tarfaya deposits are among the largest of the

Moroccan oil shales, and are located strategically relative to major cities, potential ports and mining configuration (2). The Timahdit deposit is situated in the Middle Atlas region in the north central part of Morocco, 155 miles southeast of Rabat and 22 miles south of Azrou, and occur in two northeast-southwest trending geosynclines (2). The Tarfaya deposit is located in the south west region along the Atlantic Coast of the Moroccan Sahara. The coastal location is a significant factor in the potential development of this deposit. A comprehensive summary of the previous research relative to the Tarfaya and Timahdit oil shale activities is presented elsewhere (1, 2, 5).

Marlstones, silicious marlstones and limestones comprise the bituminous rocks of the Tarfaya and Timahdit oil shale regions (1, 2). Representative samples from Tarfaya and Timahdit deposits utilized in this study are derived from seven oil shale zones which are further distinguished in 21 sub-zones (Table 1). A considerable variation in zone thickness occurs among the individual beds (Table 1). Samples representative of two lithologic units (M_1 and T_4 , see Table 1), which comprise only part of the hydrocarbon section of the Timahdit deposit (2), were available for study. These two shale beds contain predominantly argillaceous marls. In contrast, the Tarfaya oil shales consist mainly of chalks with varying kerogen contents and are characterized by higher moisture contents compared to those of Timahdit (2). The richest Tarfaya oil shale zone, R-zone, is subdivided into 5 lithologic units (R_0 , R_1 , R_2 , R_3 and R_4), all of which were available in this study (see Table 1).

The seven oil shale samples under investigation were obtained from master batches which were produced from bulk samples derived from individual shale beds. The shales were crushed, blended and screened to 18 x 20 mesh for the pyrolysis study. The shale was stored under argon to retard oxidation. Fixed bed, N_2 -swept fixed bed and fluidized bed runs were conducted using representative sample aliquotes with the same grain size to allow for more precise comparison of the oil yields.

EXPERIMENTAL.

Modified Fischer Assay

A single fixed bed retorting system was used to determine the Fischer Assay pyrolysis characteristics of the seven oil shale zones. A single retort was utilized to eliminate unaccountable systematic errors and to obtain an unbiased base for comparison. Modifications to standard Fischer Assay procedures were employed because it had been previously shown that these running conditions provide for more reproducible results for eastern US oil shales (9, 12). This study's operating conditions included a linear heating rate of 12 °C/min during oil evolution and a 30 minute soak time at maximum retort temperature of 550 °C. The purpose of the modified Fischer Assay experiments was to establish oil yield data for the shale samples that will be used in the fluid bed retort experiments.

N_2 -Swept Fixed Bed Experiments

The fixed bed retorting system is described in detail elsewhere (9). Operationally, a continuous stream of N_2 -gas was allowed to enter the pyrolysis zone after being heated to run temperature (550°C). Preheating of the purge-gas was achieved while passing it through a spiral coil that was encased in the reactor furnace. The N_2 -stream swept oil vapors and a small amount of fines into the product collection system. The purpose of the N_2 -swept fixed bed runs was to determine variations in oil yields caused when the contact time between oil vapors and shale particles was reduced.

Bench Scale Fluidized Bed Experiments

Apparatus: A 1.5 inch diameter reactor as used for fluid bed pyrolysis of Eastern Shales was used in this study. The apparatus has also been described in detail elsewhere (9) and only a brief description is offered here. The retort itself was constructed of 316 stainless steel and has a 100 micron stainless steel filter at the bottom which serves as distributor plate. A stand pipe controlled the spent shale overflow from the bed. To closely monitor the retort conditions three thermocouples were located above the distributor plate at lower, medium and upper bed heights. The retort was enclosed in an electrically heated furnace which further accommodates a gas preheater and a fines trap. The preheater served to heat the fluidizing gas to bed temperature before entering the shale zone. The baffled fines trap helped to remove shale particulates from the oil vapor to diminish coke formation before vapors exit the high temperature zone provided by the furnace. A screw feeder was calibrated to add raw shale at a feeding rate of 2.0 ± 0.1 g/min into the reactor. N_2 purge-gas was passed down from the feed bin and up through the spent shale reservoir into the reactor. A purge-gas flow rate of 0.25 - 0.30 STP L/min was sufficient to prevent oil vapors from escaping through either inlet or exit pipes. Helium gas was used as fluidizing medium. The volumetric He-flow rate at bed temperature (550°C) and pressure (1 atmosphere) was adjusted to 28 L/min and in combination with a shale feed rate of 2.0 g/min provided for a shale residence time of approximately 20 minutes.

The above fluidized bed pyrolyser provides all of the following: good mixing of the shale solids including both raw shale and pyrolysed ash particles; excellent heat transfer; rapid heating rates of the shale particles; and, a uniform pyrolysis temperature of 550°C. In addition, short residence time of oil vapor in the hot zones favors low oil cracking.

Product Collection Traps: The same configuration of product traps used for eastern US oil shales was employed in this study and the reader is referred to the original work (9). Four traps were used to condense the products generated in the fluidized bed retort. The trap closest to the reactor exit pipe, an air-cooled stainless steel tube, condensed a tarry product. The second trap, an Ice/bath, is designed to remove both oil and H_2O from the vapor phase and consists of a closed pyrex tube with gas in- and outlet openings. The third trap, was developed to condense large amounts of products and utilizes thermal wells and densely coiled stainless steel wire spirals for increased precipitation surface (10, 11). The trap itself was immersed in a Dry Ice/isopropanol bath (-78°C). The final trapping system consists of a 50 ml pyrex tube, sealed with a rubber stopper and was immersed in a Dry/Ice isopropanol bath. The exit tube is connected into a hood system and allows non-condensable vapors to be removed. A gas sample can be drawn for analysis of the vapor phase. Gases leaving the product collection apparatus were monitored on a Carle Gas analyser (Series SX-AGC) to determine off-gas weight.

RESULTS AND DISCUSSION. Operating parameters employed in this study are not necessarily optimum running conditions. They were chosen as a basis for this investigation because a large data base is available from previous bench scale fluidized bed retorting on similar materials.

Ultimate and proximate analyses indicate major differences in moisture, ash and sulfur contents between the Timahdit and Tarfaya oil shales under investigation (Table 2). Results of material balances for modified Fischer Assay runs (Table 3) and N_2 -swept fixed bed experiments (Table 4) demonstrate that the latter pyrolysis method caused a slight enhancement in oil recovery. Modified Fischer assay for the shales resulted in oil yields ranging between 13.2 and 20.4 gal/ton and oil yields obtained in the N_2 -swept fixed bed retorting experiments were in the range of 15.7 - 21.6 gal/ton. Therefore, a maximum oil yield increase of 21 percent was achieved by

mobilizing oil vapors with a continuous flow of N_2 gas which reduced the overall residence time of the oil vapors on the shale particles. Also, a decrease in off-gas emission was recorded when N_2 gas mobilized the oil vapors (Table 3, 4), suggesting that vapor phase cracking was reduced. In general, a slightly greater reduction in off-gas emission was recorded for the Tarfaya oil shale samples compared to those of Timahdit. The difference may be related to the higher carbonate and moisture and lower sulfur contents of Tarfaya shales. The results further indicate that oil densities increase for the N_2 -swept fixed bed runs (0.956 - 0.971 g/cm³, Table 4) compared to modified Fischer Assay (0.944 - 0.968 g/cm³, Table 3).

Fluidized bed pyrolysis resulted in oil yields in excess of the modified Fischer Assay and N_2 -swept fixed bed pyrolysis (Table 6 and Figure 1). At this point of study, fluidized bed retorting was performed for three of the seven shale samples. Oil yields obtained from the bench scale fluid bed retort (Table 6) were based on oil collected in the trapping system. The moisture collected simultaneously with the oil was resolved during Karl Fischer water analysis. The C_5^+ hydrocarbon fraction in the off-gas phase was not accounted for in the mass-balance calculations at this time. The C_5^+ concentration was determined to be insignificantly small in the off-gas for either of the fixed bed retort methods employed.

Using the 1.5 inch diameter fluid bed retort, at 550°C operating temperatures 55 to 60 percent of the carbon was removed from the Timahdit shale samples (M_1 and T_4) and 65 percent of the carbon was removed from the Tarfaya shale (R_4). Material balances indicated oil yields for the Timahdit and Tarfaya shale samples to vary between 133 to 157% of those of the Fischer Assay runs (Table 6). A comparison with Eastern shale fluidized bed retorting shows great similarities with respect to overall oil yield and processing behavior.

The fluidized bed retorting of Moroccan oil shales appears very promising from a view point of oil yields. Fluidized beds provide not only enhanced oil yields under relatively non-severe conditions (moderate temperatures of 550°C at atmospheric pressures), but also leave the pyrolysed shale with much less remaining sulfur. This has two potential advantages. The first is lower environmental risks do to lower acid release after exposure to atmosphere. A second is the potential recovery of elemental sulfur, a needed raw material in Morocco.

ACKNOWLEDGEMENTS

The authors gratefully acknowledge the work of D. Thomas and M. Moore for analytical support and D. McLean for sample preparation.

REFERENCES

- 1 Russell P.L., (1990). Oil shales of the world. Their Origin, Occurrence and Exploitation, Chap. 3, Pergamon Press, Oxford, p. 15-30.
- 2 Bekri, O. and Ziad, M.,(1992). Proceedings of the 1991 Eastern Oil Shale Symposium, Lexington, KY (in press).
- 3 Bouchta, R. and Marcil, A., (1981). Moroccan oil shale development program, 6th IIASA Resources Conference, Golden Colorado, pp. 24.
- 4 Bouchta, R., (1985). Oil shale programme in Morocco, Office National de Recherches et d'Exploitations Pétrolières, Oil shale Division, Rabat, Morocco, pp. 21
- 5 Bouchta, R. and Bekri, O., (1981). Oil shale activities in Morocco, Office National de Recherches et d'Exploitations, Rabat, Morocco, pp. 24.
- 6 Anon, (1986). Oil shale in Morocco, research and development activities. A brochure by Office National de Recherche et d'Exploitations Pétrolières, Rabat, Morocco.

- 7 Rubel, A.M. and Carter, S.D., (1984). Symposium on Characterization and Chemistry of Oil Shales, American Chemical Society, St. Louis, 202.
- 8 Margolis M.J., (1982). Proceedings of the 1981 Eastern Oil Shale Symposium, Lexington KY.
- 9 Rubel A.M., Margolis M.J., Haley J.K. and Davis B.H., (1983). Proceedings of Eastern Oil Shale Symposium, IMMR, 89.
- 10 Wallman P.H., Tamm P.W. and Spars B.G., (1981). Oil shale retorting kinetics. Symposium on Oil Shale, Tar Sands, and Related Materials, American Chemical Society, Washington D.C., 163.
- 11 Richardson J.H., Nuss E.B., Ott L.L., Clarkson J.E., Bishop M.O., Gregory L.J., and Morris C.J.,(1982). Fluidized bed pyrolysis of oil shale, oil yield, composition and kinetics. UCID-195648, Lawrence Livermore National Laboratory.
- 12 Coburn T.T., Rubel A.M. and Henson T.S.,(1981). Eastern oil shale retorting: Pyrolysis of the Sunbury shales of Kentucky. IMMR Reprint no. IMMR 81/062, University of Kentucky, Lexington, KY.

TABLE 1 OIL SHALE ZONES FROM TARFAYA AND TIMAHDIT DEPOSITS

DEPOSIT TYPE	SAMPLE ID [sub-zone]	OIL- SHALE ZONES	ZONE THICKNESS [meter]
TARFAYA OIL SHALE DEPOSITS	RON	I RO	1.1
	R-1A	II R1	7.45
	R-1B		
	R-1C		
	R-1D		
	R-1E		
	R-1F		
	R-1G		
	R-2A1	III R2	4.4
	R-2A3		
	R-2B1		
	R-2B2		
	R-2C	IV R3	4.85
	R-3A1		
	R-3A2		
R-3A3			
R-3A4			
R-3A5	V R4	2.2	
R-4B1			
TIMAHDIT OIL SHALE DEPOSITS	T-4	VI T	42.15
	M1-COUCH	VII M	67.35

TABLE 2 PROXIMATE AND ULTIMATE ANALYSES OF MOROCCAN OIL SHALE DEPOSITS

SAMPLE ID	MOISTURE wt %	VOLATILES wt %	ASH wt %	FIXED CARBON wt %	1*		2*	
					C wt %	H wt %	N wt %	S wt %
TARFAYA OIL SHALE DEPOSIT								
RON	2.39	40.3	56.33	1.1	16.88	1.41	0.63	0.19
R-1A	2.77	41.8	54.86	0.6	18.88	1.92	0.84	0.98
R-1B	3.91	39.4	55.87	0.8	14.82	1.29	0.62	0.15
R-1C	4.67	41.8	52.86	0.7	19.02	2.07	0.83	0.35
R-1D	6.61	42.3	49.76	1.3	19.06	2.44	0.76	0.39
R-1E	4.44	44.1	51.73		19.93	2.14	0.83	0.48
R-1F	2.47	47.7	49.62	0.2	21.84	2.01	0.82	0.47
R-1G	7.04	43.2	49.96	0	19.14	2.23	0.79	0.46
R-2A1	1.98	41.5	55.38	1.2	14.7	0.94	0.52	0.17
R-2A3	4.68	39.7	53.37	2.2	17.4	1.74	0.7	0.32
R-2B1	8.12	40.7	49.71	1.5	15.44	1.8	0.52	0.08
R-2B2	5.45	42.9	51.31	0.3	15.43	1.46	0.54	0.19
R-2C	3.01	42.2	53.77	1.1	13.9	1.03	0.57	0.13
R-3A1	6.47	43.6	49.71	0.2	18.31	1.95	0.76	0.29
R-3A2	5.15	40.9	52.83	1.1	17.6	1.78	0.7	0.37
R-3A3	3.54	48.1	48.14	0.3	22.23	2.27	0.31	0.52
R-3A4	5.91	47.1	46.13	0.9	20.98	2.36	0.81	0.39
R-3A5	7.75	38.9	52.36	1.1	15.16	1.8	0.53	0.23
R-4B1	7.05	44.1	48.59	0.3	19.16	2.19	0.67	0.39
TIMAHDIT OIL SHALE DEPOSIT								
T-4	2.79	29.5	65.31	2.4	15.65	1.63	0.78	1.44
M1-COUCH	1.8	36.4	60.94	0.9	19.77	1.85	0.77	1.9

1* organic + inorganic C

2* organic + inorganic S

TABLE 3 MATERIAL RECOVERY FROM MODIFIED FISCHER ASSAY

SHALE MATERIAL	R0	R1	R2	R3	R4	M	T
	wt %	wt %	wt %	wt %	wt %	wt %	wt %
SPEND SHALE	81.4	76.55	89.57	77.08	75.11	85.07	83.16
H2O	9.26	12.08	4.11	14.02	13.01	4.44	7.27
OIL	6.72	7.94	5.33	8.22	8.19	7.09	6.19
GAS	1.82	3.45	1.02		3.75	3.33	3.41

TABLE 4 MATERIAL RECOVERY FROM N2-SWEPT FIXED BED

MATERIAL	R0 wt %	R1 wt %	R2 wt %	R3 wt %	R4 wt %	M wt %	T wt %
SPEND SHALE	81.45	76.21	88.89	77.52	75.05	83.17	81.74
H2O	9.35	12.99	3.99	14.29	14.11	4.97	7.31
OIL	7.41	8.27	6.31	8.41	8.25	8.69	7.88
GAS	1.77	2.56	0.77		2.61	3.12	3.06

TABLE 5 OIL YIELD AND OIL DENSITY OF PYROLOYSED SHALES

ZONE	FA		N2-FA	
	[gal/ton]	OIL DENSITY	[gal/ton]	OIL DENSITY
R0	16.97	0.949	18.57	0.956
R1	19.92	0.955	20.66	0.959
R2	13.29	0.959	15.68	0.964
R3	20.39	0.966	20.79	0.969
R4	20.27	0.968	20.38	0.971
T	15.71	0.944	19.66	0.61
M	17.92	0.948	21.58	0.965

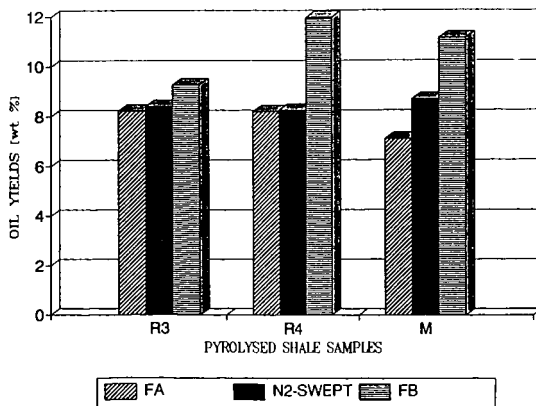
TABLE 6

YIELDS FOR FLUID BED RETORT

ZONE	OIL wt %	1* FB vs. FA %
R3	9.28	133
R4	11.96	146
M	11.13	157

1* percent oil yields of Fischer Assays

FIGURE 1 COMPARISON OF OIL YIELDS



**THE OXIDATION OF THE KEROGEN OF CHATTANOOGA SHALE
WITH ALKALINE PERMANGANATE AND CHROMIC ACID**

Melissa Rogers and Chris W. McGowan

Department of Chemistry, Tennessee Technological University
Cookeville Tennessee 38505

Keywords: oil shale, kerogen, oxidation

INTRODUCTION

The majority of the organic material in oil shales is present in the form of kerogen. Kerogen is a high molecular weight heteropolymer which is insoluble in common organic solvents. Due to the interferences inherent in the analysis of such material, data obtained from raw kerogen concentrates is somewhat limited and valid only on a statistical basis. One method used to more thoroughly characterize the kerogen structure is to break down the polymeric matrix by controlled oxidation followed by analysis of the oxidation products.

Several methods have previously been used to oxidize Chattanooga Shale and kerogen concentrates derived from the shale. Leonard (1) used 3.5 percent ozone to oxidize shale samples and a kerogen concentrate. Water and ether soluble acids were extracted from the oxidized material. Products consisted primarily of aliphatic hydroxy acids. A later study by Kinney and Leonard (2) produced highly oxygenated ether and water soluble acids. Kinney and Schwartz (3) oxidized Chattanooga Shale with air at 200°C for 200 hours in order to maximize the production of humic acids. The acids obtained were quinoid in nature and similar to those obtained from coal. Stanton and co-workers (4,5,6) utilized a stepwise oxidation with perchloric acid to oxidize Chattanooga Shale. The primary products were highly polar, unsaturated carboxylic acids. A model for the structure of the kerogen in Chattanooga Shale was proposed by Stanton et al. (6). The model consisted of highly condensed aromatic material with alkyl side chains. Ether oxygen was a major crosslink in the kerogen matrix.

This paper describes the characterization of two kerogen samples derived from Chattanooga Shale by oxidative degradation with alkaline potassium permanganate and chromic acid. The oxidation products were separated into acidic and basic fractions. Samples were analyzed by fourier transform infrared spectrophotometry (FTIR) and gas chromatography (GC). Selected samples were analyzed by gas chromatography coupled to mass spectrometry (GC-MS).

EXPERIMENTAL

A sample of the Gassaway member of the Chattanooga Shale was obtained from the Eastern Highland Rim area of Tennessee. The sample was ground to minus 60 mesh in preparation for demineralization and bitumen extraction. A 1000-g sample was demineralized using a combination of hydrochloric and hydrofluoric acids (5). Bitumens were removed by soxhlet extractions with benzene and methanol. The kerogen concentrate obtained had a mass of 235.1 g. A kerogen concentrate previously prepared by Stanton (4,5) was also used in this study.

Both kerogen samples were oxidized with alkaline permanganate solution. Samples having a mass of approximately two grams were oxidized in a stepwise manner using 100-mL aliquots of a 0.06 molar potassium permanganate solution in 1.6 percent potassium hydroxide. The solution was heated to 90°C until complete permanganate consumption was indicated by the loss of purple and green colors in the reaction flask. The mixture was filtered at the end of each reaction step and the residue washed with 1.6 percent potassium hydroxide to insure complete product removal. Neutral and basic molecules were separated from the aqueous product mixture by ether extractions. The remaining aqueous phase was then acidified and extracted with ether to remove the ether soluble acids. Precipitated acids which formed at this stage were also collected. All extractions were performed in three steps with one hour allowed for partitioning between the phases in each step. The remaining aqueous solution was essentially colorless, indicating a low concentration of water soluble acids. No effort was made to recover these compounds. The residue from alkaline permanganate oxidation contained large amounts of manganese dioxide, which was removed by treatment with oxalic acid in order to determine the mass of the remaining organic material. The residue from one sample dissolved completely, indicating that the kerogen sample had been entirely converted to soluble species.

A 14-g sample of the kerogen concentrate was also oxidized in a stepwise manner using 3.0 M chromic acid solution and successively longer oxidation steps. The time periods of the oxidation steps were 3, 6, 12, 24, and 48 hours. The oxidation products were separated at the end of each step by a series of extractions. Heptane and ether extractions removed the oxidation products from the aqueous solution. These extracts were then extracted with 6.0 M sodium hydroxide in order to separate the basic fraction of the products. The sodium hydroxide solutions were then back-extracted with heptane or ether to isolate the basic products.

The raw kerogen concentrate was analyzed by X-ray diffraction (XRD) and scanning electron microscopy using energy dispersive X-rays (SEM-EDX) in order to determine the identity of any resistant mineral material. Oxidation products obtained from alkaline permanganate and chromic acid oxidations were analyzed using FTIR, GC, and GC-MS. Infrared spectra were obtained by

using thin films and potassium bromide pellets with a Nicolet 20 DXB FTIR Spectrometer. Gas chromatograms of the neutral and basic fractions, and of the methyl esters of the ether and heptane soluble acids were obtained on a Perkin-Elmer 8500 Gas Chromatograph with an SGE SPB-5 capillary column. Selected samples were analyzed by GC-MS using a Hewlett Packard 5987 gas chromatograph/mass spectrometer with a similar column.

RESULTS AND DISCUSSION

The kerogen concentrate was 17.1 percent ash. The ash was brick red in color. After dissolution, iron was determined spectrophotometrically with 1,10-phenanthroline (7). The ash was found to be 55.4 percent iron(III) oxide. Scanning electron microscopy of the kerogen concentrate indicated the presence of iron and sulfur. X-ray diffraction confirmed these findings and indicated that the mineral material consisted almost exclusively of pyrite. This was expected as pyrite is not removed by the demineralization procedure. By comparison, inorganic ash made up 33.8 percent of the kerogen concentrate prepared by Stanton. The difference is due mainly to the somewhat irregular distribution of pyrite in the Chattanooga Shale.

The oxidation products obtained from both alkaline permanganate and chromic acid oxidations were separated into basic and acidic fractions. Chromic acid oxidation products were further separated into heptane and ether soluble fractions. Alkaline permanganate oxidation also produced considerable high molecular weight acids which precipitated from solution. These precipitated acids remained complex enough to make analysis difficult. Therefore, 50-mg samples of precipitated acids from several steps were further oxidized with 10-mL portions of 0.06 alkaline permanganate. These reactions were carried out using microscale apparatus. Products were separated in a manner similar to the original permanganate oxidations, the exception being that any precipitated acids formed were returned to the reaction flask.

Product mass data for the alkaline permanganate oxidations reveal some interesting differences between the two samples. While the recovery of basic material and soluble acids is very similar, that of precipitated acids and residual material is quite distinct. The kerogen concentrate with 33.8 percent ash (Table 1) produced only moderate amounts of precipitated material and left no residue. Slightly less than 30 percent of the original sample weight was recovered as oxidation products. This suggests that large amounts of the structure were oxidized to carbon dioxide and other light molecules which would be lost. The kerogen concentrate with 17.1 percent ash (Table 2) produced large amounts of precipitated acids as well as considerable residual material. One hundred thirty percent of the initial sample weight was recovered as oxidation products and residual material. This represents not only the retention of much of the initial structure but also the incorporation of large amounts of oxygen. This data appears to indicate some significant

heterogeneities in the kerogen of the Chattanooga Shale, although no definite conclusions may be drawn on the basis of two samples. Chromic acid oxidation of the 17.1 percent ash sample (Table 3) produced generally low product recovery. This is consistent with oxidation of only the more reactive sites of this resistant material.

Infrared spectra were obtained for all fractions. Spectra for both acidic and basic fractions indicated the presence of both aromatic and aliphatic material. Basic fractions were found to contain hydroxyl and amide groups, as well as various substituted benzenes. The presence of ether functionalities and both aromatic and aliphatic ester groups was indicated, as were quinone structures. Spectra of acidic fractions were dominated by peaks attributable to carboxylic acid groups. Aromatic ethers, alcohols, phenols, and thiols were also present. The spectra of precipitated acids were similar to those of soluble acids. The major difference between the two was that oxygen containing functional groups were more dominant in the precipitated acid fraction and aliphatic material was greatly reduced.

Gas chromatograms were obtained for all basic fractions. The acidic fractions were converted to methyl esters using boron trifluoride in methanol (8). Gas chromatograms were then recorded for the methyl esters of all acidic fractions with the exception of the precipitated acids produced by alkaline permanganate oxidation. Chromatograms were obtained for the degradation products of the precipitated acids. Gas chromatography data indicated a broad diversity of products.

Selected samples from each product type were analyzed by gas chromatography-mass spectrometry. Preliminary analysis of the mass spectra obtained has confirmed the presence of both aromatic and aliphatic material. Both acidic and basic fractions contained multisubstituted benzenes, saturated and unsaturated cyclic structural units, and long alkyl chains. n-Alkane chains containing up to thirty carbons have been identified. The basic fractions were found to contain amines, alcohols, thiols, and esters. Hydrocarbons and alcohol functionalities were dominant. Carbon skeletons consist primarily of disubstituted benzenes, multisubstituted cyclohexanes, and n-alkyl chains. Molecular sizes range from sixteen to twenty-seven carbons. The acidic fractions were esterified prior to analysis, and the spectra of these samples were characterized by peaks attributable to the ester functionality. The compounds were interpreted as originally being mono- and poly-carboxylic acids. Carbon skeletons consisted of mono-, di-, and tri-substituted benzenes, phenols, cyclic groups, and n-alkyl chains. Molecular sizes range from ten to thirty carbons.

CONCLUSIONS

A kerogen concentrate derived from the Chattanooga Shale was oxidized in a stepwise manner with alkaline potassium permanganate and chromic acid. Infrared analysis of the oxidation products indicated the presence of aromatic and aliphatic material. Functionalities included alcohols, thiols, phenols, ethers, esters, quinones, and carboxylic acid groups. Gas chromatography-mass spectrometry analysis of selected oxidation products confirmed that both aromatic and aliphatic material was present in the oxidation products. Carbon skeletons of the products were found to consist of substituted benzenes, saturated and unsaturated cyclic structures, and n-alkyl chains. Molecular sizes ranged from ten to thirty carbons. The largest molecules were interpreted as n-alkanes and n-saturated monocarboxylic acids. Aromatic material was typically multifunctional, and was probably responsible for most of the cross-linking within the kerogen. This data will be used to suggest modifications to the structure of Chattanooga Shale kerogen proposed by Stanton (6). Several basic modifications to the structure are in order. Sulfur and nitrogen containing compounds are confirmed in the oxidation products and amine, amide, and thiol groups should be introduced into the model. Alkyl chains of up to thirty carbons should also be included, essentially doubling the length of those in the present model. Other groups which should be accommodated include carbon chains with multiple double bonds, phenols, quinones, and disubstituted benzene rings.

ACKNOWLEDGEMENTS

This work was supported by a Tennessee Tech Faculty Research Grant. The authors would like to thank Scott Schlorholtz, Glenn Oren and Warren Straszheim of Iowa State University for the XRD and SEM-EDX analyses. The authors appreciate the efforts of Robin Bright at Tennessee Tech University for developing some of the GC methods. The authors would also like to thank Susana Harwood of the Water Center at Tennessee Tech University for running the GC-MS system. Donation of the samples of Chattanooga Shale by H. Wayne Leimer of the Earth Sciences Department at Tennessee Tech is gratefully acknowledged.

REFERENCES

1. Leonard, J.T., "Ozonolysis of the Organic Matter of Chattanooga Black Shale," Univ. Microfilms (Ann Harbor), L.C. Card No: Mic 59-2987, 1288 (1959).
2. Kinney, C.R. and J.T. Leonard, "Ozonization of Chattanooga Uraniferous Black Shale," J. Chem. Eng. Data, **6**, 474 (1961).
3. Kinney, C.R. and D. Schwartz, "Partial air Oxidation of Chattanooga Uraniferous Shale," Ind. Eng. Chem., **49**, 1125 (1957).

4. Stanton, B.J. and C.W. McGowan, " The Analysis of the Organic Matter in Chattanooga Shale by Oxidation with Perchloric Acid," Prepr. Pap.-Am. Chem. Soc., Div. Fuel Chem., **33**, 449 (1988).
5. Stanton, B.J., R.M. Morris and C.W. McGowan, "The Characterization of the Kerogen of Chattanooga Shale, Part I - the Oxidation of the Chattanooga Shale with Boiling Perchloric Acid," Fuel Process. Technol., **29**, 85 (1991).
6. Stanton, B.J., D.J. Davidson and C.W. McGowan, "The Characterization of the Kerogen of Chattanooga Shale, Part II - Analysis of Oxidation Products and Proposal of a Model of the Structure of Kerogen in Chattanooga Shale," Fuel Process. Technol., **29**, 97 (1991).
7. Diehl, H. and G.F. Smith, Quantitative Analysis, John Wiley and Sons, Inc., New York, 368 (1952).
8. McGowan, C.W. and H. Diehl, "The Oxidation of Green River Oil Shale with Perchloric Acid. Part II - The Analysis of Oxidation Products," Fuel Process. Technol., **10**, 181 (1985).

TABLES

TABLE 1. Product masses (in mg) resulting from the alkaline permanganate oxidation of the kerogen concentrate with 33.8 percent ash

	Basic Fraction	Soluble Acids	Precipitated Acids	Total Product
Step 1	10.2	12.6	8.6	31.4
Step 2	7.0	14.9	69.3	91.2
Step 3	5.0	19.0	33.9	57.9
Step 4	4.0	19.1	43.5	66.6
Step 5	10.6	31.6	55.1	97.3
Step 6	13.5	23.5	61.4	98.4
Step 7	3.7	32.3	48.5	84.5
Step 8	3.3	25.3	35.4	64.0
Step 9	3.4	24.1	19.7	47.2
Step 10	4.4	11.1	0	15.5
Residue				0
Total	65.1mg	213.5mg	375.4mg	654.0mg
Initial sample: 2.2106g				

TABLE 2. Product masses (in mg) resulting from the alkaline permanganate oxidation of the kerogen concentrate with 17.1 percent ash

	Basic Fraction	Soluble Acids	Precipitated Acids	Total Product
Step 1	7.5	22.0	27.1	56.6
Step 2	12.1	21.0	185.2	218.3
Step 3	6.9	21.1	78.9	106.9
Step 4	5.9	32.0	555.7	593.6
Step 5	3.9	32.6	30.8	67.3
Step 6	10.5	29.9	37.2	77.6
Step 7	11.9	29.1	54.5	95.5
Step 8	3.2	31.0	32.4	66.6
Step 9	3.6	14.0	0	17.6
Step 10	8.8	6.0	0	14.8
Residue				1380.3mg
Total	66.8mg	216.7mg	974.7	2638.5mg

Initial sample: 2.0164g

TABLE 3. Product masses (in mg) resulting from the chromic acid oxidation of the kerogen concentrate with 17.1 percent ash

Oxidation Step	Water Soluble Bases	Ether Soluble Bases	Heptane Soluble Bases	Ether Soluble Acids	Heptane Soluble Acids
3 hour	1.0	2.5	0.4	2.3	4.3
6 hour	2.0	41.1	1.1	5.8	3.5
12 hour	43.2	43.3	40.5	6.2	35.2
24 hour	8.4	11.6	7.7	10.4	10.1
48 hour	9.1	8.9	6.9	14.5	6.0
Total	63.7mg	107.4mg	56.6mg	39.2mg	59.1mg

Total product: 326.0mg Residue: 14.1458g
Initial sample: 14.4139g

COKING AND CRACKING REACTIONS OF OIL VAPOR OVER HOT OXIDIZED OIL SHALE

M. F. SINGLETON, C. J. MORRIS, P. H. WALLMAN, and C. B. THORSNESS
Lawrence Livermore National Laboratory, Livermore, California 94550

Keywords: coking, cracking, mineral surfaces, shale oil

ABSTRACT

The investigation of cracking and coking reactions of shale oil vapor in the presence of hot oxidized oil shale is conducted both for its intrinsic importance and in support of the modeling effort on the oil shale process. The model includes mass transfer of vapor through the gas film surrounding the shale particles with countercurrent flow of cracked low-molecular weight products, diffusion through the pore system, adsorption onto the internal surfaces, chemical reaction of the adsorbate, and desorption of oil and light gas. Results from two experimental configurations are related to the model calculations, and the application of coking and cracking in the retort process to upgrade oil product are discussed.

INTRODUCTION

Hot-Recycle-Solids (HRS) oil shale processes^(1,2) provide the heat for reaching pyrolysis temperatures through recycle of a burned shale stream. The intimate contact between primary oil vapors and recycled burned solids results in oil property changes that are mostly favorable but can also result in oil yield loss to coke and noncondensable gases. Previous work at LLNL^(3,4) and at CSIRO in Australia^(5,6) has shown that partial coking of shale oil vapors over oxidized shale minerals can have a favorable oil upgrading effect due to cracking of heavy oil to lighter components. Hence the degree of coking in HRS oil shale processes may provide an opportunity to improve oil quality and at the same time control the undesirable loss of product to excess coking and cracking. As a guide to this optimization we have developed a coking model that is based on the HRS pilot plant process developed at LLNL.

The coking process is quite complex because of its heterogeneous character coupled with its dependence on both oil properties and surface properties⁽³⁾. In many respects it resembles catalytic petroleum crackers in that both processes involve the contact of oil vapors with a hot porous solid. Similar to the deactivation of many solid catalyst, the surface reactions on oxidized shale have been shown⁽⁴⁾ to change with coke buildup leading to a slowdown of the overall coking rate with time.

In the model we assume that the oil is a mixture of three pseudocomponents each with a different boiling point. The diffusion rates and the adsorption equilibria are different for the three components, but the intrinsic coking kinetics are assumed to be the same since experimental data on intrinsic coking rates of specific oil components are not available. We also assume that the three oil components undergo the same coking reaction on the surface to produce coke and light gas with the same stoichiometry (2/3 coke and 1/3 gas). No production of lighter oil components from adsorbed heavy oil has been included since basic kinetic data do not exist. Even with these simplifying assumptions the current model has several adjustable parameters which are determined by matching the model to experimental results.

In our previous study⁽⁴⁾ we used a simple packed-bed reactor with a constant oil feed. With that apparatus, the oil upgrading effect was established: Fig. 1 shows a sample result that compares the boiling point distribution of the feed oil with the product oil distribution after 27% of the oil is coked. The partially coked oil is considerably lighter, and hence more valuable, than the starting oil. In modeling this effect, we make use of the fact that the result in Fig. 1 can be predicted by postulating that coke originates from the heavy end of the boiling point distribution without production of any light oil components. Such an explanation is no doubt a simplification of the real coking/cracking reactions that probably both produce and remove light oil. Nevertheless, this result provides a basis for the simple reaction stoichiometry adopted for the model. In the same study⁽⁴⁾ we determined the intrinsic coking rate of shale oil adsorbed on a non-porous quartz surface. This coking rate was determined on a well-

coked surface, because the fresh surface is covered with coke in a fraction of the total elapsed time of each experiment. For this same reason, the apparatus used in Ref. 4 did not allow determination of coking kinetics over fresh-oxidized porous shale surfaces. In order to relax this limitation we took a different experimental approach in our current work.

EXPERIMENTAL APPROACH

The apparatus shown schematically in Fig.2 consists of a fluidized bed for pyrolyzing a small shale sample followed by a packed bed of oxidized shale where coking reactions occur. An oil-vapor pulse from the fluidized bed enters the packed bed at the inlet and emerges as an altered oil pulse from the outlet. The hydrocarbon concentrations of both of these pulses are determined in separate experiments by oxidizing the oil pulse to $\text{CO}_2 + \text{H}_2\text{O}$ in a combustion tube and monitoring the combustion products by a rapid mass spectrometer. Coke deposited in the packed bed is quantitatively determined by subsequent oxygen addition and burnoff with quantification of the combustion products. A disadvantage of this apparatus relative to the apparatus of Ref. 4 is that the products are destroyed and cannot be used for studying oil property changes. Another experimental limitation is that only dilute vapors (i.e., low oil concentrations) can be studied.

The system was standardized on an Anvil Points, Green River Formation oil shale with a grade of about 24 gallons/ton. Shale sample drops varied from 0.5 to 1.6 grams each. Most of the experiments included a series of sample drops into the fluidized bed with the resulting oil pulses passing through the packed bed followed by burnoff of both beds at the end of each series of drops. Consequently the first oil pulse in each series encountered a freshly oxidized shale surface whereas subsequent oil pulses saw an increasingly coked surface. The size of the packed bed was varied, so that the coke yield would differ relative to the oil pulse. Shorter beds were used for small particles because small particles showed a greater overall coking tendency than did large particles.

COKING MODEL

The basis for the current coking model is a computer code developed at LLNL⁽⁷⁾ for heterogeneous reactions in a porous sphere. This code is quite rigorous; i.e., it incorporates the Stefan-Maxwell relationships for describing diffusion of gas species in the multi-component system. The code also allows for a film resistance around the particle, but this resistance proved to be insignificant for the cases studied here. This general code and the numerical scheme employed for its solution are not discussed in this paper. Rather the emphasis here is on the relationship of the experimental data to the results obtained from the code.

Table 1. Oil Component Properties Used in Model

Component	Boiling Point °C	Molecular Weight	Fraction Wt%	Diffusivity @ 500° C cm ² /s
1	200	155	50	0.27
2	400	338	25	0.17
3	500	451	25	0.15

Properties of the three oil pseudocomponents are specified in Table 1. This selection of components implies a three-point discretization of the continuous boiling-point curve of the shale oil. More components could easily be added. Molecular diffusivities predicted by theory⁽⁸⁾ are also given in Table 1. The effective diffusivities for porous shale are based on the ϵ^2 model⁽⁹⁾. A typical porosity (ϵ) and total surface area of oxidized Green River formation oil shale are 0.3 and 5 m²/g, respectively.

The adsorption equilibrium relationships are based on the Langmuir isotherm⁽⁹⁾ and are given by:

$$K_i \cdot P_i^* = \frac{\theta_i}{1 - (\theta_1 + \theta_2 + \theta_3)}, \quad i = 1, 2, 3 \quad (1)$$

where

K_i = Equilibrium constant of component i (kPa^{-1} , function of temperature)

P_i^* = Equilibrium vapor pressure of component i (kPa)

θ_i = Surface coverage factor for component i ($[\text{Oil}_i, \text{ads}] / [\text{Oil}_{\text{max,ads}}]$)

K_i correlates to the heat of adsorption ΔH_i according to the van't Hoff relationship:

$$K_i = k_0 \exp\left(\frac{\Delta H_i}{RT}\right) \quad (2)$$

where

$$\frac{\Delta H_i}{R} = 10 \cdot T_{\text{boiling point}} \quad (\text{Trouton's rule for heat of condensation})$$

The equilibrium relationships, Eqs. 1 and 2, contain two adjustable parameters: the pre-exponential factor k_0 in Eq. 2 and the total number of sites for adsorption $[\text{Oil}_{\text{max,ads}}]$ appearing in the definition of θ_i .

A third adjustable parameter is the preexponential factor A appearing in the first-order coking rate, Eq. 3, for the intrinsic coking rate on a freshly oxidized surface. The activation energy is assumed to be the same as for the coking rate on a coked surface from Ref. 4 shown for reference in Eq. 4:

$$\frac{d[\text{Oil}_i, \text{ads}]}{dt} = -A \cdot \exp\left(-\frac{19270 \text{ K}}{T}\right) \cdot [\text{Oil}_i, \text{ads}] \quad (\text{mineral surface}) \quad (3)$$

$$\frac{d[\text{Oil}_i, \text{ads}]}{dt} = -10^9 \cdot \exp\left(-\frac{19270 \text{ K}}{T}\right) \cdot [\text{Oil}_i, \text{ads}] \quad (\text{coked surface}) \quad (4)$$

The model uses a weighted average of Eqs. 3 and 4 for the case of a partially coked surface.

RESULTS

The fitted parameters are: $k_0 = 3 \cdot 10^{-7} \text{ kPa}^{-1}$, $[\text{Oil}_{\text{max,ads}}] = 0.6 \text{ mg/m}^2$, and $A = 10^{10} \text{ s}^{-1}$. This set of parameters produces the match of model results (shown as drawn curves) to experimental results (shown as individual points) in Figs. 3 and 4. For plotting the exposure time in these figures, the actual oil pulses have been approximated by assuming rectangular oil pulses instead of the true pyrolysis-kinetic pulses used in both experiment and model calculations.

Figure 3 shows that oxidized shale particle size has a strong effect on overall coking rate and that the overall coking rate declines significantly at a coke coverage of approximately 3 mg/g. The slowdown is particularly strong for the 1-mm particles because the initial overall coking rate for this small particle size is not dominated by pore diffusion. The model matches the slowdown by switching from a combination of Eq. 3 and Eq. 4 to Eq. 4 kinetics only at a coke coverage of 3 mg/g. (There is an order of magnitude change in intrinsic coking rate between the two equations.) The coke coverage of 3 mg/g is equivalent to 0.6 mg/m^2 and corresponds approximately to a monolayer. It is significant that the matching of the model produced the same monolayer limit for the maximum adsorbed oil concentration on the surface.

The two sets of 5-mm particle data in Fig. 3 show the importance of differential reactor conditions. The diamond series used a larger bed than the triangle series, and the consequence is a significant

depletion of cokable reactants across the bed (hence less coke per g of oxidized shale) for this series of experiments.

Figure 4 shows the results of varying the temperature of the oxidized-shale bed. Increasing temperature increases the overall coking rate but not in proportion to the increase in intrinsic coking rate that Eqs. 3 and 4 predict. Pore diffusion is only partially responsible for limiting the overall coking rate increase with temperature; another effect particularly important at low oil coverage of the surface is the reduced adsorbate equilibrium concentration on the surface which is modeled by the equilibrium constant in Eq. 2. (The surface is assumed to be in equilibrium with the local oil vapor within the pore system.)

Figure 4 also shows a result of varying oil concentration at a constant temperature of 502 °C. Oil concentration is seen to have a significant effect on the overall coking rate for the 5-mm particles.

Figure 5 contains model results that address the question of coking at higher oil concentrations. The maximum oil concentration expected in HRS oil shale processes is a few hundred mg oil/l. (The exact concentration depends on the amount of stripping gas.) Fig. 5 shows that increasing oil concentration increases the coke yield but with a proportionality much less than first-order; this result has also been confirmed by experiment. Comparison of Fig. 5(a) and Fig. 5(b) reveals that the increased coke yield with higher oil concentration is due mostly to increased coking in the large particles. This is explained by pore diffusion responding to a higher driving force. The pore-diffusion effect is also evident in the coke profiles of the larger particle sizes: a coke wave penetrates gradually into the 5- and 7.5-mm particles. A distinct coke layer extending from the surface partway into the particle has also been observed visually in partially coked shale bed samples.

CONCLUSIONS AND FUTURE PLANS

We compared experimental data with a model based on physical and chemical phenomena that govern coking of oil vapors over a porous medium. We conclude that mass transfer, phase equilibria and intrinsic chemical kinetics are all important in determining the overall coking rates for oil shale processes where the product-oil vapor contacts an oxidized recycle solid stream. We have used our model to extrapolate the experimental data to higher oil concentrations typical of the HRS processes and to larger particle sizes. Although these extrapolations remain to be confirmed in a newly constructed laboratory apparatus, we are relatively confident that oil losses to coke in the HRS process can be kept to a level of 10-15% of primary oil produced (assuming recycle ratios of 2 to 3). We have also concluded that the physical adsorption step is at least partially responsible for the observed selectivity toward high-boiling components in the heterogeneous coking process. It is likely that the high-boiling components also have higher reactivities than the low-boiling components, and we intend to study possible differences in reactivity as a function of molecular structure. Different reactivities also lead to the question of reaction products: adsorbed oil will no doubt produce lighter oil, not just coke and noncondensable gas. Hence cracking reactions for oil adsorbed on the surface should be added to the two competing processes, coking and desorption, included in this study.

ACKNOWLEDGEMENTS

We wish to thank our colleagues who provided support throughout this project: Bob Cena for his technical and supervisory support, Doug Fields for technical skills and practical advice, Bob Taylor and Bruce Watkins for technical insight and discussion, Roz Swansiger for analytical support. Special thanks to Sharon Crowder for preparing this document and for taking care of a myriad of administrative details. This work performed under the auspices of the U.S. Department of Energy by the Lawrence Livermore National Laboratory under contract number W-7405-Eng-48.

REFERENCES

1. P. W. Tamm, C. A. Bertelsen, G. M. Handel, B. G. Spars and P. H. Wallman "The Chevron STB Oil Shale Retort," *Energy Progress* 2, 37 (1982).

2. A. E. Lewis and R. J. Cena "LLNL Pilot Plant Development – Part I," *Proc. of the Oil Shale and Tar Sand Contractor's Review Meeting*, pp. 72-85, T. C. Bartke, Ed., DOE/METC-90/6111, Morgantown, West Virginia (1990).
3. M. F. Singleton, P. H. Wallman, and R. Mallon, "Oil Cracking and Coking Experiments," *Proc. of the Sixth Briefing on Oil Shale Research*, Lawrence Livermore National Laboratory, Livermore, California, pp. 103-140 (1989).
4. P. H. Wallman, M. F. Singleton, and R. W. Taylor, "Cracking and Coking of Shale Oil Vapors," *23rd Oil Shale Symposium Proc.*, Colorado School of Mines, Golden, Colorado, pp.125-132 (1990).
5. G. C. Wall and P. Udaja, *Fuel* 67, 1340-1343 (1988).
6. P. Udaja and G.J. Duffy, Chensee, M.D. *Fuel* 69, pp. 1150-1154 (1990).
7. S. H. Johnson and A. C. Hindmarsh, "MSRS: A Fortran Code for the Numerical Solution of Solid/Fluid Reactions in Nonisothermal Multispecies Porous Spheres with Stefan-Maxwell Diffusion," *UCRL-21002*, Lawrence Livermore National Laboratory, Livermore, California (1988).
8. R. C. Reid, J. M. Prausnitz, and T. K. Sherwood, *The Properties of Gases and Liquids*, McGraw-Hill, New York (1977).
9. M. Suzuki, *Adsorption Engineering* (Chemical Engineering Monograph 25), Elsevier, Amsterdam (1990).

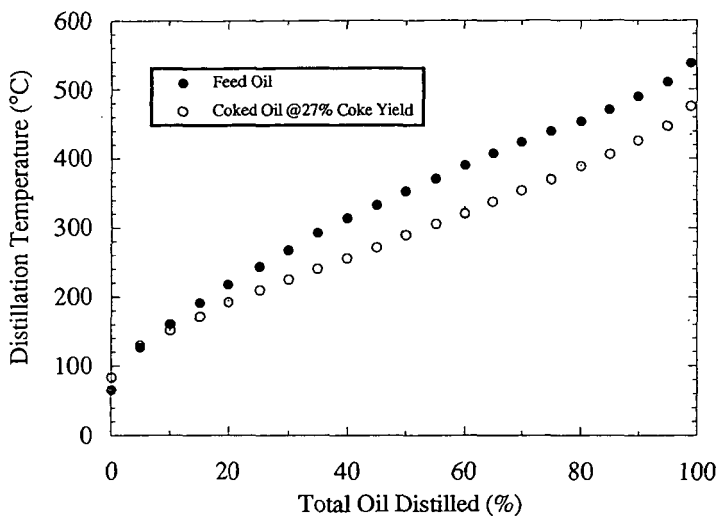


Figure 1 Effect of coking on shale oil boiling point distribution.

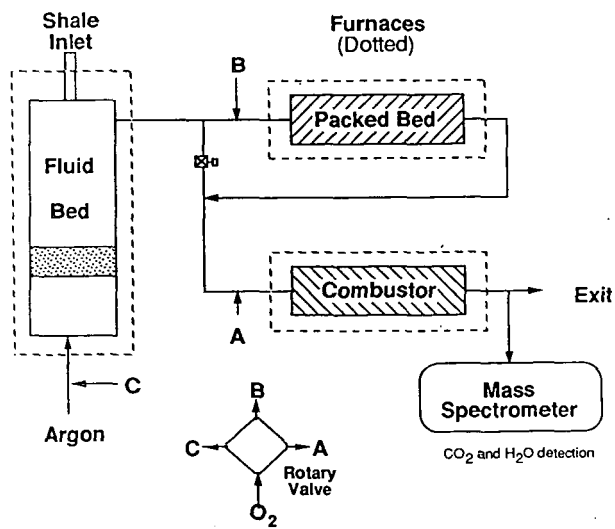


Figure 2 Apparatus for studying coking kinetics.

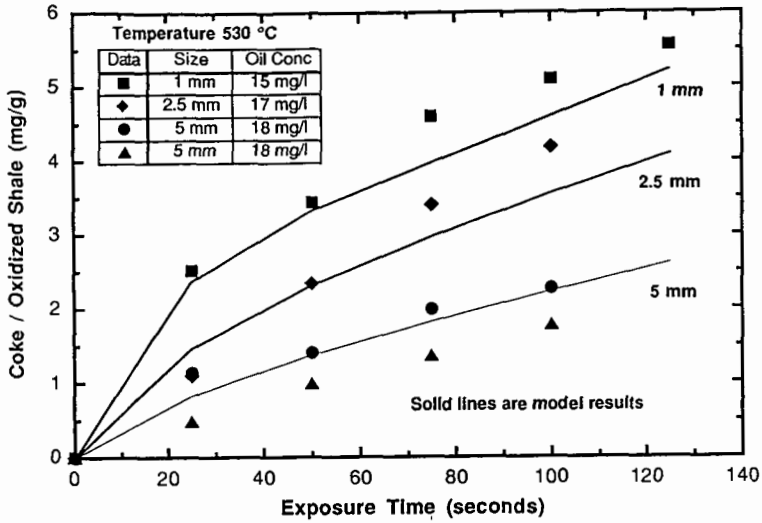


Figure 3 Particle-size effect on coke buildup.

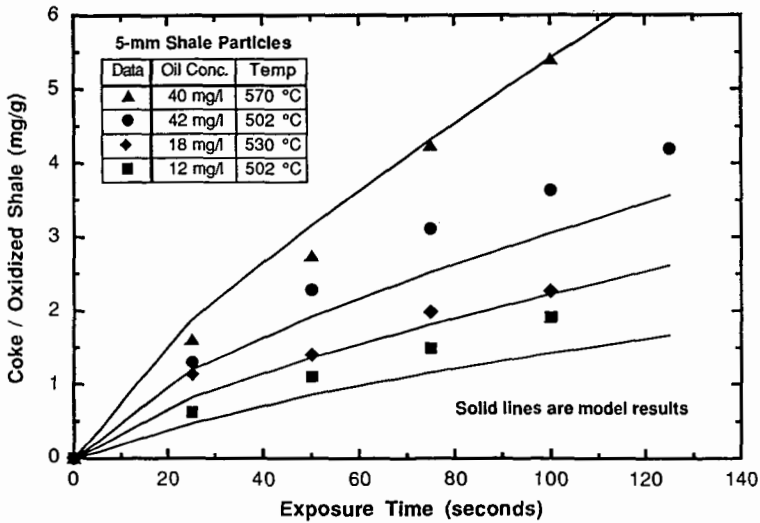


Figure 4 Temperature and oil-concentration effects on coke buildup.

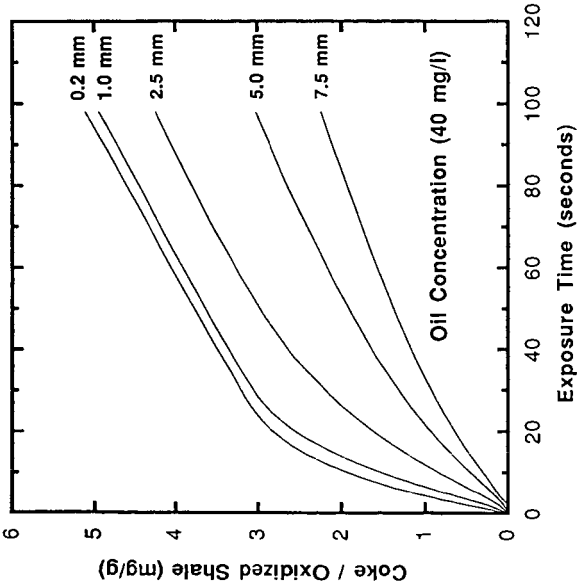


Figure 5 (a)

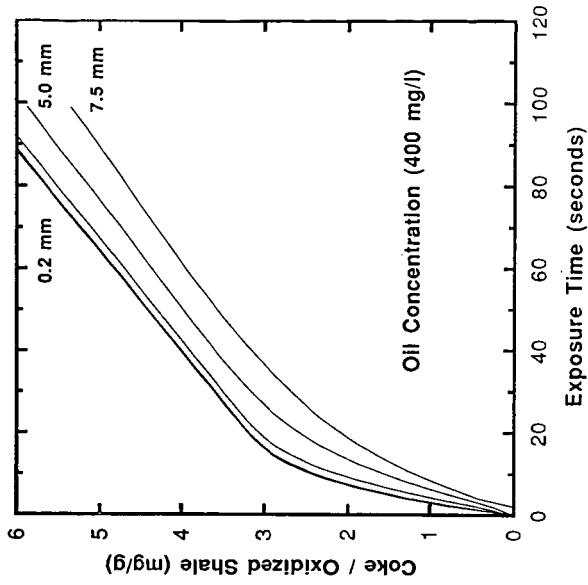


Figure 5 (b)

Figure 5 Model-predicted coke buildup with constant oil vapor concentration at (a) 40 mg oil/l, (b) 400 mg oil/l.

Investigation of product coking induced by hot recycle solids
in the KENTORT II fluidized bed retort.

D.N. Taulbee and S.D. Carter
University of Kentucky-Center for Applied Energy Research
Lexington, KY 40511

Keywords: coke, shale oil coke, fluidized bed.

ABSTRACT. The mechanism and extent to which oil shale pyrolysis products undergo secondary coking reactions is governed to a large degree by the nature and temperature of the surfaces with which these products interact. Since the composition and temperature of the solids utilized to transfer heat in the KENTORT II fluidized-bed reactor can, to some extent, be controlled, it is important to determine the relative coke forming activity of these solids at process temperature in order to maximize product yield. With this objective, an apparatus has been constructed that permits shale oil vapors generated in one fluidized bed to pass over selected substrates in a second fluidized bed. The reactivity of the solid as a function of exposure time is monitored with an on-line mass spectrometer while total carbon deposition is determined post-run by ultimate analysis of the substrate. Over the temperature range of 530-660^o C, the order of substrate reactivity was determined to be kaolinite > combusted shale > illite > gasified shale > pyrolyzed shale > sand. Surface area/pore volume data for the various substrates will be presented and discussed in terms of coking activity.

INTRODUCTION. One of the factors that ultimately controls oil yield during oil shale pyrolysis is the extent of secondary reactions, i.e., cracking and coking, that occur within the reactor¹. These reactions in turn, are governed by several factors including reactor temperature, product residence time, resource properties, and the types of solid surfaces which the vapor phase hydrocarbons contact at elevated temperature. For a given resource, short of resorting to high H₂ partial pressures, the simplest means of enhancing liquid yield is to reduce the product residence time. For this reason, among others, fluidized bed retorting is regarded as an attractive technology for processing the eastern US oil shales, and consequently, has been under continuing development at the UK-CAER since about 1982² in a process termed KENTORT II.

Since one of the more effective means to transfer heat in a fluidized bed reactor is through direct addition of heat carrying solids, solids recycle is thought to be the most practical approach for a large scale operation. Accordingly, a KENTORT II prototype operated at the CAER was designed to simulate commercial operation by recycling hot solids to the pyrolyzer from both a fluidized bed gasifier and combustor. However, delivery of hot solids to the pyrolyzer promotes secondary cracking and coking reactions resulting in lower oil yield. Therefore, since the temperature, concentration, and composition of the heat transfer solids can, to some extent, be controlled in the KENTORT design, it is vital that the reactivity of the heat-carrying solids be characterized at process temperature in order to minimize these detrimental reactions.

Several, often ingenious, strategies have been used to investigate the cracking and coking of shale oil over a solids substrate bed. However, all these techniques have suffered from an inability to closely simulate the solids/HC product interactions that take place in a continuous, solids recycle operation. For example, Levy et al.³ continuously injected Fischer assay shale oil into a reactor where the shale oil was vaporized then passed through a bed of solids. Though informative, the HC stream does not have the same composition or tendency toward coke formation as freshly generated

shale oil vapors, particularly for shale oils that contain significant amounts of non-volatile components. In an investigation reported by Coburn et al.,⁴ a pulse of oil shale was dropped into a fluidized bed pyrolyzer with the resulting vapors passed through a packed bed of solids. While this technique lends itself well to kinetic measurements, it suffers from the fact that the pyrolysis products differ in nature and concentration (and therefore reactivity) as a function of time. Rubel et al.⁵ connected a packed bed pyrolyzer in series with a packed bed of solids in the same furnace then subjected both beds to the same heating profile. While this technique provides information on the relative substrate reactivity, its transient nature is unsuitable for kinetic measurements, nor does it simulate fluidized bed conditions.

To realistically examine both the kinetics and reaction mechanisms, an apparatus has been constructed which permits shale oil vapors generated in one fluidized bed to pass over selected substrates in a second bed. Since the oil product is at no time cooled or removed from the reactor and the time for non-catalyzed secondary reaction to occur is minimal, product loss reactions are thought to closely simulate those that occur within a circulating solids fluid bed reactor. Substrates can be fed in either a batch or continuous mode. In the batch mode, a given substrate is heated to reaction temperature then exposed to shale oil vapors for a selected time period. Carbon deposition onto the solid is monitored in real-time using an on-line mass spectrometer and total deposition verified by elemental analysis of the substrate following exposure.

Because the KENTORT concept utilizes a combination of gasified and combusted shale particles as the heat transfer medium, examination of these materials is emphasized.

EXPERIMENTAL. The oil shale used in this study was the CLE003 master sample from Fleming County, Ky.⁶ The solid substrates examined and reactor conditions used are given in Tables 1 and 2. In addition to examining all of the substrates without pretreatment, aliquots of the gasified and combusted shale were placed in a solution of either 0.005 N NaOH or HCl overnight, thoroughly rinsed with deionized H₂O, then dried prior to testing.

The coking apparatus and procedures used are described in detail elsewhere.⁷ Following is a condensed description.

Apparatus. The apparatus consists of two vertically aligned fluidized beds (7.6 cm i.d.) that share a common fluidizing medium and are heated externally by two dual-zone electrical furnaces (Figure 1). The fluidizing gas, N₂ in this study, is preheated then routed to the lower fluidized bed maintained at 530^o C for all runs. Raw oil shale is metered by a N₂-purged screwfeeder into the lower fluidized bed where the level of solids is maintained at 7.6 cm by an exit standpipe.

In the upper portion of the apparatus, a vertical baffle divides the pipe into two unequal sections (73% and 27% of the cross sectional area). The larger section contains a fluidized bed of solids, and the smaller section provides a bypass-path for the fluidizing stream. A semi-butterfly valve beneath the baffled section selects the upward path for the pyrolysis product stream and is coupled to a three-way valve that routes a balancing gas to injection ports on either side of the baffle such that gas flows through both chambers regardless of the butterfly valve position. The balancing gas flow serves to maintain a constant total N₂ flow from the reactor, fluidize the upper bed, provide a gas seal for the semi-butterfly valve, and in some experiments, is used as a pretreatment gas for the substrate. A purge gas, argon, is introduced into the seal assembly of the semi-butterfly valve to inhibit coke formation and serve as a tracer gas to facilitate mass spectrometer analyses by correcting for pressure surges, changing flowrates, and instrumental fluctuations.

The balancing gas and the pyrolysis/fluidization stream are joined in the uppermost portion of the reactor. A split of this stream is drawn through a heated combustion tube (600^o C) filled with a Pt/Al₂O₃ catalyst to expedite combustion. Downstream from the combustion tube, a heated

(280°C), 0.3 mm fused silica capillary continually samples the combustion gases and routes them directly to the inlet of a VG model EGA 300MM quadrupole mass spectrometer (QMS) operating in the multiple ion monitoring (MIM) mode. The masses selected for continuous monitoring include 40 (Ar); 12 (C-to confirm mass 44); 18 (H₂O); 28 (N₂); 32 (excess O₂ from combustion); 44 (CO₂); 46 (NO₂); 64 (SO₂); and 42 (C₂H₆-to verify combustor performance). All selected masses were sampled at approximately 1.5 second intervals. Total product transit time from the reactor to the QMS detector was roughly 1 second.

Procedure. Following system heat-up, raw shale feed is initiated with the semi-butterfly valve positioned so that pyrolysis products bypass the upper, substrate bed (i.e. "bypass" position). At this point, the QMS is used to verify combustor operation and check overall system performance.

Next, ~100 g of substrate is loaded to the upper bed which is fluidized by the balancing N₂ gas. When the substrate reaches reaction temperature, QMS data collection is initiated and a baseline established. After approximately 3 minutes (>100 QMS scans), the semi-butterfly valve is rotated so that the upper bed is now fluidized by the pyrolysis stream from the lower bed and maintained in the 'fluidize' position for a selected time interval (5-15 minutes is typical). The valve is then returned to the bypass position and the substrate solids are immediately drained from the bed into a purged collection flask. QMS data collection is continued for at least 3 minutes to re-establish the baseline. The solids receiver flask is removed and replaced with an empty one and the procedure repeated.

Following exposure and recovery, each batch of substrate is weighed and ultimate analyses are performed using standard methods. Surface area and pore volume measurements by N₂ adsorption and Hg porosimetry are conducted on selected substrates. Total surface area data shown in this report represent the sum of meso and macro surface area from Hg porosimetry and BET micro surface area from N₂ adsorption. Pore volume data are from Hg porosimetry.

Part of the post-run data manipulation involves taking the ratio of the combustion gas the tracer gas intensity. By doing so, changes in selected elemental concentrations, particularly carbon, could be observed with minimal interference from changing measurement conditions that frequently occur during a run. These uncontrolled measurement variations include pressure fluctuations, changing combustor or capillary transfer tube flowrates, QMS drift, etc., and result in variations in the absolute level of combustion gases reported by the QMS that are not related to coking loss.

Results and Discussion. The method as described in this manuscript detects only those coking losses resulting from interaction between HC pyrolysis products and the solid substrate to which they are exposed. The apparatus was not configured to probe cracking reactions which will be examined in future experiments involving continuous substrate feed and model compound investigations. Nevertheless, because coking losses account for a significant reduction in oil yield in solid recycle systems and carbon deposition can affect the solids reactivity, the study of coking kinetics is crucial to yield optimization.

Two independent measures of carbon deposition were obtained. The first was calculated from ultimate analysis of the substrate prior to and following HC exposure. The main disadvantage with this approach is that numerous runs are required to establish the deactivation rate for a particular solid under a given set of conditions. Further, at low carbon concentrations, the analytical scatter of the ultimate analysis becomes significant and trace O₂ in the fluidizing gas is a potential problem. Therefore, a complementary measure of carbon deposition is required to provide an on-line determination of coke formation that is less prone to error at low conversion.

In the system described, the rate of carbon deposition onto a solid substrate can be inferred by measuring the total vapor phase carbon that exits the reactor in the by-pass mode (pyrolysis stream by-passes substrate bed) and comparing to the carbon that exits in the coking mode (pyrolysis stream

passes through substrate bed). However, accurately measuring total vapor phase carbon in a pyrolysis stream is not trivial. Collecting the product oil with the required precision is impractical in a fluid bed process due to numerous parameters that affect collection efficiency, i.e. HC concentration, fluidizing velocity, compositional changes due to cracking, etc. Attempts to measure the total HC product with a flame ionization detector (FID) have been reported.^{8,9,10} However, FID measurement suffers from a variety of quantitative flaws including a small, nonlinear response to HC's of differing size or type, insensitivity to heteroatoms, and problems with aerosol formation and condensation of larger components prior to measurement. In comparison, the combustion/QMS approach utilized in this work, rapidly combusts the product stream before condensation or aerosol formation can occur and avoids non-linearity problems by monitoring a single species (CO₂) over a reasonably narrow concentration range. In addition, total N and S deposition can potentially be measured as NO₂ and SO₂ though problems with apparent reaction between H₂S and substrate iron have been encountered.

A typical coking sequence is illustrated by the QMS CO₂/Ar ratio in Figure 2b. With the semi-butterfly valve in the initial bypass position, the CO₂/Ar ratio is near constant. Upon switching the valve to 'fluidize', the ratio immediately drops to a minimum then makes an asymptotic approach to a new constant ratio. The initial plunge in the CO₂/Ar ratio is apparently due to rapid transport of oil vapor into the substrate pores. The ratio rises as the concentration within the pores nears the extraparticle concentration. When the valve is returned to bypass, the original baseline is restored.

There is a good deal of scatter apparent in the CO₂/Ar ratio of Figure 2b (likewise for NO₂ and SO₂). However, the measured fluctuations are real and due to rapid changes in the CO₂ concentration since the absolute intensity of Ar tracer, fluidizing N₂, and excess combustion O₂ remain relatively constant. This rapid change in CO₂ intensity is assigned to a number of sources including fluctuations in the shale feed rate over short time intervals, the chaotic nature of a bubbling fluid bed reactor, fines carryover to the combustor, and perhaps particle-to-particle kerogen content variations. The first two are believed to account for the bulk of the observed scatter.

Although the QMS baseline scatter is pronounced, conversion of shale oil vapor to coke was higher than the scatter under all study conditions. However, due to the data scatter, instead of directly integrating the raw data, a least-squares curve was first fitted to the data and the area between the fitted curve and a least-squares line fitted to the baseline data was determined. The 2-parameter functional form (excluding the intercept) that best fit the response curves for all runs was a decaying exponential form (Eq. 1).

$$C_{solid} = a + b(1 - \exp(-ct)) \quad (1)$$

The area between the region described by this curve and the CO₂/Ar baseline was then integrated and related to the increase in carbon content of the substrate through a proportionality constant. This constant was calculated by taking the ratio of the rate of volatile carbon production from the pyrolysis zone (determined by elemental analysis of the pyrolyzed shale) to the baseline CO₂/Ar ratio.

The coke formation data from integration of Equation 1 was then averaged with the substrate ultimate analysis. These average values are shown plotted in Figures 3 as a function of exposure time and substrate bed temperature. With the possible exception of sand, all substrates showed a higher coking rate with temperature. However, this change was small enough to suggest that coke formation was, for the most part, mass transfer limited.

Also shown in Figure 3, are coke deposition data for combusted and gasified shales that were pretreated in either NaOH or HCl (0.005 N). In all cases, coking onto the treated substrates was not significantly different than coking onto the untreated substrate. This suggests that the rate of coke

formation on the combusted or gasified shale substrates was not dominated by ionic surface sites.

The plots of Figure 3 indicate the relative coking activity to follow the order of Sand < pyrolysed < gasified < illite < combusted < coarse kaolinite < fine kaolinite. In an attempt to relate coking activity to substrate properties, total surface area data are shown in Figure 4a plotted in the above order. With the exception of sand, it is apparent that coking activity does not follow the total surface area series of Figure 4a. However, the macro pore surface area shown in Figure 4b does appear to track coke formation with the exception of illite.

Figure 5a shows the sum of meso and macro pore volume (pores > 2 nm) for each substrate. With two exceptions, illite and coarse-grained kaolinite, this plots also tracks the order of relative coking activity from Figure 3. The coarse-grained kaolinite had a greater pore volume than did the fine-grained kaolinite but showed relatively less coking activity. The reason for this anomaly may be due to the substantial difference in surface area between these two samples (Figure 4). That is, even though the coarse-grained kaolinite had a larger pore volume, the substantially lower surface area perhaps countered the larger pore volume. In the case of illite, the relatively high coking rate cannot be explained by either surface area or pore volume. We cannot explain the relatively high coke formation rate for illite though we suspect there may be a significant difference in active surface site concentration (or perhaps the absence of a carbon coating) relative to the other substrates.

Finally, Figure 5b shows the changes in the combusted shale pore volume as a function of exposure time at 620° C. As might be expected, this value steadily declines with increasing exposure time suggesting that the rate of coke formation may be decreasing as well. Such a decline was not detected by curve fitting the QMS data though data scatter could easily have obscured a small effect. Longer exposure times planned for future experiments should help clarify this point.

Acknowledgments. The authors gratefully acknowledge the work of D. Smith and J. Fannin for assisting with the experiments and data reduction, and M. Stewart, G. Thomas and M. Moore for analytical support. This work was supported in part by the Morgantown Energy Tech. Ctr., USDOE, under Coop. Agreement DE-FC21-90MC27286 (such support does not constitute an endorsement by the USDOE of the views expressed in this manuscript).

References

1. Taulbee, D.N. and Carter, S.D., *Fuel*, **70**, 1991, p. 1245-51.
2. Carter, S.D., Robl, T.L., Rubel, A.M., and Taulbee, D.N., *Fuel*, 1990, **69**, p 1124.
3. Levy, J.H., Mallon, R.G., and Wall, G.C., *Proc. 3rd Australian Workshop on Oil Shale*, Lucas Heights, NSW, 1986, p. 133.
4. Coburn, T.T., Taylor, R.W., Morris, C.J., and Duval, C., *Proc.: Int. Conf. on Oil Shale and Shale Oil*, Beijing, China, 1988, Colorado Sch. Mines Press.
5. Rubel, A.M., Rimmer, S.M., Keogh, R., Robl, T.L., Carter, S.D., and Derbyshire, F.J., *Fuel*, 1991, **70**, 1352.
6. Carter, S.D., Taulbee, D.N., Rubel, A.R., Abner, R.T., *Proc.: 1988 Eastern Oil Shale Symp.*, **IMMR88/101**, Inst. Min. & Minerals Res., Lexington, Ky., May., 1989, p. 333-340.
7. Carter, S.D., and Taulbee, D.N., submitted to *Fuel*, Jan. 1992.
8. Richardson, J.H., Huss, E.B., Ott, L.L., Clarkson, J.E., Bishop, M.O., Taylor, J.R., Gregory, L.J., and Morris, C.J., **Report UCID-19548**, 1982, LLNL, Livermore, Ca.
9. Wallman, P.H., Tamm, P.W., and Spars, B.G., *ACS Symp. Ser.* **163**, 1981, p. 93.
10. Carter, S.D., *ACS Div. of Pet. Chem. Prep.*, 1987, **32**, #1, p. 133.

Table 1. Substrate properties. Substrates are 20X60 mesh unless otherwise noted.

<u>Substrate</u>	<u>Origin</u>	<u>Preparation/comment</u>
Pyrolyzed Shale	Cleveland oil shale	530C in N ₂ /10 min
Gasified Shale	Cleveland oil shale	800C in Steam/20 min
Combusted Shale	Cleveland oil shale	700C in air/10 min
Sand	Ottawa, Canada	20X30 mesh
Illite	Carbon deficient Huron Shale (Three Lick Member), Rowan Co, KY	
Kaolinite-F	Fine grained, Georgia, USA	
Kaolinite-C	Course grained, Georgia, USA	

Acid/base treated substrates were placed in an excess of .005 N NaOH or HCl overnight, exhaustively rinsed with distilled H₂O, and dried prior to exposure.

Table 2. Reactor Conditions.

PYROLYZER:

Shale Feedrate	12 g/min
Superficial gas velocity	0.46 m/s
Temperature	530°C
Bed Height	7.6 cm

SUBSTRATE BED:

Substrate load	100 g (~3 cm depth)
Temperature	530-660°C
Solid Residence Time	5, 10, 15 min

Figure 2. Schematic of reactor configuration during coking sequence-Top.
 CO_2/Ar ratio (44/40 m/e) during typical coking sequence-Bottom.

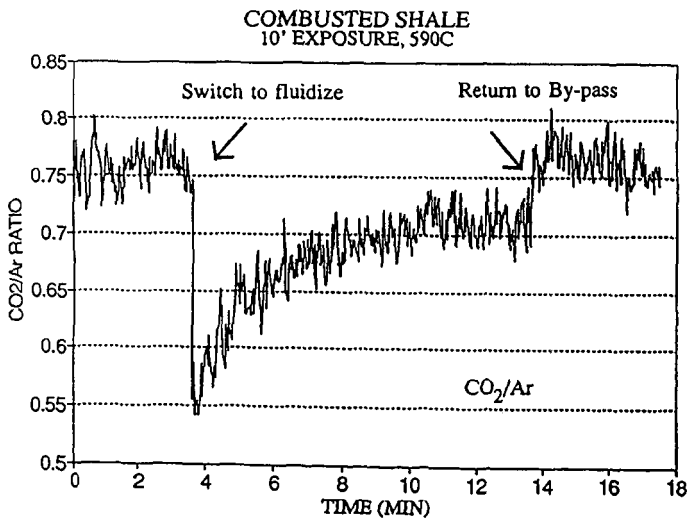
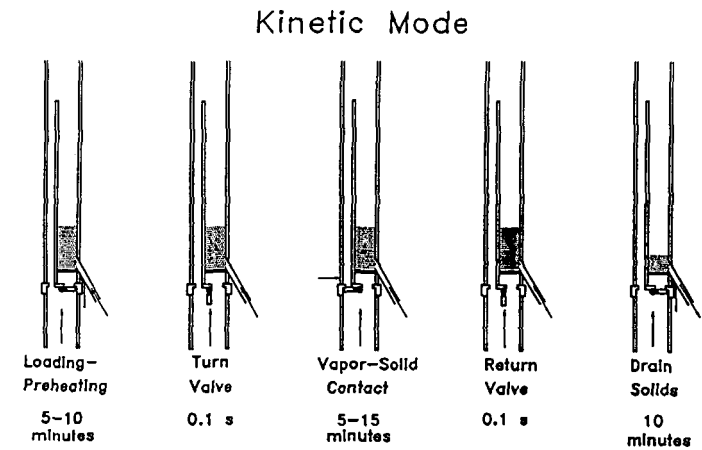
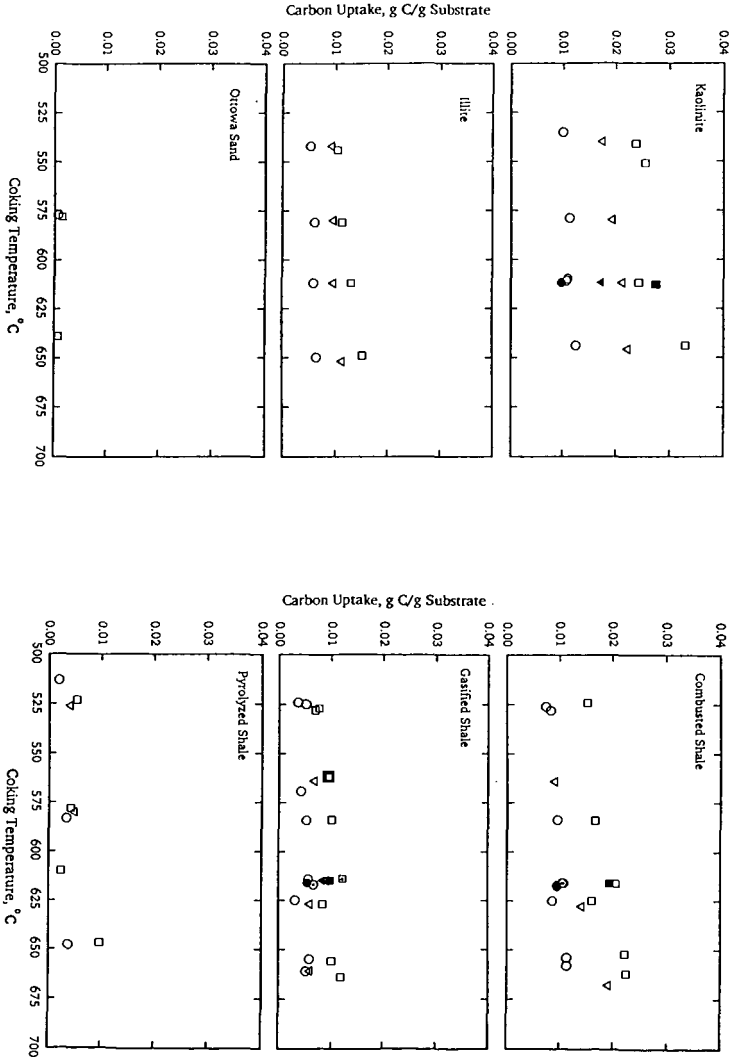


Figure 3. Average coke deposition as a function of exposure time and substrate temperature. \circ -5 min, ∇ -10 min, \square -15 min. Filled symbols represent either coarse-grained kaolinite (kaolinite plot) or base treated combusted or gasified substrate, symbols with \cdot represent acid treatment.



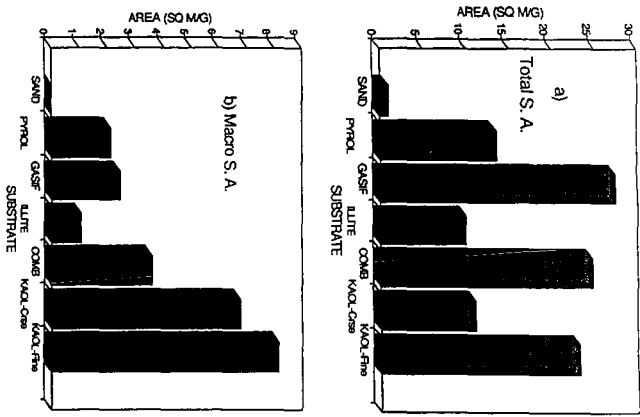


Figure 4. a) Total surface area. b) Surface area within macro pores. Substrates shown in order of increasing coking activity.

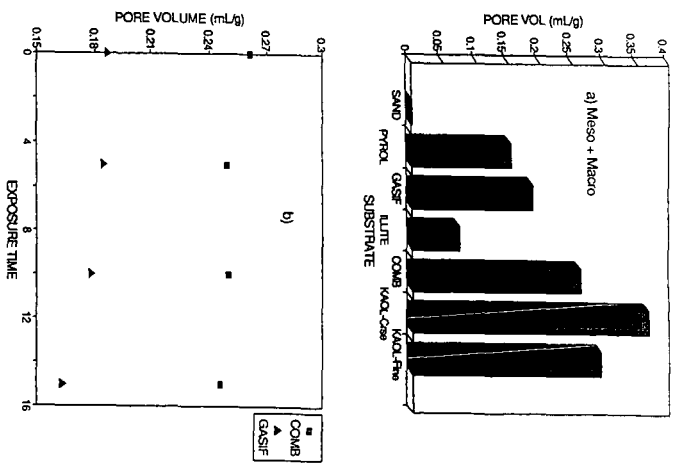


Figure 5. a) Meso + macro pore volume (mL/g substrate). b) Changes in the meso + macro pore volume for combusted and gasified substrates as a function of exposure time at 620° C.

Molecular Transformations in the Processing Sequence
Pyrolysis-Hydrotreating with Utah Oil Sands

by

F.V. Hanson, M.D. Deo, D.C. Longstaff and C.H. Tsai
Department of Fuels Engineering
University of Utah

INTRODUCTION

The utilization of Utah's Uinta Basin oil sands resource will most likely involve a combination of in-situ and mining-surface recovery techniques. It has been reported that 15-30% of Utah's oil sands are amenable to mining-surface recovery processes.⁽¹⁾ The mining-surface recovery processes include aqueous separation,⁽²⁻⁴⁾ solvent extraction^(5,6) and pyrolysis.⁽⁷⁻¹⁹⁾ The production of refinery feedstocks from mined oil sands can be accomplished by a number of processing sequences: aqueous separation or solvent extraction followed by coking or hydrotreating of the full range bitumen and rotary kiln or fluidized bed pyrolysis followed by hydrotreating of the bitumen-derived liquid.

The objective of this investigation was to explore the molecular transformations that occurred in the processing sequence pyrolysis of the mined oil sand ore in a fluidized bed⁽¹⁵⁾ followed by hydrotreating of the bitumen-derived liquid⁽²⁰⁾.

EXPERIMENTAL METHODS AND MEANS

Fluidized Bed Pyrolysis System

The bitumen-derived liquid used in the hydrotreating studies was produced from the Whiterocks tar sand ore in a large diameter fluidized bed pyrolysis reactor. The reactor temperature ranged from 773 to 813 K, and the average feed sand retention time was 17.2 minutes during the course of the production run.

The production of the bitumen-derived hydrocarbon liquid from the Whiterocks tar sand has been described in detail by Sung⁽¹⁵⁾.

Hydrotreater Process Unit

Process studies were conducted in a fixed bed reactor which operated in an upflow mode to minimize thermal gradients in the catalyst bed and to ensure complete wetting of the catalyst. A schematic of the hydrotreater system is presented in Figure 1. The reactor was designed for operation at a maximum pressure of 34.5 MPa at 773 K. The catalyst was diluted with quartz sand (50% by volume) in the inlet region of the bed (~20%) to trim the exotherm caused by olefin hydrogenation reactions.

The base case operating conditions for the hydrotreating study were as follows: reaction temperature, 619 K (653 °F); liquid hourly space velocity (LHSV), 0.5 h⁻¹; total reactor-pressure, 13.7 MPa (1980 psia) and hydrogen-to-hydrocarbon feed ratio, 890 m³/m³ (5000 scf/bbl). The API gravity of the total liquid product was constant at 23.2 °API after the reactor was on-stream for 94 hours at the base case conditions. At this point, it was assumed that the catalyst had attained a stationary state and that 95% of the coke deposition had occurred. A series of experiments were conducted in which the system was operated in a cyclic mode (base case condition/desired reaction condition/base case condition) for approximately 1000 hours. The total liquid product from each experiment was collected for analyses. The analytical test procedures conformed to those outlined in the ASTM manuals.

Mass balances were taken for 3 hours at the end of a 16-hour line-out period after the system had attained a stationary state at the new reaction conditions. The mass balances were conducted by monitoring the liquid fed to the reactor system for discrete time periods. At the conclusion of each mass

balance the collected gas and liquid samples were weighed and the gas sample was weathered into a vapor collector and analyzed by gas chromatography. All the mass balances were greater than 97.5 wt%.

The extent of nitrogen removal was the key reactivity parameter followed during the course of the study; however, the key operating parameter followed on the catalyst testing unit during the run was the specific and/or API gravity of the total liquid product.

Catalyst

A UNOCAL quadralobe Ni/Mo/Al₂O₃ hydrodenitrogenation (HDN) catalyst was used in this study. The catalyst contained 3.3 wt% NiO, 12.8 wt% MoO₃, and 0.8 wt% P₂O₅. It had a surface area of 241 M²/g and a pore volume (Hg porosimetry) of 0.55 cm³/g. The sulfiding conditions were specified by the catalyst manufacturer. A solution of dimethyl disulfide in kerosene (~ 2 wt% sulfur) was used to sulfide the catalyst at a LHSV of 1.0 h⁻¹. The hydrogen-to-sulfiding solution ratio was 890 m³/m³ (5000 scf/bbl). The reactor temperature was adjusted to the initial run temperature after sulfur breakthrough at which point the sulfiding solution was discontinued.

A description of the experimental apparatus and operating procedures; a description of the catalyst and the catalyst activation procedures; and a summary of the process variable study have been reported by Longstaff, et al²¹. The design, construction and operation of the hydrotreater catalyst testing unit have been discussed in detail by Longstaff²⁰.

Analysis of Liquid Products

Simulated Distillation The boiling point distributions of the hydrotreated products were determined by simulated distillation. The samples were dissolved in dichloromethane and the analyses were performed on a programmed Hewlett-

Packard Model 5730 A gas chromatograph: the oven temperature was programmed from 243 to 623 K at 11°C/minute and was held at 623 K for 16 minutes; the injector temperature was initially set at 523 K and raised to 633 K after 12 minutes and the FID detector temperature was 673 K. The boiling point temperatures were calibrated with a standard mixture of normal paraffins (C₅ - C₄₄).

Gas Chromatography-Mass Spectrometry Analysis The bitumen-derived liquid feed and the hydrotreated total liquid products were analyzed with a gas chromatograph (Hewlett-Packard Model 5890 A) using a fused silica capillary column coated with 5% phenyl methyl silicone bonded stationary phase (30m x 0.25mm ID, DB-5, J & W scientific). The temperature program was ranged from 323 K to 573 K at 3°C min⁻¹, with a hold at 573 K for 20 minutes.

Gas chromatography - mass spectrometry analyses were performed on a Finnigan MAT95 high resolution gas chromatograph/mass spectrometer (Finnigan MAT ICIS II operating system) fitted with a DB-5 gas chromatographic column (30m x 0.25mm ID).

RESULTS AND DISCUSSION

The bitumen-derived liquid was significantly upgraded relative to the native bitumen (Table 1): 19.1 °API versus 11.9 °API; a viscosity of 85.4 cps @ 289 K, versus 2665 cps @ 358 K; a volatility (<811 K) of 82.2 wt.% versus 40.5 wt.%; a Conradson carbon residue of 4.7 wt% versus 8.1 wt%; etc., respectively. The atomic hydrogen-to-carbon (H/C) ratio of the bitumen-derived liquid was lower than that of the native bitumen. This reduction was related to dealkylation reactions during pyrolysis which resulted in the production of a more aromatic hydrocarbon liquid and consequently a lower H/C ratio. Furthermore, the asphaltene fraction in the native bitumen was assumed to be the primary precursor of the carbonaceous residue deposited on the spent sand thus the coking tendency

of the bitumen-derived liquid during hydrotreating was expected to be less than that of the native bitumen.

Identification of individual compounds in the volatile fractions (811 K) of the Whiterocks bitumen, the bitumen-derived liquid and the hydrotreated total liquid was based on the comparison to known spectra from the literature or were tentatively assigned based on interpretation of the mass spectrum.²²⁻³⁴ Major compound types found in the 1000°F minus fraction of the native Whiterocks bitumen were substituted and unsubstituted cyclohexanes, benzenes, decalins, tetralins, naphthalenes perhydrophenanthrenes (tricyclic terpanes), octahydrophenanthrenes, tetrahydrophenanthrenes, phenanthrenes, phenyl (cyclohexyl) alkanes, indan (cyclohexyl) alkanes, perhydrochrysenes (17,21-secohopanes), steranes (C₂₇ - C₂₉), hopanes (C₂₇ - C₃₅) and traces of paraffins. Heterocyclics such as benzofuran, indoles, quinolines, carbazoles and tricyclic and pentacyclic carboxylic acids were also detected.

Basically, the compounds types identified in the Whiterocks bitumen-derived liquid were similar to those identified in the volatile fraction of the bitumen. Several additional compound types were also identified: normal alkanes (C₇ - C₃₀) and α -alkenes, branched alkanes (C₇ - C₂₈) and alkenes, cyclopentanes, styrenes, indenenes, dihydronaphthalenes, dihydrophenanthrenes, and the olefin related to perhydro- β -carotane. The amounts of alkyl naphthalenes and alkylphenanthrenes increased in the bitumen-derived liquid compared with the bitumen. The hydrotreated bitumen-derived liquid consisted primarily of saturated compounds, such as alkanes (normal and branched) and cycloalkanes (1-5 rings). It also contained low concentrations of aromatic compounds which were predominantly monoaromatics.

The task of identifying the thermal reactions pathways in bitumen pyrolysis

was difficult due to the complexity of the native bitumen. However, several pathways were rationalized through the structural identifications of these three samples. These reactions included cleavage of long side chain, dehydrogenation, polymerization and condensation, and decarboxylation.

The normal and branched (mostly isoprenoid) alkanes and normal and branched-1-alkenes generated in the pyrolysis reactions probably originated as alkyl groups attached to aromatic rings in multi-ringed aromatics and naphenoaromatics and/or from alkyl bridges between two aromatic clusters, two naphenic clusters, and/or an ermoatic cluster and a naphenoaromatic cluster. Since these types of compounds were not found in the 811 K minus fraction of the bitumen, it was presumed that they were present in the high boiling, residual fraction of the bitumen.

The speculation regarding the pyrolysis reaction pathways was confirmed by gradient elution chromatography⁽³⁵⁻³⁷⁾ analysis of the native bitumen and the bitumen-derived liquids produced during the rotary kiln pyrolysis⁽¹⁸⁾ of the Whiterocks tar sand (Table 2). The breaking of alkyl linkages between clusters followed by dealkylation led to a reduction in the asphaltene content of the bitumen-derived liquid and to a large increase in the mono-, and dinuclear aromatic contents of these liquids.

The presence of alkyl indenenes, dihydronapthalenes, dihydrophenathrenes and the increased amounts of the alkyl naphthenes and phenanthrenes suggested that step-wise dehydrogenation of hydroaromatics occurred. The hydroaromatics present in the bitumen could have acted as hydrogen donors during pyrolysis.

Hydrogen was produced during the pyrolysis of oil sand. The formation of hydrogen was believed to have occurred via a gas phase reaction, coincident with light oils production and a solid reaction, associated with the formation of the

carbonaceous residue on the sand grains.⁽³⁸⁾ The clays in the solid substrate may have been activated at pyrolysis conditions and may have catalyzed polymerization and condensation of aromatics and hydroaromatics during pyrolysis. These reactions would be expected to be accompanied by the formation of hydrogen.

Small amounts of carbon dioxide were detected in the produced gases during pyrolysis of the Whiterocks oil sand. It was presumed that the CO₂ was produced by thermal decomposition of carboxylic acid functional groups present in the native bitumen. The decomposition of the R-COOH bonds readily occurred at the pyrolysis temperatures (723-823 K).⁽³⁸⁾ It was presumed that the CO₂ concentration would have been higher if the source of CO₂ had been related to the decomposition of mineral carbonates which were present in the reservoir rock.

Hydrogenation, hydrogenolysis and heteroatom removal were the principal reactions which occurred in the hydrotreater. The absence of olefins in the hydrotreated products and the heat released in the inlet region of the catalyst bed, suggested that hydrogenation of olefinic bonds occurred readily during hydroprocessing. The predominance of hydroaromatic species in the total liquid product indicated that polycyclic aromatics underwent partial hydrogenation. The naphtha and middle distillate fractions were formed via thermal and catalytic reactions at hydrotreating conditions.

ACKNOWLEDGEMENTS

John E. Fausett is thanked for providing the ore from the Whiterocks tar sand deposit. Dr. K.R. Chen is thanked for his contribution to the preliminary design and fabrication of the hydrotreating catalyst testing unit. The Wright Aeronautical Laboratories at the Wright-Patterson Air Force Base are acknowledged for the sponsorship of the work which led to the initial design of the hydrotreating unit. The financial support of the U.S. Department of Energy

through the Laramie Projects Office of the Morgantown Energy Technology Center is gratefully acknowledged. Dr. John Ward of UNOCAL, Inc., is gratefully acknowledged for providing the catalyst and for numerous, helpful discussions.

REFERENCES

1. Resnick, B.S., Dike, D.H., English, L.M., and Lewis, A.G., "Evaluation of Tar Sand Mining; Vol. 1. An Assessment of Resources Amenable to Mine Production," DOE/ET/30201-1 (DE82010249).
2. Miller, J.D. and Misra, M., "Hot Water Process Development for Utah Tar Sands," Fuel Proc. Technol. 6, 27-59 (1982).
3. Miller, J.D. and Misra, M., "Concentration of Utah Tar Sands by an Ambient Flotation Process," Internat. J. Miner. Proc. 2, 269-287 (1982).
4. Rendall, J.S., "Hot Water Bitumen Extraction Process" U.S. Patent No. 4,875,998 (October 24, 1989).
5. Rendall, J.S., "Solvent Extraction Process," U.S. Patent No. 4,160,718 (July 10, 1979).
6. Rendall, J.S. "Method and Apparatus for Solvent Extraction," U.S. Patent No. 4,424,112 (January 3, 1984).
7. Taciuk, W., Turner, L.R., and Wright, B.C., "Oil Shale Processing with the AOSTRA Taciuk Processor," Proc. 4th UNITAR/UNDP Intern. Conf. on Heavy Crude and Tar Sands, 5(237), 439-447. (1989).
8. Taciuk, W., "Process for Thermal Cracking a Heavy Hydrocarbon," U.S. Patent 4,180,455 (1977).
9. Boyer, L.D., Sooter, M.C., and Sage, F.E. "Method for Production of Distillable Hydrocarbonaceous Fuels and Carbonaceous Agglomerates from Heavy Crude Oil," "U.S. Patent 4,473,464 (1984).
10. Zimmermann, K.F., "Rotary Kiln for Drying and Deoiling Oil Sands and Oil Shales," Germany Patent DE 3,042,146 (1980).
11. Cha, C.Y. and Guffey, F.D., "Recycle Oil Pyrolysis and Extraction of Tar Sand," Proc. of 4th UNITAR/UNDP Intern. Conf. on Heavy Crude and Tar Sands, 5(106), 449-456 (1987).
12. Venkatesan, V.N. Fluidized-bed thermal recovery of synthetic crude from bituminous sands of Utah. Ph.D. dissertation. University of Utah, Salt Lake City, Utah. (1979).

13. Wang, J. The production of hydrocarbon liquids from a bitumen-impregnated sandstone in a fluidized bed pyrolysis reactor. M.S. thesis. University of Utah, Salt Lake City, Utah. (1983).
14. Dorius, J.C. The pyrolysis of bitumen impregnated sandstone from the P.R. Spring (Utah) deposit in a fluidized bed. Ph.D. dissertation. University of Utah, Salt Lake City, Utah, (1985).
15. Sung, S.H. The fluidized bed pyrolysis of bitumen-impregnated sandstone in a large diameter reactor. M.S. Thesis, University of Utah, Salt Lake City, Utah. (1988).
16. Shun, D. Fluidized Bed Pyrolysis of The Bitumen-Impregnated Sandstone from the Circle Cliff Deposit. Ph.D. Dissertation, University of Utah, Salt Lake City, Utah. (1990)
17. Cha, S., Hanson, F.V., Longstaff, D.C. and Oblad, A.G., "Pyrolysis of Bitumen Impregnated Sandstones: A Comparison of Fluidized Bed and Rotary Kiln Reactors." Proc. 1990 Eastern Oil Shale Conf., 136-145 (1991); Fuel 70, 1357 (1991).
18. Cha, S., "Pyrolysis of Oil Sands from the Whiterocks Tar Sands Deposit in a Rotary Kiln", Ph.D. Dissertation. University of Utah, Salt Lake City, Utah (1991).
19. Hanson, F.V. and Oblad, A.G., (1989), "The Fluidized Bed Pyrolysis of Bitumen-Impregnated Sandstone from the Tar Sand Deposits of Utah," Proc. Fourth UNITAR/UNP Internat. Conf. on Heavy Crude and Tar Sands, Vol. 5, 421-438.
20. Longstaff, D.C., (1992)., "Hydrotreating the Bitumen and Bitumen-Derived Liquid from the Whiterocks Oil Sand Deposit" Ph.D. Dissertation, University of Utah, Salt Lake City, Utah.
21. Longstaff, D.C., Deo, M.D., Hanson, F.V., and Oblad, A.G., (1992) "Hydrotreating the Bitumen-Derived Hydrocarbon Liquid Produced in a Fluidized-Bed Pyrolysis Reactor", Proc. 1991 Eastern Oil Shale Symp.
22. Philp, R.P., (1985)., "Fossil Fuel Biomarkers - Applications and Spectra," Methods in Geochemistry and Geophysics, 23, Elsevier, Amsterdam.
23. Henderson, W., Wollrab, V. and Eglinton, G., (1968)., "Identification of Steroids and Triterpenes from a Geological Source by Capillary Gas-Liquid Chromatography," Chem. Commun., 710.
24. Anderson, P.C., Gardner, P.M. and Whitehead, E.V., (1969)., "The Isolation of Steranes from Green River Shale," Geochim. Cosmochim. Acta, 33, 1304.
25. Anders, D.E. and Robinson, W.E., (1971)., "Cycloalkanes Constituents of the Bitumen from Green River Shale," Geochim. Cosmochim. Acta, 35, 661.

26. Gallegos, E.J., (1971)., "Identification of New Steranes, Terpanes and Branched Paraffins in Green River Shale by Combined Capillary Gas Chromatography and Mass Spectrometry," Anal. Chem., 43(10), 1151.
27. Gallegos, E.J., (1973)., "Identification of Phenylcycloparaffin Alkanes and Other Monoaromatics in Green River Shale by Gas Chromatography-Mass Spectrometry," Anal. Chem., 45(8), 1399.
28. Reed, W.E., (1977)., "Molecular Compositions of Weathered Petroleum and Comparison with its Possible Sources," Geochim. Cosmochim. Acta, 41 237.
29. Trendel, J.M., Restle, A., Connan, J. and Albrecht, P., (1982)., "Identification of Novel Series of Tetracyclic Terpene Hydrocarbons (C₂₄-C₂₇) in Sediments and Petroleum," J. Chem. Soc., Chem. Commun., 304.
30. Ekweozor, C.M. and Strausz, O.P., (1982)., "18,19-Bisnor-13 β H, 14 α H-Cheilanthane: A Novel Degraded Tricyclic Sesquiterpenoid-Type Hydrocarbon from the Athabasca Oil Sands," Tetrahedron Letters, 23(27), 2711.
31. Whitehead, E.V., (1974)., "The Structure of Petroleum Pentacyclanes," in Advances in Geochemistry.(eds. B. Tissot and F. Bienner), Editions, Technip, Paris, 225.
32. Bendoraitis, J.G., (1974)., "Hydrocarbons of Biogenic Origin in Petroleum - Aromatic Triterpanes and Bicyclic Sesquiterpenes," Advanced in Geochemistry, (eds. B. Tissot and F. Bienner), Editions, Technip, Paris, 209.
33. Kimble, B.J., Maxwell, J.R., Philp, R. P. and Eglinton, G., (1974)., "Identification of Steranes and Triterpanes in Geolipid Extracts by High-Resolution Gas Chromatography and Mass Spectrometry," Chem. Geology, 14, 173.
34. Aquino Neto, F.R., Restle, J., Connan, J., Albrecht, P. and Ourisson, G., (1982)., "Novel Tricyclic Terpanes (C₁₉-C₂₀) in Sediments and Petroleum," Tetrahedron Letters, 23(19), 2027.
35. Middleton, W.R., 1967, Gradient Elution Chromatography Using Ultraviolet Monitors in the Analytical Fractionation of Heavy Petroleum, Analytical Chemistry. 39 (14), 1839-1846.
36. Callen, R.B., Benderatis, J.G., Simpson, C.H., and Voltz, S.E., 1976. "Upgrading Coal Liquids to Gas Turbine Fuels I. Analytical Characterization of Coal Liquids," Ind. Eng. Chem., Prod. Res. Dev., 15 (4) 22.
37. Utley, J.K. 1980, The Adaptation of Gradient Elution Chromatography to the Analysis of the Bitumen and Synthetic Liquids Derived from Bituminous Sand, Senior Project Report, Department of Mining and Fuels Engineering, University of Utah, Salt Lake City, Utah.
38. Ritchie, R.G.S., Roche, R.S., and Steedman, W. "Non-Isothermal Programmed Pyrolysis Studies of Oil Sand Bitumens and Bitumen Fractions," Fuel, 1985, 64 391.

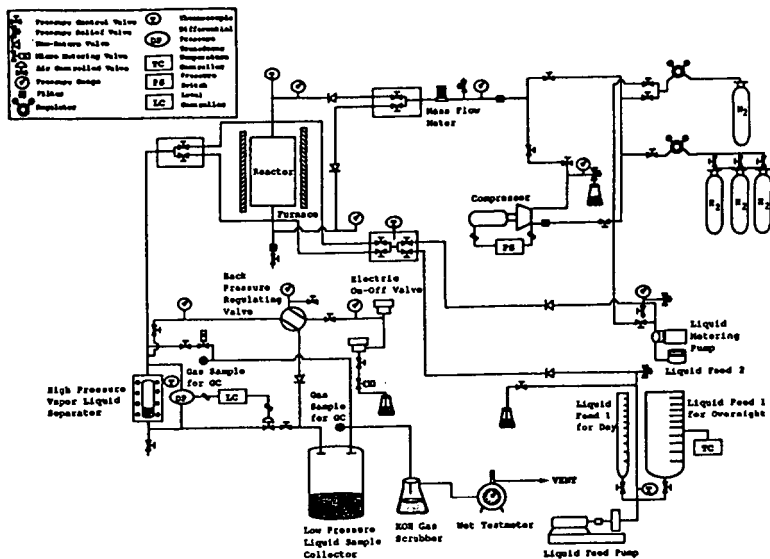


Figure 1 Flow diagram for a hydrotreating/hydrocracking unit

Table 1
Properties of Bitumen and Bitumen-Derived Liquids
from the Whitecourt Deposit Tar Sand

	Native Bitumen	Bitumen-Derived Liquid	Hydrotreated Bitumen-Derived Liquid
API Gravity	11.9	18.3	33
Conradson Carbon Residue wt%	8.1	4.7	NA
Pour Point, °C	330	378	339
Distillate Distillation			
Refluxivity, wt-%	40.3	62.2	67.6
133 °C	513	434	318
178 - 227 °C, wt%	8.9	6.7	12.5
217 - 218 °C, wt%	4.9	10.3	46
218 - 219 °C, wt%	33.6	39.8	34.9
>219 °C, wt-%	39.3	17.8	2.6
Elemental Analysis			
C, wt%	85.1	85.0	86.7
H, wt%	12.3	12.1	13.3
S, wt%/ppm	3.0	5.1	63 ppm
N, wt%/ppm	0.4	0.4	18 ppm
O, wt%	1.1	1.5	0
NI, ppm	63	0	NA
V, ppm	0	0	NA

Table 2
Chemical Composition of the Bitumen-Derived Liquids from the Whitecourt Tar Sands

Run ID	Native Bitumen	WH-02-1	WH-02-2	WH-02-3	WH-02-4
Reactor Temperature, °C					
		396	396	396	396
Reactor Retention Time, min.					
		31	31	18	9
H₂ Gas Flow Rate, SCFH					
		37.5	37.5	37.5	37.6
Reaction Station Characteristics					
Conversion, wt-%					
NI, wt-%	10.3	10.3	11.7	9.4	13.5
NI, ppm					
oil, wt-%	3.3	39.7	41.7	41.4	39.7
NI Gas Flow Rate, SCFH					
		31.3	18.1	18.6	11.9
NI Gas Flow Rate, SCFH					
		13.0	13.4	12.9	13.0
NI Gas Flow Rate, SCFH					
		3.0	0.9	1.5	1.3
NI Gas Flow Rate, SCFH					
		1.6	1.3	1.7	1.3
Asphaltenes, wt-%					
		19.4	12.9	12.9	13.1
Numbered Asphaltenes, wt-%					
		10.9	0.4	2.2	0.3

The Effect of Cosolubilizing Lighter Components on the Asphaltene Content of Heavy Oils

Milind D. Deo, Jonsic Hwang and Francis V. Hanson
Department of Fuels Engineering
University of Utah, Salt Lake City, Utah, 84112.

Introduction

Asphaltenes are precipitates that separate from petroleum, petroleum residua or bituminous materials on treatment with low-boiling liquid hydrocarbons¹. The solvents for effecting this separation are n-pentane and n-heptane, although other light hydrocarbon solvents have also been used². The amount and composition of asphaltene fractions are important from processing considerations. In petroleum refining, asphaltene fractions can precipitate in heat exchangers and/or can deposit on catalysts causing excessive coke formation. A number of physical properties of the crude oils are also determined by the asphaltenes. In petroleum production operations, asphaltenes can precipitate and cause extensive formation damage. Asphaltene precipitation in oil reservoirs has proved to be a difficult problem to define and study^{3,4}.

Speight¹ provided a detailed discussion on the influence of solvent type on asphaltene separation. Yields of precipitate using various solvents and a western Canadian bitumen indicated that when the solvent carbon number was increased, the yields (wt% bitumen) decreased. This was particularly true for the n-alkane homologous series and was applicable to a lesser degree to naphthenic and aromatic compounds. The amount of precipitate correlated well with two types of solubility parameters defined by the following equations:

$$\delta_1 = \gamma V^{-1/3} \quad (1)$$

$$\delta_2 = \left(\frac{\Delta H^v - RT}{V} \right)^{1/2} \quad (2)$$

where, γ is the solvent surface tension, V is the molar volume, ΔH^v is the heat of vaporization, R is the universal gas constant and T is the absolute temperature. Burke et al.³ used Equation 1 to define solubility parameters.

Fractionation of asphaltenes using solvent mixtures also exhibited varying yields depending on the ratio of the solvents used². This data suggests that the amount of asphaltene precipitate will be influenced by the lighter cosolubilizing components in the petroleum or bitumen. The work reported in this paper on the continuous supercritical fluid extraction (SFE) of an oil sands bitumen with propane provides direct evidence on the influence the lighter components have in keeping the asphaltene fractions in solution.

Experimental

The SFE system was custom-built for the University of Utah by Autoclave Engineers, Inc. A schematic of the apparatus is shown in Figure 1. Central to the system was a temperature controlled extractor with a capacity of 300 cc and rated to a pressure of 37 MPa at 615 K. The extractor was equipped with a magnetic-drive packer-less stirring device. Propane was charged into the extractor and the system was brought to the desired pressure using a high-pressure liquid pump. Pressure control is achieved by incorporating a back pressure regulator in parallel with the pump. The pump-head was cooled by a circulating cooling bath to ensure that the propane was maintained in a liquid state at the pump-head.

Initially 50 g of Whiterocks native bitumen was charged into the extractor. Selected properties of the bitumen are presented in Table 1. Once the initial equilibrium state was attained, propane was continuously pumped into the extractor. Commercial grade propane containing about 96% propane and

4% of other C₁ - C₄ hydrocarbon gases was used in this work. A heated metering valve was used to transfer the extracted phase from the extractor to the separator. The separator was held at ambient pressure. The solvent separated from the extract phase in the separator was vented through a flow totalizer which measured the cumulative volume of solvent withdrawn from the separator. The oil in the separator was collected and weighed. In all the experiments, a known amount of bitumen was charged into the extractor and the continuous extraction process was started. After about 25 liters of solvent (at room temperature) had passed through the totalizer, the amount of oil accumulated in the separator was collected and weighed. When the amounts of oil extracted became small relative to the amount extracted in the first 25 liters, the extraction was stopped. The extractor was depressurized and the residue was weighed and analyzed for maltenes and asphaltenes. In each extraction sequence, seven to eight extract samples were collected, each sample corresponding to an *extraction window* of 25 liters of propane vented through the totalizer or about 20 minutes of extraction time.

Asphaltene contents of the residual fractions produced during the propane extraction of the native bitumen were measured by the analytical method developed by AOSTRA⁵. Two grams of the residual oil sample were dissolved in an equal volume of toluene. Forty volumes of n-pentane were added for each volume of toluene. The AOSTRA method recommends benzene as the diluent; however, toluene was used in place of benzene for safety reasons. The precipitate was filtered from the solution, dried and weighed.

Results and Discussion

Experiments were performed at three different pressures (5.5 MPa, 10.3 MPa and 17.2 MPa) at a constant temperature of 380 K and at three different temperatures (339 K, 380 K and 422 K) at a constant pressure of 10.3 MPa. The critical temperature of propane is 369.8 K and its critical

pressure is 4.25 MPa. The effect of pressure on the extraction yields at 380 K is presented in Figure 2 and the effect of temperature on the extraction yields at 10.3 MPa is shown in Figure 3. Attempts have been made to link the extraction performance of dense gases to solvent density^{6,7}. The densities of pure propane at the experimental conditions, as calculated by the Peng-Robinson equation of state⁸ is presented in Table 2. It can be observed from Figures 2 and 3, and Table 2 that density did affect the extraction yields. However, pure solvent density was not the only parameter that governed the extraction process. The density variations for an increase in pressure from 5.5 MPa to 17.2 MPa at a temperature of 380 K and for an increase in temperature from 339 K to 422 K at a pressure of 10.3 MPa were almost identical (44%). However, Figures 2 and 3 indicated that pressure appeared to have a stronger influence on the extraction yields than temperature. The highest extraction yield was obtained at 380 K and 17.2 MPa.

The compositional variation in the extracted material as a function of time can be determined by examining the carbon number distributions of the first, middle and the last extracts for the experiments at 10.3 MPa and 380 K (Figure 4). The middle and the last extracts contained compounds heavier than the first fraction. The carbon number distributions of the middle extracts as a function of pressure (Figure 5) indicated that heavier compounds are extracted at higher pressure. No significant compositional changes in the middle extracts were observed as a function of temperature (Figure 6). This behavior appeared to be consistent with the extraction yield information, where it was observed that pressure had a stronger influence on the extraction process than temperature in the range of pressures and temperatures examined in this work.

Residual oils from all the extraction experiments were dark black solids. The asphaltene contents of the residual oils are listed in Tables 3 and 4 along with the elemental analyses of the residual oils. It should be noted

that the asphaltene content of the feed material was 5.9%. The asphaltene contents of all the residual oils were significantly higher than the original heavy oil. The asphaltene content of the residual oils increased with pressure. This was consistent with the observation that increased extraction of heavier compounds occurred as the extraction pressure was increased. The highest asphaltene content was found in the residual oil from the extraction at 380 K and 17.2 MPa where the extraction yield was also the highest. The asphaltene contents of the extracts were not measured in this study. The percentage of asphaltenes as a fraction of the original oil feed are also listed in Tables 3 and 4. These values were also considerably higher than the asphaltene content of the original oil. Obviously, compounds that did not precipitate from the original oil as pentane insolubles were precipitating from the residual oils.

These experiments established the fact that asphaltenes, as defined in this study (pentane insolubles), are not a definite compound class but were a collection of compounds specific to a given mixture. Lighter compounds in these mixtures helped keep the asphaltene fraction in solution when a pentane solubility test was performed on the mixture. During the extraction process, these lighter compounds were stripped from the original mixture, thus decreasing the tendency of the heavier molecules to be in solution. As a result of this, the pentane insolubles fraction increased in the residual oils. It is apparent from this reasoning that the asphaltene content of the residual oils would be higher for the residuals produced at conditions that led to more efficient extraction of the lighter components. The data demonstrated this with the exception of the extraction at 5.5 MPa and 380 K. In this experiment, despite an extraction of only about 20% of the material which consisted of relatively lighter compounds (Figures 2 and 5), an asphaltene fraction of 14% was observed in the residual oil. Extractions in the vicinity of the critical temperature of propane (T_c for 380 K is 1.03) and the quality of the compounds extracted may explain this data point. However, detailed

compositional information on the extracts (possibly by gas chromatography - mass spectrometry), their asphaltene contents, etc. would be required to evaluate this.

The elemental analysis of the residual oils reported in Tables 3 and 4 indicated that the H/C ratio of the residual oils decreased relative to the H/C ratio of the original bitumen. This suggested that saturated compounds are preferentially extracted by propane and that the heavier portion of the bitumen is relatively more unsaturated than the bitumen as a whole. It was also seen from the data that the nitrogen and sulfur contents of residual oils were higher than the original bitumen. This indicated that the heteroatomic species are concentrated in the unextractable heavier portion of the bitumen.

The solubility parameters (Equations 1 and 2) increase with carbon number¹. As the extraction pressure increased more of the heavier hydrocarbons are extracted (Figures 2 and 5). Thus the increase in the asphaltene content of the residual oils for increased extraction pressures was expected. The effect of solubilizing co-solvents² led us to presume that as lighter components are extracted, more of the heavier components ought to precipitate. Thus the data reported in this work were intuitive. However, the data did point out that it would be misleading to perform material balances on the asphaltene portions of the fractionated oils (as reported by Burke et al.³) since the type and amounts of asphaltenes in different fractions would depend on the solubility character of the specific fractions. Since residual oils recovered in the extractions were dark black solids, it may be wrong to presume that only the pentane insolubles asphaltene fraction of the original oil is susceptible to precipitate in any given recovery or refining process. The solubility parameter approach would also have to be modified to account for the different compound types that precipitate depending on the state of the mixture.

Conclusions

1. When an oil sand bitumen was subjected to supercritical extraction with propane, the residual oils left in the extractor exhibited significantly higher values of asphaltene fractions than the original oil (bitumen). The loss of cosolubilizing lighter components from the original oil during the extraction process caused more of the heavier components to precipitate thus increasing the apparent asphaltene content. This established that pentane-insoluble asphaltenes were not a definite compound class and that their nature and quantity in a given mixture was determined by the overall solubility character of the mixture.
2. As the extraction pressure increased at a constant temperature of 380 K, the asphaltene content of the residual oil also increased. This was consistent with the observation that the extraction yields increased with pressure and that heavier compounds were extracted at higher pressures.
3. The H/C ratio in the residual oils was lower than the original oil establishing that saturated compounds were preferentially extracted leaving the residual oils richer in unsaturated compounds than the original oil. The nitrogen and sulfur contents of the residual oils were also higher which indicated that heteroatomic compounds concentrated in the heavier (unextractable) portion of the original oil.
4. This study indicated that care should be exercised when performing material balances on asphaltenes from fractionated oils and that it may be inappropriate to presume that only the pentane-insoluble asphaltene fractions of the original oils are susceptible to precipitate in a given recovery (enhanced oil recovery) or refining process.

Acknowledgements

The financial support of the U.S. Department of Energy through the Laramie Project Office of the Morgantown Energy Technology Center is gratefully acknowledged. The authors wish to thank Professor Alex G. Oblad, Director of the Utah Tar Sand Program for his support and encouragement. The authors would also like to acknowledge support from the mineral leasing funds from the College of Mines and Earth Sciences, University of Utah and the Research Support Committee, University of Utah.

References

1. Speight, J. G., *The Chemistry and Technology of Petroleum*, Second Edition, Marcel Dekker, New York, NY.
2. Mitchell, D. L. and Speight, J.G., Fuel, 1973, **52**, 151.
3. Burke, N. E., Hobbs, R. E. and Kashou, S. F., Journal of Petroleum Technology, 1990, **42**, 1440.
4. Chaback, J. J., Journal of Petroleum Technology, 1991, **43**, 1519.
5. AO STRA, *Syncrude Analytical Methods for Oil Sand and Bitumen Processing*, 1979, Edmonton, Alberta, Canada.
6. Orr, F. M., Jr. and Silva, M. K., SPEJ, 1983, **23**, 272.
7. Orr, F. M., Jr. and Silva, M. K. and Lien, C., SPEJ, 1983, **23**, 281.
8. Peng, D. Y. and Robinson D. B., Ind. Eng. Chem. Fund., **15**, 59, (1976).

Table 1
Selected Properties of the Whiterocks Bitumen

Specific Gravity (288 K)	0.98
Conradson Carbon (wt%)	9.50
Pour Point, K	327
Viscosity (323 K), Pa-s	27
Simulated Distillation	
Volatility, Wt%	32.5
IBP, K	520
IBP-477 K, Wt%	0.0
478-616 K, Wt%	5.6
617-811 K, Wt%	26.9
> 811 K, Wt%	67.5

Table 2
Densities of Propane (g cm^{-3}) at Experimental Conditions
Calculated by the Peng-Robinson Equation of State

Temperature (K)	339	380	422
Pressure			
5.5 MPa	-	0.2585	
10.3 MPa	0.4782	0.3825	0.2672
17.2 MPa	-	0.4416	-

Table 3
Selected Properties of the Residual Oils After
Propane Extractions of Bitumen: Pressure = 10.3 MPa

Extraction	Bitumen		
Temperature (K)	339	380	422
Product Yield(%)			
Extract Phase	40	39	24
Residual Phase	59	58	73
Asphaltene/Maltene			
Asphaltenes, Wt%	12.5	15.0	9.8
Maltenes, Wt%	87.5	85.0	90.2
Asphaltenes Wt% Original Oil	7.4	8.7	7.16
5.9			
Elemental Analysis			
C, Wt%	86.74	86.69	86.66
H, Wt%	10.81	10.80	11.08
N, Wt%	1.95	2.02	1.79
S, Wt%	0.50	0.49	0.47
H/C Atomic Ratio	1.50	1.49	1.53
1.56			

Table 4
Selected Properties of the Residual Oils After
Propane Extractions of Bitumen: Temperature = 380 K

Extraction	Bitumen		
Temperature (K)	339	380	422
Product Yield(%)			
Extract Phase	20	39	48
Residual Phase	79	58	50
Asphaltene/Maltene			
Asphaltenes, Wt%	14.0	15.0	20.2
Maltenes, Wt%	86.0	85.0	79.8
Asphaltenes Wt% Original Oil	11.0	8.7	10.1
5.9			
Elemental Analysis			
C, Wt%	86.78	86.69	86.80
H, Wt%	10.97	10.80	10.58
N, Wt%	1.78	2.02	2.12
S, Wt%	0.47	0.49	0.50
H/C Atomic Ratio	1.52	1.49	1.46
1.56			

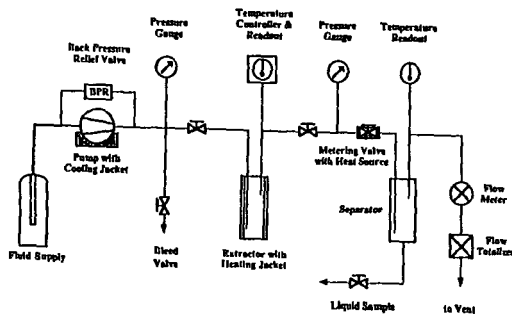


Figure 1: Schematic diagram of the supercritical fluid extraction system

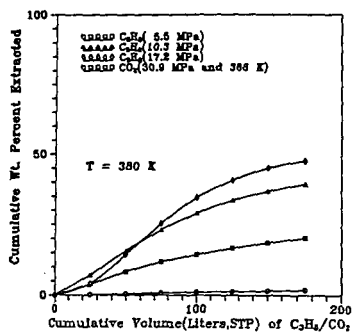


Figure 2: Extraction yields for the native bitumen with propane as function of pressure at 380 K.

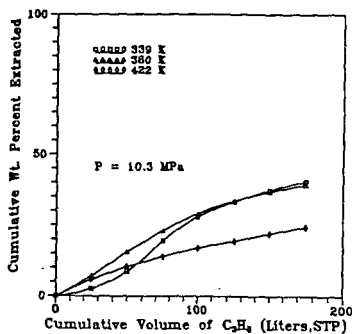


Figure 3: Extraction yields for the native bitumen with propane as function of temperature at 10.3 MPa.

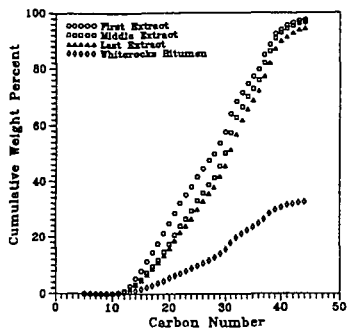


Figure 4: Changing compositions as a function of time for the native bitumen propane extracts at 350 K and 10.3 MPa.

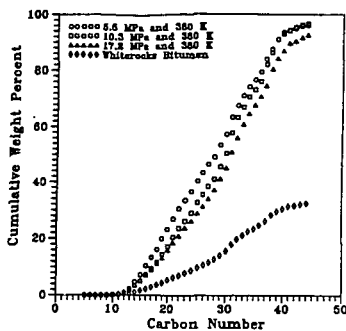


Figure 5: Compositional changes as a function of pressure for the native bitumen propane extractions at 380 K.

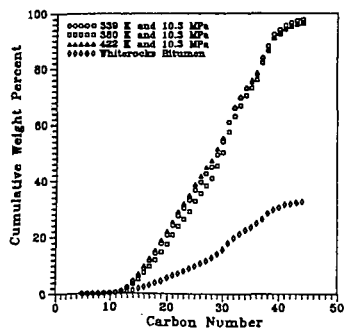


Figure 6: Compositional changes as a function of temperature for the native bitumen - propane extractions at 10.3 MPa.

SMALL ANGLE X-RAY SCATTERING STUDY OF ASPHALTENES

David A. Storm, Eric Y. Sheu and Maureen M. DeTar

Texaco R&D, Beacon, N.Y. 12508

INTRODUCTION

Asphaltenes are molecules that can be precipitated from carbonaceous liquids by certain non-polar solvents¹⁻³. Traditionally they were those molecules in petroleum residuum that were soluble in benzene and insoluble in pentane, but over the years molecules precipitated by other solvents, usually heptane², and molecules precipitated from other materials, such as coal and oil shale liquids have been called asphaltenes³. As such there can be many kinds of asphaltenes, each a mixture of a number of molecules. In this work we have studied the heptane insolubles of vacuum residue from Ratawi crude oil.

Although petroleum asphaltenes have been studied for some time⁴, their physical nature, or macrostructure, in petroleum is poorly understood. Small angle X-ray scattering(SAXS) is a technique that can be used to study asphaltenes in their natural state. Early SAXS experiments confirmed the colloidal nature of crude oil^{5,6}, atmospheric residue⁷, and solid asphaltic materials⁸. Scattering centers were observed with radii of gyration in the range of 30-70 Å, indicating either the presence of macromolecules⁷, or micelle-

like particles.⁸ In more recent studies the authors have tried to obtain more information by fitting the observed scattering intensity with an intensity calculated for model particles.^{9,10} Senglet et al. however noted that polydispersity complicates the analysis.¹⁰ For example the well-known Guinier analysis failed in their study of asphaltenes in toluene, or gas oil.¹⁰ Applying a method suggested by Vonk¹¹, they extracted histograms for the radii of gyration that are quite broad.¹⁰ Recently Sheu¹² suggested some ambiguity can be removed by applying a constraint that follows from the assumption of homogeneous particles. Operationally we have:

$$I(Q) = A \langle F_o^2(Q; \text{shape, size}) \rangle \quad (1)$$

where $I(Q)$ is the measured scattering intensity, and $\langle F_o^2 \rangle$ is the normalized form factor for a particular particle shape and size distribution function. Equation (1) defines A, which also depends on the shape and size parameters used in the fitting. Since the scattering intensity is:

$$I(Q) = N(\Delta\rho)^2 V_p^2 \langle F_o^2 \rangle \quad (2)$$

for identical particles, where N is the number of particles per unit volume, $\Delta\rho$ is the contrast between particles and fluid, V_p is the particle volume and $\langle F_o^2 \rangle$ is the square of the normalized form factor averaged over orientation angles, we would expect for a polydispersed sample that:

$$\alpha - A(shape, size) / (N(size) \langle V^2(shape, size) \rangle \langle F_o^2(shape, size) \rangle) \quad (3)$$

is independent of the shape and size parameters for the right shape and distribution function, since Eq.(3) express the fact that the contrast is constant for homogeneous particles. The constraint is applied by requiring that Eq.(3) remain constant as the concentration is varied; i.e., the parameters of the distribution may change, but the form of the distribution function, and the particle shape can not change. This procedure was used to fit the scattering data obtained with natural and synthetic Ratawi vacuum residue. The asphaltenic particle sizes (radii) are distributed according to a Schultz distribution. The average radius agree well with the radii of gyration reported earlier⁵⁻⁸, and the spherical shape agrees with the recent rheological studies for Ratawi asphaltenes in vacuum residue¹³, and in toluene.¹⁴

EXPERIMENTAL

Ratawi crude oil comes from the Neutral Zone in the Middle East. The vacuum residue was obtained by vacuum distillation; it is the fraction that has an apparent boiling point above 1000 °F. Samples of synthetic vacuum residue were prepared by dispersing appropriate amounts of vacuum residue in the corresponding non-asphaltenic portion. The non-asphaltenic fraction was prepared by first mixing heptane with the vacuum residue in the ratio of 40 parts of heptane for each part of vacuum residue, then stirring overnight at room temperature, and finally removing the asphaltenes by filtration. Heptane was removed from the non-asphaltenic portion by vacuum distillation.

The SAXS measurements were made with the ten meter small angle scattering spectrometer at Oak Ridge National Laboratory. The X-ray generator was a Rigaku-Demki rotating anode with a copper target; the power was 4KW. The K_{α} wavelength of 1.54 Å was selected using a pyrolytic graphite monochromator. The input collimator and a series of pinholes produced a 1 mm² spot at the sample position. The sample to detector distance was 112.6 cm. The detector was a 20 x 20 cm² continuously wired area detector purged by P10 gas. With this configuration the scattering wave vector Q ranged from 0.1 to 0.25 Å⁻¹. The samples were heated to 125 °C and then injected into a Kapton sandwich circular cell with a path length of 1 mm. The temperature was maintained at 93 °C during the experiment. Scattering from empty cells with and without Kapton windows was also measured for subsequent use during data reduction. A

calibrated polyethylene standard of known cross section at the peak position was used to obtain the absolute intensity (differential cross section per unit volume of sample)

RESULTS AND DISCUSSION

As discussed above, the measured scattering intensities were fit according to the procedure suggested by Sheu.¹² The fit obtained for spherical particles with sizes distributed according to the Schultz distribution for the Ratawi vacuum residue is shown in Figure 1. Other particle shapes and distributions were tried, but the alpha values defined in Eq.(3) were not constant. For example, the data for a particular sample could be fit by monodispersed cylinders, but the alpha values were not constant as the concentration was changed.

The Schultz distribution functions is shown in Figure 2. The Schultz distribution is defined as follows:

$$D(R) = [(z+1)/\langle R \rangle]^{z+1} R^z e^{-(z+1)R/\langle R \rangle} / \Gamma(z+1)$$

where $\langle R \rangle$ is the average radius, $\Gamma(z+1)$ is the gamma function, and z is a width parameter related to the polydispersity as

follows:

$$\text{polydispersity} = \sqrt{(\overline{R^2}) - (\overline{R})^2} / (\overline{R}) = 1/\sqrt{z+1}$$

The average radius and the degree of polydispersity is 33.8 Å and 15.4%. There are particles with radii as small as 20 Å and as large as 50 Å in this distribution. The average radius agrees very well with the radii of gyration reported by others for crude oil^{5,6}, atmospheric residue⁷, asphaltic materials⁸, and asphaltenes in solvents.⁵⁻⁸ The distributions are broad, as also found by Senglet et al.¹⁰ using the method due to Vonk.¹¹ The spherical shape for the asphaltenic particles is in agreement with the rheological measurements for these asphaltenes in vacuum residue¹³ and in toluene.¹⁴

ACKNOWLEDGMENT

We thank the Solid State Division of Oak Ridge National Laboratory for granting us beam time, and Dr. J. S. Lin for special assistance during the measurement. The SAXS experiments performed at Oak Ridge National Laboratory are partially supported by the Division of Material Sciences, U. S. Department of Energy under contract number DE-AC05-84OR21400, with Martin Marietta Energy Systems, Incorporated.

REFERENCES

- (1) Long, R. B. 1981. The Concept of Asphaltenes. In: J. W. Bunger and C. Norman (Editors), Chemistry of Asphaltenes. Advances in Chemistry Series 195:17-27
- (2) Speight, J. G. and S. E. Moschopedis, 1981. On The Molecular Nature of Petroleum Asphaltenes. In: J. W. Bunger and Norman C. Li (Editors) Chemistry of Asphaltenes, Advances in Chemistry Series 195:1-15
- (3) Yen, T. F. 1981. Structural Differences Between Asphaltenes Isolated from Petroleum and from Coal Liquid. In: J. W. Bunger and N. C. Li, Chemistry of Asphaltenes, Advances In Chemistry Series 195:39-51
- (4) Speight, J. G. 'The Chemistry and Technology of Petroleum,' Second Edition, Marcel Dekker, Inc., 1991
- (5) Dwiggin, C. W. Jr. *J. Appl. Cryst.* 1978, **11**, 615
- (6) Dwiggin, C. W. Jr. *J. Phys. Chem.* 1965, **69**, 3500
- (7) Klm, Hyo-gun and Long, R. B. *Ind. Eng. Chem. Fundam.* 1977, **18**, 60
- (8) Pollack, S. S. and Yen, T. F. *Anal. Chem.* 1970, **42**, 623
- (9) Herzog, P., Tchoubar, D. and Espinat, D. *Fuel* 1988, **67**, 245
- (10) Senglet, N., Williams, C., Faure, D., Des Courieres, T. and Guillard, R. *Fuel* 1990, **69**, 72
- (11) Vonk, C. G. *J. Appl. Cryst.* 1976, **9**, 433
- (12) E. Y. Sheu, "Polydispersity Analysis of Scattering Data from Self-Assembled Systems", to appear in *Phys. Rev A*
- (13) Storm, D. A., Sheu, E. Y., Barresi, R. J. and DeTar, M. M. International Symposium on the Chemistry of Bitumens, Rome,

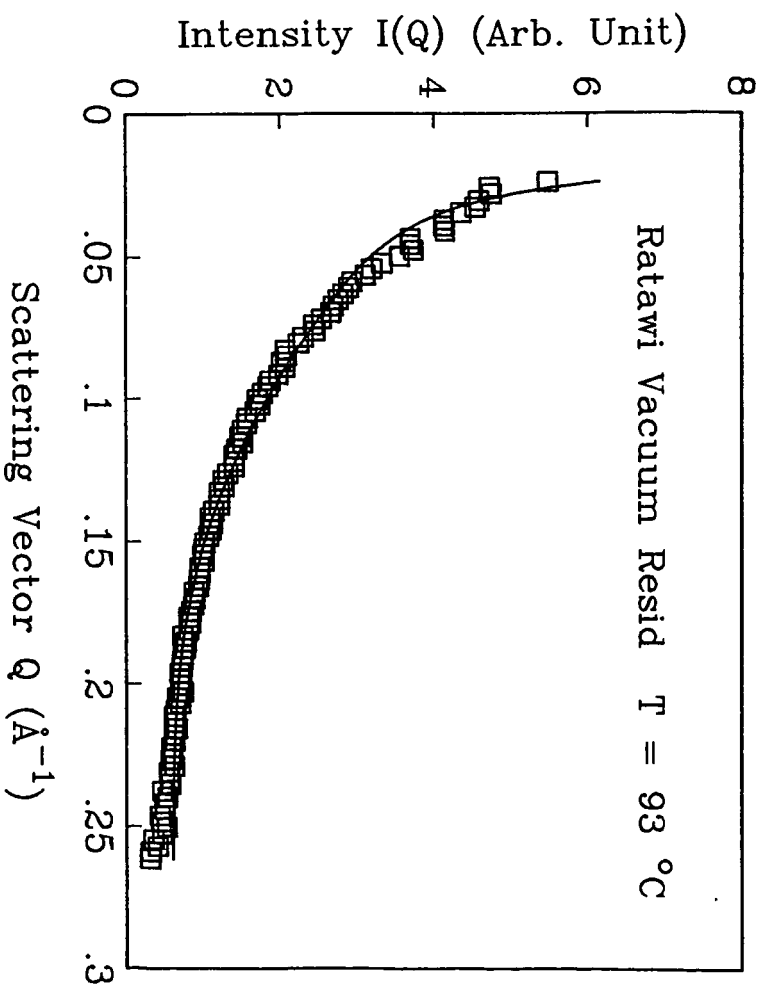
Italy, June 5-8, 1991

(14) Sheu, E. Y., DeTar, M. M. and Storm, D. A. *Fuel* 1991, 70, 1151

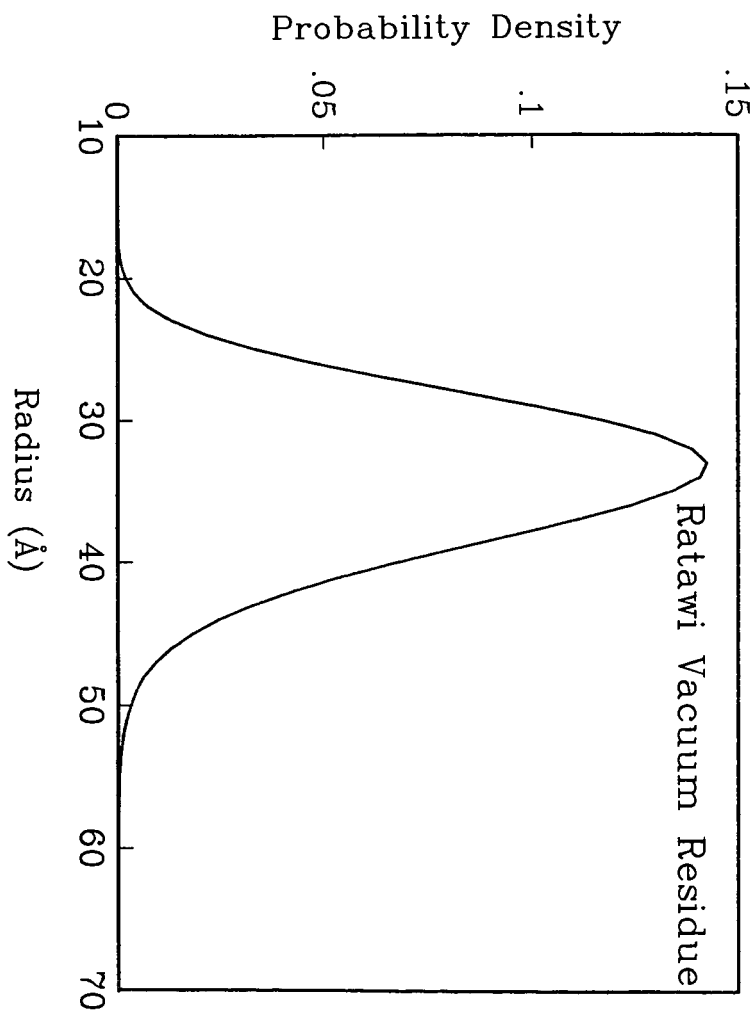
FIGURE CAPTIONS

Figure 1 Scattering intensity for Ratawi vacuum residue at 93° C

Figure 2 Distribution of radii of asphaltenic particles



Particle Size Distribution



COLLOIDAL STRUCTURE OF VACUUM RESIDUE IN SOLVENTS

Eric Y. Sheu, M. M. De Tar, and D. A. Storm
Texaco R & D Dept. P.O. Box 509, Beacon, N. Y. 12508

Key Words: asphaltenes, colloids, small angle neutron scattering (SANS).

I. Introduction

Petroleum asphaltenes form colloidal particles in organic solvents through self-association, when the concentration exceeds a threshold value [1-5]. The self-association process is very similar to the micellization process of surfactant systems [6]. Since the structure, size and the polydispersity of the asphaltene colloids are important parameters for developing technology to upgrade vacuum residue, it is necessary to establish an analytical technique capable of accurately evaluating these parameters. Small angle neutron scattering (SANS) has been successfully applied to the structural characterization of micellar solutions [7]. We employed this technique in this study to investigate asphaltenes. Unfortunately, the polydispersity and the intercolloidal interactions often complicate the data analysis, and lead to ambiguous results, due to local convergence in the data fitting process. Recently, Sheu [8] developed a self-consistent scheme, by which the particle size distribution can be unambiguously determined from a scattering measurement. This technique however, can only be applied for dilute systems, since the intercolloidal interactions were not taken into account.

In this study, we followed up on the polydispersity work of Sheu, with the interparticle interaction taken into account. We also studied the effect of solvent permittivity on particle structure, polydispersity and interparticle interactions.

II. Experimental

A. Sample Preparation

Asphaltene fractions were extracted from Ratawi (Neutral Zone) vacuum residue, by mixing with heptane (1 gram of vacuum residue with 40 cm³ of heptane) at room temperature. After stirring overnight, the solution was filtered with Whatman number 5 filter paper. The insoluble portion was dried under a stream of nitrogen, until constant weight was maintained for a 48 hour period. This insoluble fraction was taken as the asphaltene fraction.

To prepare the samples for the SANS measurement, asphaltenes were dissolved in deuterated toluene/pyridine mixtures of various volume ratios, and aged for several days to ensure thermodynamic equilibrium [9]. Toluene has a permittivity of 2.4, while pyridine is 12, the samples were prepared to exhibit the following permittivities: 2.4, 3.84, 5.28, 6.72, and 9.12.

B. SANS Measurement

The SANS experiment was conducted on the small angle diffractometer (SAD) at Argonne National Laboratory. The neutrons were generated by a neutron generator via Pu-Be reaction. The generated neutron wave lengths were sorted by the time-of-flight method, in order to fully utilize the generated neutrons. The scattering vector Q ($Q = (4\pi/\lambda) \sin \theta$) was computed by built-in software using neutron

energy. Therefore, the sample-to-detector distance was fixed. The temperature was maintained at 22 °C.

III. Scattering Theory

The intensity as a function of the scattering vector, $I(Q)$, represents the differential cross section per unit volume of the sample. $I(Q)$ is a function of concentration, particle-solvent contrast, particle structure, and interparticle interactions [10],

$$I(Q) = C (\Delta\rho)^2 \left[\frac{\langle V_p^2 \rangle}{\langle V_p \rangle} \langle P(Q) \rangle \langle S(Q) \rangle \right] \quad (1)$$

where C is concentration, $\Delta\rho$ is the particle-solvent contrast, $\langle V_p^2 \rangle$ is the second moment of particle volume, and $\langle V_p \rangle$ is the average particle volume. $\langle P(Q) \rangle$ is the average form factor, governed by particle structure, and $\langle S(Q) \rangle$ is the average structure factor, governed by interparticle interactions. The evaluation of $\langle V_p^2 \rangle$, $\Delta\rho$, $\langle V_p \rangle$ and $\langle P(Q) \rangle$ are described in references 1 and 9.

To calculate $\langle S(Q) \rangle$, we approximated $\langle S(Q) \rangle$ by $S(Q)$ (the monodispersed particle structure factor) using $\langle R \rangle$ (the average particle radius) as the particle size. This approximation is generally plausible [10].

We computed $S(Q)$ by solving the Ornstein-Zernike equation using a mean spherical approximation ansatz. A one-tailed Yukawa potential was used as a direct correlation function [10]. A fortran program was developed to compute $S(Q)$, along with $\langle P(Q) \rangle$. This program enabled us to unambiguously determine both particle structure and interparticle interactions.

IV. Results

Fig. 1 displays the scattering intensity $I(Q)$ (open circles) and the fitted curve (solid line). The fitting is reasonable for Q up to $\sim 0.2 \text{ \AA}^{-1}$. Fig. 2 shows the average radius $\langle R \rangle$ and the Yukawa parameter, K , as a function of solvent permittivity. K represents the "diffusiveness" of the Yukawa potential,

$$V(r) = A \cdot \text{Exp}(-Kr)/Kr, \quad r > \langle R \rangle$$

where A is an amplitude factor representing the contact potential at $r = \langle R \rangle$. As one can see from Fig. 2, the average radius does not depend on solvent permittivity, but the diffusiveness of the interparticle interaction increases (K decreases). This indicates that the range of interaction increases. Obviously, this is due to "effective" charges on the asphaltene colloids, which result in long range interactions when solvent permittivity increases. Fig. 3 shows the polydispersity as a function of solvent permittivity. It was found to increase substantially as a function of solvent permittivity. From Gibbs' equilibrium condition this result clearly indicates that for permittivities up to ~ 9.0 , the solvent quality decreases as a function of permittivity [10].

V. Discussion

In aqueous solutions, the K in Yukawa potential is equal to kR , where k is the Debye screening length. In our case, the solvents were oil-like, which may change the meaning of K . Therefore, K can only be visualized as a parameter characterizing the "diffusiveness" of the the potential.

As for the polydispersity, we argue based on the first principle given by Gibbs, about thermal equilibrium. Based on Gibbs' equilibrium condition, the polydispersity should increase when the solvent quality becomes poorer, in order to optimize the free energy through eutropic energy [10.11]. This finding leads us to conclude that the asphaltene colloids behave similarly to surfactant solutions, and by tuning the solvent permittivity, dispersion of asphaltene colloids may be possible. This conclusion may shed light on the upgrading of vacuum residue.

References

- [1] E.Y. Sheu, D.A. Storm and M.M. De Tar, *J. Non-Cryst. Solids*, **131** 341 (1991).
- [2] R.E. Overfield, E.Y. Sheu, S.K. Sinha and K.S. Liang, *Fuel Sci. and Tech. Int'l.*, **1** 611 (1989).
- [3] P.D. Herzog, and D. Espinot, *FUEL*, **67** 245 (1988).
- [4] J. C. Ravey, G. Docouret, and D. Espinot, *FUEL*, **67** 1560 (1988).
- [5] T.F. Yen, *Energy Sources*, **1** 447 (1974).
- [6] E.Y. Sheu, M.M. De Tar, and D.A. Storm, "Aggregation and Kinetics of Asphaltenes in Organic Solvents," to appear in *FUEL*.
- [7] S.H. Chen and E.Y. Sheu, in "Statistical Mechanics and Thermodynamics of Micelle and Microemulsion Systems" ed. by S.H. Chen and P. Rajagopalan, Spring-Verlag (1990).
- [8] E.Y. Sheu, "Particle Size Distribution for a Non-Interacting Dispersed System, Studied by Small Angle Scattering," to appear in *Phys. Rev. A*.
- [9] E.Y. Sheu, K.S. Liang, S.K. Sinha, R.E. Overfield, "Polydispersity Analysis of Asphaltenes in Toluene," submitted to *J. Coll. Int. Sci.*
- [10] E.Y. Sheu and S.H. Chen, "The Hydrophobic Effect, Formation of Micelles and Biological Membranes," *J. Wiley A. Sons, N.Y.* (1980).

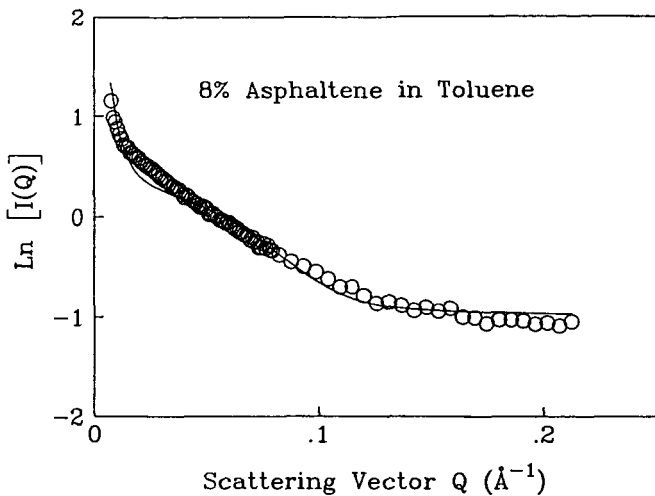


Fig. 1. Fitting of a 8% asphaltene solution. The SANS data (circles), and the theoretical curve (solid line) agree reasonably well, indicating that a one-tailed Yukawa potential is an appropriate representation of the interactions between asphaltene colloids .

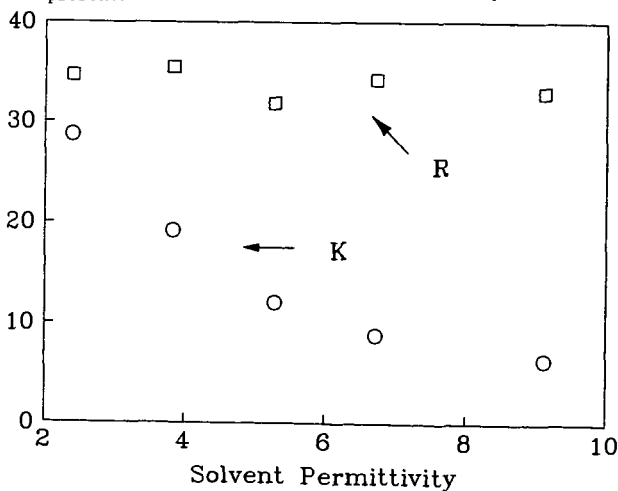


Fig. 2. Average particle radius and potential diffusiveness as a function of the solvent permittivity. The diffusiveness increases (K decreases) as a function of the solvent permittivity, while the average radius remains nearly unchanged.

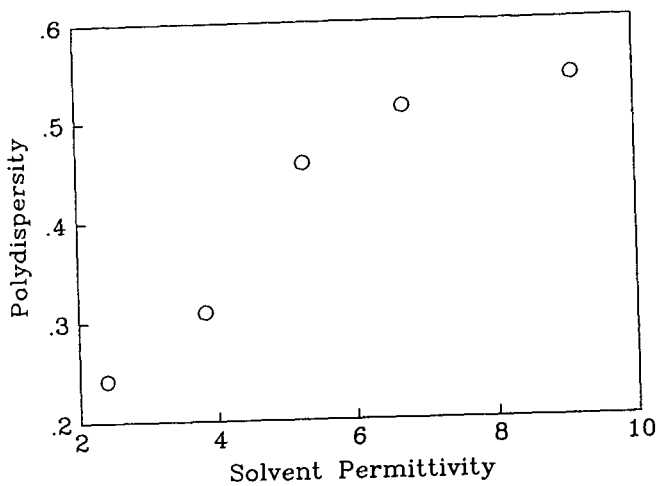


Fig. 3. Polydispersity, as a function of the solvent permittivity, for an 8% asphaltene concentration.

THE ARGONNE COALS DO NOT HAVE AN EXTENDED INTER-CONNECTED PORE NETWORK

John W. Larsen & Patrick C. Wernett
Department of Chemistry
Lehigh University
Bethlehem, Pennsylvania 18015

Keywords: pore structure, gas adsorption, surface area

ABSTRACT

The sorption of N_2 , CO_2 , ethane, cyclopropane, cyclobutane, cyclopentane, and cyclohexane has been studied on all of the Argonne premium coals. For all of the bituminous coals, the CO_2 BET surface areas are as expected and much higher than all of the other molecules studied. Plots of \log (moles adsorbate in monolayer) vs. \log (cross section area of adsorbate) are straight lines whose slopes are very steep (-5.5 to -11.6) and inconsistent with the known fractal dimensionalities of the coal pore surfaces. For Zap lignite, the CO_2 BET surface area is $274m^2/g$, while all of the hydrocarbons give lignite surface areas of $8 \pm 3m^2/g$. These data are inconsistent with adsorption in an inter-connected pore network. For bituminous coals, the dependence of the amount sorbed vs. molecular diameter is similar to the dependence of diffusivities through glassy polymers on molecular diameter. We conclude that the pores in coal are isolated from each other and can only be reached by diffusion through the solid, glassy, macromolecular coal.

INTRODUCTION

It is widely accepted that coals contain an inter-connected network of slit like pores and that the connections between pores are often bottlenecked.¹ This conclusion is based almost entirely on experimental studies of gas adsorption. We have recently completed a study of the adsorption of a series of gases on the Argonne coals and obtained results which are inconsistent with this model. Our data for Illinois #6 coal have already been published and we will here discuss our results for some of the other Argonne coals.²

Small angle X-ray studies have been carried out on all of the Argonne coals and demonstrate that the pore surfaces are well behaved fractals.³ Being surfaces, their fractal dimensionalities are constrained to lie between 2 and 3. Fractal dimensionalities can also be obtained by determining the dependence of measured surface area on the size of the adsorbate molecule.⁴ Fractal dimensionalities obtained in this way should agree with those obtained by other techniques. The basis of the measurement is that small molecules will follow a rough surface more precisely than will larger molecules and thus report a larger surface area. The difference between the surface areas reported by a small and a large molecule will increase with the degree of surface roughness, that is with the fractal dimensionality. The fractal dimensionalities calculated from adsorption measurements carried out using ethane, cyclopropane, cyclobutane, cyclopentane, and cyclohexane

are reported in Table 1. The dimensionalities do not lie between 2 and 3 demonstrating that the process under investigation cannot be a simple equilibrium surface adsorption.

Perhaps the most impressive feature of these data are the great size of the calculated "fractal dimensionalities". They vary from 11 to 23. The amount of gas adsorbed varies with the cross sectional area raised to at least the 5th power. Stated another way, the amount of gas sorbed by these coals exhibits an extraordinarily steep dependence on gas molecular size, that dependence being between the 5th and 12th power of the cross sectional area. Any model for coal structure must rationalize this extraordinary fact.

This enormous sensitivity to molecular size is rare. Diffusivities through glassy polymers are known to have similar and even greater sensitivities to molecular size.⁵ We propose that the process occurring here is not gas adsorption on the surface, but rather diffusion of the gases through a glassy polymer to reach an internal pore surface. We are suggesting that the BET surface areas measured using these gases are not equilibrium values, but are controlled by the rate of diffusion of these gases through the glassy coal. This was confirmed by following the uptake of ethane by Illinois No. 6 coal at 177°K which had not reached equilibrium after 5.5 days.

We look to the surface areas measured using the individual gases for confirmation of the idea that it is diffusion through glassy polymers which is occurring, not diffusion through a more-or-less rigid pore network. We have already pointed out for Illinois No. 6 coal that we were unable to rationalize the reported surface areas based on diffusion through a interconnected network.² Figure 1 contains the data for Bruceton coal and the results are similar. CO₂, which is known to swell coals, has a ready diffusion pathway and reports a high surface area.⁶ Ethane, which differs in size from CO₂ by only 16% and which has a similar cylindrical shape, reports a much lower surface area. It is hard to rationalize this difference if both materials are diffusing through a rigid pore network. Cyclopropane has the same surface area as ethane, but a significantly different shape. It is hard to believe that two materials, one planar and the other cylindrical, would pass equally through a rigid pore system and report the same surface area. Similar results have been obtained for all of the other Argonne bituminous coals. These data support the notion that the coals do not have an interconnected pore network, but rather isolated pores like bubbles in a solid which are reached only by diffusion through the solid coal.

Finally, we consider the surface area measurements for ZAP lignite shown in Figure 2. Hydrocarbon gases should be essentially insoluble in this high oxygen, highly polar low rank coal. If the pore structure is a rigid network, this should have no effect on the surface areas measured. The data are shown in Figure 2 and reveal that within experimental error, all of the hydrocarbon gases report the same surface area, 8 ± 3 m²/g. This is to be contrasted with the CO₂ area which is 274 m²/g. We are unable to rationalize these data using a pore network structure. They are nicely consistent with a pore model which involves

isolated pores which can be reached only by diffusion through the solid.

We conclude that the pore structure of these coals is isolated pores which can be reached by diffusion through the coals and that an interconnected pore network which provides access to a large internal surface by pore diffusion does not exist. This structure model has a number of consequences, a few of which can be elaborated here. The first is that CO₂ surface areas are approximately correct. Because it is somewhat soluble in coals, CO₂ has a rapid diffusion pathway and can quickly reach all of the pore surfaces where it is adsorbed as it would be on any surface. These reported surface areas are undoubtedly somewhat in error because of the amount of CO₂ dissolved in the coal. We believe these errors are small compared to the fundamental uncertainties of the measurement. Likewise, we believe that helium densities give accurate pore volumes. Diffusion rates vary inversely with molecular size and helium is small enough to have reasonably rapid passage through the coal and reasonable equilibrium times. Because coal surface areas depend on the diffusion rate of the molecules used to probe it, measured surface areas will depend on the nature of the molecular probe. This would be true in any case because the surfaces are fractal, but we are concerned with a much greater sensitivity to molecule size and polarity. Molecules which interact with coals (are soluble in them) will have a rapid diffusion pathway and will report much greater surface areas than will non-polar hydrocarbons and other molecules which do not interact specifically.

EXPERIMENTAL

Complete experimental descriptions of all procedures used may be found in the Ph.D. thesis of Patrick Wernett.⁷

ACKNOWLEDGEMENTS

This work was supported by the U. S. Department of Energy Contract #DE-AC22-38PC89757. We gratefully acknowledge this support. Numerous discussions with Dr. Peter Hall played an important role in the development of our ideas and we are grateful to him.

REFERENCES

1. Bond, R. L. Nature **1956**, 104-105. Mahajan, O. P.; Walker, P. L., Jr. Analytical Methods for Coal and Coal Products, **1**, C. Karr Jr., Editor, Academic Press: New York, NY, 1979. Marsh, H. Carbon **1987**, 25, 49-58.
2. Larsen, J. W.; Wernett, P. Energy & Fuels **1988**, 5, 719-720.
3. Hall, P.J.; Wernett, P.C.; Larsen, J.W. unpublished.
4. Farin, D.; Peleg, S.; Yavin, D.; Avnir, D. Langmuir **1985**, 1, 399-407. Farin, D.; Volpert, A.; Avnir, D. J. Am. Chem. Soc. **1985**, 107, 3368-3370. Pfeifer, P.; Avnir, D. J. Chem. Phys. **1983**, 79, 3558-3565.

5. Crank, J.; Park, G. S. Diffusion in Polymers Academic Press: New York, NY, 1968. Van Krevelen, D. W.; Hoftyzer, P.J. Properties of Polymers Elsevier Scientific Publishing Company: New York, NY 1976. Berens, A. R.; Hopfenberg, H. B. J. Membr. Sci **1982**, 10 283-303.
6. Reucroft, P. J.; Patel, H. Fuel, **1986**, 65, 816-820. Walker, P.L., Jr.; Verma, S.K.; Rivera-Utrilla, J.; Khan, M.F. Fuel, **1988**, 67, 719-726.
7. Wernett, P. C. Ph.D. Thesis, Lehigh University, 1991.

Table 1. Fractal Dimensionality of Argonne Coal Surfaces Measured by BET Adsorption of Ethane, Cyclopropane, Cyclobutane, Cyclopentane, and Cyclohexane

Coal	%C dmmf	Dimensionality	Correlation Coefficient
Pocahontas #3	91.8	12	0.998
Upper Freeport	88.1	11	0.995
Lewiston-Stuchton	85.5	15	0.942
Pittsburgh No. 8	85.0	16	0.987
Blind Cargon	81.3	14	0.990
Illinois No. 6	80.7	23	0.999
Wyodak	76.0	11	0.867

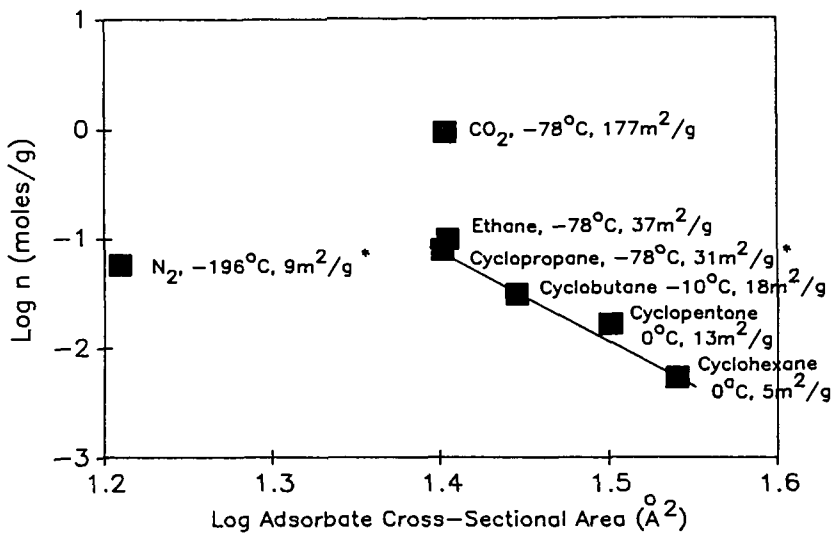


Figure 1. Fractal Analysis of the Cyclic Hydrocarbon Gas Adsorption on Argonne Pittsburgh No. 8 Coal (n is the Number of Moles Required for Monolayer Surface Coverage Obtained from the BET Equation). The Adsorbate Gas is Given Followed by the Adsorption Temperature and the Measured BET Surface Area.

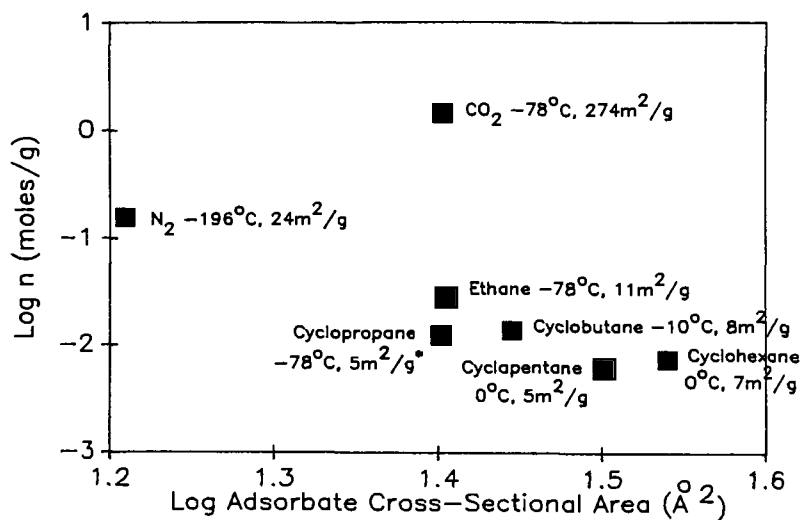


Figure 2. Fractal Analysis of the Cyclic Hydrocarbon Gas Adsorption on Argonne Beulah Zap Lignite (n is the Number of Moles Required for Monolayer Surface Coverage Obtained from the BET Equation). The Adsorbate Gas is Given Followed by the Adsorption Temperature and the Measured BET Surface Area.

Structural Changes in High-rank Bituminous Coals Caused by Solvent Swelling and Heat

Yongseung Yun and Eric M. Suuberg
Division of Engineering, Box D
Brown University, Providence, RI 02912

(Key Words: Bituminous coal structure, Solvent swelling, Differential Scanning Calorimetry)

INTRODUCTION

High-rank coals (>86 %C daf) have been known to exhibit fundamentally different response characteristics to heat and solvent treatments than lower-rank coals (< 86 %C daf). Sakurovs et al.[1] reported that heat is more effective than pyridine for creating mobility in coal structure, for coals of 86-90 %C daf. Also Iino et al.[2] showed that extraction yields using solvent mixtures of CS₂/N-methyl-2-pyrrolidinone(MP) (1:1 v/v) increase with carbon content up to 86 %C daf and then fall rapidly with further increase in carbon content.

High-rank coals do not significantly swell in pyridine, while most lower-rank coals show a substantial amount of swelling in that solvent. However, some combinations of solvents, especially with CS₂, yield for the higher-rank coals similar swelling ratios as can be obtained in lower-rank coals. The work of Iino et al.[2-4] is especially noteworthy, since they first reported the benefit of mixing CS₂ (which is a known good solvent for fats, resins, and rubbers) with several solvents (i.e., pyridine, dimethylsulfoxide, dimethylformamide, dimethylacetamide, MP), in enhancing extraction yield and volumetric swelling of coal, particularly around 86 %C daf.

It has also been demonstrated that the structure of high-rank bituminous coals can be thermally loosened, to yield high volumetric swelling ratios in pyridine (when the coals are heated to above 350°C)[5,6]. These swelling ratios are similar to those which can be obtained at room temperature in mixtures of CS₂/pyridine, CS₂/dimethylsulfoxide, or CS₂/dimethylformamide as will be shown in this paper.

In order to understand the underlying structural changes caused both by mixed solvents and heat, as well as to explore possible effective pre-liquefaction strategies for these high-rank bituminous coals, two coals, viz., Upper Freeport (mvb) and Pocahontas No. 3 (lvb), were studied using differential scanning calorimetry (DSC) and solvent swelling techniques.

EXPERIMENTAL

Aliquots of several coal samples, obtained from the Argonne National Laboratory - Premium Coal Sample Program, were analyzed by DSC and solvent swelling techniques. These samples included Illinois No. 6 (-20 mesh), Blind Canyon (-20 mesh), Upper Freeport (-100 mesh), and Pocahontas No. 3 (-20 mesh) coals. They were used as-received. Detailed petrographic, chemical, and physical analysis data on these coals can be found elsewhere [7].

Differential Scanning Calorimetry A DuPont 2910 DSC system with a liquid nitrogen cooling accessory (LNCA-II) was employed in this study. The sample cell was operated under a nitrogen flow rate of 90 ml/min in order to keep the cell free of oxygen during measurement. Aluminum sample pans were used in an unsealed mode. This was done by just pushing down the

top sample pan cover gently onto the bottom pan containing the coal. Samples were initially isothermal for five minutes and then heated from 30°C at 8 °C/min or 10 °C/min. Typically 6-9 mg of sample was used in an experiment. Cooling of the cell between consecutive heating scans normally involved air convection in the heating assembly, but the sample itself was always kept under nitrogen.

Solvent Swelling Coal samples were placed in constant diameter tubes (3 mm i.d., ca. 5 cm long) and centrifuged at 7500 rpm for 3 min in a roughly 30 cm horizontal rotor (SAVANT HSC-10K high speed centrifuge), after which the initial height of the sample was measured by a caliper. The choice of 7500 rpm was rather arbitrary and selected only to be as high as could be comfortably tolerated by the equipment. Solvent was then added and stirred until a visual check showed the total submergence of coal in solvent. The stirring was repeated frequently (normally 3 times) during the first 30 min following solvent addition. At the desired measurement times, the sample tubes were centrifuged again (7500 rpm for 3 min), the swollen coal height measured, and the solvent replaced with the clean solvent. This assured that the concentration of extractable was not so high as to interfere with the measurement.

Samples (22-28 mg) for solvent swelling were prepared in the DSC at a heating rate of 8 °C/min under a nitrogen flowrate of 90 ml/min. After reaching the desired temperature, each sample was cooled immediately by contacting the bottom of the sample pan with ice or cold water. Swelling solvents employed were all reagent grade and were used without any further purification.

Sample Pretreatment In order to determine the main parameters governing the relaxation of coal structure, several treatments were performed before subjecting the samples to DSC or solvent swelling. These include preswelling by solvent, pyridine Soxhlet extraction, acetylation, and heat treatment. Solvent preswelling was performed in two ways. One method involved swelling coal samples in the constant diameter glass tubes, which were used in the normal swelling experiments described earlier. The swelling was performed in excess solvent at room temperature for about 3-4 days with frequent replacement of extract-laden solvent with fresh solvent. The samples were subsequently dried under vacuum (<30 inHg) at room temperature for about two days. Another approach involved Soxhlet extraction of samples with pyridine for about two days, until the color of pyridine in the extraction tube indicated no further extraction. Then the sample was washed with deionized water, filtered using a water aspirator, and dried under vacuum (<30 inHg) at room temperature for about two days. Thus in the first case the samples were swelled but not exhaustively extracted, whereas in the second case the samples were exhaustively extracted (as well as presumably being fully swelled). Acetylation of hydroxyls was accomplished by mixing coal with excess pyridine and excess acetic anhydride at room temperature for about three days, and then excess acetic anhydride was destroyed by reaction with water while excess pyridine was removed by washing the sample with water. The acetylated sample was subsequently dried under vacuum at room temperature for about two days.

RESULTS AND DISCUSSION

Figure 1 shows difference DSC spectra, solvent swelling ratios in pyridine and tetrahydrofuran (THF), and pyrolytic mass loss for the Upper Freeport and Pocahontas No. 3 coals. The mass loss curves indicate the total loss observed from individual samples heated at 8°C/min and then immediately quench-cooled from the specified temperature by contacting the bottom of the sample pan with ice or cold water. The mass loss around 100°C shows the loss of moisture (around 1% in each sample) and the upturn at around 300°C heralds the onset of pyrolytic weight loss. It is presently unclear at what temperature pyrolysis reactions actually begin in these samples, since the mass loss at near 300°C might include physical evaporation of small molecules, in a manner analogous to the loss of water at 100°C. This point will be further discussed below.

The solvent swellability of the raw Upper Freeport and Pocahontas No. 3 samples is very low, prior to heat treatment (see middle panels of Figure 1). Both exhibit a volumetric swelling ratio of roughly 1.1 in pyridine, prior to heat treatment. As we discussed in our earlier papers [5,6], heat treatment appears to irreversibly "relax" the coal structure somewhat, such that both swellability in pyridine and THF is greatly enhanced, as is also seen in Figure 1. The temperature at which increased swellability is first observed is around 300°C in both the Upper Freeport coal and the Pocahontas No. 3 coal, although it takes considerably higher temperatures to achieve maximum swellability in the latter.

As we earlier noted [5], such irreversible changes in swellability correspond with events observed by DSC (see the top panels of Figure 1). In both coals, the dramatic rise in swellability coincides with a significant endothermic peak in the DSC spectra. The spectra are shown as difference spectra, obtained by scanning through the same temperature range three times with the same sample. The first minus second and first minus third scan spectra show the peaks distinctly, centered at 350°C in the Upper Freeport coal and at around 425°C in the Pocahontas No. 3 coal. The peaks around 100°C involve moisture loss. The second minus third scans show the absence of these peaks, confirming the irreversibility of the processes.

Figure 2 shows the actual raw DSC spectra for the two coals of interest here, compared with two spectra for lower-rank bituminous coals. While somewhat less distinct in feature than the subtracted spectra of Figure 1, the curves in the top panel show the clear endothermic peaks at 350°C and 425°C for the Upper Freeport and Pocahontas No. 3 coals, respectively. Such distinct peaks are not visible in the spectra of the lower rank coals in the lower panel in Figure 2, in which water evaporation process (endothermic) is followed by a more or less straight DSC response curve corresponding to the heat capacity of coal, and then followed by thermal degradation process where a peak occurs in the exothermic direction, in part due to weight loss. What is notable from the top panel is that the endothermic peaks corresponding to the irreversible relaxation of the structures of the higher rank coals are well separated from the main pyrolysis events, seen as major disturbances in the DSC curves. The sharp peak into the exothermic direction in the Upper Freeport coal is mainly caused by the sudden expansion of sample volume, with the development of plasticity.

The above observations do not establish the nature of the events resulting in the endothermic peaks coinciding with the relaxation event in the high-rank coals. They might be reaction endotherms, occurring prior to the main pyrolysis reactions, or they could be physical events of an endothermic nature (such as "melting"). The fact that the events are irreversible does not necessarily rule out an explanation based on physical processes, since the coal obviously does not have to reassume the same physical form upon cooling as it had in the raw state. We believe that the events have a high probability of having physical origin, based upon other observations. First, the endothermic peaks for two high-rank bituminous coals are similar to the "hysteresis" peak normally occurring just after the glass transition temperature in stressed polymers [8]. The hysteresis peak is mainly caused by stress relief of the structure by heat, quite often observed in amorphous polymers, e.g., epoxies, polycarbonate, polystyrene. Second, we believe that the behavior of one of the coals in certain solvents supports the hypothesis of a physical process.

It has been noted [2-4] that higher rank bituminous coals show a remarkably high degree of extractability in mixtures of certain solvents with CS₂. The Upper Freeport coal shows a sharp increase in room temperature swellability in a mixture of pyridine and CS₂, as noted in Figure 3. There is no need to heat treat the coal to achieve significant swellability, which suggests that a physical relaxation of the structure is all that is involved. There is, of course, the possibility that CS₂ undergoes chemical reaction with the coal, cleaving similar numbers of bonds as are cleaved

during heat treatment, but there is no strong reason to believe that this should be so. Moreover, as the data of Figure 3 show, there is a maximum in swelling ratio for the 1:1 by volume mixture of pyridine and CS₂. It would be difficult to understand why, if CS₂ is a chemically reacting agent, such a stoichiometry would be needed, when solvent is in large excess. We thus are led to the tentative conclusion that the CS₂/pyridine mixtures are effective mainly because of specific solvent properties.

The fact that the CS₂/pyridine mixture relaxes the coal structure in a manner similar to heat, is established in Figure 4. Treating the coal with CS₂ alone, pyridine alone, or chloroform/pyridine mixtures leaves intact the DSC peak, corresponding to the relaxation of the structure. The Upper Freeport coal treated in CS₂/pyridine, however, no longer shows such a relaxation event at 350°C. The CS₂/pyridine mixture is not nearly as effective a swelling agent for Pocahontas No. 3 coal as for Upper Freeport coal. This, too, is confirmed by the DSC which still records a significant relaxation event for the previously pyridine/CS₂ treated Pocahontas No. 3 coal (see lower panel of Figure 4). Apparently this specific solvent combination is only effective for a certain range of ranks. This is consistent with the observations of Iino et al.[3].

There is nothing particularly unique about the choice of pyridine in mixture with CS₂. As Iino et al. earlier showed [2,3], N-methyl-2-pyrrolidinone/CS₂ mixtures are also effective. We have established, as Iino et al. noted, that CS₂/dimethylsulfoxide(DMSO) and CS₂/dimethylformamide are also effective mixtures (see Table 1). Thus the solvent pair need not even include a nitrogen base, since DMSO is not. All the effective solvents in CS₂ mixtures are, however, fairly good electron donors.

Pyridine was tried in admixtures with other solvents of similar solubility parameter to CS₂, and with other solvents that could serve as effective electron acceptors (see Table 1). None of these other combination rivaled the ability of the CS₂/pyridine mixture to swell the Upper Freeport coal. Of course, these solvents did not yet include particularly strong electron acceptors (strong acids) and work on this point continues.

Pretreatment of the coal by pyridine extraction has little effect on its subsequent behavior in CS₂/pyridine (see Table 1). Pretreatment of the coal by acetylation does little to change the behavior of the coal with respect to swelling in CS₂/pyridine mixtures. This means that the structure is not irreversibly expanded to a significant extent by the acetylation alone. This suggests that it is not, for example, a xanthate formation type of process [9-11] involving CS₂ and the hydroxyl groups in the coal that results in the greater swellability of the coal in CS₂/pyridine mixtures. The completeness of our acetylation has not yet been established, so its conclusion is still tentative.

Pretreatment of the coal in CS₂, followed by removal of the CS₂ by evaporation and then subjected to pyridine swelling, showed again the importance of the interaction of pyridine and CS₂. The sequence resulted in pyridine swelling comparable to that of the raw untreated coal (see Table 2). Reversing the order of sequential exposure was also not effective (again see Table 2).

When the coal was "relaxed" by exposure to CS₂/pyridine mixtures, it was more swellable than in the raw state, by either of these solvents (see Table 2). The fact that the swellability was not as great as that induced by the thermal treatment to 350°C is also seen in Table 2. This is because

once swollen in pyridine/CS₂ mixture, it is difficult to fully remove all of the pyridine from the coal by vacuum drying. Thus the coal is already in a partially swollen state, due to the irreversibly bound pyridine. Heating a CS₂/pyridine swollen coal to 350°C results in a higher subsequent pyridine swellability (relative to the vacuum dried CS₂/pyridine swelled coal), because the pyridine is fully lost upon heating.

Results of swelling by solvents for low volatile bituminous Pocahontas No. 3 coal (91.1 %C daf) are illustrated in Table 3. As can be expected from DSC responses for CS₂/pyridine-swollen Pocahontas No. 3 coal (see Figure 4), even CS₂/pyridine mixture was not as effective in swelling as for Upper Freeport coal. However, heat treatment up to 450°C can relax the coal structure enough to induce swelling of more than 60% by THF and pyridine. At present, only heat appears to be an effective agent for loosening the structure of low volatile bituminous coal significantly.

CONCLUSIONS

- Two high-rank bituminous (Upper Freeport: mvb, Pocahontas No. 3: lvb) coals exhibit a distinct endothermic DSC peak corresponding to the irreversible relaxation of the structure. The endothermic peaks are well separated from the main pyrolysis events and appear to originate from physical processes rather than from chemical reaction processes.
- Even strong solvents (e.g., pyridine) cannot swell the structure of high-rank coals more than ten percent at low temperatures (<250°C). Heat treatment above 300°C can enhance the swelling of both Upper Freeport and Pocahontas No. 3 coals significantly. Solvent swelling by mixtures of solvents (e.g., with CS₂) is effective in relaxing the structure of medium volatile bituminous Upper Freeport coal, but not for low volatile bituminous Pocahontas No. 3 coal.
- The efficacy of mixed solvents containing CS₂ and certain solvents (e.g., pyridine, dimethylsulfoxide, dimethylformamide) appears to be physical. The work to confirm more conclusively this hypothesis is in progress.

ACKNOWLEDGEMENT The work reported here was financially supported by the Department of Energy Contract No. DE-AC22-91PC91027.

REFERENCES

1. Sakurovs, R.; Lynch, L.J.; Barton, W.A. In *Coal Science II*; Schobert, H.H., Bartle, K.D., Lynch L.J., Ed.; ACS Symposium Series 461; ACS: Washington, DC, 1991; Chapter 9, p 111.
2. Iino, M.; Takanoashi, T.; Ohsuga, H.; Toda, K. *Fuel* **1988**, *67*, 1639.
3. Takanoashi, T.; Iino, M. *Energy Fuels* **1990**, *4*, 452.
4. Iino, M.; Matsuda, M. *Fuel* **1983**, *62*, 744.
5. Yun, Y.; Otake, Y.; Suuberg, E.M. *Prepr. Pap.- Am. Chem. Soc., Div. Fuel Chem.* **1991**, *36(3)*, 1314.
6. Suuberg, E.M.; Otake, Y.; Deevi, S.C. *Prepr. Pap.- Am. Chem. Soc., Div. Fuel Chem.* **1991**, *36(1)*, 258.
7. Vorres, K.S. *User's Handbook for the Argonne Premium Coal Sample Program*; Argonne, Illinois, 1989.
8. Meesiri, W.; Menczel, J.; Gaur, U.; Wunderlich, B. *J. of Polymer Science* **1982**, *20*, 719.
9. Petrucci, R.H. *General Chemistry*; The Macmillan Co.: New York, 1972.
10. Morrison, R.T.; Boyd, R.N. *Organic Chemistry*; Allyn and Bacon, Inc.: Boston, 1983.
11. Roberts, J.D.; Caserio, M.C. *Modern Organic Chemistry*; W.A. Benjamin, Inc.: New York, 1967.

Table 1. Volumetric Swelling Ratio by Mixed Solvents (1:1 v/v) for Upper Freeport Medium Volatile Bituminous Coal

Pretreatment	Solvent mixture (1:1 v/v)	Solvent characteristics			Q**
		Solvent	Acceptor Number	$\delta(H)^*$	
None	CS ₂ /pyridine	pyridine	14.2	10.4	1.95
	CS ₂ /dimethylsulfoxide	dimethylsulfoxide	19.3	12.8	1.75
	CS ₂ /dimethylformamide	dimethylformamide	16.0	11.5	1.92
	CS ₂ /n-butylamine	n-butylamine	-	-	1.21
	pyridine/water	water	-	9.4	1.08
	pyridine/methanol	methanol	41.3	12.9	1.09
	pyridine/chlorobenzene	chlorobenzene	-	9.5	1.12
	pyridine/chloroform	chloroform	-	9.3	1.13
	pyridine/methylene chloride	methylene chloride	-	9.7	1.14
	pyridine/nitroethane	nitroethane	-	11.1	1.09
	Pyridine Soxhlet extracted	CS ₂ /pyridine	CS ₂	-	10.0
Acetylated	CS ₂ /pyridine	CS ₂	-	10.0	1.71

* δ : solubility parameter in Hildebrand which is equivalent to $\text{cal}^{1/2}\text{cm}^{-3/2}$ **Q: volumetric swelling ratio

Table 2. Solvent Swelling Results for Upper Freeport Medium Volatile Bituminous Coal

Pretreatment	Solvent	Solvent Properties				Q*	Swelling number** ($\times 10^3$)
		Donor No.	Acceptor No.	$\delta(H)^*$	Molar Vol.(cc/mol)		
None	pyridine	33.1	14.2	10.4	80.9	1.14	1.73
	CS ₂	-	-	10.0	60.3	1.08	1.33
	n-butylamine	-	-	-	99.8	1.12	1.20
	THF	20.0	8.0	9.1	81.1	1.08	0.99
	dimethylsulfoxide	29.8	19.3	12.8	71.0	1.09	1.27
	dimethylformamide	26.6	16.0	11.5	77.4	1.08	1.03
CS ₂ swelled	pyridine	33.1	14.2	10.4	80.9	1.12	1.48
Pyridine Soxhlet extracted	pyridine	33.1	14.2	10.4	80.9	1.19	2.35
	CS ₂	-	-	10.0	60.3	1.07	1.16
CS ₂ /pyridine (1:1 v/v) swelled	pyridine	33.1	14.2	10.4	80.9	1.40	4.94
	CS ₂	-	-	10.0	60.3	1.30	4.97
Heated under N ₂ up to 350°C	THF	20.0	8.0	9.1	81.1	1.82	10.11
	pyridine	33.1	14.2	10.4	80.9	2.17	14.46
	CS ₂	-	-	10.0	60.3	1.50	8.29
	dimethylsulfoxide	29.8	19.3	12.8	71.0	1.49	6.90
	chlorobenzene	-	-	9.5	101.7	1.40	3.93
CS ₂ /pyridine swelled and heated up to 350°C	pyridine	33.1	14.2	10.4	80.9	1.83	10.26
Acetylated	pyridine	33.1	14.2	10.4	80.9	1.10	1.24
	CS ₂	-	-	10.0	60.3	1.06	0.99

* δ : solubility parameter in Hildebrand which is equivalent to $\text{cal}^{1/2}\text{cm}^{-3/2}$ *Q: volumetric swelling ratio **Q-1/molar volume

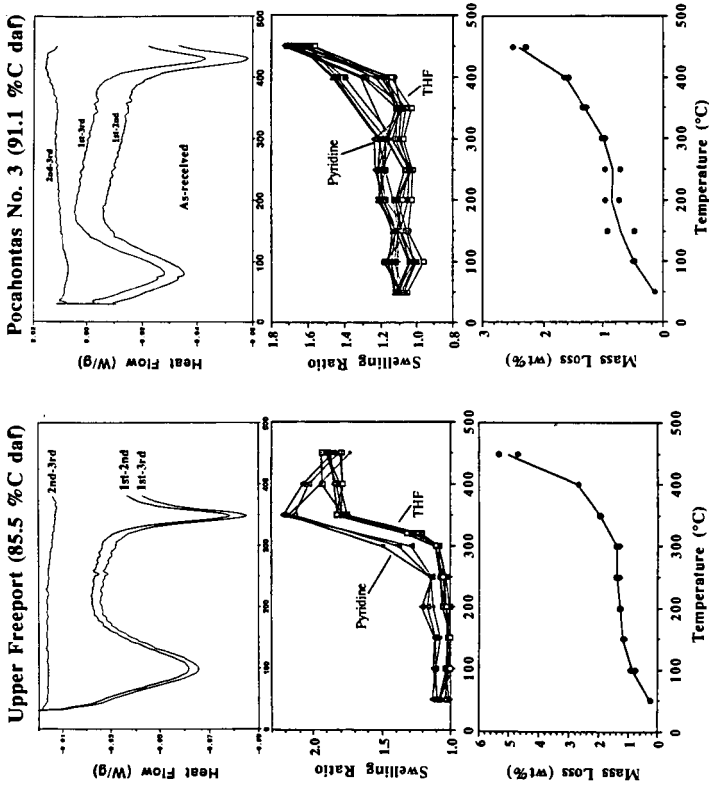


Figure 1. DSC difference thermograms as well as profiles of swelling ratio and weight loss for Upper Freeport (~100 mesh) and Pocahontas No. 3 (~20 mesh) coals. DSC was performed at 8°C/min under N₂ atmosphere.

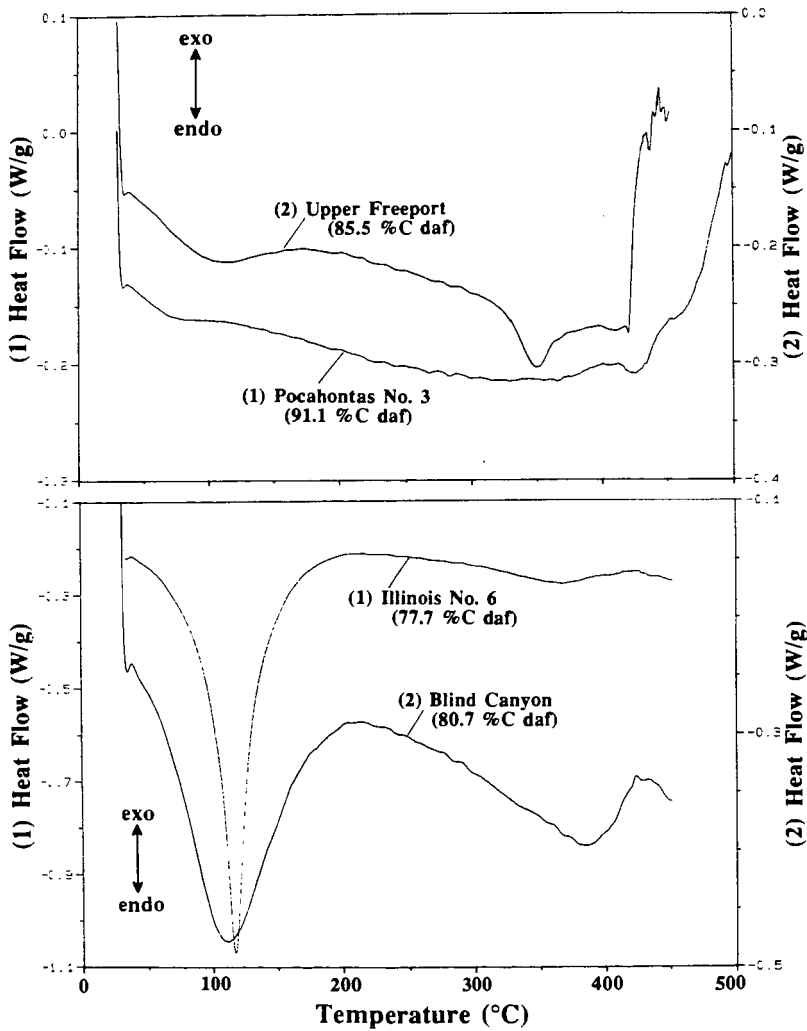


Figure 2. Comparison of DSC thermograms obtained at 8°C/min for different rank bituminous coals.

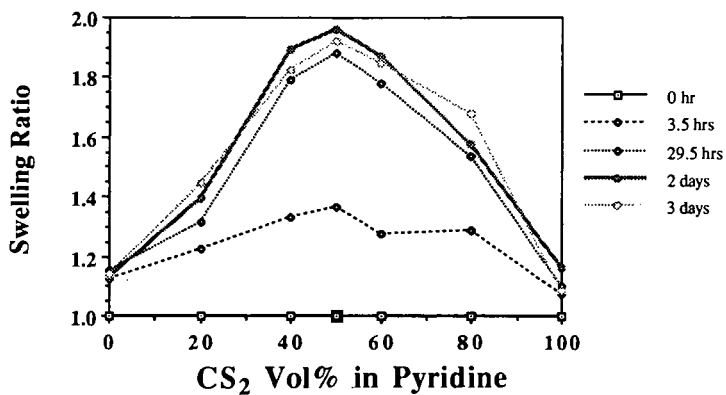


Figure 3. Changes of volumetric swelling ratio by mixed solvents of CS₂ and pyridine for Upper Freeport coal.

Table 3. Solvent Swelling Results for Pocahontas No. 3 Low Volatile Bituminous Coal

<u>Pretreatment</u>	<u>Solvent</u>	<u>Q</u>	<u>Swelling number (x10³)</u>
None	pyridine	1.12	1.48
	CS ₂	1.16	2.65
	THF	1.10	1.23
	CS ₂ /pyridine (1:1 v/v)	1.16	-
CS ₂ swelled	pyridine	1.13	1.61
Heated under N ₂ up to 450°C	THF	1.65	8.01
	pyridine	1.72	8.90

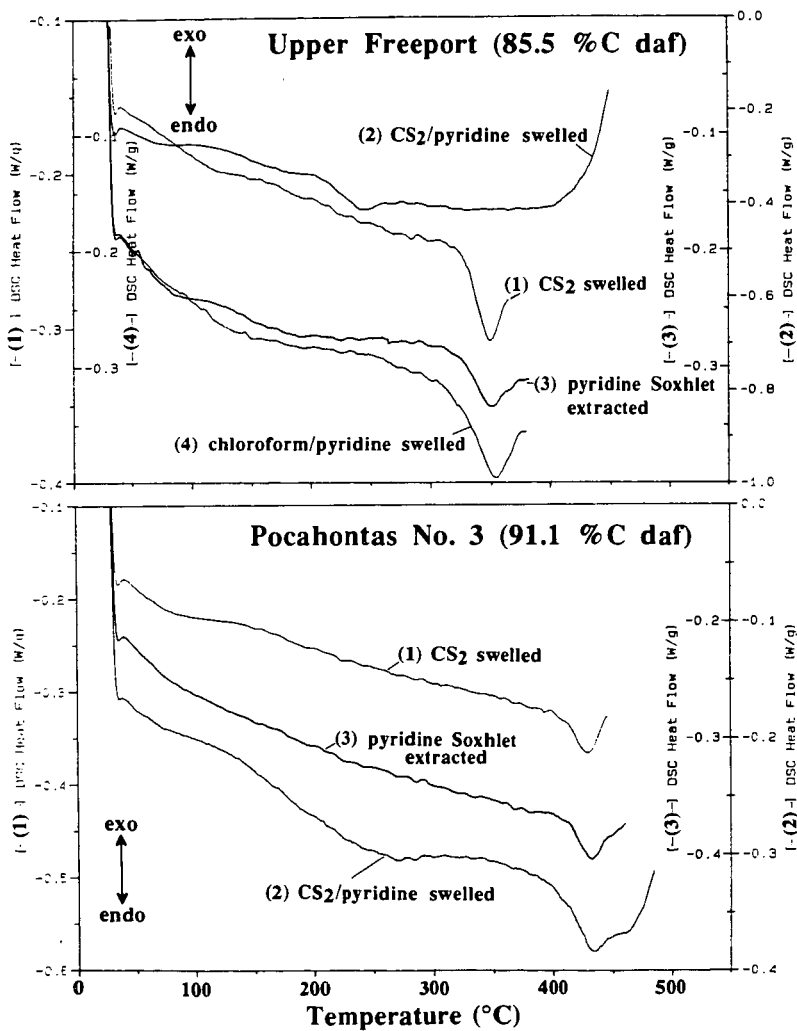


Figure 4. DSC thermograms obtained at 10°C/min for differently pretreated samples, illustrating the relaxed coal structure already at room temperature in CS₂/pyridine (1:1 v/v) swelled Upper Freeport Coal.

THE VISCOELASTIC BEHAVIOR OF SOLVENT-SWOLLEN COAL

George D. Cody, Alan Davis, Semih Eser,
Patrick G. Hatcher, Paul Painter
The Pennsylvania State University
University Park, PA

Keywords: Coal, Macromolecular Structure, Viscoelasticity

Introduction

Under conditions typical of most industrial processes, such as liquefaction, coal is subjected to thermal and pressure-driven stresses. Deformation, diffusion, and chemical reaction all occur simultaneously during liquefaction; in order to optimize process conditions, it is important to understand the nature of such internal processes occurring within coal. Details on the time dependences of such processes could reveal much about the architecture of coal's macromolecular network.

Viscoelasticity is an important time-dependent phenomenon in terms of elucidating aspects of coal's structure. Coal's viscoelastic properties in the glassy state have been measured by numerous researchers¹⁻⁵; under such conditions the measurements only detect deformational mechanisms which are rapid and correlate over a very short contour interval, where the contour describes the spatial arrangement of a macromolecular chain. At higher temperatures ($T > 250$ °C) deformational mechanisms involving larger scale contour relationships become important. It is these larger scale motions which dominate coal's physical response to process conditions. The thermo-mechanical behavior of coals has also been measured; in addition to viscoelastic behavior at elevated temperatures thermal degradation also accompanies the viscoelastic deformation. The presence of such parallel processes greatly hinders interpretation of macromolecular characteristics, i.e. under conditions of thermal degradation the state of the coal's network structure is also time dependent. The optimum experiment would be to characterize coal in a rubbery state at room temperature. Brenner demonstrated that coals immersed in appropriate solvents, such as pyridine, exhibit rubbery characteristics. He subsequently quantified this observation by measuring coal's elastic modulus while in the swollen state⁶; the magnitude of this was shown to lie in the range of stiff rubber. The experiments of Brenner constituted an important step towards characterizing coal's macromolecular structure. This present paper continues the investigation and focuses on a set of simple experiments designed to highlight aspects of the viscoelastic behavior of solvent swollen coals.

Experimental

The experiments described in this presentation involve monitoring creep (i.e. time-dependent strain) under compressive

stress. The two samples used in this study were procured from the Penn State Coal Sample Bank; both coals are high volatile C bituminous in rank from the Illinois No. 6 and the Lower Kittanning seams, respectively. Details on the samples are presented in table 1 under the designation PSOC-1539 and PSOC-1274, samples 1 and 2, respectively. The sample selection and preparation protocol has been described in detail elsewhere⁹. The crucial characteristics of an optimum sample for such studies are 1) that it be homogeneous, i.e. entirely vitrinite, 2) that it be exhaustively extracted in pyridine, and 3) that it be free of cracks. Using the protocol described in reference 9, these ideal characteristics are very closely approached. The instrument employed to measure strain is a microdilatometer also previously described⁹. In brief, vertical displacement of a piston is measured using a linear variable differential transformer (LVDT); the analog signal is sent to a chart recorder so that strain can be continuously monitored. All measurements reported here are made while the sample is immersed in solvent.

Two different experiments were conducted; in the first, a constant compressive stress was applied to the sample, while the resultant strain was measured as a function of time; a standard creep test. In the second, the sample was subjected to a progressively greater stress up to a maximum on the order of 0.6 MPa. Upon reaching the maximum, the stress was progressively reduced. The stress rates in both loading and unloading are on the order of 0.2 MPa/min. To avoid introducing uncertainties in the position of the piston upon complete unloading, it was necessary to unload only to approximately 0.1 MPa before initiating the next stress cycle. The subsequent stress cycle was begun only after the strain recovery rate reached zero.

The precision of the instrument is such that displacements on the order of 0.5 μm are detectable. The compliance of the instrument is very low; at the maximum stress the LVDT recorded a displacement of less than 5 μm , whereas the typical displacement of a swollen coal sample at stress maximum is on the order of 70 μm in the case of the first experiment and on the order of 300 μm in the second.

Results and Discussion

The time dependent compressive strain of solvent-swollen coal while under a constant stress can be separated into three fundamental deformational modes. These have been illustrated schematically in figure 1. The first is an instantaneous (time-independent) element (E_0 in figure 1, which here appears Hookean, but is, in fact, nonlinear, see below). The second mode is a time-dependent, reversible viscoelastic element ($K-V$ in figure 1; signifying that the strain response in this region can be described with a Kelvin-Voigt model). The third mode is a time-dependent, irreversible element (N in figure 1; indicating that strain in this region is largely viscous in nature and thus can be considered as a Newtonian fluid with a coefficient of viscosity, η).

The time-dependent strain behavior of sample 2 is presented in figure 2 (the strain presented in this figure is compressive, strain = $-(\Delta L/L)$). The applied stress is on the order of 0.1 MPa; the instantaneous elastic strain component has been factored out and only the time-dependent deformation is presented. Therefore, the magnitude of the strain is calculated from height of the instantaneously compressed sample. The magnitude of the instantaneous deformation, under a small stress applied in this manner, accounted for approximately 50 percent of the strain. As will be discussed below, however, the instantaneous strain is nonlinear and its contribution to the total strain diminishes with progressively increased stress.

The first part of figure 2 corresponds to viscoelastic deformation which can be described with a generalized Kelvin-Voigt element model (i.e. a model in which elements composed of a Hookean solid spring in parallel with a Newtonian fluid dashpot are arranged in a series). At longer times ($t > 30$ minutes) the deformation is essentially linear and can be modeled using a single Newtonian fluid dashpot. The viscosity of the "fluid" in this case is calculated to be approximately 3×10^8 centipoise.

The behavior of this coal at small strains (figure 2) suggests that linear viscoelastic models could be applied to parameterize sample 2's strain behavior. Investigations at higher stresses, however, indicate that the overall viscoelastic behavior is significantly non-linear. Non-linearity in the instantaneous reversible strain component is demonstrated in figure 3 (sample 1), where the incremental displacement accompanying incremental stress clearly decreases. A noteworthy point is that magnitude of the incremental displacement for a given stress is apparently independent of the other deformational mechanisms.

The viscoelastic behavior of sample 1 with cyclic stress loading is presented in figure 4. In this figure, the strain is presented as the ratio of the height to the original height. Several interesting features are evident. First, there is a progressive shift to greater strains with each subsequent cycle, the result of superposition of viscous irreversible deformation on the reversible viscoelastic deformation. Second, upon compression, the stress-strain slope remains essentially constant, i.e. the time-dependent compliance remains the same for each cycle. Third, the magnitude of energy dissipation evident upon stress reduction is also nearly constant. The implication is that the same retardational strain mechanisms are being utilized upon each cycle. Also, it appears that these modes are independent of the viscous strain superposed on the entire strain process.

Conclusions

Solvent swollen coals, exhibit three apparently independent strain modes. The first is reversible and time-independent; although it exhibits regular reproducible behavior it is nonlinear,

i.e. non-Hookean. The second mode is reversible and time-dependent; it is reproducible, hence predictable. The third strain mode is entirely viscous and appears to be independent of the previous two and is readily treated using a Newtonian fluid model. These results indicate that swollen coal's viscoelastic behavior can be described through a constitutive equation where the individual elements, e.g, Maxwell or Kelvin-Voigt elements, are nonlinear with respect to stress. Coal's viscoelastic behavior, therefore, can be parameterized, e.g. in terms of a retardation spectrum; this has the potential to yield fundamental information on the nature of coal's macromolecular structure.

Acknowledgement

We gratefully acknowledge the financial support of the sponsors of the Penn State Cooperative Program in Coal Research

References

1. Bangham, D. H.; Maggs, F. A. P. *Proceedings of the Conference on Ultra-fine Structure of Coals and Cokes*; British Coal Utilization Research Association: London, 1943.
2. Hiorns, F.J., *Fuel* 1953, 32, 113.
3. Terry, N. B., *Fuel* 1957, 37, 309.
4. van Krevelan, D. W., *Coal*; Elsevier Scientific: New York, 1981.
5. Weller, M.; Wert, C., *J. Appl. Phys.* 1982, 53, 6205.
6. Howell, J. M.; Peppas, N. A., *Fuel* 1987, 66, 810.
7. Brenner, D., *Fuel* 1984, 63, 1324.
8. Brenner, D., *Pre. Pap.-ACS Div. Fuel Chem. Prepr.* 1986, 16.
9. Cody, G. D.; Davis, A.; Esser, S.; Hatcher, P. G., *Pre. Pap.-ACS Div. Fuel Chem. Prepr.* 1991, 1307.

TABLE 1- SAMPLES

<u>SAMPLE</u>	<u>%C*</u>	<u>%H*</u>	<u>%O*</u>	<u>H/C*</u>	<u>O/C*</u>	<u>%R_m**</u>	<u>%Q***</u>
1539 (1)	81.0	5.5	9.4	0.8	0.1	0.58	2.3
1274 (2)	82.1	5.9	8.0	0.9	0.1	0.63	2.1

* DAF basis

** Mean-Max Reflectance in oil

*** Volumetric Swelling Ratio

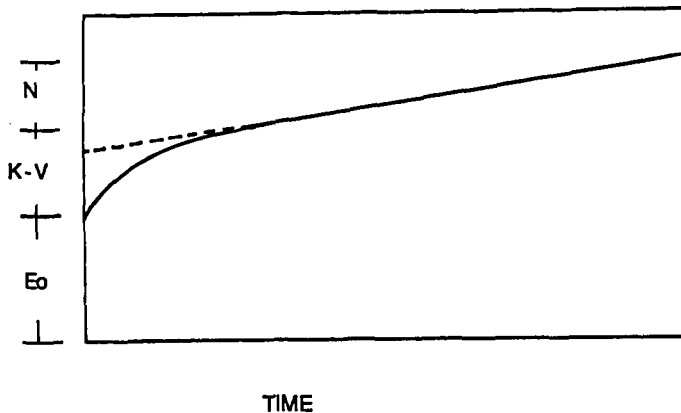


Figure 1: Typical strain vs time curve for a constant applied stress. E_0 = instantaneous elastic strain, K-V = reversible viscoelastic strain, N = irreversible viscous strain.

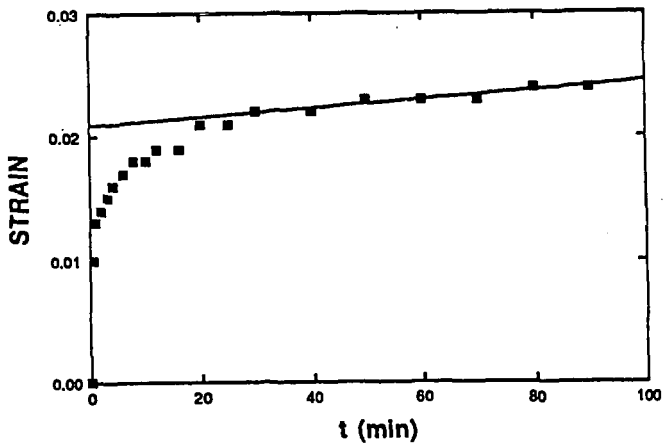


Figure 2: Characteristic Creep curve, sample 2, stress = 0.1 Mpa

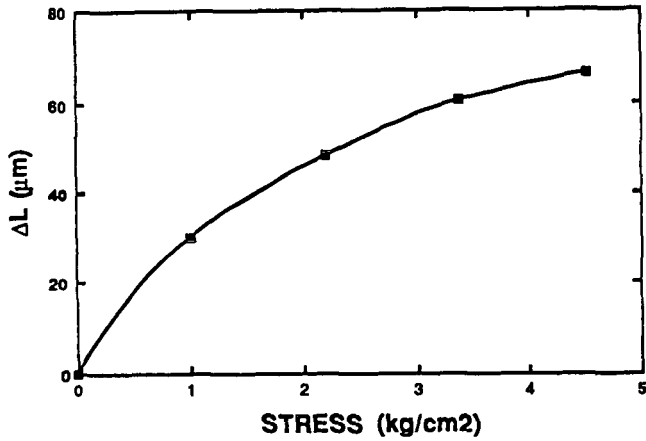


Figure 3: Incremental displacement due to instantaneous strain vs. stress, sample 1.

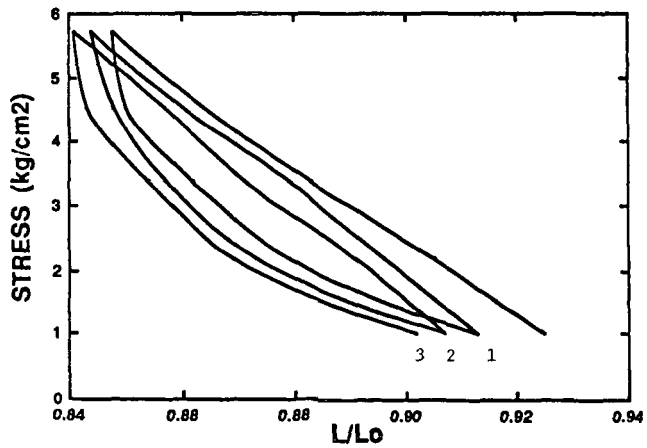


Figure 4: Compressive stress - strain cycles, sample 1. The stress rate is 0.2 Mpa/min

DO GLASS TRANSITIONS REPRESENT GLOBAL CHANGES TO COAL STRUCTURE?

Peter J. Hall and Alexander J. Mackinnon
Department of Pure and Applied Chemistry
University of Strathclyde, Glasgow G1 1XL
SCOTLAND

Key Words: Glass transition, Differential Scanning Calorimetry

Introduction

At room temperature coals are glassy solids. The existence of thermal glass to rubber transitions has been claimed for coals in a number of publications. Typically, coals have glass transition temperature (T_g) in the region of 600K. There is a certain amount of contradictory experimental data published. For example, Green *et al.*¹ have presented data which suggest a second order phase transition at 573K for APCS Illinois #6 which looks like a traditional glass to rubber transition. Conversely, Lucht *et al.*² claim a second order phase transition at 655K for PSOC Illinois #6 in which the specific heat baseline is displaced downwards. It may be claimed that this difference is due to the difference in the origin of the coal but nevertheless, this raises doubts about the reproducibility of these second order phase transitions. The existence of such transitions may be important to coal processing because diffusion rates through rubbery materials are orders of magnitude faster than through the corresponding glass.

The question to be considered here is whether glass transitions represent truly global changes in the viscoelastic properties of coals. In many polymers, which have tend to have much more uniform chemical and physical structures than coal, physical properties such as Young's moduli typically reduce by two orders of magnitude³. Direct measurement of Young's moduli for coals is difficult and unreliable because of the existence of cracks and a well defined bedding plane.

The objective here is to use Differential Scanning Calorimetry (d.s.c.) to investigate thermal and solvent effected glass transitions in coals and, by comparison with another polymer system, determine whether they represent global changes to structure.

The process of quantifying glass transitions will be achieved by interpreting specific

heat (C_p) data in terms of two component Einstein C_p models. It has been shown by Merrick⁴ and Hall and Larsen⁵ that the C_p of coals from ~100K to pyrolysis temperatures can be described by Einstein C_p models that consist of two components. One component comes from easily excited atomic vibrations and has a weighting of 1/3. The second component originates from vibrations that are harder to excite and has a weighting of 2/3. C_p at any temperature, T , is given by:

$$C_p = \left(\frac{R}{a} \right) [1/3 g_1(\Theta_1/T) + 2/3 g_2(\Theta_2/T)] \quad 1$$

where $g(\Theta/T)$ is the Einstein function:

$$g = \frac{\exp(\Theta/T) (\Theta/T)^2}{(\exp(\Theta/T) - 1)^2} \quad 2$$

a is the mean atomic weight and Θ is the Einstein temperature. Equation 1 provides a two component fit to empirical C_p data, Θ_1 and Θ_2 being adjustable parameters. One advantage of Equation 1 is that it explicitly separates the mean atomic weight and the Einstein temperatures Θ . Θ is therefore independent of the chemical structure and provides a basis for comparing chemically different structures.

Hall⁶ has shown that Equation 1 provides a good description for C_p data of a Dioxane Lignin (DL) obtained by Hatakeyama *et al.*⁷. DL is a good model for certain aspects of coal structure because it is a heterogeneous aromatic-based crosslinked polymer. However, it is simpler to understand the structure of DL because there are no analogues to coal macerals, mineral matter contamination or bedding planes. The chemical structure is more uniform than coal. Hall⁶ demonstrated that Θ_2 decreased from 1630K below T_g to 1230K above T_g , a decrease of 400K. This is taken as the bench mark figure for a material that has well-defined glass to rubber transition.

Experimental

A Mettler DSC 30 was used with standard aluminium pans. A detailed experimental procedure has been described previously⁸. The only difference was that C_p errors due to convective heating at low temperatures were minimized by minimizing the volume of the pan and reference chamber using a low temperature lid. Exhaustive calibration meant that temperatures were determined to ± 0.1 K, enthalpies were determined to ± 0.01 J/g. DSC was performed at 10 K/min in a carrier of dry nitrogen.

Coals were obtained from the Argonne Premium Coal Bank. The ultimate analyses from APCS was used for calculating mean atomic weights. The coals were dried in the DSC chamber at 373K until the heat flow indicated that no water remained.

Results and Discussion

A number of coals were tested. Ten separate samples of Illinois #6 were tested. Very slight second order phase transitions were detected in two cases. In three others displacement of the Cp baseline downwards was noted, similar to the observations of Lucht *et al.*² The temperature of these transitions varied between 520K and 630K. In the other experiments there were either no second order phase transitions observed, they were too small or ambiguous. Figure 1 shows a mean of the runs, overall there are no obvious second order phase transitions. The Einstein temperatures for fresh Illinois #6 were calculated to be 380K and 1200K. In the cases where a second order phase transition resembling a glass transition was observed, the reduction in the higher Einstein temperature following a glass transition was 50K. This is much less than the change of 400K calculated for DL⁵. Our conclusions are that if genuine glass to rubber transitions do indeed exist for Illinois #6 then they do not represent global changes to structure. Differences in the behaviour are probably due to sample inhomogeneity.

Pittsburgh #8 presented different problems in the identification of a possible glass to rubber transition. Figure 2 shows a typical d.s.c. result. The dashed lines mark what may be a second order phase transition followed by what may be a slight exotherm. Another interpretation of this is that it may be a first order endotherm caused by some pyrolysis effect. On the basis of the data presented here these possibilities cannot be distinguished. The problem is that the onset of softening in high swelling coals such as Pittsburgh #8 is accompanied by the evolution of tars. This result illustrates the difficulties of using d.s.c. alone to investigate glass transitions.

Two higher rank coals, Upper Freeport and Pocahontas were also investigated. We were not able to find any evidence of glass to rubber transitions for these coals below the onset of pyrolysis.

The only situation in which we were able to produce a significant, reproducible and well defined glass to rubber transition was for Wyodak coal following heat treatment. Figure 3 shows d.s.c. for Wyodak coal dried at 373K. Run 1 is on the dry coal and Run 2 is on the same sample of coal that has been heated to 573K in the d.s.c. and cooled to room temperature. Run 1 shows a well defined endotherm at 478K and a rather broad endotherm at 430K. Run 2 shows a well defined second order phase transition at 380K.

Equation 1 has been used to model the Cp data for Run 2 both below and above the glass transition. There was not enough sample to determine the elemental composition

of the Wyodak following Run 1 and the assumption is made that there is no significant change in the mean atomic weight. This is a reasonable assumption since the weight loss on Run 1 was only 3%. Figure 4 shows that Θ_2 values of 2250K and 1850K give the best fits. In other words, Θ_2 reduces by 400K as a result of the glass transition. This is the same as previously observed for the DL. We therefore conclude that this particular glass transition represents a global change to the Wyodak structure. The reasons for this are a matter for speculation but the following discussion is at least consistent with the experimental results presented here and with what is known about the molecular structure of Wyodak coal. It is known that Wyodak has a large oxygen content and a relatively large concentration of carboxylic acid groups. The first order phase transitions in Run 1 could be caused by the dissociation of these groups. The fact that they are very much reduced in Run 2 suggests some chemical change, rather than a melting phenomenon. In the original coal these acid groups would give rise to hydrogen bonding in the coal macromolecule. When they are removed the coal may become effectively less heavily crosslinked and therefore has a well defined glass to rubber transition.

References

- 1 T.K. Green, T.K.; Pan, W-P; Clark M.A. *ACS Fuel Div Preprints*, **1991** 36(2), 814.
- 2 Lucht, L.M.; Larson, J.M.; Peppas, N.A. *Energy and Fuels*, **1987**, 1, 56.
- 3 Billmeyer, F.W. *Text Book of Polymer Science*, Wiley, New York, 1966.
- 4 Merrick, D *Fuel*, **1983**, 62, 540.
- 5 Hall, P.J.; Larsen, J.W. submitted to *Energy and Fuels*, **1992**.
- 6 Hall, P.J. in press, *Polymer Communications*, **1992**.
- 7 Hatakeyama, H.; Nakamura, K.; Hatakeyama, H, *Polymer*, **1982**, 23, 1801.
- 8 Hall, P.J.; Larsen J.W. *Energy and Fuels*, **1991**, 5, 228.

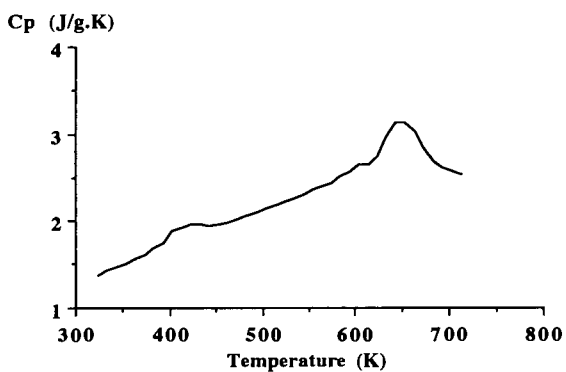


Figure 1: DSC at 10K/min for dry Illinois #6 coal.

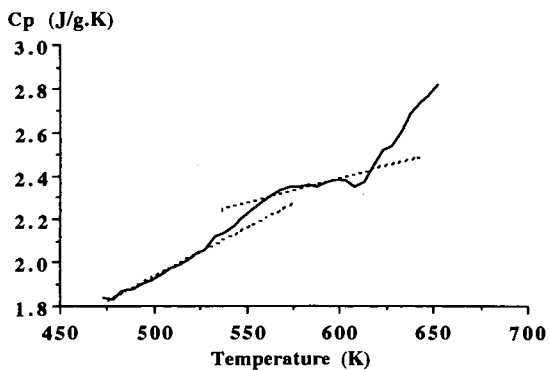


Figure 2: DSC at 10K/min for dry Pittsburgh #8 coal.

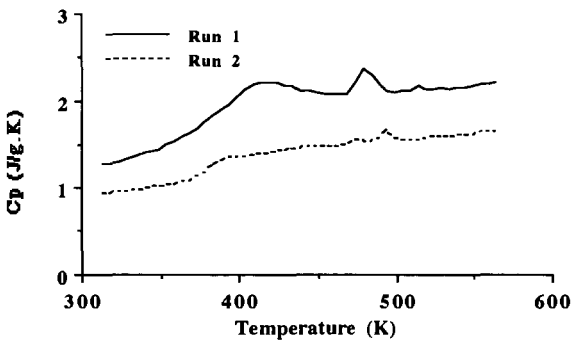


Figure 3: DSC at 10 K/min for dry Wyodak coal and a re-run of the same sample.

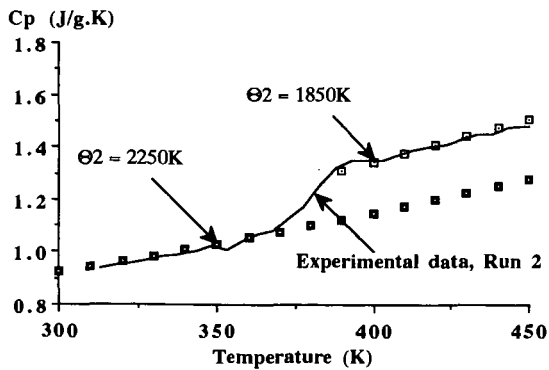


Figure 4: DSC at 10 K/min for Wyodak coal heated to 573K then cooled to room temperature together with two-component Einstein C_p theory fits to the experimental data below and above the glass transition.

THE ASSOCIATED MOLECULAR NATURE OF BITUMINOUS COAL

Masaharu Nishioka

BCR National Laboratory, 500 William Pitt Way, Pittsburgh, PA 15238

Keywords: coal structure, association, intermolecular interactions

INTRODUCTION

Coal is a complex mixture of organic material and inorganic components. Detailed characterization of the organic material is still impossible, even when using today's highly developed sophisticated analytical techniques. This is primarily due to the amorphous nature of high-molecular-mass mixtures. The understanding of the physical structure of these materials is an important step in the study of coal structure. The extent to which coal molecules may be (A) covalently cross-linked and/or (B) physically associated is illustrated in Figure 1.

A cross-linked, three-dimensional macromolecular model (Model A) has been widely accepted as a model of the organic material, with this framework occluding some solvent-extractable components. It is, however, this author's opinion that the evidence is indirect and there is little information to elucidate the real state of the physical structure of coal.

Intra- and intermolecular (secondary) interactions play an important role in Model B, but differentiation between covalent bonds and the strong secondary interactions has not been thoroughly studied. Our recent work (1-6) demonstrated the significance and importance of relatively strong secondary interactions in all ranks of coal. Therefore, the conventional coal structural Model A needs to be reinvestigated.

In this paper, our recent results will be summarized and investigated along with the relating past work. From this analysis, it is reasonable to deduce that significant portions (far more than generally believed) of coal molecules are physically associated.

EXPERIMENTAL

Most of the experimental procedures have been already reported in the previous papers (1-7). The followings are some of these outlines. American Chemical Society reagents and h.p.l.c.-grade solvents were used without purification. Coal samples were obtained from the Premium Sample Program at Argonne National Laboratory (8), the Pennsylvania State University Coal Bank and Exxon Research and Engineering Co.

Approximately 5 g of coal was placed in 100 ml of solvent in a 250 ml flask or a 300 ml autoclave and magnetically stirred under nitrogen. The mixture was either stirred at room temperature, heated, or mildly refluxed in an oil bath or in an autoclave heater. The cooled mixture was dried using a rotary evaporator, mixed with methanol, and filtered, while being rinsed with methanol several times. The coal was dried in a vacuum oven at 95°C overnight.

The experimental procedure of coal swelling is based on the earlier reported method (9,10). The measurements were performed in the disposable Wintrobe Tubes (Fisher Scientific) of 3 mm inner diameter and 115 mm in length with graduations in 1 mm divisions. After placing three weighed coal samples into the tubes, these tubes were centrifuged for 5 min (at 3600 rpm in a 30 cm diameter horizontal rotor). Bulk density of each coal under the condition was determined by the average height centrifuged. Each initial height before solvent swelling was calculated from weight of samples by using the bulk density. This is tedious compared to the conventional procedure but essential

to obtain reproducible results particularly at low coal concentration. Solvent was added to each weighed sample after measuring its volume, and the content was vigorously stirred with a thin rod. The tubes were centrifuged for 5 min at 3600 rpm. The volumetric swelling ratio (Q) was calculated by the difference between these heights of samples (9,10). Separate samples were employed for determining the extents of swelling as a function of time and coal concentration.

RESULTS AND DISCUSSION

Solvent extractability

There is a long history, over a century, of coal-solvent extraction. Only a small fraction of most coals is extractable in organic solvents. This amount may reach 20-30 wt%, and it has been thought that this limited solubility or extractability is consistent with Model A. Hydrogen bonds have been primarily considered in addition to relatively weak van der Waals' forces and they are assumed to be broken with one of the best solvents, pyridine (11,12). Caution, however, is advised against the limited extractability of coal, because it seems that the limited extractability originates from the disregard of various relatively strong secondary interactions caused by polyfunctional groups in coal.

The variety of relatively strong secondary interactions are present and their abundances are highly rank-dependent because of the dependence of the abundance of diverse functional groups on coal rank (1,4,6). It was estimated (1,4,6) that the Coulombic force is predominant in lower-rank coal due to ionized groups, that charge-transfer complexes involving non-ionizable but transferable electrons are important in medium-rank coal, and that dispersion forces involving polarizable π -electrons in polycyclic aromatics (π - π interactions) are major contributors in higher-rank coal.

Any single solvent does not appear to be able to disrupt all of these relatively strong secondary interactions and allow an efficient single step extraction. Macromolecules with relatively strong secondary interactions co-operatively interact (13). The co-operativity may make solubilization of coal more difficult. Therefore, another extraction procedure appropriate for coal needs to be explored.

A multistep sequence was proposed with the aim of minimizing various interactions step by step in the recent papers (6). Each step was selected to minimize the possibility of cleaving covalent bonds. Detailed mass balances and additional experiments to investigate the breaking of different secondary interactions were shown in the paper (6).

Each step to break or solvate relative strong secondary interactions has to be selected according to ranks of coals because of the rank dependence of the abundance of these interactions. The concept of this rank dependence may be represented as shown in Figure 2. For subbituminous coal, ionic forces and then charge-transfer interactions should be solvated step by step in addition to hydrogen bonds. For high-volatile bituminous coal, the solvation of π - π interactions would be important after breaking charge-transfer interactions.

The pyridine extraction yields for Argonne Premium coal samples by single step and multistep procedures were compared (6). Total extraction yields of 38-73 wt% (daf) were obtained by using multistep extractions except for low-volatile bituminous coal. These procedures are tedious but straightforward, and the extractabilities are much larger than those obtained by using the conventional extraction. Other results of high extractability using different methods has been available for selected ranks of coal (14-17).

Above results indicate that coal is extractable to a large extent if

various relatively strong secondary interactions are properly weakened. Therefore, limited extractability using a single step with an individual solvent may give a misleading information about coal structure. It is not logical to deduce any concept from the values.

Associative equilibria

If the relatively strong secondary interactions or physical associations are significant in coal, associative equilibria of coal should be observed in solvents. The associative equilibria, however, have not been fully appreciated for the system of coal and solvent regardless of such numerous observations for polymer solutions.

The solvent-induced association has been observed and interpreted as associative equilibria (1,2). Self-associations of high-volatile bituminous coal and its pyridine extract is induced by the solvent soaking. Heating or immersing these materials in poor solvents or in good solvents, followed by the removal of good solvents (the solvent treatment), caused decreases in their pyridine extractability. Any significant chemical reaction during the solvent treatment was experimentally ruled out.

Other associative equilibria were seen as changes in precipitation of extract solutions and molecular weight at different temperatures (3). It was observed that such associative equilibria are highly rank-dependent. This resulted in remarkable differences in extraction rate, effect of preheating on extraction and effect of solvent-soaking on extraction for A region (< ca. 87 % C), B region (ca. 87 to 90 % C) and C region (> ca. 90 % C) coals (3). This coincides with the significant rank dependence of types and abundances of relatively strong secondary interactions in coal considered for multistep extractions in the previous section.

From the above discussion, relatively strong secondary interactions exist in coal, and coal components (or molecules) equilibrate between association and dissociation due to these interactions even in good solvents such as pyridine. So, differentiation between chemical bonds and strong secondary interactions should be considered, although the quantitative assessment of their abundances is very difficult. Because of the presence of relatively strong secondary interactions, it is suggested that apparent networks experimentally observed, which have been often regarded as representing Model A, are much deviated from the phantom (real) networks, if any.

Solvent swelling

The behaviour of solvent(-induced) swelling without complete dissolution in any organic solvent has been often referred to the evidence for Model A. Sanada and Honda (18) applied the statistical theory of rubber elasticity to coal in order to estimate the average molecular weight between cross-links. Since then, solvent swelling has been used to characterize the macromolecular nature of coal by many workers (19,20). The author critiques this line of evidence for Model A on the grounds that coal swelling is not reversible and highly dependent upon coal concentration. Although a series of full papers will be reported elsewhere (21), some of recent results on these issues are shown.

1 Irreversibility of solvent swelling. Distinctively different physical phenomena have been observed in a solvent between the A and B region coals (3). Accordingly, pyridine swellings of Illinois no. 6 (IL: the A region) and Upper Freeport (UF: the B region coal) were compared. The swelling ratio Q at room temperature is very small as seen by UF-1 in Table 1, whereas the Q value at 70°C is larger and increased with time (UF-2). If the pyridine swelling is

mainly due to cross-linked covalent bonds in the coal, the significantly different Q between the two temperatures cannot be explained by elastic swelling. The result can be rationalized due to more disruption of secondary interactions at high temperature (70°C) (3).

The UF coal once swollen in pyridine, followed by the removal of pyridine, gave nearly the same Q value (UF-3) and pyridine extractability (3) as the raw coal. However, decreases in the Q value (IL-1 and 2 in Table 1) and extractability (3) were observed for the IL coal by the swelling/deswelling procedure.

Thermally induced dissociation which is significant for the B region coal was observed for UF-2 as shown above. However, if pyridine is removed from the B region coal after thermally induced dissociation by refluxing in pyridine, relatively strong association may occur as seen for the A region coal (3). The UF coal was refluxed in pyridine for 3 days, followed by the removal of pyridine, and then the swelling ratio Q of this sample was measured at room temperature (UF-4) and 70°C (UF-5). Both Q values at room temperature and 70°C of the sample were nearly equal to that of the raw coal. It is noted that an increase in the Q value was not observed at 70°C .

If pyridine solubles is removed from the coal after thermally induced dissociation, the coal may increase solvent swelling even when the coal was dried, because the solubles do not associate back with the residue. In fact, the swelling ratio Q of the pyridine extracted UF coal (PI) (UF-6) was larger than that of the raw coal. This is also notable, because PI of the IL coal (IL-3) showed the smaller Q value than the raw coal.

Therefore, solvent swelling is irreversible for the IL and the UF coals. The irreversibility is quite different between the IL and the UF coals. These distinctive differences are consistent with different physical phenomena between these ranks of coals discussed above.

2 Dependence of coal concentration on solvent swelling. The change in associative equilibria for residue may be detected by the dependence of coal concentration on solvent swelling. Therefore, swelling ratios of various coals and their PI were measured at various coal to solvent weight ratios (C/S) in room temperature pyridine.

The results for PSOC-1491 coal (high-volatile C bituminous coal) are summarized in this section. Swelling ratios of the raw coal and its PI versus C/S values are shown in Figure 3. In both cases, swelling ratios are highly dependent on coal concentration.

Most of Q by the volumetric method have been obtained at the large C/S value, and these Q can be regarded as the saturated value (Q_{∞}) (9,10). A gravimetric (18) and a piston type (22) of measurements are under the condition of the quite large C/S value without agitation. Therefore, these methods must also give the saturated swelling ratios. Because of the small dependence of concentration on solvent swelling at the larger C/S value, the conventionally obtained Q should be approximately reproducible regardless of C/S. However, caution should be exercised when coal structure is investigated by using these Q_{∞} , because the Q_{∞} are apparent values.

If soluble material during coal swelling significantly affect solvent activity and change solvent swelling, swelling of coal and residue must be significantly different against the C/S value. However, the results (Figure 3) show the approximately same dependence on sample concentration. The effect of solubles on solvent swelling was further examined. The PI from the PSOC-1491 coal was mixed with its PS, and their pyridine swelling ratios were measured at various mixing ratios at the C/S value of 0.2.

It was found that the swelling ratio Q of the mixture containing solubles

is simply determined by the additive of swelling of each fraction. As PS cannot completely dissolve in room temperature pyridine at the C/S value of 0.2, the undissolved PS behaves like residue and is swollen with pyridine. No significant effect of solubles in the solvent on the solvent activity was observed.

From these results, the dependence of coal concentration on solvent swelling indicates that secondary interactions are solvated more at lower concentration, associated coal dissociates more, and coal is swollen more.

A mono- or two-phase model?

It has been proposed that coal is composed of a macromolecular network (immobile phase) with relatively small molecules (mobile phase) occluded in the macromolecular network. This idea was recently described as the so-called two-phase mode (23,24). The essence of this model states that only some portions (ca. 10-20%) of the mobile phase can be extracted using the regular extraction procedures because of restricted orifice sizes of the immobile phase. The two-phase model is readily compatible with Model A. However, there is no direct evidence to prove the two-phase model as reviewed in a recent paper (7). The problem is that no work has differentiated (a) between the extent of covalent bonds and physical associations, and (b) between the disruption of covalent bonds and physical dissociations.

The proposed two-phase model has been studied by two different approaches (7,25). Since major portions (70-90%) of high-volatile bituminous coal can be extracted with THF after heating (350°C) in *n*-butylamine (26), the physically trapped mobile phase should be released in the extract. The Illinois no. 6 coal extract from this treatment was further pyrolyzed, and typical mobile phase compounds were semi-quantitated in these samples (7). Although the detailed solvation mechanism in *n*-butylamine is not clear, the differences in amounts of such compounds between the original extract and further pyrolyzed samples are unequivocally due to degradation of chemical bonds. As the results showed, typical mobile phase molecules such as *n*-alkanes and polycyclic aromatic hydrocarbons were not released during the *n*-butylamine treatment, but were released by the thermal degradation of coal macromolecules. From this result, it was concluded that the two-phase model is not applicable for high-volatile Illinois bituminous coal. This work and another work (25) showed that *n*-alkanes, alkylbenzenes, alkyl-naphthalenes, phenanthrene, and alkyl hydroaromatic pentacyclic triterpanes, which were regarded as the mobile phase, are important partial constituents of coal molecules regardless of molecular mass.

Consequently, coal can be regarded as a monophase rather than the two-phase model. The monophase model is more consistent with Model B rather than Model A.

CONCLUSION

On the basis of the preceding discussion, it can be suggested that the three major indications of Model A: (a) limited solvent extractability, (b) reversible solvent swelling and (c) the present concept of the two-phase model, are not entirely persuasive. It is reasonable to deduce from various results shown above that significant portions (far more than generally believed) of coal molecules are physically associated.

REFERENCES

- 1 Nishioka, M. and Larsen, J. W. Energy & Fuels 1990, 4, 100
- 2 Nishioka, M. and Larsen, J. W. Prepr. Am. Chem. Soc. Div. Fuel Chem. 1990, 35(2), 319
- 3 Nishioka, M. Energy & Fuels 1991, 5, 487
- 4 Nishioka, M., Gebhard, L. A. and Silbernagel, B. G. Fuel 1991, 70, 341
- 5 Nishioka, M. Energy & Fuels 1991, 5, 523
- 6 Nishioka, M. Fuel 1991, 70, 1413
- 7 Nishioka, M. and Gorbaty, M. L. Energy & Fuels 1990, 4, 70
- 8 Vorres, K. S. Energy & Fuels 1990, 4, 420
- 9 Green, T. K., Kovac, J. and Larsen J. W. Fuel 1984, 63, 935
- 10 Otake, Y. and Suuberg, E. M. Fuel 1989, 68, 1609
- 11 Larsen, J. W. and Baskar A. J. Energy & Fuels 1987, 1, 230
- 12 Painter, P. C., Sobkowiak, M. and Youtcheff, H. Fuel 1987, 66, 973
- 13 Tsuchida, E. and Abe, K. Adv. Polym. Sci. 1982, 45, 77
- 14 Iino, M., Takanohashi, T., Ohsuga, H. et al. Fuel 1988, 67, 1639
- 15 Mallya, N. and Stock, L. M. Fuel 1986, 65, 736
- 16 Miyake, M. and Stock, L. M. Energy & Fuels 1988, 2, 815
- 17 Chatterjee, L., Miyake, M. and Stock, L. M. Energy & Fuels 1990, 4, 242
- 18 Sanada, Y. and Honda, H. Fuel 1966, 45, 295
- 19 Larsen, J. W. and Kovac, J. in 'Organic Chemistry of Coal' (Ed. J. W. Larsen), American Chemical Society, Washington, DC, 1978, Ch. 2
- 20 Lucht, L. M. and Peppas, N. A. in 'New Approaches in Coal Chemistry' (Eds. B. D. Blaustein, B. C. Bochrath and F. Friedman), American Chemical Society, Washington, DC, 1981, Ch. 3
- 21 Nishioka, M. to be published
- 22 Aida, T and Squires, T. G. Am. Chem. Soc. Div. Fuel Chem. Prepr. 1985, 30(1), 95
- 23 Given, P. H. in 'Coal Science Vol. 3' (Eds. M. L. Gorbaty, J. W. Larsen and I. Wender), Academic Press, New York, 1984, pp. 63-252
- 24 Given, P. H., Marzec, A., Barton, W. A. et al. Fuel 1986, 65, 155
- 25 Nishioka, M. and Larsen, J. W. Energy & Fuels 1988, 2, 351
- 26 Tagaya, H., Sugai, J., Onuki, M. et al. Energy & Fuels 1987, 1, 397

Table 1 Swelling ratio (Q) in pyridine of UF and IL coals at room temperature (r.t.) and 70°C (21) (coal/solvent wt ratio: 0.20-0.25)

Code	Sample	0	2h	4h	8h	16h	24h	48h	72h
UF-1	Raw coal (r.t.)	1.2	1.1	1.1			1.2	1.1	1.1
UF-2	Raw coal (70°C)	1.2	1.2	1.4	1.7	1.8	2.2		
UF-3	Coal swollen in pyridine followed by drying (r.t.)	1.0					1.0	1.1	1.1
IL-1	Raw coal (r.t.)	2.3	2.1	2.2	2.1	2.3	2.2	2.3	2.2
IL-2	Coal swollen in pyridine followed by drying (r.t.)	2.0	2.0	2.0	2.0		2.0	2.0	
UF-4	Coal refluxed in pyridine followed by drying (r.t.)	1.0					1.1	1.0	
UF-5	Coal refluxed in pyridine followed by drying (70°C)		1.0	1.1	1.0	1.1	1.1	1.1	
UF-6	Pyridine extracted coal (r.t.)	1.4					1.4	1.3	
IL-3	Pyridine extracted coal (r.t.)	2.0	2.0				2.1	2.0	

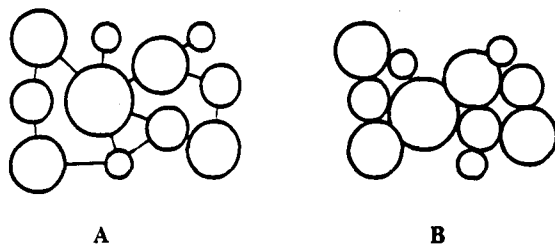


Figure 1 (A) Covalently cross-linked and (B) physically associated models of coal structure

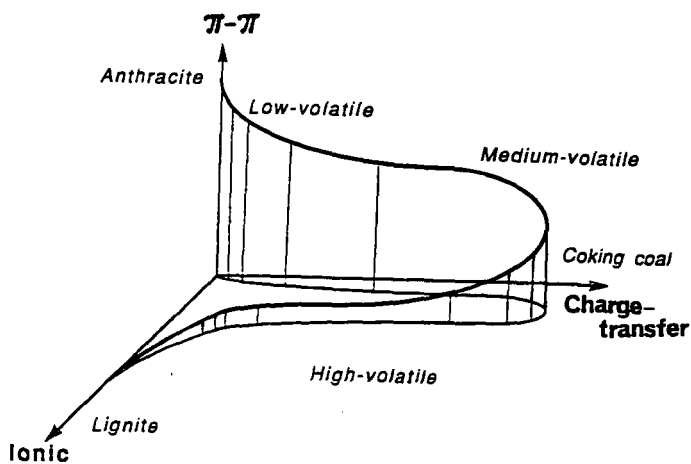


Figure 2 Proposed dependence of relatively strong intra- and intermolecular interactions on coal rank

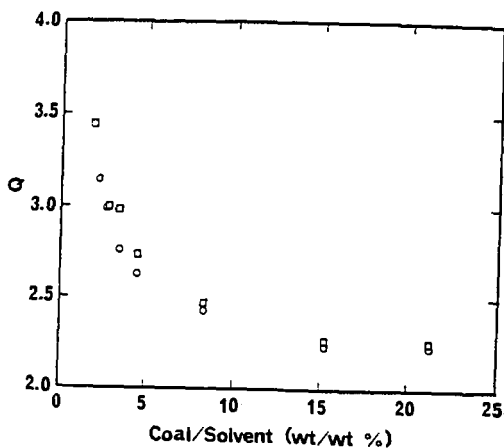


Figure 3 Swelling ratios (Q) in pyridine of PSOC-1491 native (\square) and its pyridine extracted (\circ) coals as a function of coal/solvent wt% (21)

A THREE DIMENSIONAL STRUCTURAL MODEL FOR VITRINITE FROM HIGH VOLATILE BITUMINOUS COAL

Patrick G. Hatcher, Jean-Loup Faulon, Kurt A. Wenzel
and
George D. Cody

Fuel Science Program
The Pennsylvania State University
University Park, PA 16802

Keywords: vitrinite, coal structure, molecular modeling

Introduction

In recent years, several models have been proposed for the chemical structure of coal (1-4). Some of these models have been visualized in three dimensions by use of computer graphics (5). The models have been constructed by considering elemental, spectroscopic, and pyrolysis/gas chromatography/mass spectrometry data. While the models have provided a visual framework for evaluating the kinds of structural elements that are contained in coal macromolecules, they fail to depict the chemical heterogeneity that exists in coal due to the many varied macerals. Developing structural models for individual macerals such as vitrinite would limit some of the heterogeneity, but vitrinite, a petrographically defined component, can also have a heterogeneous composition. There are numerous petrographic forms of vitrinite.

The approach towards defining a more homogeneous maceral component of coal used in our laboratory is one which has focused on coalified wood as a representative for vitrinite derived from xylem in ancient trees (6-9). Structural models were developed from a lignin template, because lignin has been determined to be the major source of chemical structures in coalified wood. By examining the chemistry of series of woods from peat to coalified woods from ancient rocks and seams, we have been able to discern changes in the lignin framework induced by coalification to the rank of subbituminous coal. The models were then developed by applying the observed changes to the lignin template. The model for lignin was that proposed by Adler (10).

Detailed examination of coalified wood samples of higher rank, high-volatile bituminous coal, have allowed us to extend the model to this rank range. This paper presents the data and the model for vitrinite from coalified wood of high volatile C bituminous coal rank. The model is constructed from elemental, solid-state ^{13}C NMR, and flash pyrolysis/gas chromatography/mass spectrometric data.

Methodology

The sample is a fossil stem which was recovered from a lacustrine shale from the Midland Formation (Triassic) near Culpeper, Virginia. Elemental and ^{13}C NMR data for this sample have been previously published, but are here reevaluated for purposes of developing a structural model. Flash pyrolysis/gas chromatography/mass spectrometry was employed in a manner analogous to that described previously (6). Pyrolysis products were quantified by integrating the total ion chromatogram (TIC), assuming equivalent response factors for individual components, and normalizing the concentrations to the total peak area for all peaks in the pyrogram.

The solid-state ^{13}C NMR data were obtained by both the method of cross polarization with magic angle spinning (CPMAS) and by a Bloch decay. The CPMAS conditions were similar to those described previously (7). The cycle time for the Bloch decay was 45 sec. Both NMR data

sets were transferred to a PC computer format and the peaks were deconvoluted by Lab Calc software available from Galactica Industries, Inc.

Results

The elemental and NMR data for the coalified wood sample are shown in Table 1. The carbon content of 85.5% and a vitrinite reflectance value of 0.6 (N. Bostick, personal communication) indicate that the rank of this sample is equivalent to high volatile C bituminous coal. The oxygen content of 5.9%, measured by direct analysis (7), is significantly lower than oxygen contents (13.9%) of coalified logs of subbituminous rank (7). A significant amount of nitrogen, 2.2%, is also observed.

Comparison of the NMR data obtained by CPMAS and by Bloch decay indicates that the two methods yield virtually identical spectra (Figure 1). The Bloch decay does show greater aromaticity and possibly a higher yield of phenolic carbon (Table 1). In both spectra the broad peaks for aromatic (100 - 160 ppm) and aliphatic (0-60 ppm) carbons dominate. Discernible shoulders at 140 and 153 ppm are observed in the aromatic carbon region, and these can be assigned to aromatic bridgehead or nonprotonated aromatic carbons and phenolic carbons, respectively. With a ratio of aryl-O to total aromatic carbon of about 0.12, it appears that nearly all aromatic rings have at least one phenolic OH or aryl ether carbon. The aliphatic carbon region also exhibits fine structure with a distinct peak at 17 ppm which can be assigned to methyl carbons. Dipolar dephasing studies confirm that this peak is that of methyl carbons (7). Deconvolution of the aliphatic region shows that approximately one third of the aliphatic carbons are methyl carbons. Due to insufficient spinning speeds of the sample rotor, spinning sidebands are observed at 260 and 0 ppm.

Flash pyrolysis data for the coalified wood sample are shown in Figure 2 and the peaks are identified and quantified in Table 2. Phenol and alkylphenols are the most readily visible pyrolysis products. Of these, the three cresol isomers, 4-ethylphenol, and 2,4 dimethylphenol predominate. Other isomers of C₂-phenols are apparently minor or trace components. Only 4 isomers of C₃-phenols predominate, trimethyl phenol, 2 isomers of ethyl, methyl phenols, and propylphenol. The specific substitution sites have yet to be discerned. As a whole, the phenols account for approximately 60% of the aromatic pyrolysis products and 40% of the total pyrolyzates. Benzene and alkylbenzenes are the second most prominent components, accounting for about 11% of the pyrolyzates. C₁, C₂, and C₃ benzenes with undetermined substitution patterns comprise the prominent components eluting in the 0-10 min retention time window.

Other pyrolysis products which account for numerous other peaks in the pyrogram are naphthalenes, alkylidibenzofurans, and n-alkane/n-alkene pairs. C₁, C₂, and C₃ alkyl naphthalenes are present as various, as yet undetermined isomers. The n-alkane/n-alkene pairs show a range of carbon numbers ranging from C₆ to C₂₂. The lower molecular weight homologs predominate and the distribution tapers off with increasing carbon number. Quantitatively, the n-alkanes/n-alkenes contribute to 33% of the pyrolyzate, a rather large percentage as a whole. At higher retention times in the pyrogram, peaks for alkylidibenzofurans are found. These contribute to only 3.5% of the pyrolyzate and 5.2% of the aromatic products.

Discussion

The quantitative information on carbon types afforded by the NMR data and the molecular-level information supplied by the flash pyrolysis data provide sufficient detail to allow construction of a molecular model from a lignin template. It is clear that the original lignin structures have been modified by coalification because the coalified wood does not show any characteristics of the lignin-derived methoxy phenol structures. Previous studies (8,9) have suggested that lignin undergoes a series of coalification reactions that include 1) B-O-4 aryl-ether cleavage, 2) demethylation to form catechol-like structures, 3) dehydroxylation of the 3-carbon side chain, and 4) dehydroxylation of catechols to form phenols. In this previous study, a structural model was developed for ranks of brown coal, lignite, and subbituminous coal, using the lignin template published by Adler (10), and modifying the aromatic structures according to the coalification reactions observed for each rank level.

It is a logical progression to take the model developed in this prior study for subbituminous coal and to alter it in a way which would reflect the changes in chemistry observed between the high volatile C coal in the present study and the subbituminous coal in the previous study whose elemental and NMR data are shown in Table 1. The major changes between the two coalified woods in going towards higher rank include 1) a decrease in oxygen content from 13.9% to 5.9% with a corresponding increase in carbon content and 2) a significant increase in benzene and alkylbenzenes in pyrolyzates. Interestingly, the carbon aromaticity does not change greatly, but the fraction of aryl-O carbon to total aromatic carbon decreases by about half. This and the significant loss of oxygen from the elemental data would imply that the primary transformation of the catechol and alkylphenolic structures in subbituminous coal is a loss of aryl-O -containing structures and a condensation of the phenols to diaryl ethers.

While tracing a template through coalification is certainly a valid approach, we have begun to investigate other approaches to molecular modeling, using primarily computer methods that have recently been described (11, 12). Using a molecular modeling software similar to the one developed by Faulon et al. (12), we have generated two models, one which will be described in this paper and the other to be described by Faulon et al. (13). The model generated here provides a three dimensional graphical display of a structure constructed from a lignin framework. Briefly, the input to the model is the quantitative NMR information and the elemental data. The pyrolysis data is not used in a quantitative sense but rather a qualitative sense to input structures found that relate to lignin structural units. The lignin skeletons and inferred bonding sites are deduced from the pyrolysis data and from the previous studies on the coalification of wood showing the reactions of the various functional groups associated with lignin. For example, it is clear that the presence of 2,4 dimethylphenol in pyrolyzates indicates a lignin-derived phenol where the attachments to other structural entities are at the 2 and 4 positions. Indeed, the three-carbon side chain of lignin is in the C-4 position and a significant number of lignin units are also linked at C-2. From previous studies of coalified woods of low rank, we have deduced that the methoxy group is lost and that the three-carbon side chain is reduced to a propenyl group.

From a practical point of view, to verify the correlation between the lignin and our structure, three molecular fragments were introduced in the computerized model: propylbenzene, 4-propylphenol, and dipropylphenol. These fragments were built and stored in a library using the molecular modeling software PCMODEL (Serena software). Then, our program was asked to generate a structure containing these fragments by taking account of all analytical data. This operation was realized in two steps. First, the program computed the correct amount of fragments and connections between fragments to obtain a structure consistent with ^{13}C NMR and elemental analysis. The model of lignin used as template in our previous publication (9) contains 115 carbon atoms, therefore we asked the program to find all the solutions between 95 and 135 carbon atoms. The best solution found is $\text{C}_{113}\text{H}_{105}\text{O}_5$ and is composed of 3 propylbenzenes, 2 propylphenols, and 2 dipropylphenols. The connections between these fragments are the following: 4 biphenyl bonds, 5 benzylphenyl ether bonds, 8 bibenzyl bonds, 3 biphenylpropane bonds, and one biphenylethane bond. In a second step, from the previous list of fragments and bonds, the program was run to generate automatically a 3D structure. The program estimated first the number of structures which can be generated. The number found was too big to build all of them, therefore one structure was chosen randomly and constructed in 3D space.

Figure 3 shows a two-dimensional projection of the 3D model built by the program. There are some important features of this model that need explanation. It is important to highlight the fact that this displayed model is only one of numerous possible models that the program has calculated, and as such should be viewed as only an example whose chemistry is consistent with the chemical information provided to the program. Note that all aryl-O carbons are phenolic ethers and that the structure is composed of principally one- and two-ring aromatic systems. Also, the presence of dibenzofurans is a characteristic feature that is consistent with the pyrolysis data. In fact, the entire structure can be visualized as providing pyrolysis fragments which match rather well with the distribution of aromatic pyrolysis products. What is conspicuously absent is the presence of long-chain aliphatic structures which could give rise to the n-alkane/n-alkene pairs observed in

pyrolysis. We feel that these components are minor components of the coalified wood and are not derived from lignin structural units. It is likely that they were incorporated into the coal from either external materials migrating into the sample or from microbial remains present within the wood as it decomposed and was later coalified. It is also likely that the flash pyrolysis accentuates these substances because they are more readily pyrolysed in comparison with the lignin-derived materials. Also absent are the nitrogen-containing structures. Elemental data for this sample shows about 2% nitrogen (8). We do not have any data concerning the types of nitrogen-containing structures that might be present in this sample. Thus, we choose to omit these structures until which time we might have enough information to include them.

The three dimensional display is not readily visualized in two dimensions, but examination of the structure in Figure 3 shows the connecting points which imply that the structure is three-dimensional. The visualization of the structure in three dimensions is important from the standpoint that we must visualize coal reactivity as a three dimensional phenomenon. The ability to utilize sophisticated computer graphics displays adds to our ability to eventually utilize such structures for the prediction of coal reactivity.

Literature Cited

1. Given, P. H., *Fuel*, **39**, 147, 1960.
2. Wisner, W. H., *Proc. of the Electric Power Research Institute Conf. on Coal Catalysis*, 1973.
3. Solomon, P.R., in *New Approaches in Coal Chemistry*, Am. Chem. Soc. Symp. Series No. 169, 61, 1981.
4. Shinn, J. H., *Fuel*, **63**, 1187, 1981.
5. Carlson, G. A., and Granoff, B., in *Coal Science II*, Advances in Coal Sciences series **461**, 159, 1990.
6. Hatcher, P.G., Lerch, H.E., III, Kotra, R.K., and Verheyen, T.V., *Fuel*, **67**, 1069, 1988.
7. Hatcher, P.G., *Energy and Fuels*, **2**, 48, 1988.
8. Hatcher, P.G., Lerch, H.E., III, and Verheyen, T.V., *Int. J. Coal Geol.*, **13**, 65, 1989.
9. Hatcher, P. G., *Organic Geochemistry*, **16**, 959, 1990.
10. Adler, E., *Wood Sci. Technol.* **11**, 69, 1977.
11. Faulon, J. L., *Prediction Elucidation and molecular modeling : Algorithm and Application in Organic Geochemistry*, PhD Thesis, Ecole des Mines, Paris, 1991.
12. Faulon, J. L., Vandenbroucke, M., Drappier, J. M., Behar, F., and Romero, M., *Advances in Org. Geochem.*, **16**, 981, 1990.
13. Faulon, J. L., Hatcher, P. G., and Wenzel, K. A., *Fuel Div. ACS, Preprints*, this volume, 1992.

Acknowledgments

Financial support for this study was provided by the U. S. Department of Energy, Sandia National Laboratories under contracts DE-AC04-76DP00789 and 12-5543. We also acknowledge financial support from DOE contract DE-AC22-91PC91042 from the Pittsburgh Energy Technology Center. We thank Jackie M. Bortiatynski for assistance in assembling the data and manuscript.

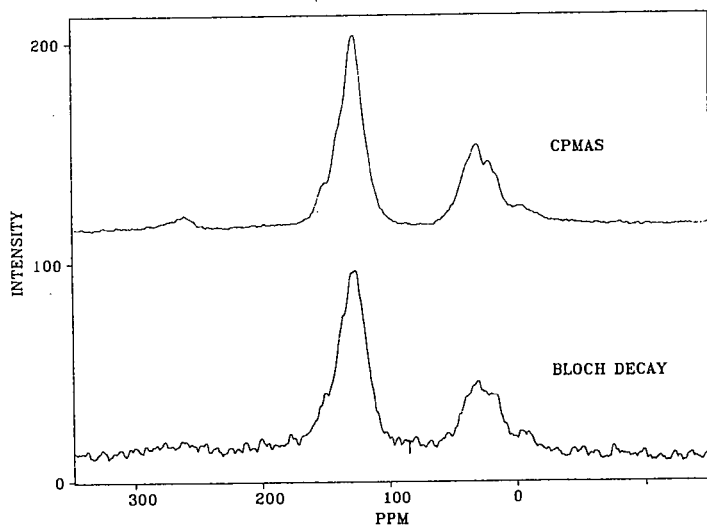


Figure 1. Solid state C NMR data for the high volatile C bituminous coalified wood obtained by the CPMAS and Bloch decay methods.

Table I. Solid-state ^{13}C NMR data for coalified wood samples.

Parameter	Hv Bituminous coal	Subbituminous coal
% carbon*	85.8	77.5
% hydrogen*	6.5	5.28
% oxygen*	5.9	13.9
% nitrogen	2.2	1.0
carbon aromaticity	0.64 (0.61)	0.59
aryl-O/aryl	0.11 (0.13)	0.22
methyl/total aliphatic	0.33 (0.28)	
aryl-H/aryl	0.44	0.40

*- moisture and ash-free values in () are for Bloch decay data

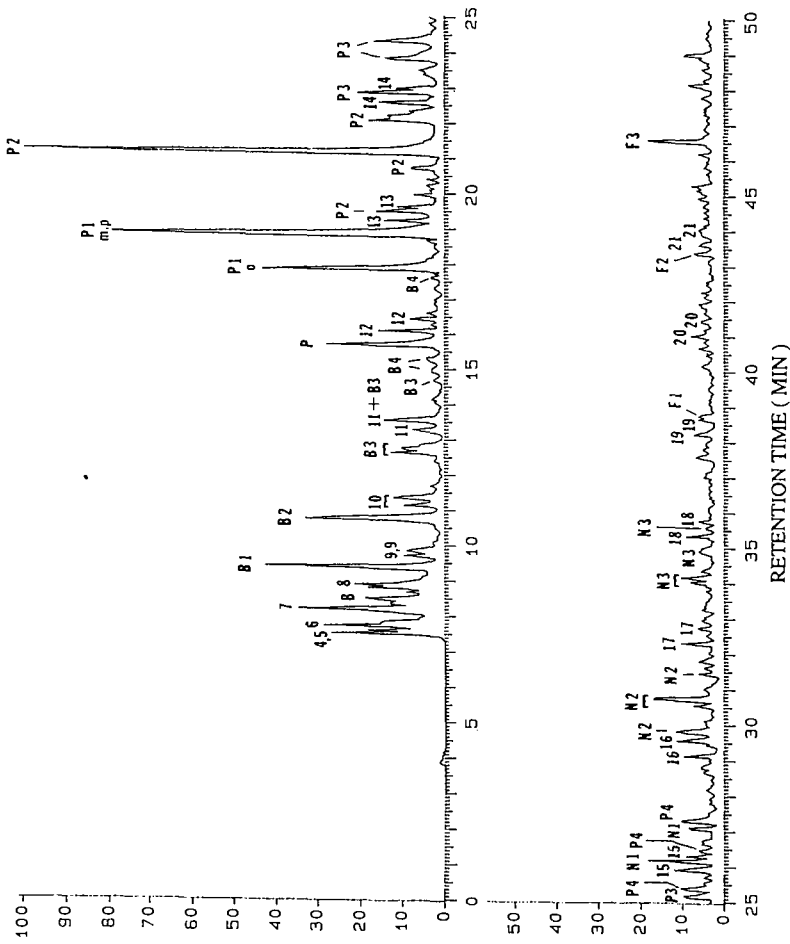


Figure 2. The pyrolysis/gc/ms trace of total ion current for the sample of Hv Bituminous coalified wood. Peak identifications are given in Table 2.

Table 2. Flash pyrolysis data for Hv C bituminous coalified wood

compound	peak designation in Figure 2	weight %	weight % normalized to aromatics
benzene	B	2.2	3.3
toluene	B1	3.2	4.8
C-2 benzenes	B2	3.4	5.2
C-3 benzenes	B3	2.6	3.9
Total benzenes		11	17
phenol	P	2.3	3.6
<i>o</i> -cresol	P1	3.7	5.7
<i>m</i> + <i>p</i> -cresol	P1	8.9	13
2,4 dimethylphenol	P2	8.2	12
other C-2 phenols	P2	6.8	11
C-3 phenols	P3	7.2	11
C-4 phenols	P4	3.2	4.8
Total phenols		40	61
alkylnaphthalenes	N1, N2, N3	11	17
alkyldibenzofurans	F1, F2, F3	3.4	5.2
C ₄ - C ₂₂			
n-alkane/alkenes	4- 22	33	

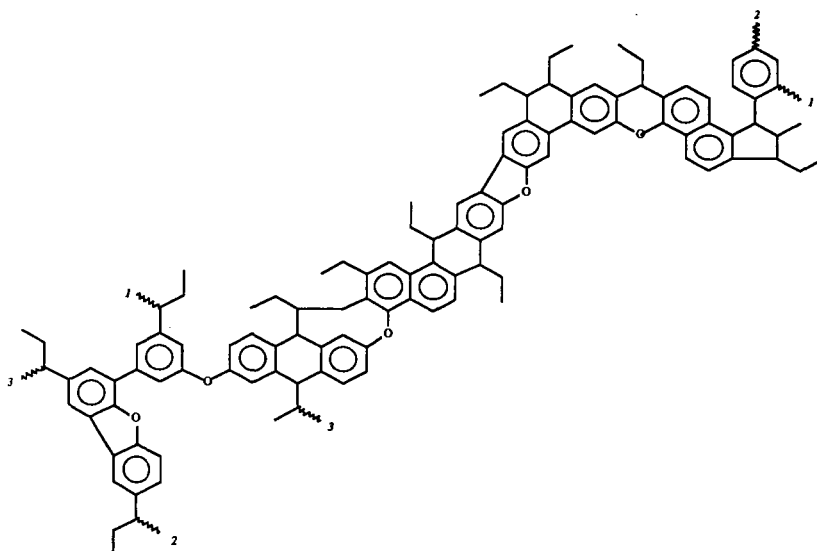


Figure 3. The two-dimensional display of the three-dimensional structural model for high volatile bituminous coalified wood.

POSITRON ANNIHILATION IN ARGONNE ILLINOIS #6 COAL

Peter J. Hall *, Alexander J. Mackinnon and Richard A. Pethrick

Department of Pure and Applied Chemistry

University of Strathclyde,

295 Cathedral Street Glasgow G1 1XL

SCOTLAND

Key Words: Electronic structure, positron annihilation.

* - To whom communications should be addressed.

Introduction

The electronic structure of coals has received little attention but has been the subject of a recent investigation by Larsen *et al.*¹ At a molecular level, the coal becomes increasingly more unsaturated with increasing rank, consistent with generation of a pseudo graphitic structure. Electronically the maturing of coal may be visualized as a transformation from an insulator to a semi conductor. Studies of coal have indicated that a decrease in resistance occurs with increasing temperature consistent with coal being classed as a semi conductor.² Recently there has been considerable interest in the electrical properties of conducting polymers generated by doping conjugated macromolecules³⁻⁵. The conductivity of these materials is influenced by the efficiency of electron diffusion within the conjugated chain structure and hopping between chains which usually involves donor-acceptor sites. Conjugated polymers are very poor semi conductors and it is only when they are doped either by the addition of strong Lewis acids or bases or alternatively the incorporation of heteroatoms into the conjugated structure that semi conductor or metallic behaviour is observed. It is reasonable to assume that similar criteria will be operative for coal, the detailed processes being a function of the rank and chemical composition of the coal. If conductivity were to be measured on a block, there would be complications from any cracks present, together with complications from the bedding plane and the local maceral structure. Direct measurement of the conductivity of powders is difficult in itself.

Positron annihilation has been used for a number of years in the investigation of the effects of radiation damage on metals and ceramic and recently in the study of free

volume in polymers and glasses. The generation or occurrence of defects on an atomic scale allows trapping of positrons as positronium. The typical positron annihilation experiment involves firstly the generation of a positron with an energy of approximately 1.28 MeV; and it is this which when it passes through an organic media will induce radiation damage, combining with a free electron and forming positronium [Ps]. In polystyrene, the diffuse Ps becomes thermally equilibrated and trapped in a molecular size void associated with free volume. Positronium can exist in two spin states; ortho [o-] and para [p-] Ps. The pPs state undergoes annihilation via an allowed transition and has a lifetime of 0.125ns, whereas the oPs state which undergoes annihilation via a forbidden transition which has been predicted by Dirac to have a lifetime of 140ns. In a molecular insulator, spin exchange processes shorten the lifetime and a proportionality with the size of the void has been established. The intensity of the oPs component is a function of the ionization potential of the molecular structure and hence reflects the ability of the thermalizing positron to induce radiation damage. In amorphous polymeric materials, the annihilation spectra are usually composed of three components. The two shortest lifetime components correspond respectively to the self annihilation of p-Ps and free positrons with lifetimes of 0.125ns and 0.4ns. In general, neither of these annihilations will have any significant interaction with media and are independent of its physical and chemical properties. The intensity of the p-Ps will be influenced by the trapping thermalization probability of the positronium which is intimately connected with the occurrence of voids. In the case of a conductor, the positron can interact with the intrinsic delocalized free electron density and trapping will only occur if the radiation spur is larger than the domain structure of the material. Studies of doped polypyrrole has shown that in contrast with the usual situation in most amorphous polymer insulators, annihilation gives rise to a two component spectrum which contrasts strongly with that of the typical amorphous polymer. In this case the positron is assumed to combine with the delocalized electronic structure of the extended conjugated backbone of polypyrrole and its annihilation is a probe of the spin states of this structure. This paper reports the first positron annihilation studies of coal and attempts to compare these observations with the results of related studies on other amorphous materials.

Results and Discussion

Materials

Illinois #6 was selected from the Argonne premium Coal bank for this study. The coal was used as supplied and was subjected to exhaustive extraction using pyridine. The pyridine was completely removed by rotary evaporation prior to use.

Positron Annihilation Spectroscopy

Figure 1 shows a schematic diagram of the apparatus used. A sealed ^{22}Na source was used to generate 1.28 MeV positrons and an accompanying gamma ray. The source was constructed by the evaporation of a concentrated solution of $^{22}\text{NaCl}$ onto a polyamide [Kapton] film. The source was then covered with a second layer of film and the sandwich sealed using a room temperature curing epoxy resin [Araldite]. The positron lifetime was determined from the time delay between the observation of the initial 1.28 MeV gamma ray and the detection of two 0.511 MeV gamma rays which mark the annihilation process. The spectrometer used in this study was a fast-slow coincidence system which incorporates a time-to-pulse height conversion unit and the data is collected using a multichannel analyser, Figure 1. The gamma rays are detected using two fast plastic scintillators coupled to fast photomultiplier tubes [PMT]. The processes are characterized by the emissions at 1.28 and 0.511 MeV which are energy selected and provide the start and stop signals respectively. Discrimination between the start and stop pulses is achieved in the slow circuit and removes any ambiguity of the nature of the pulse arriving at the photomultiplier tubes. The positron annihilation spectra used in this study were obtained from an accumulation of 10^5 counts. The spectrum obtained was analysed using the computer programme POSITRONFIT⁶. The timing resolution of the system had previously been determined using the full width at half peak maximum obtained from a ^{60}Co source. The instrumental resolution function was determined by analysing the lifetime spectrum for annihilation in benzophenone which has a single lifetime of 0.33ns. POSITRONFIT EXTENDED uses the results from the calibration experiments and fits the deconvoluted curve to a sum of exponentials:

$$f(t) = \sum_i A_i \exp(-t/\tau_i) \quad 1$$

where i represents the the number of components present. The relative intensity of

each component is calculated from the area under the corresponding lifetime curve. The adjustable variable in the computer fitting of the data can be altered allowing the selection of the number of components and whether or not each is to be fixed or allowed to be freely adjustable. The quality of the data fit is obtained from the value of σ . For these experiments the powdered coal sample as was loaded into a 5ml vial (diameter 10m) and the ^{22}Na source with its plane perpendicular to the axis of the PMT's. The glass vial was placed coaxially in a second larger vial which was itself inserted between the PMT's⁷. All measurements were carried out at room temperature.

Results and Discussion

Two samples of powdered coal were examined in this initial investigation; a sample of Illinois #6 and a sample of the same coal which has been extracted with pyridine. This extraction removes low molecular mass fractions and may be expected to increase the *free volume* in the material. Ps annihilation spectra for the two samples were obtained and fitted using two component lifetimes. Attempts to fit the data using the traditional three component fits fails, there being no appreciable long lifetime component. The lifetimes and the fits are presented in Table 1. A typical spectrum for the fresh Illinois #6 is shown in Figure 2.

The process of extraction appears to have the effect of increasing the lifetime. Increases in the lifetime of oPs in polymers such as polystyrene can be interpreted in terms of an increase in the lifetime associated with the generation of *free volume* in the matrix. However, in the case of coal the observed spectra resembles more closely that observed in doped polypropylene than that obtained for polystyrene, as shown in Table 2.

Spectra obtained from coal can therefore be seen to resemble those of the semi conducting polymer polypyrrole rather than the insulator polystyrene. The shorter lifetime τ_1 can be associated with free positron annihilation and would not be expected to be significantly influenced by the nature of the matrix. The values of 0.34 and 0.32 ns for the coal and polypyrrole can be assumed to be the same within experimental error. The second component, τ_2 is however clearly a more sensitive probe of the matrix and has a longer time in the coal than in the conducting polymer. The electron mobility may be expected to be greater in the case of the p-toluenesulphonic acid doped polypyrrole than that of the coal. However, these data would suggest that at a microscopic level these values are comparable. Extraction of the low molecular weight fraction appears to

increase slightly the lifetime and this would be consistent with a reduction in the electron mobility. It is probable that the extractable material will not only fill voids in the coal but can also aid electron mobility. Removal of this fraction may generate voids into which the positronium might be trapped and will reduce electron mobility which will further increase the lifetime. It is not possible from these preliminary observations to deduce which of these effects will dominate, however, this data does indicate that positron annihilation may be useful in obtaining information about the nature of the micro-structure of coal.

References

- 1 J.W. Larsen, R.A. Flowers, P.J. Hall, B.G Silbernagel & L.A. Gebhard **1991 Int. Coal Conf.**, Butterworth-Heinemann, (1991).
- 2 M.G.B. Mahoubin Jones & R.A. Pethrick, **Polymer Yearbook** (Ed R.A. Pethrick) Harwood, New York (1985).
- 3 J.R. Steven & A.J. Mao, **Appl. Phys.**, 41, 4273, (1970).
- 4 R.N. West, **Positron studies of Condensed Matter**, Taylor & Francis, London (1974).
- 5 S.E. Doyle, M.G.B. Mahoubin Jones & R.A. Pethrick, **Polymer Communications**, 26, 262-264, (1985).
- 6 P. Kikegaard & M. Eldrup, **Comput. Phys. Comm.**, 3.204 (1972), 7.40 (1974).
- 7 B.D. Malhotra & R.A. Pethrick, **Macromolecules**, 16, 1175-1179, (1983).

Table 1 Positron Annihilation Study of Illinois #6 Coal

	τ_1 (ns)	σ_1 (ns)	τ_2 (ns)	σ_2 (ns)	I ₁ (%)	σ_1 (%)	I ₂ (%)	σ_2 (%)
Illinois #6	0.746	0.092	0.345	0.007	10.411	3.273	89.589	3.27
Pyridine Ext. Illinois	0.843	0.101	0.345	0.005	7.987	1.785	92.013	1.78

Table 2 Lifetimes and Intensities for Related Polymer Systems

	τ_1 (ns)	τ_2 (ns)	τ_3 (ns)	I_1 (%)	I_2 (%)	I_3 (%)
Polystyrene (room temperature)	0.125	0.450	1.20	-	-	-
Doped Polypyrrole (room temperature)	0.32	0.68	-	18.0	78.0	-

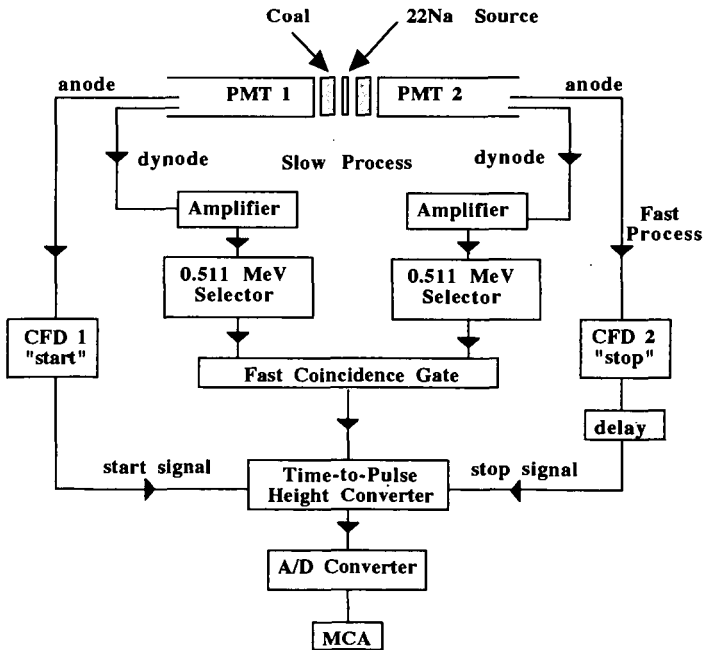
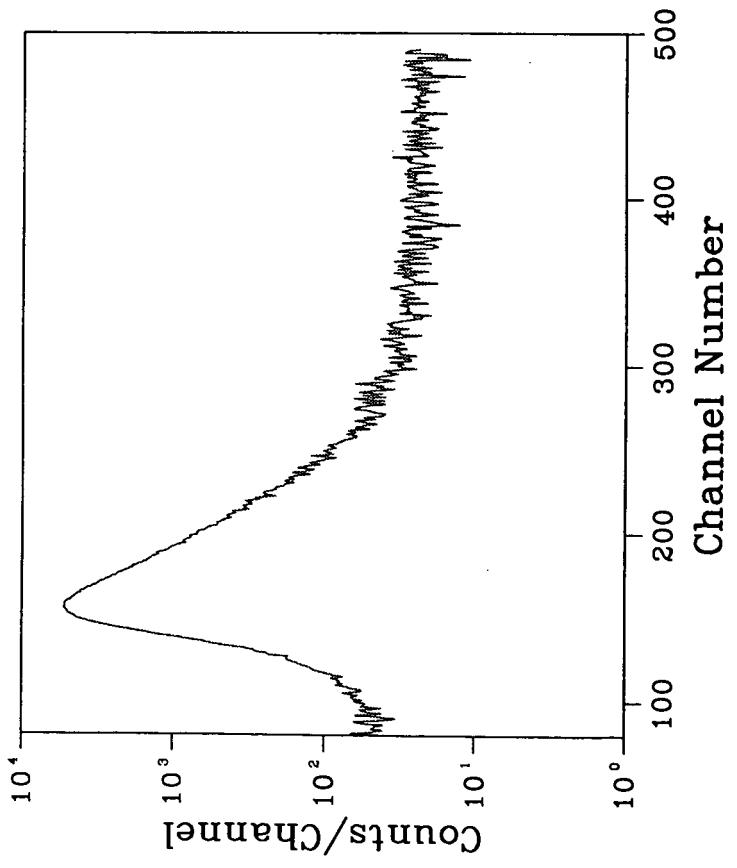


Figure 1 Schematic diagram showing the fast-slow coincidence system



A COMPUTER ASSISTED STRUCTURAL ELUCIDATION FOR COAL MACROMOLECULES.

Jean-Loup Faulon, Patrick G. Hatcher,
and Kurt A. Wenzel.

Fuel Science Program,
The Pennsylvania State University,
University Park, PA 16802.

Keywords : coal structure, molecular modeling, computer aided structure elucidation.

INTRODUCTION

Study of the chemical structure of coal has been the subject of fundamental research for decades and we are now beginning to better understand this structure. It is well recognized that coal is chemically and physically a highly heterogeneous material mainly consisting of organic matter (macerals) and some inorganic materials (minerals). Organic matter which is the object of our interest is composed of carbon, hydrogen and oxygen with lesser amounts of sulfur and nitrogen. The amount, the distribution, and the chemical structure of various macerals in coals depend on the chemical nature of the original coal forming material and the conditions of coalification. Individual macerals may themselves be heterogeneous assemblages of sub-macerals with different chemical structural compositions. The nature of each phase progressively changes during coalification (with rank). For example it is well known that the carbon content of coal increases with its degree of maturation (1). In short, coals are very diverse, and even within any given coal type there is considerable heterogeneity.

Nonetheless, because of the strong link between structure and reactivity, there have been many attempts to model the molecular structure of various coals. For example, chemical structural models have been developed for vitrinite, a major component of coal, ranging in rank from lignite to subbituminous coal (2). For bituminous coals, the most widely accepted molecular models developed during the past 30 years have been the aromatic/hydroaromatic structures. These models are formed by fragments containing about three linked aromatic and/or hydroaromatic rings including appropriate numbers and types of heteroatoms. The fragments are interconnected by hydroaromatic, etheric or aliphatic linkages (3-6). These models have been built using available chemical and structural data on coal, without the aid of computers. They are certainly not unique and the same analytical data can produce similar but different models. Because of the highly heterogeneous character of coal these models are only intended to be representative structures, or average structures. The main limitation of these molecular structures are their two dimensional nature which necessarily ignores most of the interfragment interactions and three dimensional properties such as density and porosity.

Recently Spiro (7) and Carlson (8) have constructed 3D models of several of these structures. Using a space-filling model, Spiro identified several steric difficulties in the original structures and proposed some modifications. To determine the optimal structural conformations of the previous models (3-6), Carlson has used molecular mechanic and dynamic programs. Once minimized, some characteristics such as energy, density porosity can be systematically evaluated

for each model (8). An important result is that for all the models no porosity volumes were found since bituminous coals do clearly show substantial porosity.

The result of these studies have led us to reconsider the modelization of coal. Considering the complexity and the heterogeneity of this material, our intention is not to define another new general model but more specifically to establish a set of average 3D structures which can be correlated to different macerals at different rank levels. In this paper we have chosen to modelize only one maceral of high volatile bituminous coal : the vitrinite. The sample is specifically a coalified wood sample described by Hatcher et al. (9). Our method will involve use of chemistry and a computer. By chemistry we mean we will consider all the chemical analytical results already employed in the previous models but also new techniques which were not used in the past. By computer, we will see that it is possible to generate automatically 3D models from the analytical results and characterize these models in terms of statistics.

METHOD

From a chemical point of view, the task of determining the molecular structure is becoming simpler with the advent of many spectroscopic methods such as NMR, FTIR and flash pyrolysis/gas chromatography/mass spectrometry (py/gc/ms). ^{13}C NMR with cross polarization-magic angle spinning and dipolar dephasing can be used to analyze the overall distribution of various types of carbon structures present in coal such as aliphatic, oxygen-containing, aromatic and hydroaromatic structures (2). By using dipolar dephasing techniques, we can also identify protonated and non-protonated carbons (Table I). Information on the nature of pyrolysis products produced upon heating a coal particle can be obtained using py/gc/ms (2). Results of elemental analysis, and NMR are directly conducted on the coal macromolecule (9) and we can then define what we call a signature for this macromolecule. The signature is simply a series of numbers which count different types of atoms in a specific environment (Table II). The information obtained by py/gc/ms does not describe directly the macromolecule but degradation products or fragments of this macromolecule (Fig. 1). The information given by py/gc/ms is qualitative and defines the fragments which once connected together, in an appropriate amount, constitute the macromolecule. The problem is therefore to find the correct quantity of each fragment and each connection between fragments (interfragment bonds) to form a macromolecule which is consistent with all the structural information. Retrieval of molecular structure from a set of analytical results can be accomplished by an empirical method which consists of a repetitive trial-and-error process to find the correct structure. This method was probably used by the previous authors (3-6), but it is not an entirely satisfactory technique for at least two reasons :

- 1- The process to build a structure is empirical, is accomplished through manual fitting, and can be time consuming for large molecules.
- 2- Generally, many structures can be built from the same analytical data, the reason one structure is chosen instead of an other cannot be clearly defined. This is probably one of the reasons why the coal models cited previously are so different.

Many studies have been conducted in the 30 past years to resolve by computer the general problem of retrieving a structure from analytical data. The generic name for these studies is *computer-aided structure elucidation* (10). Unfortunately the techniques used in these studies are useful only for small molecules and, therefore, cannot be helpful for coal. Recently Faulon et al. (11) have developed a technique which is efficient for macromolecules such as coal. More precisely the data used by this technique are the quantitative chemical information regarding the macromolecule (a signature) and qualitative information concerning a set of fragments. The authors have shown that it is possible from a set of chemical data to compute the amount of fragments and the connections between fragments (interfragment bond) by resolving a linear equation (signature equation). Briefly, the quantitative data given by elemental analysis and NMR defines the signature of the macromolecule, the qualitative information defined by py/gc/ms identifies the molecular

fragments. The structure of each fragment is known from mass spectrometry, therefore it is possible to calculate a signature for each of them. It is also possible to determine a signature for each possible interfragment bond. The amount of fragment and interfragment bonds is obtained by solving the signature equation :

$$\text{signature of fragments} + \text{signature of interfragment bonds} = \text{macromolecular signature}$$

This equation is defined in a discrete space and can admit several solutions. Once resolved, the equation defines the pieces (fragment) and the relations between the pieces (interfragment bonds) of the unknown model which is at that point still an unresolved "puzzle". To "reconstruct the puzzle", a combinatorial program has been developed (12). The program computes first an estimation of the number of solutions : how many models can be built considering a set of pieces and the relation between pieces. When this number is reasonable, the program calculates automatically all the models which correspond to the analytical results. Otherwise the program builds randomly one or a fixed quantity of different models. In all cases the solutions are 3D structures coherent from a chemical point of view : the bonds lengths and the angles between bonds are consistent with the values defined in the literature. These structures can be read and displayed by molecular modeling softwares such as PCMODEL (Serena software), DISCOVER (Biosym) and can be submitted to energy minimization using programs of molecular mechanics like for example MMX (13). Once minimized, physical properties, such as energy, density, porosity can be evaluated.

RESULTS

The analytical results introduced in the program are described in the paper presented by Hatcher et al.(9). From a practical point of view the atomic information (elemental analysis and NMR data listed in Tables I and II) was stored in a file. The molecular fragments (Fig. 1) and the interfragments bonds (Fig. 2) were built using the molecular modeling software PCMODEL (Serena Software) and stored in a library.

The signature equation (11) has been applied for the previous information and all the molecular structures containing a number of carbon atoms between 140 and 180 has been searched. The signature equation found 7 solutions listed in Table III. The best structure with the least error is structure number 6 (molecular formula $C_{178}H_{164}O_8$). This structure is composed of the following fragments: 2 toluenes, 3 C2 benzenes, 1 C3 benzene, 1 o-cresol, 3 m- and p-cresols, 3 C2 phenols, 1 C4 phenol, 3 alkylnaphthalenes, 3 propyls, 9 ethyls, and 7 methyls. The interfragment bonds are 6 benzene-benzenes, 8 benzene-phenols, 10 benzene-toluenes, 5 toluene-toluenes, 7 ethylbenzene-ethylbenzenes, 3 propyl-benzenes, 9 ethyl-toluenes, and 7 methyl-ethylbenzenes. The fragments and inter-fragments bonds are the structures listed in Fig. 1 and 2. Benzene and phenol which appear in the py/gc/ms results are not present in the solution but they can be obtained by pyrolysis from any alkyl benzene or alkyl phenol. C3 phenol is also not present in the solutions. This compound is formed by connecting cresol to ethyl or ethylphenol to methyl. In the same way, alkyldibenzofuran is formed by bonding alkyl benzene and alkyl phenol with a benzene-phenol bond and a benzene-benzene bond.

The combinatorial program presented in (12) has been applied to determine how many models can be built for the structure number 6. This structure is composed of 36 fragments. Considering the structure of the fragments and the global percentage of hydrogen, each fragment must be attached to the rest of the molecule by an average of 3.05 bonds. The total number of bonding sites is therefore $36 \times 3.05 = 110$; this number is also equal to the number of interfragment bonds (55) multiplied by 2. The first bonding site cannot be connected to itself, and there is $110 - 1$ or 109 possible connections. After this operation, $110 - 2$ or 108 bonding sites remain. For the same reason, there is $108 - 1$ or 107 possibilities to connect the second bonding site, 105 for the third, 103 for the fourth, and so on. Consequently the maximum number of structures that can be built is $109 \times 107 \times 105 \times 103 \dots \times 1$: this number is greater than 10^{86} ! However most of the

structures are identical and most of them do not respect the classical chemical constraints and the quantity of interfragment bonds calculated by the signature equation. By avoiding the redundancies and respecting all the analytical constraints, the program found around 1,000,000 possible structures. All these structures are composed of the same fragments and inter-fragments bonds but are different. Fig. 3 shows one of these structures randomly generated by the program. This structure has been subjected to an energy minimization to find a conformationally correct form (MMX program 13). Fig. 4 is the 3D representation of the structure after minimization. All the fragments analyzed by py/gc/ms can be retrieved in this solution, especially C3 benzene and alkyldibenzofuran which were not present in the initial data but obtained by combination of other fragments.

CONCLUSION

The conclusion which can be made from the above results is that for coal the number of models is too large to build all of them. Therefore, in such cases the following question has to be considered : *how many and which structures must be selected and built ?*

The theory of sampling assumes that when the size of a finite population is known, it is possible to extract a subset (a sample) of this population which, in terms of probability, is a good representation. Many techniques of sample design are possible : random sampling, stratified sampling, and sampling with unequal probability of selection (14). The most simple technique which can be applied as a first approximation for our problem is the simple random sampling without replacement (SRSWOR). With this technique it is possible to define an optimal size for a sample (Mean Square Error Method : 15) and extrapolate the mean sample value of a certain characteristic to the whole population. Clearly, according to the theory of sampling, it will be possible to define a sample of average structures which represents the studied coal. It will be also possible to evaluate on this sample certain characteristic such as the energy, the density, the porosity, and to extrapolate these characteristics to the whole population of coal models.

The computer program developed for this study is built in such a way that any new experimental result can be introduced, at any time, without modification of the program. The same program will be useful in the future, when from new experimental data, new models will be needed. Furthermore, we can point out that the program can be applied for any other bituminous coal maceral and any other molecule studied in coal science such as lignite, subbituminous coal, or anthracite. Because different ranks of coal can be modeled, the program can be helpful in understanding the process of coalification. In fact the method is based on an original study made for the kerogen macromolecule (11), and is a general system of structure elucidation efficient for any unknown molecular structure. Therefore, it is realistic to consider applications in organic geochemistry, fuel science and petroleum science such as modelization of humic acids, peat, asphaltenes, crude oil, jet fuel, etc.

REFERENCES

1. Van Krevelen, D. W., *Coal*, Elsevier, Amsterdam, 1961.
2. Hatcher, P. G., *Advances in Org. Geochem.*, **16**, 959, 1990.
3. Given, P. H., *Fuel*, **39**, 147, 1960.
4. Wiser, W. H., *Proc. of the Electric Power Research Institute Conf. on Coal Catalysis*, 1973.
5. Solomon, P.R., in *New Approaches in Coal Chemistry*, Am. Chem. Soc. Symp. Series No. **169**, 61, 1981.
6. Shinn, J. H., *Fuel*, **63**, 1187, 1981.
7. Spiro, C. L. *Fuel*, **60**, 1121, 1981.
8. Carlson, G. A., Granoff B., in *Coal Science II*, Advances in Coal Sciences series, 159 1990.
9. Hatcher, P. G., Faulon, J. L., Wenzel, K. A., Cody, G. D., *this volume*, 1992.

10. Smith, D. H., *Computer-Assisted Structure Elucidation*, Am. Chem. Soc. Symp. Series No. 54, 1977.
11. Faulon, J. L., Vandenbroucke, M., Drappier, J. M., Behar, F., and Romero, M., *Advances in Org. Geochem.*, **16**, 4-6, 1990.
12. Faulon, J. L., *Prediction Elucidation and molecular modeling : Algorithm and Application in Organic Geochemistry*, PhD Thesis, Ecole des Mines, Paris, 1991.
13. Alinger, N. L., *J. Am. Chem. Soc.*, **99**, 8127, 1977.
14. Dalenius, T., in *handbook of statistic 6 - Sampling*, Elsevier, Amsterdam, 1988.
15. Rao, J. N. K., in *handbook of statistic 6 - Sampling*, Elsevier, Amsterdam, 1988.

ACKNOWLEDGMENTS

Financial support for this study was provided by the U. S. Department of Energy, Sandia National Laboratories under contracts DE-AC04-76DP00789 and 12-5543. We also acknowledge financial support from DOE contract DE-AC22-91PC91042 from the Pittsburgh Energy Technology Center. We thank Jackie M. Bortiatynski for assistance in assembling the data and manuscript.

Table I. The atomic information. These values are taken from Hatcher et al.(9).

ELEMENTAL ANALYSIS			¹³ C NMR			
	WEIGHT %	for 100 C		Value 1	Value 2	AVERAGE
C	85.8	100	fa	0.64	0.61	0.63
H	6.5	91.2 ± 1	Aro-O / Aro	0.11	0.13	0.12
O	5.9	5.2 ± 1	Aro-H / Aro	0.44		0.44
			CH ₃ / Ali	0.33	0.28	0.30

Table II. The macromolecular signature. The notations used by the signature are the potential types defines in Biosym softwares : h_ represents an hydrogen atom, c_ an aliphatic carbon, cp an aromatic carbon, and o_ an oxygen atom. The values are given for 100 carbon atoms, h_ = 91.2 means that the ratio H/C is equal to 0.912, c_(c_h_h_h_) = 9.2 means that there is 9.2% of carbon which is aliphatic, linked to one other aliphatic carbon and three hydrogen atoms.

SIGNATURE

	MIN	MAX	AVERAGE
h_	90.2	92.2	91.2
o_	4.2	6.2	5.2
c_	34.2	39.8	37.0
cp	60.2	67.8	64.0
c_(c_h_h_h_)	11.1	13.3	12.2
cp(cp cp h_)	25.3	29.9	27.6
cp(cp cp o_)	6.6	8.9	7.7

Table III. The solutions of the signature equation. The error listed is the difference between the model and the analytical results

solution number	molecular formula	error for 100 C
1	C ₁₅₂ H ₁₄₀ O ₇	0.92
2	C ₁₆₁ H ₁₄₈ O ₈	0.91
3	C ₁₆₂ H ₁₄₈ O ₈	0.83
4	C ₁₇₀ H ₁₅₆ O ₉	0.94
5	C ₁₇₁ H ₁₅₆ O ₉	0.86
6	C ₁₇₈ H ₁₆₄ O ₈	0.82 (-)
7	C ₁₈₀ H ₁₆₄ O ₁₀	0.97

NAME	WEIGHT %	CHOSEN STRUCTURE	NAME	WEIGHT %	CHOSEN STRUCTURE
methyl ethyl propyl			C2 phenol	23.0	
benzene	3.3		C3 phenol	11.0	
toluene	4.8		C4 phenol	4.8	
C2 benzene	5.2		alkyl naphthalene	17.0	
C3 benzene	3.9				
phenol	3.6				
o cresol	5.7		alkyl dibenzo furans	5.2	
m and p cresol	13.0				

Fig. 1. The molecular information. These fragments are results of flash pyrolysis/gas chromatography/mass spectrometry. The weight percentages and the different isomers for the chosen structures are discussed in Haicher et al.(9). The fragments are considered by the program only as qualitative information. Once connected together in an appropriate amount these fragments form the unknown macromolecule.

BOND	STRUCTURE
benzene-benzene	
benzene-phenol	
benzene-toluene	
toluene-toluene	
ethylbenzene-ethylbenzene	
propyl-benzene	
ethyl-toluene	
methyl-ethylbenzene	

Fig. 2. The inter-fragment bonds are shown as broken lines. These bonds represent the different ways to connect the fragments listed in Fig. 2.

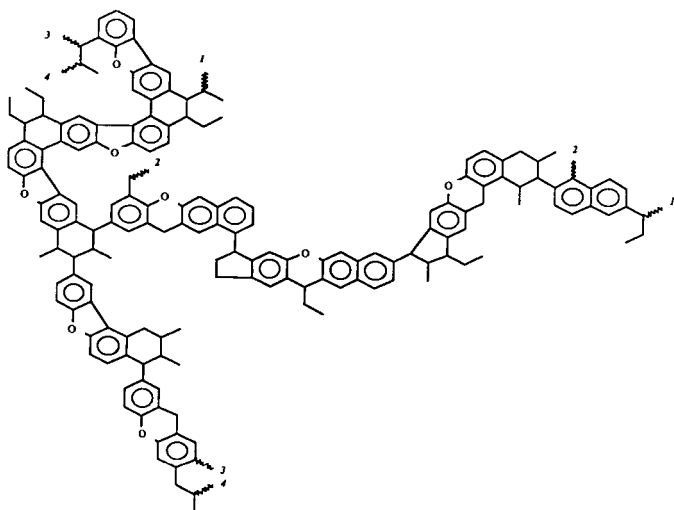


Fig. 3. One possible 2D representation for vitrinite from high volatile bituminous coal. Some other models are possible. An other possibility is given in Hatcher et al. (9). The number indicates the bonding sites (e.g. 1 -> 1).

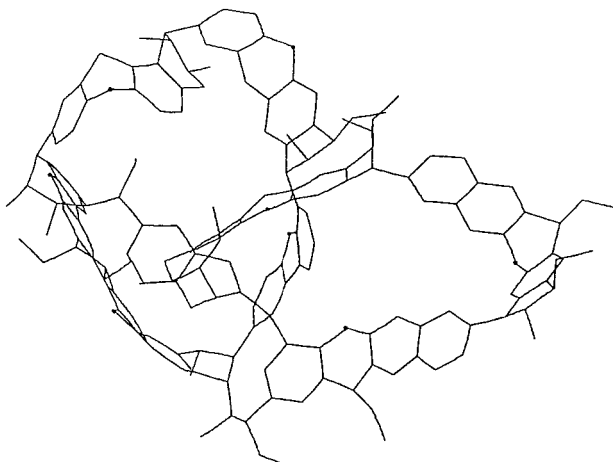


Fig. 4. One possible 3D structure for vitrinite from high volatile bituminous coal. This structure is the 3D representation of Fig. 3.

CHARACTERIZATION OF COAL LIQUEFACTION RESIDS BY FIELD IONIZATION MASS SPECTROMETRY: CORRELATING SPECTRAL FEATURES WITH PROCESSING PARAMETERS

Ripudaman Malhotra, Donald F. McMillen, and David L. Huestis
Chemical Kinetics Department, SRI International, Menlo Park, CA 94025-3493.

Keywords: FIMS, Resid analysis, Resid processing

INTRODUCTION

Under a contract with the U.S. Department of Energy, Consolidation Coal Company (Consol) has provided a range of well-documented samples obtained from process development units to various analytical researchers, who then apply their chosen methodology to determine the value of the method to process understanding and development (1). One objective of Consol's program is to provide a bridge between direct coal liquefaction process development and analytical chemistry. At SRI International, we have analyzed 15 resid samples, taken from three sampling points in five close-coupled two-stage liquefaction runs at the Wilsonville facility by field ionization mass spectrometry (FIMS) to help answer several questions relating to the chemistry of liquefaction, specifically as it relates to resid conversion, and how to improve the overall process.

The technique of field ionization (FI) consists of passing the vapors of a material through a region of intense electric field to polarize and ultimately ionize the molecules. The ions are then mass analyzed using standard mass spectrometric techniques. For most organic compounds, this procedure causes minimal fragmentation and produces only the molecular ions (2). The resulting spectra are thus true representations of the molecular weight profiles of the volatilized materials. FIMS has been used for a variety of applications relevant to coal liquefaction. However, its ability to answer the very difficult questions pertaining to the chemistry of resid reactivity has not been demonstrated. The objective of the task on FIMS analysis was to evaluate the utility of FIMS for addressing the issue of resid reactivity by analyzing a reasonably large set of related samples.

EXPERIMENTAL PROCEDURES

The samples were the vacuum resid portions of the oils samples collected at the end of the first stage, the second stage and following the ROSE-SR deashing unit. They are referred to as the interstage oil (V1235), product oil (V1067), and recycle oil (V131B) respectively. These samples are from five different two-stage liquefaction runs: Lignite (Run 255), Wyo-dak (Run 251-II), Illinois No. 6 (run 250) in the thermal-catalytic mode, and Illinois No. 6 (Run 257) and Pittsburgh (Run 259) in the catalytic-catalytic mode.

The analyses were conducted using SRI's FIMS instrument, which consists of a foil-type field ionizer interfaced with a 60-degree magnetic-sector mass analyzer and a PDP 11/23 computer for instrument control, data acquisition, and report production. The spectrometer has a resolving power ($M/\Delta M$) of 1300, although it is capable of scanning up to 3000 Da. Typically, approximately 20 μg of the sample is taken in a melting point capillary and introduced into the spectrometer with a heatable direct insertion probe. The sample is heated at a fixed rate from ambient (or $\sim 67^\circ\text{C}$ for samples with sufficiently high vapor pressure) to about 700°C . The pressure in the ion source chamber is generally in the 10^{-6} Torr range, although the pressure in the capillary sample holder is considerably higher. We estimate the sample pressure to be around 10^{-4} Torr. Under these conditions, materials with atmospheric equivalent boiling points (AEBP) up to about 1400°F are expected to vaporize completely, and those with AEBPs in between 1400° and 1600°F to vaporize at least partially. What often limits the vaporization of these high boiling materials are the coupling reactions with other species present in the sample. Hence the quoted limits should be regarded as a rough guide. (Similarly, other pyrolytic reactions can occur that produce volatile species not present at such in the original mixture.) The spectra of the evolving volatiles are continuously recorded, and at the end of a run, they are added to produce a "sum" spectrum of the total volatiles.

RESULTS AND DISCUSSION

General Spectral Features

Figure 1 shows the spectrum of the recycle oil from cat-cat run with the Pittsburgh coal (Run 259), and is typical of the entire set. All of the spectra consist of a broad distribution of molecular weights ranging from about 200 to 1000 Da. There is an additional group of peaks in the 50 to 120 Da range corresponding to small fragment ions. The total intensity of this low-mass group is typically extremely low compared to that of the main profile, reflecting the minimal ion fragmentation that is typical of most liquefaction product streams during FIMS analysis. Immediately apparent from these spectra are two profiles: a more intense profile for the even masses and the other (dark profile) corresponding to the odd masses. Peaks at odd masses generally arise due to ^{13}C , N, or fragmentation. Because FIMS does not cause much fragmentation and these spectra have been corrected for natural abundance of ^{13}C , the odd-mass profile arises mainly from compounds containing nitrogen.

At first glance, the FI mass spectra of all the resids look very similar. The similarity is reassuring because several processing requirements tend to provide resids of similar molecular weight range and polarity. Apart from being similar, the spectra also show that the resids are very complex mixtures. The bulk of the material in these samples falls in the 200-1200 molecular weight range and considering coal-origin and heteroatom content of the products, the "average" molecule at, say, m/z 600 would contain one oxygen, one-half nitrogen, and one-quarter sulfur. Therefore, most of the resid molecules are polyfunctional, and not classifiable, even in principle, according to simple chemical type or class. (3) For these reasons, we focused primarily on the overall profiles. We note here that there are a few peaks in the 240 to 340 Da range in each of the spectra that do stand out in all the spectra, and we examined them in some detail. However, before discussing this group of peaks, we first describe our attempt at a semi-quantitative characterization of the overall profiles.

In many instances, the spectra appear to be composed of two partially overlapping clusters of peaks: one such cluster, which we will call Component A, is centered around 350 Da and the other cluster, which we will call Component B, is centered around 600 Da. Relative to Component B, Component A appears to span a relatively narrower MW range. In other work, we had observed the somewhat bi-modal distribution of molecular weights in coal liquefaction resids. However, those observations were with isolated samples, and we were not sure if they were indicative of a general trend. Examination of fifteen closely related samples in this project confirmed the general nature of this distribution, and we felt encouraged to examine this distribution and see if the relative amounts of the two components can be correlated with some process-related parameters.

Several steps are involved in deconvoluting the spectra into Components A and B. First, we have to assign a general functional form to each of the component envelopes; second we perform a least-squares fit on a few selected samples to derive the parameters for the general formula describing the two components; and third we fit the spectra using these expressions while varying only the relative amplitude factors. We chose to express the rising part of each envelope as a power function of the molecular weight (m^α) and the decline as an exponential ($e^{-\beta m}$). The parameters α and β were to be different for each of the two components, but the overall functional form was constrained to be the same. The following expression gives the intensity (I_m) at any mass:

$$I_m = Q_A m^{\alpha_A} e^{-\beta_A m} + Q_B m^{\alpha_B} e^{-\beta_B m}$$

Here Q_A and Q_B are the weighting factors for the two curves. The parameters α_A , β_A , α_B , and β_B were determined by a regression analysis. Rather than fit all of the spectra by regression, we decided that a more meaningful test would be to select for regression five of the most divergent looking spectra. Once the parameters α and β were determined, they were fixed and the remaining spectra were fitted by varying only the Q 's. Figure 2 shows an example of the deconvolution. The dots are the data for the even masses in the FIMS of the recycle oil from the run with the Pittsburgh coal (Run 259). This spectrum was not among the ones used in the least-squares fit to obtain the parameters defining A and B. The continuous line through the data is the fit obtained by varying the amounts of A and B. The contributions of A and B components to the total fit are shown by the two dashed lines. The fit in this case is reasonably good over most of the mass range, except at high masses where the fit gives a lower intensity than the data. The break in the curve around 450 Da is well mimicked by the fit. Those spectra without a distinct break in the curve were not fit quite so well.

To obtain the relative *weight* fractions of the two components, A and B, we integrate the product of mass with the fitted expressions over the mass range. Thus:

$$\%A = \frac{100 \times \int Q_A m^{\alpha_A} e^{-\beta_A m} \cdot m \, dm}{\int Q_A m^{\alpha_A} e^{-\beta_A m} \cdot m \, dm + \int Q_B m^{\alpha_B} e^{-\beta_B m} \cdot m \, dm}$$

The data in Table I show the wt% A in the various samples.

Correlation of Lumped Component Levels with Process Parameters and Yields

Having in hand the deconvolution results summarized in Table I, an attempt can be made to see how the levels of Components A and B correlate with process conditions and product character and yields as previously summarized.⁽⁴⁾ The Illinois No. 6 catalytic-catalytic product oil (Run 257) has a very pronounced low-mass intensity (200-400 Da) as is also reflected in the large A content (32%). This low-mass grouping is somewhat less prominent in the "younger" interstage oil (22%). Evidently, under the catalytic-catalytic conditions, high yields of material that is low molecular weight are produced from the coal or "fresh" resid in the first-stage reactor, and most noticeably, in the second-stage reactor.

In significant contrast to the prominent low-mass intensity in the Run 257 product oil, the recycle oil (which nominally differs from the product oil only in that a portion of the stream has been split off, sent through a vacuum flash separator, and had the ash and insoluble organic matter removed in the ROSE-SR unit) has substantially less of the 200 to 400 Da intensity (13%). Whereas one expects some of the high molecular weight organic material visible with FIMS to be rejected along with the ash, and therefore for the *higher* end of the molecular weight profile to be trimmed in the recycle oil (as compared with the product oil), it is the *lower* end of the profile that has shrunk. This observation suggests significant retrogression between V1067 and V131B; in other words, that significant coupling occurs when the high temperatures are maintained during the "physical" separation process or subsequently in the holding tanks, but catalyst and H₂ pressure are largely absent.

In the case of the Pittsburgh coal, which was also processed in the catalytic-catalytic mode (Run 259), as we move from the interstage oil to the product oil, we see that Component B dominates over Component A. In this case, the fresh resid seems to be much less readily converted (in the second-stage reactor) into A; the net change in fact is for the B to become *more* important as a result of reaction in the second stage. The differences between the Pittsburgh product oil and the recycle oil seem to reflect mainly removal of high molecular weight material, B. This is as would be expected, but is in contrast to the Illinois catalytic-catalytic case, where the effect of putting a side stream through the ROSE-SR unit (and the holding tanks) was curiously to *increase* the amount of B.

The next appropriate comparison is between the Illinois catalytic-catalytic run (Run 257), and the Illinois thermal-catalytic run (Run 250). In Run 250, the level of Component A in the interstage oil is only about half that in Run 257, and passage through the Stage 2 reactor *decreases* Component A still further (rather than increasing it as in Run 257). We conclude (since Stage 2 is catalytic in both cases) that the product of the thermal first stage is less reactive. Apparently the "fresh" resid is more refractory because of the absence of catalyst and/or the slightly higher temperatures used during operation of a thermal first stage.

Moving to the two lower rank coals in this series, also processed in a therm-cat configuration, we see that for both the Wyodak coal and the lignite, second-stage reaction causes a decrease in the percentage of Component A — a change that is qualitatively similar to that seen for the Illinois therm-cat run (Run 250). With respect to changes between the product oil and the recycle stream, there is a slight increase in Component A for both the Wyodak and the lignite, whereas for the Illinois No. 6 coal (Run 250), Component A had decreased. Since we associated the decrease in Component A between the product and recycle streams for the Illinois No. 6 runs with a proclivity for retrogression, we would conclude from the slight *increase* in A that the Wyodak and lignite resids are actually less prone to retrograde reaction than the Illinois No. 6 resids. The observed increase in A supports the conclusion that PCAH species, which are expected to be less abundant in the lower rank coals and their products, are the primary candidates for retrogressive reactions in these highly processed resids. The observed increase in Component A is thus most likely due to a greater rejection of Component B as was observed with the Pittsburgh coal.

To summarize, the attempt to make a straightforward association between the amounts of Components A and B in each resid was surprisingly successful, however some loose ends remain. For instance, a decrease in

Component A as a resid moves through the processing stream can reflect not only regression to the heavier component, B, but also upgrading to distillate. For simplicity, we have simply chosen to try first to rationalize the data in terms of the possibility that is more troublesome in process terms, namely retrogression of Component A to B.

Examination of Prominent Individual Peaks

While a large part of each of the FI-mass spectral profiles is basically quite smooth, with few prominent masses, it is noteworthy that at the low mass end (240 to 350 Da), there is substantial "structure" in the spectra. Moreover, the same peaks appear as prominent in spectra of all the fifteen resids. The six major series apparent in the spectra of these resids begin at m/z 242, 276, 282, 300, 308, and 316. In Figure 1 we have labeled some of these prominent peaks.

Curiously enough, the six major peaks apparent in these resid spectra are either the same as, or closely related to, those recently identified by Sullivan, Boduszynski, and Fetzer (5) as showing substantial increases during hydrotreating of petroleum vacuum gas oil fractions. Based on the evidence presented by Sullivan et al. (5), and the very striking correspondence between the major peaks seen here and some of those identified by them, we consider it to be very likely that most of the prominent peaks noted here are causally related to the difficulty of catalytic/thermal breakdown to smaller species (distillate) and to the buildup of more refractory resid and IOM. At present, it is difficult to make a more quantitative statement regarding the importance of these peaks. However, a few of the trends that emerge from an initial examination are listed below.

- Consistent with the fact that the Pittsburgh resid is the most difficult to upgrade, the intensities for m/z 276, benzo[ghi]perylene, observed for the Pittsburgh coal (Run 259) are generally higher than those for any other sample. However, this relationship appears not to always hold. In the interstage and recycle oils for Run 259, the levels are 2 to 2.5 times higher than the respective samples for Run 257, the catalytic/catalytic Illinois No. 6 run, but for the product oil the levels are essentially equal.
- The cat/cat run with Illinois No. 6 coal (Run 257), produces more of m/z 276 by about a factor of two than the therm/cat run (Run 250), even though the resid produced in 250 was considered to have been more difficult to upgrade. If the large PCAH are produced in significant part by the cracking activity of the alumina-supported catalysts, we might rationalize that without the first stage catalyst, less benzo[ghi]perylene is formed. But if we accept this explanation, we are then forced to say that the difficulty in upgrading the Illinois therm/cat fresh resid is not due to benzoperlylenes, coronenes, etc., but is due instead to the fact that less cracking occurred in the first stage. While this latter rationalization may be correct, it is apparent that the situation is complex and not susceptible to analysis by simple inspection.
- If instead of comparing the absolute levels, we compare the ratios of peaks at m/z 276 and 300, we find that in going from the recycle stream to the interstage oil the relative amount of benzo[ghi]perylene increases in the more difficult-to-process Runs 250 and 259, while it decreases in Run 257.
- Changes in the ratios of hydroaromatic/aromatic pairs as the resid moves through the system provide an additional point for comparison. We find that the hard-to-convert Runs 250 and 259 show distinct decreases in the ratio of hexahydrobenzo[ghi]perylene to benzo[ghi]perylene. On the other hand, the "good" run 257 actually shows an increase in this hydroaromatic/aromatic ratio as a result of addition of coal to the recycle oil and reaction in the first stage reactor. The appearance of high levels of benzoperlylene in Run 259 is presumably related to the fact that the level of cyclic- β -hydrogen (i.e., hydroaromatic hydrogen, as determined by NMR) in the recycle oil was the lowest of these three runs.

These trends do not extend to the entire set of runs. In other words we were not able to construct a consistent set of correlations between the most prominent homologous series and the processing behavior in all five runs. However we believe it is very likely that the difficulty in significant part is that the run-to-run comparisons attempted are anything but all-other-things-being-equal comparisons. A more careful examination of these data is warranted. One correction that ought to be included in this analysis is for the background intensity of all other components that might be present at these specific masses. The background could be adequately represented by the "fit" to the profile described in the previous section. The correction is small for peaks at 242 Da, but probably substantial for those at 300 Da. An alternative strategy would be to perform a

factor analysis on this set of peaks and identify the major trends. We suggest that these tasks be undertaken in a future effort.

SUMMARY

During this research effort we found that FIMS of many of the liquefaction resid samples exhibited a bimodal molecular weight distribution. The relative amounts of the low and high molecular weight components differ significantly from sample to sample, and simple mathematical deconvolution into Components A and B has revealed a correlation between the variations in A and B on the one hand and coal type, process conditions, and process performance on the other. While the correspondence is not perfect, the deconvolution leads to conclusions reasonably in concert with what is already recognized in coal liquefaction. It is satisfying to see so many observations about reactivity reiterated, not on the basis of yields, but on the basis of differences in molecular weight distribution of streams that are already constrained by process conditions and product fractionation to be as similar as possible. The mass spectra consistently showed a same set of few prominent peaks in the low mass end. Interestingly, these masses were identical with those previously associated by Sullivan et al. with increased difficulties in hydrotreating vacuum gas oils. This similarity prompted us to seek correlations between processing variables the intensity of these peaks. Our partial success in finding such correlations warrants a more extensive examination of the variations in these prominent masses, which when coupled with the deconvolution into lumped low and high molecular weight components, is likely to provide substantial independent information for cross-correlation with other resid properties and processing parameters.

Acknowledgement. This work was performed as a subcontract under Consolidation Coal Company's prime contract with the U.S. Department of Energy, Contract No. DE-AC22-89PC89883. Helpful discussions with Drs. R. A. Winschel, F. P. Burke, and S. D. Brandes are gratefully acknowledged.

REFERENCES

1. Brandes, S. D.; Winschel, R. A.; Burke, F. P. "The Application of Advanced Analytical Techniques to Direct Coal Liquefaction," *Am. Chem. Soc., Div. Fuel Chem. Preprints*, 1991, 36(3), 1172.
2. St. John, G. A.; Buttrill, S. E., Jr.; Anbar, M., in *Organic Chemistry in Coal*, J. Larsen, Ed.; ACS Symposium Series 71, Washington, D. C., 1978, p. 223.
3. Boduszynski, M. M.; "Characterization of Heavy Crude Components," *Am. Chem. Soc., Div. Fuel Chem. Preprints*, 1985, 30(3), 365.
4. Burke, F. P.; Winschel, F. P.; Robbins, G. A., "Coal Liquefaction Process Solvent Characterization and Evaluation," Final Report, U.S. DOE Contract No. DE-AC22-84PC70018, 1989.
5. Sullivan, R. F.; Boduszynski, M. M.; Fetzer, J. C. *Energy Fuels* 1989, 3, 603.

Table 1

PERCENTAGE OF LOW-MOLECULAR WEIGHT COMPONENT A IN RESIDS TAKEN FROM DIFFERENT RUNS AND SAMPLING POINTS

Wt% A in the Sample Determined from Even-Mass Profile

Sample point	255	251-II	250	257	259
	Lignite Therm-Cat	Wyodak Therm-Cat	Illinois Therm-Cat	Illinois Cat-Cat	Pittsburgh Cat-Cat
Interstage oil	21.5	11.4	13.9	22.4	13.7
Product oil	18.2	9.0	10.4	32.0	9.2
Recycle oil	21.6	10.0	8.6	13.1	18.5

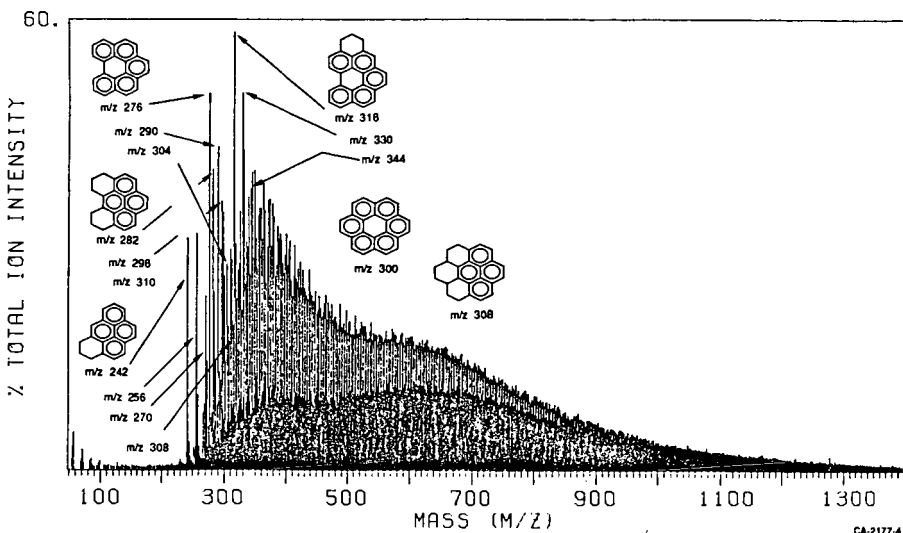


Figure 1. FIMS of the Pittsburgh (Run 259) recycle oil showing the prominent PCAH structures in the 200-350 Da range. CA-2177.4

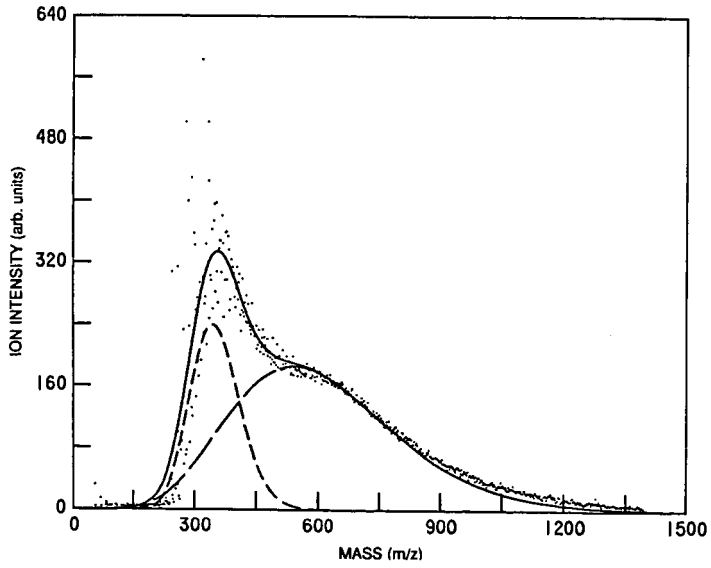


Figure 2. Deconvolution of the FIMS of Pittsburgh (Run 259) recycle oil into Components A and B.

THE EFFECT OF CROSS-LINKING ON THE THERMAL DECOMPOSITION OF DIPHENYLALKANES

Phillip F. Britt and A. C. Buchanan, III
Chemistry Division
Oak Ridge National Laboratory
P. O. Box 2008
Oak Ridge, Tennessee 37831-6197

Keywords: Pyrolysis mechanisms, model compounds, retrogressive reactions

ABSTRACT

In the early stages of the thermal depolymerization of coal, its cross-linked macromolecular structure may restrict the diffusion of reactive intermediates and alter the reaction pathways. In an effort to model the effects of restricted mass transport on the thermally induced free radical decomposition of polymethylene units bridging aromatic clusters in coal, a series of diphenylalkanes [Ph(CH₂)_nPh] have been cross-linked to an inert silica surface by the condensation of the corresponding phenol, HOC₆H₄(CH₂)_nC₆H₄OH. Results from the thermolysis of the diattached substrates at 350-400 °C will be presented and compared to the thermolysis of fluid phase and mono-attached diphenylalkanes [≈Ph(CH₂)_nPh] to highlight the impact that restricted diffusion has on the reaction mechanisms.

INTRODUCTION

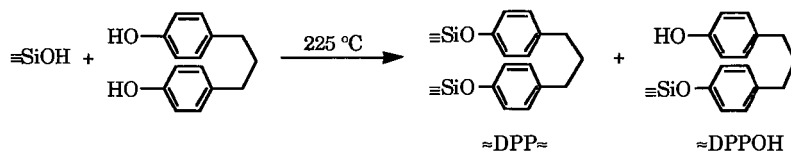
The study of the fundamental reaction mechanisms associated with the thermal decomposition of coal is hindered by its heterogeneous, cross-linked, macromolecular structure. One solution to this problem has been to investigate the thermal decomposition of model compounds representing structural features present in coal, but extrapolation of the results back to coal is difficult and sometimes unreliable.¹ In order to provide a more relevant model for exploring the reaction mechanisms associated with coal pyrolysis, some of the complexities imparted by the macromolecular network structure of coal must be taken into account.

Our research has focused on modeling the effects of restricted mass transport on thermal free radical reaction pathways.²⁻⁶ Thermolysis studies at 350-400 °C of α , ω -diphenylalkanes covalently attached to an inert silica support has provided evidence that restricted radical and substrate diffusion can alter the free radical reaction pathways as compared to their liquid or gas phase behavior. In the thermolysis of surface-immobilized 1,2-diphenylethane, unimolecular rearrangement and cyclization were favored over bimolecular coupling reactions.² Thermolysis of surface-immobilized 1,3-diphenylpropane (≈DPP)³ and 1,4-diphenylbutane (≈DPB)⁴ showed that a free radical chain reaction can efficiently occur under the effects of restricted diffusion, and an unexpected regioselectivity in the hydrogen abstraction process was observed. These studies have also shown that cross-linking reactions can occur under conditions of restricted diffusion. For example, in the thermolysis of ≈DPP and ≈DPB, surface-attached benzyl radical adds to a surface-attached styrene

to form a cross-linked DPP ($\approx\text{Ph}(\text{CH}_2)_3\text{Ph}\approx$ or $\approx\text{DPP}\approx$) after hydrogen abstraction. Although the reactions responsible for cross-linking have been investigated,⁷ the effects of cross-linking on the thermal decomposition reaction pathways has not been investigated. Therefore, in this paper, we will explore the effects of cross-linking on the thermolysis of 1,3-diphenylpropane and 1,4-diphenylbutane as model compounds for coal.

EXPERIMENTAL

1,3-di(*p*-hydroxyphenyl)propane and 1,4-di(*p*-hydroxyphenyl)butane were prepared by the procedure of Richardson⁸ and purified by repeated crystallizations from benzene/hexanes until the purity was >99.9% by GC. The surface-attached materials were prepared by the condensation (225 °C for 1-4 h) of the diphenol with the surface hydroxyls of a high purity fumed silica (Cab-O-Sil, M-5, Cabot Corp.) and sublimation



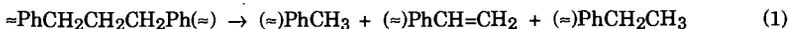
of the excess phenol under vacuum (5×10^{-3} Torr) at 275 °C, as previously described.²⁻⁴ Complete diattachment could not be obtained even at the lowest surface coverages, and the surface contains a mixture of mono- and diattached material. Surface coverages were determined by liberation of the surface-attached phenol by base hydrolysis, silylation to the corresponding trimethylsilyl ethers, and analysis by GC. Three batches of $\approx\text{DPP}\approx/\approx\text{DPPOH}$ were prepared with surface coverages of 0.465, 0.181, and 0.105 mmol of organic per gram of derivatized silica with purities of 99.9, 99.5, and 99.6%, respectively, and one batch of $\approx\text{DPB}\approx$ was prepared with surface coverage of 0.113 mmol/g and purity of 99.6%. The fraction of mono-attached substrate was determined from the quantity of HOPhCH_3 , a product from the thermolysis of $\approx\text{DPPOH}$ and $\approx\text{DPBOH}$, which distills into the cold trap.

Thermolyses were conducted in sealed, evacuated ($<5 \times 10^{-6}$ Torr) T-shaped tubes as previously described.²⁻⁴ Volatile products were collected in a cold trap and analyzed as phenols and their trimethylsilyl ethers, while surface-bound products were removed from the surface by base hydrolysis and silylated to the trimethylsilyl ethers. The samples were analyzed by GC and GC-MS with the use of internal standards.

RESULTS AND DISCUSSION

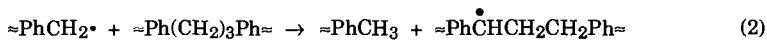
Thermolysis of $\approx\text{DPP}\approx$. In order to determine the effect of cross-linking on the thermolysis of 1,3-diphenylpropane, a series of surface-attached DPPs were synthesized in which the fraction of diattachment was varied. As shown in Table 1, the extent of diattachment increased with decreasing surface coverage, but complete diattachment could not be achieved. This is most likely a consequence of the

geometric constraints of the short aliphatic chain (see \approx DPB \approx below). Thermolysis of the high coverage \approx DPP \approx at 375 °C at low conversion produces approximately equal amounts of surface-immobilized toluene and styrene as the major products and a small amount of surface-immobilized ethylbenzene (ca.1%), eq 1. The parentheses



indicate that both a surface-immobilized species and a gas-phase species are present since the starting DPP is not completely cross-linked to the surface. At higher conversions, isomers of $\text{C}_{22}\text{H}_{22}\text{O}_3$ and $\text{C}_{23}\text{H}_{24}\text{O}_3$ (after work-up) are formed as secondary products.

The products from the thermolysis of \approx DPP \approx can be rationalized by a free radical chain reaction analogous to the one determined for \approx DPP \approx^3 and DPP.⁹ Assuming that all of the DPP is diattached to the surface, the chain propagation steps are shown in equations 2 and 3. The mono-attached DPP (\approx DPPOH) decomposes analogously, but

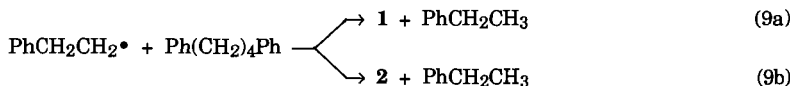
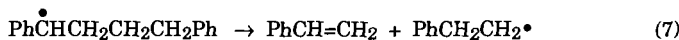
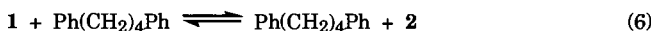
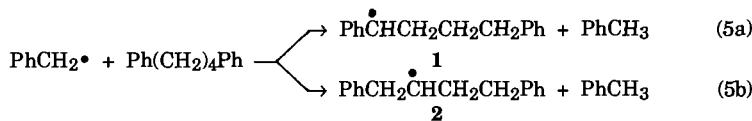


produces a mobile gas-phase (vide infra) benzyl radical (p -HOPhCH₂•). The surface-immobilized ethylbenzene could result from the initiation reaction or hydrogenation of styrene. Alkenes such as stilbene and styrene are known to be reduced to the alkane in the presence of hydrogen donors such as tetralin as well as DPP itself.^{9a} The secondary products $\text{C}_{23}\text{H}_{24}\text{O}_3$ and $\text{C}_{22}\text{H}_{22}\text{O}_3$ are formed from reaction of the diattached 1,3-diphenyl-1-propyl radical with surface-attached styrene or benzyl radical.¹⁰ Although radical addition to styrene has been observed in the thermolysis of \approx DPP and DPP, radical coupling involving a 1,3-diphenyl-1-propyl radical is a unique chain terminating reaction that has not previously been observed.

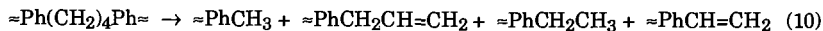
The rate of decomposition of \approx DPP \approx should be sensitive to the extent of cross-linking since the geometric constraints placed on the chain carrying benzyl radical and the neighboring DPP molecules would influence the hydrogen abstraction reaction. Comparing the rate of conversion of a high coverage \approx DPP \approx and \approx DPP (see Table 1), it is found that the small degree of cross-linking (24%) has only a modest effect on the rate. The free phenolic functionality of the mono-attached DPP is not expected to inhibit the rate of decomposition since it has been shown that in the thermolysis of DPP in the liquid phase at 350 and 400 °C, phenol and alkylated phenols have no effect on the rate of decomposition or product distribution.¹¹ Surprisingly, at lower coverages, the rate of decomposition of \approx DPP \approx is only slightly slower than that of \approx DPP. This could indicate that (1) hydrogen abstraction reactions are not more hindered by diattachment at these surface coverages, (2) gas phase HOPhCH₂•, from the decomposition of the mono-attached DPP, is an effective chain carrying radical, or (3) the rate of initiation is accelerated by strain introduced into the aliphatic chain by cross-linking. The effects of cross-linking on the rate of decomposition is under further investigation.

No new products are observed from the thermolysis of \approx DPP \approx as the fraction of cross-linking increases. However, retrogressive reactions dramatically increase as a consequence of cross-linking. A comparison of the mole % secondary products from the thermolysis \approx DPP \approx and \approx DPB at similar coverages and conversions reveals that as cross-linking increases, retrogressive reactions increase over 100-fold at the lowest surface coverage as shown in Table 2. Additionally, the mole % of \approx PhCH₂CH₃ increases with decreasing surface coverage and is approximately independent of conversion. If the ethylbenzene is formed from the reduction of styrene, the yields would likely be conversion dependent.³

Thermolysis of \approx DPB \approx . The thermolysis of a diattached 1,4-diphenylbutane (\approx DPB \approx) was used to study the effects of cross-linking on the selectivity of hydrogen abstraction. In thermolysis of 1,4-diphenylbutane (DPB), four products are formed (eq 4) by a free radical chain mechanism in which the chain propagation steps are shown in equations 5-9.



A \approx DPB \approx was prepared with a surface coverage of 0.113 mmol/g with 94% of the material cross-linked. The fraction of diattachment is larger than that found for \approx DPP \approx (82%) and must be a result of the longer aliphatic chain. Thermolysis of \approx DPB \approx at 400 °C produced the four products shown in eq 10. A mechanism similar



to that proposed for the thermolysis of DPB can be invoked for the cross-linked DPB. The selectivity of formation of 1 to 2 as determined by the PhCH₂CH₃/PhCH₃ ratio is dramatically altered compared to selectivity found for \approx DPB (see Table 3), and favors

the thermodynamically less stable aliphatic radical 2. This perturbation of selectivity could result from the geometric constraints placed on the hydrogen abstraction reaction by restricted mass transport. Additionally, the rate of decomposition is significantly reduced as a consequence of cross-linking. The impact of cross-linking on the selectivity will be studied further.

CONCLUSION

This paper presents the preliminary results from the study of the effects of cross-links on the thermolysis of coal model compounds. Our previous studies have shown that restricting mass transport can alter reaction pathways. Results from this study indicate that cross-linking can dramatically increase retrograde reactions, alter the selectivity of hydrogen abstraction reactions and reduce the rate of decomposition. Additional studies are in progress to probe the impact of restricted mass transport on retrograde reactions.

ACKNOWLEDGEMENTS

Research was sponsored by the Division of Chemical Sciences, Office Of Basic Energy Sciences, U. S. Department of Energy under contract DE-AC05-84OR21400 with Martin Marietta Energy Systems, Inc.

REFERENCES

1. Larsen, J. *Prepr. Pap.-Am. Chem. Soc., Div. Fuel Chem.* **1990**, *35*, 376.
2. Buchanan, III, A. C.; Dunstan, T. D. J.; Douglas, E. C.; Poutsma, M. L. *J. Am. Chem. Soc.* **1986**, *108*, 7703.
3. Buchanan, III, A. C.; Biggs, C. A. *J. Org. Chem.* **1989**, *54*, 517.
4. Britt, P. F.; Buchanan, III, A. C. *J. Org. Chem.* **1991**, *56*, 6132.
5. Britt, P. F.; Buchanan, III, A. C.; Hitsman, V. M. *Prepr. Pap.-Am. Chem. Soc., Div. Fuel Chem.* **1990**, *36(2)*, 529.
6. Buchanan, III, A. C.; Britt, P. F.; Biggs, C. A. *Energy Fuels* **1990**, *4*, 415.
7. (a) Suuberg, E. M.; Lee, D.; Larsen, J. W. *Fuel* **1985**, *64*, 1668. (b) Suuberg, E. M.; Unger, P. E.; Larsen, J. W. *Energy Fuels* **1987**, *1*, 305. (c) Solomon, P. R.; Hambeln, D. G.; Carangelo, R. M.; Serio, M. A.; Deshpande, G. V. *Energy Fuels* **1988**, *2*, 405. (d) Solomon, P. R.; Serio, M. A.; Deshpande, G. V.; Kroo, E. *Energy Fuels* **1990**, *4*, 42.
8. Richardson, E. W.; Reid, E. E. *J. Am. Chem. Soc.* **1940**, *62*, 413.
9. (a) Poutsma, M. L.; Dyer, C. W. *J. Org. Chem.* **1982**, *47*, 4903. (b) Gilbert, K. E.; Gajewski, J. J. *J. Org. Chem.* **1982**, *47*, 4899.
10. C₂₂H₂₂O₃ could also be formed from reaction of =PhCH=CHCH₂Ph= with =PhCH₂• but =PhCH=CHCH₂Ph= was not detected as a product.
11. (a) Gilbert, K. E. *J. Org. Chem.* **1984**, *49*, 6. (b) Stock, L. M.; King, H.-H. *Fuel* **1982**, *61*, 1172.

Table 1. Rate of Conversion of \approx DPP \approx and \approx DPP as a Function of Surface Coverage.

Compound	Coverage (mmol/g)	% Diattachment	Rate ^a (% h ⁻¹)
\approx DPP \approx	0.465	24	3.5
	0.181	60	0.56
	0.105	82	0.096
\approx DPP	0.57	-	7.0
	0.14	-	0.40
	0.10	-	0.26

^aDetermined from the slopes of the linear regression of conversion vs time

Table 2. Yield of Secondary Products as a Function of Surface Coverage.

Coverage (mmol/g)	Secondary Products: \approx DPP \approx / \approx DPP ^a	\approx PhCH ₂ CH ₃ ^c (mole %)
0.465	2.8	1.2
0.181	22	5.3
0.105	>120 ^b	8.5

^aRatio of the mole % secondary products from thermolysis of \approx DPP \approx and \approx DPP compared at similar coverages and conversion.

^bSecondary products for 0.10 mmol/g \approx DPP below detection limit of 0.05 mole %. ^cIndependent of conversion.

Table 3. Selectivity and Rate of Decomposition of \approx DPB \approx and \approx DPB.

Compound	Coverage (mmol/g)	1/2 Selectivity ^a	Rate (% h ⁻¹) ^b
\approx DPB \approx	0.113	0.60	1.1%
\approx DPB	0.117	2.0	9.5%

^aPhCH₂CH₃/PhCH₃ product ratio. ^bRate determined from the slope of a conversion vs time plot.

DIDEUTERIUM INCORPORATION DURING THE COPROCESSING REACTION OF LLOYDMINSTER PETROLEUM RESID AND ILLINOIS NO. 6 COAL IN D₂

Michael Ettinger and Leon M. Stock
Department of Chemistry, University of Chicago, Chicago, IL 60637

John G. Gatsis, UOP Research Center, Des Plaines, Illinois 60017

Keywords: Coprocessing, NMR, Liquefaction

INTRODUCTION

Coal petroleum resid coprocessing is fast becoming a cost effective means of coal liquefaction. The reaction mechanisms, however, are not well understood and are very important to the development and improvement of the technology. The coprocessing reaction is carried out at high temperatures and under a dihydrogen atmosphere that donates hydrogen to the fossil fuels to provide higher yields of liquids and to increase their hydrogen content. Accordingly, we have undertaken a study of the role of dihydrogen in the coprocessing reaction. The initial research in which Illinois No. 6 coal or Wyodak coal and Lloydminster resid or Hondo resid was mixed with a molybdenum based UOP proprietary catalyst was carried out under a 3000 psi dideuterium atmosphere at 420°C with a heat up time of 120 minutes and a residence time of 120 minutes¹. Quantitative 1H and 2H NMR analyses yielded similar results for the four combinations of coals and resids. Specifically, the degree of deuteration, (D/H+D), of the coprocessed products approached 0.25, the value that was expected for complete equilibration of the isotopes among the available positions in the oil, resin, and asphaltene. These results established the unselective character of the severe coprocessing reaction. However, we sought information on the limiting processes. Accordingly, additional coprocessing reactions with Illinois No. 6 coal and Lloydminster resid have been carried out under less severe conditions to investigate how the dideuterium utilization in the reaction products is affected by changes in the temperature and pressure.

EXPERIMENTAL

Materials. Illinois No. 6 coal was prepared by the Kentucky Center for Energy Research (KCER) and used as received (Anal. %C, 68.60; %H, 4.51; %N, 1.39; %S, 3.04; %O, 9.65; %H₂O, 3.15; %Ash, 9.65). Lloydminster Resid (Anal. %C, 83.6; %H, 11.5; %S, 4.77; %N,) was obtained by UOP Research Center and used as received. The catalyst used was a molybdenum based UOP proprietary catalyst.

Coprocessing Reaction Procedure. Weighed amounts of Lloydminster and Illinois No. 6 coal in a two to one ratio (resid/MAF coal) and the catalyst (2%wt) are added to an 1800ml rocking autoclave. The autoclave is sealed and is pressurized first with hydrogen sulfide and then with dihydrogen or dideuterium to give a 10 vol% hydrogen sulfide and 90 vol% dideuterium such that the desired pressure is obtained at reaction temperature. The autoclave is heated to the desired temperature for a residence time of 0.0, 0.5, or 2 hours. At the reaction conditions, dideuterium is added automatically so that the desired reaction pressure (1770 or 3000psi at temperature) is maintained. After the desired time-at-temperature, the autoclave is cooled to room temperature, and is then depressurized with the gas passing through a foam trap, caustic scrubbers, metering system, and then a sample is collected for analysis. To remove additional gas from the remaining reaction mixture, the material in the autoclave is stripped with dinitrogen. This gas also is passed through the foam trap, caustic scrubber, metering system, and analyzed. Any slurry product recovered in the foam trap is recovered with toluene and added to the toluene rinse solution. The slurry product from the autoclave is decanted. The material that remains in the autoclave is removed by rinsing the vessel with toluene until the autoclave is clean. The combined slurry

product is solvent separated into four fractions (oil, resin, asphaltene, and insoluble) according to a previously reported procedure¹.

Analysis. Deuterium spectra were obtained on a Varian XL 400 MHz spectrometer. Two hundred fifty six scans were acquired by using a 90° pulse and a .5 second delay between pulses. Benzaldehyde- α -d-1 was used as a quantitative internal standard. Proton spectra were obtained similarly on the same instrument by using a 90° pulse and a 20 second delay between pulses. Elemental analyses for carbon and hydrogen for each solvent separated product were obtained from Huffman Laboratories by using an instrument that detected both hydrogen and deuterium².

RESULTS

The autoclave reactions were carried out with Illinois No. 6 coal, Lloydminster resid and a molybdenum based UOP proprietary catalyst. Temperature was varied from 390 to 420°C and pressure was varied from 1770 to 3000 psi of dideuterium. The actual reaction time is a sum of the heat up time, approximately two hours, and the residence time, 0.0, 0.5, or 2 hours. The coprocessed products were solvent separated into four fractions; oil (isopentane soluble), resin (heptane soluble-isopentane insoluble), asphaltene (toluene soluble-heptane insoluble), and insolubles (toluene insoluble). The yields of each fraction, the coal conversion, and the asphaltene conversion for each reaction are provided in Table I.

The solvent separated products were quantitatively analyzed by proton and deuterium NMR methods and elemental analysis. The NMR spectra were partitioned into regions: aromatic resonances (12.0 - 6.0 ppm), total aliphatic resonances (5.0 - (-2.0) ppm), alpha aliphatic resonances (5.0 - 2.0 ppm), beta aliphatic resonances (2.0 - 1.0 ppm), and gamma aliphatic resonances (1.0 - (-2) ppm). Hydrogen content, deuterium content, and % deuteration at each position in the oil, resin, and asphaltene fractions were determined as shown in Table II, and (H+D)/C ratio is shown in Figure 1.

The data in Tables I and II clearly show the effects of temperature and pressure on the yields and conversions in the coprocessing reaction. Temperature proves to be the dominant driving force for conversion. An increase in dideuterium pressure from 1770 to 3000 psi at 390°C has essentially no effect on either coal or asphaltene conversion, or on the yields of any of the solvent separated products. However, except for the aromatic positions, an increase in pressure does increase the deuteration at all positions, and the (H+D)/C ratio increased in the oil, resin, and asphaltene fractions. Aromatic deuteration increased from 17.2 to 19.1%, mainly in the resin and asphaltene fractions. The increase in aliphatic deuteration from 9.1 to 12.1% was dominated by incorporation at the alpha position.

An increase in reaction temperature from 390 to 405°C and then to 420°C had a dramatic effect on the coal and asphaltene conversions. The coal conversion increased from 42.6 to 75.0% at 405°C, and then to 92.1% at 420°C. The coal conversion reached its maximum of about 92% at 420°C with no residence time. The same result was realized both when the residence time was 0.5 hours and 2.0 hours. The asphaltene conversion steadily increased from 13.0 to 29.6% at 405°C, and then to 40.1% at 420°C. The oil and asphaltene yields increased slightly, but most importantly the insoluble yield decreased significantly from 19.3% at 390°C to 2.7% at 420°C enabling the high coal conversions. In addition, the increase in temperature from 390 to 405°C, and from 405 to 420°C provided almost linear increases in deuteration at all positions. Approximately 9-10% increases are seen in the deuteration of all the aliphatic positions in the oil, resin, and asphaltene fractions with the exception of the alpha position in the resin and asphaltene fractions. The lack of a comparable increase in alpha % deuteration is almost certainly the result of the already high level

of deuterium incorporation in the alpha position at 390°C. Increases in the aromatic region averaged about 7.5%.

Both coal conversion and alpha D exchange reach their maximum at 420°C with no residence time. As the residence time was increased, coal conversion remained constant and % alpha deuteration declined in all three fractions while the asphaltene conversion exhibited its largest increase. As the residence time and, consequently, the asphaltene conversion were increasing, the % aliphatic and % overall deuteration remained essentially constant in the asphaltene fraction while the % aromatic deuteration and the % alpha deuteration decreased. The increase in % deuteration in the beta and gamma positions compensated for the decreases in the other positions to keep the overall % aliphatic deuteration of the asphaltene fraction constant indicating the approach to equilibrium of H and D in the asphaltenes. The alpha position was still slightly favored.

However, as the residence time at 420°C is increased, the % deuteration at the other positions (aromatic, beta, and gamma) in all three fractions increases, and lead to an increase in the overall aliphatic and total deuteration in the oil and resin fractions. In addition, (H+D)/C significantly decreases in the resin and asphaltene, and to some extent in the oil.

CONCLUSIONS

Increasing pressure and temperature both lead to increased deuterium uptake from the dideuterium atmosphere. Temperature is, however, the driving force behind the conversion chemistry. Deuterium uptake, asphaltene conversion, and coal conversion all increase as temperature is raised from 390 to 420°C. Once 420°C is reached, coal conversion chemistry and % alpha deuteration have reached their maximum levels. As residence time at 420°C is increased, the chemistry responsible for increased asphaltene conversion and the upgrading of these asphaltenes to resins and then to oils takes place. The initially high levels of deuterium atoms in the alpha positions decrease as reactions at the less reactive beta and gamma positions occur. The deuteration at all sites in the asphaltene fraction essentially remains constant at about 27% as residence time at 420°C is increased, but the (H+D)/C ratio decreases as the asphaltene conversion and upgrading of asphaltenes to resins and oils takes place. Concurrently, (H+D)/C is also decreasing in the oil and resin. However, the overall deuterium uptake is still increasing from 18.6 to 26.7% in the oil, and from 23.9 to 30.9% in the resin.

REFERENCES

1. Ettinger, M.; Stock, L. M.; Gatsis, J. G.; Prepr. Pap. - Am. Chem. Soc., Div. Fuel Chem. 1991, 36(2), 635.
2. Total %wt H+D was calculated by correcting the elemental analysis %wt H using quantitative deuterium values provided by NMR analysis. The calculation can be found in the dissertation of Michael D. Ettinger, University of Chicago Libraries.

Table I. Reaction Conditions, Yields (wt%MAF), and Conversions (wt%MAF)

Conditions	Oil	Resin	Asphaltene	Insolubles	Recovered Products	Coal Conversion	Asphaltene Conversion
0.0 hr at 390, 1770psi	53.4	3.8	17.1	18.9	93.2	43.3	15.1
0.0 hr at 390, 3000psi	54.1	3.3	17.7	19.3	94.4	42.6	13.0
0.0 hr at 405, 3000psi	59.7	1.1	21.2	8.3	90.3	75.0	29.6
0.0 hr at 420, 3000psi	55.4	3.6	22.8	2.7	84.5	92.1	40.1
0.5 hr at 420, 3000psi	60.8	1.7	19.3	2.7	84.4	91.9	47.3
2.0 hr at 420, 3000psi	62.3	3.9	8.5	2.4	77.1	92.8	74.2

Figure I. (H + D) / C

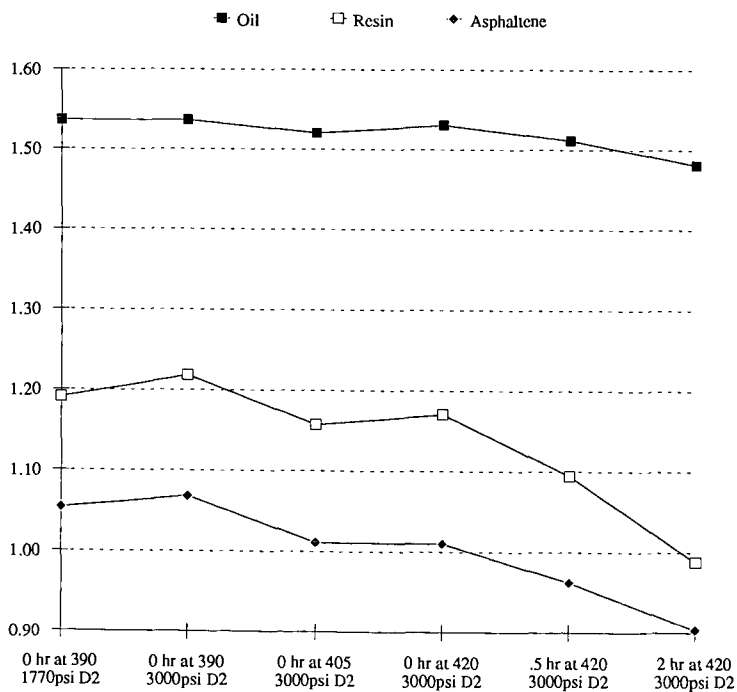


Table II. % Deuteration in Solvent Separated Products

Conditions	Oil	Resin	Asphaltene	Total
<u>% TOTAL D 12.0 - 6.0 & 5.0 (-2) PPM</u>				
0.0 hr at 390, 1770psi	6.59	10.33	14.76	10.03
0.0 hr at 390, 3000psi	8.60	13.97	17.95	12.89
0.0 hr at 405, 3000psi	13.05	17.75	24.43	17.62
0.0 hr at 420, 3000psi	18.57	23.88	27.89	22.78
0.5 hr at 420, 3000psi	20.33	25.07	26.67	23.55
2.0 hr at 420, 3000psi	26.70	30.88	27.59	28.17
<u>% AROMATIC D 12.0 - 6.0 PPM</u>				
0.0 hr at 390, 1770psi	13.28	16.30	20.38	17.23
0.0 hr at 390, 3000psi	13.25	19.10	22.69	19.14
0.0 hr at 405, 3000psi	16.97	22.05	27.42	23.00
0.0 hr at 420, 3000psi	22.50	26.22	29.47	26.70
0.5 hr at 420, 3000psi	22.00	25.47	26.58	25.18
2.0 hr at 420, 3000psi	25.30	31.25	26.66	28.12
<u>% ALIPHATIC D 5.0 - (-2.0) PPM</u>				
0.0 hr at 390, 1770psi	6.09	9.42	13.58	9.06
0.0 hr at 390, 3000psi	8.26	13.25	16.99	12.08
0.0 hr at 405, 3000psi	12.72	17.04	23.70	16.82
0.0 hr at 420, 3000psi	18.23	23.40	27.46	22.11
0.5 hr at 420, 3000psi	20.17	24.98	26.70	23.23
2.0 hr at 420, 3000psi	26.85	30.75	27.97	28.18
<u>% ALPHA D 5.0 - 2.0 PPM</u>				
0.0 hr at 390, 1770psi	19.38	21.30	25.27	22.09
0.0 hr at 390, 3000psi	25.14	29.41	30.36	28.46
0.0 hr at 405, 3000psi	29.63	31.65	34.42	32.02
0.0 hr at 420, 3000psi	36.29	35.44	36.52	36.06
0.5 hr at 420, 3000psi	35.61	34.35	33.64	34.45
2.0 hr at 420, 3000psi	34.27	35.01	31.69	33.68
<u>% BETA D 2.0 - 1.0 PPM</u>				
0.0 hr at 390, 1770psi	3.82	5.14	8.25	5.19
0.0 hr at 390, 3000psi	5.43	7.54	10.25	7.15
0.0 hr at 405, 3000psi	9.65	11.30	16.96	11.62
0.0 hr at 420, 3000psi	15.85	17.48	21.20	17.41
0.5 hr at 420, 3000psi	18.72	20.31	21.39	19.70
2.0 hr at 420, 3000psi	27.35	28.61	24.74	27.13
<u>% GAMMA D 1.0 - (-2.0) PPM</u>				
0.0 hr at 390, 1770psi	2.48	5.25	8.47	4.87
0.0 hr at 390, 3000psi	3.26	7.54	11.32	6.54
0.0 hr at 405, 3000psi	6.86	11.57	18.36	11.11
0.0 hr at 420, 3000psi	9.86	16.26	21.72	14.16
0.5 hr at 420, 3000psi	11.56	17.98	22.72	15.54
2.0 hr at 420, 3000psi	18.70	24.19	25.35	21.25

ON-LINE GC/MS ANALYSIS OF HIGH PRESSURE CONVERSION REACTIONS OF MODEL COMPOUNDS FOR COAL-DERIVED LIQUIDS

Huaying Huai, Chung H. Tsai*, Joseph Shabtai* and Henk L.C. Meuzelaar
Center for Micro Analysis and Reaction Chemistry, *Fuels Engineering Department,
University of Utah, Salt lake City, Utah 84112

Keywords: (on-line GC/MS, high pressure reaction, model compounds)

INTRODUCTION

Direct coal liquefaction involves complex and insufficiently defined chemical reactions. In order to improve direct coal liquefaction processes, it is necessary to improve our understanding of key chemical reactions. Unfortunately, due to the high pressure and high temperature requirements of most coal liquefaction processes, real-time on-line reaction monitoring by advanced spectroscopic and/or chromatographic techniques has generally been impossible until now. Thus, relatively little is known about the precise reaction pathways as well as the intermediate reaction products involved. This is particularly true for conversion reactions carried out in batch reactors such as autoclaves. Due to the relatively long residence times primary reaction products formed in batch type autoclaves are quite susceptible to secondary, or even tertiary reactions. Consequently, real-time on-line monitoring experiments are needed to elucidate reaction pathways in autoclaves.

Although several on-line systems have been developed for coal conversion at near-ambient pressure or high vacuum conditions [1-4], there are no reports of on-line chromatography/spectroscopy based systems built for monitoring high pressure conversion reactions. Therefore, the development of a direct GC/MS interface for near-real time analysis of high pressure reaction products, while minimally disturbing the reaction process, has been undertaken in our laboratory.

It is well established that coal contains fused aromatic and hydroaromatic ring clusters, composed of an average of two to four condensed ring units, connected by various alkylene, ether, sulfide and direct (Ar)C-C(Ar) bridges [5]. Liquefaction reactions are primarily thought to involve these connecting bridges, especially ether linkages and alkylene linkages [6]. In recent years, a number of workers [7-17] have subjected coal-model compounds to various coal conversion conditions in order to confirm that certain coal structures are reactive during coal conversion and to infer the conversion mechanisms of real coals from mechanisms determined for such compounds.

The present paper reports the design and testing of a newly developed on-line GC/MS monitoring system for high pressure reactions and its application to the investigation of hydrogenation and hydrodeoxygenation (HDO) of model compounds, such as diphenyl methane and dibenzyl ether, under both catalytic and thermal conditions.

EXPERIMENTAL

Instrumental Design: Figure 1 shows that the on-line system consists of: (1) a 50 ml flow-through micro-autoclave reactor (Autoclave Engineers Inc.), with a continuous stream of mixture feed flowing through a preheater, entering the reactor from the bottom, and continuously sweeping solubilized products into a collecting reservoir; (2) a pressure reduction line (15 μ m i.d. fused silica capillary) which reduces the pressure from about 1650 psig to ambient at a mass flow of approximately 1 mg/min for toluene while minimizing dead space at the high pressure end and minimally disturbing the reaction process; (3) a novel automated vapor sampling (AVS) inlet developed at the University of Utah, Center for Micro Analysis and Reaction Chemistry (U.S. Patent No. 4,970,905) for diluting

and pulsed sampling of ambient vapor sample streams; and (4) a GC/MS system with a 1 m long, 150 μm i.d. fused silica capillary "transfer line" GC column directly coupled to a Finnigan Mat Ion Trap Mass Spectrometer (ITMS) with tandem MS capabilities and electron ionization (EI) as well as chemical ionization (CI) options.

Materials: Diphenylmethane, dibenzyl ether, decalin and biphenyl, were obtained from Aldrich Chemical Co. as G.R. grade without further purification. A commercial catalyst, $3\text{Co}8\text{Mo}/\gamma\text{-Al}_2\text{O}_3$, was sulfided before use for the reaction. A protonic acid catalyst, $\text{FeCl}_3/\text{SiO}_2\text{-Al}_2\text{O}_3$, was prepared by means of a special impregnation technique in this laboratory.

Experimental procedure: About 300 ml of a mixture containing 10%(wt) feed, 86% solvent (decalin) and 4% internal standard (biphenyl) were used for each experiment. Under catalytic reaction conditions, about 1 g of the catalyst was placed in a self-containing basket with 52 wire mesh. The liquid flow was about 30 ml/hr after the first reactor fill with feed mixture. The reactor was pressurized at 1600 psi with a continuous H_2 supply. After analysis start-up, normally 10 samples were taken at 2 min/sample at ambient temperature for checking system stabilization. Then the GC/MS was started at the same time as the reactor started heating. The reactor temperature was recorded for each sample. After the reactor reached the reaction temperature, the reaction time was recorded. Detailed parameters for each reaction are listed in Table 1. Both reactor temperature and reaction time effects will be discussed.

RESULTS AND DISCUSSION

On-line system function: Aside from occasional plugging of the 15 μm i.d. capillary pressure reduction line and the protective 2.0 and 0.5 μm frits the system exceeded design specifications with regard to GC/MS performance, especially isothermal GC results (note the separation of decalin isomer peaks in Figure 2) and dynamic range (solvent peaks representing > 80 % of the reactor contents were as readily measurable as small product peaks representing less than 100 ppm thus establishing an effective dynamic range > 10^4). As also demonstrated in previous work, the combination of automated pulsed vapor sampling and short column capillary "transfer" line GC enabled repetitive recording of complete isothermal GC runs at 1-4 minute intervals. Moreover, the transfer time of nonretained sample components between reactor and detector was found to be less than 1 minute. In short, the system shown in Figure 1 is capable of detecting minute changes in sample composition in a time which is short compared to typical reaction times in autoclave reactors.

Diphenylmethane: Figure 2 shows the reactor temperature effect on diphenylmethane decomposition under thermal and acid-catalyzed reaction conditions. As seen, the first products can be detected at about 330°C for the catalytic reaction, but not for the corresponding thermal reaction (even at about 350°C). Kinetic profiles of the effect of reaction time on the decomposition of diphenylmethane at thermal and catalytic reaction conditions at 350°C are illustrated in Figure 3. As expected, the concentrations of the products and the feed are increasing and decreasing, respectively, as a function of reaction time for both thermal and catalytic reactions. At 350°C, conversion yield at the equilibrium stage (flow reactor!) is about 50% of the feed for the acid-catalyzed reaction, whereas the thermal reaction produces detectable products by GC/MS, but achieves a very low conversion yield, which is consistent with previous results [15,17]. Figure 4 shows typical single ion chromatograms with the corresponding mass spectra of the decomposition product of diphenylmethane (benzene, toluene, and xylene) under catalytic reaction conditions. Figure 5 demonstrates the concentration of benzene, toluene and xylenes as a function of reaction time under catalytically controlled conditions. Obviously, benzene is the dominant product, whereas the concentration of toluene is increasing with reaction time, and xylene concentrations attain only about 1% of the benzene concentration. The results infer that α -bond cleavages are preferable under the

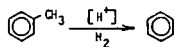
acid-catalyzed conditions which agrees with other results [11]. That the active form of the metal chloride is aqua complex [18], $H^+[MCl_4OH]^-$, has been considered. Thus, the mechanism of diphenylmethane decomposition under the acid-catalyzed condition is proposed as follows:

Main Reaction (hydrodealkylating cleavage of the α -bond)

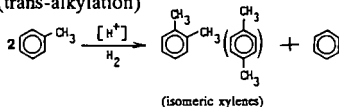


Secondary Reactions of toluene

(a) hydrodealkylation



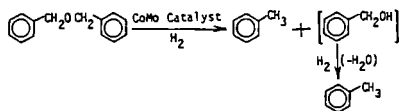
(b) disproportionation (trans-alkylation)



The rate-limiting step in the overall process is protonation of diphenylmethane to form an intermediate carbonium ion, which undergoes σ -cleavage to yield benzene and toluene. The small extent of secondary reactions of toluene can not be avoided under the acid-catalyzed reaction condition.

In the thermal reaction, toluene is the most important product and the ratio of toluene to benzene shows no clear trend with reaction time. A free radical mechanism is suggested. Due to very low conversion yields, the reaction pathway of diphenylmethane under the thermal conditions is not discussed.

Dibenzyl Ether: Figure 6 illustrates dibenzyl ether decomposition under both thermal and catalytic reaction conditions. This reaction proceeds at much lower temperatures than the diphenyl methane decomposition reaction, due to the bond energy differences listed in table 2. Figure 7 shows the kinetic profiles of the decomposition of dibenzyl ether under both thermally and catalytically controlled reaction conditions. The conversion of dibenzyl ether under catalytic reaction conditions is approximately 96%, as opposed to 30% under thermal reaction conditions. The GC/MS results reveal six products, namely: benzene, toluene, benzaldehyde, dibenzyl, 4-methyl diphenyl methane and 2-methyl diphenyl methane, from the thermally controlled reaction, while only one product, toluene, is observed from the catalytically controlled reaction. This implies that the reaction pathways under both conditions are different. The thermal decomposition of dibenzyl ether has been well defined following the free radical mechanism [8-10]. The reaction pathway of the HDO reaction of dibenzyl ether in the presence of a sulfided $3\text{Co}8\text{Mo}/\gamma\text{-Al}_2\text{O}_3$ catalyst is as follows:



The benzyl alcohol intermediate has been observed as the only intermediate at temperatures between 140-260°C in the presence of the same type of catalyst (3Co8Mo) at 1000-1500 psig H_2 [19]. Due

to the more severe conditions under which our experiment was performed (300 C), the intermediate benzyl alcohol was not detected.

CONCLUSIONS

A newly developed, on-line GC/MS monitoring system for high pressure reactions performed reliably. This represents a significant over conventional off line methods and should facilitate elucidation of the mechanisms and kinetics of coal liquefaction.

The results obtained suggest that the protonic acid catalyst, $\text{FeCl}_3/\text{SiO}_2\text{-Al}_2\text{O}_3$, acting as an aqua complex, $\text{H}^+[\text{FeCl}_3\text{OH}]$, causes cleavage of the α -bond in diphenylmethane to produce approximately 50% each of benzene and toluene, whereas very low product yields ($< 1\%$) are observed in the absence of a catalyst.

The decomposition of dibenzyl ether under catalytic conditions is almost complete (96%). The only product, toluene detected, under such conditions reveals that an HDO reaction occurred. The thermal reaction mainly breaks C-O bonds by a free radical mechanism.

ACKNOWLEDGEMENT

The authors are grateful to N. Aronld, W.H. McClennen, J. Dworzanski for technical discussions and to G. Charkol for experimental assistance. This work was supported by the Consortium for Fossil Fuel Liquefaction Science (U.S. Department of Energy).

LITERATURE REFERENCES

1. Yun Y.; Meuzelaar, H.L.C.; Chakravarty, T.; Metcalf, G. "Computer-Enhanced Pyrolysis Mass Spectrometry: A New Window on Coal Structure and Reactivity" in: *Advances in Coal Spectroscopy*, 1992 (in press).
2. Chakravarty, T.; Windig, W.; Taghizadeh, K.; Meuzelaar, H.L.C. *Energy & Fuels*, 1988, 2, 191-196.
3. Dworzanski, J.P.; Buchanan, R.M.; Chapman, J.N.; Meuzelaar, H.L.C. *ACS Preprints, Div. Fuel Chem.*, 1991, 36(2), 725-732.
4. Carangelo, R.M.; Solomon, P.R.; Gerson, D.J. *Fuel*, 1987, 66, 960.
5. Shabtai, J.; Zhang, Y. *Proc. Int. Conf. Coal Sci.*, 1989, Vol. II, 807-810.
6. Shabtai, J.; Saito, I. *U.S. Patent 4,728,418* (1988).
7. Poutsma, M.L. *Fuel*, 1980, 59, 335-338.
8. Kamiya, Y.; Yao, Y.; Oikawa, S. *ACS Preprints, Div. Fuel Chem.*, 1979, 24(2), 116-124.
9. Schlosberg, R.H.; Ashe, T.R.; Pancirov, R.J.; Donaldson, M. *Fuel*, 1981, 60, 155-157.
10. Schlosberg, R.H.; Davis, W.H.Jr.; Ashe, T. *Fuel*, 1981, 60, 201-204.
11. Taylor, N.D.; Bell, A.L. *Fuel*, 1980, 59, 499-506.
12. Ogo, Y.; Kuranuki, K. *Proc. Int. Conf. Coal Sci.*, 1989, Vol.II, 705-708.
13. Sharma, R.K.; Diehl, J.W.; Olson, E.S. *ACS Preprints, Div. Fuel Chem.*, 1990, 35(2), 414-422.
14. Futamura, S.; Koyanagi, S.; Kamiya, Y. *Fuel*, 1988, 67, 1436-1440.
15. Vernon, L.W. *Fuel*, 1980, 59, 102-106.
16. Husain, A.; Olah, G.A. *Proc. Int. Conf. Coal Sci.* 4, 1983, 191-194.
17. Wei, X.Y.; Ogata, E.; Futamura, S.; Kamiya, Y.; Niki, E. *ACS Preprints, Div. Fuel Chem.*, 1991, 36(2), 505-512.
18. Hayatsu, R.; Scott, R.G.; Moore, L.R.; Studier, M.H. *Nature*, 1975, 257, 378-
19. Shukla, Y., Ph.D. Dissertation, University of Utah, 1985.

TABLE 1
EXPERIMENTAL CONDITIONS

Reactor Conditions:	
- Pressure	1600-1650 psig
- Feed Flow Rate	30 ml/hr
- Reaction Gas	Continuous flow H ₂ 50 sccm
- Heating Speed	ambient--> 300°C in ~18 min
- Final Reaction Temperature	350°C for diphenylmethane, 340 and 300°C for dibenzyl ether under thermal and catalytic conditions, respectively
- Catalyst	~1 g sulfided 3Co8Mo/γ-Al ₂ O ₃
Pressure Reduction Line Conditions:	
- Temperature	175°C
- Pressure	1600-1650 psig--> ambient
Sample Inlet Conditions:	
- Temperature	270°C
- Pressure	ambient
- Dilution He Flow Rate	100 ml/min
- Carrier Gas He Flow Rate	40 ml/min
- Sampling Valve Flow Rate	43 ml/min
- Bleed Flow Rate	10 ml/min
- Sampling Pulse	550 ms at 2 min intervals
Transfer Line Conditions:	
- Column	1 m x 150 μm i.d. coated with 0.12 μm CP-SIL 5CB
- Temperature	105°C
- Pressure	ambient -->10 ⁻⁶ torr
MS Conditions:	
- Pressure	10 ⁻⁶ torr
- Ion Trap Temperature	96°C
- Ionization	electron impact (with automatic gain control)
- Spectrum Scanning Speed	4 spectra/s
- Mass Range	m/z 50-100

TABLE 2
PROPERTIES OF THE MODEL COMPOUNDS SOLVENT AND INTERNAL STANDARD

Name	Structure	Molecular Weight	Boiling Point (°C)	BDE (Kcal/mol)
diphenylmethane	ph-CH ₂ -ph	168	264	350 ^a ,339 ^a
dibenzyl ether	phCH ₂ -O-CH ₂ ph	198	298	330 ^b
diphenyl	ph-ph	154	256	480 ^c ,485 ^a
decalin		138	187.1-196.4	--

- a - Ross, D.S. et al., in: *Coal Liquefaction Fundamentals*, (Whitehurst, D.D., ed.), 1980, ACS Symposium Series 139, p. 303.
 b - Schlosberg, R.H., et al., *Fuel*, 1981, 60, 202.
 c - Vernon, L.W., *Fuel*, 1980, 59, 103.

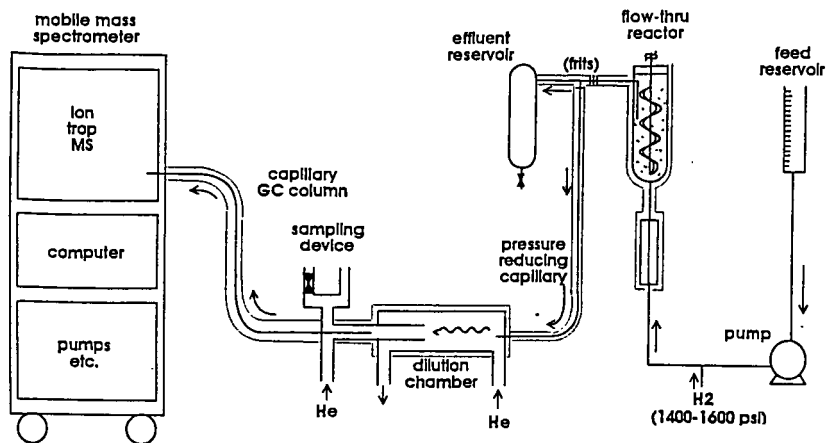


Figure 1. On-line GC/MS monitoring of high pressure reactor.

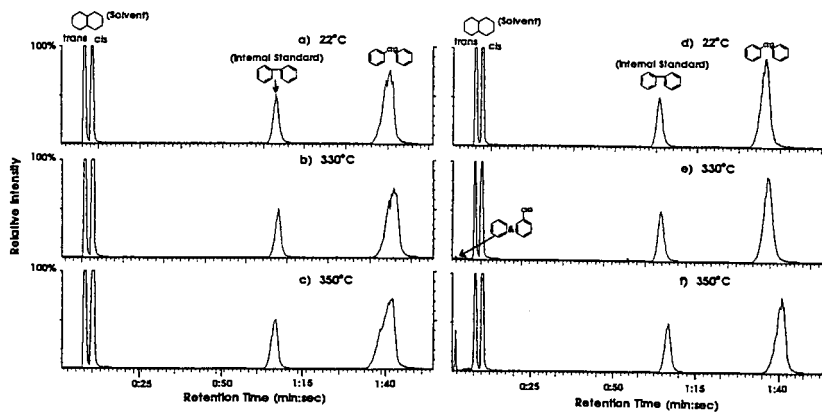


Figure 2. Total ion chromatograms of diphenylmethane at different reactor temperatures under thermal (a-c) and catalytic (d-f) conditions.

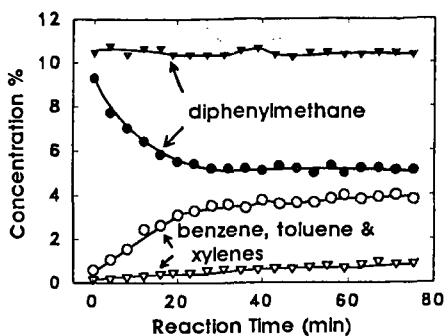


Figure 3. Kinetic profiles of the decomposition of diphenylmethane at 350 C under thermal and catalytic conditions.

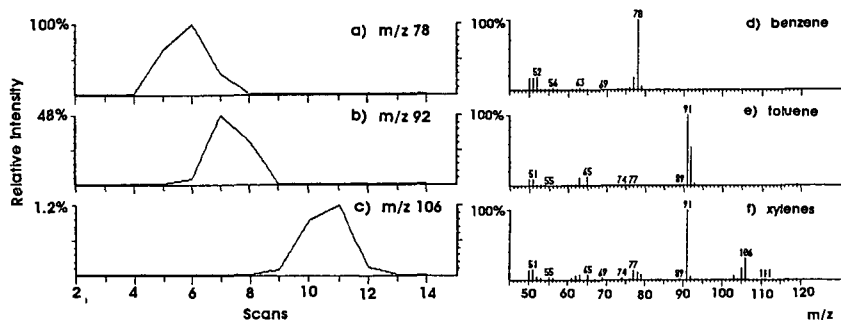


Figure 4. Typical single ion chromatograms (a-c) and corresponding mass spectra (d-f) of the products from the decomposition of diphenylmethane under catalytic conditions.

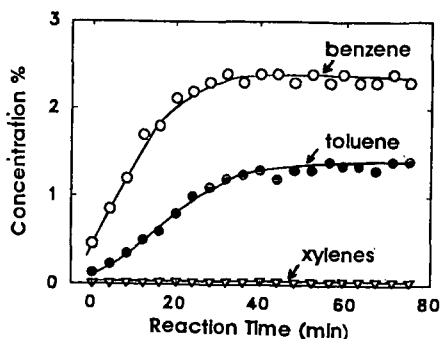


Figure 5. Relationship between reaction time at 350 C and the concentrations of the products from the decomposition of diphenylmethane under catalytic conditions.

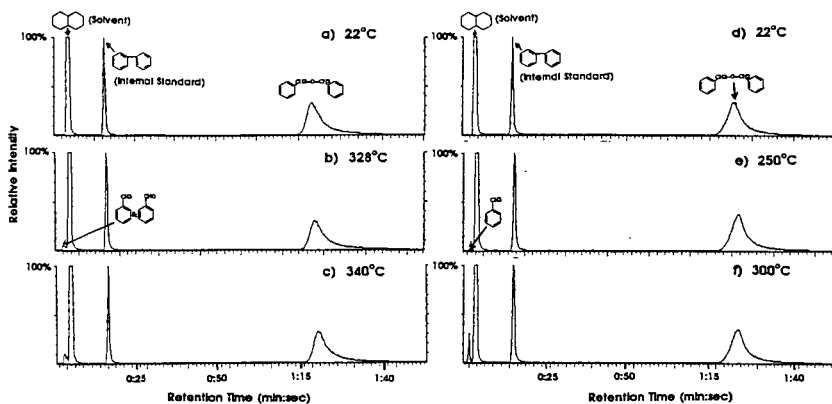


Figure 6. Total ion chromatogram of dibenzylether at different reactor temperatures under thermal (a-c) and catalytic (d-f) conditions.

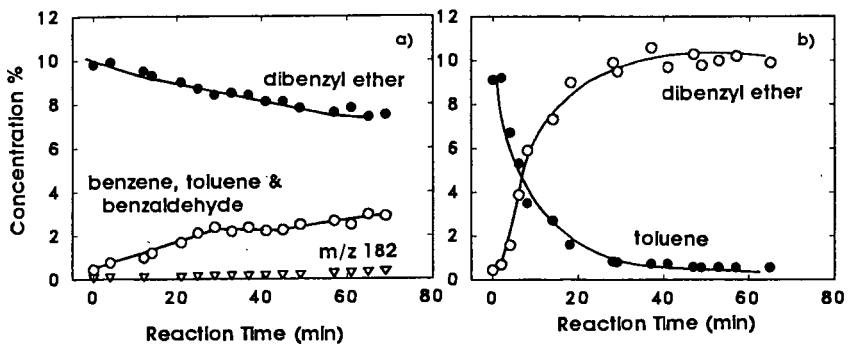


Figure 7. Kinetic profiles of the decomposition of dibenzylether under thermal (a) and catalytic (b) conditions.

MASS SPECTROMETRIC ANALYSIS OF THE REACTION OF ISOTOPICALLY LABELLED ALCOHOLS ON GAMMA ALUMINA AND MODIFIED ALUMINA MATERIALS

Vincent P. Nero and Elaine C. DeCanio
Texaco Inc, Beacon, NY 12508

INTRODUCTION

A novel temperature programmed desorption (TPD) technique has been developed in which the direct insertion probe of a mass spectrometer is used as the reactor. This technique has been used to investigate the adsorption sites of alcohols on gamma alumina by monitoring the dehydration products and has been found to provide both greater sensitivity and a more precise experimental record for these reactions than conventional TPD techniques. Reactions involving O-18 labelled alcohol produce two isotopomeric ether products ($R^{18}OR$ and $R^{16}OR$), in addition to $H_2^{18}O$, and alkene. This shows that the alcohol is initially chemisorbed onto the Al_2O_3 to form alkoxides via two routes, a) a dissociative adsorption on Lewis acid sites, and b) a nucleophilic attack by a surface oxide on an alcohol which is probably activated toward C-O cleavage.

Experiments involving either poisoning the alumina with 2,6-dimethylpyridine or modifying the alumina with fluorine treatments have been used to elucidate the mechanism of alkoxide formation and the dehydration reactions. Observed product distributions and temperature trends can be related to changes in the nature of the Lewis and Bronsted acid sites brought about by the inductive effect of fluorine and to site blocking by bulk AlF_3 phases or dimethylpyridine.

EXPERIMENT

Both a Finnigan-MAT TSQ70, operating in a single quadrupole mode, and SSQ710 mass spectrometer were used. Both instruments were operated under electron impact conditions with a 70 eV ionizing potential and 200 ua ion current. The source temperature was 150°C. A mass range from 12 to 170 Daltons was scanned every 0.5 seconds.

Norton 6375C (20/40 mesh) gamma alumina with a surface area of 221.8 m^2/g and a pore volume 1.4 cc/g was used for all experiments. The gamma alumina was calcined in flowing air (60 cc/min) at 500°C for 3 h and then stored in an air tight container. Approximately 0.2 g of the alumina was then transferred to a 5-ml beaker which was placed into a 25-ml sealed vessel containing about 0.5 ml of ethanol or ethanol- ^{18}O (99%) at room temperature and exposed to its vapor for at least 1 h. About 0.2 mg of the alumina with the absorbed alcohol was placed into a quartz insertion tube which loaded into the temperature programmed probe of the mass spectrometer. Immediately the probe was inserted into the mass spectrometer source, which is at a vacuum of 1×10^{-7} torr. The temperature of the sample was increased from 25°C to 300°C at a rate of 25°C per min. The probe tip was within 1 mm of the ionizing electrons which ensures that the desorbed species are immediately analyzed upon desorption from the alumina surface. This results in minimal diffusion losses and time delays and is therefore much more sensitive than conventional temperature programmed experiments.

For the experiment involving poisoning with 2,6-dimethylpyridine,

the calcined alumina was exposed to its vapor for 24 h. The poisoned alumina was then transferred to a clean vessel and exposed to the vapors of 0.5 ml ethanol-¹⁸O. For the experiments involving modified alumina with fluorine loading, the alumina was treated with ammonium fluoride at 2%, 5%, and 10% levels and then calcined before exposure to the alcohol.

RESULTS AND DISCUSSION

Reconstructed partial ion chromatograms of the reaction of ethanol (not enriched in ¹⁸O) on calcined alumina are shown in Figure 1. At 25°C only desorption of physisorbed water and ethanol is observed as shown in the selected ion traces of $m/z = 17, 18$ and $m/z = 45, 46$. The physisorbed water and ethanol is rapidly evolved in the vacuum of the mass spectrometer. As the temperature is increased to 100°C, diethyl ether begins to form and reaches a maximum at 200°C. This is shown in the selected ion trace $m/z = 59, 74$. At 210°C ethene starts to form, peaking at 260°C (selected ion trace $m/z = 26, 28$). These products are the result of dehydration reactions involving ethoxide. The coproduction of water is seen in the $m/z = 17, 18$ ion trace, which shows a broad peak with inflections corresponding to the formation of the ether and the ethene. The ether formation is a bimolecular reaction requiring the alkoxide groups to be on adjacent sites, while the alkene is presumably formed by the unimolecular elimination of water from isolated ethoxide species.¹

The same experimental procedure was repeated substituting ethanol-¹⁸O. The ether formation splits into distinct regions as indicated in figure 2. The reaction produces two isotopomeric ether products as evidenced by the selected ion chromatograms for $m/z = 59, 74$ and $m/z = 61, 76$, which correspond to $\text{CH}_3\text{CH}_2^{18}\text{OCH}_2\text{CH}_3$ and $\text{CH}_3\text{CH}_2^{16}\text{OCH}_2\text{CH}_3$, respectively. The ether incorporating the ¹⁸O appears first and peaks at 179°C. The ¹⁶O ether does not reach its maximum intensity until 220°C. A summary of the peak temperatures and peak areas appear in Table I. The relative amounts of these isotopomers did not change even after the Al_2O_3 -ethanol-¹⁸O was allowed to stand for several months. This indicates that the alkoxides leading to the ether products are irreversibly formed.

The two isotopomeric ethers originate from two different alkoxide species, one incorporating an ¹⁸O and the other, ¹⁶O. The presence of these two alkoxides suggest that alkoxide is formed via two routes. The first involves a direct reaction at a Lewis site resulting in deprotonation of the complexed alcohol and formation of ¹⁸O-alkoxide as shown in the upper scheme in figure 2. The second involves a reaction with a nucleophilic surface base site resulting in ¹⁸OH displacement and the formation of ¹⁶O-alkoxide, as shown in the lower scheme in figure 2. This latter pathway probably involves a secondary interaction of the alcohol hydroxyl with an adjacent acid site, since hydroxide itself is a relatively poor leaving group.

The 2,6-dimethylpyridine poisoning experiment provides further evidence for the formation of distinct alkoxide sites. This base is expected to adsorb onto either Bronsted acid sites or Lewis acid sites.² The adsorption of 2,6-dimethylpyridine prior to ethanol-¹⁸O adsorption has a significant effect on the ratio of ether-¹⁸O and ether-¹⁶O as shown in Table I. The untreated alumina yields ethers approximately 3:1 in favor of the ¹⁸O isotopomer. This ether ratio

changes to 0.6:1 for the base treated alumina. This clearly establishes that both ethers are formed from different alkoxide species and that the ether-¹⁸O is formed from an alkoxide associated with Lewis acid sites. It also shows that the relative amount of the ether-¹⁸O to the ethene actually is increased by effect of the 2,6-dimethylpyridine poisoning. This result also indicate that the ether-¹⁸O did not form at a Bronsted acid site (via protonolysis of alcohol hydroxide), since the latter would be strongly inhibited by the pretreatment with 2,6-dimethylpyridine; this would have led to a decrease in the ratio of ether-¹⁸O to ethene, rather than the observed increase.

Modification of alumina by fluorine treatment is known to increase the Bronsted acid character of the surface.³ At 2% fluorine loadings the observed ether and ethene distributions show no significant changes, although the peak temperatures of various reactions

increased substantially, probably due to the the inductive effect of the fluorine. (Table I) At the 5% fluorine level the peak temperatures have increased to the point of favoring elimination as the major reaction pathway. The yield of the ether-¹⁸O is greatly reduced since the fluorine is now occupying sites previously occupied by the ¹⁸O ethoxide. At the 10% fluorine level even the ether-¹⁸O is reduced. This can be attributed to site blocking due to the formation of bulk AlF₃ on the alumina surface.

1. Knozinger, H., Kockloefl, K. and Meyer, W., J. Catal., 28, 69 (1973)

2. Matulewicz, E. R. A., Kerhof, F. P. J. M., Moulign, J. A. and Reitsma, H. J., J. Coll. Interface Sci., 77, 110 (1980).

3. Ghosh, A. K, and Kydd, R. A., Catal. Rev. [Sci. Eng., 27 [4], 539-589 [1985]

TABLE I
PEAK TEMPERATURES AND PRODUCT DISTRIBUTIONS
FOR ETHANOL-¹⁸O ON ALUMINA AND MODIFIED ALUMINA

ALUMINA	PRODUCT	PEAK TEMP	Ethene to Et ¹⁸ OEt	Ethene to Et ¹⁶ OEt	Et ¹⁸ OEt to Et ¹⁶ OEt
UNTREATED	Et ¹⁸ OEt	179	22	69	3.2
	Et ¹⁶ OEt	220			
	Ethene	261			
2,6-DIMETHYL PYRIDINE	Et ¹⁸ OEt	220	36	23	.62
	Et ¹⁶ OEt	275			
	Ethene	286			
2% FLUORINE	Et ¹⁸ OEt	240	20	58	3.0
	Et ¹⁶ OEt	266			
	Ethene	295			
5% FLUORINE	Et ¹⁸ OEt	256	260	86	.32
	Et ¹⁶ OEt	269			
	Ethene	285			
10% FLUORINE	Et ¹⁸ OEt	260	120	290	2.4
	Et ¹⁶ OEt	280			
	Ethene	287			

FIGURE 1

ETHANOL

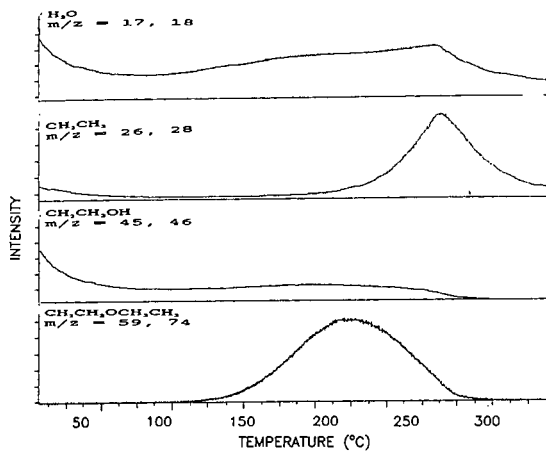
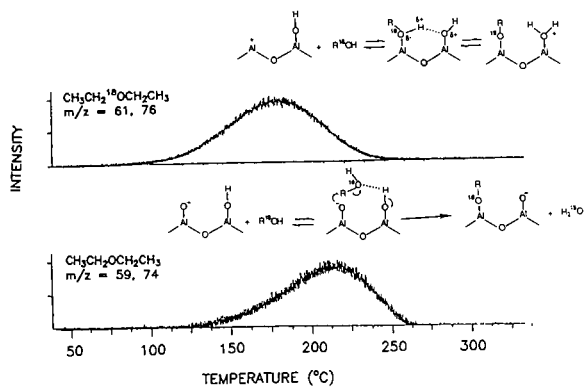


FIGURE 2

ETHANOL- ^{18}O



HYDROGENOLYSIS MECHANISMS FOR POLYCYCLIC ALKYLARENES

C. Michael Smith and Phillip E. Savage*
University of Michigan, Department of Chemical Engineering
Ann Arbor, MI 48109-2136

KEYWORDS: Alkylpyrenes, Hydrogenolysis, Pyrolysis

INTRODUCTION

Recent neat pyrolyses of polycyclic alkylaromatics have demonstrated the relatively facile cleavage of strong aryl-alkyl bonds.¹⁻⁷ Because these compounds mimic the analogous moieties in coal and oil, their reaction pathways and mechanisms provide insight to reactions occurring in co-processing, coal liquefaction and gasification, and heavy oil upgrading and coking. The hydrogenolysis mechanisms responsible for aryl-alkyl C-C bond cleavage in alkylarenes have not been fully elucidated, but the literature does provide some possibilities.⁶⁻⁸

We desired to understand this hydrogenolysis more completely and to employ this understanding to develop a general mechanistic model for alkylarene pyrolysis that was consistent with experimental observations. A general mechanistic reaction model can be developed by conducting experiments with different alkylarenes, taking advantage of results in the literature, and employing the principles embodied in thermochemical kinetics and molecular orbital (M.O.) theory. We have previously reported experimental data (e.g., product molar yields, selectivities, rate constants) for a large number of n-alkylarenes, and we proposed a general pyrolysis network.³ We also conducted experimental studies using probe molecules to explore different mechanistic scenarios for the hydrogenolysis.^{1,2} This paper reports our initial activities aimed at developing a general mechanistic model. We have relied on our experimental results and the literature to provide probable elementary reaction steps, and we used thermochemical kinetics and M.O. theory to estimate their reaction rate constants. Our initial mechanistic models explore the pyrolysis of 1-methyl- and 1-ethylpyrene. Our logic for studying these compounds is twofold. First, the mechanisms responsible for the cleavage of the aryl-alkyl bond in methyl- and ethylpyrene must also be operative during the pyrolysis of alkylarenes with longer chains. Second, the pyrolysis of these compounds leads to a smaller number of products than does the pyrolysis of long-chain alkylarenes. Thus, there is a smaller pool of species from which the hydrogenolysis agents can be chosen, and this reduces the complexity of the mechanistic models. Additionally, for methylpyrene neither α -alkylpyrene radicals nor aliphatic radicals can participate in the radical hydrogen transfer reactions that others have suggested as potential hydrogenolysis steps^{6,8} for long-chain alkylpyrenes. Thus, it is apparent that the simplicity of these pyrolysis systems makes them convenient initial tools for probing different mechanistic scenarios and developing more complex mechanistic models for long-chain alkylarenes.

EXPERIMENTAL

1-Methylpyrene and 1-ethylpyrene pyrolyses were conducted neat at 400, 425, and 450°C in constant-volume, 316 stainless steel, micro-batch reactors. The reactors were typically loaded with about 10 mg of alkylpyrene and 10 mg of *o*-terphenyl as an internal standard. After being loaded, the reactors were purged and sealed in a nitrogen-filled glove box and then placed in an isothermal, fluidized sand bath. Upon reaching the desired holding time, the reactors were removed from the fluidized bath, and the reaction was quenched. The products were recovered by repeated extraction with benzene. The reaction products were identified by gas chromatography-mass spectrometry, and their molar yields (i.e., moles of product formed/moles of reactant loaded in reactor) were quantified by capillary column gas chromatography. Details about the experimental protocol have been given previously.¹⁻⁴

EXPERIMENTAL RESULTS

1-Methylpyrene: The pyrolysis of methylpyrene led to pyrene and dimethylpyrene as the major products, and Table I lists the molar yields of these products at different reaction conditions. The minor products included a second dimethylpyrene isomer, ethylpyrene, and four trimethylpyrene isomers. Of these minor products, only the dimethylpyrene isomer was present in yields sufficiently high to quantify. Its molar yield increased steadily at all three

temperatures, and its maximum yield was 1.8% at 150 minutes at 450°C. The recovery of pyrene moieties in the quantified products ranged from nearly 100% to a low of 72% for the reaction at 450°C and 300 minutes. The failure to achieve 100% recovery at the more severe reaction conditions is likely due to the formation of high molecular weight products that did not elute from the GC.

1-Ethylpyrene: The pyrolysis of ethylpyrene led to pyrene and methylpyrene as major products, and Table II lists representative results from these experiments. The minor/trace products were diethylpyrene, methylethylpyrene, vinylpyrene, dihydropyrene and a benzene-insoluble char. The molar yield of diethylpyrene typically reached a maximum and then decreased with time. Vinylpyrene and methylethylpyrene were only observed in trace quantities, so their yields were not quantified. The lowest recovery of pyrene units in the quantified products was 72% for the reaction at 450°C and 72 minutes.

MECHANISTIC MODELING AND RESULTS

The development of mechanistic models for methyl- and ethylpyrene pyrolysis was guided by experimental observations, by previous mechanistic models for toluene and ethylbenzene pyrolysis, and by previous investigations into the pyrolysis of polycyclic aromatic hydrocarbons. We simulated the pyrolyses using *AcuChem*, a software package developed by the National Institute of Standards and Technology.⁹ The program sets up and solves the differential equations that describe species' concentrations as a function of time for reactions in a constant-volume batch reactor.

1-Methylpyrene: The 18 elementary step free-radical reaction mechanism used to describe the pyrolysis of methylpyrene is depicted in Figure 1. Methylpyrene undergoes initiation through two possible routes: unimolecular homolytic dissociation and bimolecular reverse radical disproportionation (RRD).^{10,11} Chain propagation proceeds via radical hydrogen transfer (RHT),¹² H-atom and methyl radical addition, and methyl radical and H-atom elimination. Finally, termination occurs through the recombination and disproportionation of methylpyrenyl radicals and alkyldihydropyrenyl radicals. This mechanism omits potential secondary reactions such as RRD of dimethylpyrene molecules or RHT to pyrene molecules. Thus, this model will be most valid at low methylpyrene conversions where these secondary reactions are unimportant. The Arrhenius parameters estimated for each step in Figure 1 are listed in Table III, and details of the estimation procedure are given elsewhere.⁴

Figure 2 displays the comparison of the model prediction and experimental observation for the temporal variation of product yields from methylpyrene pyrolysis at 425°C. The model (solid lines) predicts the experimental data (discrete points) well at conversions less than 30%. At higher conversions, however, the model tended to underpredict methylpyrene reactivity. This lack of quantitative agreement at higher conversions could be due to the model's omission of secondary reactions. For example, pyrene could serve as a hydrogen acceptor in RRD reactions, but the model does not include such steps. If it had, the predicted reactivity of methylpyrene would have increased. Overall, however, the agreement between the calculated and the experimental molar yields was reasonably good.

Figure 3 displays the model's prediction of the rates of RRD (reaction 2), RHT (reactions 4 and 5) and H-atom addition (reaction 8), reactions that add hydrogen to the ipso position in methylpyrene, as a function of conversion for the pyrolysis at 425°C. The results at 400 and 450°C were similar to those presented in Figure 3. It is apparent from Figure 3 that the rate of H-atom ipso substitution is typically lower than the rates of RHT and RRD. The rate of RHT by methylhydropyrenyl radicals (step 4) is initially faster than the rate of RRD, but at a conversion of about 0.1 the rate of RRD becomes more significant. The model predicted that this transition point occurred at methylpyrene conversions of about 0.2 and less than 0.1, respectively for pyrolysis at 400°C and 450°C, respectively. Thus, the importance of RHT by methylhydropyrenyl radicals relative to RRD decreases as temperature increases.

The rates of RHT by dimethylhydropyrenyl radicals (step 5) and H-atom substitution (step 8) are lower than those of steps 2 and 4. At 425°C, the rate of RHT by dimethylhydropyrenyl radicals is greater than the rate of H-atom substitution for methylpyrene conversions less than about 0.68. At conversions greater than 0.68, there is a shift in the

importance of these two steps as the rate of step 8 becomes greater than the rate of step 5. This behavior was also observed at the other temperatures studied. For example, at 400 and 450°C, respectively, this transition occurred at methylpyrene conversions of 0.85 and 0.48, respectively. This trend suggests that the importance of step 8 relative to step 5 increases as the temperature increases. This observation that H-atoms become more important as the temperature increases is consistent with previous work.^{6,13}

The results of the pyrolysis simulation have revealed that the relative importance of RHT by methylhydropyrenyl radicals decreases and the role of H-atoms increases with increases in temperature. This behavior arises because high temperatures favor β -scission of hydropyrenyl radicals to yield a hydrogen atom rather than direct hydrogen transfer by RHT. This is because the β -scission step has the higher activation energy. Thus, at higher temperatures there is a greater concentration of hydrogen atoms and consequently a higher rate of H-atom ipso substitution.

1-Ethylpyrene: The free-radical mechanism for ethylpyrene pyrolysis is shown in Figure 4, and the estimated Arrhenius parameters for each elementary step are summarized in Table IV. Details of their estimation have been discussed elsewhere.⁴ As was the case for methylpyrene pyrolysis, initiation in ethylpyrene proceeds through both homolytic dissociation and RRD. The resulting radicals propagate the chain through hydrogen abstraction, RHT, and addition/elimination reactions. Termination proceeds through radical disproportionation.

Figure 5 compares the model predictions and the experimental molar yields of ethylpyrene at 400, 425, and 450°C. Inspection of Figure 5 reveals essentially quantitative accord between the model calculations and the experimentally determined yields of ethylpyrene. Although the model accurately predicted the kinetics of ethylpyrene disappearance, it underpredicted the amount of pyrene and methylpyrene formed, and it overpredicted vinylpyrene formation. For example, at a batch holding time of 150 minutes and at a pyrolysis temperature of 425°C, the predicted molar yields of vinylpyrene, pyrene, and methylpyrene are 0.36, 0.36 and 0.008 respectively. Experimentally, however, vinylpyrene was not observed, and the molar yields of pyrene and methylpyrene were 0.47 and 0.08. One reason for this discrepancy is that the model, which focuses on the primary reactions, does not include the secondary decomposition reactions available for vinylpyrene. Omitted reactions include vinylpyrene polymerization, its reduction to ethylpyrene, and its decomposition to pyrene or methylpyrene. The kinetics and mechanisms of these reactions are not completely resolved and it is for this reason that they were not included in the model. If such steps were included, however, the model would predict a much lower yield of vinylpyrene and increased molar yields of methylpyrene and pyrene as observed experimentally.

Examination of Figure 6, which displays the rates of different elementary reaction steps at 425°C as a function of ethylpyrene conversion, reveals the relative importance of each of the different hydrogen addition mechanisms. Step 15, RHT by ethylhydropyrenyl radicals has the fastest rate of reaction. The next fastest hydrogenolysis step is RRD (step 2) followed by H-atom addition (step 13), RHT by ethyl radicals (step 20), and RHT by α -ethylpyrene radicals (step 19). The trends that are depicted in Figure 6 were also observed for the simulations at 400 and 450°C. As was observed for the pyrolysis simulation of methylpyrene, RHT by alkylhydropyrenyl radicals and RRD are the major steps that lead to aryl-alkyl bond cleavage. The rates of the other hydrogenolysis steps, however, are not insignificant and can not be ignored. Indeed, the relative importance of H-atoms in ethylpyrene pyrolysis at high conversions stands in contrast to the model results for 1-methylpyrene where H atoms had a less significant contribution to the total hydrogenolysis rate. The increased role of H-atoms in ethylpyrene pyrolysis is likely due to their production through the β -scission of α -ethylpyrene radicals. To summarize, the results of this simulation suggest that all of the modes of hydrogenolysis included in the simulation can be important in engendering aryl-alkyl bond cleavage in 1-ethylpyrene pyrolysis.

CONCLUSIONS

1. Hydrogenolysis was the dominant reaction during the neat pyrolysis of methylpyrene. The major pyrolysis products were pyrene and dimethylpyrene. This experimental observation is noteworthy because radical hydrogen transfer by alkyl radicals or by α -alkylpyrene radicals is not an operable mechanism in this system.

2. The pyrolysis of ethylpyrene led to pyrene and methylpyrene as the major products with pyrene being present in much higher yields. The rate of hydrogenolysis for ethylpyrene was greater than that for methylpyrene.

3. Mechanistic modeling of methylpyrene and ethylpyrene pyrolysis revealed that RRD played an important role in adding hydrogen to the ipso-position and in generating alkylhydropyrenyl radicals that then participated in radical hydrogen transfer steps. In the pyrolysis of methylpyrene, alkylhydropyrenyl radicals generated from methyl radical addition were also hydrogenolysis agents. In ethylpyrene pyrolysis alkylhydropyrenyl radicals were also largely responsible for hydrogenolysis along with contributions from H-atoms, ethyl radicals, and α -ethylpyrene radicals.

ACKNOWLEDGEMENTS

We thank Steven Sherman and Joseph Gullo for performing the methylpyrene pyrolysis experiments. This work was supported in part by the Link Foundation, the Shell Faculty Career Initiation Fund, and the National Science Foundation (CTS-8906859). Acknowledgement is also made to the donors of the Petroleum Research Fund (ACS-PRF # 23744-AC4), administered by the ACS, for the partial support of this research.

LITERATURE CITED

1. Smith, C. M.; Savage, P. E. *Ind. Eng. Chem. Res.* **1991**, *30*, 331-339.
2. Smith, C. M.; Savage, P. E. *Energy & Fuels* **1991**, *5*, 146-155.
3. Smith, C. M.; Savage, P. E. *AIChE Journal* **1991**, *37*, 1613-1624.
4. Smith, C. M.; Savage, P. E. *Energy & Fuels* **1992**, *6*, in press.
5. Savage, P. E.; Jacobs, G. E.; Javanmardian, M. *Ind. Eng. Chem. Res.* **1989**, *28*, 645-652.
6. Freund, H.; Maturro, M. G.; Olmsted, W. N.; Reynolds, R. P.; Upton, T. H. *Energy & Fuels*. **1991**, *5*, 840-846.
7. Vlasnik, V. J.; Virk, P. Paper 139D *AIChE Annual Meeting*, Chicago, 1990.
8. McMillen, D. F.; Malhotra, R.; Tse, D. S. *Energy & Fuels* **1991**, *5*, 179-187.
9. Braun, W.; Herron, J. T.; Kahanen, D. K. *Int. J. Chem. Kinet.* **1988**, *20*, 51-62.
10. Billmers, R.; Brown, R. L.; Stein, S. E. *Int. J. Chem. Kinet.* **1989**, *21*, 375-389.
11. Billmers, R.; Griffith, L. L.; Stein, S. E. *J. Phys. Chem.* **1986**, *90*, 517-523.
12. McMillen, D. F.; Malhotra, R.; Chang, S. J.; Olgier, W. C.; Nigenda, S. E.; Fleming, R. H. *Fuel* **1987**, *66*, 1611-1620.
13. McMillen, D. F.; Malhotra, R.; Nigenda, S. E. *Fuel* **1989**, *68*, 380-386.

TABLE I: MOLAR YIELDS OF MAJOR PRODUCTS FROM 1-METHYLPYRENE PYROLYSIS

TEMP (°C)	400	400	400	400	400	400	400
TIME (min)	30	60	90	120	150	240	300
PYRENE	0	0.01	0.01	0.01	0.02	0.05	0.06
DIMETHYLPYRENE	0	0.00	0.01	0.01	0.01	0.03	0.04
METHYLPYRENE	1.01	1.05	0.98	1.03	0.95	0.87	0.85
TEMP (°C)	425	425	425	425	425	425	425
TIME (min)	30	60	90	120	165	240	300
PYRENE	0.01	0.05	0.07	0.1	0.15	0.22	0.22
DIMETHYLPYRENE	0	0.04	0.04	0.06	0.09	0.12	0.11
METHYLPYRENE	0.97	0.90	0.90	0.83	0.67	0.57	0.54
TEMP (°C)	450	450	450	450	450	450	450
TIME (min)	30	60	90	120	150	240	300
PYRENE	0.06	0.15	0.22	0.26	0.31	0.39	0.37
DIMETHYLPYRENE	0.03	0.08	0.10	0.10	0.09	0.01	0.01
METHYLPYRENE	0.88	0.66	0.50	0.42	0.41	0.35	0.35

TABLE II: MOLAR YIELDS OF MAJOR PRODUCTS FROM 1-ETHYLPYRENE PYROLYSIS

TEMP (°C)	400	400	400	400	400	400	400
TIME (min)	45	70	90	110	150	200	320
PYRENE	0.20	0.47	0.13	0.37	0.44	0.61	0.60
METHYLPYRENE	0.02	0.05	0.01	0.04	0.05	0.11	0.11
ETHYLPYRENE	0.91	0.80	0.82	0.52	0.47	0.41	0.26
TEMP (°C)	425	425	425	425	425	425	425
TIME (min)	65	80	115	135	150	180	205
PYRENE	0.52	0.49	0.54	0.64	0.47	0.61	0.62
METHYLPYRENE	0.07	0.08	0.10	0.11	0.09	0.07	0.13
ETHYLPYRENE	0.55	0.41	0.32	0.33	0.18	0.13	0.17
TEMP (°C)	450	450	450	450	450	450	450
TIME (min)	20	30	42	50	60	72	80
PYRENE	0.45	0.48	0.56	0.47	0.68	0.48	0.74
METHYLPYRENE	0.08	0.08	0.10	0.10	0.14	0.11	0.13
ETHYLPYRENE	0.58	0.46	0.25	0.19	0.17	0.13	0.13

TABLE III: ARRHENIUS PARAMETERS FOR 1-METHYLPYRENE PYROLYSIS

Reaction Number in Figure 1	$\log_{10} A$ (s^{-1} or Liter mole $^{-1}$ s $^{-1}$)	Activation Energy (kcal mole $^{-1}$)	Reaction Path Degeneracy
1	16	82.9	3
2	8	45.8	6
3	8	45.8	18
-3	9.5	0	-
4	8.1	16.5	2
5	8.1	16.5	1
6	8.1	16.5	3
7	10.4	2.3	3
8	10.4	2.3	1
9	8.8	4.1	3
-9	13.9	29.4	1
10	13.9	35.3	2
11	13.9	29.4	1
12	11.1	5.6	3
13	8.5	6.9	3
14	9.5	0	-
-14	16	51.2	1
15	9.5	0	-

TABLE IV: ARRHENIUS PARAMETERS FOR 1-ETHYLPYRENE PYROLYSIS

Reaction Number in Figure 4	$\log_{10} A$ (s^{-1} or Liter mole $^{-1}$ s $^{-1}$)	Activation Energy (kcal mole $^{-1}$)	Reaction Path Degeneracy
1	16	69.6	1
2	8	42.8	4
3	8	42.8	12
4	14.0	53.6	3
5	13.9	35.3	2
6	14	20	1
7	12.9	38.4	3
8	11.1	5.6	2
9	8.5	5.4	2
10	8.5	8.9	2
11	8.8	15.5	2
12	10.3	2.3	3
13	10.3	2.3	1
14	9	6	3
15	8.1	16.5	2
16	8.1	16.5	1
17	8.1	16.5	3
18	8.1	25	9
19	8.1	25	3
20	8.4	14.5	3
21	8.4	14.5	9
22	9.5	0	-
23	9.5	0	-

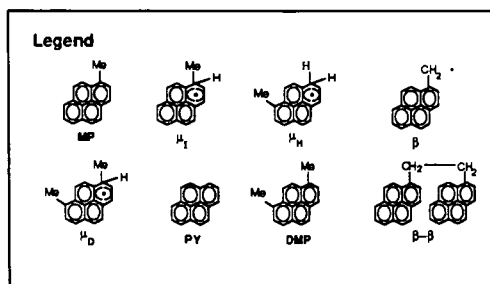
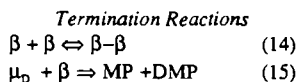
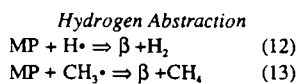
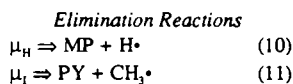
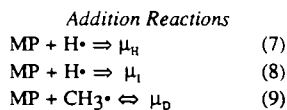
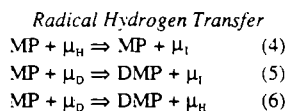
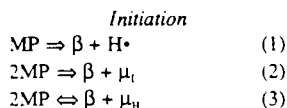


Figure 1: 1-Methylpyrene Pyrolysis Mechanism

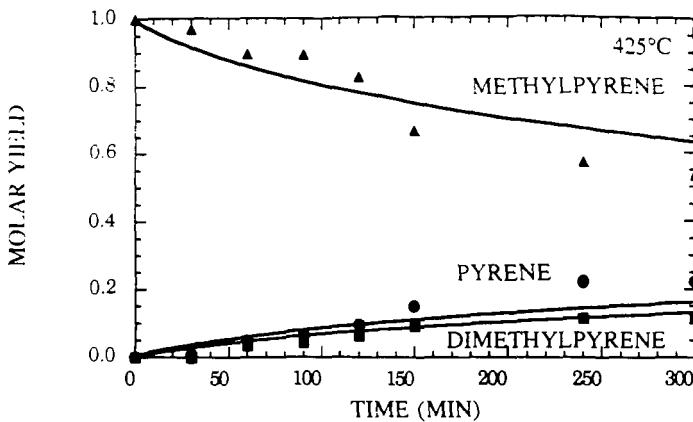


Figure 2: Model and Experimental Results for 1-Methylpyrene Pyrolysis at 425°C

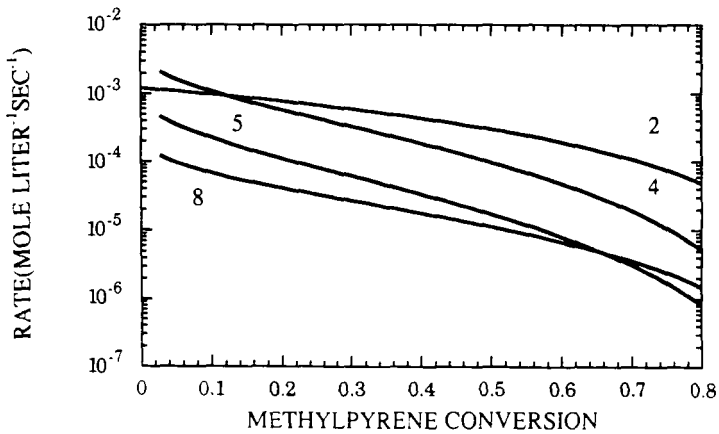


Figure 3: Hydrogenolysis Rates Calculated for 1-Methylpyrene Pyrolysis at 425°C (step 2 is RRD, steps 4 and 5 are RHT, step 8 is H atom addition)

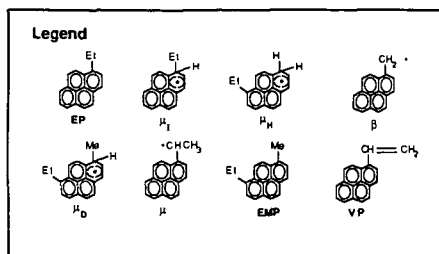
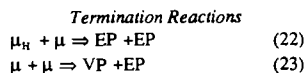
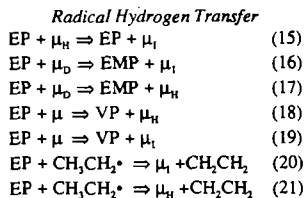
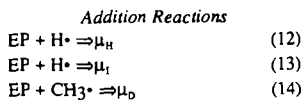
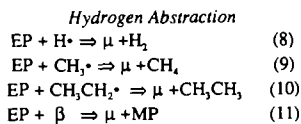
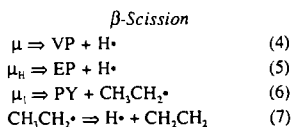
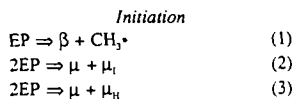


Figure 4: 1-Ethylpyrene Pyrolysis Mechanism

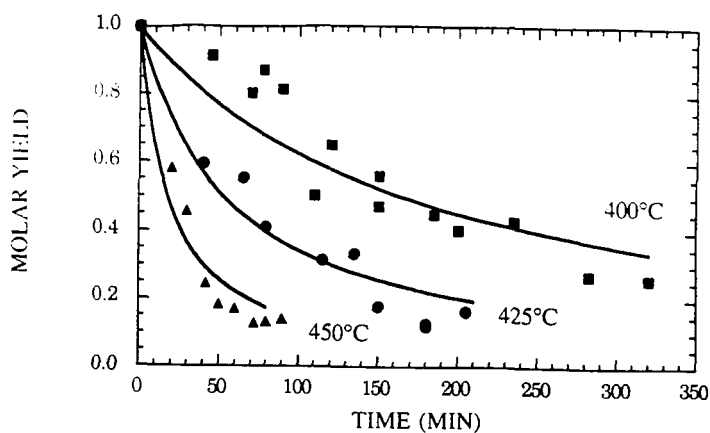


Figure 5: Model and Experimental Results for 1-Ethylpyrene Pyrolysis Kinetics

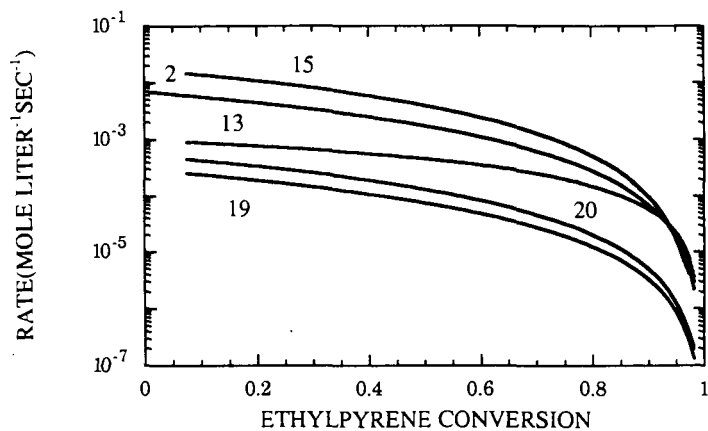


Figure 6: Hydrogenolysis Rates Calculated for 1-Ethylpyrene Pyrolysis at 425°C (step 2 is RRD, step 15 is RHT by ethylhydropyrenyl radicals, step 13 is H atom addition, step 20 is RHT by ethyl radicals, and step 19 is RHT by α -ethylpyrene radicals)

PATHWAYS FOR THERMOLYSIS OF 9,10-DIMETHYL-ANTHRACENE.

P.S. Virk and V.J. Vlastnik

Department of Chemical Engineering, M.I.T., Cambridge, MA 02139.

Keywords: Reaction Paths, Pyrolysis, Kinetics, Demethylation

ABSTRACT. We report experiments on thermolysis of 9,10-dimethyl-anthracene (DMA) at temperatures from 315-409 C with initial concentrations from 0.1-3.0 M. Substrate conversions ranged from 0.05 to 0.98 with quantitative assays of major products. The substrate appears to decompose primarily by two parallel pathways, namely, demethylation (major) to 9-methyl-anthracene (MA) plus methane and disproportionation (minor) to MA plus tri-methyl-anthracenes (TMA). These reactions are also associated with hydrogen transfer, as inferred from the detection of 9,10-dihydro-9,10-dimethyl-anthracenes (DHDMA). At the higher substrate conversions, the primary reaction products appear to be secondarily operated upon by a parallel pathway pair analogous to the primary pair, eventually forming anthracene (ANT). Also, minor amounts of the 1- and 2-methyl-anthracenes (1MA, 2MA) were detected, both arising subsequent to the appearance of the parent acene. A preliminary mechanism is presented for DMA thermolysis, based on elementary free-radical and molecular reactions relevant to the present conditions, combined with the experimentally observed kinetics and product selectivities. Also, frontier-orbital theory is applied to model the observed 1MA and 2MA isomer distributions.

INTRODUCTION

The present work on DMA thermolysis is part of a continuing study of simple substrates that mimic the chemical moieties found in complex fossil materials of engineering interest. DMA was chosen for two reasons. First, its acene aromatic ring system is prototypical of the aromatic molecules found in fossil fuels, and its methyl moieties model the electron donating substituents commonly pendant on the aromatic rings of natural materials. Second, its thermal destruction is of environmental interest, the intermediate decomposition product, MA, being far more toxic than either the original DMA or the final ANT.

There appear to be no previous studies of DMA thermolysis in the literature, save for a preliminary investigation in our laboratories (Pope 1987) that is elaborated here. However, the literature does contain references to pyrolyses of the related MA (Pomerantz 1980) and ANT (Stein 1981) substrates.

In outline, we briefly describe the experimental approach and present representative results for the concentration histories and product selectivities observed during DMA thermolysis. Reaction pathways inferred from these results are then summarized, leading to a preliminary mechanism for the early stages of DMA thermolysis. Finally, frontier orbital theory is applied to understand the formation of certain minor methylated products.

EXPERIMENTAL

The chemicals used, DMA (Aldrich 99% purity), biphenyl (BIP) (Aldrich 99% purity) and methylene chloride (EM Science omnisolv), were all obtained commercially and used as received.

Pyrolyses were conducted in batch reactors, volume 0.49 ml, made from 1/4" stainless steel Swagelok parts. The reactors, purged with inert gas, were charged with weighed amounts of biphenyl (internal standard) and DMA substrate totalling 0.30 g, sealed, and placed in an isothermal, fluidized-sand, bath for the appropriate holding time, after which they were quenched in ice-water, and their contents extracted into methylene chloride. Based on their

melting and critical properties, the biphenyl and DMA reactor contents were in the liquid phase during all experiments.

Products were identified and assayed by an HP-5890 Series II Gas Chromatograph equipped with flame ionization (FID) and thermal conductivity (TCD) detectors and on-column and split/splitless injectors. Liquid products were analysed using on-column injection, a 25m HP-101 column, and the FID. Product concentrations were calculated from experimentally determined response factors, using biphenyl as internal standard. Identified compounds typically accounted for >90% of total product mass at low fractional substrate conversions, $X < 0.4$, but only about 70% of total product mass at the highest conversions, $X > 0.8$.

Figure 1 shows the experimental grid traversed, DMA being pyrolysed at initial concentrations from 0.1 to 3.0 M, temperatures between 315 and 409 C, and holding times from 450 to 28800 s.

RESULTS

Representative concentration histories obtained during DMA pyrolysis at $T = 409$ C and $[DMA]_0 = 1.0$ M are chronicled in Figure 2, with coordinates absolute mols of each identified compound, j , versus time, s . The plot clearly depicts the continuous decay of substrate DMA, the initial growth, maximum, and final decay exhibited by the primary product MA, and the initial absence and final growth of the secondary product ANT. The major thermolysis pathways evidently involve the demethylation sequence $DMA \rightarrow MA \rightarrow ANT$. Closer scrutiny reveals small amounts of TMA at low times, and the formation of methyl-anthracenes, with $1MA > 2MA$. Also, though not seen in Figure 2, small amounts of DHDMA were clearly visible at lower temperatures. The minor thermolysis pathways thus involve methylations of both the DMA substrate and the ANT final product, as well as hydrogen transfers that lead to DHDMA.

Additional insights into the operative pathways are offered by the selectivity diagram in Figure 3, which shows the selectivity $S(j)$, that is, (mols j formed/mol DMA reacted), versus conversion. For low $X < 0.6$, it is seen that both $S(MA) \sim 0.5$ and $S(TMA) \sim 0.1$ are essentially constant, implying that MA and TMA are both primary products of DMA thermolysis, resulting from parallel pathways that are respectively fast and slow. For high $X > 0.6$, the mirror-image decrease in $S(MA)$ and increase in $S(ANT)$ is evidence that ANT is a secondary product, arising from the primary product MA. Too, $S(1MA)$ and $S(2MA)$ are each essentially zero for $X < 0.6$, where $S(MA)$ is large, and increase only for $X > 0.6$, when $S(ANT)$ becomes appreciable. This timing implies that the 1MA and 2MA arise from methylation of ANT, and not from isomerization of MA.

PATHWAYS

Pathways for thermolysis of DMA, inferred from results over the entire experimental grid, are summarized in Figure 4. The main demethylation sequence, shown bold, cascades from DMA to MA to ANT. Compounds in the main sequence are all subject to methylation, forming the various methyl substituted anthracenes shown to the right, but neither MA nor DMA isomerize to their positional isomers. DMA is also hydrogenated to DHDMA (cis- and trans-isomers not distinguished). In overall, unbalanced, terms, based on detected products, the primary parallel reactions of DMA are:

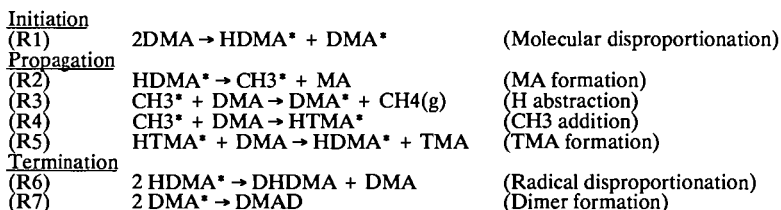
- | | | |
|--------------------------|------|---|
| (RO1) Demethylation | fast | DMA \rightarrow MA (+ CH ₄ + heavy products) |
| (RO2) Disproportionation | slow | DMA \rightarrow MA + TMA |
| (RO3) Hydrogenation | slow | DMA \rightarrow DHDMA |

A similar set of three pathways presumably operates on MA, by analogy, but we have evidence only of the demethylation step, forming ANT.

Kinetic information was also derived from the experiments that delineated the DMA thermolysis pathways. At $T = 355\text{ C}$, initial conversion data for $0.1 < [\text{DMA}]_0 < 3.0\text{ M}$ suggested that the overall decomposition was $\sim 3/2$ order in DMA. For fixed $[\text{DMA}]_0 = 1.0\text{ M}$, initial conversion data at temperatures $315 < T < 409\text{ C}$, showed an apparent activation energy $\sim 55\text{ kcal/mol}$.

MECHANISM

A possible mechanism for the early stages of DMA thermolysis, that is consistent with the present pathway and kinetic observations, is enumerated below and illustrated by the "Tolman clock" formalism in Figure 5. The elementary molecular and free-radical steps are:



The initiation reaction, (R1), involves H atom transfer from the methyl of one DMA molecule to the 9 position of another, forming the corresponding DMA^* and HDMA^* radicals. The propagation sequences involve two parallel clocks that respectively form either $\text{MA} + \text{CH}_4$ (R2 + R3) or $\text{TMA} + \text{MA}$ (R2 + R4 + R5); the latter slower than the former by the kinetic ratio $R_4/R_3 \sim S(\text{TMA})/S(\text{MA}) \sim 0.2$. Of the termination steps, (R6), the disproportionation of chain-carrying HDMA^* radicals, accounts for the observed DHDMA product. However, there is yet no independent evidence for (R7), the combination of DMA^* radicals to form dimer, although unidentified heavy products do indeed arise.

Steady-state analysis of the preceding mechanism indicates that the observed reaction orders wrt $[\text{DMA}]$ should respectively be 1 and 2 for terminations controlled by (R6) and (R7); these bracket the experimentally observed order of $3/2$.

FRONTIER ORBITAL MODEL

The observed formations of 1MA and 2MA from ANT during DMA thermolysis at high severities invite interpretation according to frontier orbital theory, as examples of periselective methyl radical attack on the ANT nucleus. Following Fukui (1975), an interaction diagram for this system is shown in Figure 6. The corresponding expression for the FMO stabilization energy is given in the bottom line of the figure, using the coefficients and energies of the CH_3 radical SOMO (singly-occupied MO) and the ANT HOMO and LUMO (highest occupied and lowest unoccupied MOs). The evaluation of these expressions is depicted graphically in Figure 7. Here each position on the ANT ring framework is decorated with its HOMO coefficients, $C_t(\text{HO})$, derived from MINDO calculations (Clark 1985, Dewar 1970), and then positions 9, 1, and 2 are shown interacting with the methyl radical SOMO, having $C_u(\text{SO}) = 1$. The resulting, favourable, nondimensional stabilization energy, denoted $\Delta E'(\text{FMO})$, is respectively 0.232 and 0.117 at positions 1 and 2 (position 9 is not in contention here). FMO theory thus predicts methyl radical attack favoured in the order position 1 >

position 2. The latter inequality accords with the experimental observation, from Figures 2 and 3, that $1MA > 2MA$.

CONCLUSIONS

1. Thermal decomposition of DMA was experimentally studied at $0.1 < [DMA]_0 < 3.0$ M, $315 < T < 409$ C, covering fractional substrate conversions $0.05 < X < 0.98$.
2. DMA decomposition pathways included:
 (RO1) Demethylation fast $DMA \rightarrow MA (+ CH_4 + \text{heavy products})$
 (RO2) Disproportionation slow $DMA \rightarrow MA + TMA$
 (RO3) Hydrogenation slow $DMA \rightarrow DHDMA$
3. The MA product decomposed by pathways analogous to DMA.
4. At low conversions, DMA decomposition was $\sim 3/2$ order in DMA, with apparent activation energy $E^* \sim 55$ kcal/mol.
5. A mechanism was devised for DMA decomposition, comprizing 7 elementary steps. This accounted for the reaction products and kinetics observed at low DMA conversions.
6. Minor products 1MA and 2MA observed at high DMA conversions appeared to arise from ANT methylation rather than 9MA isomerization.
7. The relative amounts of 1MA and 2MA observed experimentally were interpreted by FMO theory, as periselective methyl radical additions.

REFERENCES

- Clark, T.: "A Handbook of Computational Chemistry", Wiley, New York (1985).
 Dewar, M.J.S.; Haselbach, E.; Worley, S.D.: *Proc. Roy. Soc. Lond.* **A315**, 431 (1970).
 Fukui, K: "Theory of Orientation and Stereoselection", Springer-Verlag, Berlin (1975).
 Pomerantz, M.; Combs, G.L.; Fink, R.: *J. Org. Chem.*, **45**, 143 (1980).
 Pope, J.M.: Sc.D. Thesis, Dept. of Chem. Eng., MIT, Cambridge, MA (1987).
 Stein, S.E.: *Carbon*, **19**, (6) 421 (1981).

FIGURES

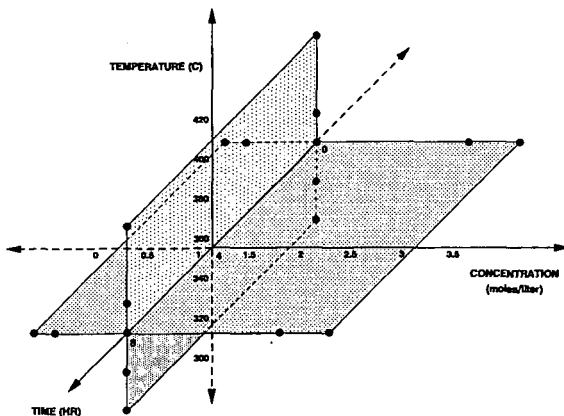


Figure 1. Experimental Grid.

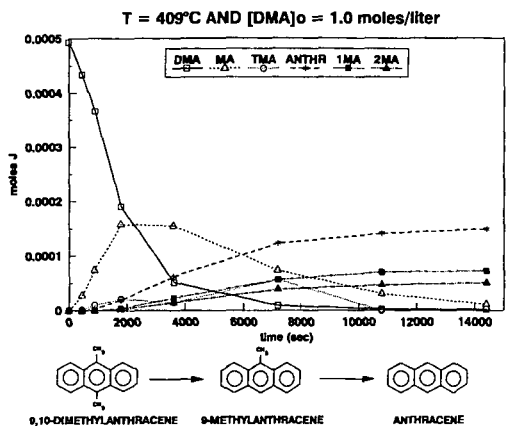


Figure 2. Concentration Histories.

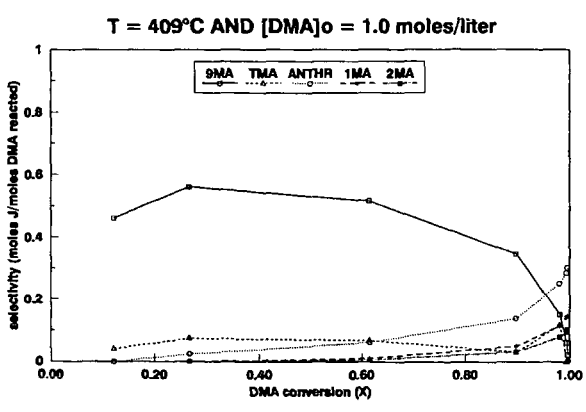


Figure 3. Selectivity Diagram.

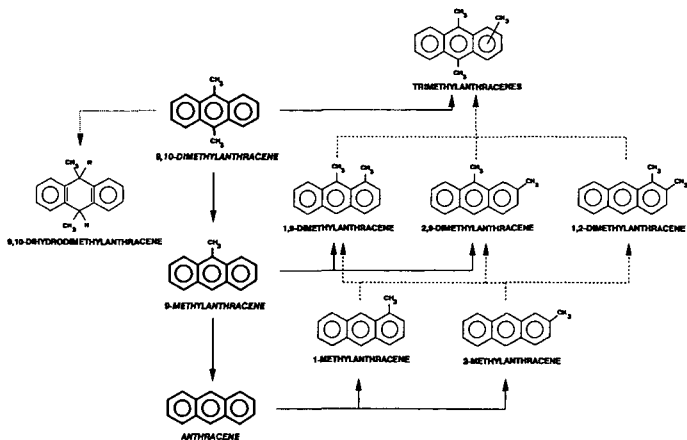


Figure 4. DMA Pyrolysis Pathways.

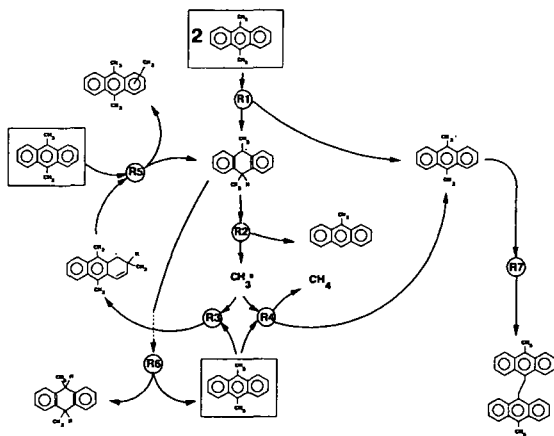


Figure 5. DMA Pyrolysis Mechanism.

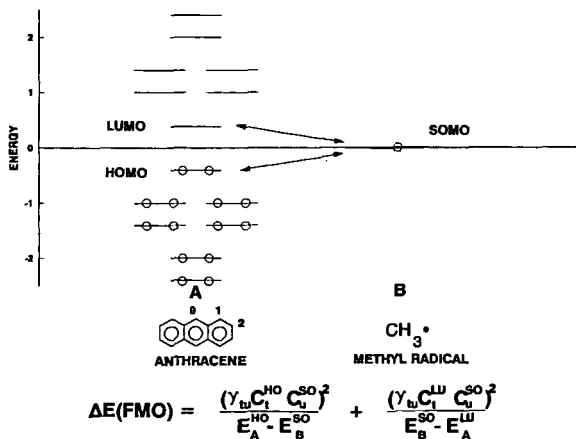


Figure 6. Frontier Orbital Interaction Diagram.

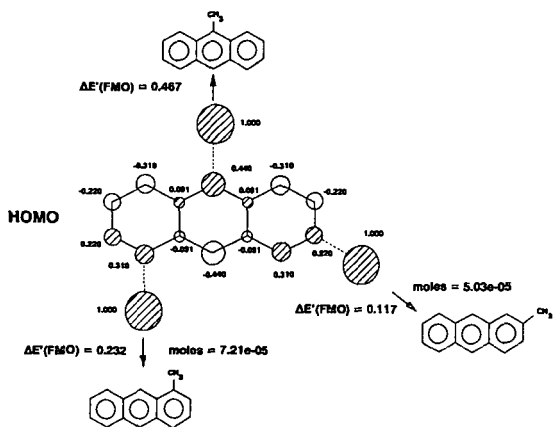


Figure 7. Periselectivity of Methyl-Anthracenes.

HYDROGEN TRANSFER PATHWAYS UNDER RESTRICTED DIFFUSION

A. C. Buchanan, III and P. F. Britt
Chemistry Division
Oak Ridge National Laboratory
P. O. Box 2008
Oak Ridge, Tennessee 37831-6197

Keywords: Pyrolysis mechanisms, hydrogen transfer, restricted mobility

ABSTRACT

The impact of restricted mass transport on the thermal processing of coal is being explored through the study of organic model compounds that are covalently anchored to an inert silica surface. Two-component surfaces are being prepared and pyrolyzed at 375 °C that contain a thermally reactive component [$\text{Ph}(\text{CH}_2)_n\text{Ph}$, $n=2-4$] in the presence of a second component that is either thermally inert [biphenyl or naphthalene] or contains reactive C-H bonds [diphenylmethane (DPM) or 9,10-dihydrophenanthrene (DHP)]. Reactions are found to be highly sensitive to the spatial distribution of hydrogen donors and nondonors that surround immobilized free-radical intermediates. In the presence of DPM or DHP, rapid serial hydrogen transfer steps allow radical intermediates to migrate across the surface overcoming normal diffusional limitations. Studies with DHP also reveal a minor reaction channel in which strong bond cleavage reactions occur via hydrogen transfer in these diffusionaly constrained environments.

INTRODUCTION

Our research has been concerned with the development of model systems¹⁻⁴ that probe the potential perturbations in free-radical reaction pathways that may arise in coal as a result of its cross-linked, network structure.⁵ This effect may be particularly important in thermal conversions of coals at low temperatures, e.g., 350-400°C, where bonds begin to break but most of the residual framework is retained.⁶ Important mechanistic insights have now been gained through the study of representative organic compounds that are covalently immobilized on an inert silica surface through Si-O-C_{org} linkages.

In order to maximize the production of hydrogen-rich products during liquefaction or pyrolysis of coal, it is important to understand and potentially control the reactions of native, reactive hydrogen-containing molecules. Our current studies employ two-component surfaces to address the influence of the structure and distribution of neighboring molecules on pyrolysis decay pathways in diffusionaly restricted environments, particularly with respect to key hydrogen transfer steps. We have focused on the thermolysis of surface-immobilized diphenylalkanes, $\text{-Ph}(\text{CH}_2)_n\text{Ph}$ [$n=2-4$], in the presence of the surface-immobilized spacer molecules, biphenyl, naphthalene, diphenylmethane, and 9,10-dihydrophenanthrene.

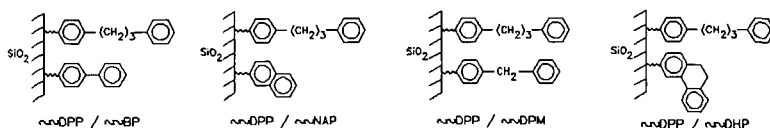
EXPERIMENTAL

The surface immobilization, pyrolysis, and product analysis procedures have been described in detail previously.^{1,2} The syntheses of $p\text{-HOC}_6\text{H}_4(\text{CH}_2)_n\text{C}_6\text{H}_5$, $n=2^1$, 3^2 , and 4^3 have also been described.

The starting materials, *p*-HOC₆H₄C₆H₅, *p*-HOC₆H₄CH₂C₆H₅, and 2-HOC₁₀H₇, were commercially available, and were purified to >99.9%. A multistep synthesis was employed to prepare 3-hydroxy-9,10-dihydrophenanthrene,⁷ which contained about 0.5% of the 3-hydroxyphenanthrene as impurity. The two-component surfaces were prepared by co-attachment in a single step, and had final purities >99.5%. Gas-phase pyrolysis products were collected in a cold trap (77K) as they formed and were analyzed by GC and GC-MS with the use of internal calibration standards. Surface-attached products were liberated as phenols following digestion of the silica in base, silylated to the corresponding trimethylsilyl ethers, and analyzed as above.

RESULTS AND DISCUSSION

Surface-Immobilized 1,3-Diphenylpropane (≡DPP). Our most detailed results come from studies of the free-radical chain decomposition pathway for ≡DPP in the presence of the surface spacer molecules shown below. Pyrolysis of ≡DPP alone in sealed, evacuated (2x10⁻⁶ torr) tubes at 375°C and low conversions produces the cracking products shown in Eq. 1.² No new products are detected



in the presence of the co-attached ≡BP, ≡NAP, or ≡DPM, while a minor new reaction channel is observed in the presence of ≡DHP (vide infra). The long chain, free-radical decay pathway (propagation steps shown in Eqs. 2-4) cycles through the two distinct benzylic radicals, ≡PhCH•CH₂CH₂Ph (1) and ≡PhCH₂CH₂CH•Ph (2) that undergo subsequent rapid unimolecular



decay via β-scission (Eqs. 2-3).² Selectivity in the product distribution is determined by the relative concentrations of the two benzylic radicals, [2]/[1], and is experimentally monitored by the PhCH=CH₂/PhCH₃ yield ratio, S. In related fluid phase studies of *p*-Me₃SiOPh(CH₂)₃Ph at 375 °C,

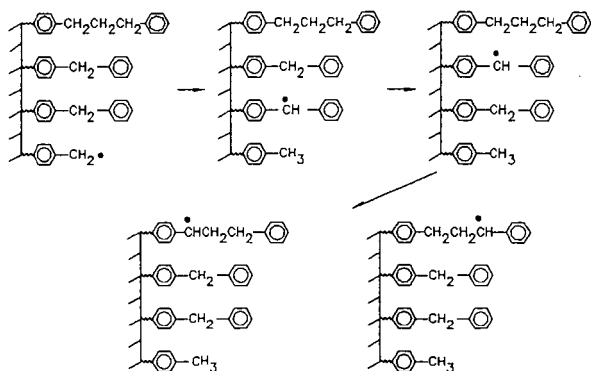


a substituent effect, S=0.91, was observed indicating a slight inherent stabilization of the benzylic radical para to the siloxy substituent.²

The initial rates and selectivities for thermolysis of ≡DPP at 375°C as a function of surface coverage and co-attached aromatic are given in Table 1.⁴ For surfaces containing only ≡DPP, the thermolysis rate decreases dramatically with decreasing surface coverage, while S increases indicating an increasing preference for abstracting the more accessible benzylic hydrogen farthest from the surface. As shown in Table 1, the presence of ≡BP or ≡NAP results in reaction rates and selectivity values comparable with surfaces containing only ≡DPP at similar ≡DPP surface coverages. On the other hand, the

presence of \sim DPM leads to a dramatic rate acceleration compared with the \sim BP or \sim NAP spacers, and gives rate and selectivity values more typical of saturated coverages of \sim DPP (see Table 1).

These results suggest that rapid hydrogen transfer steps involving \sim DPM are occurring that allow radical centers to "migrate" on the surface as illustrated below. The result of this process is to effectively decrease the distance between a \sim DPP molecule and a radical center on the surface. This



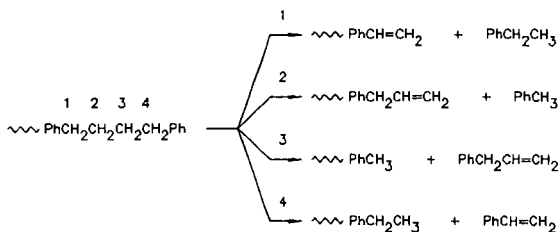
enhances the rate at which \sim DPP reacts by increasing the rate of the hydrogen transfer propagation step, which probably contains a distance dependence in the rate constant when the hydrogen abstracting radical is also surface attached. In contrast, the presence of a hydrogen donor such as tetralin⁸ or diphenylmethane⁹ had essentially no effect on the pyrolysis rate of liquid-phase DPP at ca. 350 °C at similar dilutions, and behaved similarly to liquid biphenyl⁸ as diluent. The values of $S < 1.0$ for \sim DPP/ \sim DPM surfaces are also consistent with a reduced separation between \sim DPP molecules and radical centers on the surface. Radical migration effectively removes the distance dependent conformational constraints on the hydrogen abstraction reactions from \sim DPP that resulted in the unexpected regioselectivity in product formation at lower coverages.

Supporting evidence for the involvement of \sim DPM in the radical relay mechanism depicted above comes from studies of surfaces containing \sim DPP/ \sim DPM- d_2 .⁴ Consistent with the results for \sim DPM, we find $S < 1.0$ and a substantial rate enhancement, although the rate enhancement is slightly less than the protium analog perhaps due to a small kinetic isotope effect. Furthermore both the gas-phase and surface-attached toluene products show substantial deuterium incorporation providing direct evidence for the involvement of H(D) transfer between \sim DPM- $h_2(d_2)$ and both chain carrying gas-phase and surface-attached benzyl radicals.

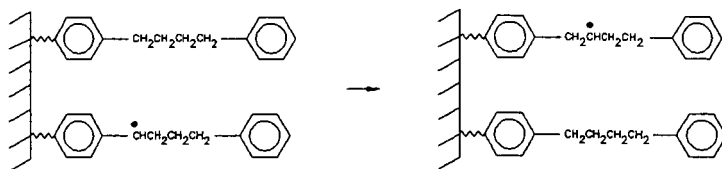
As evidenced by the rate and selectivity parameters in Table 1, the hydroaromatic \sim DHP is also very effective in promoting the radical relay pathway even for an extremely low surface coverage of \sim DPP. In addition, a second reaction channel is observed (accounting for about 2.5% of the \sim DPP reacted) that results in hydrodealkylation of \sim DPP to form \sim PhH + PhC₃H₇, and \sim PhC₃H₇ + PhH in comparable amounts. This strong bond cleavage likely results from transfer of hydrogen atoms from intermediate surface-immobilized hydrophenanthryl radicals which, as opposed to diphenylmethyl

radicals, are known to possess hydrogenolysis activity.¹⁰ Additional studies are in progress that examine the influence of α -DHP/ α -DPP surface coverage and reaction temperature on the selectivity for this reaction channel.

Surface-Immobilized 1,4-Diphenylbutane (α -DPB). A detailed analysis of the influence of restricted mobility on the pyrolysis of α -DPB at 400 °C has been recently reported.³ At low conversions α -DPB cracks to form four main sets of products, as shown below, resulting from a long chain radical decay pathway analogous to that for α -DPP that cycles through both benzylic and nonbenzylic radicals at positions 1-4.



Data for initial rates and selectivities as a function of surface coverage and co-attached spacer molecule are summarized in Table 2. The selectivities again depend on the relative concentrations of the radicals centered on carbons 1-4. The benzylic selectivity, C_1/C_2 , shows the same trend with decreasing surface coverage and the type of spacer present as did the related selectivity for α -DPP. The lack of selectivity between benzylic and nonbenzylic sites at high coverage (as typified by the values for C_1/C_2), and the increase in this selectivity with decreasing surface coverage, necessitates a rapid hydrogen transfer step that interconverts benzylic and nonbenzylic radical sites prior to β -scission as illustrated below. This interconversion step is most efficient at high surface coverages.



The C_1/C_2 product selectivity is found to be quite sensitive to the nature of the co-attached spacer present. The presence of α -BP provides a barrier that inhibits the hydrogen transfer step that interconverts benzylic and nonbenzylic radicals on the surface and results in a substantially increased value of C_1/C_2 . On the other hand, as in the case of α -DPP, the presence of α -DPM enhances the rate of radical interconversion and leads to a decreased value of C_1/C_2 identical with that of a high surface coverage of α -DPB alone.

SUMMARY

Investigations of pyrolysis reactions employing two-component surfaces have provided fundamental insights into the influence of the structure of neighboring molecules on free-radical decay pathways in diffusionally constrained environments. The rates and selectivities of key hydrogen transfer steps can be profoundly effected by the structure and spatial distribution of hydrogen donors surrounding immobilized free-radical intermediates. The results give dramatic evidence that intervening molecules containing reactive C-H bonds can act as "relay catalysts" for radical intermediates allowing them to "migrate" under conditions where classical diffusion is prohibited. Diffusional limitations for similar intermediates in coal may also be overcome by similar processes. Related studies are now in progress for α -BB, which has been found to primarily undergo retrogressive rearrangement and cyclization reactions when pyrolyzed under conditions of restricted mass transport.¹

ACKNOWLEDGEMENTS

We wish to thank C. A. Biggs and K. B. Thomas for their technical support. Research was sponsored by the Division of Chemical Sciences, Office of Basic Energy Sciences, U.S. Department of Energy under contract DE-AC05-84OR21400 with Martin Marietta Energy Systems, Inc.

REFERENCES

1. Buchanan, III, A. C.; Dunstan, T. D. J.; Douglas, E. C.; Poutsma, M. L. *J. Am. Chem. Soc.* **1986**, *108*, 7703.
2. Buchanan, III, A. C.; Biggs, C. A. *J. Org. Chem.* **1989**, *54*, 517.
3. Britt, P. F.; Buchanan, III, A. C. *J. Org. Chem.* **1991**, *56*, 6132.
4. Buchanan, III, A. C.; Britt, P. F.; Biggs, C. A. *Energy Fuels* **1990**, *4*, 415.
5. Green, T. K.; Kovac, J.; Brenner, D.; Larsen, J. W., In *Coal Structure*; Meyers, R. A., Ed.; Academic Press: New York, 1982; Chapter 6.
6. Berkowitz, N. *The Chemistry of Coal, Coal Science and Technology*; Elsevier: Amsterdam, 1985; Vol. 7, Chapter 7.
7. Takaki, K.; Okada, M.; Yamada, M.; Negoro, K. *J. Org. Chem.* **1982**, *47*, 1200.
8. Poutsma, M. L.; Dyer, C. W. *J. Org. Chem.* **1982**, *47*, 4903.
9. Gilbert, K. E.; Gajewski, J. J. *J. Org. Chem.* **1982**, *47*, 4899.
10. McMillen, D. F.; Malhotra, R.; Chang, S.-J.; Ogier, W. C.; Nigenda, S. E.; Fleming, R. H. *Fuel* **1987**, *66*, 1611.

Table 1. Rate and Selectivity in Pyrolysis of -Ph(CH ₂) ₃ Ph at 375 °C			
Surface Composition	Coverage (mmol/g)	Rate x 10 ⁴ (% s ⁻¹)	S ^a
-DPP	0.57	18	0.96
	0.14	1.1	1.09
	0.10	0.72	1.21
-DPP / -NAP	0.12 / 0.44	1.9	1.08
-DPP / -BP	0.13 / 0.51	2.3	1.14
	0.10 / 0.51	1.2	1.18
-DPP / -DPM	0.17 / 0.42	21	0.82
	0.13 / 0.37	16	0.93
-DPP / -DPM-d ₂	0.16 / 0.36	13	0.98
-DPP / -DHP	0.065 / 0.47	13	0.89

^a Measured by PhCH=CH₂ / PhCH₃ yield ratio.

Table 2. Rate and Selectivity in Pyrolysis of -Ph(CH ₂) ₄ Ph at 400 °C				
Surface Composition	Coverage (mmol/g)	Rate x 10 ⁴ (% s ⁻¹)	S ^a (C ₁ /C ₂)	S ^b (C ₄ /C ₁)
-DPB	0.485	43	1.19	0.96
	0.087	17	2.0	1.01
	0.054	9.2	2.07	1.08
-DPB / -BP	0.072 / 0.566	20	2.9	1.06
-DPB / -DPM	0.060 / 0.465	49	1.19	0.96

^a Measured from PhCH₂CH₃ / PhCH₃ yield ratio.

^b Measured from PhCH=CH₂ / PhCH₂CH₃ yield ratio.

A SIMPLIFIED REACTION MECHANISM FOR PROPANE COMBUSTION

*J. M. Deur
Sverdrup Technology, Inc.
Lewis Research Center Group
Brook Park, Ohio*

*K. P. Kundu
National Aeronautics and Space Administration
Lewis Research Center
Cleveland, Ohio*

Keywords: Reduced Mechanisms, Propane Combustion, Nitrogen Oxides

Abstract

A simplified reaction mechanism for propane combustion has been derived. This scheme is based on two competitive fuel decomposition reactions. Further, the combustion of hydrogen has been used to derive the concentrations of the intermediate reactive species, and the kinetic parameters for the rate equations are estimated through comparison of the species concentrations calculated using detailed mechanisms available in the literature. Calculated concentrations of nitrogen oxides (NO_x) and carbon monoxide found using this mechanism agree well with previously published experimental data.

Introduction

The principal pollutants released in hydrocarbon combustion are carbon monoxide, oxides of nitrogen, organic compounds (unburned and partially burned), and particulates, e.g., soot. In general, the observed concentrations of these various pollutant species differ from calculated equilibrium level concentrations, indicating the importance of reaction kinetics in determining pollutant emissions.

The formation and decomposition of some pollutants (carbon monoxide, organic compounds, soot, etc.) are important aspects of the overall combustion process. To understand the chemistry of these pollutant species, some knowledge of the hydrocarbon fuel combustion process is required. However, other pollutants, e.g., nitrogen oxides, form independently of the combustion process itself. Under these circumstances, it becomes possible to decouple the description of their formation from the combustion process. Even so, the reactions involving these pollutants are controlled by the environment established by the combustion process, and hence, their chemistry is still intimately connected to combustion.

Over the last decade, numerical combustion modeling has become an essential part of many research and development programs. Although combustion involves a complex coupling of chemistry and transport processes, early combustion modeling efforts treated the former in a very simplistic fashion. Unless the characteristic times for the flow field and the chemistry are widely disparate, the details of the flow field and the finite rate chemistry must be simultaneously taken into account. However, the computational burden soon becomes excessive since the level of complexity involved in such coupled calculations increases proportionately with the number of reacting species. One way to improve tractability is to reduce the number of reactions considered in a coupled solution with the flow field.

Hydrocarbon combustion is a very complex process, and any attempt to obtain a simplified reaction scheme can easily become a daunting task. During combustion, a fuel molecule breaks down into many different hydrocarbon fragments. Any reaction mechanism which aims to consider all of these fragments tends to become very large. While there have been attempts to simplify the detailed kinetic mechanisms by algebraic (1,2,3) and other techniques (4,5), it is difficult to say if any such simplified scheme can substitute the detailed mechanisms, and while a few global reaction mechanisms (6,7,8,10) have been reported, their utility in practical applications where the levels of pollutants must be calculated has not been established.

The level of detail required to obtain the concentrations of species, particularly minor constituents such as the oxides of nitrogen, is difficult to determine. Although a detailed kinetic mechanism is sometimes required to understand the process, a global reaction scheme involving a few reaction species will often suffice.

Of course, it must be emphasized that all descriptions of chemical kinetics are in real sense only approxima-

tions. Even detailed kinetic mechanisms are constructed on the basis of reproducing observable phenomena which are not necessarily singular events. Moreover, evaluation of specific rate constants over ranges of temperatures and pressures adequate for combustion modeling is a difficult problem. Thus, it cannot be assumed that any validated mechanism can be divided and the parts used to describe independent phenomena, unless the detailed mechanism was constructed in that way.

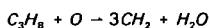
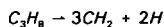
The objective here is to develop a semi-global reaction mechanism that can predict overall temperatures and concentrations of pollutants such as NO_x and CO .

A Simplified Reaction Mechanism

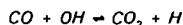
The formation of thermal NO_x is generally slow when compared to combustion itself(9). Therefore, the NO_x formation mechanism can be divided into two stages: initiation and NO_x formation.

In the initiation phase, the hydrocarbon molecule (propane in the current discussion) is broken down into hydrocarbon fragments (10), followed by hydrogen combustion reactions to generate the free radicals. For simplicity, only one type of hydrocarbon fragment, i.e., CH_2 , will be tracked in the present mechanism.

The key steps in these reactions are:

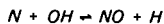


These steps generate two key radical species, CO and H_2 . Further reactions of these species lead to the formation of CO_2 and H_2O , the most important reaction for the disappearance of CO being:

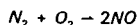


In the second stage, the NO_x is formed. The two principal sources of nitrogen oxide are: (1) oxidation of atmospheric nitrogen at high temperatures (thermal NO_x), and (2) reactions between hydrocarbon fragments and atmospheric nitrogen (prompt NO_x).

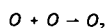
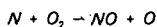
The principal reactions for thermal NO_x involve two radical species, O and OH , which are formed during the initiation stage and are near equilibrium with the corresponding molecular species.



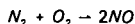
The above reactions do not correctly explain the effect of residence times on NO_x formation. To overcome this problem, the following semi-global reaction has been incorporated into the present mechanism:



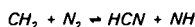
which follows from the series of reactions:



Thus, the present mechanism postulates the following reactions for thermal NO_x formation:



In fuel-rich flames, the rapid formation of NO near the flame zone cannot be explained by the equilibrium concentrations of O and OH. Although there is uncertainty in the mechanisms for such prompt NO_x formation, it is normally hypothesized that the principal product of initial reaction is HCN. In the present mechanism, it will be assumed that HCN is formed through the reaction between the hydrocarbon fragment CH_2 and N_2 :



The product species, HCN and NH, are subsequently transformed into other species by other reactions in the fuel rich combustion environment. In the current mechanism, these steps have not been considered. Instead, we have assumed that HCN and NH are the representative nitrogenous species themselves.

Combining the above description of the thermal and prompt NO_x formation with the previous characterization of the hydrocarbon combustion, the reduced mechanism summarized in Table I results.

Reaction Rates

Most reaction rates are taken from the literature with minor adjustments to match ignition delay times, flame temperatures, and concentrations of species formed during reactions. The activation energy for the fuel fragmentation reaction is taken to be equivalent to the activation energy reported by Lefebvre (11) in an ignition delay measurement.

Validation of Mechanism

The purpose of this mechanism is to compute NO_x emissions, which as noted earlier, depend on temperature and concentrations of radicals. To examine the fidelity of the mechanism, studies based on well stirred reactor calculations have been performed using the LSENS program (12), with sensitivity analyses generated via the decoupled direct method of Radhakrishnan (13). Flame temperatures (Fig. 1) and species concentrations (Figs. 2 through 5) for various test conditions have been compared with results found with a standard detailed mechanism of Miller and Bowman (14).

However, since agreement between experimental data and computed results using the Miller and Bowman mechanism is less than satisfactory in the case of NO_x formation, direct comparisons between calculations based on the present mechanism and experimental data obtained by Anderson (15) have been made (Figs. 6 and 7). These experiments were conducted at an initial pressure of 5.5 atmospheres and initial temperatures of 600 K and 800 K, although comparisons are only shown at 800 K in the above figures.

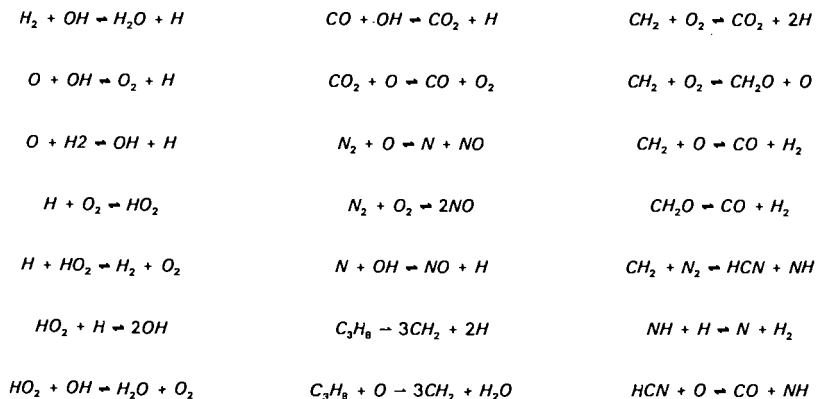
Finally, since the ultimate use of the reduced mechanism is multi-dimensional reacting flow field calculations, the Anderson burner geometry has been modeled using KIVA-II (16) with the current mechanism. Favorable comparisons (Fig. 8) have been obtained with regards to the NO_x emission levels over the range of equivalence

ratios and residence times reported by Anderson.

References

1. Peters, N., and Kee, R. J., *Comb. and Flame*, Vol. 68, 1987, p. 7.
2. Paczko, G., et. al., *21st Sym. (Intl.) Comb.*, 1988, p. 739.
3. Chen, J. Y., and Dibble, R. W., *SAND-90-8447*, 1990.
4. Lam, S. H., *Recent Advances in Aerospace Sciences (C. Casci, Ed.)*, Academic Press, 1985.
5. Lam, S. H., and Goussis, D. A., *MAE Report No. 1799*, Princeton U., 1988.
6. Ying, S. J., and Nguyen, H. L., *AIAA Paper No. 90-0546*, 1990.
7. Westbrook, C.K., and Dryer, F. L., *Comb. Sci. Tech.*, Vol. 27 (1-2), 1989, p. 31.
8. Reitz, R. D., and Bracco, F. V., *Num. Fluid Mech.*, Vol. 5, 1982, p. 130.
9. Bowman, C. T., *Fossil Fuel Combustion (W. Bartock and A.F. Sarofim, Eds.)*, Wiley, 1991.
10. Kieheue, T. M., et. al., *Comb. Sci. Tech.*, V. 54, 1987, p. 1.
11. Freeman, G. and Lefebvre, A. H., *Comb. and Flame*, V. 58, 1984, p. 153.
12. Radhakrishnan, K., *Prog. in Astro. and Aero.*, V. 135, 1991, p. 83.
13. Radhakrishnan, K., *NASA-CR-179636*, 1987.
14. Miller, J. A., and Bowman, C. T., *Prog. in Energ. and Comb. Sci.*, V. 15, 1989, p. 287.
15. Anderson, D. A., *NASA-TM-X-71592*, 1975.
16. Amsden, A. A., et. al., *LA-11560-MS*, 1989.

Table I. Reduced Reaction Mechanism for Propane Combustion.



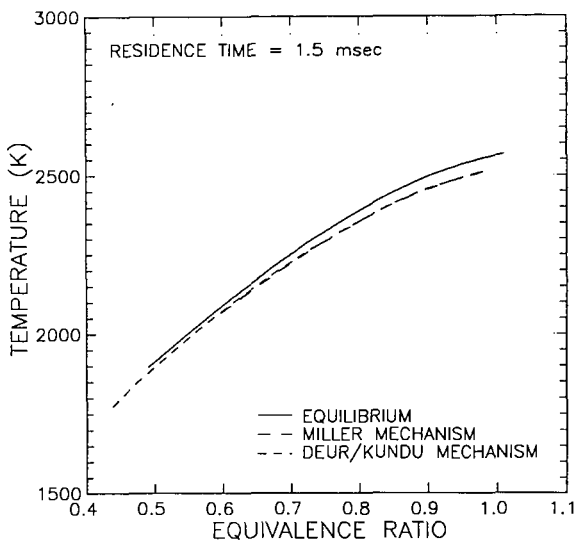


Figure 1. Equilibrium and Adiabatic Flame Temperature Comparison.

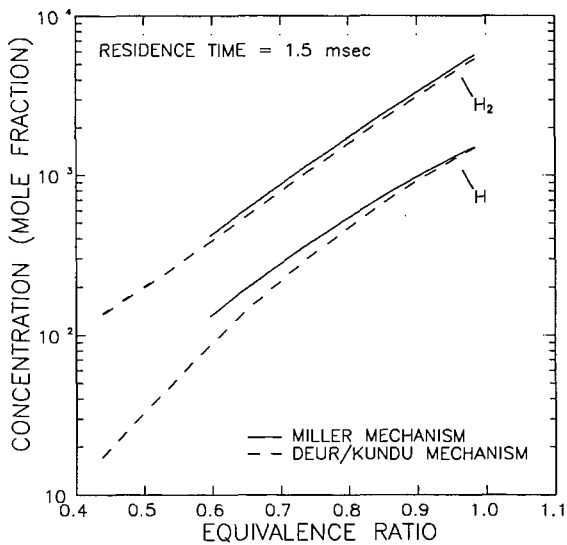


Figure 2. H and H₂ Species Concentration Comparison (Residence Time = 1.5 msec).

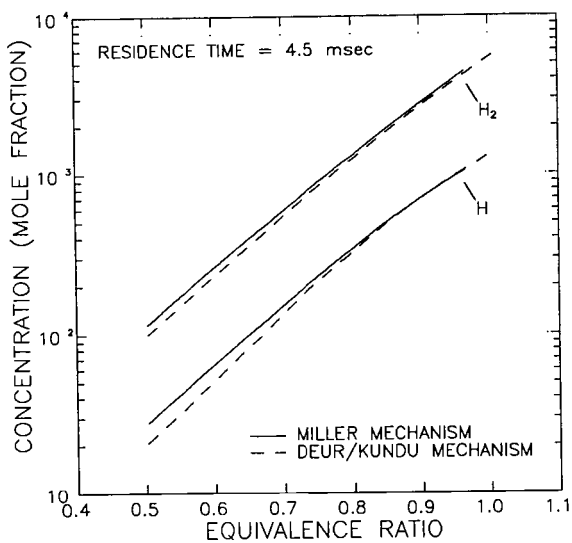


Figure 3. H and H₂ Species Concentration Comparison (Residence Time = 4.5 msec).

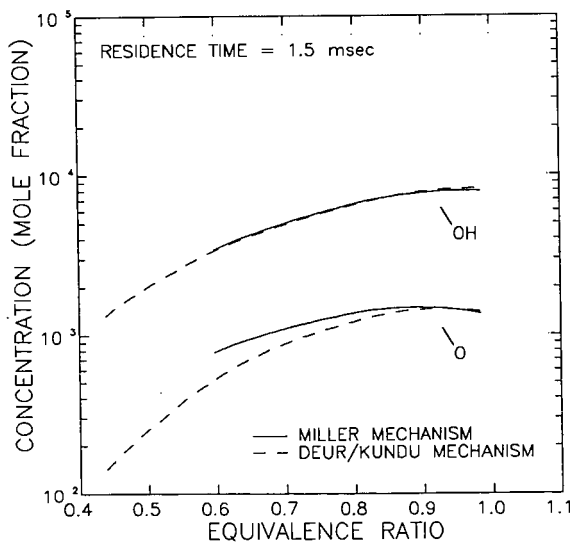


Figure 4. O and OH Species Concentration Comparison (Residence Time = 1.5 msec).

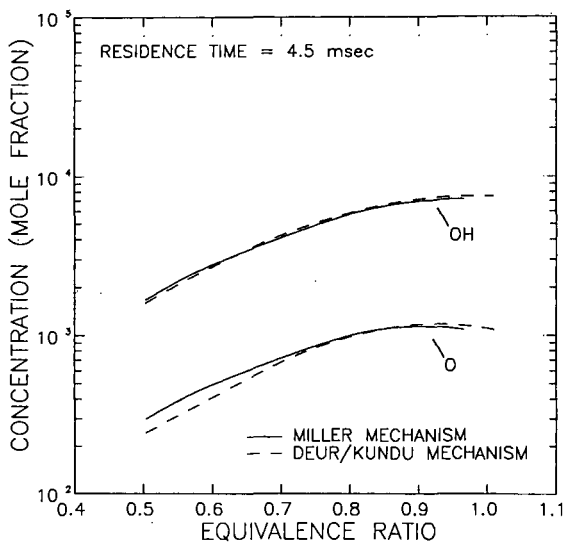


Figure 5. O and OH Species Concentration Comparison (Residence Time = 4.5 msec).

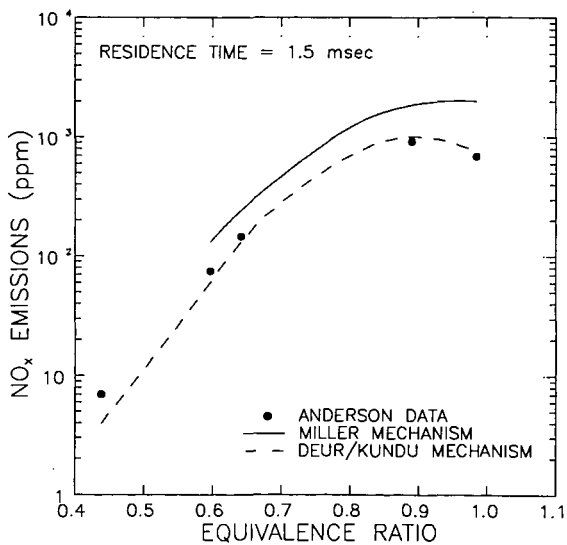


Figure 6. NO_x Emissions Comparison (Residence Time = 1.5 msec).

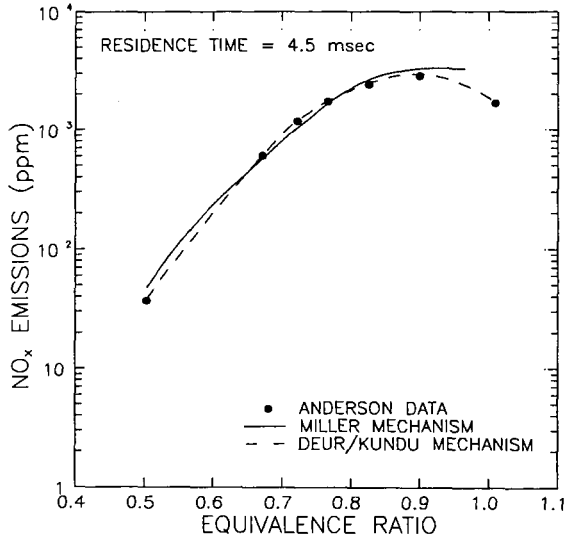


Figure 7. NO_x Emissions Comparison (Residence Time = 4.5 msec).

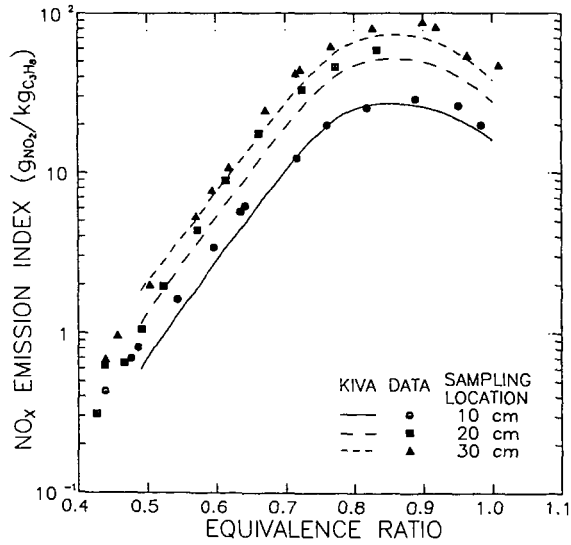


Figure 8. NO_x Emissions Comparison: Anderson Experimental Data vs. KIVA-II Predictions.

Mechanisms of Hydrogen Donation from Cyclic Olefins
to Pittsburgh No. 8 Coal

Michael W. Bedell, Exxon Research and Development Laboratories
Baton Rouge, LA 70821
Christine W. Curtis, Chemical Engineering
Auburn University, AL 36849-5127

Keywords: Hydrogen Donation, Cyclic Olefins, Coal Liquefaction

INTRODUCTION

Hydrogen donation is considered to be an important mechanism by which hydrogen is transferred from the solvent to coal during coal liquefaction (Bockrath, 1982). Hydrogen donation from cyclic olefins such as 1,4,5,8,9,10-hexahydroanthracene (HHA) and 1,4,5,8-tetrahydronaphthalene or isotetralin (ISO) to coal has been shown to be both rapid and effective (Bedell and Curtis, 1991). This investigation examined the mechanisms and kinetics by which HHA and ISO transfer their hydrogen to Pittsburgh No. 8 coal and compared these effects with those of hydroaromatic donors. The cyclic olefins readily converted to hydroaromatics at liquefaction conditions but still remained more effective than most conventional hydroaromatic donors in converting coal. Combinations of cyclic olefins and conventional hydroaromatic donors produced effective hydrogen donor combinations providing hydrogen rapidly and sustaining hydrogen donation throughout the reaction time. The universality of the effectiveness of the cyclic olefin donation was examined with a set of eight coals from the Argonne Premium Coal Bank that are of different rank and reactivity. The cyclic olefins effectively converted the coals of different rank, being most effective with the coals of intermediate reactivity.

Efficient coal liquefaction processing requires that hydrogen be transferred to the dissolving coal matrix at the rate that it can be accepted by the reacting coal molecules and effectively used donors. A key to obtaining high coal conversion in liquefaction through donation from solvent is the matching of the rate that hydrogen is released by the donor and accepted by the coal. When these rates are not matched, inefficient usage of the hydrogen results. When hydrogen is released by the donor too quickly, the hydrogen is not used by the dissolving coal and forms gaseous hydrogen; when hydrogen is released too slowly, retrogressive reaction of the dissolving coal molecules can occur forming refractory coke precursors.

The goals of this research were to evaluate the effects of different rates of hydrogen donation by evaluating the hydrogen donation from a cyclic olefin, 1,4,5,8,9,10-hexahydroanthracene (HHA) in combination with the hydroaromatic, 9,10-dihydroanthracene (DHA). The acceptor used in this study was Pittsburgh No. 8 coal. Liquefaction reactions were performed with the combined donor system as well as with individual cyclic olefins, HHA and ISO, and hydroaromatic donors, DHA, octahydroanthracene (OHA) and tetralin (TET). The rate of hydrogen acceptance by Pittsburgh No. 8 coal was determined in terms of coal conversion to THF solubles after different reaction times.

These same hydrogen donors were evaluated with eight coals from the Argonne Premium

Coal Sample Bank. These coals were of different rank and reactivity. The various degrees of hydrogen acceptability and, hence, reactivities of the coals were evaluated.

EXPERIMENTAL

Reactions with Pittsburgh No. 8 Coal. The reactions of cyclic olefins, HHA and ISO, and hydroaromatic donors, DHA, OHA, and TET were performed with Pittsburgh No. 8 coal from the Argonne Premium Coal Sample Bank. Information concerning Pittsburgh No. 8 coal properties is given in Table 3. Reactions were performed in 50 cm³ stainless steel tubular reactors that were agitated at 700 cpm. The reaction conditions used were 30 minutes reaction time, 1250 psig H₂ atmosphere at ambient temperature, 380°C reaction temperature, 2.0g coal, 4.0g total solvent mixture including 0.5 weight percent donable hydrogen of the donor with the balance being hexadecane as the diluent solvent.

Reactions with Argonne Coals. Reactions were performed with the hydrogen donors, both cyclic olefins and hydroaromatic donors, and eight Argonne Premium Sample Bank coals. Another coal, Western Kentucky No. 9, from the PSU/DOE sample bank was used for comparison. The reactions were performed using the same type of reactor and conditions as those with Pittsburgh No. 8 coal.

Materials and Analysis. The hydrogen donors used were obtained from the following manufacturers and were used as received: tetralin, 1,4,5,8,9,10-hexahydroanthracene, 1,2,3,4,5,6,7,8-octahydroanthracene, 9,10-dihydroanthracene, and hexadecane from Aldrich Chemical Co.; 1,4,5,8-tetrahydronaphthalene (isotetralin) from Wiley Organics Inc.; and Pittsburgh No. 8, Illinois No. 6, Upper Freeport, Pocahontas No. 3, Lewiston Stockton, Blind Canyon, Wyodak and Beulah Zap coals from the Argonne Premium Coal Sample Bank. Western Kentucky No. 9 coal was obtained from the PSU/DOE Coal Sample Bank.

The hydrogen donor compounds and their products produced during coal liquefaction were analyzed by gas chromatography using a Varian 3400 gas chromatograph equipped with a HT-5 column from SGE and FID detection. The internal standard method with biphenyl as the internal standard was used. The peaks were identified by comparing retention times with authentic compounds and by GC mass spectrometry using a VG 70EHF mass spectrometer.

Coal conversion is defined as

$$\text{Conversion} = [1 - [\text{IOM (maf)}] / \text{coal charge (maf)}] \times 100$$

where IOM is the THF insoluble organic matter remaining after reaction and maf is defined as moisture and ash free.

RESULTS AND DISCUSSION

Cyclic olefins, as donors for coal liquefaction, have been shown to release their hydrogen readily and quickly to the dissolving coal matrix. The conversion of cyclic olefins occurred very rapidly at liquefaction temperatures, forming a number of reactions products including

hydroaromatic and aromatic compounds (Bedell and Curtis, 1991). HHA converted quickly at temperatures of 380°C and above, forming reaction products of DHA, OHA, and anthracene (ANT). DHA has also been shown to be very effective in converting coal at liquefaction temperatures (Bedell, 1991); however, the conversion and subsequent release of hydrogen from DHA was not nearly as rapid as that from HHA. The purpose of this research was to investigate the possible synergism between the hydrogen donating rate of HHA and DHA on coal conversion. The idea being explored was that HHA released its hydrogen very quickly making it readily available to the coal as it initially began to dissolve while DHA released its hydrogen more slowly making hydrogen available to the less reactive components of the coal.

The reactions performed as shown in Table 1 were comprised of varying amounts of HHA and DHA. The reactions were configured to maintain a constant level of 0.5 weight percent donable hydrogen. Hence, the amount of donable hydrogen remained the same although the relative amount of each donor was varied from 75% HHA and 25% DHA to 75% DHA and 25% HHA. The reaction that produced the highest coal conversion to THF solubles contained equal levels of donable hydrogen from HHA and DHA. Nearly 12% more coal conversion was obtained from the combined HHA/DHA system than with HHA alone, while nearly 7% more conversion was obtained with the combined system than with DHA alone. The reactions containing 75% HHA and 25% DHA produced more coal conversion than the reaction with HHA alone, and nearly equivalent coal conversion as the reaction with DHA alone. The reaction containing 75% DHA and 25% HHA produced more conversion than either HHA or DHA alone.

These increases in coal conversion with the combined systems suggested that combining the two donors provided a synergism in both the amount and rate of hydrogen released in the system. Additional reactions were performed to evaluate the effect of time on the behavior of the hydrogen donors. Reactions were performed with the combined HHA and DHA system and with the individual donors of HHA, DHA, OHA, ISO and TET for reaction times of 5, 15, 30 and 60 minutes. Hydrogen donation was monitored by evaluating the reaction products from the donors. Hydrogen acceptance was measured by evaluating coal conversion to THF solubles. At the short reaction time of 5 minutes, HHA produced the most coal conversion, producing slightly more than the HHA/DHA combined system, 5% more than the DHA system, and 16% more than OHA. Analysis of the reaction products from hydrogen donors showed that more than 70% HHA converted while less than 25% DHA converted after 5 minutes of reaction. In the combined system, almost all of the HHA had converted after 5 minutes. Comparison of the cyclic olefin, ISO, to the hydroaromatic donor, TET, again showed much higher coal conversion at short reaction time. ISO converted very rapidly forming a reaction products of 1,2-dihydronaphthalene (DHN) and naphthalene (NAP) while TET remained essentially unreacted. These experimental results indicate that the rapid release of hydrogen by cyclic olefins promoted coal conversion at shorter reaction times compared to the slower hydrogen release by the hydroaromatic donors.

The liquefaction reactions of Pittsburgh No. 8 coal at 15, 30 and 60 minutes with the two types of donors are also compared in Table 2. At the short reaction time of five minutes, the cyclic olefin HHA produced the highest coal conversion to THF solubles. At longer reaction times of 15 and 30 minutes, the combined HHA/DHA reaction produced the highest coal

conversion. At the longest reaction of 60 minutes, the combined HHA/DHA and the individual DHA and HHA systems all produced similar coal conversions. Even in the system with no hydrogen donor present, the amount of coal conversion increased with time. Hence, coal conversion in a hydrogen atmosphere increased with time regardless of the presence or type of hydrogen donor present. However, the presence of the hydrogen donor increased the amount of coal conversion achieved by 13 to 22% at the long reaction time. Greater benefits were observed with some of cyclic olefin donors or the combined cyclic olefin/hydroaromatic donors at shorter reaction times.

Each of the hydrogen donors underwent reactions that released hydrogen from themselves. HHA showed the most reactivity while OHA showed the least amount of reactivity for the conversion of the donor to other species. In the reaction times of 15 minutes and longer, HHA formed OHA, DHA, and ANT; OHA formed DHA and ANT and DHA formed OHA and ANT. At short reaction time of 5 minutes, tetrahydroanthracene (THA) was observed in the individual reactions of OHA, HHA and DHA.

The reactions using the two ring donors, ISO and TET, yielded the same trends. ISO converted coal much more quickly than did TET and showed substantial increases in coal conversion compared to the amount produced by TET. However, at longer reaction times of 15 and 30 minutes, both ISO and TET showed similar coal conversion which was substantially more than without any donor. ISO was highly reactive forming TET and naphthalene (NAP) at reaction times of 15 minutes and longer, but forming 1,2-DHN rather than TET at the short reaction time (5 min.). TET converted very little and only formed small amounts of NAP.

Argonne Coals. Cyclic olefins have been shown to be effective hydrogen donors for bituminous coals, Western Kentucky (Bedell and Curtis, 1991) and for Pittsburgh No. 8 coal. To establish the universality of these donors, a series of reactions was performed in which cyclic olefins were reacted with eight coals from the Argonne Premium Coal Sample Bank. The efficacy of the hydrogen donation from the cyclic olefins to coals of different rank was compared to the efficacy of hydrogen donation from hydroaromatic donors. These reactions were performed using an equivalent amount of donable hydrogen for each hydrogen donor species and a reaction time of 30 minutes. The efficacy of hydrogen donation for each hydrogen donor for each coal was evaluated in terms of coal conversion to THF solubles.

The coals, themselves, had considerably different reactivities. Reactions in hydrogen and hexadecane without an added hydrogen donor ranked the reactivity of the coals for conversion as Illinois No. 6 > Western Kentucky No. 9 > Pittsburgh No. 8 > Blind Canyon > Wyodak-Anderson and Upper Freeport > Beulah-Zap and Lewiston-Stockton >> Pocahontas No. 3. The reactivity ranking of the coals became less distinct when the different donors were added to the reaction system. The addition of hydrogen donors to the system increased the amount of coal conversion obtained for most of the coals. The most active donors were the cyclic olefins, HHA and ISO, and the hydroaromatic donor, DHA. The hydroaromatic donors, OHA and TET, contributed less hydrogen to the system and resulted in less coal conversion.

The coals of high inherent reactivity, Kentucky No. 9, Illinois No. 6, and Pittsburgh No. 8 showed similar coal conversions with DHA and HHA. These coals were evidently sufficiently

reactive to be able to utilize the hydrogen that was quickly released from the cyclic olefin, HHA. The coals of lower reactivity, Upper Freeport, Lewiston-Stockton, Blind Canyon, Wyodak, and Beulah Zap, showed a much wider disparity between the coal conversion obtained with DHA and that from HHA. For these coals, the quick release of hydrogen from HHA was not effective in promoting coal conversion, most probably because these coals were slow to react and could not utilize the hydrogen released from the cyclic olefin quickly enough to promote coal conversion.

SUMMARY

The combination of the cyclic olefin, HHA, with the hydroaromatic donor, DHA, was the most effective hydrogen donor system, producing the most coal conversion in the least amount of time. HHA released its hydrogen rapidly to produce high initial levels of coal conversion to THF solubles. Although coal conversion increased with increasing reaction time, the combined HHA/DHA yielded a high level of coal conversion at very short time with only small increases being observed with increased time. The high level of reactivity of the cyclic olefins resulted in quick release of hydrogen that could then be incorporated into the dissolving coal matrix of the reactive coals. However, the coals of lesser reactivity did not benefit to nearly the same degree to the quick release of the hydrogen by the cyclic olefin. The slower release of DHA was more effective in promoting the desired reactions between donated hydrogen and the less reactive coals.

REFERENCES

- Bedell, M.W. and Curtis, C.W., *Energy and Fuels*, 1991, 5, 469.
 Bedell, M.W., Ph.D. Dissertation, Auburn University, 1991.
 Bockrath, B., *Coal Science*, Vol. 2, Academic Press, New York, NY, 1982.

Table 1. Effect of Hydrogen Donor Content on Coal Conversion

Percentage of Hydrogen Donor		Coal Conversion
Dihydroanthracene	Hexahydroanthracene	
%	%	%
100	0	56.4 ± 0.1
75	25	60.8 ± 1.6
50	50	63.7 ± 0.1
25	75	55.5 ± 0.3
0	100	51.8 ± 0.6
0	0	20.1 ± 3.3

Reaction Conditions: Pittsburgh No. 8 coal, hexadecane as solvent, 1250 psig H₂ at ambient temperature, 380°C, 30 minute reaction time.

Table 2. Effect of Time and Hydrogen Donor Content on Coal Conversion

Hydrogen Donor	Coal Conversion (%) at Specific Reaction Times (min)			
	5	15	30	60
HHA + DHA*	30.9±0.3	58.0±0.5	63.1±1.0	63.7±0.1
DHA	27.5±1.1	55.2±0.3	56.4±0.1	67.7±1.6
HHA	32.3±1.4	44.6±4.0	51.8±0.6	65.0±0.7
OHA	15.5±1.2	25.9±0.9	38.8±1.0	58.5±0.9
ISO	19.1±0.6	37.1±1.6	42.3±5.2	58.8±0.2
TET	6.0±0.4	17.4±1.0	30.5±3.8	56.9±2.6
No Donor	7.9±0.2	20.9±0.1	20.1±3.3	44.2±3.1

Reaction Conditions: Pittsburgh No. 8 coal, hexadecane as solvent, 1250 psig H₂ at ambient temperature, 380°C.

*HHA and DHA present in a 1 to 1 weight ratio.

Table 3. Proximate Analysis of the Argonne Premium Sample Coals

Coal	Moisture %	Ash %	Volatile Matter %	Sulfur %	BTU	Rank
Kentucky No. 9	7.12	10.97	35.77	4.50	11936	HVB
Illinois No. 6	7.97	14.25	36.86	4.45	10999	HVB
Upper Freeport	1.13	13.03	27.14	2.29	13315	MVB
Pocahontas No. 3	0.65	4.74	18.48	0.66	14926	LVB
Pittsburgh No. 8	1.65	9.10	37.20	2.15	13404	HVB
Lewiston Stockton	2.42	19.36	29.44	0.69	11524	HVB
Blind Canyon	4.63	4.49	43.72	0.59	13280	HVB
Wyodak	28.09	6.31	32.17	0.45	8426	Sub B
Beulah Zap	32.24	6.59	30.45	0.54	7454	LIG

All values are weight percents for the as-received coals.

HVB = high volatile bituminous
MVB = medium volatile bituminous
LVB = low volatile bituminous
Sub B = subbituminous
LIG = lignite

Table 4. Coal Conversion for Reactions of Argonne Coals with Hydrogen Donors in Hexadecane

Coal Reacted	Coal Conversion: (%) with						No Donor Added
	DHA	HHA	OHA	ISO	TET		
Kentucky No. 9	68.3(1.0)	65.0(3.3)	49.7(1.0)	37.2(0.4)	29.8(0.2)		25.6(1.8)
Illinois No. 6	69.6(2.0)	67.7(0.2)	66.1(2.8)	65.5(1.6)	62.1(2.0)		55.7(0.1)
Upper Freeport	47.1(2.0)	15.8(1.2)	13.0(1.7)	20.9(2.5)	8.3(0.7)		11.4(0.5)
Pocahontas No. 3	4.5(0.1)	-4.4(0.1)	-6.1(2.0)	-6.7(1.5)	-3.1(1.0)		-5.7(1.7)
Pittsburgh No. 8	56.4(0.1)	51.8(0.6)	38.8(1.0)	42.3(5.3)	30.5(3.8)		20.1(3.3)
Lewiston Stockton	41.7(1.9)	25.2(2.1)	19.6(1.2)	20.9(1.1)	9.1(2.6)		6.0(3.1)
Blind Canyon	64.8(3.9)	41.6(1.6)	27.9(0.7)	25.3(0.2)	15.2(2.0)		17.4(0.4)
Wyodak (dried)*	50.6(0.6)	40.5(1.3)	21.4(1.2)	21.1(2.9)	14.9(1.5)		11.7(1.5)
Beulah Zap (dried)*	35.6(3.0)	20.8(3.0)	13.3(1.0)	13.8(0.1)	5.0(2.5)		8.1(2.1)

Reaction Conditions: hexadecane as solvent, 1250 psi, hydrogen at ambient temperature, 30 minute reaction time, 380°C
 * dried to approximately 4% moisture content

Temperature-Programmed Liquefaction of Low-Rank Coals in H-Donor and Non-Donor Solvents

Chunshan Song and Harold H. Schobert

Fuel Science Program, Department of Materials Science and Engineering,
209 Academic Projects Building, The Pennsylvania State University,
University Park, PA 16802

Keywords: Temperature-programming, Coal Liquefaction, H-donor

Introduction

U.S. production of low-rank coals including lignite and subbituminous coals has increased tenfold over the last two decades, and production is poised for a further step increase [1]. Recently there has been increasing interest in finding ways to improve conversion of low-rank coals, which are often less readily liquefied than bituminous coals [2]. In coal liquefaction, the thermally derived reactive fragments (radicals) must be stabilized to achieve molecular weight reduction, otherwise they will promptly recombine or crosslink to form more refractory materials [3]. The rate of thermal fragmentation is mainly determined by coal reactivity, temperature, and time, while its balance with the rate of radical capping by hydrogen-donation is a critical factor [3,4]. It is now recognized that low-rank coals are more reactive than had been thought previously, and their conversion in high-severity processes is accompanied by significant retrogressive reactions [5].

Due to the presence of various C-O and C-C bonds in coals, there may be a relatively broader distribution of dissociation energies of bonds connecting the structural units in low-rank coals, as can be visualized from the dissociation energies of various C-O, C-C and C-H bonds that are believed to be relevant to coal and coal conversion processes [6]. The concept of distribution of bond energies for coals is also supported by the results of temperature-programmed pyrolysis (TPP) of coals ranging from brown to bituminous coals [6,7]. TPP data show that more bonds in low-rank coals are thermally broken at lower temperatures as compared to bituminous coals [6]. The question that arises for liquefying low-rank coals is how to balance the rates of bond cleavage with the rates of hydrogen transfer to the radicals. Of some importance to the present work are several recent reports showing that using relatively slow heating rates [3,4,8] is effective for liquefying low-rank coals. In catalytic liquefaction, temperature-staged conditions have been shown to improve coal conversion and oil yields [9-11], even in the aqueous liquefaction system [12].

For a given reaction system, controlling the conditions is important for maximizing the yield and quality of products and minimizing retrogressive reactions. The retrogressive reactions may include the crosslinking of thermally generated radicals and condensation of thermally sensitive compounds. The temperature-programmed liquefaction (TPL) reported here seeks to efficiently liquefy low-rank coals by controlling the rate of pyrolytic cleavage of weak bonds while minimizing the retrogressive crosslinking of radicals and thermally sensitive groups. In preliminary communications, we reported that temperature-programming appears to be promising for more efficient conversion of low-rank coals in tetralin [13,14]. This paper reports on the temperature-programmed and non-programmed liquefaction (N-PL) of a subbituminous coal and a lignite in H-donor and non-donor solvents. Reported separately are the solid-state ^{13}C NMR and pyrolysis-GC-MS studies of coal structure and the TPL reactions [15], and catalytic TPL of a low-rank coal using dispersed Mo catalyst [16].

Experimental

The coals used were a Montana subbituminous coal and a Texas lignite obtained from the DOE/Penn State Coal Sample Bank (DECS-9 / PSOC-1546; DECS-1 / PSOC 1538). Table I shows the characteristics of these coals. The coals were recently collected and stored under argon atmosphere in heat-sealed, argon-filled laminated foil bags consisting of three layers (polyethylene plus aluminum foil plus polyethylene) [17]. The coals were crushed to less than 60 mesh and dried in vacuo at 95°C for 2 h (before use) by placing a flask containing the fresh coal into a preheated vacuum oven. Our preliminary data showed that vacuum dried coal gave similar or slightly higher conversion than the fresh coal. The H-donor vehicle used was tetralin, a known H-donor. As non-donor, naphthalene and 1-methylnaphthalene were used. The products from low temperature runs with naphthalene at $\leq 350^\circ\text{C}$ were rock-like and

difficult to remove from the reactors. However, there were no such experimental problems with 1-methylnaphthalene because it is a liquid. Liquefaction was carried out in 25 mL microautoclaves using 4 g coal (< 60 mesh) and 4 g solvent under 6.9 MPa H₂ using a given temperature program. The liquid and solid products were separated by sequential Soxhlet extraction with hexane, toluene and THF for about 24 h. The THF-insoluble residues were washed with acetone, then with pentane to remove THF completely, and subsequently dried in a vacuum oven at 100°C for over 6 h before weighing. The conversions of coal into THF-solubles were determined from the amount of THF-insoluble residues and are based on the dmmf basis. The yields of preasphaltene (THF soluble but toluene insoluble) and asphaltene (toluene soluble but hexane insoluble) are given as the yields of recovered products, and the yields of oil plus gases are determined by difference between total conversion and the sum of preasphaltene and asphaltene yields.

Results and Discussion

Temperature-Programming

Figure 1 shows the reactor heat-up profiles for temperature programmed liquefaction. Although the temperature inside the reactor was not measured, the pressure change of the reactor during the heat-up can give a direct measure of the temperature change. Figure 2 shows the change of sandbath temperature and pressure of the reactor for a TPL run of DECS-9 in tetralin with 6.9 MPa cold H₂ at final temperature of 400°C. The sandbath temperature was controlled manually such that the heating ramp would be the same for all the runs. It can be seen from Figures 1 and 2 that the programming was successfully achieved. The t-p profile in Figure 2 is typical for a thermal run, but a catalytic run shows a different t-p change pattern [6]. No catalyst was used in the present work. The selected temperature program consisted of a low-temperature soak at 200°C for 15 min, programmed heating to a final temperature at about 7°C/min, followed by a 30 minute hold at the final temperature (300, 350, 375, 400, and 425 °C). We expect few chemical reactions to occur at 200°C. The rationale for selecting such a low temperature for soaking is to allow the solvent molecules to penetrate into the interior of coal particle (diffusion and swelling), before they are needed as hydrogen donors for stabilizing the radicals and thermally labile compounds in the subsequent heat-up period and high temperature stage.

Temperature-Programmed Liquefaction

Figure 3 shows the yields of THF-, toluene- and hexane-soluble products plus gas from duplicate runs of Montana coal, as a function of final TPL temperature. At 300°C, the yield of THF-solubles is only slightly higher than that of the original coal. It should be noted that the low temperature TPL did not cause considerable increase in coal conversion, but did result in some desirable change in coal structure. As shown in Figure 3, the conversion of coal to THF-solubles increased significantly with increasing final temperature from 300 °C (9%) to 400 °C (about 79%), but rose to a much lesser extent from 400 to 425°C (about 82%). On the other hand, the conversion to toluene solubles displayed a monotonic increase from 300 to 425 °C.

Figure 4 shows the product distribution from TPL runs in tetralin as a function of final temperature. It is clear from Figure 4 that from 300 to 350°C, the increase in conversion was due mainly to gains in preasphaltene and asphaltene yields, while the oil yields rose substantially with increasing temperature from 350 to 425°C. It is likely that under the TPL conditions, increasing temperature up to 350°C contributed to cleavage of the weak bonds that released the larger molecules of asphaltene and preasphaltene classes from macromolecular network; increasing temperature from 350 to 400 directly promoted the formation of oil from coal; and further increasing temperature from 400 to 425°C further enhanced oil formation from both coal depolymerization and the thermal cracking of preasphaltene and asphaltene.

We also conducted the control runs under the conventional non-programmed (N-PL) conditions (rapid heat-up from 23°C to reaction temperature in 2-3 minutes) at the temperatures of 350-425°C. Figure 5 compares the TPL and N-PL data for DECS-9 coal in tetralin. As can be seen from Figure 5, relative to N-PL, TPL afforded more preasphaltene at low temperatures between 350-375°C, and more toluene solubles and more oil between 375-425°C. It should be noted that the data in Figure 5 are average of duplicate runs for both TPL and N-PL. The raw data from the duplicate runs show the same trend. For example, the THF conversions from duplicate experiments of N-PL are 70.6 and 72.2% for runs at 400°C, and 75.0, 75.7 and 78.4% for runs at 425°C in tetralin under H₂. A longer N-PL run at 400°C for extended time period (60 min) only increased the THF conversion by about 2-3 % as compared to the 30 min N-PL run. However, the THF conversions from duplicate TPL runs are 77.0 and 81.4% for TPL at 400°C, and 81.4 and 83.1% for TPL at 425°C. In the case of DECS-1 Texas lignite, TPL runs also gave considerably higher conversions than N-PL runs in tetralin. The average values from duplicate runs of DECS-1 in tetralin are shown in Table 2.

In order to understand the beneficial effects of TPL in H-donor tetralin, we also conducted both TPL and N-PL runs in

non-donor solvents. The data in Table 2 and Table 3 shows that temperature-programming in a non-donor solvent such as naphthalene or 1-methylnaphthalene does not appear to have any significant impact on coal conversion and product distribution. This indicates that beneficial effects of TPL as compared to N-PL in tetralin solvent are closely associated with hydrogen transfer from tetralin.

The above results demonstrated that in the presence of H-donor solvent, TPL can afford considerably higher conversion than the conventional run at the same or even higher final temperatures. This comparison clearly showed that the programmed heat-up is superior to the rapid heat-up for conversion of the low-rank coals in tetralin under H₂, although it is known that in coal pyrolysis *ultrarapid* heating increases tar yields [18]. These results indicate that the temperature-programming is a promising approach for converting low-rank coal in H-donor solvent, and further improvement may be achieved by finding the optimum program and by using a catalyst. In fact, we also demonstrated that catalytic TPL of DECS-9 is superior to N-PL in the presence of a dispersed Mo catalyst and a process solvent which has much lower H-donating ability compared to tetralin [16]. Analytical characterization of the residues using CPMAS ¹³C NMR and pyrolysis-GC-MS [15] points to the progressive loss of oxygen functional groups and aliphatic species from the macromolecular network of the subbituminous coal during its depolymerization in tetralin under TPL conditions. The higher conversions in TPL runs (relative to the conventional runs in tetralin) suggest that the removal of carboxylic and catecholic groups from the coal during the programmed heat-up in tetralin may have contributed to minimizing the retrogressive crosslinking at higher temperatures.

Mechanistic Considerations

Comparative examination between the TPL and N-PL runs using different solvents established that the beneficial effects of temperature-programming in tetralin are not due to thermal treatment but are closely associated with low temperature hydrogen-transfer during programmed heat-up. Although H-transfer is a chemical process, both the physical and chemical mechanisms can be responsible for the desirable effects of TPL as compared to N-PL in tetralin. Our initial idea in designing the temperature program was to meet the physical as well as chemical requirements for conversion of coals which are macromolecular in chemical nature but are microporous in physical nature. The rationale of selecting a low temperature soak is associated with the characteristics of coal pore structure. A large part of pore volume of low-rank coals is located in mesopores (20-500 Å in diameter) and macropores (>500 Å). However, most of the surface area of coals is enclosed in the micropores (<20 Å); hence rates of reaction are limited by rates of diffusion through the micropores [19,20]. Spears et al. [20] reported that the micropore walls contain polar functional groups, and their abundance is higher for low-rank coals. It is considered that soak at 200°C for 15 min will facilitate the diffusion of tetralin into the micropores (< 20 Å) and smaller mesopores (>20 Å). Also, possibility exists that tetralin could induce swelling at 200°C which may open up some pores that are solvent-inaccessible at room temperature. However, such physical effects would be smaller for liquefaction of bituminous coals.

The chemically beneficial effect of TPL compared to N-PL in H-donor lies in the programmed heat-up. The H-transfer from H-donor could stabilize the thermally derived radicals and thermally sensitive groups. Because of the bond dissociation energy distribution, one could selectively break certain bonds at certain temperature range by using temperature programming, which would provide time for radical to abstract H from H-donor. Low-rank coals are characterized by low aromaticities and high oxygen functionalities [21]. Suuberg et al. [22], Solomon et al. [18] and Lynch et al. [23] have indicated that during coal pyrolysis, decarboxylation is accompanied by crosslinking reactions and the formation of CO₂. McMillen et al. [24] have provided some insights into the retrogressive reactions involving polyhydroxy structures. It is likely that the retrogressive reactions occurring during liquefaction of low-rank coals under conventional high-severity conditions are, at least in part, associated with the reactions of their oxygen functional groups. It seems possible from comparative examination of the coal conversion data that the TPL conditions may facilitate the reduction of crosslinking reactions of the thermally sensitive groups such as oxygen-functional groups at low temperatures in H-donor. Both the present and previous results [3,4,8] strongly suggest that very fast heating would result in too fast a thermal fragmentation of low-rank coals at high temperatures to be balanced by H-donation, which consequently leads to enhanced retrogressive reactions.

Acknowledgements

Financial support for this work was provided by the Cooperative Program for Coal Research (Fund No. 424-04-2404 LG-4-91) at Pennsylvania State University. We gratefully acknowledge the assistance of Mr. J. McConnie in liquefaction experiments. We also wish to thank Dr. A. Davis and Mr. D.C. Glick for providing the samples and data of the coals from Penn State Coal Sample Bank.

References

- Sondreal, E.A., Paper presented at the *Information Transfer Session*, Cooperative Program in Coal Research, The Pennsylvania State University, Nov. 18-19, 1991.
- Derbyshire, F.; Davis, A.; Lin, R., *Energy & Fuels* 1989, 3, 431.
- Song, C., Hanaoka, K. and Nomura, M., *Fuel* 1989, 68, 287.
- Song, C., Nomura, M. and Hanaoka, K., *Coal Sci. Technol.* 1987, 11, 239.
- DOE COLIRN Panel, "Coal Liquefaction", Final Report, DOE-ER-0400, Vol. I & II, 1989
- Song, C.; Nomura, M.; Ono, T., *Am. Chem. Soc. Div. Fuel Chem. Prepr.* 1991, 36(2), 586
- Song, C.; Nomura, M., *Fuel*, 1986, 65, 922.
- Masunaga, T and Kageyama Y. *Proc. 1989 Int. Conf. Coal Sci.*, Tokyo, 1989, 819.
- Derbyshire, F.J.; Davis, A.; Epstein, M.; Stansberry, P.G. *Fuel* 1986, 65, 1233
- Derbyshire, F.J.; Davis, A.; Schobert, H.; Stansberry, P.G. *Am. Chem. Soc. Div. Fuel Chem. Prepr.* 1990, 35, 51.
- Burgess, C.E. and Schobert, H. *Am. Chem. Soc. Div. Fuel Chem. Prepr.* 1990, 35, 31.
- Stenberg, V.I., Gutenkurt, V., Nowok, J. and Sweeny P.G. *Fuel* 1989, 68, 133.
- Song, C.; Schobert, H.H.; Hatcher, P.G., *Proc. 1991 Int. Conf. Coal Sci.*, 1991, UK, p.664.
- Song, C.; Schobert, H.H.; Hatcher, P.G., *Energy & Fuels* 1992, in press.
- Song, C.; Schobert, H.H.; Hatcher, P.G., *Am. Chem. Soc. Div. Fuel Chem. Prepr.* 1992, 37, in press.
- Huang, L.; Song, C.; Schobert, H.H., *Am. Chem. Soc. Div. Fuel Chem. Prepr.* 1992, 37, in press.
- Davis, A.; Glick, D.C.; Mitchell, G.D., Proceedings of DOE Liquefaction Contractors' Review Meeting, Sept. 3-5, 1991, Pittsburgh, p.398-410.
- Solomon, P.R.; Serio, M.A.; Despande, G.V.; Kroo, E. *Energy & Fuels* 1990, 4, 42.
- Mahajan, O.P.; "Porosity of Coals and Coal Products", in *Analytical Methods for Coal and Coal Products*, Vol. I, C. Karr, Ed., Academic Press, New York, 1978, p.125-162.
- Spears, D.R.; Sady, W.; Kisperi, L.D., *Am. Chem. Soc. Div. Fuel Chem. Prepr.* 1991, 36 (2), 1277.
- Schobert, H.H., *Resources, Conservation and Recycling* 1990, 3, 111.
- Stuoberg, E.M.; Unger, P.E.; Larsen, J.W. *Energy & Fuels* 1987, 1, 305.
- Lynch, L.J.; Sakurovs *Proc. 1991 Int. Conf. Coal Sci.*, Newcastle upon Tyne, 1991, 592.
- McMillen, D.F.; Chang, S.; Nigenda, S.E.; Malhotra, R. *Proc. 1985 Int. Conf. Coal Sci.*, Sydney, 1985, 153.

Table 1. Representative Analyses of DOE / Penn State Coal Samples

Sample No.	DECS-9 or PSOC 1546	DECS-1 or PSOC 1538
Proximate (wt%)		
Volatile Matter	33.5 (47.1) ^a	33.2 (55.5) ^a
Fixed Carbon	37.1 (52.9) ^a	25.8 (44.5) ^a
Moisture	24.6	30.0
Ash	4.8	11.1
Ultimate (wt%, dmmf)		
Carbon	76.1	76.1
Hydrogen	5.1	5.5
Nitrogen	0.9	1.5
Organic Sulfur	0.3	1.1
Oxygen (by diff)	17.6	15.8
Source & Rank		
State	Montana	Texas
County	Bighorn	Freestone
City	Decker	Fairfield
Seam	Dietz	Bottom
Age of Seam	Paleo	Eocene
ASTM Rank	Subbit B	Lig A / Sub C
Sampling Date	6/12/90	12/1/89

a) On a dry, mineral matter free (dmmf) basis.

Table 2. Temperature-Programmed (TPL) and Non-programmed Liquefaction (N-PL) with H-Donor Teralin and Non-donor 1-Methylnaphthalene (1-MN) Solvents at 400 °C for 30 min

Coal	DECS-9	DECS-9	DECS-1	DECS-1	DECS-9	DECS-9
	Mont Sub	Mont Sub	Texas Lig	Texas Lig	Mont Sub	Mont Sub
	TPL	N-PL	TPL	N-PL	TPL	N-PL
Solvent	Tetralin	Tetralin	Tetralin	Tetralin	1-MN	1-MN
Prod. dmmf wt%						
THF-Conv ^a	79.2	71.4	78.0	69.8	34.1	32.2
Tolue-Conv ^b	55.5	50.1	66.1	58.0	27.1	25.4
Oil + Gas	34.4	29.4	48.5	45.1	18.9	16.0
Asphaltene	21.1	20.6	17.5	12.9	8.2	9.4
Preasphaltene	23.7	21.4	11.9	11.8	7.0	6.8

a-b) Total conversion to a) THF-solubles and b) toluene-solubles plus gas.

Table 3. Temperature-Programmed (TPL) and Non-programmed Liquefaction (N-PL) with H-Donor Teralin and Non-donor Naphthalene Solvents at 350 °C for 30 min

Coal	DECS-9	DECS-9	DECS-9	DECS-9
	Mont Sub	Mont Sub	Mont Sub	Mont Sub
	TPL	N-PL	TPL	N-PL
Solvent	Tetralin	Tetralin	Naphthalene	Naphthalene
Prod. dmmf wt%				
THF-Conv ^a	42.0	31.9	21.3	21.4
Tolue-Conv ^b	19.2	17.0	13.7	14.2
Oil + Gas	2.7	4.0	9.3	7.9
Asphaltene	16.5	13.0	4.4	6.3
Preasphaltene	22.8	14.9	7.6	7.2

a-b) Total conversion to a) THF-solubles and b) toluene-solubles plus gas.

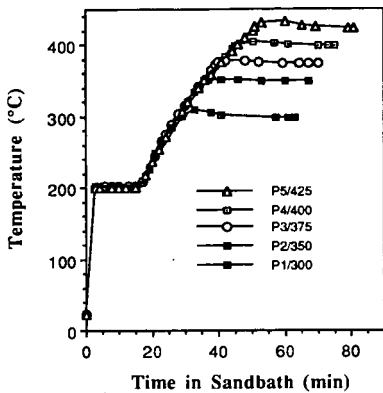


Figure 1. Temperature programs examined in TPL of DECS-9 coal.

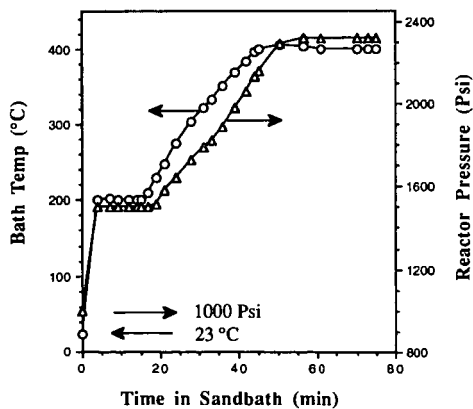


Figure 2. Typical temperature-pressure profile during programmed heat-up and holding for non-catalytic TPL of DECS-9 coal in tetralin at a final temperature of 400 °C.

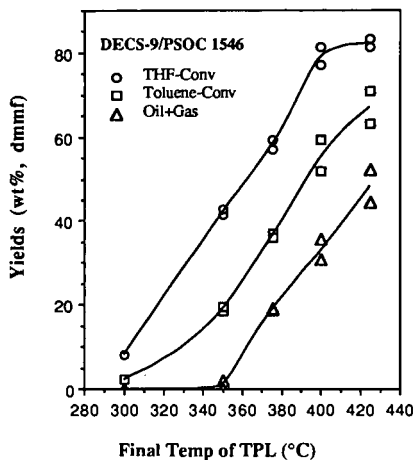


Figure 3. Relationship between final temperature of TPL and coal conversion to THF-, toluene- and hexane-solubles plus gases.

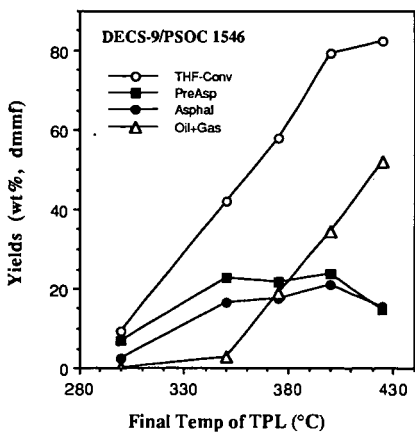


Figure 4. Product distribution from TPL of DECS-9 in tetralin at different final temperatures ranging from 300 to 425°C.

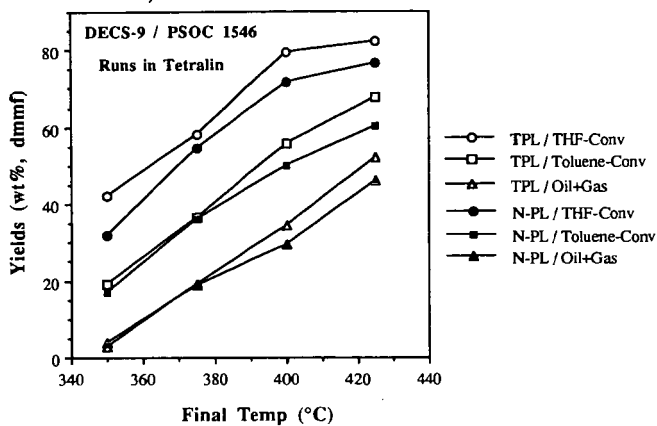


Figure 5. Comparison between temperature-programmed (TPL) and non-programmed (N-PL) runs of DECS-9 coal in tetralin solvent.

STUDIES OF THE REACTIONS OF DIBENZYL ETHER UNDER
PRECONVERSION PROCESSING CONDITIONS*

Frances V. Stohl and Richard J. Kottenstette
Process Research Division 6212
P.O. Box 5800
Sandia National Laboratories
Albuquerque, NM 87185

Keywords: retrogressive reactions, dibenzyl ether, pyrite, kaolinite

INTRODUCTION

The occurrence of retrogressive reactions during direct coal liquefaction processing is harmful because these reactions result in the formation of high molecular weight material that is refractory to further processing. Therefore, the yields of desired products are decreased, downstream processing conditions must be more severe than if retrogressive reactions did not occur, and in some cases, an accumulation of solids causes process shutdown.⁽¹⁾ The objectives of this research project are 1) to determine the causes of retrogressive reactions during the initial processing of coal (known as preconversion processing) in direct liquefaction and 2) to devise methods for minimizing these undesired reactions. The first objective involves evaluating the effects of process conditions and additives on retrogressive reactions. The approach to completing this objective is twofold. Initial scoping studies have been done using the model compound dibenzyl ether (DBE). Subsequent work will use coal. Work on the second research objective will be performed in conjunction with the evaluation of the effects of process variables and additives on coal. Research for completing the second objective will involve several different approaches such as the use of cleaned coals, and the use of different coal pretreatments.

DBE was chosen for the initial scoping studies for three reasons: 1) ether linkages represent one type of bonding reported to be present in coal⁽²⁾; 2) other investigators have analyzed the kinetics and mechanism of thermolysis of DBE^(3,4) and have also used DBE to study effects of process variables in coal liquefaction⁽⁵⁾; and 3) DBE is known to undergo retrogressive reactions. In the work reported here, experiments have been performed to evaluate the impacts of different types of mineral matter (including low temperature ash (LTA) separated from Illinois #6 coal, kaolinite (a clay mineral commonly found in coal), and pyrite) on the reaction of DBE. The preconversion processing conditions used in this work are similar to those that occur between the time the coal is mixed with recycle solvent and the time the coal slurry enters the first-stage reactor at the Wilsonville Advanced Direct Coal Liquefaction R & D Facility. This includes the preheating step in which the coal slurry is heated up to first-stage reaction temperatures. The initial temperature for preconversion processing is about 180°C (the temperature of the solvent-coal mixture just prior to entering the preheater at Wilsonville). The final temperature has not been reported because the temperature of the feed to the

* This work was supported by the U.S. Department of Energy at Sandia National Laboratories under contract DE-AC04-76DP00789.

first-stage reactor is proprietary. However, it must be less than the average first-stage temperature, which is approximately 425°C. The slurry blend tank and feed tank are both at atmospheric pressure; pressurization with hydrogen occurs prior to the slurry entering the preheater.

EXPERIMENTAL

Materials

The commercial hydrotreating catalyst used in these experiments was Shell 324N, a NiMo/Al₂O₃ catalyst with 12.4 wt% Mo and 2.8 wt% Ni. Prior to use, this catalyst was presulfided with a 10 mol% H₂S/H₂ mixture at 380°C and atmospheric pressure for 2 h, and was then ground to -200 mesh. Three types of fine-grained mineral matter were utilized: coal-derived mineral matter, kaolinite (Al₂Si₂O₅(OH)₄), and a coal-derived pyrite sample. The coal-derived mineral matter was separated from Illinois #6 coal, which was obtained from the Argonne Premium Coal Sample Program, by using an LFE Corp. low temperature ashier (model LTA 504). The kaolinite, in the form of a Georgia kaolin, was used as received. The pyrite sample was obtained by beneficiation of coal at the Robena Laboratory of the U. S. Steel Corporation and was subsequently pulverized under nitrogen to a particle size of -5 microns by means of a four inch orbital "Micron-Master Jet Pulverizer" at the Jet Pulverizer Co., Palmyra, New Jersey. The pyrite sample was cleaned by low-temperature ashing to oxidize the associated organic matter. After low-temperature ashing, the pyrite was separated from the other mineral matter by using the acid cleaning procedure, which consists of washing and filtration using hydrochloric acid, followed by hydrofluoric acid, and a repeat of the hydrochloric acid treatment, reported by Bishop and Ward⁽⁶⁾. X-ray diffraction was used to check the purity of pyrite samples.

Hydrotreating Experiments

All reactions with DBE were performed in 26 cm³ 316 stainless steel microautoclaves. The heat up time and quench time for each reaction were less than 2 minutes each. Nominal reactant and catalyst loadings for most experiments (unless otherwise noted) were 100 mg DBE, 50 mg catalyst, and 50 mg mineral matter. The microautoclaves for all experiments were charged with 1000 psig H₂ cold charge pressure. Reaction times at temperature for all experiments were 15 minutes; reaction temperatures ranged from 180°C to 300°C.

Product Analyses

Products from the microautoclave experiments were dissolved in carbon disulfide (CS₂) and analyzed using a combination of gas chromatography (GC) and GC/mass spectrometry (GC/MS). Recoveries of products from runs were determined quantitatively by GC using dodecane as an internal standard and response factors determined for DBE and toluene. Recoveries of products from the DBE reactions included quantitation of all non-CS₂ related peaks that were detected by GC (Figure 1). Unidentified compounds with GC retention times less than DBE are classified as low molecular weight unknowns, i.e. the molecular weight (MW) is less than 198, which is the MW of DBE. The total amount of low molecular weight material is equal to the sum of DBE, additional identified compounds (all of which have MWs less than DBE), and the low molecular weight unknowns. The unidentified compounds with retention times greater than DBE represent compounds with MWs greater than DBE, which were formed by retrogressive reactions. The total amount of high molecular weight material (HMWM) formed by retrogressive reactions is defined in this work as the sum of the amount of unidentified compounds detected by GC that had higher retention times than DBE

and the amount of material that was not detectable by GC. This non-detectable material, which did not elute from the GC column, was determined by difference.

Field Ionization Mass Spectrometry (FIMS) analyses, which provide molecular weight distributions for products vaporized using a mild ionization source, were performed on the products from several of the experiments. These analyses were done by Ripu Malhotra of SRI International.

RESULTS and DISCUSSION

The Impact of Low Temperature Ash from Illinois #6 Coal on DBE Reactions

Results of an experiment performed at 300°C with the low temperature ash separated from the Illinois #6 Argonne coal are shown in Figure 2. This reaction had a DBE:LTA ratio of 2.25:1. The total recovery of all products detectable by GC analysis was only about 9 wt%, of which about 4 wt% was low molecular weight products (including toluene, diphenyl methane (DPM), and C₁₄H₁₄ compounds) and about 5 wt% was unidentified material with a MW greater than DBE. The remainder of the reaction product (91 wt%) did not elute from the GC column. Therefore, the total amount of HMWM in the product was about 96 wt% indicating the occurrence of significant retrogressive reactions. The results of this experiment were compared to those of a similar experiment with Shell 324M catalyst. The experiment with Shell 324M had a 2:1 DBE:Shell 324M ratio; other conditions were the same. The total recovery of all products detectable by GC was 83 wt%, of which about 71 wt% was low molecular weight material (42 wt% toluene, 1 wt% DPM, 11 wt% bibenzyl, 9 wt% other C₁₄H₁₄ compounds, 8 wt% low molecular weight unknowns). The presence of a catalyst and no mineral matter yields a significant improvement in recoveries of low molecular weight material. (Previous work has shown that the presence of a good hydrogen donor with the Shell 324M would give a significantly higher yield of low molecular weight material.) A similar thermal reaction with no additives gave about 98 wt% recovery of low molecular weight material of which 89 wt% was DBE.

The results of the experiment with Illinois #6 LTA showed that mineral matter in coal can produce significant amounts of retrogressive reactions with DBE. Since coal-derived mineral matter contains many different components, additional experiments were performed with several of the components.

The Effects of Pyrite on DBE Reactions

The effects of pyrite on the reaction of DBE were studied because it has known catalytic activity in direct coal liquefaction. Results of an experiment with freshly cleaned Robena pyrite and DBE are shown in Figure 3. The DBE:pyrite ratio was 2:1. Results show that pyrite yields about the same total recovery of material on the GC (about 84 wt%) as Shell 324M. However, the pyrite gives more low molecular weight material than Shell 324M (77 wt% versus 71 wt%), and the distribution of low molecular weight material is significantly different; pyrite gave about 60% more toluene than Shell 324M. Both of these reactions were run in duplicate and showed excellent reproducibility.

An additional experiment was performed with an oxidized sample of Robena pyrite. This sample had been low temperature ashed and acid cleaned in 1980 using the same procedures as the freshly cleaned pyrite. It was stored under air in a glass sample vial without any special precautions to prevent oxidation. A comparison of the DBE reaction product distributions from experiments with these two pyrite samples is shown in Figure 4. The aged pyrite yielded about 95 wt% HMWM whereas the freshly cleaned pyrite gave only

23 wt% HMWM. X-ray diffraction analyses of both pyrite samples showed that the aged sample had significant amounts of iron sulfate hydrate present, whereas the freshly cleaned sample was pure pyrite.

The Effects of Kaolinite on DBE Reactions

Kaolinite was also chosen for additional experiments because it is a clay mineral present in coal, and clays usually are the most abundant minerals in coal. In addition, a previously reported study⁽⁷⁾ has shown that the acidic components of coal mineral matter enhance DBE conversion. Figure 5 shows the product distributions for five reactions of DBE with varying amounts of kaolinite present. These results show that retrogressive reactions occur for all the experiments. With the least amount of kaolinite only about 15 wt% of the product is HMWM. However, for higher concentrations of kaolinite, as much as 93 wt% of the product can be HMWM. An additional set of experiments was performed to determine the impact of reaction temperature on product distribution with 36 wt% kaolinite on a weight of DBE basis (Figure 6). The results show that even at a temperature of 180°C significant retrogressive reactions occur with about 75 wt% HMWM formed. A FIMS analysis of the product from the 180°C reaction is shown in Figure 7. The number average MW for the product was 804, significantly higher than the MW of DBE (198). The spectrum shows that the reaction product had compounds with MWs greater than 1300 amu. In addition, it shows groups of peaks that are separated by 90 amu. This distribution is indicative of the occurrence of benzylation reactions, which are known to occur in the presence of strong Lewis acids.

Three experiments were performed to determine the impact of water on the reaction of DBE with kaolinite. These results, shown in Figure 8, indicate that water does decrease the formation of HMWM. However, the effect is not very large and large amounts of water are required.

CONCLUSIONS

The results of these experiments indicate that the mineral matter in coal can have a significant effect on retrogressive reactions. Kaolinite yields high amounts of retrogressive reactions that occur down to reaction temperatures at least as low as 180°C. These retrogressive reactions are due to benzylation reactions. Pyrite, in contrast, can be either beneficial or harmful. If the pyrite is unoxidized, it can give high yields of desired product. However, if the pyrite is oxidized, it can yield significant amounts of retrogressive reactions. It has been demonstrated that retrogressive reactions can occur under currently used preconversion processing conditions and that improved processing techniques need to be developed to prevent these harmful reactions. Coal cleaning involving removal of the clays and readdition of unoxidized pyrite may be one technique for improving coal liquefaction.

REFERENCES

1. Gollakota, S. V., Vimalchand, P., Davies, O. L., Lee, J. M., Corser, M. C., Cantrell, C. E., Proc. Liquefaction Contractors' Review Meeting, 504-531, Pittsburgh, PA, September 3-5, 1991.
2. Shinn, J.H., Fuel 63(9), 1187-96, 1984.
3. Korobkov, V.Y., Grigorieva, E.N., Senko, O.V., Kalechitz, I.V., Fuel Proc. Tech. 19, 243-52, 1988.
4. Cronauer, D.C., Jewell, D.M., Shah, Y.T., Modi, R.J., Ind. Eng. Chem. Fundam. 18(2), 153-162, 1979.

5. Panvelker, S.V., Shah, Y.T., Cronauer, D.C., Ind. Eng. Chem. Fundam. 21, 236-42, 1982.
6. Bishop, M., Ward, D. L., Fuel 37, 191-200, 1958.
7. Kamiya, Y., Nagae, S., Oikawa, S., Fuel 62, 30-3, 1983.

LOW MOLECULAR WEIGHT MATERIALS

- TOLUENE Cc1ccccc1
- ADDITIONAL IDENTIFIED PRODUCTS
 - BENZALDEHYDE O=Cc1ccccc1
 - BENZYL ALCOHOL OCCc1ccccc1
 - BIBENZYL Cc1ccccc1Cc2ccccc2
 - DIPHENYL METHANE Cc1ccccc1Cc2ccccc2
- UNIDENTIFIED GC PEAKS (RT < DBE)

HIGH MOLECULAR WEIGHT MATERIALS

- UNIDENTIFIED GC PEAKS (RT > DBE)
- NOT DETECTABLE BY GC

Figure 1. Distribution of reaction products used for quantification.

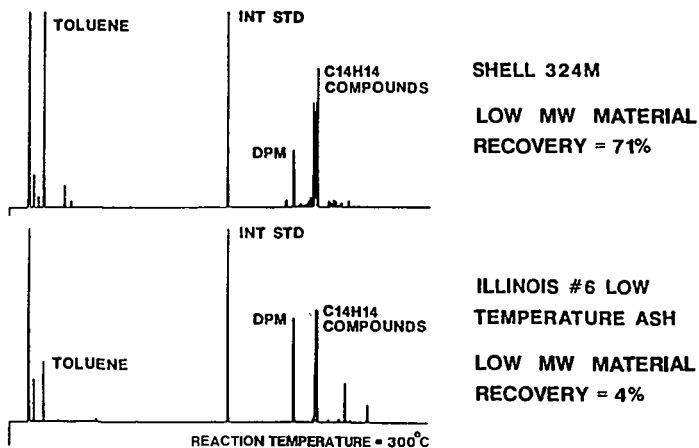


Figure 2. Mineral matter addition gave much higher yields of HMWM than Shell 324M.

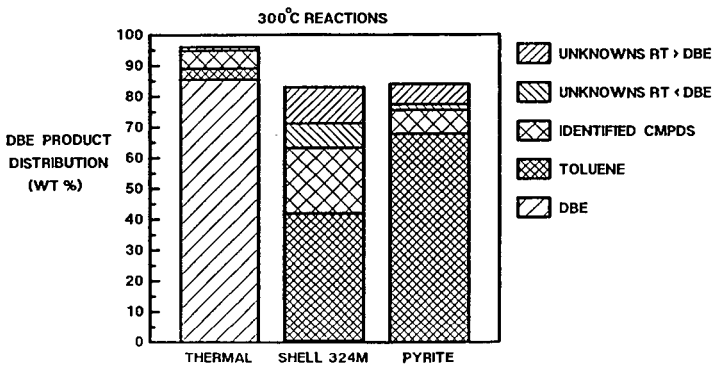


Figure 3. Pyrite addition gave 60% more toluene than Shell 324M at 300°C.

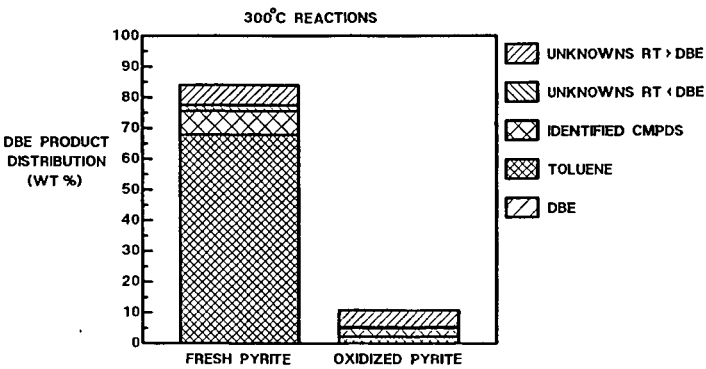


Figure 4. Oxidized pyrite causes significantly more retrogressive reactions than fresh pyrite.

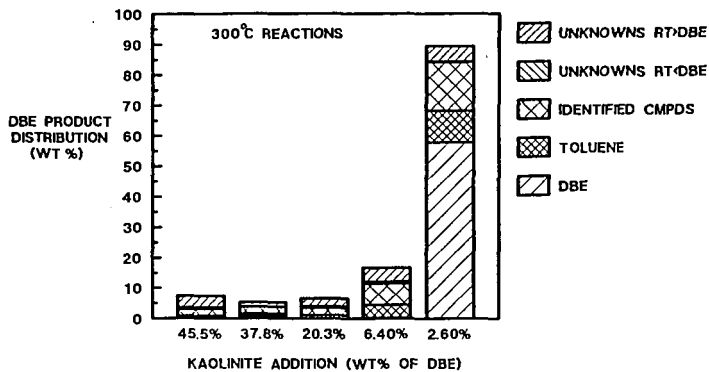


Figure 5. Kaolinite addition at 300°C causes the formation of HMWM.

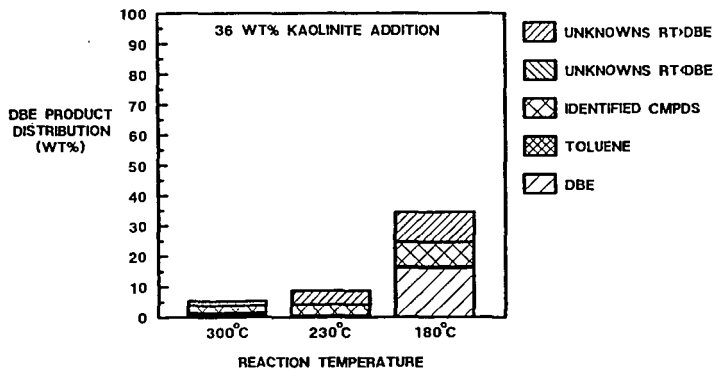


Figure 6. Kaolinite addition causes retrogressive reactions at temperatures as low as 180°C.

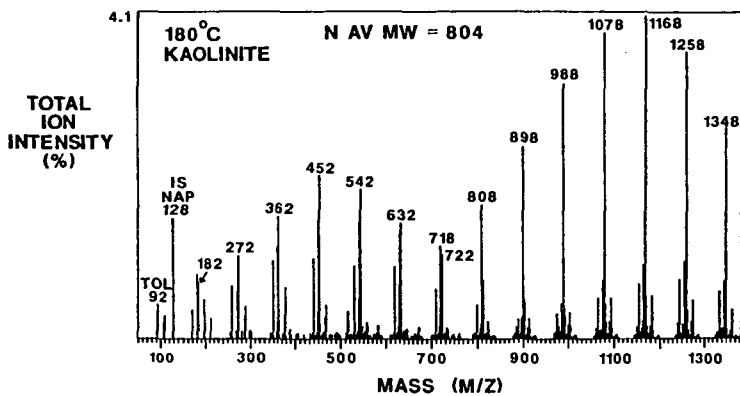


Figure 7. At 180°C, kaolinite gives benzylated products with molecular weights greater than 1300 amu.

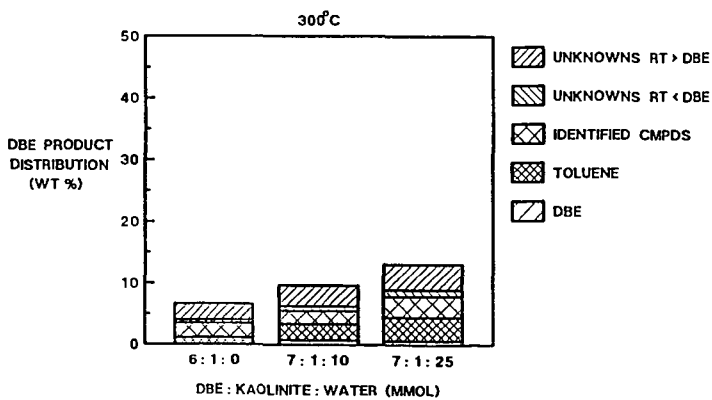


Figure 8. Addition of water appears to decrease the effect of kaolinite on retrogressive reactions.

CATALYSTS FOR AQUEOUS/CO LIQUEFACTION OF SUBBITUMINOUS COAL

Ramesh K. Sharma and Edwin S. Olson

University of North Dakota Energy and Environmental Research Center
Grand Forks, ND 58202

Key Words: Aqueous/CO liquefaction, homogeneous catalysts, sodium aluminate

ABSTRACT

Coal liquefaction has been effectively carried out with carbon monoxide reductant in an aqueous solvent (CO steam process). Australian workers demonstrated that sodium aluminate is able to catalyze the conversion of Australian coals in the CO/H₂O system and in water/hydrogen donor solvent mixtures. To demonstrate an economical process for liquefaction of Wyodak subbituminous coal, aqueous sodium aluminate has been utilized as the catalyst. High conversions comparable with those obtained with hydrogen donor solvents and hydrogen sulfide were obtained. The product consists of a large distillate fraction composed of oxygenated compounds and many aromatics. The asphaltene and oil fractions are suitable for second-stage catalytic hydrogenation. Reactions utilizing hydrogen as the reductant gave low conversions with sodium aluminate. The nature of the reductive reactions catalyzed by the sodium aluminate in aqueous/carbon monoxide systems are currently being investigated with various model compounds.

INTRODUCTION

The goal of the UNDEERC coal science group is the development of new homogeneous catalysts for first-stage coal liquefaction. These catalysts are expected to aid in solubilization and preliminary reduction of low-rank coals to a high quality intermediate product that can be easily converted to distillate fuels with low heteroatom content.

Catalysis of the first stage of coal liquefaction involves improving the rates of bond cleavage reactions leading to improved solubility and of preliminary reduction reactions so that oils and asphaltene are produced without extensive retrogressive reactions. These materials should be able to interact effectively with the solid and colloidal coal matter, catalyzing the conversion to soluble oils at moderate temperature, while minimizing problems with low surface areas or mass transfer. Thus various inorganic agents that are soluble in the reaction vehicle or solvent are being investigated. Some of these (e.g., sodium aluminate) are polymeric at the reaction conditions and are precursors for the clays and zeolites that are currently under investigation as second-stage liquefaction catalysts.

EXPERIMENTAL

Catalytic Liquefaction of Coal

A slurry consisting of 5.0 g of coal (as received Wyodak-Clovis Point) and a solution of the desired catalyst in 20 g solvent (water) was placed in a 70-ml

Parr reactor. The reactor was evacuated and charged with a mixture of 1000 psi of desired gas. The reactor was heated to 400°C in a rocking autoclave (initial heatup time = 11 minutes) and left at this temperature for 30 minutes. At the end of the reaction, the reactor was cooled to room temperature, and the gases were removed. The reactor was attached to a set of two traps cooled in ice and liquid nitrogen. The product slurry was distilled to remove water. The distillate was saturated with NaCl and extracted with ether. The extract was mixed with appropriate internal standard and analyzed by GC and GC/FTIR/MS.

The residue was extracted with pentane, toluene, and tetrahydrofuran (THF). The pentane-soluble fraction was mixed with appropriate internal standard and analyzed by GC. The toluene-soluble, THF-soluble, and THF-insoluble fractions were dried in vacuo at 110°C overnight and weighed. The percent conversion was calculated on the basis of the coal (maf) that did not appear in the THF-insoluble fraction. The conversion and yield data are given in Table 1.

Catalytic Hydrotreating of Model Compounds

In a typical run, 0.5 g of model compound, 2 g of solvent (water), and the desired amount of catalyst (if needed) were placed in a tubing bomb (12-mL microreactor). The microreactor was evacuated, pressurized with 1000 psig of carbon monoxide, placed in a rocking autoclave, and heated to 400°C. At the end of the specified reaction period, the microreactor was cooled in a dry ice-acetone slurry, degassed, and opened. The resulting slurry was acidified with dilute HCl. The desired amount of the internal standard was added to the product slurry, and the product slurry was extracted with methylene chloride. The methylene chloride extract was dried over molecular sieves (4Å) and analyzed by GC/FID and GC/FTIR/MS.

Instrumentation

Quantitative GC/FID analyses were performed with a Hewlett Packard 5880A gas chromatograph equipped with a Petrocol capillary column. A mixture of iso-octane and n-octadecane was the internal standard. GC/FTIR/MS was performed on a Finnigan 800 ITD ion trap detector with a HP 5890A gas chromatograph and a J&W 30-m x 0.32-mm (ID), 1.0-micron film of DB-5. A 15-m x 0.25-mm (ID), 0.25-micron DB-5 film capillary column was used for the analysis of high boiling components.

RESULTS AND DISCUSSION

In the first part of our study of homogeneous catalysts for first-stage coal liquefaction, catalysts for improving the conversion and product quality of liquefactions carried out in aqueous systems were investigated. Aqueous reactions that utilize carbon monoxide as the reductant gas have been extensively investigated in this and other laboratories over many years (1-3). Basic catalysts have been employed to achieve higher conversions. The aqueous/CO reduction has been shown to be superior to hydrogen for the first stage of liquefaction.

Little is understood about the mechanism of the aqueous/CO reaction with coal or even with model organic compounds. Jones and others have shown that an aryl ketone (benzophenone) and an aryl carbinol are reduced (4). Bases were required for reduction of the ketone, and higher conversions were obtained for the carbinol reduction in the presence of base. Reduction of anthracene and quinoline were also effected with aqueous CO; however, higher conversions of

anthracene were obtained in the absence of base (5). The reduction of ketones with CO in aqueous sodium carbonate can be explained by sodium ion activation of the CO to give an intermediate such as formate that can donate hydride to the carbonyl. Reduction of anthracene or other hydrocarbons would appear to proceed by a different mechanism.

In screening a number of candidates for improving the conversion in aqueous/CO liquefaction processing, Jackson and others (6,7) found that aqueous sodium aluminate gave good conversions of brown coal to oils at temperatures of 350° to 400°C. Factors such as pH and concentration in aqueous systems of the materials are critical in determining the actual aluminate structures present; however, Jackson did not report the pH of his system. Being amphoteric, the polymeric aluminate form may have Lewis acid sites at moderate pH values of 8-12 that would be effective in cleavage of covalent bonds in coals. Whether the sodium aluminate is able to activate the carbon monoxide so as to produce a hydride- or hydrogen-donating intermediate or some other form of activated hydrogen is still not certain.

The first priority in our work was to verify that sodium aluminate is also effective in improving the aqueous-CO liquefaction of low-rank western U.S. coals and to measure the solubilities and product qualities of the reaction products from these U.S. coals. Since high conversions to THF solubles are easily obtained at 400°C without any promoter or catalyst with the low-rank coals, the conversion to oils, asphaltenes, and distillate needs to be accurately determined. The composition of the distillate, oil, and asphaltene product obtained after first-stage liquefaction in aqueous CO must be determined for comparison with that obtained in organic solvents with CO or with hydrogen. Previous studies have indicated that the volatile first-stage product from aqueous liquefaction should contain large amounts of phenolics rather than hydrocarbons, as for organic solvent liquefaction. If this is the case, the distillate can be removed and used elsewhere, so that hydrogen is not wasted in deoxygenation of phenols.

The conversion of Wyodak subbituminous coal to THF solubles in the aqueous/CO liquefaction with sodium aluminate was 89% (Table 1). This was substantially higher than that obtained with no added sodium aluminate (78%). The high conversion with sodium aluminate is consistent with that observed by Jackson and others for Australian brown coals (6,7). Conversion in an aqueous/CO liquefaction experiment with sodium hydroxide catalyst was actually much lower than expected on the basis of previously reported work. Under the same conditions as the sodium aluminate experiments, only 72% of the Wyodak coal was converted to THF solubles with sodium hydroxide catalyst. After stirring the sodium aluminate and sodium hydroxide solutions with the coal at room temperature, the pH of the reactions was measured, and both reactions were at a pH of 11. At the end of the reactions, the pHs of the aqueous portions of the products were between 6 and 7 as a result of carbon dioxide generation during the liquefaction from decarboxylation and water-gas shift reactions. It is likely that the sodium aluminate is polymeric during the reaction, but further information is needed to understand the nature of the aluminate catalyst under these conditions.

The liquefaction product quality as determined by the distribution of solubility fractions was good for the sodium aluminate-catalyzed reaction. As shown in Table 1, the toluene solubles amounted to 20% of the maf coal, and 42% of the coal was converted pentane solubles, CO₂, and H₂O. The major products in the distillate were oxygenated compounds, such as methanol, 2-propanol (from

acetone), and phenolics. In addition, there were hundreds of hydrocarbon components that are typically found in coal-derived products. A similar distribution was obtained for the NaOH-catalyzed reaction, but the amounts in each of the fractions were much lower.

Reactions were conducted to verify that carbon monoxide was the most effective gas for the liquefaction of Wyodak under the mildly basic conditions. Hydrogen (1000 psi at room temperature) gave only a 43% conversion to THF solubles. Since nitrogen (1000 psi) gave a similar conversion (41%) and a similar product solubility distribution, it is unlikely that hydrogen had any effect at all in the liquefaction and was not activated by the sodium aluminate.

The second priority in our program was to understand something about the nature of the sodium aluminate catalysis. Sodium aluminate could probably activate CO for hydride reduction as well as sodium carbonate, perhaps better. But does it also activate CO so that hydrogenation of hydrocarbons occurs? Can it lower activation energies for cleavage of bonds such as in ether and carboxylate groups? The reactions of several model compounds were investigated in aqueous/CO conditions, and the results were compared with those obtained in the absence of the sodium aluminate.

Anthracene was heated in water at 400°C (2 hr) with 1000 psi of carbon monoxide (measured at room temperature). In the reaction with no promotor, a 79% conversion of the anthracene was observed (Table 2). The main reaction product was 9,10-dihydroanthracene, with 1,2,3,4-tetrahydroanthracene being a minor product. When sodium aluminate (1.25 mmole/g of substrate) was added, the conversion of anthracene increased to 82%. An anthracene reaction carried out with an equivalent amount of sodium hydroxide gave a lower conversion (64%). The lower anthracene conversion with sodium hydroxide is consistent with the lower conversion Stenberg and others reported for reactions of anthracene carried out with added sodium carbonate (5). Stenberg's results were obtained at more severe conditions (425°C, 1500 psi CO at room temperature), and the main product was tetrahydroanthracene, rather than dihydroanthracene. Dihydroanthracene may be an intermediate in the formation of tetrahydroanthracene, and more transformation of the initial dihydroanthracene may occur at the higher temperature. The sodium aluminate can, therefore, promote the reaction of carbon monoxide with polynuclear aromatic hydrocarbons somewhat better than water in a process that is retarded by the presence of other basic compounds and, in addition, can catalyze the reaction of carbon monoxide in the reduction of carbonyl groups in a process that is catalyzed by sodium carbonate or hydroxide.

Substituted naphthalenes were not significantly reduced by CO with the sodium aluminate promotor under the same conditions used for anthracene. Sodium 1-naphthoate was converted to naphthalene with complete decarboxylation and only 2% reduction to tetralin and to 1-methylnaphthalene. Sodium 1-naphtholate and 1-naphthol were recovered mostly unreacted, with 3% reduction to naphthalene and to tetralin. Increasing the amount of sodium aluminate tenfold in the naphthol reduction resulted in only a slight increase in the yield of tetralin.

Further work on the mechanisms and nature of the intermediates involved in these reactions is in progress.

ACKNOWLEDGEMENT

The support of the US Department of Energy is gratefully acknowledged.

REFERENCES

1. Appell, H.R.; Wender, I.; Miller, R.D. Prep. Pap.--Am. Chem. Soc., Div. of Fuel Chem. 1969, 13, 39-44.
2. Sondreal, E.A.; Knudson, C.L.; Schiller, J.E.; May, T.H. Proc. 9th Biennial Lignite Symp.: DOE/GFERC/IC-77/1, 1977, 129-158.
3. Ross, D.S.; Green, R.K.; Monsani, R.; Hum, G.P. Energy Fuels 1987, 1, 287.
4. Jones, D.; Baltisberger, R.J.; Klabunde, K.J.; Woolsey, N.F.; Stenberg, V.I. J. Org. Chem. 1978, 43, 175-177.
5. Stenberg, V.I.; Wang, J.; Baltisberger, R.J.; Van Buren, R.; Woolsey, N.F. J. Org. Chem. 1978, 43, 2991-2994.
6. Jackson, W.R.; Lim, S.C.; Stray, G.J.; Larkins, F.P. Proc. 1989 Internat. Conf. on Coal Sci.; Tokyo, Dec. 1989, Vol. II, pp 815-818.
7. Hughes, C.P.; Sridhar, T.; Chuan, L.S.; Redlich, P.J.; Jackson, W.R.; Larkins, F.P. USA/Australia Workshop on Use of Low-Rank Coals; Billings, MT, May 1991.

Table 1 Catalytic Liquefaction of Wyodak Coal

Reaction Temp. = 400°C, Reaction Time = 30 min Coal (as rec.) = 5.0 g, Reductant gas = 1000 psi (at room temp.)					
Catalyst (mmol/g coal)	Reductant	Conv. (%)*	Products (%)		
			Tol.-S	THF-S	Pent.-S#
NaAlO ₂ (0.5)	CO	89	20	27	42
NaOH (0.5)	CO	72	16	22	34
None	CO	78	n	44	34
NaAlO ₂ (0.5)	N ₂	41	n	18	23
NaAlO ₂ (0.5)	H ₂	43	n	17	25

* = Conversions are based upon the amount of initial coal (maf).

= Pentane solubles are by difference, also includes the products extracted by ether from the distillate.

n = Not determined.

Table 2 Reactions of Anthracene

Reaction Temperature = 400°C, Reaction Time = 2 hours Solvent (Water) = 2 g, CO = 1000 psig			
Catalyst (mmol/g substr)	Substr. (mmol)	Conv. (%)	Major Products (mmol)
None	2.77	79	9,10-Dihydroanthracene (2.02) Tetrahydroanthracene (0.11)
NaAlO ₂ (1.25)	2.81	82	9,10-Dihydroanthracene (2.19) Tetrahydroanthracene (0.13)
NaOH (1.25)	2.79	64	9,10-Dihydroanthracene (1.70) Tetrahydroanthracene (0.10)

DRYING OF BEULAH-ZAP LIGNITE.
PRETREATMENT WITH SOLVENTS AND REHYDRATION

Karl S. Vorres
Chemistry Div., Bldg. 211
Argonne National Lab.
Argonne, IL 60439

Keywords: Drying, Solvent pretreatment, Rehydration

ABSTRACT

Lignite (-100 mesh from the Argonne Premium Coal Sample Program) was dried in nitrogen under various conditions in a Cahn 121 thermobalance as part of a program on drying low rank coals for liquefaction. Samples were pretreated with solvents to determine the solvent's ability to displace water from the pores. Toluene had little effect. Acetone and methanol, selected because of water miscibility, were examined also. The methanol accelerated the drying, apparently because it was able to diffuse into the pores. The effect of drying on reactivity was examined by determining the rate of rehydration. Hysteresis was also examined. Rehydration is slow, and incomplete within a 23 hour period. The ability of carbon dioxide to substitute for nitrogen was examined. The behavior was similar with slight advantages for using nitrogen.

INTRODUCTION

Liquefaction of coals at low severity conditions is an important goal of coal research to maintain an economical, stable, long term supply of liquid fuels. Lignite is an abundant and reactive U. S. coal. One of the detracting properties of lignite is the high moisture content. Drying is usually carried out to minimize the impact of this constituent in the conversion process. Drying affects the reactivity of the coal. This effect is thought to be due to physical changes, such as irreversible pore collapse and/or other structural changes. Earlier work has indicated changes in the oil yield derived from raw, partly dried and more completely dried lignite samples (1).

Comments by some speakers to the effect that carbon dioxide can more effectively displace moisture from coal than nitrogen, reminiscent of use for surface area measurements or oil displacement from source rock, led to tests of the substitution of carbon dioxide for nitrogen in drying experiments.

It has also been suggested that the use of light oil to agglomerate coal prior to liquefaction may be beneficial in terms of moisture removal. There are benefits in terms of mineral reduction. Some added experiments were carried out to determine the capability of a light aromatic hydrocarbon and some other small hydrophilic molecules to accelerate drying rates.

The reactivity of the product coal is always of concern. A loss in reactivity due to a drying method, even though drying is improved, may preclude the use of the drying method. A standard

test adopted here for comparison of reactivity has been the ability to rehydrate the sample, as measured by the rate under a standard set of conditions.

EXPERIMENTAL

Coal drying was done with a Cahn model 121 thermobalance attached to an IBM PC/XT microcomputer. Vendor-supplied software was used to monitor the progress of individual runs, and convert data files to a form that could be further studied with Lotus 123.

The data were obtained as files of time, temperature and weight at 10 second intervals. Run times varied from 7-23 hours. Sample sizes started as about 80 mg. Temperatures were 30 or 40 C. The gas velocity past the sample was typically 80 cc/min in the 25 mm diameter tube. The sample was placed in a quartz flat bottom pan. The sample was the -100 mesh Argonne Premium Coal Sample - Beulah-Zap lignite (5).

Samples were quickly transferred from ampoules which had been kept in constant humidity chambers with water at room temperature (293°K). In the thermobalance system a period of about 5 minutes was used to stabilize the system and initiate data acquisition. A condenser was made to replace the usual quartz envelope that surrounds the sample. An antifreeze solution was circulated from a constant temperature bath through the condenser to maintain constant temperature during the experiments. This was more stable than the original furnace and provided very uniform temperature control during the experiments.

The gas atmosphere for the nitrogen gas runs was cylinder nitrogen (99.99%) or "house" nitrogen from the evaporation of liquid nitrogen storage containers used without further purification. For the carbon dioxide the gas was 99.9% carbon dioxide from a gas cylinder. The gas velocity was measured with a float-type flowmeter and adjusted for the density difference between carbon dioxide and air.

Data were analyzed as reported earlier (1,2,3,4). The best fit was obtained with a first order or unimolecular expression. Regression analysis was used to obtain the kinetic constants. Lotus 123 was used for analysis of individual run data. Approximations to a first and second derivative of the rate expressions were made in Lotus 123 by averaging over 20 of the 10 second time intervals before and after the point of interest. These derivatives were plotted with the rate data for further interpretation of the data.

Experiments with solvents were carried out by weighing the samples as usual and then adding solvent so that the sample was just covered with liquid. This was done on a balance to determine the amounts of solvent. The sample was then transferred to the TGA and a drying run was carried out in nitrogen as with earlier samples. There was about five minutes of contact time before the beginning of the drying run.

The reactivity of the sample was checked by measuring the rate of hydration. Tests of rehydration or humidification involved switching the gas atmosphere by passing the same gas flow through a coarse fritted gas bubbler filled with distilled water at room temperature (293°K). Typical times for the change were about 5 minutes. Finally hysteresis checks were made by redrying the humidified sample following the procedure for the initial drying.

RESULTS AND DISCUSSION

Earlier work by the author with higher rank coal samples (3,4) included studies of humidification of dried samples to determine hysteresis, observe consistency or changes in mechanism of reaction and compare rates of moisture loss and gain.

Basis for Comparison

The solvent based runs were carried out at 30°C and the runs with carbon dioxide were carried out at 40°C and a gas flow rate of 80 cc/min with sample sizes of about 80 mg. Runs with nitrogen at those conditions were used for comparison. The sets of runs include 135-7, 145-146, 150-2.

In this series of runs the sample was initially dried in nitrogen, then the gas atmosphere was changed to humid nitrogen to allow humidification to take place, and then the sample was redried to compare with the original drying. Three series of runs are summarized in Table 1.

Table 1. Runs in Nitrogen for Comparison

Run #	Coal type	k_1 dry	Moisture	k_{humid}	k_{redry}	Temp
135-7	raw	.00269	31.86%	.00264	not run	30 C
145-6	equil	.00323	29.6%	.00445	not run	30 C
150-2	equil	.00503	32.25%	.0092	.00367	40 C

MC?

A typical run series in which the three runs are superimposed is shown in Figure 1. The runs indicate that the raw coal (fresh from the ampoule) does not lose moisture as rapidly as the sample which has been allowed to equilibrate with water in a desiccator chamber at room temperature for at least a few days. Under similar conditions the equilibrated coal does not lose as much moisture as the fresh one. The rate of hydration of the equilibrated coal is greater than the rate for the raw coal. The indicated rate reflects the speed of approach to the final state for the system. The final state for rehydration or humidification involves a significantly lower moisture content than the starting material (i.e. 5% vs 31%). Therefore a comparison, per unit time, of the mass of water initially lost with the amount regained by the coal indicates that the rate of loss in the initial drying surpasses the rate of rehydration by a significant amount.

The rate of humidification of the dried coal from experiments at 40 C increases more than the rate of drying compared to the rates at 30 C. The shape of the rate function versus time curve is different for the redrying of the humidified coal than for the

original drying of the coal, implying a change, probably to a desorption mechanism. A slightly higher amount of moisture is removed by drying at higher temperature.

Drying in Carbon Dioxide

Two samples (about 80 mg) were each placed through a series of three runs without removing them from the TGA. The purpose was to establish the drying rate, rehydration rate and hysteresis by measuring the redrying rate of the humidified sample (one was at 57 cc/min gas flow, while the other was at 80 cc/min). These rates were to be compared to those in nitrogen.

A comparison of the data with that indicated above using nitrogen indicated that the drying behavior in carbon dioxide is very similar. The CO₂ drying rate (run 166) was .00398 based on mg water/gm sample per 10 second interval at 40°C with a gas flow rate of 57 cc/min. The weight loss amounted to 30.12% moisture removal. The indicated rate followed an induction period of about 1800 seconds while the rate slowly increased from .00333 to .00398. Following the initial 4,200 seconds of the run the rate gradually slowed so that in the period from 28,000 to 44,000 seconds the rate was .00056 based on mg water/gm sample/10 second interval. The rate slowed even further after that and the run was ended after 68,040 seconds.

Following a five minute changeover to humid CO₂, data on hydration were obtained. The rate of hydration (run 167) following drying in carbon dioxide also followed a first order expression. About 200 seconds were needed for the moist carbon dioxide to displace the dry gas. The rate gradually increased over about 1600 seconds until it became constant at about .00521 mg water/gm sample/10 second interval at the 57 cc/min flow rate. After 3600 seconds the rate gradually decreased. It should be noted that the rate of rehydration was greater than the rate of drying. The moisture addition resulted in restoration of the moisture content to only 4.45% compared to 30.1% originally.

The humidified sample was redried in run 168 to compare the behavior with the raw sample and establish hysteresis effects. The weight loss data no longer followed a first order expression, so a direct comparison of rates was not possible. The data appear to be closer to a desorption kinetic form, indicating a significant change in mechanism. Figure 2 shows the weight change data for the three runs.

Another sample was run through the same three steps of drying, rehydration and redrying to check the reproducibility of results and compare the behavior at 80 cc/min gas flow. Runs 169-171 showed the same behavior and the weight curves superimpose very well.

When the gas flow rate was 80 cc/min the drying rate increased from .00326 to .00403. The duration of the interval for the high rate was about 3,300 seconds and then the rate gradually decreased to .00177, about three times the rate for run 166.

The rate constant for humidification in run 170 at 80 cc/min was initially .0053 and increased to .0062.

The redrying of the humidified sample in run 171 indicated that the mechanism has again shifted as the rate constantly decreased if a first order plot was attempted. Again, desorption kinetics seem more appropriate.

The initial changes in the rate during the first drying prompted a re-examination of a number of runs to determine if the rate change might be due to some induction step or thermal lag as the sample changed temperature or possibly induced by the gas flow. Runs 135 at 30°C in nitrogen and 150 at 40°C in nitrogen were studied for this purpose. Each of these involved sample sizes of about 80 mg with the same flat bottom quartz bucket and 80 cc/min gas flow past the sample.

A superposition of Figures 1 and 2 indicates that similar runs in nitrogen show a more rapid loss of moisture.

Drying with Solvents

Several solvents were used to explore the effects of treatment with volatile hydrocarbons and water miscible solvents (toluene, acetone and methanol). A run using water in place of a solvent was carried out for a check on the experimental procedure. The experimental results are indicated in Table 2.

The rates of drying for the toluene treated sample appear to be less than that for the others. Treatment with acetone is essentially similar to the base water case. Treatment with water appears to cause a slight increase. The addition of methanol apparently permits diffusion of the miscible solvent into the pores such that the measured mass change is accelerated. The change can be due to a combination of a real rate increase and the increase in mass of methanol compared to water (neglecting volume effects).

The solvents rapidly evaporated following a linear weight loss with time. The drying then appeared to be similar to normal drying in mechanism and in terms of rates, except as noted above. Humidification and redrying were similar also to the cases of nitrogen drying of normal samples.

Table 2. Drying Lignite After Exposure to Solvents at 30°C

Solvent	Run #	k_1 dry	Moisture
Toluene	137-9	.00317	29.0%
Acetone	140-2	.00333	30.3%
Methanol	142-4	.00397	31.1%
Water	147-8	.00363	30.4%

Drying in Humid Nitrogen

A series of runs were carried out in humid nitrogen to determine the limits of water reabsorption, and search for changes in rate or mechanism. Runs 154-5 at 40°C and 156 at 60°C are summarized in Table 3.

Table 3. Drying Lignite in Humid Nitrogen

Run #	Temp°C	k_{humid}	Moisture Loss	$k_{\text{dry N}}$	$k_{\text{humid 2}}$
154	40	.00414	23.7%		
156	60	.01227	28.5%	.00531	.01736

It is no surprise that the rates of drying are less than those under dry conditions, in this case about 80% of the rate at 40°C. The amount of moisture lost at 40°C is about 7-8% less than that lost using dry nitrogen.

CONCLUSIONS

A base set of rates is available to compare the results of thermogravimetric analysis (TGA) experiments over the temperature range of interest.

The curves for drying and humidification with moist nitrogen or carbon dioxide are very similar.

The curves for redrying humidified samples are different from the drying of the original sample, implying a different mechanism for the second moisture loss, probably following a desorption rate control.

The use of solvents to accelerate the rate of drying does not seem to be beneficial with a non-miscible aromatic light hydrocarbon like toluene. A water miscible solvent like acetone was not beneficial either when the contact time before the experiment was only five minutes. A smaller water miscible molecule did have an effect, indicating that the rate would increase.

The use of humid nitrogen in place of nitrogen reduces the amount of moisture that will be removed in an initial drying. The amount that can be restored in humidification at a given temperature is also reduced indicating a limited reactivity compared to a nitrogen dried material.

ACKNOWLEDGMENTS

The author gratefully acknowledges the support of the U. S. Department of Energy, Pittsburgh Energy Technology Center.

REFERENCES

1. Vorres, K. S., Wertz, D., Joseph, J. T. and Fisher, R., Am. Chem. Soc. Preprints Fuel Chem. Div. 36 (3), 853 (1991).
2. Vorres, K. S., Molenda, D., Dang, Y. and Malhotra, V. M., Am. Chem. Soc. Preprints Fuel Chem. Div. 36 (1), 108 (1991).

3. Vorres, K. S., R. Kolman, and T. Griswold, Am. Chem. Soc. Preprints Fuel Chem. Div. 33 (2), 333 (1988).
4. Vorres, K. S. and R. Kolman, Am. Chem. Soc. Preprints Fuel Chem. Div. 33 (3), 7 (1988).
5. Vorres, K. S. Energy & Fuels, 4 (5) 420 (1990).

Fig. 1, Lignite in N₂, 40 C

ND150-2, -100 mesh, 81 mg, 80 cc/min, fbb

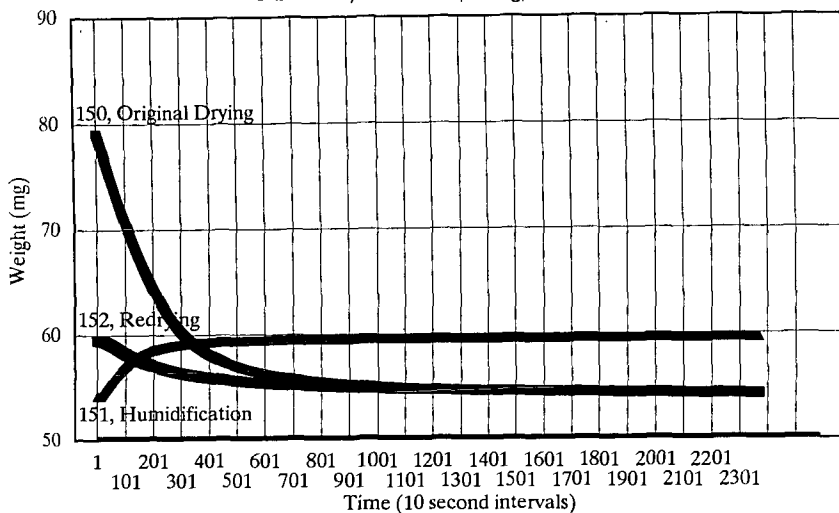
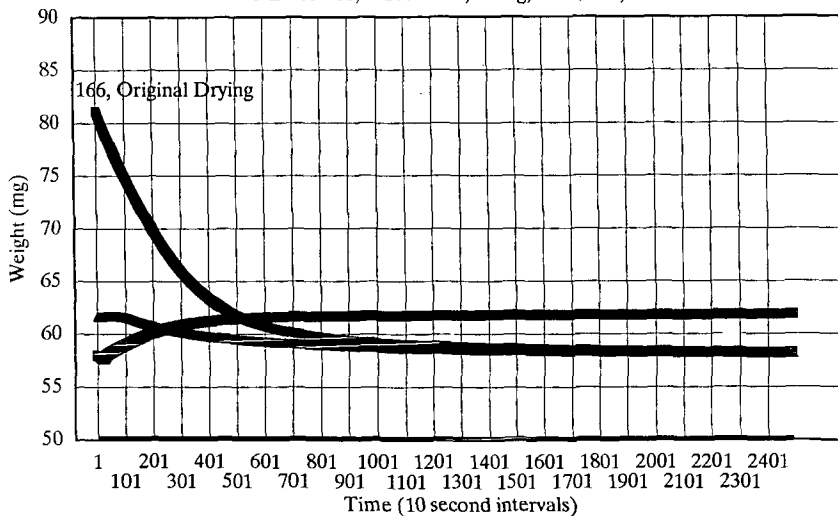


Fig. 2, Lignite in CO₂, 40 C

ND166-68, -100 mesh, 83 mg, 57 cc/min, fbb



HOT VAPOR TREATMENT OF GULF PROVINCE LIGNITES

Stanley D. Merritt, John P. Wagner, Tibor G. Rozgonyi and Jerome H. Zoeller, Jr. Engineering Biosciences Research Center, Texas Engineering Experiment Station, College Station, Texas TX 77843-2476

Keywords: Coal, desulfurization, fluidized bed.

INTRODUCTION

Fluidized steam beds are used in Germany (1, 2), Australia (3), Hungary (4) and more recently in The United States (5) for the drying of low rank coal. The technologies developed for this process can be carried out on a continuous mode, and provides an economical alternative to dewatering the fuel before, or during, the combustion operation. Fuels which contain sulfur do produce sulfurous effluent gases under steam drying conditions. It has long been known that treatment of coals with hot hydrogen produces hydrogen sulfide, and sulfur dioxide with hot oxygen. In fact, sulfurous fumes are sometimes noted when sulfur-containing coals are heated in air at temperatures below 200 °C. The present work is to study conditions under which this effect could be enhanced. The possibility of achieving significant desulfurization under the comparatively mild thermal conditions in a fluidized steam bed - typically 160 °C. with a wide range of residence times - prompted a search for vapor phase reagents that would induce chemical desulfurization of coal under hot vapor conditions.

Studies of chemical reagents for coal desulfurization are of several types. Chemicals of promise to us are the redox reagents, studied in water solution. Notable examples of these include the CO/H₂O water gas shift couple (6), numerous mineral acids (7, 8), alkali bases (9, 10), transition metal cations (11), peroxy radical generators (12, 13), and the HBr/Br₂ redox couple (14). Perchloroethylene is a reagent that has demonstrated desulfurization potential (15), and can be vaporized. EPRI has in fact sponsored research into the behavior of coals under hot vapor treatment (16). For our initial experiments, nitrous oxide, trimethylamine and dimethyl ether were selected. All three are well-documented electron transfer reagents.

Two reactors were constructed for the study (17). A fixed bed reactor was made from stainless steel tubing. The reactor is fed with premixed hot vapor, heated continuously, and monitored for temperature and pressure. It is the results of these experiments that will be discussed here. A fluidized bed was made from a section of tubing seven cm. in diameter, to study the process under more realistic conditions. Three typical Gulf province lignites were used. The hot vapor reagents consisted of nitrogen or air mixed with 0.2 % steam and 15 to 30 % of the reagent.

EXPERIMENTAL

Reactors A fixed bed reactor was fabricated from stainless steel tubing 1.9 cm. in diameter by 15.2 cm. long. Sintered stainless steel plates threaded at the bottom (100 um. pores) and top (90 um. pores) of the unit contain the sample and the fines that are generated. Line connections leading to and from the reactor are 1.27 cm. in diameter. Figure 1 is a diagram of the apparatus. Close to the entrance and exit ports to the reactor are thermal wells for thermocouples, and ports for the differential flow meter probes. The reactor is wrapped with heating tape. Gases are led through flowmeters into a section of 3/4" stainless steel tubing wrapped with heating tape. Water is also metered into this preheater. The heated vapors are led into the bottom of the reactor.

A fluidized bed system was made from a stainless steel tube 7 cm. in diameter and 12 inches high, fitted at the bottom with a removable distributor plate of sintered stainless steel. A 90 um. pore filter at the exit contained the fines. This unit takes a much larger gas volume than the fixed bed unit. The preheater is a series of parallel tubes positioned inside of a Lindberg tubular furnace. The reactor itself is heated by a tubular furnace as well.

Lignites Yegua sequence lignite was a polydisperse run-of-mine sample from the Texas Municipal Power Authority generating plant at Gibbon Creek. Particals as large as 7 mm. are present with intermediate and fine particals. Wilcox sequence lignites were also provided by TMPA, from their mines in Freestone County and Martin Lake. These two lignites were sieved to 16 X 30 mesh and 30 X 200 mesh respectively, and deslimed. Table 1 lists the properties of these lignite samples.

Reagents Nitrous oxide was obtained from the Nitrous Oxide Corporation. Trimethylamine and dimethyl ether were supplied by the Aldrich Chemical Company. The gas mixtures consist of nitrous oxide in moist air, trimethylamine in moist nitrogen, and dimethyl ether in moist nitrogen. The composition of the gases is given in Table 2.

Hot Vapor Treatment Temperatures under which the lignites were treated are shown in Table 3. Also shown here are the sulfur contents and calorific values of the untreated, nitrogen control, and treated lignites. Treated samples were sealed under nitrogen until their analyses.

Analysis Proximate analysis were done on all samples, with analysis for total sulfur. In selected experiments, samples of the effluent gases were analysed by gc-ms.

RESULTS AND DISCUSSION

Results from the gas mixtures in Table 2, at the temperatures listed in Table 3, for the three lignites treated in the fixed bed reactor, are listed in Table 3. Here is listed the total sulfur content, calorific value and the sulfur emissions parameter. Although none of these experiments show significant desulfurization, some aspects of the data deserve note. None of the Gibbon Creek samples show a change in their calorific value, but both the Freestone County and Martin Lake samples increase in calorific value by 15 to 20%.

Analysis of selected samples of the effluent gases (Freestone County, N_2 ; Martin Lake, NMe_3 and Martin Lake Me_2O) showed that hydrogen sulfide is evolved. The apparent increase in the sulfur content of the treated lignites indicates that mass loss is occurring. The volatile matter yield of the treated samples is never more than 3 to 4% higher than the values given in Table 1. Tar does collect in the effluent gas tubing. All this suggests that mass loss from the samples, by decarboxylation or resin devolatilization, is larger than any desulfurization effect.

When heated at 110 °C. for an hour, all the treated samples show an increase in mass, typically from 2 to 5%. The treatment of Martin Lake lignite in the fluidized bed at 110 °C. results in the formation of dust, which is not present in the original lignite.

ACKNOWLEDGEMENTS

This research is made possible through the support of the Texas Higher Education Coordinating Board, through their Texas Advanced Technology Program. The continuing support of the Center for Energy and Mineral Resources, of Texas A&M University, is also gratefully acknowledged.

REFERENCES

1. Wolf, B., Energietechnik 1988, 7, 245
2. Militzer, K.-E., and Nebelung, M., Drying Technology 1988, 4, 675
3. Huggins, R.S., Allerdice, D.J. and Perry, G.J. "Upgrading Experience and Studies on Australian Brown Coals" In Proceedings of the Opportunities in the Synfuels Industry, University of North Dakota Energy and Minerals Research Center; Bismark, North Dakota, August 28-31, 1988

4. Rozgonyi, T.G. and Szigeti, L.Z. (1985) , Fuel Processing Technology 1985, 1
5. Land, G.W. and Brown, G.J., "The First Commercial Application of Fluid Bed Drying to Subbituminous Coal", COALPREP 89 the sixth International Coal Preparation Exhibition & Conference, May 2-4, 1989; Lexington, Kentucky
- 6.. Ross, D.S., Blessing, J.E., Nguyen, Q.C. and Hum, G.P. Fuel 1984, 9, 1206
7. Salem, G.F. and Schmidt, A.M. "Chemical Beneficiation of Coal", U.S. Patent 4,741,741 to Standard Oil Company, Cleveland, May 3, 1988, Filed Oct 17, 1977
8. McGowan, C.W., Cates, K.Q. and Markuszewski, R (1988) "The Conversion of Organic Sulfur in Coal to Sulfate using Perchloric Acid", Prepr. Pap. - Div. Fuel Chem., Amer. Chem Soc. 1988, 1, 225
9. Markuszewski, R., Miller, L.J., Strazheim, W.E., Fan, C.W., Wheelock, T.D. and Greer, R.T., "Evaluation of the removal of Organic Sulfur from Coal", pp 401-414 in New Approaches to Coal Chemistry, ACS Symp. Series 169
10. Mazumder, B., Saikia, P.C., Baruah, B.D. and Bordolo, C.S., Fuel 1989, 5, 610
11. Janikowski, S.K., Skrobbutt, A.T. and Vorres, K.S. "Ultrafine Coal Cleaning with Metal Salt Solutions", In Processing and Utilization of High Sulfur Coals, Y. P. Chugh and R. D. Caudle, Editors. Proceedings of the Second International Conference on Processing and Utilization of High Sulfur Coals, Sept. 28 - Oct. 1, 1987, Carbondale, Illinois.
12. Venkata Swamy, Y. and Chandra, D. J. Inst. Fuel 1986, 107, 120
13. Brubaker, I.M. and Stoicos, T. "Precombustion Coal Desulfurization with Sodium Hypochlorite", In Processing and Utilization of High Sulfur Coals, Y. A. Attia, Editor. Proceedings of the First International Conference on Processing and Utilization of High Sulfur Coals, Columbus, Ohio, Oct. 13 - 17, 1985. pp 311
14. Schuetz, G.H. and Serrini, G., Fuel 1988, 12, 1595
15. Buchanan, D.H. "Coal Desulfurization using Perchloroethylene", Quarterly Reports for the period ending May 31, 1989, July 17, 1989, to The Center for Research on Sulfur in Coal.
16. Tewksbury, T.L., Carlton, H.E. and Oxley, J.H. (1988) "Progress Report on the Selective Oxidation of Pyrites in Coal", Proceedings: Twelfth Annual EPRI Contractors' Conference on Fuel Science and Conversion, Report AP-5460-SR, 1988 pp4-1 to 4-16, Palo Alto, California, May 13-14, 1987, Electric Power Research Institute, Palo Alto
17. Merritt, S.D., "Development and Evaluation of Two Reactors Designs for Desulfurization of Texas Lignites", M.S. Thesis submitted to Texas A&M University, May, 1991.

Table 1: Properties of the Lignites Studied.

Lignite	H ₂ O % Whole	S _{tot} % Dry	Ash Yield % Dry	Volatile Matter % DAF	Calorific Value Btu/#
Gibbon Creek	30.5	1.45	37.0	58.7	7630
Freestone County	12.2	0.73	9.2	50.0	9421
Martin Lake	11.8	1.79	10.7	51.0	9219

Table 2: Hot Vapor Treatment Conditions. Temperatures are listed in Table 3.

Label	Treatment	Vapor Composition	Residence Time, Min.
UN	Untreated Lignite	-	-
N ₂	Wet Nitrogen Control	N ₂ /H ₂ O = 99.8/0.2	20
N ₂ O	Nitrous Oxide	N ₂ O/Air/H ₂ O = 24.8/75.0/0.2	20
NMe ₃	Trimethyl Amine	NMe ₃ /N ₂ /H ₂ O = 19.2/80.6/0.2	20
Me ₂ O	Dimethyl Ether	Me ₂ O/N ₂ /H ₂ O = 23.9/75.9/0.2	20

Table 3: Treatment temperatures, Sulfur contents and calorific values for the untreated lignites (UN), wet nitrogen controls (N₂), and representative samples of the treated lignites.

Lignite	Treatment (Table 2)	Temp. °C.	S _{tot} % Dry	Calorific Value, BTU/#	#SO ₂ MBTU
Gibbon Creek	UN	-	1.45	7630	3.8
	N ₂	220	1.33	7666	3.5
	N ₂ O	220	-	-	-
	NMe ₃	130	1.36	7666	3.6
	Me ₂ O	220	1.44	7623	3.8
Freestone County	UN	-	0.73	9421	1.6
	N ₂	220	1.00	11335	1.8
	N ₂ O	220	1.27	11466	2.2
	NMe ₃	130	0.91	11063	1.7
	Me ₂ O	220	0.93	11213	1.7
Martin Lake	UN	-	1.79	9219	3.9
	N ₂	120	2.15	10909	3.9
	N ₂ O	110	2.39	10784	4.4
	NMe ₃	110	2.29	10837	4.2
	Me ₂ O	120	2.09	10919	3.8

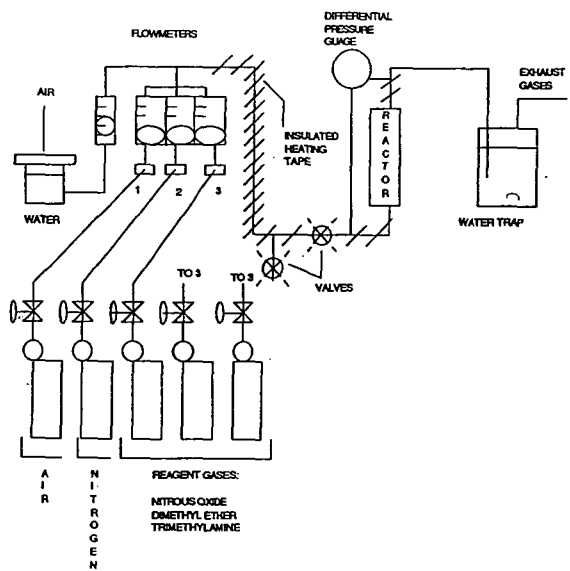


Figure 1: Diagram of the Fixed Bed Reactor. In the Fluidized Bed Reactor, the preheater and Reactor are heated by Lindberg tubular furnaces.

COAL SOLUBILIZATION USING METAL ALKOXIDES IN REFLUXING ALCOHOLS

Kuntal Chatterjee, Sao Jiralerspong and Leon M. Stock
Department of Chemistry, The University of Chicago
5735 South Ellis Ave., Chicago, IL 60637

INTRODUCTION

The inability to quantitatively solubilize coal in common organic solvents has been a detriment to the use and study of this vast fuel resource. Our efforts in the past few years have been directed toward its solubilization through O- and C-alkylation and base-promoted depolymerization.¹ O-Alkylation, which completely disrupts intermolecular hydrogen bonding, only increases the solubility of low rank coals such as Wyodak and Illinois No. 6 coals to the 35% level.¹ C-Alkylation, which can be extremely effective for the solubilization of high rank coals, is only moderately more effective for these coals than O-alkylation alone.² We were intrigued by the possibility that their solubilization could be improved by basic reagents without alkylation when we found that two high rank coals were rendered about 40% soluble merely by treatment with strong bases (most notably Lochmann's base).³ We concluded that this procedure was effective because the carbanions generated by the strong bases underwent carbon-carbon bond cleavage and produced smaller, more soluble coal fragments.³ Our prior work with basic reagents did not convert the two low rank coals to soluble products and we reasoned that the carbanions that are produced by very strong bases also undergo condensation reactions to retrogressively increase the size of the coal molecules. We, therefore, sought to eliminate this undesirable reaction by trapping the carbanions with a proton donor. The present study describes an approach to solubilize Illinois No. 6 coal (APCSP 3) by base treatment with metal alkoxides in refluxing proton donating alcohols.

EXPERIMENTAL SECTION

Materials. The Illinois No. 6 coal (APCSP 3) was obtained from the Premium Sample Program at Argonne National Laboratory.⁴ Elemental analysis (wt.%) of moisture-free coal: C, 65.7; H, 4.2; N, 1.2; S, 4.8; O (by difference) 9.8; Ash, 14.3. Pyridine was purified by distillation over barium oxide. Sodium, potassium, sodium methoxide, *n*-octanol, and benzyl alcohol were used as received from Aldrich Chemical Company. Methanol, *n*-butanol, and *tert*-butanol were used as received from J.T. Baker Inc.

General Reaction Procedure. In general, the alcohol (420 mmol) and solid potassium (80 mmol) were added to a flame-dried round-bottom flask and stirred under dinitrogen at room temperature for 30 to 45 minutes to form the metal alkoxide. The coal (2 g) was then added and the reaction mixture was stirred for 5 minutes before heating to reflux. Usually, a small pool of potassium was visible when the coal was added. The reaction mixture was refluxed for 24 hours. It was cooled in a 0 °C bath and any remaining base was diluted with *tert*-butanol followed by methanol and water. It was then acidified with dilute hydrochloric acid (2 M) until the pH was less than 1. This acidified mixture was stirred under dinitrogen for 48 hours and the solvents were removed from the reaction product either by rotary evaporation or by vacuum distillation, depending upon the boiling points of the solvents. The reaction product was then washed under dinitrogen on a Nucleopore polycarbonate membrane filter (pore size 0.8 mm) with dilute hydrochloric acid (2 M, 5 L), with methanol until the filtrate was colorless (8 L), and with aqueous methanol (50% by

volume) until the filtrate was free of halide ions (12 L). Finally, the reaction product was dried at 110°C under high vacuum for 48 hours. A sample was submitted for elemental analysis.

A portion of the product was subjected to pyridine extraction and unless otherwise mentioned, the solubility of the reaction product was determined from the weight of the insoluble portion.

Analysis of Products. Elemental analyses were performed by Commercial Testing and Engineering Company of South Holland, Illinois. Infrared spectroscopy was carried out on a Nicolet 20SXB FTIR spectrometer. ²H NMR spectroscopy was carried out on a Varian XL-400 spectrometer.

RESULTS AND DISCUSSION

Significant work has been done with alcohols as solvents and reagents for the liquefaction of coal. Use of low boiling alcohols under super critical conditions or in hydrogen donor solvents in the presence or absence of bases has been investigated by a number of workers.⁵⁻⁷ Ross *et al.* have investigated potassium isopropoxide in isopropanol and potassium hydroxide in methanol at 400 °C.⁵ More recently, Ouchi and his coworkers have reported the reactions of coals with ethanolic sodium hydroxide at temperatures ranging from 260 to 450 °C.⁶ Similar reactions were also performed with ethylene glycol as solvent by Winans *et al.*⁷ The yields of the liquified coals in these studies were high but the conditions were also severe. We sought milder conditions for the conversion so that the side reactions, if any, could be minimized. Also, some investigators have neglected the possibility that alcohols transform and adduct to coal molecules. Accordingly, we measured the conversion exclusively on the basis of the weight of the insoluble coal residue.

Potassium or sodium alkoxides, as described in the Experimental Section, were used in different alcohols at reflux for 24 hours and then the products were quenched with dilute acid. The results are presented in Table 1.

The reaction of Illinois no. 6 coal with sodium methoxide in refluxing methanol yielded a product which was only 33% soluble in pyridine. The pyridine solubility of the raw coal is 27%. Treatment with potassium *n*- and *tert*-butoxide in *n*- and *tert*-butanol with boiling points 118 and 83°C, respectively, increased the solubility of the coal to 42%. There was no significant difference between the effectiveness of the two isomeric butanols. Potassium *n*-octoxide in *n*-octanol (b.p. 196°C) gave an even more soluble product, 53%. Finally, potassium and sodium benzoxide in refluxing benzyl alcohol (b.p. 205°C) provided more than 70% soluble material.

We also briefly investigated the optimum conditions. There were differences in the yields at 6 and 24 hours, so we adopted the 24 hour reaction time for all our reactions. Selected other results are shown in Table 2. With sodium benzoxide, concentrations from 40 to 120 mmol per gram of coal gave good results and the product obtained was about 70% soluble in pyridine. However, higher concentrations of the base resulted in reaction products with masses much greater than those of the starting materials. Thus, it was evident that at higher base concentration, chemical addition reactions take place.

The results also show that the extent of solubilization does not depend on the basicity of the alkoxides. Rather, the differences in their effectiveness apparently arise as a consequence of the differences in their boiling points. There are two lines of evidence. First, the two higher-boiling alcohols, benzyl alcohol and *n*-octanol with boiling point near 200°C, gave more soluble products than the lower-boiling alcohols. Second, the use of sodium methoxide in refluxing benzyl alcohol was as effective as sodium benzoxide in the same solvent (Table 1). These results strongly suggest that there is a significant activation energy for the key conversion reaction.

We believe that there are two underlying reasons for the success of this strategy. First, hydrogen is probably transferred from the solvent to the coal. Previous work performed by the Argonne group demonstrated that the aromatic rings in coal underwent reduction in proton donor solvents with alkali hydroxides.⁷ In this study, benzaldehyde was detected among the reaction products. The microanalytical data for the reaction products, however, indicate that the increase in

the hydrogen content is modest. Second, subtle base-catalyzed carbon-oxygen, carbon-sulfur and carbon-carbon bond cleavage reactions fragment the low rank coals. It has been shown previously that strong bases such as Lochmann's base, can cleave carbon-carbon bonds in hydrocarbons if the resulting carbanions are stable.¹ Also, it has been shown that sulfidic carbon-sulfur bonds undergo cleavage under basic conditions.⁸ In presence of proton donor solvents, the anions formed in such bond scission processes are trapped and the possibility for their recombination to yield a condensation product is reduced.

A major point of interest was the large decrease in the total sulfur content of the products.⁸ The reduction ranged from 16% for *tert*-butoxide in *tert*-butanol (4.1 wt% S) to 80% for benzoxide in benzyl alcohol (1.0 wt% S). This result implies that all the pyrite and at least 50% of the organic sulfur were removed. The extent of sulfur removal for the various alkoxides in the corresponding alcohols paralleled their ability to solubilize the coal.

CONCLUSIONS

Treatment of Illinois No. 6 coal with alkoxides in refluxing alcohols yields products that are 40 to 70% soluble in pyridine, compared to 27% for the starting material. The extent of solubilization depends upon the boiling point of the alcohol and not upon the structures of the alkoxide and the alcohol. The best results were obtained with 40 mmol of sodium or potassium benzoxide per gram of coal in benzyl alcohol. Significant sulfur removal was achieved, an 80% reduction from 4.8 to 1.0 wt% S by using the benzoxide. Thus, base-catalyzed reactions at temperatures near 200 °C solubilize and desulfurize this Illinois No. 6 coal.

ACKNOWLEDGEMENTS

The authors wish to acknowledge support of this work from the United States Department of Energy under contract no. DOE/AG22-87PC79938.

REFERENCES

1. Chatterjee, K., Ph.D Dissertation, The University of Chicago, 1991.
2. Chatterjee, K.; Miyake, M.; Stock, L. M., *Energy and Fuels*, 1990, 4, 242.
3. Chatterjee, K. and Stock, L. M., manuscript in preparation.
4. Vorres, K.S. *Energy and Fuels*, 1990, 4, 420.
5. Ross, D.S. and Blessing, J. E., *Fuel*, 1979, 58, 433; 58, 438.
6. Makabe, M., Hirano, Y., Ouchi, K. *Fuel*, 1978, 57, 289; 57, 801; Makabe, M., Ouchi, K. *Fuel*, 1979, 58, 43.
7. Winans, R.E.; Hayatsu, R.; Mcbeth, R. L.; Scott, R. G.; Moore, L. P. and Studier, M. H. Ed. M.L.Gorbaty and K.Ouchi. *Advances in Chemistry Series* 1981, 192, pp 133.
8. Chatterjee, K. and Stock, L. M. *Energy and Fuels*, 1991, 5, 704.

TABLE 1.
RESULTS FOR ALKOXIDE TREATMENT OF ILLINOIS NO. 6 COAL IN REFLUXING
ALCOHOLS. DETERMINING THE OPTIMUM REACTANT-SOLVENT SYSTEM.

reaction conditions: base, solvent, time	reaction temperature, °C	coal recovered, wt%, db	pyridine solubility, wt%
raw coal	-	-	27
NaOMe (40 mmol/g), MeOH, 24 h, protonation	65	86	33
KO <i>n</i> -Bu (40 mmol/g), <i>n</i> -BuOH, 24 h, protonation	118	76	42
KO <i>r</i> -Bu (40 mmol/g), <i>t</i> -BuOH, 24 h, protonation	83	83	42
KO <i>n</i> -Oct (40 mmol/g), <i>n</i> -OcOH, 24 h, protonation	196	79	53
KOBz (40 mmol/g), BzOH, 24 h, protonation	205	43 ^a	82
NaOBz (40 mmol/g), BzOH, 24 h, protonation	205	51 ^a	74
KOBz (40 mmol/g), BzOH, 24 h, protonation	205	95	66
NaOMe (40 mmol/g), BzOH, 24 h, protonation	205	68 ^a	64

^aThe recovery of the products after the reaction was low since a significant portion of the coal was soluble in the alcohol, and this material was removed during washing and filtration.

TABLE 2.
 RESULTS FOR SODIUM BENZOXIDE TREATMENT OF ILLINOIS NO. 6 COAL IN
 REFLUXING BENZYL ALCOHOL AT 205 °C. EFFECT OF CHANGING THE BASE
 CONCENTRATION.

concentration of sodium benzoxide (mmol/g coal)	coal recovered, wt%, db	pyridine solubility, wt%
raw coal	-	27
40	51 ^a	74
74	77 ^a	52
121	63 ^a	70
253	285	31
486	457	35

^aThe recovery of the products in these experiments was low since a significant portion of the coal was soluble in the alcohol and this material was discarded in these experiments.

ENHANCED LOW SEVERITY COAL LIQUEFACTION USING SELECTIVE CALCIUM REMOVAL

K. Shams, R.L. Miller, and R.M. Baldwin

Chemical Engineering and Petroleum Refining Department
Colorado School of Mines
Golden, Colorado 80401

ABSTRACT

This paper reports results from an on-going process development study in which coal is converted to liquid products at relatively mild reaction conditions. The process consists of three main steps: 1) mild pretreatment of the feed coal at ambient conditions using methanol (or other common organic solvent) and a trace amount of hydrochloric acid to enhance dissolution reactivity and dry the coal, 2) low severity thermal dissolution to obtain a very reactive coal-derived residual intermediate product amenable to upgrading, and 3) catalytic upgrading of the residual products to distillate liquids. We have found that mild pretreatment of Wyodak subbituminous coal using methanol/HCl can provide an improvement in THF conversion of greater than 30 wt% at 350° C reaction temperature. Analysis of treated Wyodak and Illinois #6 coal samples indicates that no organic phase alteration such as alkylation occurs during pretreatment, but that over 90 wt% of the calcium is removed from each coal. Calcium is thought to catalyze retrogressive reactions during coal pyrolysis, and thus calcium removal prior to low severity liquefaction minimizes the production of THF-insoluble products.

INTRODUCTION

Much of the recent research in direct coal liquefaction seeks to develop methods for dissolving coal at low reaction severity (defined as temperatures below 350° C and pressures of 1000-1500 psi). The incentives for developing a viable low severity liquefaction process are numerous; they include: 1) reduced hydrocarbon gas production resulting in reduced feed gas consumption and enhanced hydrogen utilization efficiency, 2) suppressed retrogression of primary coal dissolution products resulting in enhanced distillate and residuum product quality, 3) production of high boiling residuum which is less refractory and thus more amenable to catalytic upgrading in a conventional second-stage hydrocracker, 4) substitution of less expensive off-the-shelf vessels, piping, valves, pumps, etc. in place of expensive, custom-designed units, and 5) less severe slurry handling and materials of construction problems as a result of lower operating temperatures and pressures.

However, as shown schematically in Figure 1, lowering the liquefaction severity reduces coal conversion and liquid product yields unless the intrinsic coal reactivity can be sufficiently enhanced using some method of physical or chemical pretreatment. The main challenge to developing a viable low severity liquefaction process scheme involves finding an efficient and inexpensive means of coal pretreatment which will provide high levels of conversion and liquid product yields at low reaction severity. Researchers at several locations including the Pittsburgh Energy Technology Center (1), the University of North Dakota Energy and Environmental Research Center (2), Carbon Resources, Inc. (3), and the Colorado School of Mines (4) have investigated various methods for improving coal reactivity and liquid yields at mild reaction conditions. These studies showed that coal can be readily converted to tetrahydrofuran (THF) soluble products via selective chemical attack rather than thermal bond scission, but that the rate and extent of coal dissolution at mild conditions is strongly dependent upon intrinsic coal reactivity.

Numerous chemical treatments including reductive and non-reductive alkylation (5,6), acylation (7), partial oxidation (8), alkali hydrolysis (9), and solvent swelling (10) have been used to disrupt the coal's organic structure and increase solvent solubility. Limited work has been reported in which the liquefaction reactivity of alkylated coals has been studied. Schlosberg et al. (11) measured the reactivity of alkylated Wyodak subbituminous and Illinois #6 bituminous coals in tetralin at 427° C, 1500 psi hydrogen pressure and 130 min. reaction time. A 10-21 wt% (maf and alkyl group-free basis) increase in cyclohexane conversion was noted for the alkylated coals.

More recently, the effect of chemical pretreatment on the inorganic constituents of coal via a vis liquefaction reactivity has been studied. Mochida (12) reported that hydrochloric acid can be used to destroy cationic bridges present in low rank coals, thereby reducing coordination between oxygen-containing functional groups and allowing better contacting between coal and solvent during the initial stages of dissolution. Joseph (13) reported that removal of sodium, potassium, and calcium from low rank coals enhances liquefaction reactivity. He attributes this effect to inhibited hydrogen transfer in the presence of these cations.

The objective of this paper is to present experimental results from a study in which mild chemical pretreatment using methanol and hydrochloric acid was used as a method to improve intrinsic coal reactivity at low liquefaction reaction conditions. Possible explanations for the observed reactivity enhancement will also be discussed.

EXPERIMENTAL PROCEDURE

The entire suite of eight coals from the Argonne Premium Coal Sample Bank was used as the source of feed coals for this study. Ultimate analyses for these coals are listed in Table I (14). Coal samples were stored under argon in sealed ampules prior to pretreatment and liquefaction experiments.

Coal was pretreated by suspending 5 g of undried coal in 40 cm³ of methanol and 0.6 cm³ of concentrated hydrochloric acid in a 100 cm³ round bottom flask and continuously stirring the coal/methanol slurry on a magnetic stirring plate for 3 hrs. The flask was connected to a cooling water condenser to reduce solvent losses by evaporation. Several experiments were completed in which dry nitrogen was used to blanket the coal/methanol slurry; elemental analyses of the treated coals showed no difference in the extent of oxidation when the system was purged with nitrogen and when it was vented to the atmosphere. Several experiments using hexane or acetone in place of methanol were also completed.

After pretreatment, most of the organic solvent was decanted off and the moist coal sample washed with three 50 cm³ aliquots of fresh solvent to remove residual acid. Any remaining solvent was recovered by vacuum drying (50° C, 10-20 millitorr pressure, 24 hrs.). Untreated coal samples were vacuum dried at the same conditions before liquefaction. After drying, all treated and untreated coal samples were stored at room temperature in a vacuum desiccator (0.1 torr) before analysis or liquefaction. Reactor runs were scheduled so that each coal sample was stored for less than 12 hours before use. Portions of each untreated coal and pretreated coal were subjected to elemental analysis and ash analysis, as well as ¹H CRAMPS and ¹³C CP/MAS NMR, FTIR, Mossbauer, and XRD spectroscopy.

Liquefaction experiments were conducted in a 20 cm³ tubing bomb reactor attached to an agitator and immersed in a fluidized sandbath. Low severity reaction conditions were set at 350° C reaction temperature, 1000 psig initial cold hydrogen pressure, and 30 min. reaction time. Dihydrophenanthrene (DHP) was used as hydrogen donor solvent (2/1 solvent/coal wt. ratio) in these runs. Coal conversion was measured using THF extraction data corrected for the intrinsic THF solubilities of treated and untreated coals. Solubility measurements were conducted at ambient conditions and consisted of three steps: 1) sonicating the liquid products from the tubing bomb reactor (or feed coal sample) in excess THF for 10 min., 2) centrifuging the mixture at 2000 rpm for 15 min., and 3) decanting THF-soluble products and excess THF from the THF-insoluble residuum. This procedure was repeated at least two times until no additional THF-soluble products were recovered. Remaining THF-insolubles were dried at 100° C for 24 hours to remove residual THF, weighed, and finally ashed. Coal conversion to THF-soluble products was computed on a moisture and ash-free basis, correcting for the intrinsic solubility of the feed coal.

RESULTS AND DISCUSSION

Effect of pretreatment on low severity liquefaction reactivity. Reactivity data for the untreated and treated Argonne coals are shown in Figure 2. Each of these data points represents the average of 2-3 reactor experiments; conversion differences of 2.1 wt% or greater (maf basis) represent statistically significant differences in liquefaction reactivity at the 95% confidence level. At the low severity reaction conditions studied, three of the high volatile bituminous coals [Illinois #6

(72.1 wt%), Blind Canyon (69.6 wt%), and Pittsburgh #8 (57.0 wt%)] gave the highest THF conversions. Wyodak subbituminous coal was the next most reactive coal (44.4 wt%), while Pocahontas low volatile bituminous coal was the least reactive sample studied (15.6 wt%). These reactivity data follow the same trends reported for the Argonne coals by other investigators (15).

Pretreatment with methanol and HCl using the procedure described earlier enhanced low severity liquefaction reactivity for all eight Argonne coals. The absolute increase ranged from only 5.5 wt% for Blind Canyon coal to 31.5 wt% for Wyodak coal, and averaged 18.0 wt% for the eight coals. No simple trends in reactivity improvement with chemical or physical properties of the coals were obvious, although the reactivity of pretreated low rank coals (Wyodak and Beulah-Zap) increased much more than reactivity of the six bituminous coals.

Although vapor phase methanol/HCl mixtures have been shown to partially alkylate bituminous coals (16), NMR and FTIR measurements indicated no alkylation occurred during our pretreatment experiments. This result was confirmed by replacing methanol with hexane or acetone (two solvents which cannot participate in acid catalyzed alkylation chemistry) during pretreatment; the reactivity of coals pretreated with hexane/HCl and acetone/HCl was also enhanced.

In an attempt to separate the effects of methanol and HCl on reactivity enhancement, a series of experiments was completed in which samples of Wyodak subbituminous coal and Illinois #6 bituminous coal were pretreated using methanol only (no HCl addition) and HCl only (1.5 wt% HCl in distilled water, no methanol addition). Results of low severity liquefaction experiments using these treated coals are summarized in Figure 3. As expected, no reactivity enhancement occurred when coal samples were pretreated with only methanol. However, coal samples treated with HCl/water exhibited significant reactivity improvement, although less than observed using methanol/HCl. Blank pretreatment using only distilled water did not affect the low severity reactivity of either coal. Thus, we can conclude that, while the presence of a small concentration of HCl is essential for successful pretreatment, the addition of methanol or other organic solvent such as hexane or acetone improves pretreatment effectiveness. Mochida (12) attributes this effect to improved wettability of the coal surface by the organic solvent and thus better contacting between coal and acid.

Effect of pretreatment on coal composition. To begin elucidating the cause of the reactivity enhancement shown in Figure 2, we used several analytical techniques to study changes in the organic and inorganic phases of Wyodak and Illinois #6 coals during pretreatment. NMR and FTIR analyses indicated no measurable organic phase alterations with one exception. The Wyodak FTIR spectra indicated formation of carboxylic function groups during pretreatment, probably as a result of divalent (Ca,Mg) cationic bridge destruction (12,13). Mossbauer spectroscopy results demonstrated that pyrite was largely unaffected by treatment with methanol and HCl, eliminating the possibility that $FeCl_3$, a known coal dissolution catalyst, was being formed in the treated coal.

X-ray diffraction measurements were conducted on the low temperature ash (LTA) from untreated and treated Wyodak and Illinois #6 coals. These results indicated that over 90 wt% of the calcium was leached from each coal during pretreatment. In these spectra, calcium was observed only as $CaCO_3$ with no CaO or $CaSO_4$ present. This observation agrees with a report by Miller and Givens (17) that organically-bound calcium will convert to $CaCO_3$ rather than CaO during low temperature ashing. Elemental analyses of treated coal samples confirmed the extent of calcium loss during pretreatment, and also showed that a lesser amount of magnesium was also extracted.

Effect of calcium content on low severity liquefaction reactivity. To study further the effect of calcium content on liquefaction reactivity, Wyodak and Illinois #6 coal samples with varying calcium contents were prepared by varying the amount of acid used during pretreatment. Other pretreatment conditions were the same as described earlier. Results of low severity liquefaction runs using these samples are shown in Figure 4. The reactivity of both coals was enhanced as calcium was removed; once again, the effect was more pronounced for Wyodak coal, particularly at a calcium content of less than about 0.2 wt%.

Several low severity liquefaction experiments were completed in which calcium as CaCO_3 was added back to the reactor prior to liquefaction. In each experiment, the amount of calcium added was equivalent to the amount extracted during pretreatment. Results of these experiments are summarized in Figure 5. As these data show, the beneficial effect of MeOH/HCl pretreatment was almost completely negated by adding CaCO_3 to the liquefaction reaction system. A similar effect was observed when CaO was added during low severity liquefaction of pretreated Wyodak and Illinois #6 coals.

The mechanistic role of calcium during low severity coal dissolution is not completely understood. Mochida (12) attributed accelerated rates of low rank coal dissolution to the destruction of calcium dicarboxylate structures and therefore, less coordination of oxygen-containing function groups. Joseph (13) speculated that calcium and other exchangeable alkaline and alkaline earth cations impeded hydrogen transfer during coal dissolution; removal of these cations would improve the rate of hydrogen transfer to coal free radicals as they form, and thus improve the extent of coal conversion. Joseph also cited the propensity of calcium dicarboxylate structures to undergo cross-linking reactions during the initial stages of coal dissolution.

We hypothesize that, in addition to the effects cited above, the presence of calcium can directly catalyze retrogressive reactions involving coal-derived free radical species during low severity liquefaction. Numerous studies have cited the role of calcium (as CaCO_3 or CaO) in increasing char yields and reducing tar yields during coal pyrolysis; the char yield enhancement has been attributed to catalysis of metaphast recombination prior to devolatilization (18) and catalysis of repolymerization and secondary cracking reactions (19). We are presently conducting a series of model compound studies to help elucidate the mechanistic effects of calcium during low severity liquefaction.

ACKNOWLEDGMENT

We wish to acknowledge financial support from the U.S. Department of Energy under Contract Nos. DE-AC22-88PC88812 and DE-FG22-90PC90289.

LITERATURE CITED

1. Bockrath, B.C.; Illig, E.C.; Finseth, D.H.; Sprecher, R.F. Prepr. Pap. - Am. Chem. Soc., Div. Fuel Chem., **29**, 5, 76, 1984.
2. Farnam, S.A.; Wolfson, A.C.; Miller, D.J.; Gaides, G.E.; Messick, D.D. Prepr. Pap. - Am. Chem. Soc., Div. Fuel Chem., **30**, 2, 354, 1985.
3. Porter, C.R.; Knudson, C.L.; Rindt, J.R. Prepr. Pap. - Am. Chem. Soc., Div. Fuel Chem., **31**, 4, 70, 1986.
4. Miller, R.L.; Baldwin, R.M. Prepr. Pap. - Am. Chem. Soc., Div. Fuel Chem., **31**, 4, 152, 1986.
5. Sternberg, H.; Delle Donne, C.L. Fuel, **53**, 172, 1974.
6. Liotta, R. Fuel, **58**, 724, 1979.
7. Hodek, W.; Kolling, G. Fuel, **52**, 220, 1973.
8. Hessley, R.K. 'Co-Oxidative Depolymerization of Coal,' Final Report for EPRI Project No. 2383-2, June 1985.
9. Mirza, Z.B.; Sarkar, M.K.; Sharma, D.K. Fuel Proc. Tech., **9**, 149, 1984.
10. Sanada, Y.; Honda, H. Fuel, **65**, 295, 1986.
11. Schlosberg, R.H.; Neavel, R.C.; Maa, P.S.; Gorbaty, M.L. Fuel, **59**, 45, 1980.
12. Mochida, I.; Shimohara, T.; Korai, Y.; Fujitsu, H.; Takeshita, K. Fuel, **62**, 659, 1983.
13. Joseph, J.T.; Forrai, T.R. Fuel, **71**, 75, 1992.
14. Vorres, K.S. Energy & Fuels, **4**, 5, 420, 1990.
15. Shin, S.C.; Baldwin, R.M.; Miller, R.L. Energy & Fuels, **3**, 193, 1989.
16. Sharma, D.K.; Sarkar, M.K.; Mirza, Z.B. Fuel, **64**, 449, 1985.
17. Miller, R.N.; Givens, P.H. 'A Geochemical Study of the Inorganic Constituents in Some Low Rank Coals,' Technical Report for DOE Contract No. EX-76-C-01-2494, February 1978.
18. Tyler, R.J.; Schafer, H.N.S. Fuel, **59**, 487, 1980.
19. Franklin, H.D.; Peters, W.A.; Howard, J.B. Prepr. Pap. - Am. Chem. Soc., Div. Fuel Chem., **26**, 121, 1981.

Table I
Ultimate Analysis of Feed Coals

Wt% Dry Basis	Wyodak	Beulah-Zap	Illinois #6	Pittsburgh #8
Carbon	68.4	65.9	65.7	75.5
Hydrogen	4.9	4.4	4.2	4.8
Nitrogen	1.0	1.0	1.2	1.5
Sulfur	0.6	0.8	4.8	2.2
Oxygen	16.3	18.2	8.6	6.7
Ash	8.8	9.7	15.5	9.3
Coal Rank	Subbit.	Lignite	HVB	HVB
Symbol	WY	BZ	ILL	PIT

Table I (cont.)
Ultimate Analysis of Feed Coals

Wt% Dry Basis	Blind Canyon	Lewiston-Stockton	Upper Freeport	Pocahontas
Carbon	76.9	66.2	74.2	86.7
Hydrogen	5.5	4.2	4.1	4.2
Nitrogen	1.5	1.3	1.4	1.3
Sulfur	0.6	0.7	2.3	0.7
Oxygen	10.8	7.8	4.8	2.3
Ash	4.7	19.8	13.2	4.8
Coal Rank	HVB	HVB	MVB	LVB
Symbol	BC	LS	UF	POC

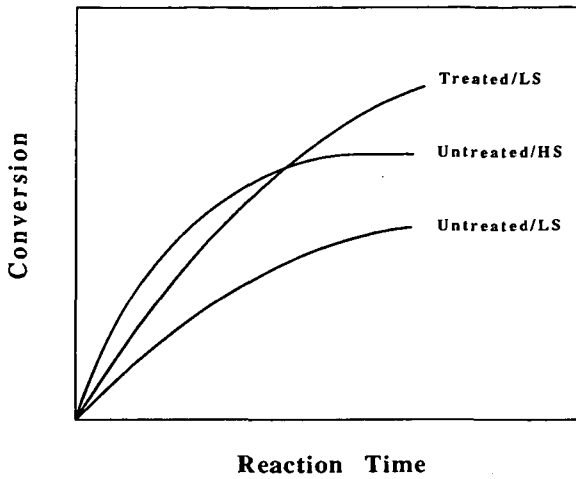


Figure 1 - Schematic Representation of Reactivity Enhancement Using Coal Pretreatment (LS = low reaction severity, HS = high reaction severity)

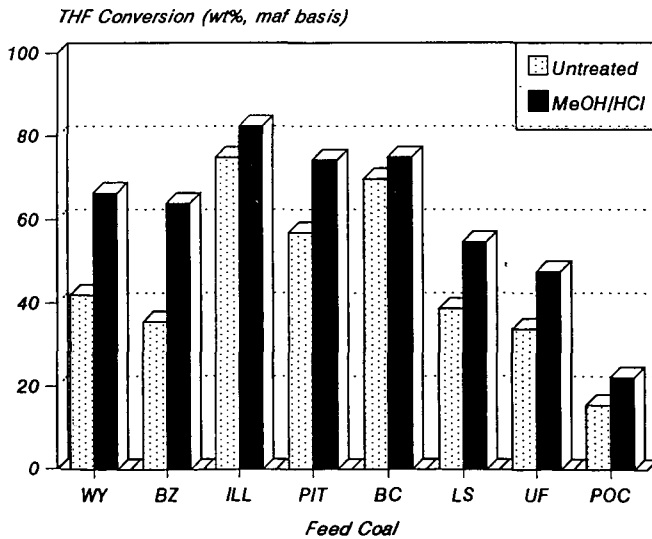


Figure 2 - Effect of Pretreatment with MeOH/HCl on Low Severity Liquefaction Reactivity of Argonne Coals

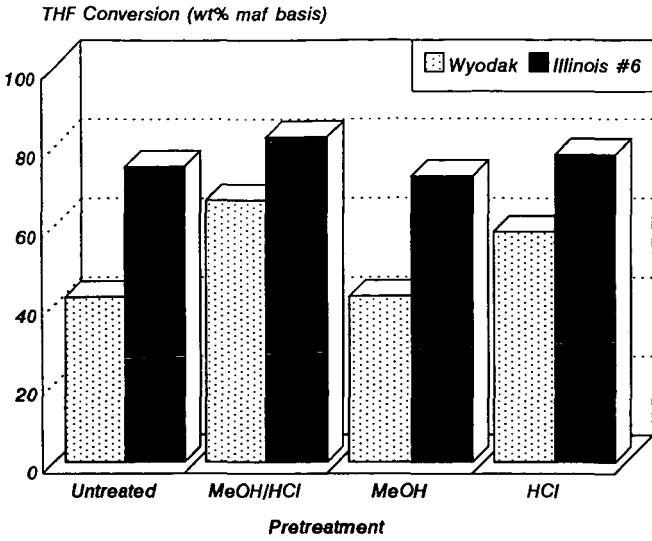


Figure 3 - Effect of Pretreatment with MeOH/HCl, MeOH, or HCl on Low Severity Liquefaction Reactivity of Wyodak and Illinois #6 Coals

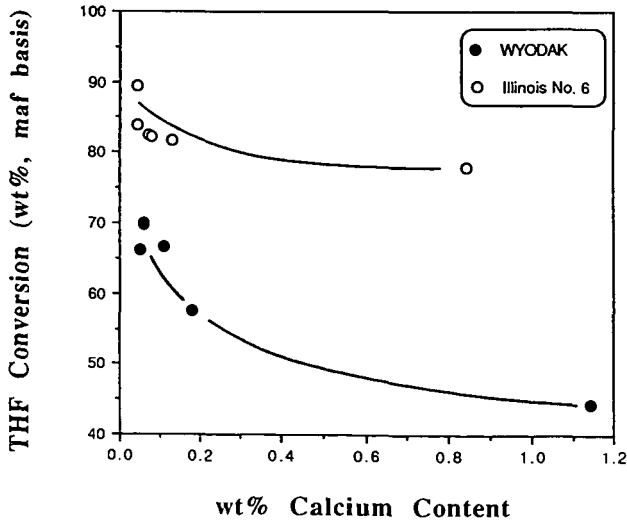


Figure 4 - Effect of Calcium Content on Low Severity Liquefaction Reactivity of Wyodak and Illinois #6 Coals

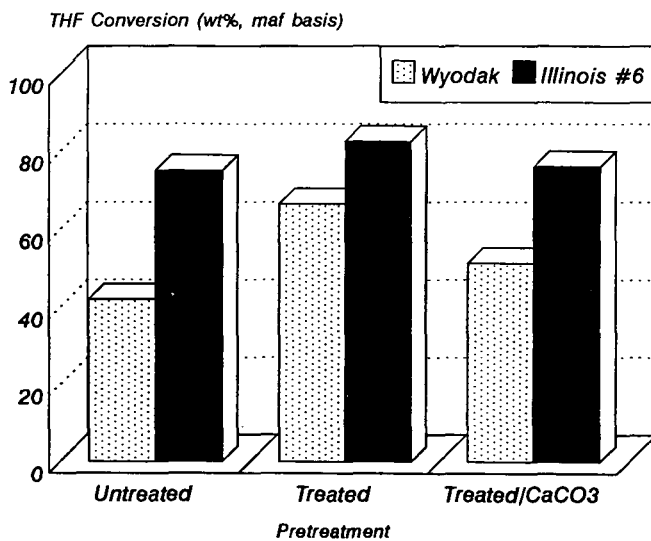


Figure 5 - Effect of Calcium Carbonate Addition on Low Severity Liquefaction Reactivity of Wyodak and Illinois #6 Coals